TERRESTRIAL HEAT FLOW STUDIES
IN EASTERN AFRICA AND THE NORTH SEA

A Thesis

By

Thomas Richard Evans

Submitted for the Degree of

Doctor of Philosophy

to the

University of London

The Geology Department

Imperial College

London, U.K.

November, 1975

Terrestrial Heat Flow Studies in Eastern Africa and the North Sea

Abstract

A detailed feasibility study of the use of oil exploration borehole temperatures and cutting samples as primary data in the computation of heat flow forms the major part of this work. The temperature data consists entirely of bottom hole temperatures (BHTs) measured by commercial logging companies during breaks in drilling. Conductivity samples were largely drill cuttings.

The thermal disturbance due to drilling and the consequent non-equilibrium state existing during temperature logging is discussed. Theoretical models and practical examples suggest that BHT derived geothermal gradients are, on average, unlikely to be more than 10-15 percent in error and thus are suitable for heat flow determinations.

A rigorous study of the reliability of conductivity values obtained from measurements on drill cuttings is presented. An empirical relation between the thermal conductivity measured at laboratory temperatures to its in-situ temperature value was derived from a large number of experimental measurements in the range 10-90^{o}C.

Sixty-eight heat flow values of variable quality were computed from all available oil exploration wells in the coastal sedimentary basins of the Sudan, Somalia, Ethiopia, Kenya, and Tanzania. Eight new Red Sea results considerably extend the heat flow coverage from the zone of axial spreading in this young proto-ocean. The results, averaging 113 mW$\cdot$m^{-2}, are consistent with a lithospheric spreading model. Two previously unknown thermal anomalies are reported; a low, mean 44 mW$\cdot$m^{-2}, in the Eastern Ogaden region of Ethiopia and Somalia and a high, mean 89 mW$\cdot$m^{-2}, in the Garissa region of Kenya.

A regional assessment of the heat flow was made by a trend surface analysis of the data and that of the surrounding seas. One dimensional modelling indicates that the lithosphere may be sufficiently thick beneath the Ogaden to impede plate motion; shallow partial melt zones are postulated under the Red Sea shelf and the Garissa region. Two dimensional modelling suggests that the Ogaden and Garissa anomalies could arise from heat production-conductivity contrast structures within the crust.

Three heat flow values are presented for the North Sea; their preferred mean is 63 $mW \cdot m^{-2}$. Extensive conductivity measurements were combined with detailed geothermal gradient and sedimentary structure maps to produce heat flow profiles.

One dimensional modelling indicates an 80 kilometre thick lithosphere beneath the North Sea. A two dimensional model of a salt dome emphasizes the importance of local structure on heat flow determinations made in oil exploration boreholes.

The mechanisms of subsidence for both Eastern Africa and the North Sea are discussed and evaluated in the context of the tectonic setting and surface heat flow of these two regions.

Table of Contents

Page			
1	Introduction		
7	Chapter 1		Temperature Measurements
7		1.1	Introduction
8		1.2	The Drilling of an Oil Exploration Well; a Description of the Resulting Thermal Disturbance
12		1.3	Temperature Measurements Routinely Made in Oil Exploration Wells
19		1.4	Model One to Predict Temperature Variations Resulting from Drilling Disturbances - The Continuous Line Heat Source
23		1.5	Model Two to Predict Temperature Variations Due to Drilling Disturbances - The Region Bounded Internally by the Continuous Cylinder Heat Source
29		1.6	The Time Required for a Borehole to Return to Thermal Equilibrium - Practical Examples
42		1.7	Other Sources of Possible Error in The Temperature Measurements
47		1.8	The Error in the Determination of The Geothermal Gradient From Oil Exploration Borehole BHTs

Page			
54		1.9	Regional Geothermal Gradient Studies and Their Significance
55		1.10	Suggestions for Future Research
57	Chapter 2		Thermal Conductivity Measurements
57		2.1	Introduction
58		2.2	The Measurement of Thermal Conductivity
60		2.3	The Divided Bar
68		2.4	Calibration of the Divided Bar
72		2.5	The Preparation and Measurement of Discs
73		2.6	The Calculation of the Contact Resistance
77		2.7	The Measurement of Rock Chips - Theory
79		2.8	The Measurement of Rock Chips - Practice
83		2.9	The Calculation of Nonporous and Porous Conductivities with a Direct Comparison with Discs
89		2.10	Porosity Determinations From Commercial Well Logs

Page			
99		2.11	Comparison of Porosity Determinations From Various Logs
105		2.12	Measurement of Soluble Rock Chips
108		2.13	The Repeatibility of Disc and Chip Conductivity Measurements
111		2.14	Interlab Checks and Fluid Comparisons
115		2.15	Errors in the Determination of Thermal Conductivity - an Assessment
126		2.16	Predicting Thermal Conductivities From Other Known Rock Properties
129		2.17	Suggestions for Future Research
131	Chapter 3		The Calculation of and The Corrections Applied to the Heat Flow Values
131		3.1	Introduction
132		3.2	The Calculation of Heat Flow - Methods
135		3.3	The Topographic Correction
138		3.4	The Climatic Correction
147		3.5	The Uplift and Erosion or Downwarp and Sedimentation Correction
153		3.6	The Correction of Thermal Conductivity Data for In-Situ Pressure

Page			
158		3.7	The Correction of Thermal Conductivity Data for In-Situ Temperature
175		3.8	Estimation of Parameters in the Calculation of Heat Flow
180		3.9	The Computation and Correction of Heat Flow Values - Computer Use, Data Presentation and Errors
185		3.10	Recommendations for Future Research
186	Chapter 4		Eastern Africa Heat Flow Results and Interpretation
186		4.1	Introduction
188		4.2	The Regional Geology of Eastern Africa (South of 15^{o}N)
195		4.3	Regional Geophysical Studies of Eastern Africa (South of 15^{o}N)
201		4.4	The Central and Southern Red Sea Regions
204		4.5	Plate Tectonics of Eastern Africa and the Surrounding Seas
208		4.6	Previous Heat Flow Studies in Eastern Africa and the Surrounding Seas
211		4.7	New Heat Flow Data from Eastern Africa
229		4.8	Heat Production Measurements

Page		
232	4.9	Coastal Red Sea Heat Flow
245	4.10	The Guban Region Heat Flow
252	4.11	The Darror and Nogal Valley Region Heat Flow
264	4.12	The Obbia Embayment Region Heat Flow
270	4.13	The Eastern Ogaden Region Heat Flow
283	4.14	The Benadir Coast Region Heat Flow
295	4.15	The Mandera-Lugh Basin Region Heat Flow
301	4.16	The South-West Somalia Basin Region Heat Flow
307	4.17	The Lamu Embayment Region Heat Flow
317	4.18	The Coastal Tanzania Region Heat Flow
324	4.19	Trend Surface Analysis of Heat Flow Data Between $10^{o}S$, $15^{o}N$, and $35^{o}E$, $70^{o}E$
338	4.20	Heat Flow and the Subsidence of the Eastern Africa Continental Margin
343	4.21	Crust and Upper Mantle Temperature Profiles

Page			
352		4.22	Two Dimensional Crust and Upper Mantle Temperature Models
360	Chapter 5		Preliminary Heat Flow Studies in The North Sea
360		5.1	Introduction
360		5.2	The Geology of the North Sea Basin
366		5.3	Geophysical Studies of the North Sea
368		5.4	North-West European Heat Flow
378		5.5	Crust and Upper Mantle Thermal Profiles
386		5.6	Heat Flow and the Subsidence of the North Sea Intracratonic Basin
388		5.7	The Effect of Local Structure on Heat Flow Determination
391	Chapter 6		Conclusions
391		6.1	Objectives
392		6.2	Significant Results
394		6.3	Suggestions for Future Research
396	List of References		

Page		
432	Omissions from Reference List	
433	Appendix 1	A Discussion of the Paper by E.C. Bullard (1947) entitled 'The Time Necessary For A Borehole To Attain Temperature Equilibrium'
436	Appendix 2	Equations and Tables for the Unit Functions $T(t_d)$, $Q(t_d)$ and $q(t_d)$
439	Appendix 3	Derivation of the Nonporous Rock Conductivity From the Maxwell Spheres Relation
442	Appendix 4	Solution of the Subsidiary Heat Equation for the Semi-Infinite Region Moving With a Velocity, u.
446	Appendix 5	Tabulation of Eastern Africa Temperature and Conductivity Data
487	Appendix 6	Tabulation of North Sea Temperature and Conductivity Data
	Inside Back Cover Pocket	'North Sea Geothermal Gradients', a Paper by T.R. Evans and N.C. Coleman (1974)
	Inside Back Cover Pocket	'Heat Flow and Heat Production in North-East Africa', a Paper by T.R. Evans and H.Y. Tammemagi (1974)

List of Figures

Page	Number	Title
4	0.1	Sedimentary Basins and Shelves of The World
10	1.1(a)	Schematic of Circulating Fluid in Oil Exploration Well
10	1.1(b)	Drill Pipe Temperatures During Circulation
11	1.1(c)	Circulating Temperatures
11	1.1(d)	Temperature versus Time (During and Post Circulation)
13	1.2	Flowline Temperatures (An Example)
15	1.3	Examples of Continuous Temperature Logs
16	1.4	Typical Log Heading
18	1.5	Comparison of BHT and Flowline Temperatures
28	1.6(a)	Graphical Representation of Equation 1.21
28	1.6(b)	Graphical Representation of Equation 1.22
28	1.6(c)	Contour Integral Path for Equation 1.31

Page	Number	Title
33	1.7(a)	Cylinder Model Dimensionless Temperature Disturbance versus the ratio of Shut In to Total Time
34	1.7(b)	Line Source and Cylinder Models - Comparison of Dimensionless Temperature Disturbance
36	1.8(a)	Examples of the Return to Thermal Equilibrium in Oil Exploration Wells
37	1.8(b)	Examples of the Return to Thermal Equilibrium in Oil Exploration Wells
39	1.9	Dimensionless Temperature Disturbance versus Dimensionless Time
43	1.10(a)	Critical Gradients for Onset of Convection in a Borehole
43	1.10(b)	Example of Well Disturbed by Water Flow
45	1.10(c)	Example of Temperatures Disturbed by Gas Flow
45	1.10(d)	Example of Temperature Disturbance by Lost Circulation
48	1.11	Maximum Per Cent Error in Two Point Gradient Determination
62	2.1	Vertical Cross Section of the Divided Bar Assembly
64	2.2	Schematic of Divided Bar Measuring System

Page	Number	Title
66	2.3	Plate of the Divided Bar
74	2.4	Contact Resistance Results
76	2.5	Contact Resistance Study
80	2.6	The Chip Thermal Conductivity Cell
85	2.7	Porous Rock Conductivity Versus Porosity
87	2.8	Porous Rock Conductivity, K_{pr} versus Disc Conductivity, K_d
91	2.9	Microlog Interpretation Chart
92	2.10	Porosity and Formation Factor Nomogram (Clean Formations)
95	2.11	Neutron Departure Curves, GNT F, G, or H
96	2.12	Neutron Porosity Equivalence Curves
100	2.13(a)	Porous Rock Conductivity, K_{pr} versus Disc Conductivity, K_d - Neutron Log Porosity Corrected Only
101	2.13(b)	Porous Rock Conductivity, K_{pr} versus Disc Conductivity, K_d - Microlaterolog Porosity Corrected Only
109	2.14	The Repeatability of The Measurement of Thermal Conductivity of Chips and Discs

Page	Number	Title
117	2.15(a)	Fractional Error (K_r'/K_r) in Nonporous Conductivity from Fractional Error (ϵ) in Bar Calibration
117	2.15(b)	Fractional Error (K_r'/K_r) in Nonporous Conductivity from Fractional Error (Ψ) in Volume Fraction of Water
122	2.15(c)	Error in Porous Rock Conductivity (K_{pr}) versus Absolute Error in Porosity (η_n)
124	2.16	Error in Porous Rock Conductivity as a Function of Nonporous (K_r) Conductivity and Porosity (η_n)
128	2.17	Example of an Empirical Conductivity Relation
137	3.1	Topographic Gradient Correction versus Depth (For Axis of Various Lee's Hills)
142	3.2	North Sea Bottom Temperature Model (Temperature versus Time)
142	3.3	North Sea Climatic Model Temperature and Geothermal Gradient Disturbances
144	3.4	Central North Sea Mean Annual Sea Bottom Temperature
144	3.5	European and African Pleistocene Climates
150	3.6	Schematic Illustration of Temperature Regime Disturbed by Downwarp and Sedimentation - (Cont'd)

Page	Number	Title
		(Cont'd)
		(a) Downwarp without sedimentation
		(b) Downwarp with contemporaneous sedimentation with constant surface temperature, T_o
		(c) Downwarp and sedimentation cease, thermal regime at time infinity
152	3.7	The Effect of Various Sedimentation/ Downwarp Models on the Geothermal Gradient
155	3.8	Absolute Change in Conductivity (K) due to Pressure (P) versus per cent Porosity, Constructed from Equation (3.37), Table 3.3, and Models Below
160	3.9	General Relations Proposed for Variation of Thermal Conductivity (K) with Temperature (T)
163	3.10	Thermal Conductivity as a Function of Temperature for 3 Empirical Relations
166	3.11	Thermal Conductivity versus Temperature - Control Samples -
		(a) Halite
		(b) Polymers
169	3.12	Thermal Conductivity of Various Rocks Measured in the Temperature Range 10-90°C
170	3.13	Thermal Conductivity of Various Rocks Measured in the Temperature Range 10-90°C
171	3.14	Thermal Conductivity of Various Rocks Measured in the Temperature Range 10-90°C

Page	Number	Title
181	3.15	Schematic Processing Flow Chart for Heat Flow Data
187	4.1	Borehole Location Map - Eastern Africa
191	4.2	Geological Map - Eastern Africa
193	4.3	Schematic Structural and Tectonic Map of Eastern Africa
196	4.4	A Bouguer Gravity Anomaly Map of Eastern Africa
199	4.5	Eastern Africa Seismicity Map
205	4.6	Plate Tectonic Map of Eastern Africa and the N.W. Indian Ocean
210	4.7	Summary of Heat Flow Values for Eastern Africa and the Surrounding Seas
213	4.8(a)	Eastern Africa Heat Flow (Coded by Reliability)
213	4.8(b)	Eastern Africa Heat Flow (Coded by Region)
215	4.9	Change in Heat Flow from Uncorrected Q_o, to Corrected Q_n, Value and Improvement in Percentage Error, ϵ, of Fit of Equation (3.1) for Corrected Heat Flow Values Q_n
216	4.10	Eastern Africa and Surrounding Seas Heat Flow Data (5 x 5 Degree Square Means)

Page	Number	Title
217	4.11	Eastern Africa Heat Flow and Local Region Division Map
233	4.12	Coastal Sudan and Red Sea Heat Flow
234	4.13	Composite Heat Flow Plot - Dungunab-1
235	4.14	" " " " - Maghersum-1
236	4.15	" " " " - Abu Shagara-1
237	4.16	" " " " - Marafit-1
239	4.17	Coastal Ethiopia and Red Sea Heat Flow
240	4.18	Composite Heat Flow Plot - Amber-1
241	4.19	" " " " - B-1
242	4.20	" " " " - C-1
243	4.21	" " " " - C-1A
244	4.22	Heat Flow Models for a Spreading Lithosphere
247	4.23	Composite Heat Flow Plot - Berbera-1
248	4.24	" " " " - Dagah Shabel-1
249	4.25	" " " " - Dagah Shabel-2
250	4.26	" " " " - Dagah Shabel-3

Page	Number	Title
251	4.27	Composite Heat Flow Plot - Biyo Dader-1
254	4.28	N.E. Somalia and Gulf of Aden Heat Flow
255	4.29	Composite Heat Flow Plot - Buran-1
256	4.30	" " " " - Burhisso-1
257	4.31	" " " " - Faro Hills-1
258	4.32	" " " " - Las Anod-1
259	4.33	" " " " - Yaguri-1
260	4.34	" " " " - Darin-1
261	4.35	" " " " - Sagaleh-1
262	4.36	" " " " - Hordio-1
263	4.37	" " " " - Cotton-1
265	4.38	" " " " - El Hamurre-1
266	4.39	" " " " - Obbia-1
267	4.40	" " " " - Endebirre-1
268	4.41	" " " " - Gira-1
269	4.42	" " " " - Maria Ascia-1
272	4.43	" " " " - XF-5

Page	Number	Title
273	4.44	Composite Heat Flow Plot - Bokh-1
274	4.45	" " " " - Galcaio-2
275	4.46	" " " " - Idole-1
276	4.47	" " " " - Dusa Mareb-1
277	4.48	" " " " - Dusa Mareb-2
278	4.49	" " " " - Bulo Burti-1
279	4.50	" " " " - Abred-1
280	4.51	" " " " - Callafo-1
281	4.52	" " " " - Magan-1
282	4.53	" " " " - Calub-1
285	4.54	" " " " - Gal Tardo-1
286	4.55	" " " " - Bio Addo-1
287	4.56	" " " " - Duddumai-1
288	4.57	" " " " - Uarsciek-1
289	4.58	" " " " - Merca-1
290	4.59	" " " " - Afgoi-1
291	4.60	" " " " - Dobei-1

Page	Number	Title
292	4.61	Composite Heat Flow Plots - Dobei-2
293	4.62	" " " " - Coriole-1
294	4.63	" " " " - Coriole-2
297	4.64	" " " " - El Kuran-1
298	4.65	" " " " - Hol-1
299	4.66	" " " " - Gheferson-1
300	4.67	" " " " - Das Uen-1
302	4.68	" " " " - Lach Bissigh-1
303	4.69	" " " " - Lach Dera-1
304	4.70	" " " " - Brava-1
305	4.71	" " " " - Giamama-1
306	4.72	" " " " - Oddo Alimo-1
310	4.73	Heat Flow Values for the Lamu Embayment and Adjacent Regions
311	4.74	Composite Heat Flow Plots - Wal Merer-1
312	4.75	" " " " - Garissa -1
313	4.76	" " " " - Walu-2
314	4.77	" " " " - Dodori-1

Page	Number	Title
315	4.78	Composite Heat Flow Plots - Pate-1
316	4.79	" " " " - Kipini-1
319	4.80	" " " " - Pemba-5
320	4.81	" " " " - Zanzibar-1
321	4.82	" " " " - Mafia-1
322	4.83	" " " " - Mandawa-7
323	4.84	" " " " - Kiswere
326	4.85	1st Order Trend Surface of Eastern Africa Heat Flow
327	4.86	2nd Order Trend Surface of Eastern Africa Heat Flow
328	4.87	3rd Order Trend Surface of Eastern Africa Heat Flow
329	4.88	4th Order Trend Surface of Eastern Africa Heat Flow
330	4.89	6th Order Trend Surface of Eastern Africa Heat Flow
332	4.90	2nd Order Trend Surface Residuals of Eastern Africa Heat Flow
333	4.91	3rd Order Trend Surface Residuals of Eastern Africa Heat Flow

Page	Number	Title
334	4.92	Eastern Africa Composite Gravity - Magnetic Map
336	4.93	Heat Flow - Gravity - Magnetic Profiles
341	4.94	Metamorphic Phases, Heat Flow and Crustal Structure; plus Isostatic and Metamorphic Phase Stable Crustal Models at Various Ambient Heat Flow Levels
341	4.95	Subsidence in Response to a Rise in Heat Flow Above 33.5 $mW \cdot m^{-2}$
346	4.96	The Variation of Temperature (T), Viscosity, Mantle Conductivity (K), and Heat Flow (Q) with Depth (Z) for an Average Eastern Africa Model, the Eastern Ogaden, and a Typical Continental Shield
349	4.97	Red Sea Temperature Profiles
350	4.98	Kenya Temperature Profiles
354	4.99	Surface Heat Flow and Isotherm Configuration for an Eastern Ogaden Model
357	4.100	Surface Heat Flow and Isotherm Configuration for a Garissa Region Model
358	4.101	Surface Heat Flow and Isotherm Configuration for a Second Garissa Region Model
362	5.1	Major Structural Elements of the North Sea
365	5.2	North Sea Summary Chart

Page	Number	Title
369	5.3	North West European Heat Flow
372	5.4	Composite Heat Flow Plot - 7/3-1
373	5.5	Composite Heat Flow Plot - 47/15-2
374	5.6	Composite Heat Flow Plot - 27/3-1
379	5.7	North Sea Geothermal Gradients
380	5.8(a)	Central North Sea Profile
381	5.8(b)	Southern North Sea Profile
384	5.9	The Variation of Temperature (T), Viscosity, Mantle Conductivity (K), and Heat Flow (Q) with Depth (Z) for the North Sea and the Surrounding Regions
390	5.10	Anomalous Heat Flow and Isotherm Configuration in and about a Model of a North Sea Salt Dome

List of Tables

Page	Number	Title
40	1.1	Initial Temperature Disturbances, T_o
41	1.2	Summary of Other Researchers Calculated and Observed Values of Initial Temperature Disturbance, T_o
52	1.3	Borehole Temperature Disturbances
53	1.4	Temperature Errors in Various Heat Flow Techniques/Sites
67	2.1	Dimensions of the Component Materials of the Divided Bar
70	2.2	Thermal Conductivity of Fused and Crystalline Quartz
71	2.3	Divided Bar Calibration Summary (1972 - 1974)
80	2.4	The Chip Thermal Conductivity Cell Typical Dimensions
82	2.5	Conductivity of Cell Materials (24^oC)
88	2.6	Comparison of the Geometric Mean and Maxwell Spheres Models
98	2.7	Sonic Log Parameter, Δt_{ma}, for Various Lithologies
103	2.8	Porosity Determination Methods

Page	Number	Title
104	2.9	Comparison of K_{pr} and K_d where ϕ_n Determined from Various Porosity Logs
104	2.10	Comparison of K_{pr} and K_d where ϕ_n Determined for an Increasing Number of Logs
107	2.11	Nonporous Chip Measurements of Thermal Conductivity - A Comparison of Brine and Water as Second Phase Components with Nonsoluble Chips
110	2.12	Repeatibility of Chip and Disc Measurements
113	2.13	Interlab Conductivity Checks
114	2.14	Thermal Conductivity of Fluids ($24^{o}C$)
125	2.15	Fluid Conductivities and the Effect of Cell Shortening
125	2.16	Summary of Error in Nonporous Rock Conductivity, K_r
146	3.1	Holocene Climatic Model Geothermal Gradient Disturbance (Depth = 100 metres)
146	3.2	Holocene Climatic Model Geothermal Gradient Disturbance (Depth = 1000 metres)
157	3.3	Coefficients for Equation (3.37)
157	3.4	Percentage Increase of Conductivity Due to a Pressure Increase Equivalent to One Kilometre of Sediments

Page	Number	Title
172	3.5	Divided Bar Calibrations at Various Mid-Point Temperatures
172	3.6	Coefficients a and b in the Equation $K = (a + bT)^{-1}$, (3.40) - for Halite (NaCl)
173	3.7	Descriptions of Samples Measured for Thermal Conductivity in the Range 10-90°C
174	3.8	Thermal Conductivity of Various Sedimentary, Igneous and Metamorphic Rocks in the Temperature Range 10-90°C
178	3.9	Mean Annual Surface Temperatures for Eastern Africa
179	3.10	Summary of Thermal Conductivity for Various Rock Types
184	3.11	Classification of Thermal Conductivity Data
194	4.0	Mesozoic/Cenozoic Structural and Depositional History: Eastern Africa
219-221	4.1	Eastern Africa - Borehole Descriptions
222-224	4.2	Eastern Africa - Raw Data Results
225-227	4.3	Eastern Africa - Corrected Heat Flow Values
228	4.4	Mean Heat Flow Values for the Individual Regions; Eastern Africa

Page	Number	Title
231	4.5	Heat Production Measurements of Eastern Africa Samples
337	4.6	Trend Surface Statistics
377	5.1	North Sea - Borehole Descriptions
377	5.2	North Sea - Raw Data Results
377	5.3	North Sea - Corrected Data Results
385	5.4	Thermal Conductivity of North Sea Sedimentary Rocks
435	A.1.1	Time necessary for a Borehole to Return to Thermal Equilibrium (Bullard, 1947) Determined From Equation (A.1.1)
435	A.1.2	Values of t_2/t_1 for Equation (A.1.2) for Bullard's (1947) parameters
435	A.1.3	Values of t_2/t_1 for a Line Source Model Insuring Sufficient Orders of the Argument of Exponential Integral, Equation (A.1.3), for Accuracy to Within 10^{-5}
435	A.1.4	Cylindrical Source Model
438	A.2.1	Unit Functions, $Q(t_d)$ and $T(t_d)$

System of Units

In general, the SI units system, based on the kilogram-metre-second, has been used throughout this thesis. However, in a few instances, both CGS (gram-centimetre-second) and British Units (pound-foot-hour) have been used to facillitate direct comparisons with other workers' results. Where CGS or British Units (BU) have been used the units are clearly stated. Where a value is quoted with no following system of units it may be assumed to be SI.

Tables of conversion factors for the three unit systems, unit abbreviations and prefix abbreviations for common units used in this thesis are given below. Units used and not listed below are defined in the appropriate place in the text.

Conversion Tables for Thermal Parameters

(one unit of the row parameter equals the table value of the column parameter)

Heat Flow	SI	CGS	BU
	$mW \cdot m^{-2}$	$\mu cal \cdot cm^{-2} \cdot s^{-1}$	$Btu \cdot ft^{-2} \cdot hr^{-1}$
$mW \cdot m^{-2}$	1.	2.39×10^{-2}	3.17×10^{-4}
$\mu cal \cdot cm^{-2} \cdot s^{-1}$	4.19×10^{1}	1.	1.33×10^{-2}
$Btu \cdot ft^{-2} \cdot hr^{-1}$	3.15×10^{3}	7.53×10^{1}	1.

Temperature Gradient	SI	CGS	BU
	$K \cdot km^{-1}$	$^{o}C \cdot km^{-1}$	$^{o}F \cdot 10^{2} ft^{-1}$
$K \cdot km^{-1}$	1.	1.	5.48×10^{-2}
$^{o}C \cdot km^{-1}$	1.	1.	5.48×10^{-2}
$^{o}F \cdot 10^{2} ft^{-1}$	1.82×10^{1}	1.82×10^{1}	1.

Thermal Conductivity	SI	CGS	BU
	$W \cdot m^{-1} \cdot K^{-1}$	$mcal \cdot cm^{-2} \cdot s^{-1} \cdot {}^{o}C^{-1}$	$Btu \cdot ft^{-1} \cdot hr^{-1} \cdot {}^{o}F^{-1}$
$W \cdot m^{-1} \cdot K^{-1}$	1.	2.39	5.81×10^{-1}
$mcal \cdot cm^{-1} \cdot s^{-1} \cdot {}^{o}C^{-1}$	4.18×10^{-1}	1.	2.42×10^{-1}
$Btu \cdot ft^{-1} \cdot hr^{-1} \cdot {}^{o}F^{-1}$	1.72	4.13	1.

Thermal Diffusivity	SI	CGS	BU
	$mm^{2} \cdot s^{-1}$	$cm^{2} \cdot s^{-1}$	$ft^{2} \cdot hr^{-1}$
$mm^{2} \cdot s^{-1}$	1.	1.00×10^{-2}	3.88×10^{-2}
$cm^{2} \cdot s^{-1}$	1.00×10^{2}	1.	3.88
$ft^{2} \cdot hr^{-1}$	2.58×10^{1}	2.58×10^{-1}	1.

Heat Production	SI	CGS	BU
	$\mu W \cdot m^{-3}$	$10^{-13} cal \cdot cm^{-3} \cdot s^{-1}$	$Btu \cdot ft^{-3} \cdot hr^{-1}$
$\mu W \cdot m^{-3}$	1.	2.39	9.67×10^{-8}
$10^{-13} cal \cdot cm^{-3} \cdot s^{-1}$	4.19×10^{-1}	1.	4.05×10^{-8}
$Btu \cdot ft^{-3} \cdot hr^{-1}$	1.03×10^{7}	2.47×10^{7}	1.

Common Parameter Unit Symbols

Used Throughout This Thesis

Parameter	Unit	Symbol
Length	millimetre	mm
	centimetre	cm
	metre	m
	kilometre	km
	foot	ft
Mass	kilogram	kg
Time	second	s
	hour	hr
Temperature	Degree Centigrade	^{o}C
	Degree Kelvin	K
	Degree Farenheit	^{o}F
Energy	Calorie	cal
	British Thermal Unit	Btu
Power	Watt	W

Parameter Fractional Unit Symbol Abbreviations

Fraction	Prefix	Symbol
10^{-6}	micro	μ
10^{-3}	milli	m
10^{3}	kilo	k
10^{6}	mega	M

Acknowledgments

This thesis would not have been possible without the kind cooperation of several oil companies and their employees. In particular I would like to thank:

AGIP (Milan)	- Dr. V. Fois, Dr. U. Accorsi, and Mr. E. Pacchiarotti
Amerada Hess U.K. (London)	- Mr. R.J.L. Stephens
Amoco Europe (London)	- Dr. M.L. Harper
Amoco U.K. (London)	- Mr. J.B. Thomas
British Petroleum Co. (London)	- Miss Hilary Roe, Mr. P. Threadgold, Mr. C.C.S. Davies, and Mr. M.W. Unstead
Burmah Oil Co. (Swindon)	- Mr. B.I.D. Hale
Conoco Europe (London)	- Mr. W.A. Branderdorf, and Mr. D.D. Skeels
Gewerschaft Elwerath (Hanover)	- Mr. I. Nodop and Mr. F. Koch
Gulf Oil Co.- Eastern Hemisphere (London)	- Dr. M.D. Beltrandi
Marathon International Oil Co. (Findlay, Ohio)	- Mr. L.S. Miller
Mobil North Sea (London)	- Mr. E.L. Jones, and Mr. D.W. Maclean
Mobil Oil Exploration & Production Services International(Dallas)	- Mr. P.B. Taylor
Phillips Petroleum Co. Europe & Africa (London)	- Mr. J.F. Settle

Tenneco Ethiopia
(Addis Ababa) - Mr. P.W. Cayce and Mr. E.L. Howard

I wish to thank Mr. J. Wheildon, the project supervisor, who initiated this study by gathering solid core conductivity samples and BHT data for the Kenya wells presented in this thesis. Mr. Wheildon is also thanked for his critical review of the manuscript.

I would also like to thank my colleagues Dr. Paul Morgan and Dr. Ken Williamson for stimulating discussion and encouragement during the writing of this thesis. I also thank Dr. Williamson for permission to use his unpublished heat flow data from Kenya.

Dr. H.Y. Tammemagi is thanked for his invaluable assistance in the measurement of radioactive heat production.

Miss Rosemary Spragg and Mr. J. Dare are thanked for assistance with the thermal conductivity sample preparation and measurement.

Dr. Paul Morgan, Dr. A. Jessop and Dr. S. Richardson are thanked for various interlaboratory checks of thermal conductivity and heat production measurements.

I thank the British Petroleum Co. for my scholorship and the Natural Environment Research Council for its partial support of my study.

My parents are gratefully acknowledged for their financial support during the final year of this research.

Miss Linda Murphy is thanked for her typing of this thesis.

Miss Linda Wookey, Mr. K. Bamford, and Mr. B. Holt are thanked for their drafting of the thesis diagrams.

Introduction

The measurement and implications of terrestrial heat flow first attracted earth scientists' attention in the nineteenth century when the physicist Lord Kelvin completed the problem begun by Fourier of calculating the age of the earth assuming that it had cooled, without internal heat sources, from a uniform molten state. Kelvin's relation was (Thompson, 1890),

$$t = \frac{T_o^2}{\pi k G^2} \qquad (0.1)$$

where T_o is the molten temperature, k the thermal diffusivity, G the earth's present geothermal gradient and t the time to cool to that gradient. The computed period, 20 to 40 million years, raised great controversy with geologists of the day who required a much longer span of time to account for, amongst other phenomena, the vast accumulation of sediments. The dispute was finally resolved with the discovery of radioactivity and recognition of its importance as a source of heat production in rocks (Holmes, 1915).

Today it is recognised that the terrestrial temperature regime plays an important if not fundamental role in most geologic processes associated with the earth's evolution and tectonism. Any attempt to formulate a thermal history of the earth, such as those of Jacobs and Allan (1954), MacDonald (1959), and Lubimova (1969), must utilise the surface heat flux as a boundary condition. Tectonic movements, such as subsidence and uplift, may well be a complex interaction of gravity, through isostatic compensation and/or hot creep, and temperature, through thermal expansion or contraction, combining to produce troughs for sedimentary basins and mountains to be eroded into them (Sleep, 1971, and Bott, 1971b).

Terrestrial heat flow values are determined from the product of two parameters; the rate of increase of temperature with depth, the geothermal

gradient, and the thermal conductivity of the rocks in which the gradient has been measured. Some thirty years prior to the first modern heat flow measurements by Bullard (1939), Joly (1909) closely estimated the earth's mean heat flux at 52 $mW \cdot m^{-2}$, little different from the value of 63 $mW \cdot m^{-2}$ obtained by Lee (1970) from some 3,127 determinations.

The distribution of heat flow measurements is, however, far from uniform. The most prevalent disparity occurs in the numbers of continental values (15%) versus oceanic results (85%). This difference has arisen for two reasons; the first being the relative ease and speed of oceanic determinations, the second being the dearth of suitable boreholes for continental measurements. For these and other reasons Africa, South America, Antarctica, and all of the continental shelves are still very poorly represented thirty-five years after the first modern heat flow determinations were made.

It has long been recognised that the relatively deep boreholes drilled for oil exploration were potential continental heat flow sites. Many early heat flow researchers, Coster (1947), Birch (1947, 1950), Meisner et al. (1951), Herrin and Clark (1956), Joyner (1960), and Garland and Lennox (1962), have made use of such wells. All of these workers have, however, measured the well temperature some considerable time after drilling ceased, though in many instances they have been forced to estimate the thermal conductivity of the various rock strata penetrated.

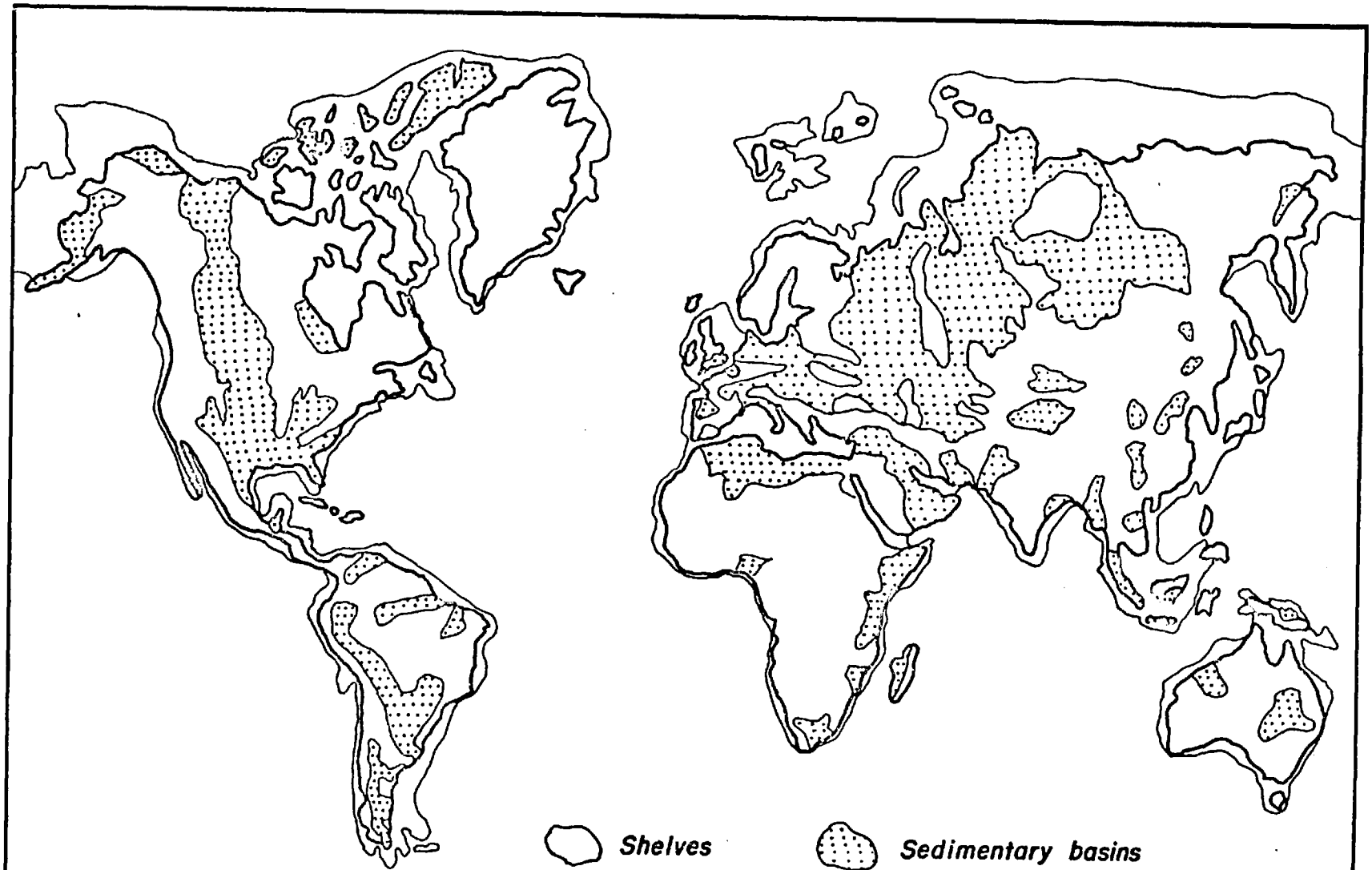
It has been routine practice in the oil industry, since about 1943, for the well logging contractor to make temperature measurements with maximum mercury-in-glass thermometers at or near the bottom of the well during breaks in drilling. These measurements, required for quantitative interpretation of electric logs, are referred to as Bottom Hole Temperatures (BHTs) and are often made many times and at several depths in a single well. When one considers that the oil industry is, at present, drilling some 4×10^4 wells, with a total depth of about 6×10^7 metres, per year (World Oil, 1974), and if, as is typical, 3 or 4 BHTs are recorded in each, then a great deal of

crustal temperature data is being largely ignored by heat flow researchers.

There are, however, two major drawbacks to the use of oil well data for heat flow determinations. The first is that there is no common opinion or authorative study as to the degree of reliability which may be placed in BHT derived geothermal gradients (cf. Uyeda and Horai, 1960, Anglin and Beck, 1965). The second is the lack of core from oil exploration wells for thermal conductivity determinations. Except for short, and generally unrepresentative sections of the hole lithology, oil wells are not cored - only small rock chips, referred to as drill cuttings, are recovered; typically every metre or two. Recent developments in the technique of thermal conductivity measurement of rock fragments by Sass et al. (1971) now permit relatively accurate determinations.

The prime objective of this thesis was to evaluate oil exploration well data, that is the BHTs recorded during breaks in drilling and the drill cuttings available for thermal conductivity determinations, as primary data for the computation of heat flow values. The success or failure of such data as components in a useful heat flow value have significant ramifications for the extension of the global coverage. Fig. 0.1, after Fairbridge (1957) with additions, illustrates the enormous area of continental crust topped by sedimentary basins and continental shelves - the sites of potential oil accumulation.

The continental margin of Eastern Africa, including the coastal basins of the Sudan, Ethiopia, Somalia, Kenya and Tanzania, was chosen as the principal region from which oil well data would be sought for this study. The area was selected for a variety of reasons. Apart from those few results of Girdler (1970) and Evans and Tammemagi (1974) there are no reported values for the sedimentary basins of these countries. The area itself lies between a well surveyed heat flow region (oceanic) and a geophysically anomalous area, a continental rift, currently under investigation. Further, the search for oil in Eastern Africa has been long and largely unsuccessful, thus resulting



SEDIMENTARY BASINS AND SHELVES OF THE WORLD
(after Fairbridge, 1957, with modifications)

FIG. 0.1

in a large number of deep, temperature logged, boreholes for which data is no longer considered confidential. Finally the region is, in itself, an interesting continental margin.

Heat flow data from Africa, or more correctly the African plate, are of special interest in the identification of sublithospheric heat sources which require about 10-100 m.y. to permeate the overlying crust and mantle by conduction alone. Piper and Richardson (1972) have shown that the paleomagnetic polar wander path for Africa suggest that it has remained stationary for the past 40 m.y., isolated between two opposed spreading ridges with no intervening zone of subduction. Briden and Gass (1974) have correlated this pause, and others in the African plate's motion, with periods of continental magmatism. Pollack and Chapman (1974) have examined the effect of lithospheric movement over lateral asthenospheric temperature variations on the surface heat flow.

The primary data for this study were 300 BHTs and 733 conductivity samples (some cores, mostly chips) from 68 Eastern Africa exploration wells. Data quality was highly variable. Interpretation of the results was made in conjunction with other available regional geological and geophysical surveys. Crust and upper mantle temperature models are proposed and related to the evolution and tectonism of the Eastern Africa margin.

The third, and final, objective of the study was to pursue a limited program of heat flow determinations from the North Sea. This was principally to follow up some of the author's views given in Evans and Coleman (1974) on the basis of a regional geothermal gradient study. Well data obtained from the North Sea consisted of 191 conductivity samples (mostly cuttings) from three boreholes. The results, which must be regarded as strictly preliminary, were used to convert profiles along the gradient map into heat flow. The technique, which was first suggested by Judge (1971), consists essentially of extrapolating conductivity data over continuous lithologic units in a single depositional environment where the sedimentary

structure is reasonably well known. The procedure of interpretation was similar to that carried out on the Eastern Africa data, though in less detail.

Chapter 1

TEMPERATURE MEASUREMENTS

1.1 Introduction

The estimation of heat flux requires a value of the increase of temperature per unit depth; the geothermal gradient. With the advent of accurate mercury-in-glass thermometers, developed principally for meteorology early in the nineteenth century, the first reliable subsurface temperature data were obtained. Many of the early measurements were made in mines or tunnels; as techniques and equipment improved temperatures were recorded in boreholes. The history, development and present status of temperature measuring equipment and techniques for the purpose of heat flow determinations are well summarized in Beck (1965).

The use of oil well exploration boreholes as sites for geothermal gradient and, later, heat flow determinations, began in the United States with the work of Van Ostrand (numerous papers in the 1920's and 1930's). These measurements, recorded with maximum mercury-in-glass thermometers, were made in wells which had returned to thermal equilibrium having been left undisturbed for extended periods after drilling had ceased.

However, by the 1940's, new legislation demanded that on completion of drilling, oil companies cemented closed all wells to prevent the interconnection of aquifers. Except for the relatively small number of wells that are retained for observation purposes, such as monitoring pressure changes in a producing field, few, if any deep unsuccessful oil exploration boreholes are left open for extended periods after completion

of drilling. Thus the heat flow researcher investigating this sort of borehole is now dependent on those temperature measurements made by the logging contractor and the oil company during breaks in the drilling of a well.

Previous researchers have been in notable disagreement about the usefulness of such data. Anglin and Beck (1965), in a survey of oil well temperatures from Western Canada, state explicitly that such data is of little or no use for heat flow purposes while a completely contrary opinion was held by Uyeda and Horai (1960) in a similar study in Japan.

This chapter will be largely concerned with the thermal disturbance induced in a borehole drilled by the rotary method and the effect it has on the geothermal regime. Of particular interest will be the degree of thermal disturbance persisting for periods of twelve to forty-eight hours after cessation of drilling; the interval when temperature data is often gathered at the bottom of an oil exploration well. The chapter's primary objective will be to evaluate the degree of confidence that can be placed in such data and to quantify the error introduced into the heat flow calculation by its use.

1.2 The Drilling of an Oil Exploration Well; a Description of the Resulting Thermal Disturbance

By the process of drilling the geothermal temperature field is disturbed, both in the hole itself and for some small distance about it, by conductive heat transfer through the face of the well resulting from the difference in temperature between the adjacent rocks and the drilling fluid. Frictional heat generated by the drill bit may, by comparison, be regarded as negligible, Lachenbruch and Brewer (1959), Holmes and Swift (1970).

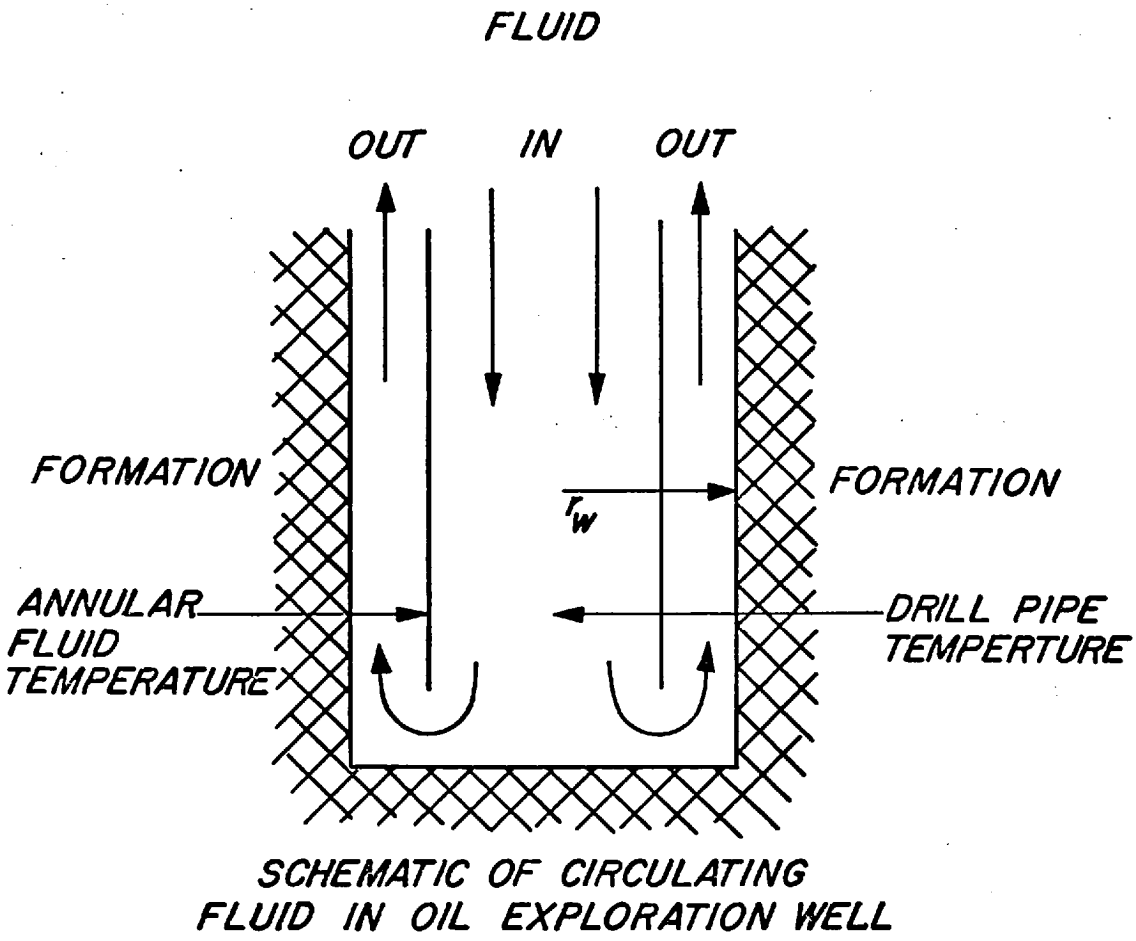
The drilling fluid, or mud, is pumped or circulated in the course of sinking the well. This circulation may be separated into three

distinct phases; the fluid enters the borehole at the surface and passes down through the drill pipe, the fluid exits through the bit, and finally returns through the drill pipe/borehole wall annulus, to the surface. This flow pattern is schematically illustrated in Fig. 1.1(a).

During drilling and mud circulation, the temperature of the fluid passing down the pipe is determined by the heat convection down the drill pipe, the rate of heat exchange between the drill pipe and the annulus and time. The temperature of the fluid rising in the annulus is a function of the convection up the annulus, the rates of heat exchange with the drill pipe and the adjacent rock strata and time. Numerous theoretical studies of the distribution of temperature in a circulating mud column have been made; Tragesser et al. (1967), Raymond (1969), Holmes and Swift (1970), and Keller et al. (1973). Figs. 1.1(b) and 1.1(c), from Raymond (1969) and Holmes and Swift (1970), respectively indicate the inferred temperatures, calculated from numerical and analytical models, of such a circulating mud system as described above.

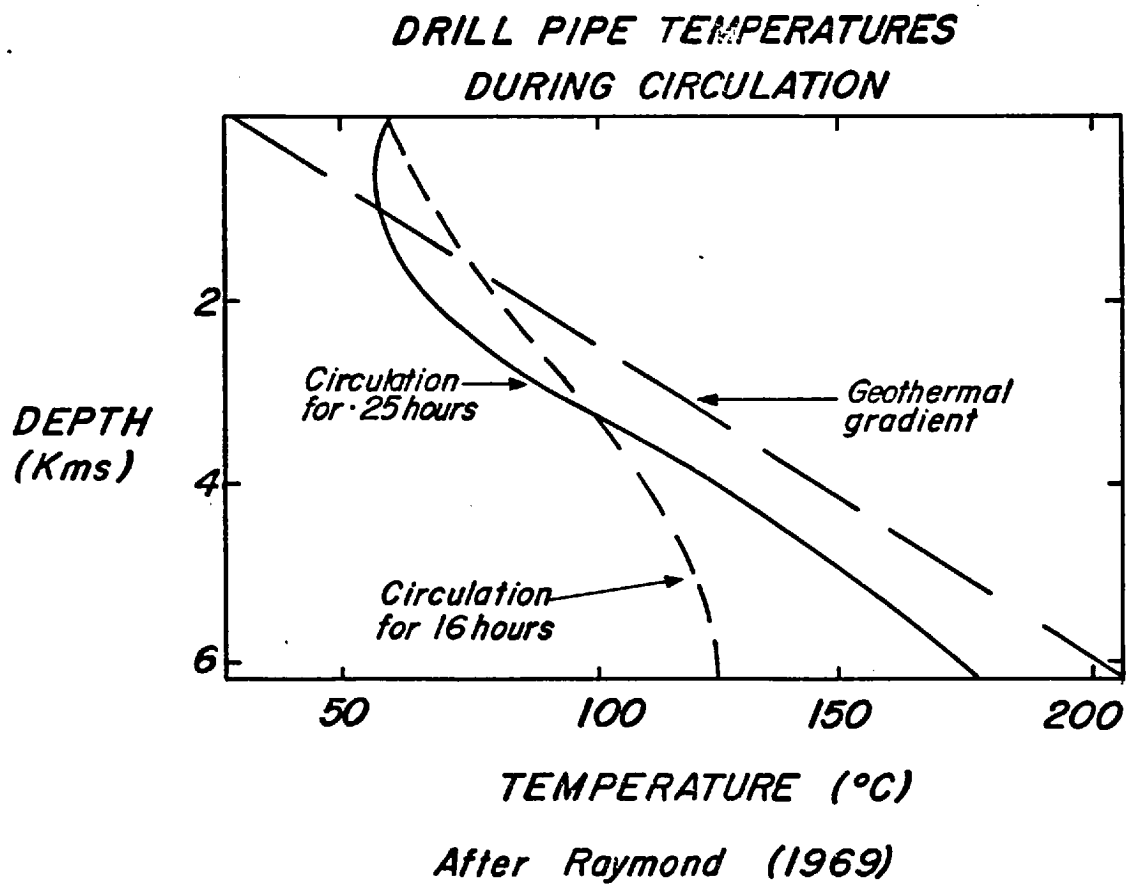
When drilling ceases and the mud circulation stops, the temperature gradient in the borehole is nonlinear and lower than the geothermal gradient. Heat diffuses out of the adjacent rock formation in the lower portion and out of the well in its upper section as the geothermal regime is re-established. Lachenbruch and Brewer (1959) state that the return to thermal equilibrium is a complex function of several variables including variations, during circulation, of the drilling fluid temperature and flow rate, ie. the history of heat extraction or input to the rock strata, together with the thermal properties of the adjacent formations. Fig. 1.1(d) from Raymond (1969), illustrates the thermal history of three depth points in a well during and after fluid circulation.

Two conclusions common to all the above mentioned circulating mud temperature studies are; that during circulation the temperature at the well bottom is much less than geothermal, and during breaks in circulation the system returns rapidly to its undisturbed state with a temperature gradient



SCHEMATIC OF CIRCULATING FLUID IN OIL EXPLORATION WELL

FIG. I.I (a)



After Raymond (1969)

FIG.I.I (b)

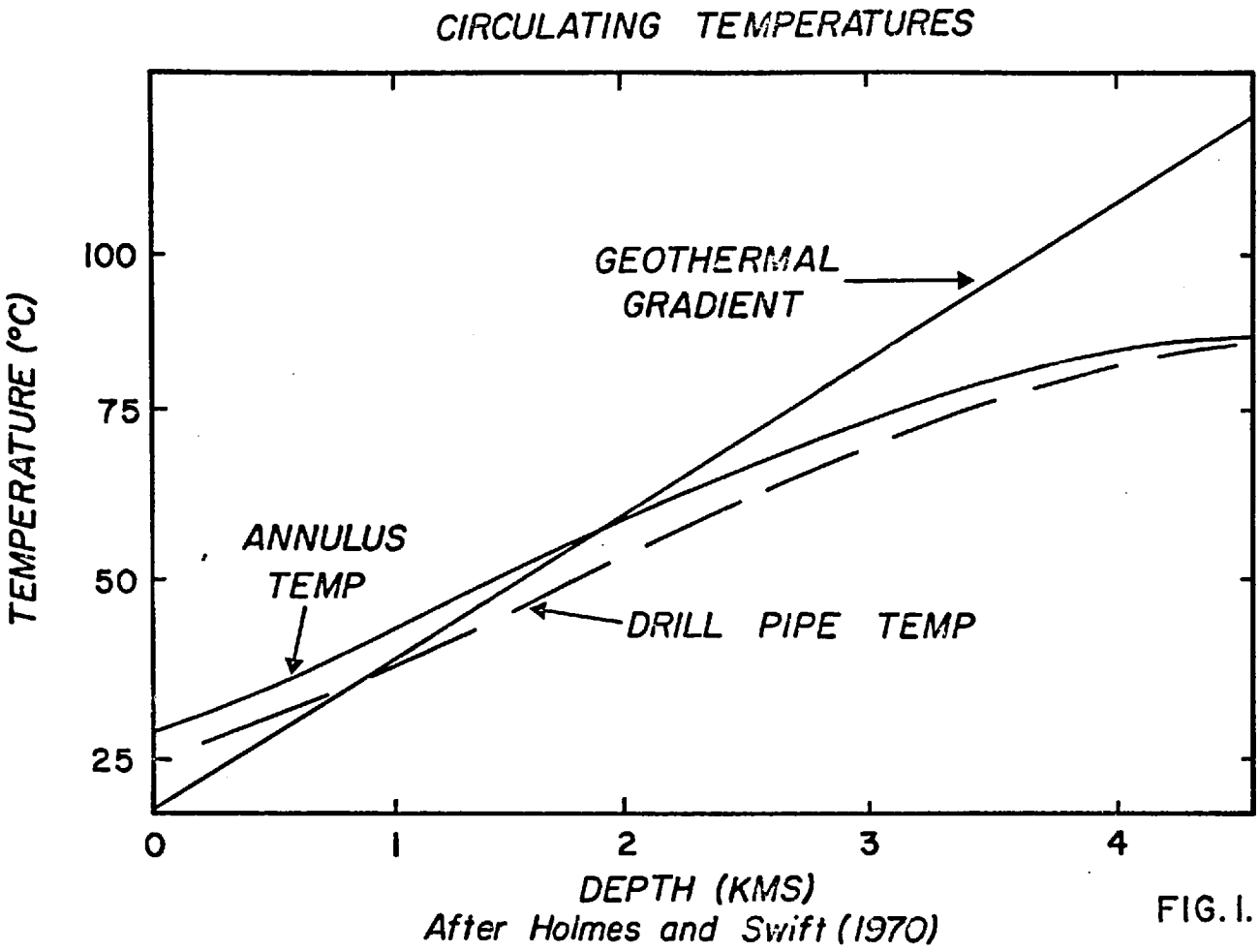


FIG. I.1 (c)

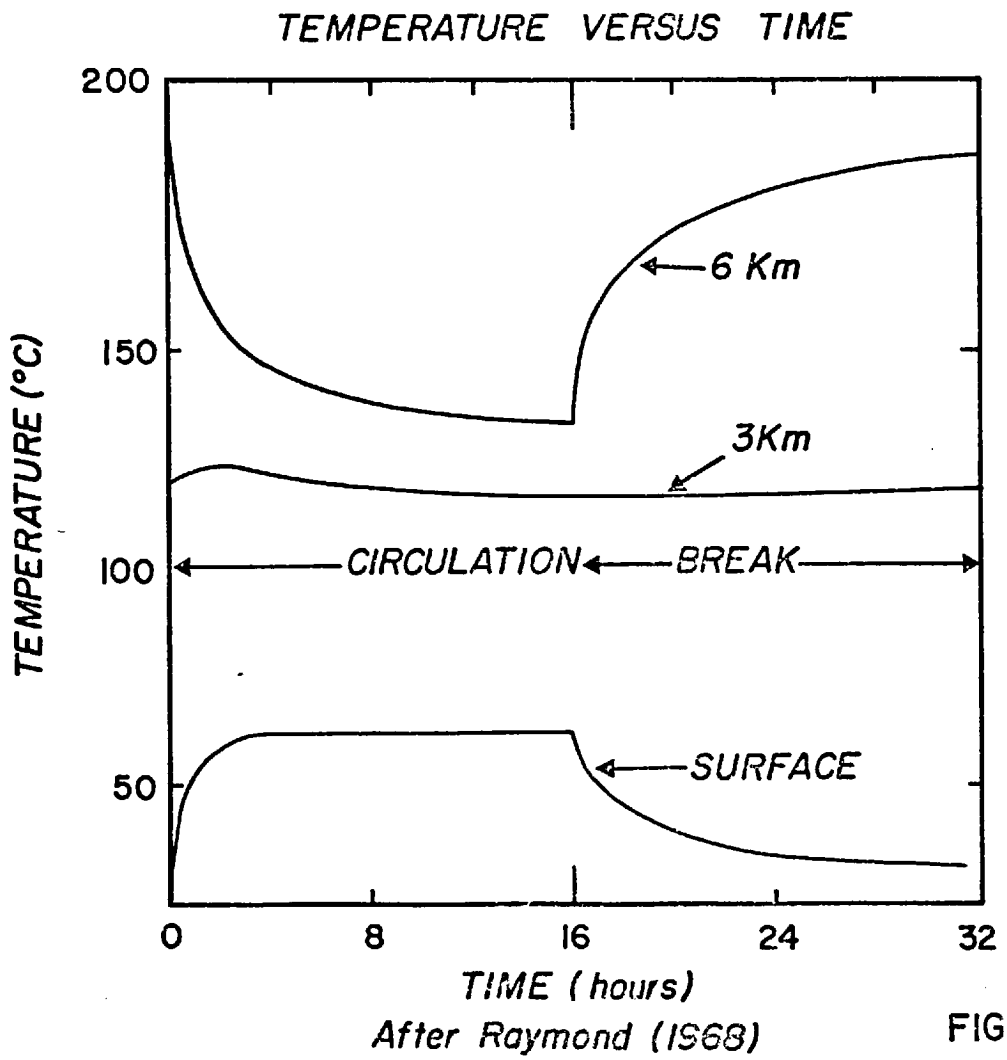


FIG. I.1 (d)

within ten percent of geothermal in sixteen hours. Maximum circulating fluid temperatures occur one quarter to one third of the distance off bottom hole.

It should, of course, be remembered that although the temperature disturbance is largest at bottom hole during fluid circulation, the total heat exchanged at the well bottom is considerably less than that of the region immediately above it. We will return to these considerations of circulating temperatures in connection with quantitative estimates of error in geothermal gradients, Section 1.6.

1.3 Temperature Measurements Routinely Made in Oil Exploration Wells

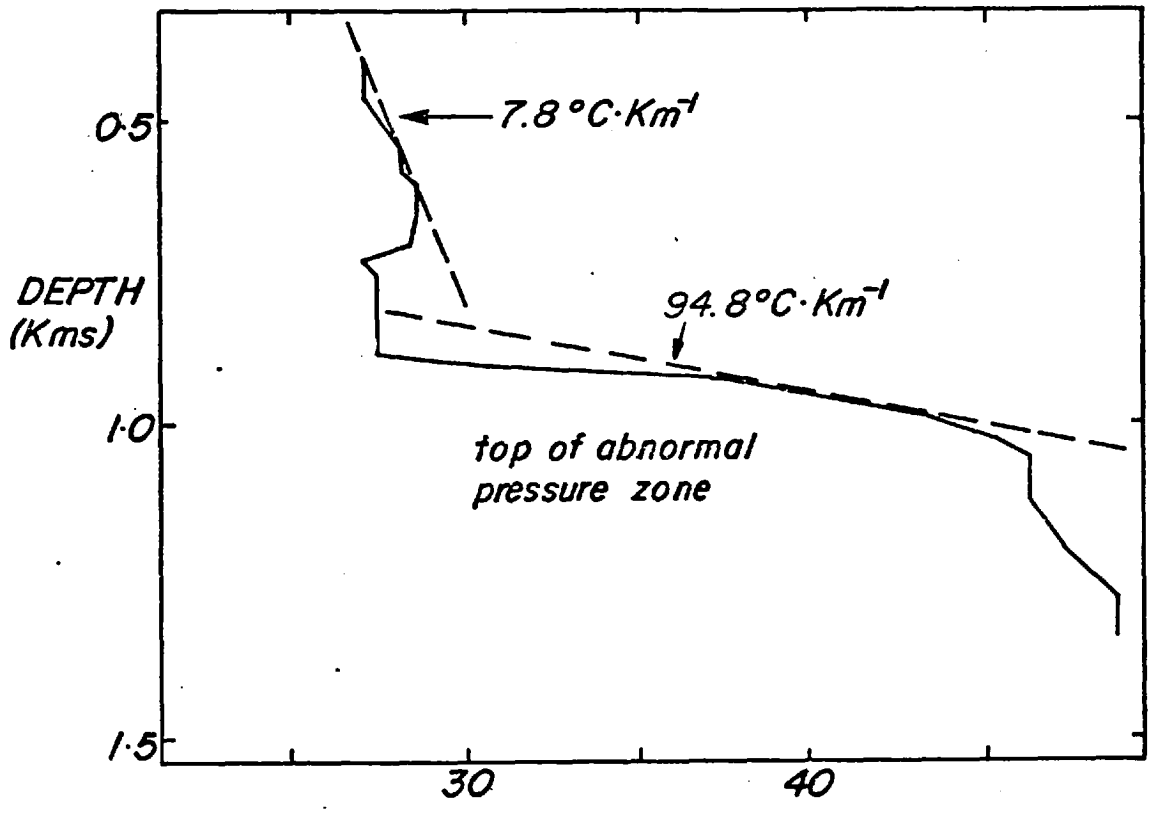
There are, typically, three basic types of temperature measurements made in oil wells; flow line, continuous log, and bottom hole recordings.

The flow line temperature measurement is a continuous record of the circulating drilling fluid temperature. It is made at the surface as the mud emerges from the drill pipe/bore face annulus. The temperature of the mud is, of course, less than the down hole circulating temperatures which are in turn different from the geothermal temperatures. The flow line temperature gradient is a function of the geothermal gradient, circulation rate, heat capacity of the mud, and numerous other, often poorly defined, parameters (Wilson and Bush, 1973).

Fig. 1.2 is a graph of flow line temperatures from a North Sea borehole illustrating one of the measurement's uses; the sharp increase commonly observed prior to the well penetrating an over-pressured shale. Flowline temperatures for a well in Kenya are shown in Fig. 1.5; note the discontinuities associated with changes in hole diameter. However, as flow line temperatures can only yield a crude estimate of the geothermal gradient, Haliburton, API (1956), they will not be discussed here further.

FLOWLINE TEMPERATURE

(AN EXAMPLE)



FLOWLINE TEMPERATURES (°C)

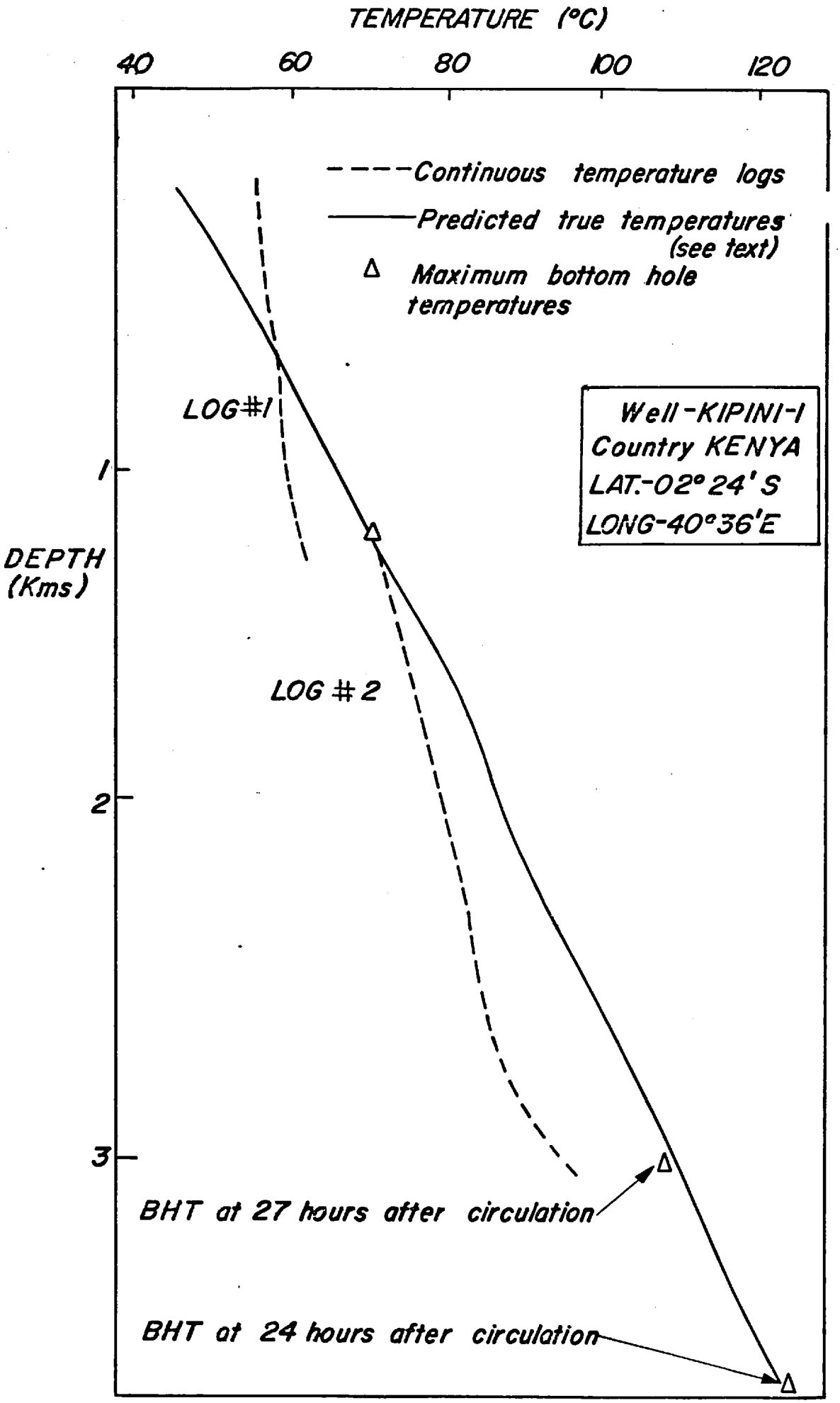
(north sea well)

After Wilson and Bush (1973)

FIG.1.2.

The second type of oil exploration borehole temperature data are continuous recordings made with a logging device which is similar to that employed by heat flow researchers being essentially an electrical bridge system using an exposed thermistor as the fourth arm of a Wheatstone bridge. During a break in drilling and circulation, this logging tool is lowered to the bottom of the hole and temperatures are recorded as it is winched up. Its principal uses, in oil exploration technology, are to detect gas entry or fluid flow, to define production or injection zones and to locate setting cement tops behind the casing. Figs. 1.10(c) and 1.10(d), which form part of a later discussion, are examples of continuous temperature logs.

The measuring unit has an accuracy of about .3^{o}C (Schlumberger, 1973) which, for the hole depths to be considered in this study, would yield reasonable temperature gradient estimates. However, these logs are commonly run some three to forty-eight hours after circulation ceases, when the greater portion of the well is still considerably out of thermal equilibrium. This is illustrated in Fig. 1.3 for a well from Kenya, East Africa, where two continuous temperature logs have been run, one when the borehole was at 1281 metres and again at 2996 metres. Clearly the recorded temperatures are high compared to geothermal values in the upper half of the borehole, at the time of logging, and vice-versa in the lower section. These two logs are in good agreement with the temperature variation with depth predicted by Raymond (1969), Fig. 1.1(d), who proposed only a very small departure from geothermal conditions at the midpoint of the borehole. Many other authors, Edwardson et al. (1962), Mongelli (1964), Schoeppel and Gilliranz (1966), Keller et al. (1967), Baldarassi (1967), and Holmes and Swift (1970), have shown, either by direct measurement or by theoretical considerations, that the thermal disturbance pattern illustrated in Fig. 1.3 is invariably present on continuous temperature logs. The geothermal gradient indicated on Fig. 1.3 has been computed from reliable temperatures and thermal conductivity data. Discussion of the method will be given in Chapter 3.



EXAMPLES OF CONTINUOUS TEMPERATURE LOGS

FIG.1.3

TYPICAL LOG HEADING

SCHLUMBERGER

BOREHOLE COMPENSATED SONIC LOG WITH CALIPER

COUNTY ETHIOPIA
FIELD or LOCATION WILDCAT
WELL RED SEA B-1
COMPANY MOBIL

COMPANY MOBIL PETRLEUM OF ETHIOPIA

WELL RED SEA B-1

FIELD WILDCAT

COUNTY ERITREA STATE ETHIOPIA

LOCATION

Sec. _____ Twp. _____ Rge. _____

Other Services:
FDC

Permanent Datum: M.S.L., Elev. 0
Log Measured From RT, 35 Ft. Above Perm. Datum
Drilling Measured From RT

Elev.: K.B. _____
D.F. _____
G.L. _____

Date	OCT 4. 1969			
Run No.	THREE			
Depth—Driller	9055			
Depth—Logger	9052			
Btm. Log Interval	9040			
Top Log Interval	8000			
Casing—Driller	13 3/8@3155	@	@	@
Casing—Logger	3154			
Bit Size	12 1/4			
Type Fluid in Hole	SALT			
	SATURATED			
Dens. | Visc.	108 40			
pH | Fluid Loss	10 | 48 ml	ml	ml	ml
Source of Sample	FLOWINE			
R_m @ Meas. Temp.	.051 @ 113 °F	@ °F	@ °F	@ °F
R_{mf} @ Meas. Temp.	.035 @ 102 °F	@ °F	@ °F	@ °F
R_{mc} @ Meas. Temp.	.091 @ 102 °F	@ °F	@ °F	@ °F
Source: R_{mf} R_{mc}	MEAS | MEAS			
R_m @ BHT	.016 @ 318 °F	@ °F	@ °F	@ °F
Time Since Circ.	16 HRS			
Max. Rec. Temp.	318 °F	°F	°F	°F
Equip. | Location	2052 | ETI			
Recorded By	R. POGGESI			
Witnessed By	G. ENGELS			

t_2
BHT

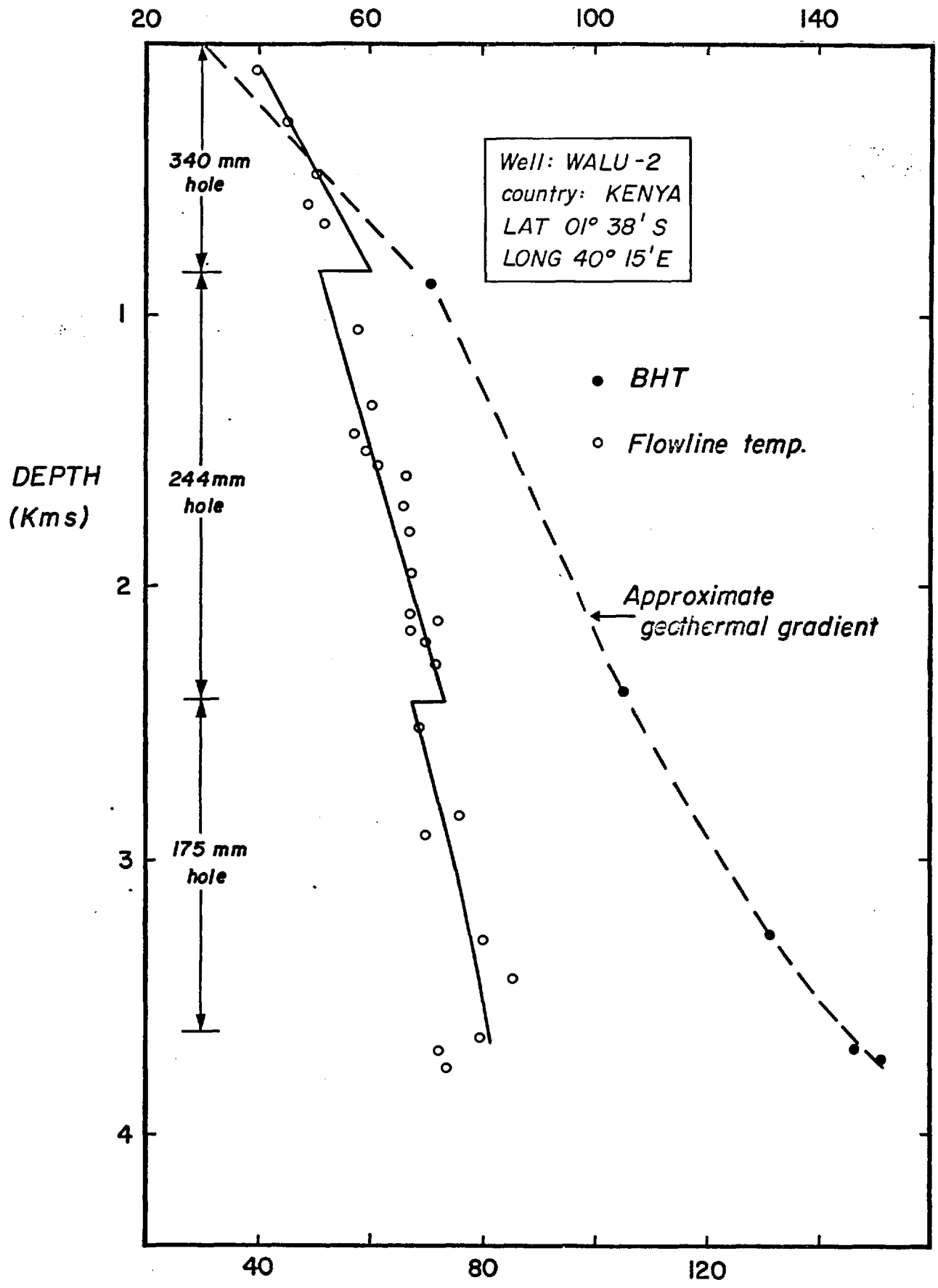
FIG. 14

Well temperatures during the recording of typical continuous logs are often further disturbed as a result of the exothermic reaction of setting casing cement, the location of which is a prime use of this log.

Another feature often observed on continuous temperature logs is the so called 'bottom hole efect' first described by Schlumberger et al. (1937), where the temperature trace exhibits a dramatic increase in proximity to the bottom of the well (cf. log two, Fig. 1.3). This tending of near bottom well temperatures to geothermal lends support to the widely held opinion that a very rapid re-establishment of geothermal conditions occurs at bottom hole. However, it is clear that continuous temperature logs are, in general, unsuitable for the determination of geothermal gradients.

Bottom hole temperatures (BHTs), the third type of routinely gathered oil exploration borehole temperature data, are measured with maximum mercury-in-glass thermometers. The standard reference for the field procedure in the use of such thermometers for borehole temperature measurements is that of Van Ostrand (1924). Where great care is taken, readings accurate to about .1^{o}C may be obtained though values measured by commercial logging companies are never quoted to be better than .5^{o}C.

Such a thermometer, on occasions two or more may be used together, is inserted into a pressure tight steel container which is in turn attached near the top of a logging tool at a point about nine metres from its base. When drilling and mud circulation have ceased the drill string is withdrawn and the logging tool is run in. Depending on hole depth, this procedure will require about three to twelve hours - the minimum period which will elapse between cessation of the thermal disturbance, fluid circulation, and the thermometer arriving at bottom hole. Often a number of such logging runs are made; five or six is not unusual. Current recommended practice by the API (1956) is to obtain a BHT on each log thus yielding, in theory, a record of the re-establishment of the geothermal temperature at bottom hole.



COMPARISON OF BHT AND FLOWLINE TEMPERATURES

FIG. 1.5

The final BHT may be recorded as much as forty-eight hours or more after the cessation of circulation.

Maximum mercury-in-glass thermometers have a thermal lag in terms of the time taken for them to respond to a sudden temperature change. Birch (1947) and Hilchie (1968) have both found that such thermometers, when in their steel pressure housing, require three to seven minutes to record true temperature. Both Hilchie (1968) and Coleman (1973) state that the logging tool is typically held at bottom hole for about twenty minutes, during which time various calibration checks are made, thus ensuring a sufficient period for the thermometer to achieve thermal equilibrium.

A well log heading, Fig. 1.4, in this case an exploration hole from Eritrea, Ethiopia, illustrates where BHT data, temperature and time since circulation, are typically recorded. Virtually all the temperature data presented in this study was obtained from similar log headings. Fig 1.5 is an example of BHT data and flow line temperature results from a deep hole in Kenya.

Depth measurement control in the logging of oil exploration wells is very good, Schlumberger (1973), and is considered a negligible source of error in this study. Likewise variations of hole verticality were never sufficient to justify applying a correction, although deviation data was not available for all of the wells presented here.

In view of the probable rapid re-establishment of the thermal regime at bottom hole, it appears that BHTs present the only source of routinely gathered oil exploration borehole temperature data which might be usefully exploited for heat flow purposes.

1.4 Model One to Predict Temperature Variations Resulting From Drilling Disturbances - The Continuous Line Heat Source

One of the first models proposed in an attempt to quantify the drilling disturbance to geothermal temperatures was the continuous line

heat source (Bullard, 1947). The fundamental premise is that at any point in the borehole, the drilling fluid circulation may be assumed to act as a constant continuous line heat source or a sink along the axis of the well. At a given depth the heat source is to act from the time the drill bit reaches that point until drilling fluid circulation ceases.

An implicit assumption in the method is that the thermal properties of the drilling fluid are the same as those of the adjacent rock formation. This is however, of relatively minor consequence due to the low heat capacity of the drilling fluid. It is further assumed that the thermal properties of the adjacent rock formations are radially homogeneous and infinite.

In the arguments that follow the initial temperature distribution will everywhere be constant and zero; thermal disturbances will begin at time zero. With these simplifying assumptions we may now derive, from first principles, the line heat source model. One dimensional time dependent heat flow is described by,

$$\frac{\partial^2 T}{\partial x^2} - \frac{1}{k} \cdot \frac{\partial T}{\partial t} = 0 \qquad (1.1)$$

Where T is temperature, x is distance, and k is thermal diffusivity. Thermal diffusivity is defined as $k = K/pc$ where K is thermal conductivity (see Chapter 2), p is density, and c is specific heat.

A so called 'source solution', which may be verified by substitution, for (1.1) is given by Carslaw and Jaeger (1959),

$$T = t^{-\frac{1}{2}} \cdot e^{-x^2/4kt} \qquad (1.2)$$

For a three dimensional semi-infinite region (1.1) becomes,

$$(1.3) \qquad \nabla^2 \cdot T - \frac{1}{k} \cdot \text{grad } T = 0$$

which has a corresponding instantaneous point source solution

$$(1.4) \qquad T = \frac{Q}{8(\pi k t)^{\frac{3}{2}}} \cdot e^{-\left[r^2 + (z-z')^2\right]/4kt}$$

in cylindrical co-ordinates where $r^2 = (x-x')^2 + (y-y')^2$, and T is the temperature at (x, y, z) at time t due to an instantaneous heat source of strength Q at(x', y', z'). The source strength Q has units of temperature volume; the heat liberated by the source is given by Qpc.

Now to obtain the analogous solution for an instantaneous line source of strength Qdz' along z' we integrate (1.4) over dz from $-\infty$ to $+\infty$ and employ the error function identity to obtain,

$$(1.5) \qquad T = \frac{Q}{4\pi kt} \cdot e^{-r^2/4kt}$$

where in this case Qpc is the heat liberated per unit length of line.

The continuous line source may be obtained from (1.5) by integrating w.r.t. t. Where Qpc is the heat liberated per unit time per unit length of line parallel to the z axis and through point (x', y');

$$(1.6) \qquad T = Q/4\pi k \cdot \int_0^t e^{-r^2/4k(t-t')} \frac{dt'}{(t-t')}$$

Setting $u = r^2/4k(t-t')$ and noting values of u at $t' = o$ and $t' = t$, we obtain,

$$(1.7) \qquad T = Q/4\pi k \cdot \int_{r^2/4kt}^{\infty} e^{-u} \frac{du}{u}$$

where the integral may be expressed as a series.

The exponential integral, Ei (-x),

$$(1.8) \qquad -Ei\,(-x) = \int_x^\infty e^{-u}\,\frac{du}{u}$$

may be evaluated by,

$$(1.9) \qquad Ei\,(-x) = \gamma + \ln x - x + \frac{x^2}{2.2!} - \frac{x^3}{3.3!} \ldots$$

where γ is Eulers constant, .5772. Selby (1967) has tabulated Ei(-x) for $.01 \leq x \leq 2.0$ and IBM (1970) have produced a computed program subroutine for its evaluation.

Neglecting terms of order x and higher (1.7) may be rewritten as,

$$(1.10) \qquad T = Q/4\pi k \cdot \left[\log\,(4kt/r^2) - \gamma \right]$$

which is approximate and valid for large t.

In practice the line source will act for a period t_1, the circulation time, and be zero thereafter. We may simulate this by invoking Duhamel's theorem of superposition and adding a negative heat source at time t_1, thus modifying (1.7) and (1.8) to,

$$(1.11) \qquad \frac{T(t)}{T_o} = \frac{Ei(-r^2/4kt_2) - Ei(-r^2/4kt)}{-Ei(r^2/4kt_1)}$$

where $t_2 = t - t_1$ and T_o and T(t) are temperatures at times t_1 and t respectively. As before, omitting terms of order x and higher in (1.9) and substituting, (1.11) becomes,

$$(1.12) \qquad T(t) = C \cdot \log\,(1 + t_1/t_2) + T(\infty)$$

where C is a constant equal to the reciprocal of the simplified denominator in (1.11), (Lachenbruch and Brewer, 1959). The term $T(\infty)$, the undisturbed geothermal temperature has been added as in the original statement of the

problem, the semi-infinite solid was initially at uniform and zero temperature. Clearly for very large t, $\log (1 + t_1/t_2) \simeq \log (1) = 0$ and $T(t) = T(\infty)$ as it should.

We will return to the line source in connection with practical examples in section 1.6.

1.5 Model Two to Predict Temperature Variations due to Drilling Disturbances - The Region Bounded Internally by the Continuous Cylinder Heat Source

Another model, that of the internal cylinder in a homogeneous infinite medium, is perhaps a closer approximation to the physical situation; the temperature disturbance resulting from the drilling of a vertical hole. The first solution of this problem was by Nicholson (1921); Van Everdingen and Hurst (1949) applied the theory to pressure and flow problems in oil and gas reservoirs; Edwardson et al. (1962) exploited these solutions to estimate the thermal disturbances in and around oil exploration wells. The following treatment incorporates aspects of the above authors' discussions together with those of Carslaw and Jaeger (1959) and Schneider (1973).

The equation of heat flow (1.3) may be transformed to cylindrical co-ordinates,

$$(1.13) \qquad \frac{\partial^2 T}{\partial r^2} + \frac{1}{r}\cdot\frac{\partial T}{\partial r} = \frac{C_p \rho}{K} \cdot \frac{\partial T}{\partial t}$$

where Cp, p and K are the rock formation specific heat, density and thermal conductivity respectively, t is the time, T temperature, and r radial distance. As with the line source the solution of (1.13) requires some simplifying assumptions. First the rock formation about the well is radially infinite and homogeneous and secondly there will be no radial component of heat flow after circulation ceases. Of course the implicit assumptions are that cylindrical symmetry exists and transfer of heat is by conduction only.

For the purpose of the argument to follow it is convenient to replace r and t with dimensionless terms r_d and t_d,

$$(1.14) \qquad t_d = Kt/C_p r_w^2 p$$

$$(1.15) \qquad r_d = r/r_w$$

where r_w is the cylinder radius. This modifies (1.13) to,

$$(1.16) \qquad \frac{\partial^2 T}{\partial r_d^2} + \frac{1}{r_d} \cdot \frac{\partial T}{\partial r_d} = \frac{\partial T}{\partial t_d}$$

which is a form which lends itself to solution by Laplace transforms. Where $\bar{T}$ is the Laplace transform of T, (1.16) becomes,

$$(1.17) \qquad \frac{\partial^2 \bar{T}}{\partial r_d^2} + \frac{1}{r_d} \cdot \frac{\partial \bar{T}}{\partial r_d} - p\bar{T} = 0$$

where p is the Laplacian operator.

Before solving (1.17) it is necessary to consider the boundary conditions that we wish to apply to the model. Two obvious cases are constant terminal temperature and constant terminal heat flow. In the former, at time zero, the temperature at the well face, $r_d = 1$, is instantaneously lowered to zero and remains so for the duration of the drilling fluid circulation; in the latter heat is exchanged with the formation at a constant rate at $r_d = 1$ from time zero.

From first order theory, we find that, for the constant terminal temperature case, the cumulative heat, Q(t), exchange per unit length of borehole is, at time t,

$$(1.18) \qquad Q(t) = 2\pi C_p \cdot r_w^2 \cdot p \cdot \Delta T(o) \cdot Q(t_d)$$

where $\Delta T(o)$ is the initial temperature change, and $Q(t_d)$ the dimensionless cumulative heat change resulting from a unit temperature drop,

$$(1.19) \qquad Q(t_d) = \int_0^{t_d} \left(\partial T / \partial r_d\right)_{r_d = 1} \, dt_d$$

For the constant terminal heat flow, Δq_o, per unit length of hole case, the resulting temperature disturbance is,

$$(1.20) \qquad T(t) = 1/(2\pi K) \cdot \Delta q(o) \cdot T(t_d)$$

Where $T(t_d)$ is the analogous unit temperature change due to a unit flow of heat (Edwardson et al., 1962).

Where the flow of heat or temperature change is not a terminal constant but varies with time (1.18) and (1.20) modify to,

$$(1.21) \qquad Q(t) = 2\pi C_p r_w^2 \, p \cdot \left[\Delta T(o) \cdot Q(t_d) + \Delta T(1) \cdot Q(t_d - t_{d1}) + \Delta T(2) \cdot Q(t_d - t_{d2}) \cdots\cdots\right]$$

and

$$(1.22) \qquad T(t) = 1/2\pi K \cdot \left[\Delta q(o) \cdot T(t_d) + \Delta q(1) \cdot T(t_d - t_{d1}) + \Delta q(2) \cdot T(t_d - t_{d2}) + \cdots\cdots\right]$$

respectively, by the superposition theorem. Figs. 1.6(a) and 1.6(b) schematically illustrate the two cases.

Now to solve (1.17) we first note that the general solution of Bessel's equation,

$$(1.23) \qquad x^2 \cdot \frac{d^2y}{dx^2} + x \cdot \frac{dy}{dx} - (x^2 + v^2)\, y = 0$$

for $v = 0$ or a positive integer, is,

$$(1.24) \qquad y = c_1 \cdot I_n(x) + c_2 \cdot K_n(x) \quad n = 0, 1, 2 \cdots\cdots$$

Where I_n and K_n are modified Bessel functions of the first and second kinds respectively and c_1 and c_2 are constants to be determined from initial or boundary conditions.

This clearly presents a solution to (1.17) with $v = 0$, viz.

$$\bar{T}(t_d) = c_1 \cdot I_0 (r_d p^{\frac{1}{2}}) + c_2 \cdot K_0 (r_d p^{\frac{1}{2}}) \tag{1.25}$$

Solving first for the constant rate case, at infinite radius $\bar{T}(t_d)$ should approach zero. $I_0(r_d p^{\frac{1}{2}})$ and $K_0 (r_d p^{\frac{1}{2}})$ become increasingly large and small respectively for increasing $r_d p^{\frac{1}{2}}$ thus $c_1 = 0$. The second boundary condition, constant rate,

$$\left(\frac{dT}{dr_d} \right)_{r_d = 1} = -1 \tag{1.26}$$

implies,

$$\left(\frac{d\bar{T}}{dr_d} \right)_{r_d = 1} = -\frac{1}{p} \tag{1.27}$$

But,

$$\frac{\partial K_0 (z)}{\partial z} = -K_1 (z) \tag{1.28}$$

Thus (1.25) becomes,

$$\bar{T}(t_d) = \frac{K_0 (r_d p^{\frac{1}{2}})}{p^{\frac{3}{2}} K_1 (p^{\frac{1}{2}})} \tag{1.29.a}$$

Similar arguments lead to the constant terminal temperature equivalent,

$$\bar{T}(t_d) = \frac{K_0 (r_d p^{\frac{1}{2}})}{p K_0 (p^{\frac{1}{2}})} \tag{1.29.b}$$

Equations (1.29.a) and (1.29.b) may readily be solved for $T(t_d)$ using Mellin's inversion formula which takes the form,

$$(1.30) \qquad T(t_d) = \frac{1}{2\pi i} \int_{\alpha-i}^{\alpha+i} e^{\lambda t_d} \bar{T}_\lambda \, d\lambda$$

Fig. 1.6(c) illustrates the contour integral path used to solve (1.30) where integration is carried out in the complex plane $\lambda = x + iy$, along a parallel, AB, to the y axis at a distance α from the origin with all poles to the left of this line. Such an integral may be represented by a semi-circle of infinite radius where the result is zero over the path segments AC and FB. This leaves only the cuts CD and EF joining the pole to the semi-circle.

Where we consider a temperature change, ΔT, as in (1.22) we may rewrite (1.29.a) and (1.30) for the upper cut, EF, as,

$$(1.31) \qquad \Delta T(t_{d_1} - t_{d_2}) = \frac{1}{\pi i} \int_0^\infty \frac{(e^{-u^2 t_1} - e^{-u^2 t_2}) \cdot K_0(u e^{i\pi/2} r_d)}{u^2 e^{i\pi/2} \cdot K_1(u e^{i\pi/2})} \, du$$

with an analogous result for the lower cut where $\lambda = u^2 e^{i\pi}$.

The Bessel function indentities (Watson, 1944),

$$(1.32) \qquad K_0(Ze^{\pm i\pi/2}) = i\pi/2 \, (-J_0(Z) \pm i \, Y_0(Z))$$

and,

$$(1.33) \qquad K_1(Ze^{\pm i\pi/2}) = i\,\pi/2 \, (J_1(Z) \pm iY(Z))$$

are substituted in (1.31) and the analogous expression for the lower cut. Their sum is given by,

T - TEMPERATURE

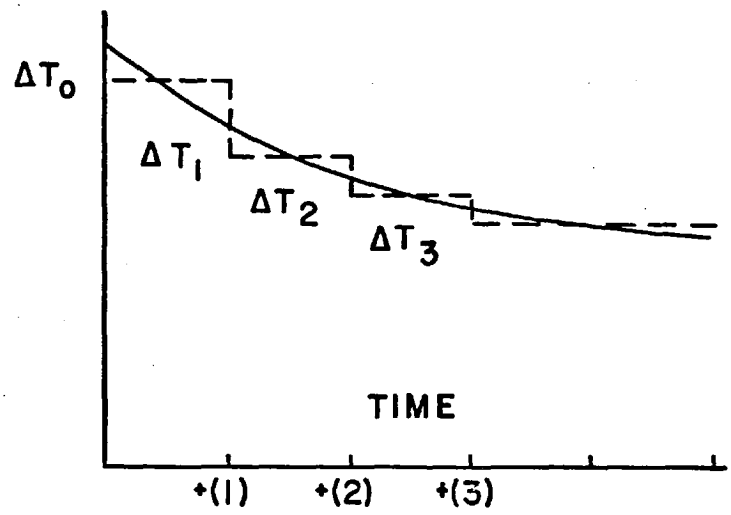


FIG. 1.6 (a)

GRAPHICAL REPRESENTATION OF EQN. 1.21

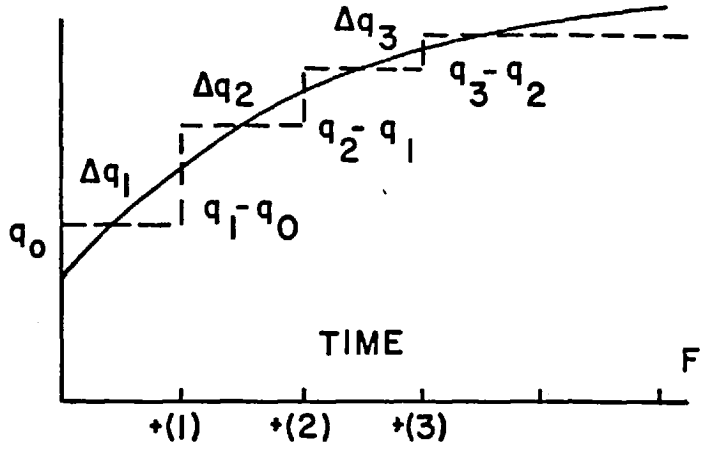


FIG. 1.6 (b)

GRAPHICAL REPRESENTATION OF EQN. 1.22

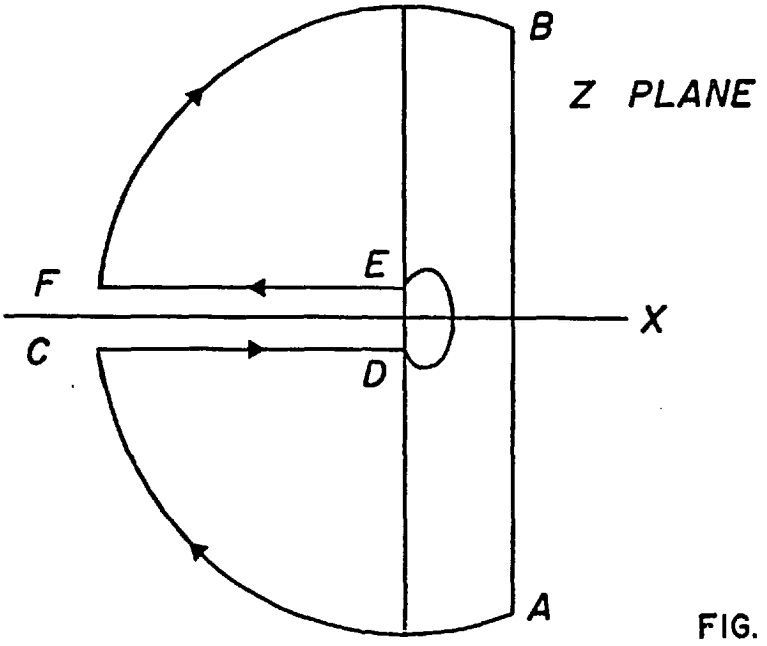


FIG. 1.6 (c)

CONTOUR INTEGRAL PATH FOR EQN. 1.31

$$(1.34)\quad \Delta T(t_{d_1} - t_{d_2}) = \frac{2}{\pi} \cdot \int_0^{\infty} \frac{(e^{-u^2 t_1} - e^{-u^2 t_2}) \left[Y_1(u)J_0(ur_d) - Y_0(ur_d)J_1(u)\right] du}{u^2 \left[J_1^2(u) + Y^2{}_1(u)\right]}$$

Where J_0, J_1, Y_0, and Y_1 are Bessel functions of the first and second kinds of order one and two respectively. Where the following recurrence formula (Watson, 1944),

$$(1.35)\quad J_1(u) \cdot Y_0(u) - J_0(u) \cdot Y_1(u) = 2/\pi \cdot u$$

is substituted, setting $r_d = 1$, and noting that at time zero the temperature change is zero, we obtain a more general form of the temperature change, $T(t_d)$, since time zero,

$$(1.36)\quad T(t_d) = 4/\pi 2 \int_0^{\infty} \frac{(1-e^{u^2 t})}{u^3 \left[J_1^2(u) + Y_1^2(u)\right]}\, du$$

A similar treatment of the constant terminal temperature case yields,

$$(1.37)\quad Q(t_d) = 4/\pi 2 \int_0^{\infty} \frac{(1-e^{-u^2 t})}{u^3 \left[J_0^2(u) + Y_0^2(u)\right]}\, du$$

Both $T(t_d)$ and $Q(t_d)$ have been tabulated by Van Everdingen and Hurst (1949) and approximated as polynomials by Edwardson et al. (1949). This allows equations (1.21) and (1.22) to be used directly for solutions of $T(t)$ and $Q(t)$. These discussions will be expanded on in section 1.6 and Appendix 2.

1.6 The Time Required for a Borehole to Return to Thermal Equilibrium - Practical Examples

In the preceeding sections, we have considered two idealised models which might be used to predict the length of time taken to re-establish borehole thermal equilibrium or to predict geothermal temperatures from non-

equilibrium BHT data.

The line source model, Section 1.4, equation (1.11), may be rewritten, (Bullard, 1947),

$$(1.38) \quad \frac{T(t)}{T_o} = \log\ (1 + t_1/t_2) \Big/ (\log\ (4kt_1/r^2) - \gamma)$$

for large values of time. However, this approximation is generally not valid for the relatively small values of time and consequent large values of the argument of the exponential integral in equation (1.11), of three to forty-eight hours to be expected in this study. Further comments on the Bullard (1947) paper are to be found in Appendix 1.

Before modifying (1.38) for small values of time, it is necessary to define a standard oil exploration well in terms of its radius, r_w, and the thermal diffusivity, k, of the rocks it penetrates. Edwardson et al. (1962), in a similar study, used r_w = 100 mm. and k = 1.1 $mm.^2 s^{-1}$, the latter value being arrived at by averaging data from Ingersoll et al. (1954), Ziefus and van der Vliet (1956) and Sommerton (1958). These values are adopted for the following discussion.

Where the exponential integral, Ei(-x) equation (1.8) has an argument of greater than .1 it is necessary to include terms $-x$, $x^2/2\cdot 2!$, $-x^3/3\cdot 3!$ ····· . For times of the order of one hour, the minimum period to be considered here, and the above mentioned values of diffusivity and well radius the maximum exponential integral argument will be,

$$(1.39) \qquad x = r^2/4kt \lesssim .63$$

which is adequately evaluated by second order terms in equation (1.8).

Thus we may modify (1.38) to,

$$(1.40) \quad \frac{T(t)}{T_o} = \frac{\log\ (1 + t_1/t_2) - u\left(\frac{t_1}{t_2(t_1 + t_2)}\right) - u^2\left(\frac{1}{t_2^2} - \frac{1}{(t_1 + t_2)^2}\right)}{\log\ (t_1/u) - \gamma + u/t_1 - u^2/t_1^2}$$

where $u = r^2/4k$ and the remaining terms are as previously defined in Section 1.4.

Now for the region bounded internally by the cylinder, Section 1.5, we may rewrite equation (1.22) as,

$$(1.41) \quad T(t) = Aq(o)\, T(t_d) + A \sum_n \delta q(t_n) \cdot T(t_d - t_{d_n})$$

and differentiating (1.18),

$$(1.42) \quad T_o q\,(t_d) = Aq(t)$$

where $A = 1/2\pi k$ and $\delta q(t_n) = q(t_n) - q(t_n - 1)$; combining (1.41) and (1.42) we obtain,

$$(1.43) \quad \frac{T(t)}{T_o} = q(o)\, T(t_d) + \sum_n q(t_{d_n}) \quad T(t_d - t_{d_n})$$

as was demonstrated by Edwardson et al. (1962), where $q(t_d)$ and $T(t_d)$ may be adequately evaluated by polynomial expressions (see Appendix 2.)

Both models, the line source and cylinder, may now be used to calculate the dimensionless temperature change, the left hand terms in (1.38) and (1.43), as a function of dimensionless time where,

$$(1.44) \quad t_d = (kt/r_w^2) = .4t$$

with values of r_w and k as previously defined. The calculation of the line source curves was made by computing Ei(-x) to sufficient orders of x to ensure an accuracy of one part in 10^3. Typically, this would involve first, second or third order terms; equation (1.40), of second order, is an example.

In the case of the cylinder a problem arises with the term $q(t_d)$, the heat flow into the well when the temperature drop is a constant, which is infinite for time $t_d = o$. The calculation was made by breaking $q(t_d)$ up into a large number of small dimensionless time steps with a mean value $\bar{q}(t_d)$, computed for each such that the cumulative heat, $\int q(t_d)\, dt_d$, gives a correct value for $Q(t_d)$, equation (1.37). Edwardson et al. (1962) have shown this to be a valid technique (see also Appendix 2). The effect of stopping fluid circulation is simulated by adding a negative value of $\bar{q}(t_d)$ to the value of $\bar{q}(t_d)$ existing at time t_1. Fig. 1.7(a) illustrates the cylinder model where the dimensionless temperature drop, $T(t)/T_o$ of equation (1.43) has been shown as a function of the ratio of the shut-in or post-circulation time, t_2, to the total time, t. Fig. 1.7(b) compares the line source and cylinder model dimensionless temperature drops, as in Fig. 1.7(a) with the same values of r_w and k applied (see Appendix 1 for comments).

The obvious question to be asked is do oil exploration boreholes return to equilibrium along traces similar to those shown in Figs. 1.7(a) and 1.7(b). Eighteen wells, from both Eastern Africa and the North Sea, for which multiple BHTs at a given depth were available have been analyzed. Values of $T(t)$, t_1 and t_2 were known, while the k/r_w^2 was estimated from the previous average values; this assumption introduces only a minor uncertainty.

The results, Figs. 1.8(a) and 1.8(b) were computed using equation (1.40) where the right hand numerator has been fitted by least squares to the term $T(t)$; the slope equaling the T_o term divided by the right hand numerator while the intercept equals the undisturbed geothermal temperature, $T(\infty)$. The obvious good agreement suggests that the idealized models do, to a degree, describe the return to thermal equilibrium at bottom hole in these boreholes.

It is of particular interest to be able to estimate the average residual temperature disturbance, due to drilling, remaining after the final

CYLINDER MODEL

DIMENSIONLESS TEMPERATURE DISTURBANCE

VERSUS

THE RATIO OF SHUT IN TO TOTAL TIME

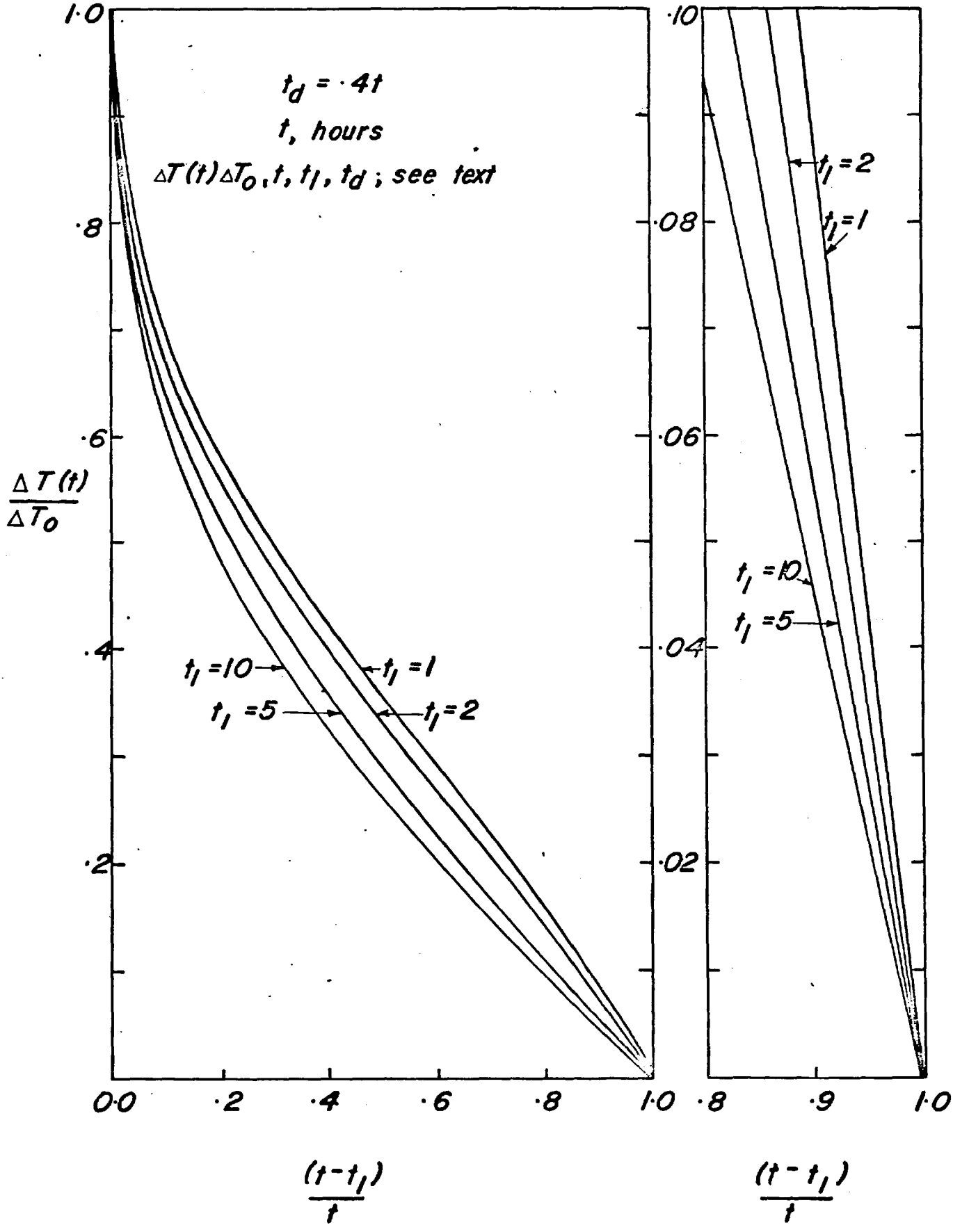


FIG. 1.7 (a)

LINE SOURCE AND CYLINDER MODELS
COMPARISON OF DIMENSIONLESS TEMPERATURE DISTURBANCE

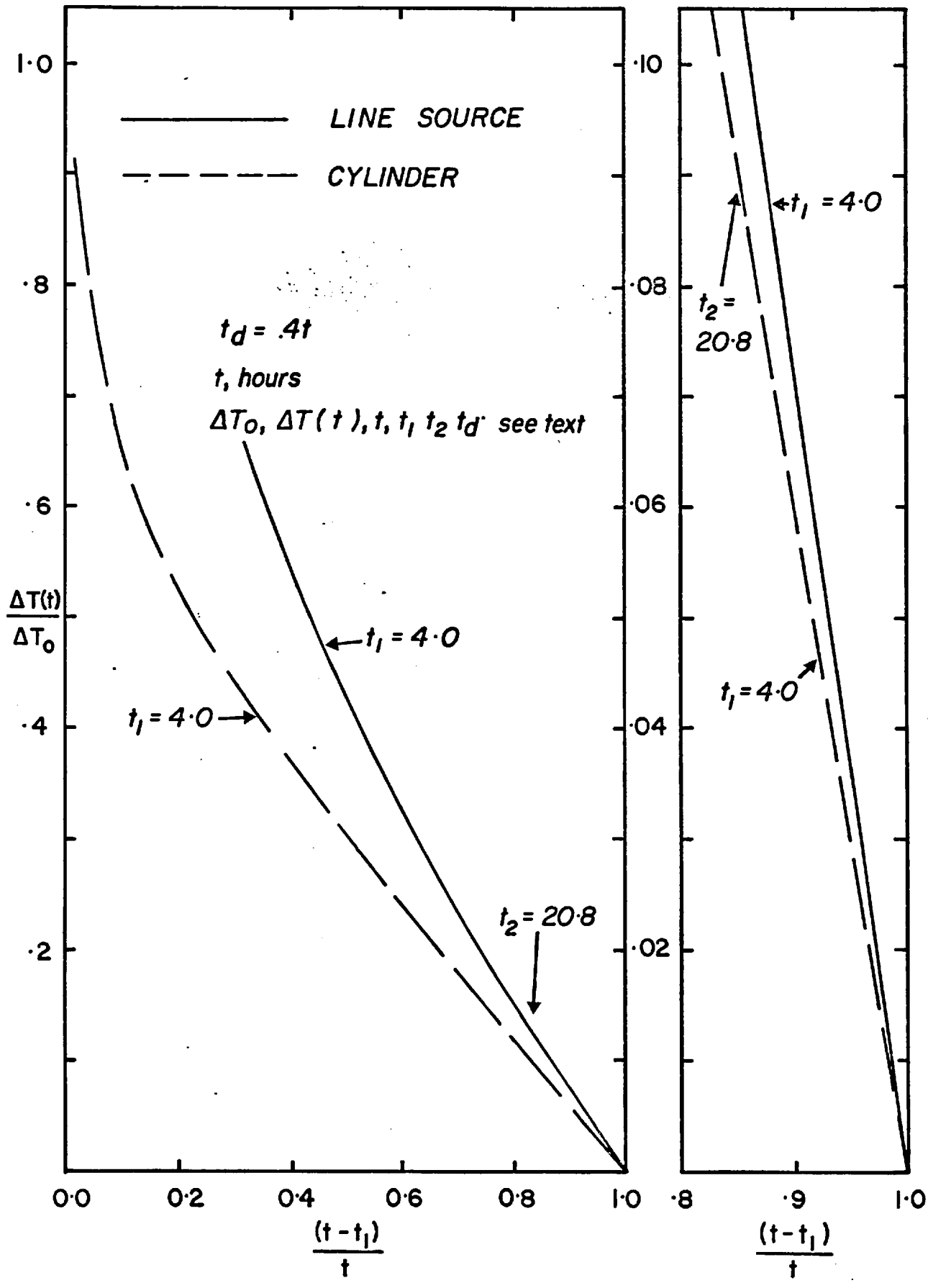


FIG 1.7 (b)

BHT log is run. This is due to the fact that despite recommended practice this is often the only temperature recorded; temperature data of the quality presented in Figs. 1.8(a) and 1.8(b) being only occasionally available. Thus the quantification of T_o, the initial temperature disturbance at time t_1, is necessary in order to assign a value to T(t) when t_1 and t_2 are known. The slope of the lines in Figs. 1.8(a) and 1.8(b) were multiplied by the right hand denominator in equation (1.40) to give an estimate of T_o. Similarly, values of T_o were also estimated for these wells from the cylinder model where the term T(t) was fitted to the r.h. expression in equation (1.43) by least squares.

Results have been compiled in Table 1.1, columns four and five, for the line source and cylinder models respectively. Clearly wells number 6, 8, and 18 were inferior in terms of data quality, ie. large error of fits for both models, and, when eliminated, result in a significantly smaller standard deviation in the mean of T_o, the initial temperature disturbance.

Larger standard deviations are associated with the T_o values computed from the cylinder model. This has two possible explanations; the cylinder model is inherently inferior to the second order line source, or, more probably, since the range of the dependent variable in (1.43) is smaller for the cylinder than that of (1.40) for the line source, the former is more sensitive to small errors in T(t). This is especially obvious in the case of well 7, where a clearly unrealistic T_o has resulted from the cylinder calculation where there was only a tiny range of the right hand term of equation (1.43).

Thus the 'preferred' value of average T_o is the 41.5^{o}C result of column four, Table 1.1. Table 1.2 is a review of other workers' estimates of T_o, all of which have been observed and/or theoretically estimated. The

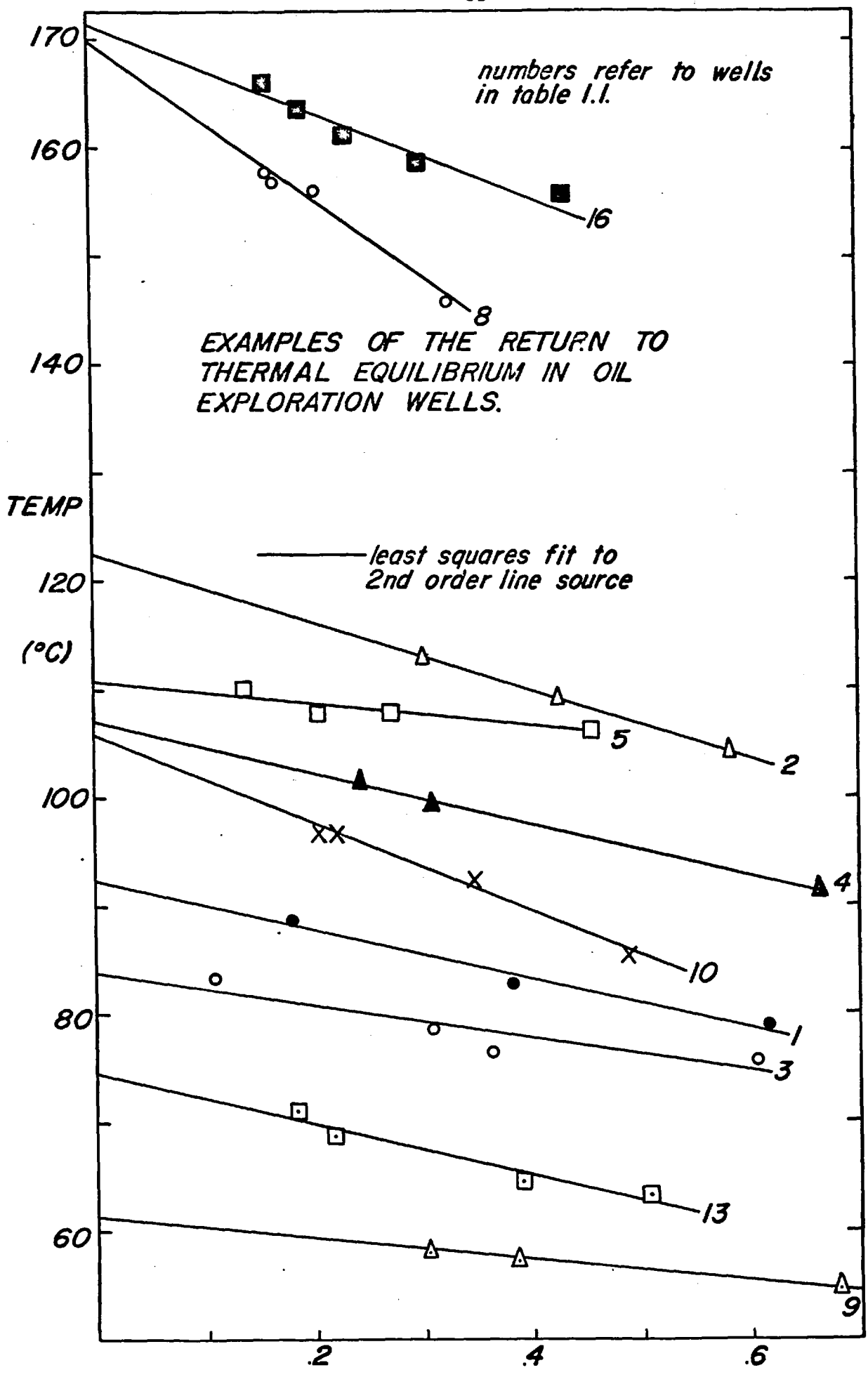

170
160
140
120
100
80
60
TEMP
(°C)
numbers refer to wells in table I.I.
16
8
EXAMPLES OF THE RETURN TO THERMAL EQUILIBRIUM IN OIL EXPLORATION WELLS.
least squares fit to 2nd order line source
2
5
4
10
1
3
13
9
.2
.4
.6
NUMERATOR IN 2nd ORDER LINE SOURCE
(DIMENSIONLESS)

FIG. 1.8 (a)

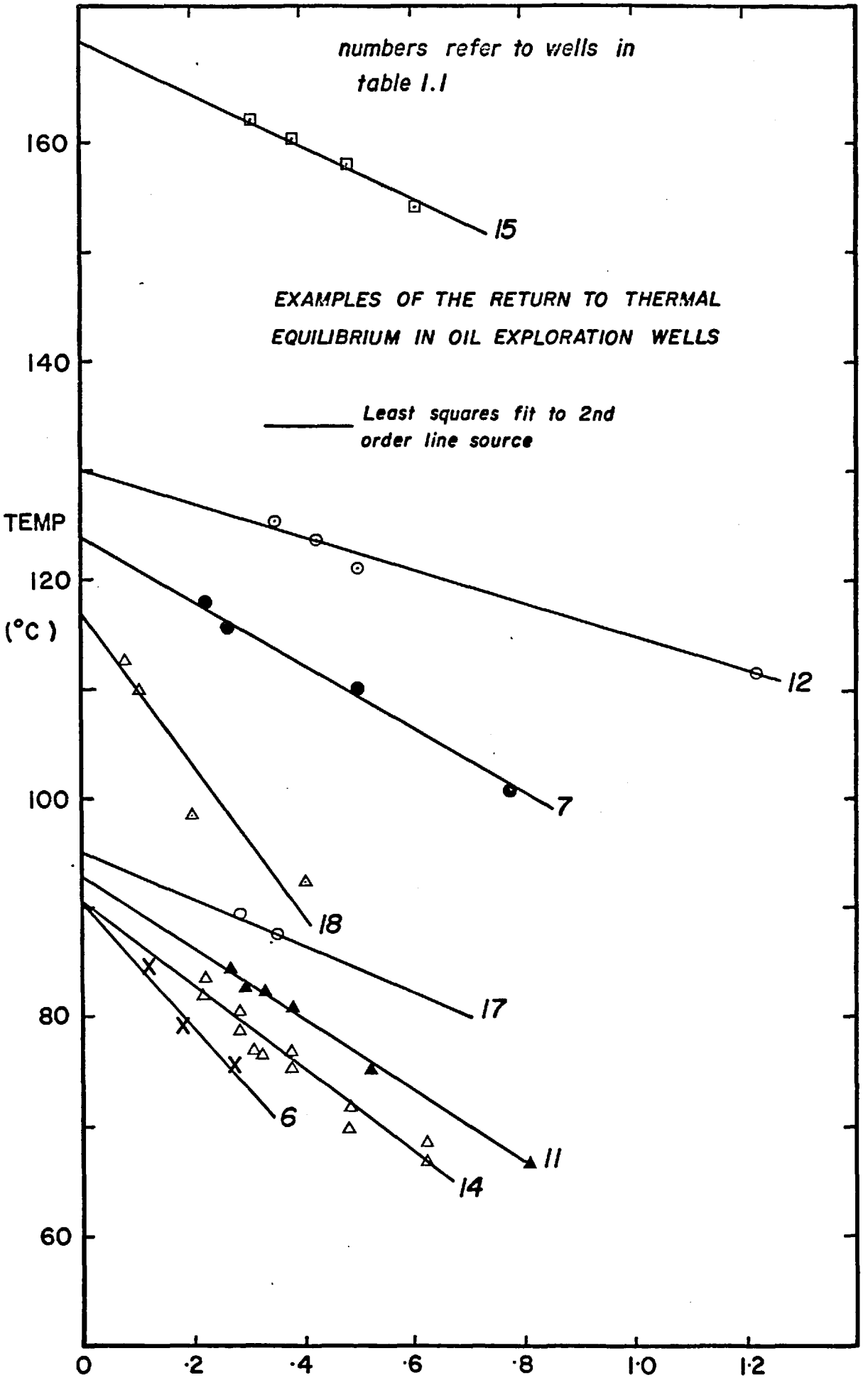

numbers refer to wells in table 1.1
EXAMPLES OF THE RETURN TO THERMAL EQUILIBRIUM IN OIL EXPLORATION WELLS
Least squares fit to 2nd order line source
TEMP (°C)
160
140
120
100
80
60
15
12
7
18
17
11
14
6
0
·2
·4
·6
·8
1·0
1·2
NUMERATOR IN 2nd ORDER LINE SOURCE
(DIMENSIONLESS)

FIG. 1.8 (b)

results suggest a reasonable agreement with that value of average T_o given here.

In table 1.1, columns six and seven, average values of t_1 and t_2, the circulation and post circulation times respectively, have been tabulated for the eighteen wells. The mean t_1 value of 4.0 hours has been used in the computation of the curves of Fig. 1.7(b); the comparison of the line source and cylinder dimensionless temperature disturbances.

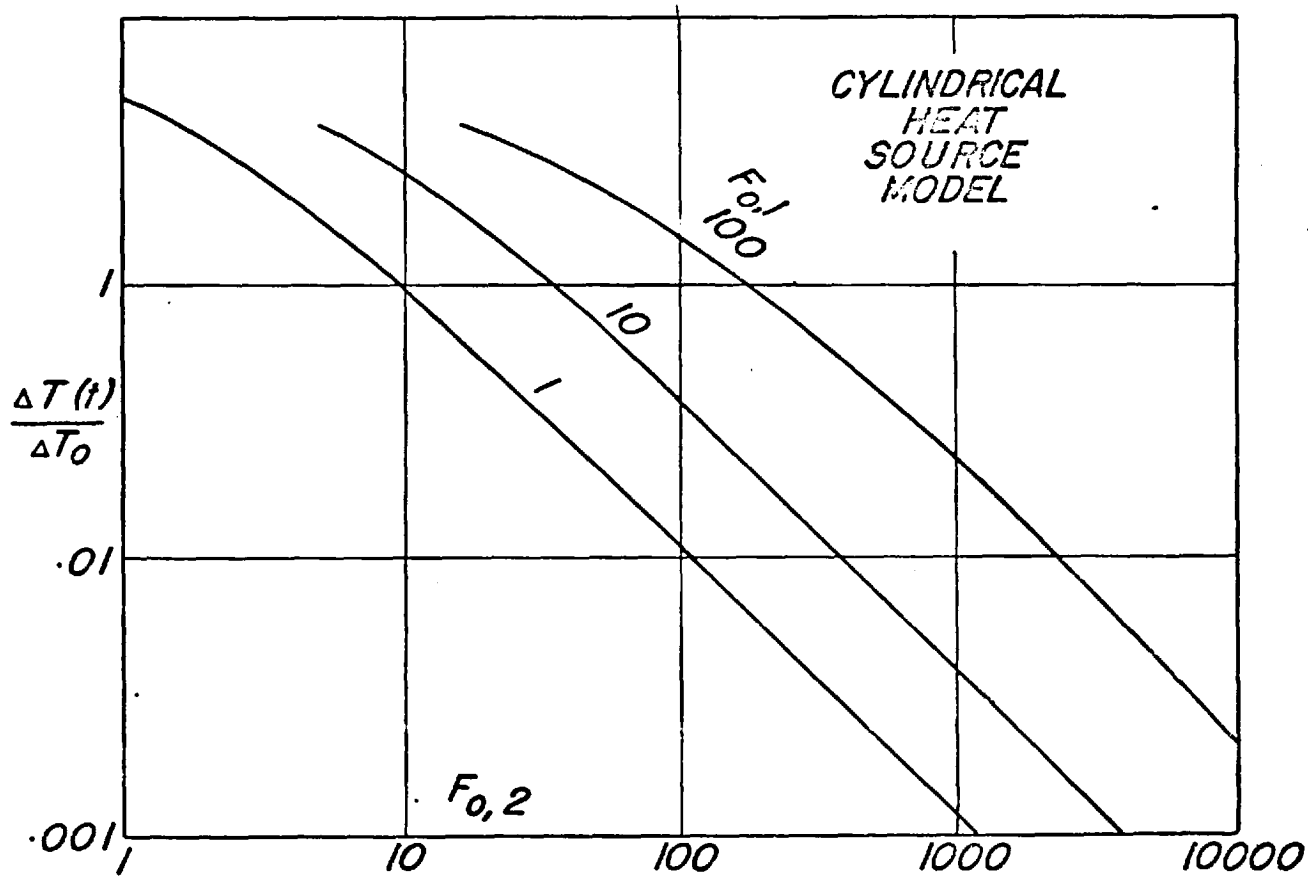
At the time t_2 = 20.8 hours, the mean value from table 1.1, the term $(t-t_1)/t$, equals .84 for average t_1, and the dimensionless temperature disturbance ratio, Figs. 1.7(a) and 1.7(b), has been reduced to about .1. Where $T_o \approx 40^oC$, this implies that, on average, a BHT, measured on the last log run, will be about 4^oC lower than geothermal. It should be emphasized though that this value of 4^oC is only a rough guide to the possible residual temperature disturbance at bottom hole at a given post-circulation time.

Mundry (1964) has extended the theory of the cylindrical source solution to incorporate the original geothermal gradient in the calculation. His solution is, at r_w,

$$(1.45) \qquad T(t)/T_o = 1 - 2/\pi \int_0^\infty \frac{\left[Y_o(u)\, J_o(u) - J_o(u)\, Y_o(u)\right] e^{-F_{o,1} u^2}\, du}{u \left[Y_o^2(u) + J_o^2(u)\right]}$$

where the derivation is similar in form to that of (1.34), Section 1.5, and J_o and Y_o are Bessel functions of the first and second kinds, k is the thermal diffusivity, t_1 is the circulation time, r_w is the well radius and $F_{o,1} = kt_1/r_w^2$. Fig. 1.9 is a graphical representation of (1.45); for a well of radius 100 mm., a diffusivity of 1.0 $mm^{-1} \cdot s^{-1}$, t_1 = 4.0 hours and $t_2 = t - t_1$ = 20.8 hours, all as before and used in Fig. 1.7(b), we obtain a dimensionless temperature disturbance ratio of about .1. This is identical with the value predicted by the previously discussed line source and cylinder models.

DIMENSIONLESS TEMPERATURE
DISTURBANCE VERSUS
DIMENSIONLESS TIME



Where $F_{0,1} = Kt_1/r_w^2$ (~1 for oil well)

$F_{0,2} = Kt_2/r_w^2$ (~10 for oil well)

And $\Delta T(t)/\Delta T_0, K, t_2, t_1$ and r_w defined in text

AFTER MUNDRY (1964)

FIG. 1.9

Table 1.1

Initial Temperature Disturbances, T_o

No.	Well Name	Number of Temps.	To (°C) Line Source	To (°C) Cylinder	t_1 hours	t_2 hours (maximum value)
1	49/17-4	3	- 31.8 ± 4.4	- 49.9 ± 6.0	4.0	20.
2	7/9-1N	3	- 45.2 ± 1.4	- 71.7 ± 1.7	4.1	11.
3	47/13-1	4	- 24.6 ± 6.9	- 36.1 ± 9.1	4.7	40.
4	22/11-2	3	- 30.0 ± 1.2	- 50.6 ± 1.7	3.5	12.
5	N-21-3	4	- 9.8 ± 2.8	- 17.3 ± 4.5	2.7	18.
6	N-25-4	3	- 88.4 ± 28.8	-158.8 ± 50.6	2.0	24.
7	N-11-3	4	- 67.1 ± 3.2	-313.5 ± 16.9*	0.7	30.
8	N-20-3	4	-126.8 ± 15.5	-159.6 ± 20.3	6.0	33.
9	N-3-1	3	- 13.3 ± 0.5	- 22.6 ± 0.8	3.6	9.5
10	N-3-3	4	- 54.7 ± 3.1	- 86.8 ± 5.8	3.6	15.
11	21/10-5	6	- 56.3 ± 1.9	- 82.2 ± 2.9	5.9	18.
12	30/1-1	4	- 34.2 ± 1.9	- 48.9 ± 2.1	8.8	20.
13	Garissa	4	- 28.2 ± 3.8	- 47.7 ± 5.9	3.1	15.
14	21/9-1	12	- 65.2 ± 5.3	- 92.8 ± 7.2	5.6	20.6
15	Wal Merer	4	- 84.0 ± 5.6	-124.8 ± 9.0	3.1	28.
16	Wal Merer	5	- 44.8 ± 4.5	- 74.1 ± 6.6	3.1	18.
17	49/13-1	3	- 33.3 ± 0.3	- 51.0 ± .9	4.9	14.
18	N-1-1	4	- 74.2 ± 13.3	-123.0 ± 20.1	2.9	28.
MEAN OF ALL DATA			- 50.7 ± 29.8	- 89.5 ± 70.0	4.0 ± 2.	20.8 ± 8.
MEAN, EXCLUDING 6, 8, 18			- 41.5 ± 20.8	- 61.2 ± 29.3		

* Result unrealistic, See Text

t_1, t_2, See Text

Table 1.2

Summary of Other Researchers

Calculated and Observed Values of

Initial Temperature Disturbance, T_o

ΔTo (^oC)	Reference	Remarks
20-40	Edwardson et al. (1962)	from calculations and results in a 3km. hole
38	Schoeppel and Gilliranz (1965)	calculated for a 3 km. hole
19-43	Tragesser et al. (1967)	measured and theoretical values
61-83	Raymond (1969)	detailed numerical analysis of circulating temperatures
23-56	Holmes and Swift (1970)	analytical analysis of circulating temperatures
22-56	Keller et al. (1973)	numerical study of circulating fluid temperatures in well annulus
42	MEAN VALUE	

1.7 Other Sources of Possible Error in the Temperature Measurements

Convective instabilities in a borehole arise when the geothermal gradient exceeds a critical value. Equation (1.47), after Hales (1937) and Krige (1939), predicts the critical gradient for a long tube filled with a liquid,

$$\left(\frac{\partial T}{\partial z}\right)_{\text{critical}} = \frac{\alpha_e T}{Cp} + \frac{Bvk}{g \cdot \alpha_e \cdot r^4} \qquad (1.47)$$

where,

- g – acceleration due to gravity
- α_e – volume coefficient of thermal expansion
- T – absolute temperature
- Cp – specific heat
- B – a constant $\approx$ 216
- k – thermal diffusivity
- v – kinematic viscosity
- r – borehole radius

The first right hand term is the adiabatic gradient, which is almost always less than geothermal while the second term is the borehole fluid viscosity factor which, of course, tends to increase the critical gradient. Fig. 1.10(a) is a suite of critical gradient curves as a function of temperature for both oil and water filled holes, where values of v, Cp, α_e, and k for both fluids have been obtained from Kaye and Laby (1948) and Ibele (1973). Values of v, α_e, Cp and k are not readily available for drilling fluids; however, water and oil are thought to represent the end points of the range of its thermophysical properties.

Clearly, Fig. 1.10(a) predicts that oil exploration boreholes will, almost invariably, be thermally unstable due to fluid convection. However, Hales' equation only predicts the onset of borehole convection

CRITICAL GRADIENTS FOR ONSET OF CONVECTION IN A BOREHOLE

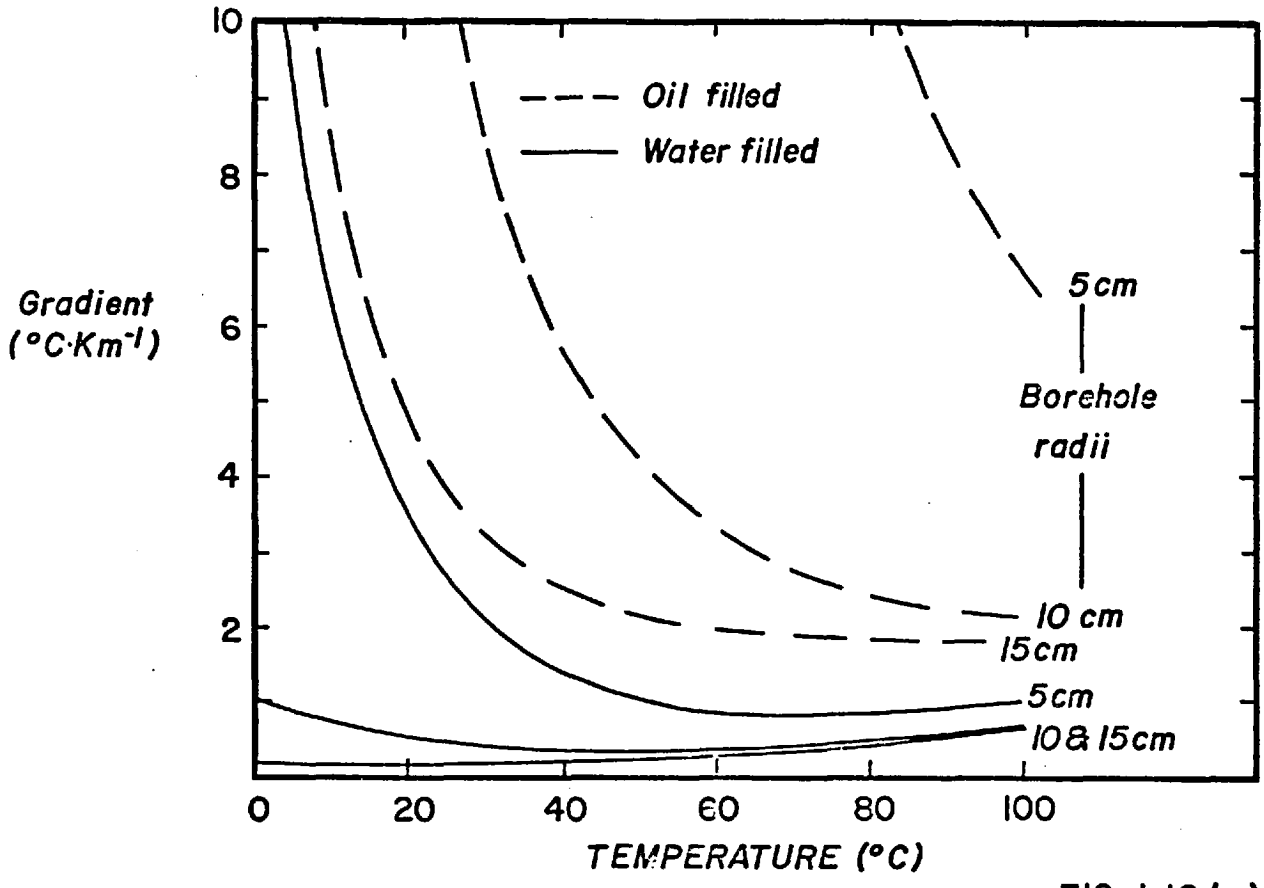
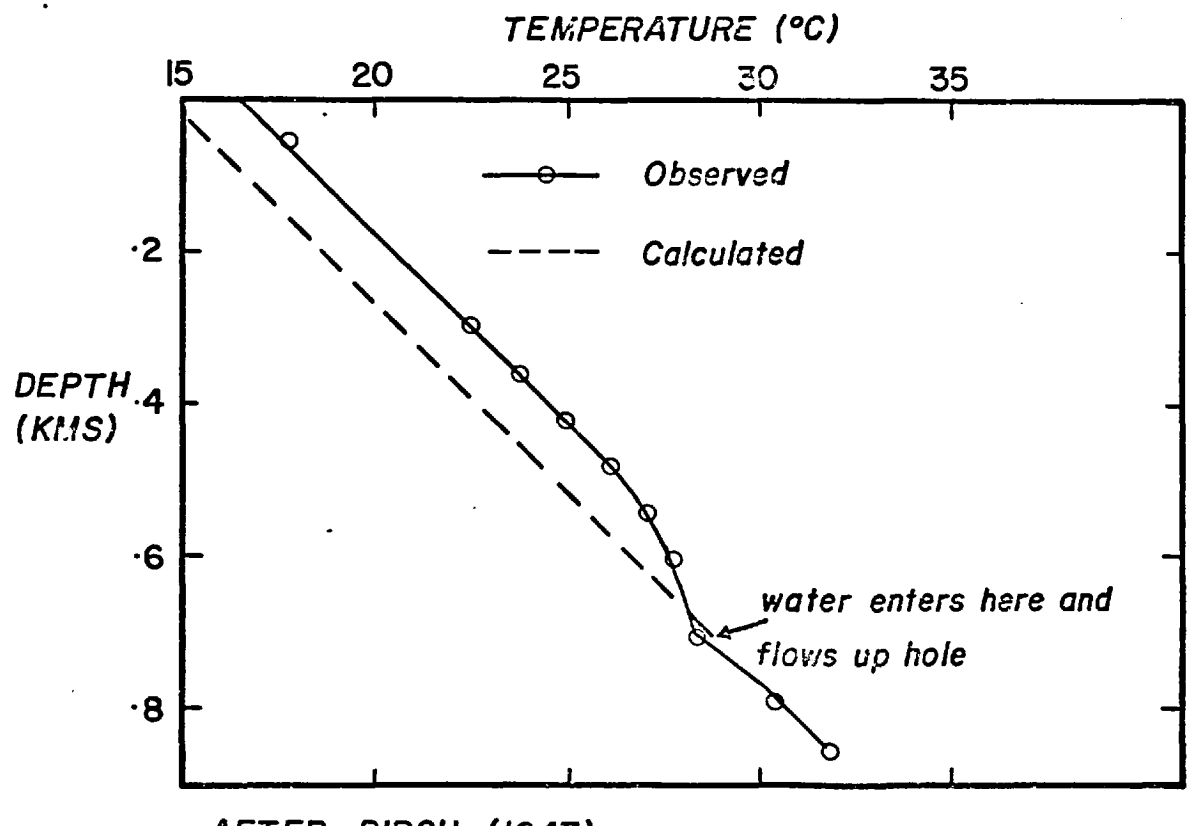


FIG. 1.10 (a)

EXAMPLE OF WELL DISTURBED BY WATER FLOW



AFTER BIRCH (1947)

FIG. 1.10 (b)

and not the magnitude of the resulting temperature disturbance. Both Gretener (1967) and Diment (1967) have investigated this problem by direct measurement and concluded that the convective movement does not exceed a few hole diameters, that the movement is cyclic with a fundamental period of about fifteen minutes and that the amplitude of temperature variation does not exceed a few hundredths of a degree Centigrade. However, Hilchie (1968) has investigated a large number of oil exploration boreholes and found a weak relationship between changes in hole diameter and variations in BHT derived geothermal gradients. He has tentatively ascribed this phenomenon to borehole convection. However, in light of the much more definitive work of Gretener (1967) and Diment (1967), it was felt that borehole convective disturbances were a negligible source of error in this study.

The flow of water into a borehole is a second possible thermal disturbance source. Depending on the point of entry and the direction of flow the net effect may be either a positive or negative disturbance. The magnitude of the temperature disturbance is a function of the flow rate, the thermal properties of the adjacent rocks and time. Birch (1947) has shown that for modest flow rates, the temperature disturbance will be of the order of 1 - 2^{o}C. Fig. 1.10(b) is a temperature depth profile for a borehole disturbed by flowing water. However it is the author's experience that there is, in general, insufficient BHT data from oil exploration wells to recognize a water flow disturbance.

This factor also limits any attempt to identify gas entry into the well. A sudden reduction in hole pressure may result in gas entry into the well where it expands, and, by the general gas law, cools, producing a significant drop in borehole temperature. Again the magnitude is dependent on several, often poorly known factors; radial pressure distribution, thermal properties of the producing formation, quantity of gas, etc. (Kunz and Tixier, 1955). Fig. 1.10(c) after Hutchins and Kading (1969) is an example of a gas entry thermal disturbance.

EXAMPLE OF TEMPERATURES
DISTURBED BY GAS FLOW

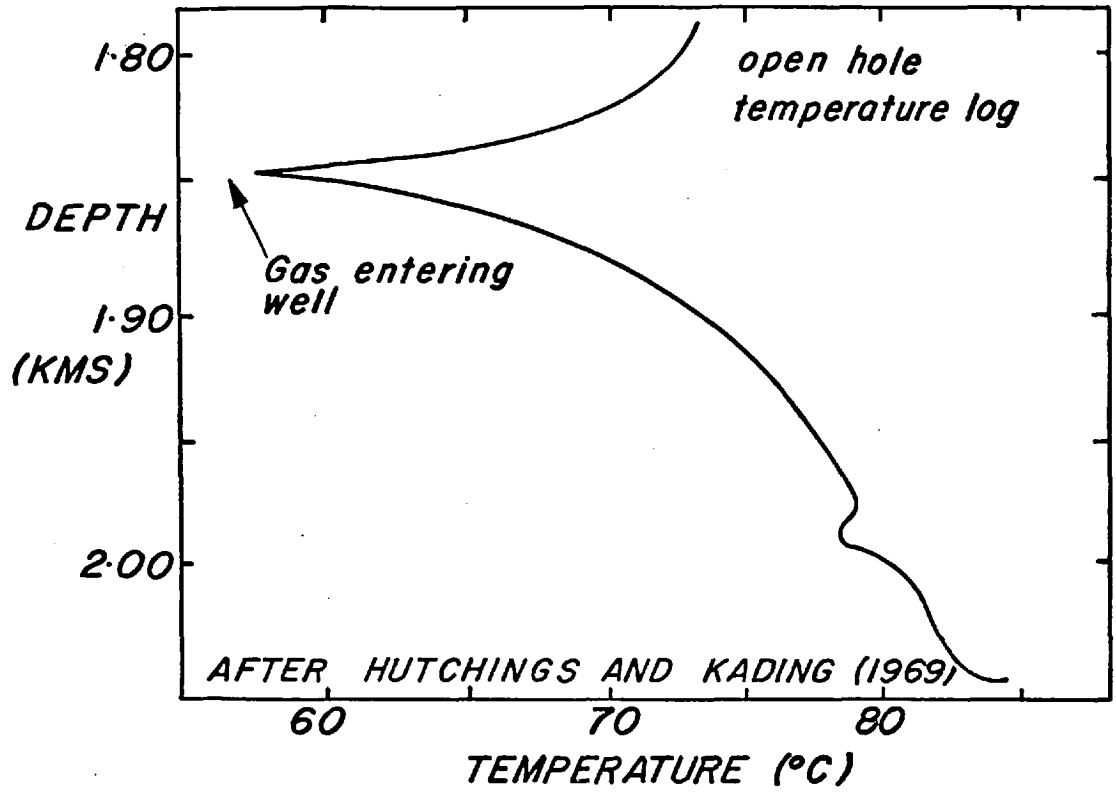


FIG.1.10(c)

EXAMPLE OF TEMPERATURE
DISTURBANCE BY LOST CIRCULATION

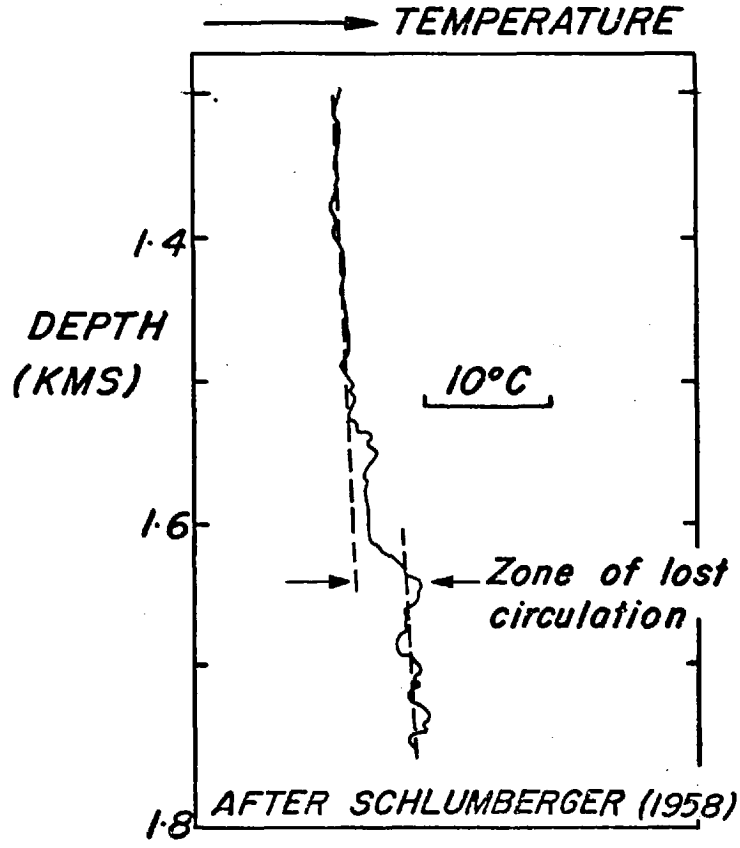


FIG.1.10(d)

Other factors affecting temperature encountered in oil exploration wells are setting casing cement and, where a well is to be produced, hydraulic or acid fracture treatments. In this study temperature data recorded to evaluate cement jobs was rejected while none of the wells considered here had reached production status. The reader is referred to Hutchins and Kading (1969) for a full discussion of temperature disturbances resulting from the above mentioned factors.

The discussion of thermal disturbances in boreholes due to drilling, Sections 1.4 through 1.6, required that no drilling fluid be lost during circulation. In general this criterion is never achieved. Where drilling fluid has been lost there is a decrease in mud volume and a concomitant reduction in the cooling effect of circulation. Fig. 1.10(d), from Schlumberger (1958), illustrates the typical result; a temperature discontinuity.

Where drilling fluid is lost to adjacent porous and permeable formations, another temperature dependent factor is introduced when drilling ceases. When circulation stops a pressure drop will occur within the well as conditions change from hydrodynamic to hydrostatic. The drilling fluid, which has been lost during circulation, will have migrated some distance laterally into the rock. This fluid will, depending on the depth, have considerably warmed or cooled but, in either case, have approached geothermal as a result of the large radial temperature gradient about the well during circulation (Edwardson et al., 1962). With the cessation of drilling, the fluid, referred to as mud filtrate, will return to the borehole and significantly speed the re-establishment of the geothermal regime.

We will return to these discussions in Sections 1.8 and 1.10.

1.8 The Error in the Determination of the Geothermal Gradient From Oil Exploration Borehole BHTs.

The possible sources of temperature error resulting from borehole disturbances and their magnitudes are summarized in table 1.3. Clearly the most significant error involved in the calculation of a geothermal gradient from BHTs is that due to the temperature disturbance of drilling. If we consider the drilling disturbance and temperature measurement errors only, disregarding the others as insignificant, undetectable or not applicable, then BHTs are, for this study, likely to be about 3-5^{o}C less than the true undisturbed formation temperature. This is, of course, only true on 'average' and only for that BHT recorded last in any suite of logs run to a particular bottom hole depth.

The obvious consideration is how do such temperatures compare with those obtained from the more traditional techniques of obtaining heat flow data. Table 1.4 summarizes the types of boreholes used in heat flow determinations, their typical associated temperature errors and the usual depth range over which the gradients are determined. Fig. 1.11 was constructed from table 1.4 where the gradient is assumed to be calculated from two temperature points with the maximum and opposite error at either end of the depth range. Although the error inherent in BHTs is about two orders of magnitude greater than those for temperatures measured expressly for heat flow, their much greater hole depth results in gradients with comparable accuracies for all the techniques/sites. Oil exploration boreholes will typically have gradients in error by 11%; this is inferior to deep continental boreholes (<1%), shallow continental boreholes (5%), and Oceanic Ewing probes (3%), though better than Bullard probes (26%). It is emphasized that this comparison is made on the assumption that the only error in those temperature measurements made in sites other than oil wells results from the degree of precision in their measurement. As we shall see

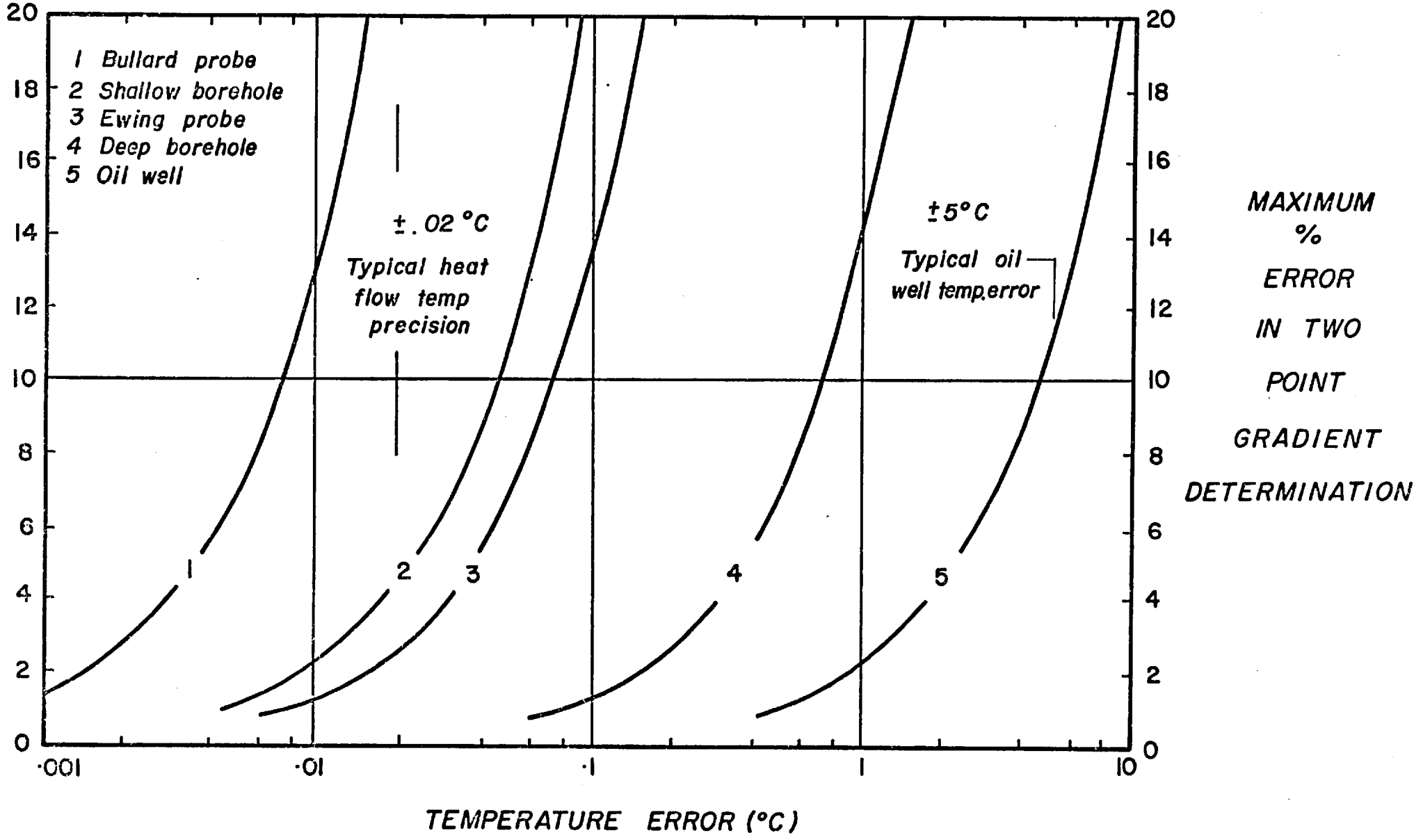

1 Bullard probe
2 Shallow borehole
3 Ewing probe
4 Deep borehole
5 Oil well
±.02 °C
Typical heat flow temp precision
±5°C
Typical oil well temp.error
1
2
3
4
5
0
2
4
6
8
10
12
14
16
18
20
·001
·01
·1
1
10
TEMPERATURE ERROR (°C)
MAXIMUM % ERROR IN TWO POINT GRADIENT DETERMINATION

FIG. I. II

in Chapter 3, temperatures measured in sites such as shallow continental boreholes may be significantly affected by local topography and recent climatic changes - effects which will not measurably perturb temperatures in the typical three to five kilometre deep oil exploration well.

To attempt to bring any further degree of sophistication to the estimate of error in geothermal gradients determined from BHTs is pointless. The lack of uniformity in the gathering of the data, the absence of detailed temperature profiles with which to detect disturbances such as water flow and gas entry, and the paucity of published data on bottom hole circulating mud temperatures prevent any refinement of the estimate of error.

It is, perhaps, more appropriate to note the findings of other workers who have studied the same problem. Harper (1971) in a study of North Sea geothermal gradients states that BHTs will give gradients within 10%; in a later study (Harper, 1973) of several wells, with long shut-in times, this figure was confirmed. Hough and Couvillon (1966) found that the return to thermal equilibrium was so rapid at the bottom of a six kilometre deep Texas well that it was not possible to lower the logging sonde rapidly enough to record temperatures less than geothermal, in this case 274^{o}C. Tragesser et al. (1967) in a study of the effects of rates and duration of circulation on drilling mud temperatures found that BHTs were essentially static, that is in equilibrium, after at twelve hour shut-in period in a three kilometre hole. Cooper and Jones (1959) found that bottom hole temperatures, when recorded twelve to twenty-four hours after drilling, gave reasonable geothermal gradients when compared with much later data. Raymond (1969), in a detailed numerical analysis of circulating fluid temperatures, concluded that the entire well was with ten percent of the geothermal gradient sixteen hours after circulation. Hedemann (1968), in a series of nonequilibrium borehole temperature measurements in Germany, found that the return to equilibrium was rapid at bottom hole with gradients accurate to better than ten percent after twenty-four hours. Many other authors

(Schlumberger et al., 1937, Uyeda and Horai, 1960, Mongelli, 1964, Schoeppel and Gillarranz, 1966, and Summers, 1972) have shown that BHTs, when used with discrimination, can give reasonable approximations to geothermal gradients.

Reel and Griffin (1971) have examined several hundred BHTs in Florida and found them qualitatively reliable though expressed some doubt as to individual determinations unless they were substantiated by several measurements. Hilchie (1968) also states that care must be exercised in the interpretation of BHT determined gradients; individual results being unreliable. Anglin and Beck (1965) report that BHTs are of little or no use in determining gradients. Kehle et al. (1970) find good and bad BHT data indistinguishable but where sufficient data exists, as in the United States, then regional geothermal gradient maps may be produced from them and the end product enhanced through spatial filtering techniques. The author's own experience suggests that in many instances only a small temperature disturbance is recorded by multiple BHTs run to bottom hole during a break in drilling.

Obviously no common opinion exists. It was, therefore, thought reasonable to attempt a heat flow study based solely, in terms of temperature data, on BHTs and to assess their suitability for heat flow determinations by the internal consistency of the heat flow values themselves.

The selection of BHT data for this study followed the following guidelines,

1) Only the last recorded BHT, the one nearest equilibrium, in any suite of logs was used.

2) Only where the thermometer reached bottom hole was the BHT used.

3) Temperature data obtained during cement jobs was eliminated.

4) No temperature data was obtained from a producing well.

None of the BHT data gathered was corrected for thermal nonequilibrium effects due to drilling as outlined in Sections 1.4 - 1.6. This was primarily due to the fact that multiple BHTs recorded on each log were very few; the normal practice being to obtain only a single reading on the last log at a given depth. In those few holes where such data was available it would be inappropriate to use it as any computed equilibrium temperature would, then, be not strictly comparable with other nonequilibrium BHTs at higher and lower levels in the hole. To obtain a temperature profile and hence a gradient it was thought to be more consistent to use the BHT at each depth which was thought to be closest to equilibrium. As BHTs will be consistently lower than geothermal this would tend to only shift the temperature profile hopefully leaving the gradient little different from its undisturbed value. The estimated error in BHT determined gradients of eleven percent is thus not unreasonable and agrees with many of those previously mentioned authors' estimates of error.

Table 1.3

Borehole Temperature Disturbances

Source of Temperature Disturbance	Error °C	Chapter Section	Remarks
Measurement Error	± 1.0	1.2	random
Drilling Disturbance	- 4.0	1.4 - 1.6	average case - lowers BHTs
Gas Entry	?	1.7	can drastically lower temperatures
Borehole Convection	± .02	1.7	undetectable with BHTs
Water Flow	± 1-2	1.7	magnitude varies with flow
Hydraulic Fracture	-	1.7	not applicable
Casing Cement	-	1.7	not applicable

Table 1.4

Temperature Errors in Various

Heat Flow Techniques/Sites

	Heat Flow Technique/Site	Typical Gradient	Error in Temp.	Depth Range	Reference
		$^{o}C \cdot km^{-1}$	^{o}C		
1	Oceanic - Bullard Probe	75	± .02	2 m.	Langseth (1965)
2	Continental - Shallow Hole	30	± .02	30 m.	Judge and Beck (1967)
3	Oceanic - Ewing Probe	75	± .02	20 m.	Langseth (1965)
4	Continental - Deep Hole	30	± .02	500 m.	Beck (1965)
5	Continental - Oil Exploration Hole	30	3-5	3 km.	This Thesis

1.9 Regional Geothermal Gradient Studies and Their Significance

Before discussing the calculation of heat flow values from BHTs it is both appropriate and useful to examine previous studies which have incorporated such data.

Regional compilations of BHT derived geothermal gradients have been the subject of several recent papers (Moses, 1961, Schoeppel and Gilliranz, 1966, Harper, 1971, Reel and Griffin, 1971, Summers, 1972, Evans and Coleman, 1974, Grisafi et al., 1974). The typical format has been to grid average data and to then map contours of isotherms or isogeotherms.

Herrin and Clark (1956) put forth the hypothesis that a correlation between geothermal gradients and sedimentary basin structure should exist; this has largely been confirmed by the above mentioned authors. In general the results have indicated relatively high geothermal gradients over sedimentary troughs and corresponding lows over the margins and intra-basin ridges.

Griffin et al. (1969) in such a study of Florida and Georgia found parallelism of geothermal, magnetic and gravity trends. Anglin and Beck (1965) found a correlation of high gradients with granite basement intrusions in western Canada. Kehle et al. (1970) have commented on the accuracy and uses to which BHT derived geothermal gradient maps might be put. Jones (1970), on the basis of a regional study of BHTs, has pointed out a possible economic reservoir of heat trapped beneath the widespread low thermal conductivity over-pressured shale units of the Gulf Coast region.

Regional geothermal gradient maps are not directly interpretable in terms of heat flow; gross lateral variations of thermal conductivity of near surface rocks, regional water flow, geologic structure and localized sources of heat production are all significant factors which will influence a geothermal gradient map. However, in most of the studies, one is struck by the seeming consistency of the data when considered in a regional context.

It is prudent to bear in mind though that many of the authors of such studies have emphasized the need to exercise care and discrimination in the use of BHT data. As with a single seismic record, gravity station, or magnetic traverse, individual BHT values having little meaning. It is only when such geophysical data are compiled in a wider context that trends emerge and a degree of confidence may be placed in its interpretation.

1.10 Suggestions for Future Research

The disturbance of the thermal regime by the drilling of a well is obviously of considerable importance to heat flow researchers. However, as is seen in Appendix 1, the standard paper on the subject clearly has some major inconsistencies. Thus a detailed theoretical analysis of the re-establishment of geothermal conditions in a borehole should be made. The recommended starting points would be the analytical work of Mundry (1964) and the numerical analysis study of Raymond (1969).

It would be pointless to pursue such a study without a series of practical experiments. Morgan (1972) has devised a disposable multiple thermistor cable suitable for siting in an oil exploration borehole when it is cemented shut. Recent developments in exploration drilling in southern England offer suitable one or two kilometre deep boreholes for such a string. An accurate record of the re-establishment of geothermal conditions could then easily be made and would provide a useful comparison with a theoretically predicted result. As a bonus, a heat flow value could be made in an area where none exists. Hopefully such a study would provide for rotary drilled holes what the Jaeger (1961) work has for diamond drill holes - a clear definition of the time necessary for a sufficient return to equilibrium for heat flow purposes.

The second suggestion is that a working relationship be formed between major oil companies and heat flow researchers. The oil companies

should then be urged to insist that logging contractors follow the API (1956) recommended procedure for recording BHTs. If the temperature measurements were systematically and carefully recorded, together with appropriate data on circulation and well size, accurate formation temperatures could be estimated as has been demonstrated by Timko and Fertl (1972). Where such data could be provided on a regular basis, ideally coded on a standard form, regional gradient maps could be easily produced and up-dated. Results would be of considerable interest to both academics and oil companies as Klemme (1972) has pointed out.

Such co-operation is unlikely to emerge unless formal arrangements are made. The recently compiled AAPG (1974) geothermal gradient map of North America is an indication of the potential of such a project.

Chapter 2

Thermal Conductivity Measurements

2.1 Introduction

Heat is a form of energy-thermal energy-in the process of transfer from one body to another. This transfer takes place in the presence of a temperature difference or gradient and is vectorial in the sense that it flows from regions of higher to lower temperature. Three basic mechanisms for such a transfer exist; convection, radiation, and conduction.

Convection is that mode of heat transfer effected by mass motion, the mass being either in its liquid or gas phase. Discussion of convection and its implications to surface heat flow is deferred to Chapters 4 and 5.

Radiation is the transfer of thermal energy by electromagnetic waves; the process is, for an ideal radiator, independent of the material medium and is governed by the Stefan-Boltzman law. For solids this radiation is insignificant for earth materials below 500^{o}K (Schatz and Simmons, 1972). This value is some 25^{o}K greater than the highest recorded borehole temperature considered here. Discussion of radiation is also left to Chapters 4 and 5 where it is incorporated into the calculation of crustal temperature models.

This leaves only conduction as a heat transfer mechanism of any consequence, in solids, for the temperature range 300-500^{o}K. The mode of transport at the molecular level consists of the transfer of energy during thermal motions from a more energetic high temperature molecule to its lower temperature neighbour. At the macroscopic level we may state that the heat flux, q, is proportional to the temperature difference, or gradient, $\partial T/\partial X$, with the constant of proportionality being defined as the thermal conductivity, K,

$$q = -K \cdot \partial T/\partial X \qquad (2.1)$$

The negative sign results from the definition of the direction of flow (Carslaw and Jaeger, 1959). In general, for geophysical considerations, the heat flux is quoted as a positive value and this convention will be followed here.

It is the measurement of this quantity, thermal conductivity, that is the subject of this chapter. The discussion will be limited to the value of thermal conductivity of materials at laboratory temperatures and pressures. In-situ effects will be considered in Chapter 3.

The measurement of the thermal conduction of samples retrieved from oil exploration boreholes posed a variety of problems; measurement technique, sample preparation, reconstruction of whole rock conductivity from measurements on rock fragments, porosity corrections and soluble samples. These and many other aspects of the laboratory work are discussed.

The chapter has been composed with initial sections dealing with general aspects, the middle with techniques, and the remainder with particular problems and sources of error.

2.2 The Measurement of Thermal Conductivity

That the measurement of the thermal conduction of samples from the borehole in which temperatures are obtained is essential to the calculation of a reliable heat flow has long been recognized (Birch, 1950, Beck, 1965). Various measuring techniques have been devised most of which may be classified as either of the transient or steady-state type.

Transient methods, as the name would suggest, are measurements made at a time when the system has yet to reach thermal equilibrium. The needle probe method (Von Herzen and Maxwell, 1959) is one of the most commonly used transient methods being essentially the introduction of a continuous line source of heat (section 1.4) into the sample. Carslaw and Jaeger (1959) show that for large times, of the order of 10-100 seconds, the continuous line source will produce, at any radial distance, a linear increase of tempera-

ture with time. The rate of this temperature increase is a function of the measured heat input and the thermal conductivity. The method, despite its obvious advantages of quick measurement and simple equipment, was not considered suitable for use in this study as the volume of sample required is more than that which could typically be made available for analysis by the various oil companies.

The measurement of conductivity by transient in-situ methods has attracted considerable attention (Blackwell, 1954, Beck et al., 1956, Wright and Garland, 1968, Oelsner and Sippel, 1971, Beck et al., 1971). However, despite numerous attempts, the equipment remains unreliable and prohibitively bulky for most field work. The question of making such in-situ measurements was never seriously considered as the oil exploration wells discussed here were all plugged with cement on completion. However, the prospect of deep wells open and undisturbed for long periods is about to be a reality in the North Sea with the advent of production platforms and observation wells. A suggestion for an improved in-situ conductivity apparatus, to take advantage of such boreholes, is given in section 2.17.

Steady state methods, of which the divided bar apparatus is the most common, were the alternative. Samples to be measured in this study were either solid core or drill cuttings (rock chips of about 1 mm.). With the recent development of the Sass et al. (1971) technique, both types of sample could be conveniently measured with the same apparatus - the divided bar.

The principle of the divided bar is straight-forward being based on the following hypothesis of Carslaw and Jaeger (1959). A solid is bounded by two planes of such an extent that they may be regarded as infinite. The two planes are maintained at different temperatures for a sufficient time such that for points well removed from the ends of the planes the temperature of the solid will remain unchanged along lines parallel to these planes. If the solid is bounded by a cylinder of Area A, normal to the planes at temperatures T_0 and T_1, and if the planes are seperated by a distance X, then

the quantity of heat, Q, flowing through the cylinder in time t is,

$$(2.2) \qquad Q = \frac{K \cdot (T_0 - T_1) \cdot A \cdot t}{X}$$

where K is the thermal conductivity of the solid and where no heat is presumed to flow in and/or out of the cylinder through its generating lines.

The divided bar apparatus was developed by a number of workers beginning with Clement and Peclet (1841) and Landsberg (1853). The modern apparatus is essentially the so called 'Forbes bar' (Forbes, 1845), used later by Lodge (1878). Lees (1892) was the first to use the divided bar for the measurement of rocks.

2.3 The Divided Bar

The current divided bar apparatus has evolved little in basic design from that described by Birch (1950). That design consists of two vertical brass cylinders both of which are held at different but constant temperatures. In the space between the cylinders are situated the two 'stacks', each typically consisting of a reference disc of known conductivity with a brass thermocouple locating disc on either side of it. In older bar designs the thermocouples were inserted directly into solid brass cylinders which also served as the reference material.

The sample, a cylindrical disc of 5 to 15 mm. in length and the same diameter as the bars, is inserted between the upper and lower stacks. The determination of its conductivity is made when steady state conditions have been reached, ie. when there is uniform axial heat flow in the cylinders/stacks/sample system. The flow of heat in the sample then equals that through the reference discs. Equation (2.2) may be invoked equating the ratio of the temperature gradients, measured by thermocouples, across the sample and reference discs to the ratio of the sample's and references' conductivities.

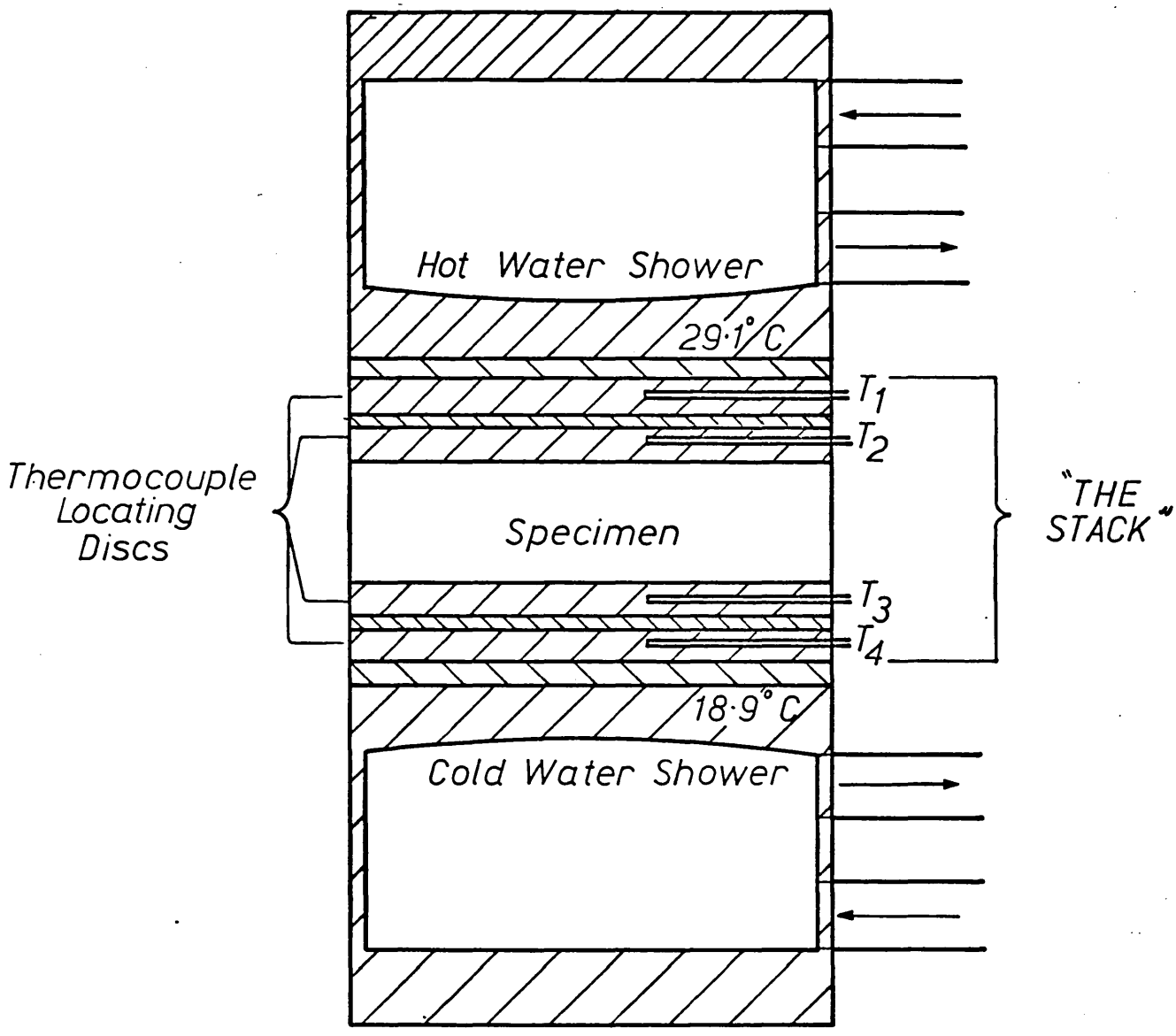
Significant developments in divided bar design have included; the replacement of electrical heaters with thermostatically controlled water showers in the brass cylinders, (Beck, 1957), the use of plastic as a reference material, (Roy et al., 1968), and the development of a fully automated measuring system, (Kresl and Vesely, 1971).

Fig. 2.1 is a schematic illustration of the divided bar used throughout this study. The design most closely resembles that of Roy et al. (1968). Table 2.1 gives dimensions for the various component parts of the bar shown in Fig. 2.1. The bar diameter used throughout this study was 34.92 mm.

The hot and cold water showers were maintained at 29.1^{o}C and 18.9^{o}C respectively with the upper bar being the hot end to prevent any convective instability. The hot and cold showers were fed from the reservoirs of two COLORA thermostatically controlled baths (Model NB) with self-heating and cooled by a COLORA immersion unit (Model TK64, modified).

Copper-constantan thermocouples were used and arranged so as to measure the temperature differences $T_1 - T_2$, $T_2 - T_3$, and $T_3 - T_4$ (Fig. 2.1). The thermocouples themselves were of 40 SWG wire with a sensitivity of approximately 40 $\mu V \cdot {}^{o}C^{-1}$ in the temperature range 20-30^{o}C (ASTM, 1970). The thermocouples were cemented into hollow brass cylinders about 17 mm. long and 1 mm. in diameter and inserted into the brass thermocouples locating discs shown in Fig. 2.1. The thermocouple wire emerging from the bar was carried one full turn around its (the bars) circumference at the level of the thermocouple. This ensured that the thermocouple and the first several centimetres of its leads were virtually at the same temperature thus preventing any conductive effects along the wire disturbing the measurement.

The measurement of the thermocouple potentials, or temperature differences, was made with a vernier potentiometer, model P10, and a galvonometer both manufactured by Croydon Precision Instruments Co. Ltd. The thermocouple differential voltages were nulled against a constant voltage



Vertical Cross Section of the Divided Bar Assembly

FIG. 2.1

with the measurement of potential difference being obtained to a precision of .1 μV, or about .003^{o}C, the limit of the thermal stability of the galvonometer. The thermocouple differential voltage measuring circuit is schematically illustrated in Fig. 2.2.

The 'stack' or reference and thermocouple locating discs were cemented together with an epoxy resin, the reference material being a plastic polycarbonate with the trade name Lexan. Good bar design demands that the thermal resistance of each reference disc should be comparable to that of the sample to be measured (Jessop, 1970). Most of the material to be measured on the bar would have a conductivity of about 2.5 $W \cdot m^{-1} \cdot K^{-1}$ and be of the order of 10 mm. in length. The Lexan material was known to have an approximate conductivity of .2 $W \cdot m^{-1} \cdot K^{-1}$ (ASTM, 1971) thus implying an optimum reference disc thickness of .8mm. (see table 2.1). The brass thermocouple locating discs do not contribute significantly to the resistance of the reference.

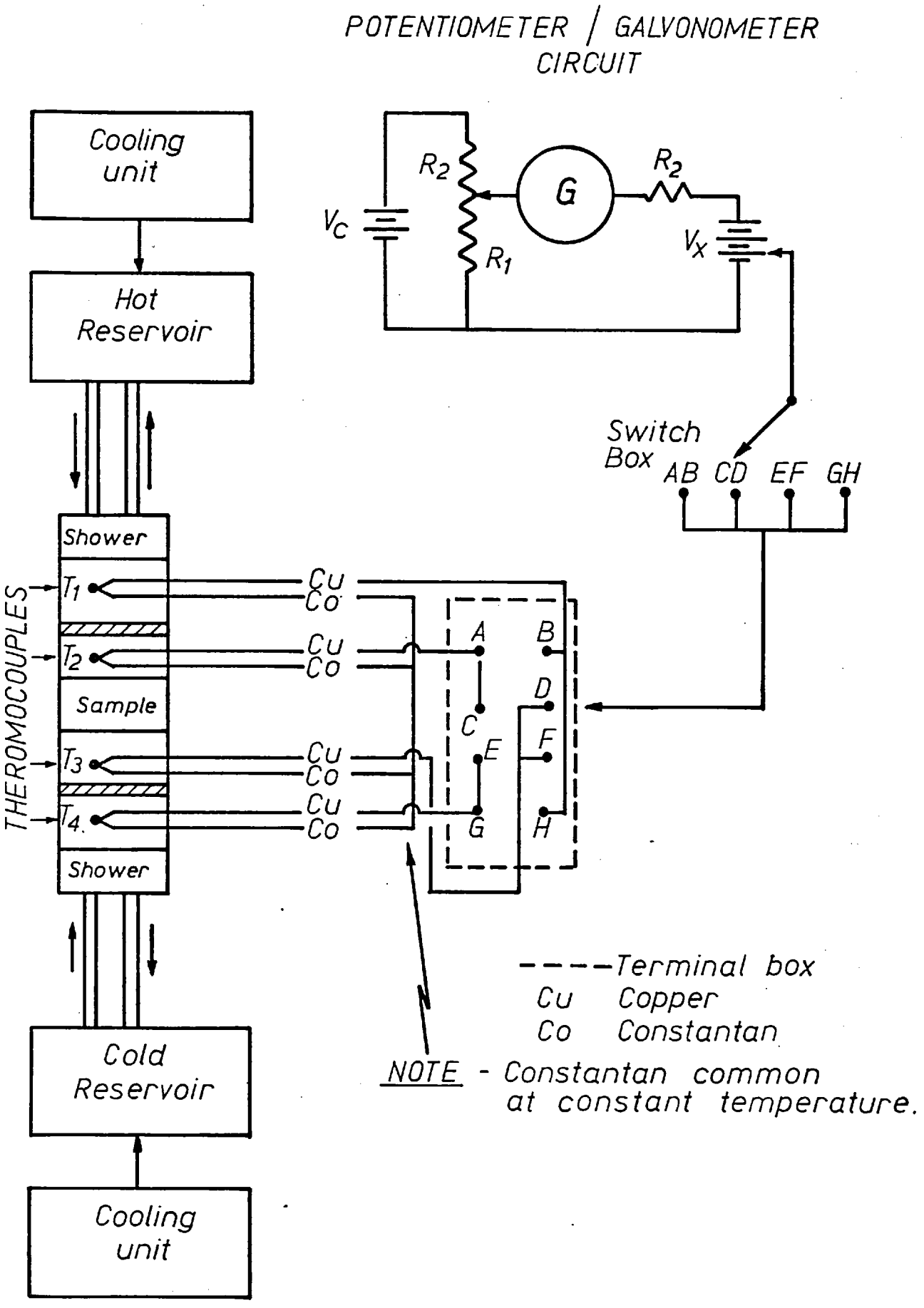
In addition, two further Lexan discs were cemented between the upper and lower stacks and the hot and cold showers (Fig. 2.1). These discs were necessary to effect thermal damping as it was found that the COLORA baths had a periodicity of approximately 10 seconds with an observed amplitude of .03^{o}C. The relatively small temperature drop of about 2^{o}C across each reference disc meant that such oscillations were significant. The thickness of damping material (Lexan) was chosen to obtain an order of magnitude drop in observed amplitude. For a uniform half space the amplitude of a sinusoidally varying temperature at the surface decreases with depth, x, as,

$$e^{-2\pi x/\lambda} \tag{2.3}$$

where

$$\lambda = (4\pi k/n)^{\frac{1}{2}} \tag{2.4}$$

and,



SCHEMATIC OF DIVIDED BAR MEASURING SYSTEM

FIG 2·2

(2.5) $$n = w/2\pi$$

where k is the material thermal diffusivity, and w is the angular frequency of the temperature variation. An assumed thermal diffusivity of .1 $mm^2 \cdot s^{-1}$, based on the conductivity value of .2 $W \cdot m^{-1} \cdot K^{-1}$, would not be unreasonable for Lexan. This led to a minimum thickness of 1.3 mm to effect an order of magnitude drop in the observed temperature variation (see table 2.1).

The upper and lower stacks were set in a rectangular steel frame with the upper unit suspended from the cross member and in a ball joint while the lower unit was situated on the end of a hydraulic pump. With a sample between the stacks the lower unit would be driven up to create a uniaxial pressure of up to 7 $MN \cdot m^{-2}$, the upper stack in the ball joint self-adjusting to compensate for any slight non-parallelism of sample faces.

Figure 2.3 is a plate of the entire divided bar and baths units.



The divided bar apparatus used in this study. The upper and lower bars are wrapped in white tape and are visible in the rectangular metal press. The hot and cold reservoirs with their connecting hoses are seen at the bottom of the plate.

Fig. 2.3

Table 2.1

Dimensions of the Component Materials

Of The Divided Bar

(see Fig. 2.1)

Component	Material	Thickness (mm.)
Upper Damping disc	Lexan	1.636
No.1 Thermocouple locating disc	Brass	2.527
Upper Reference disc	Lexan	0.821
No.2 Thermocouple locating disc	Brass	2.555
No.3 Thermocouple locating disc	Brass	2.403
Lower Reference disc	Lexan	0.827
No.4 Thermocouple locating disc	Brass	2.527
Lower Damping disc	Lexan	1.635

2.4 Calibration of the Divided Bar

As was mentioned in section 2.3 the divided bar is a comparative, as opposed to absolute, measuring system thus necessitating its calibration. The previously mentioned reference material Lexan must be assigned a conductivity by the measurement of some standard material.

The most commonly used standards are fused quartz and crystalline quartz which has been cut perpendicular to its c crystallographic axis. These two materials span the range of thermal conductivity of most rocks. Table 2.2 gives values, for both materials, which have been measured by various workers using both absolute and comparative methods.

The values selected for this study were those of Ratcliffe (1959) who proposed the following empirical relations,

$$K_{fq} = 1.323 + .00193 \cdot T - .0000067 \cdot T^2 \qquad (2.6.1)$$

$$K_{cq} = (.145 + .000578 \cdot T)^{-1} \qquad (2.6.2)$$

where T is the temperature in degrees Centigrade, and K_{fq} and K_{cq} are the fused and crystalline quartz conductivities, respectively, in $W \cdot m^{-1} \cdot K^{-1}$. The temperature at the midpoint of the bars was determined by direct measurement with an absolute thermocouple. The mean midpoint value for several measurements was $23.92^{o}C \pm .03$ which by (2.6.1) and (2.6.2) yields conductivities of 1.365 and 6.296 $W \cdot m^{-1} \cdot K^{-1}$ for fused and crystalline quartz respectively.

The standard approach to the calibration of a divided bar has been described by Beck (1965). Briefly, it consists of the measurement of several discs of fused and crystalline quartz each of a different thickness. The following relation may easily be derived (Jessop, 1970),

$$\frac{L \cdot V_2}{V_1 + V_3} = \frac{d_s \cdot K_b}{K_s} + R \cdot K_b \qquad (2.7)$$

where d_s is the thickness of the standard disc, L is the total thickness of the two reference discs, K_b is the reference material conductivity, K_s is the standard material conductivity, V_1, V_2, V_3 are the temperature drops across the upper stack, standard disc and lower stack respectively and R is any additional thermal resistance, or contact resistance, between the standard disc and stacks. The left hand term of equation (2.7) may be fitted by least squares to d_s and the resulting slope multiplied by K_s to yield a value of K_b, the reference conductivity. The intercept gives a value of contact resistance; this will be discussed further in section 2.6.

Values of K_b were determined for both fused and crystalline quartz as standards. The results of several such calibrations carried out during the course of this research, October, 1972 to July, 1974, are given in table 2.3. The value of .222 $W \cdot m^{-1} \cdot K^{-1}$, the mean of the fused and crystalline quartz values, was used as the K_b value for all measurements made at 23.92°C.

An alternative calibration method utilising a criterion of a minimum variance sum (Topping, 1962) for the terms K_b and R is equation (2.7) yielded results insignificantly ($< 1\%$) different from those given above.

As can be seen from table 2.3 the inferred values of fused and crystalline quartz are about 1.5 percent low and high respectively compared with the Ratcliffe (1959) values used to compute the standard conductivity. These inferred values are comparable with those of other workers (Beck, 1965, Jessop, 1970, Judge, 1971). Furthermore, the inferred results differ from the Ratcliffe values by little more than the typical uncertainty in a single calibration fit of equation (2.7), or from the standard deviation of the individual results in table 2.3. These values will be discussed in the estimation of errors in section 2.15.

Table 2.2

Thermal Conductivity of Fused and Crystalline Quartz*

$W \cdot m^{-1} \cdot K^{-1}$

Reference	Method	Fused Quartz	Crystalline* Quartz
Kaye and Higgins (1926)	Divided Bar (Aluminium)	1.356	6.312
Birch and Clark (1940)	Thermopile (Absolute)	1.398	6.199
Beck (1957)	Divided Bar (Copper)	1.352	-
Ratcliffe (1959)	Thermopile (Absolute)	1.369	6.270
Devyatkova et al. (1960)	Divided Bar (Copper)	1.352	-

* at $25^{o}C$

* cut perpendicular to the c crystallographic axis

Table 2.3

Divided Bar Calibration Summary (1972 - 1974)

FUSED QUARTZ			CRYSTALLINE QUARTZ			DATE d/m/y
FQ3(3)	FQ4(5)	FQ5(5)	CQ1(3)	CQ4(5)	CQ5(5)	
.219			.214			09-10-72
.222			.218			13-10-72
			.218			09-11-72
			.224			22-11-72
	.229					16-03-73
				.219		18-03-73
			.222			19-03-73
		.224			.218	23-04-73
		.225			.220	29-05-73
		.226			.218	12-06-73
		.227			.217	02-07-73
		.229			.221	21-11-73
		.226			.221	24-01-74
		.228			.219	07-02-74
					.224	20-03-74
			.218		.216	09-07-74
.221	.229	.227	.219	.219	.219	AVERAGES
.2256 ± .0031			.2192 ± .0027			
MEAN VALUE = .222 $W \cdot m^{-1} \cdot K^{-1}$ (26 calibrations) (124 measurements)						

Inferred fused quartz conductivity = 1.344 $W \cdot m^{-1} \cdot K^{-1}$

Inferred cryst. quartz conductivity = 6.383 $W \cdot m^{-1} \cdot K^{-1}$

FQ3, CQ1, etc.; name of calibration set

(3), (5); number of calibration discs in a set

2.5 The Preparation and Measurement of Discs

The core samples obtained from the various oil companies ranged in size from 50 - 120 mm. in diameter. This necessitated their being re-cored to the bar diameter of 34.9 mm. with care being taken to obtain a sample with the orientation of the original core. Discs were then cut with a diamond saw, the sample being held and rotated in the chuck of a lathe. Each disc was lapped with carborundum powder in an automatic machine. The finished discs consistently had faces parallel and flat to a tolerance of about .03 mm. Judge (1971) has shown that where a disc surface is flat and parallel to .04 mm. no significant change in conductivity will result from further improvement in the surface finish of the disc.

Where possible three or more discs ranging in thickness from 3 to 16 mm. were cut from each sample thus allowing a determination of conductivity independent of the contact resistance term in equation (2.7). However, this criterion could not always be met due to the friable and semi-consolidated nature of some of the cores.

Each disc was water saturated prior to measurement to simulate in-situ conditions. This was accomplished by evacuating the sample to a pressure of 130-400 $N \cdot m^{-2}$ and covering it with water from which all dissolved gases had been removed. The disc/water system was then returned to atmospheric pressure forcing water into the sample pore spaces. The necessity of such precautions has been discussed elsewhere (Walsh and Decker, 1966).

Prior to inserting the sample in the divided bar both faces of the disc were smeared with a mixture of one part glycerol to two parts water to insure an effective thermal contact. The sample was then immediately placed in the bar and the system loaded to an axial pressure of approximately 7 $MN \cdot m^{-2}$.

Typically a sample required five to six minutes to attain thermal equilibrium, a value comparable with that found by other workers (Kresl and Vesely, 1972). A measurement of the differential voltages was then made

(section 2.3) and was repeated three to four minutes later to ensure that steady state conditions did in fact exist. If any significant differences, changes of greater than .2 μV, were observed, measurements were repeated until consistent values were obtained.

The disc was then removed from the bar and its thickness measured with a micrometer to a precision of .02 mm.

2.6 The Calculation of the Contact Resistance

When three of more discs were prepared from a core, the calculation of thermal conductivity was straight-forward. Equation (2.7) was used with the left hand term being fitted by least squares to the various disc thicknesses. The resulting slope was divided into the reference conductivity (section 2.4) to obtain the sample conductivity.

Where only one or two discs were available, a value of the term $K_b \cdot R$ in equation (2.7) was required. This value, referred to as the contact resistance, was computed from measurements made on one hundred and twenty-one multiple set discs, that is those samples having three or more discs each. As mentioned above, the conductivity determination of these multiple disc sets was by least squares with the intercept value equalling the contact resistance. On plotting in histogram form, Fig. 2.4, it emerged that the R values had a large scatter and a small positive mean of 77.2 $m^2 \cdot K \cdot MW^{-1}$. Beck (1965) has shown that relatively small compositional changes, involving materials of differing conductivity, which often occur in discs from the same core, will yield spurious conductivities and contact resistances when these values are computed by the least squares technique. An obvious method to circumvent this difficulty was to reject any result where the error in fit in the least squares calculation of equation (2.7) exceeded some arbitrary value, the implication being that those disc sets with compositional variations would have poorer fits than more homogeneous samples. The values chosen were percentages of the error of fit in the calculated conductivity.

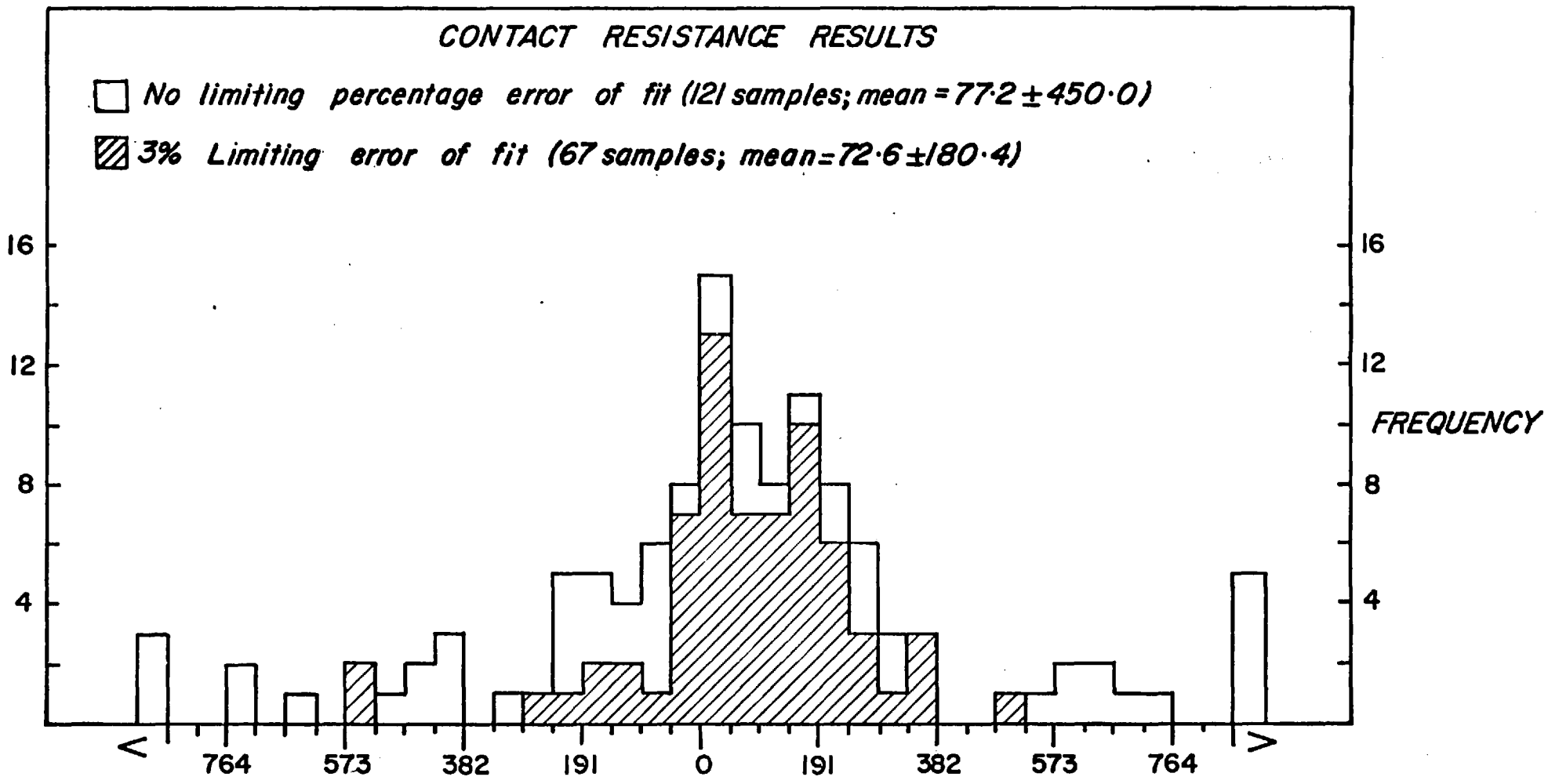

CONTACT RESISTANCE RESULTS
No limiting percentage error of fit (121 samples; mean = 77·2 ± 450·0)
3% Limiting error of fit (67 samples; mean = 72·6 ± 180·4)
16
12
8
4
FREQUENCY
< 764 573 382 191 0 191 382 573 764 >
CONTACT RESISTANCE
(m²·K·MW⁻¹)

FIG 2.4

In one percent steps from one to ten percent and two percent steps from ten to twenty percent the contact resistance data were analyzed for mean and standard deviation values with any individual value which exceeded the step level percentage standard error of fit being excluded. The results are shown in Fig. 2.5 with number of sets satisfying the criterion, the mean contact resistance, and the standard deviation plotted against the limiting percentage error of fit. Large variations of the mean resistance occur until a limiting error of fit of about seven percent is reached. At this point, twenty-nine of the original one hundred and twenty-one sample sets have been eliminated and the standard deviation considerably reduced. From seven to one percent limiting error of fit there was only a small variation of the mean but a further substantial decrease in the amount of scatter.

The result obtained with a limiting percentage error of fit of three percent, with sixty-seven multiple disc sets, was adjudged optimum as that at two percent gave a slightly greater standard deviation while that at one percent so severely reduced the number of multiple sets, to twenty-five, that it was now of questionable significance, statistically. Those values satisfying the three percent limiting error of fit have been shaded in in Fig. 2.4.

The mean value of 72.6 $m^2 \cdot K \cdot MW^{-1} \pm 180.4$ was adopted as the $\bar{R}$ value throughout this work. This value is in close agreement to that obtained by Cermak and Jessop (1971) for a similar divided bar.

The value itself is equivalent to about 1.6×10^{-2} mm. of the bar reference material Lexan or roughly .2 percent of the resistance of a typical measurement. In the extreme case of a thin, 3 mm., disc of high, 6.3 $W \cdot m^{-1} \cdot K^{-1}$, conductivity it represents fifteen percent of the measured sample resistance.

The contact resistance was not determined from the calibration results using fused and crystalline quartz (section 2.4) as the values obtained differed so markedly, the fused quartz value being about 100 $m^2 \cdot K \cdot MW^{-1}$ and

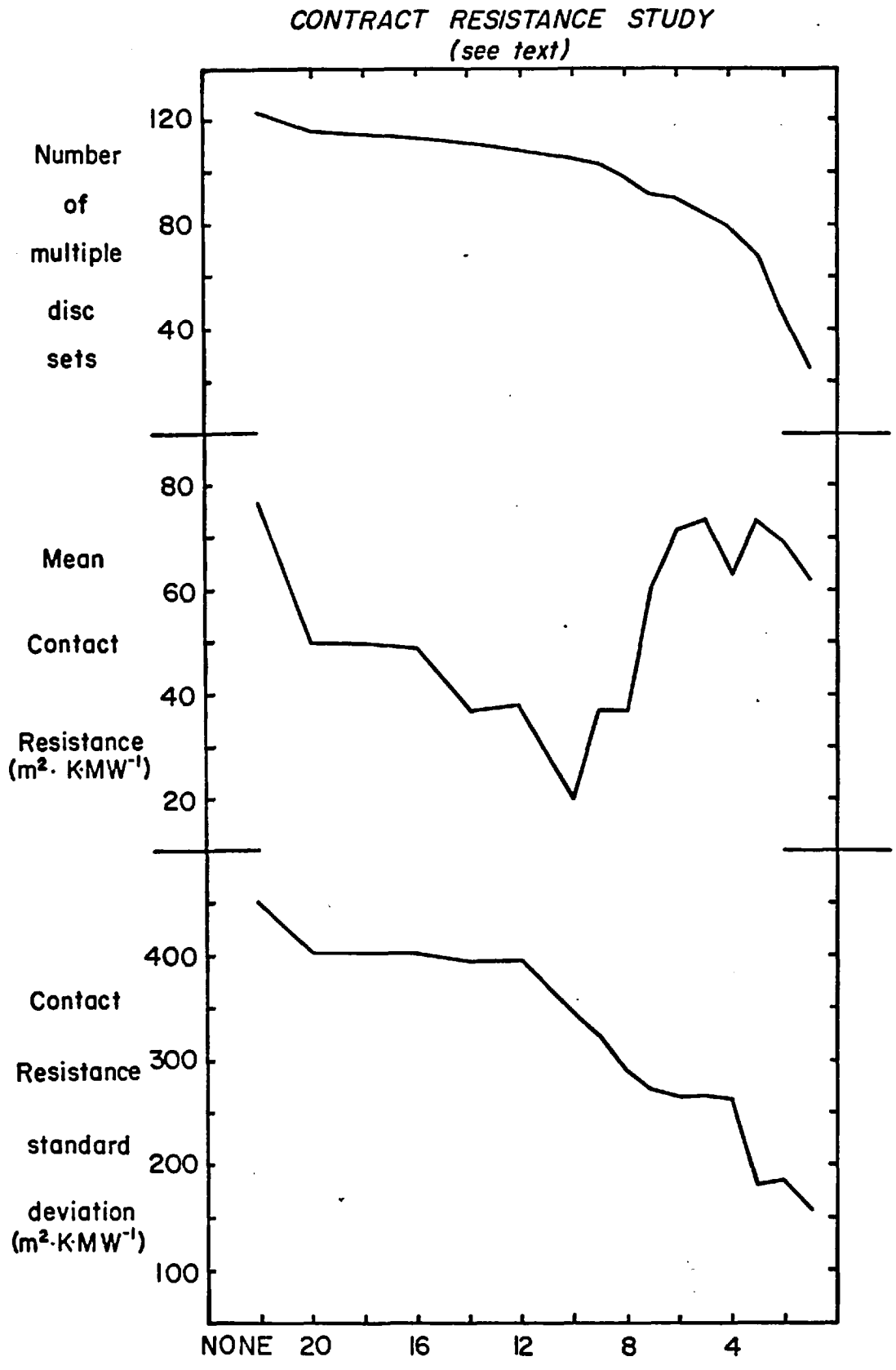

CONTRACT RESISTANCE STUDY
(see text)
Number of multiple disc sets
120
80
40
Mean Contact Resistance (m².K.MW⁻¹)
80
60
40
20
Contact Resistance standard deviation (m².K.MW⁻¹)
400
300
200
100
NONE
20
16
12
8
4
LIMITING ERROR (PER CENT) IN FIT OF EQUATION (2·7)
(3 DISCS OR MORE PER SET)

FIG. 2.5

some four times greater than that of the crystalline quartz. Judge (1971) has explained this large difference by assuming a contact thickness, X_c, composed of parallel arrangements of the fused or crystalline quartz and the water/glycerol contact mixture. Thus,

$$R = X_c/K_c \tag{2.7.1}$$

and

$$K_c = \alpha \cdot K_Q + (1 - \alpha) \cdot K_{gw} \tag{2.7.2}$$

where R is the contact resistance, K_c, K_Q and K_{gw} are the conductivities of the contact, the quartz and the glycerol/water mixture respectively and α is the proportion of parallel paths. Where α is one-half, the ratio of contact resistances observed for fused and crystalline quartz is roughly obtained. However, to obtain contact resistances equal to those observed an unreasonably large value of X_c (.08 mm) is required.

2.7 The Measurement of Rock Chips-Theory

The estimation of whole rock thermal conductivities from measurements on rock fragments has been investigated in depth (de Vries, 1952, Assad, 1955, Woodside and Messmer, 1961, Beck and Beck, 1965, Horai and Simmons, 1969, and Sass et al., 1971). To date, the basis of all of the workable techniques has been the measurement of a two component system, the conductivity of one being known and the other being calculated.

The calculation of the second phase depends on how accurately the original two phase system can be represented by a physical model which is mathematically definable. Various relationships have been proposed to describe the effective thermal conductivity of a two phase system, (Woodside and Messmer, 1961), the most widely used being the geometric mean model, (Sass et al., 1971), and the mean of the upper and lower bounds given by

Maxwell's relation, (Maxwell, 1904), for noninteracting spheres of one conductivity in a matrix of another (Hashim and Strikman, 1962, and Horai and Simmons, 1969).

The geometric mean model may be described as the weighted arithmetic mean of the logarithms of the constituent individual conductivities. The aggregate conductivity, K_a, in which the i^{th} constituent occupies the volume fraction, v_i, is given by Sass et al. (1971) as,

$$K_a = K_1^{v_1} \cdot K_2^{v_2} \cdots K_n^{v_n} \tag{2.8}$$

For a two component system this reduces to,

$$K_a = K_1^{1-v_2} \cdot K_2^{v_2} \tag{2.9}$$

or, as was stated in the definition,

$$\log K_a = (1 - v_2) \cdot \log K_1 + v_2 \cdot \log K_2 \tag{2.10}$$

The Maxwell spheres model is based on the mean of two limiting cases, a lower bound, K_l, for the aggregate conductivity, K_a, being spheres of the higher conductivity, K_1, phase dispersed in a continuous matrix of the lower conductivity, K_2, phase and an upper bound, K_u, being the opposite, (Hashim and Strikman, 1962).

$$K_l = K_2 + (1 - v) \cdot \left\{ (K_1 - K_2)^{-1} + v \cdot (3K_2)^{-1} \right\}^{-1} \tag{2.11}$$

$$K_u = K_1 + v \cdot \left\{ (K_2 - K_1)^{-1} + (1 - v) \cdot (3K_1)^{-1} \right\}^{-1} \tag{2.12}$$

and

$$K_a = \tfrac{1}{2} \cdot (K_u + K_l) \tag{2.13}$$

Where ϕ is the volume fraction of the lower conductivity material.

Both the geometric mean and Maxwell spheres models are limited in their ability to predict aggregate conductivities of multi-phase systems. In the case of the geometric mean model the constituent conductivities should differ by less than an order of magnitude while for the Maxwell spheres relation the result is only strictly valid for intermediate values of ϕ.

2.8 The Measurement of Rock Chips-Practice

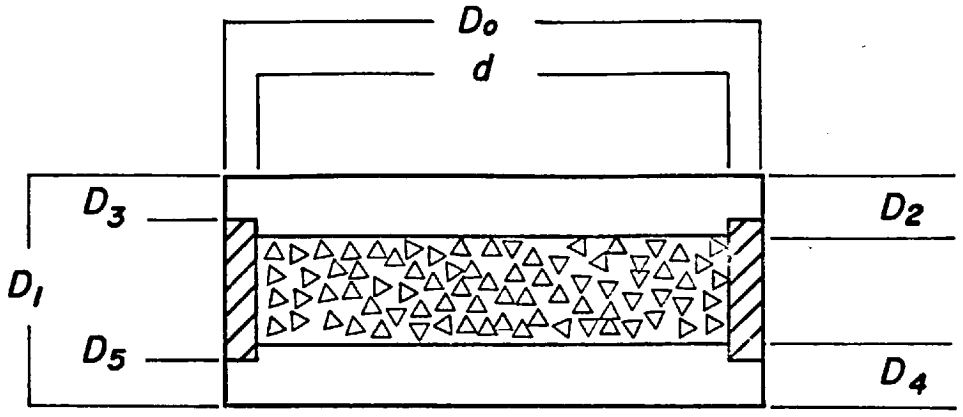
The method of measurement of the thermal conductivity of rock chips adopted for this study was by the technique developed by Sass et al. (1971). The method was judged most suitable as it required only a small amount of sample, about 20 cc., and the measurement could be made on the already existing divided bar.

The measurement procedure was to pack the chips into a cylindrical cell (Fig. 2.6) of the same diameter as the divided bar. The packed cell was then water saturated in exactly the same manner as a disc. Thus a two phase chip/water system was to be measured for its aggregate conductivity, K_a, with the conductivities of water, K_w, and rock, K_r, replacing the K_1 and K_2 terms respectively of equations (2.8) - (2.13).

The calculation of the chip/water aggregate conductivity was accomplished by subtracting the thermal resistances of the various components of the cell from its total measured thermal resistance. Utilising the cell dimensions D_1 - D_5 defined in Fig. 2.6 and where the conductivity of the plastic and copper cell components are K_p and K_c respectively, we may define,

$$(2.14) \qquad K_y = D_1 / \left[(D_3 + D_5) / K_c + (D_1 - D_3 - D_5) / K_p \right]$$

where the square bracketed term of (2.14) represents the total thermal resistance of a cell composed entirely of plastic and copper in series. K_y is the conductivity of such a cell of thickness D_1. Further,



Scale : x 2

Plan : circular.

Copper

Perspex

Rock chip - water aggregate

THE CHIP THERMAL CONDUCTIVITY CELL

FIG 2.6

TABLE 2·4

THE CHIP THERMAL CONDUCTIVITY CELL
TYPICAL DIMENSIONS

D_o	=	3.49 cm
d	=	3.20 cm
D_1	=	1.40 cm
D_2	=	0.40 cm
D_3	=	0.30 cm
D_4	=	0.40 cm
D_5	=	0.30 cm

(2.15) $$K_s = D_1 \cdot K_b / (R_c - R) \cdot K_b$$

where K_s is the apparent conductivity of the packed saturated cell, K_b is the bar reference conductivity and R_c and R are the cell thermal resistance and the cell contact resistance respectively.

Now where the inside and outside diameters of the cell are d and D_o respectively, (Fig. 2.6), we may subtract the conductivity K_y from K_s where the outer annulus of plastic and copper is in parallel with the inner cell of copper and chip/water aggregate. Thus,

(2.16) $$K_x = D_o^2 \cdot K_s / d^2 - (D_o^2 - d^2) \cdot K_y/d^2$$

Finally to compute the chip/water aggregate conductivity, we must subtract the component of thermal resistance, which is in series, of that section of the copper discs immediately above and below the aggregate.

(2.17) $$K_a = (D_1 - D_2 - D_4) / \left[D_1/K_x - (D_2 + D_4) / K_c \right]$$

Table 2.4 gives typical dimensions for a cell. These dimensions were measured to an accuracy of .02 mm. and were determined for each of the twenty cells used. Table 2.5 summarizes the copper, K_c, and plastic, K_p, conductivities used to compute K_a.

Table 2.5

Conductivity of Cell Materials ($24^{o}C$)

Material	Conductivity $W \cdot m^{-1} \cdot K^{-1}$	Reference
Copper	383.6	Ibele (1973)
Copper	398.3	Weast and Selby (1968)
Copper	387.7	Kaye and Laby (1966)
Copper Ave.*	388.5	- VALUE USED -
Perspex	.211	Determined from divided bar measurement of four discs

* Mean copper value computed from temperature adjusted values

2.9 The Calculation of Nonporous and Porous Chip Conductivities with a Direct Comparison with Discs

In the discussion of section 2.7 it was noted that the calculation of a rock conductivity, K_r, from an aggregate value, K_a, required a value ϕ, in this instance the volume fraction of water. This was determined by measuring, to a precision of .001 gram, the weights of the packed cell both before, WD, and after, WW, water saturation. Where V is the volume of the cell and taking the density of water as 1.00,

$$\phi = (WW - WD)/V \tag{2.19}$$

The value of K_r, which may now be determined, either by equations (2.8) - (2.10) or (2.11) - (2.13), represents a nonporous rock value. This is due to the fact that some of the water entering the cell is taken into the natural porosity of the chips. Thus, whether the geometric mean or Maxwell spheres model is used, an estimate of natural porosity, ϕ_n, will be required to correct the term K_r to K_{pr}, the porous rock conductivity.

The relevant equations to compute K_r and K_{pr}, assuming water to be the interstitial fluid, are, for the geometric mean,

$$K_r = e^{\left[\log (K_a/K_w^{\phi}) \,/\, (1 - \phi)\right]} \tag{2.20}$$

and

$$K_{pr} = K_w^{\phi_n} \cdot K_r^{1 - \phi_n} \tag{2.21}$$

and, for the Maxwell spheres model,

$$K_r = \tfrac{1}{2} \cdot \left[K_w + (1 - \phi)\cdot(K_a - K_w)^{-1} - \phi\cdot(3K_w)^{-1}\right]^{-1} + \tfrac{1}{2}\cdot \left[\frac{-B - \left\{B^2 - 4\cdot(2\phi - 2)\cdot K_w\cdot K_a\cdot(1 - \phi)\right\}^{\frac{1}{2}}}{2\cdot(2\phi - 2)}\right] \tag{2.22}$$

where $B = K_a \cdot (2 + \phi) - K_w \cdot (1 + 2\phi)$

and,

$$(2.23) \quad K_{pr} = \tfrac{1}{2} \cdot \left[K_r + \phi_n \cdot \left\{ (K_w - K_r)^{-1} - (\phi_n - 1) \cdot (3K_r)^{-1} \right\}^{-1} \right] + \tfrac{1}{2} \cdot \left[K_w + (1 - \phi_n) \cdot \left\{ (K_r - K_w)^{-1} + \phi_n \cdot (3K_w)^{-1} \right\}^{-1} \right]$$

Equations (2.20), (2.21) and (2.23) follow directly from (2.8)-(2.12); equation (2.22) is discussed in Appendix 3. Fig. 2.7 graphically illustrates the two relations described by (2.21) and (2.23).

The natural porosity, ϕ_n, was calculated throughout this study by the application of standard interpretation techniques to commercial well logs run in the holes comprising this study. These techniques, in widespread use throughout the oil industry, are briefly described in section 2.10.

The choice of models to compute the conductivity, and indeed to check whether either model was valid, was made by comparing results obtained by measuring discs and chips obtained from the same core. From theoretical considerations there is nothing to recommend one method to the other so that preference must be made on one or the other's ability to successfully predict a porous rock conductivity. The equivalent disc conductivity, K_d, has been chosen as the standard as it is widely held to be accurate to a value of two percent or better (Beck, 1965, Judge, 1971). The errors implicit in these measurements will be discussed further in section 2.15.

Samples used in this study comprised a variety of sedimentary rocks; sandstones, limestones, shales, claystones, mudstones, and marls. Their natural porosities ranged from virtually nothing to in excess of forty percent.

There were ninety samples in all, for which multiple disc conductivity determinations were available from sixty-six, the remainder being calculated from a single disc. Where there were only two discs or, where the error fit of

POROUS ROCK CONDUCTIVITY

VS

POROSITY

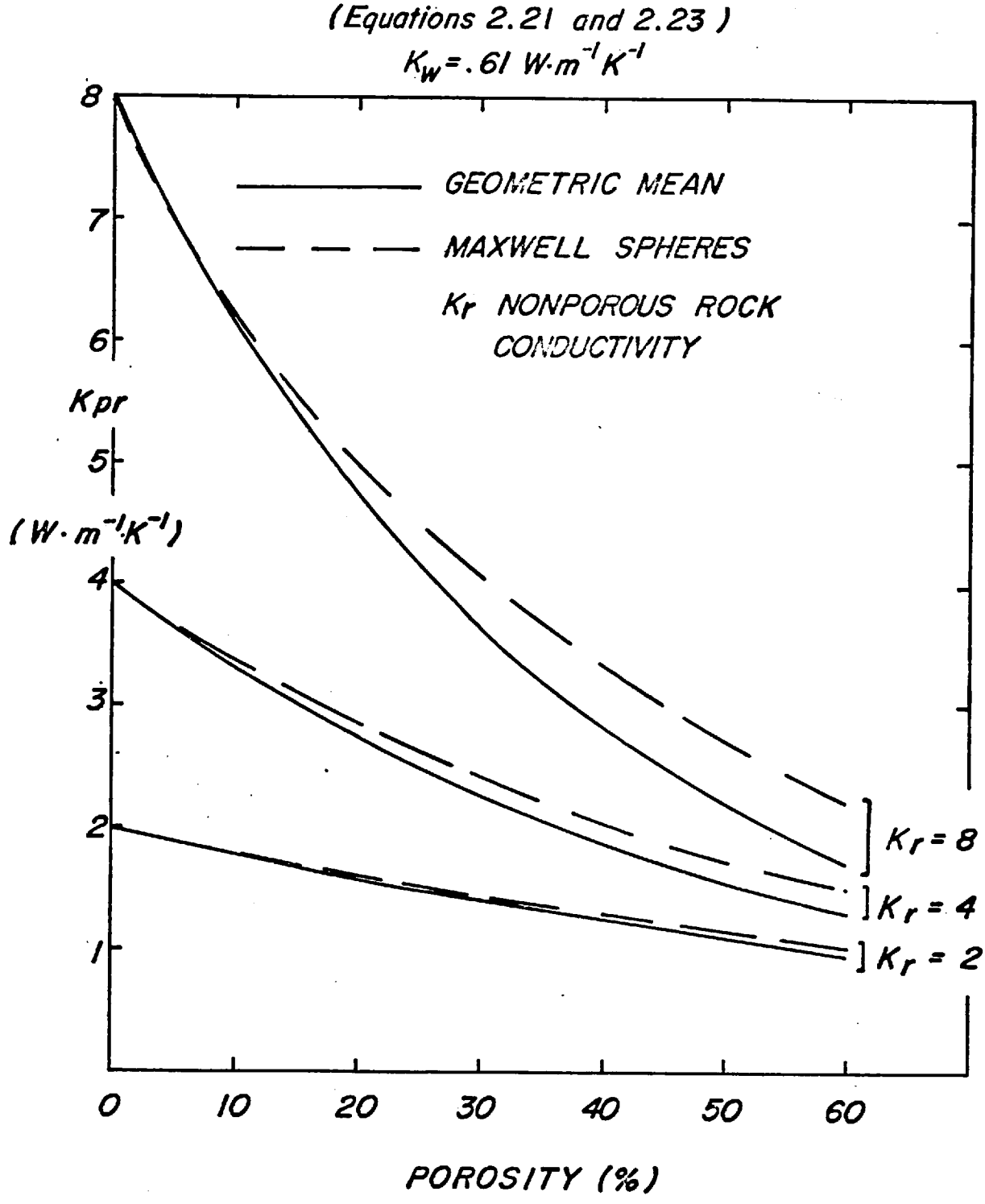


FIG 2.7

equation (2.7) exceeded three percent of the computed conductivity, the harmonic mean value of the single disc determinations was used for the comparison (see section 2.6).

The results of this comparison, for both geometric mean and Maxwell spheres models, are summarized in Fig. 2.8 and table 2.6. The obvious conclusion is that both models are quite acceptable, the geometric mean being marginally the better. The mean of differences, column one, table 2.6, were computed by subtracting the disc conductivity, K_d, from the porous chip value, K_{pr}, summing these differences and calculating the mean and standard deviation. The mean of absolute differences, column two, table 2.6, were computed in an analogous manner except that the absolute values of the differences were summed. The mean of the differences indicates, that for both methods, little, if any apparent bias was introduced into the calculated porous rock conductivities when compared to their equivalent disc values. The mean of the absolute differences suggests that the values of K_{pr} typically differ from those of K_d by less than ten percent. This latter result agrees well with that obtained in a similar study by Sass et al. (1971) although they noted that the Maxwell spheres model did introduce a significant bias producing results consistently lower than those measured on equivalent disc samples.

On the basis of these results it was decided to use the geometric mean model for the calculation of all porous rock conductivities determined from chips in this study.

The individual results for the geometric mean model are shown in Fig. 2.8 and are coded to differentiate the mode of determination of K_d. A similar plot for the Maxwell spheres model was omitted as it was insignificantly different.

The values lying above the 10% positive error line and below $K_d = 2.5$ on Fig. 2.8 may be the effect observed by Sass et al. (1971) of low conductivity anisotropic shales. The discs, cut perpendicular to the bedding would, in general, always yield lower values than a computed porous rock conducitivity from randomly oriented chips.

POROUS ROCK CONDUCTIVITY, K_{pr} versus DISC CONDUCTIVITY, K_d

(GEOMETRIC MEAN MODEL)

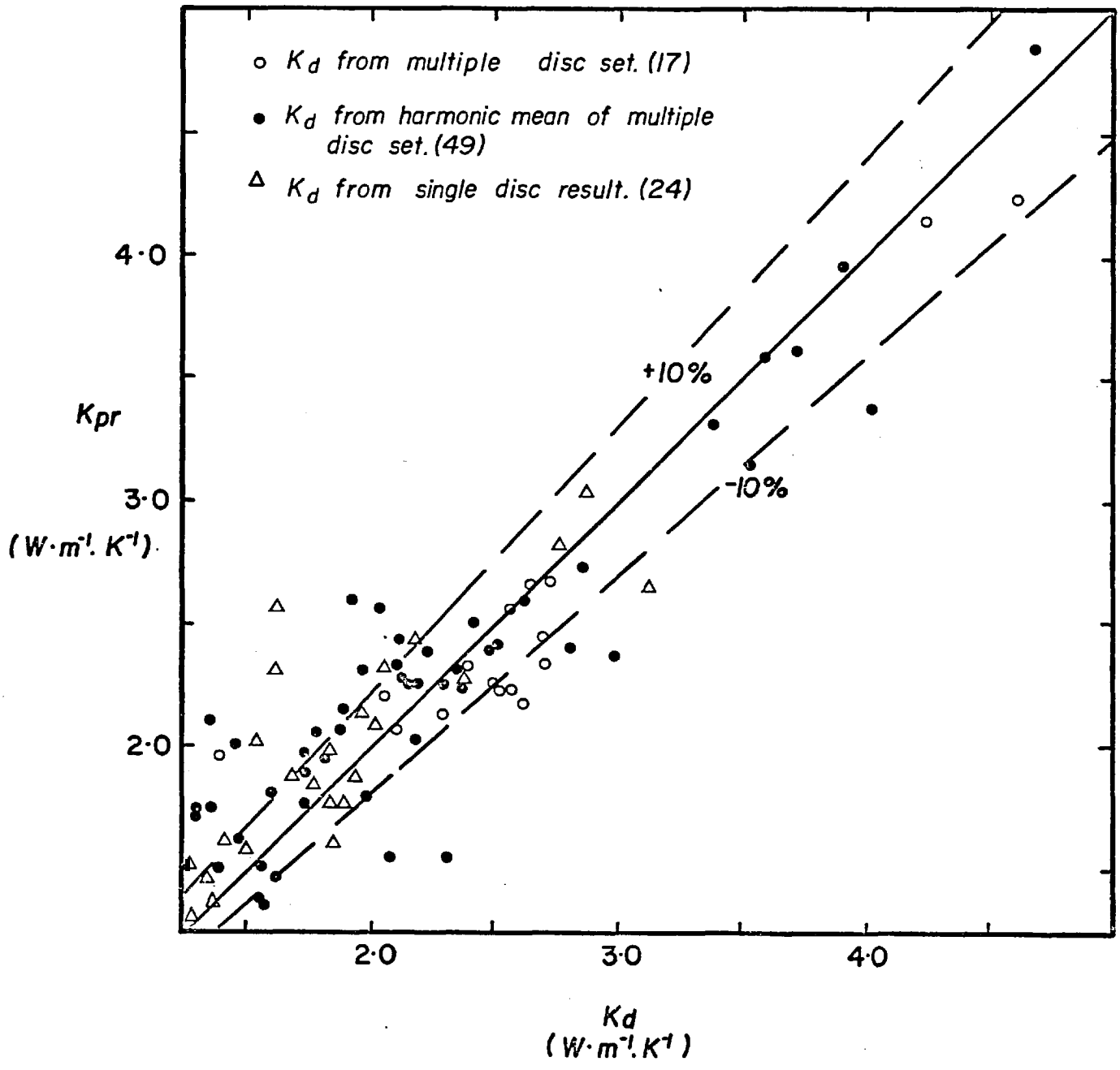


FIG. 2.8

Table 2.6

Comparison of the Geometric Mean

and Maxwell Spheres Models

Model	Mean* of Differences ($W \cdot m^{-1} \cdot K^{-1}$)	Mean* of Absolute Differences ($W \cdot m^{-1} \cdot K^{-1}$)
Geometric Mean	$.01 \pm .10$	$.24 \pm .04$
Maxwell Spheres	$.03 \pm .11$	$.25 \pm .05$

* See text for definitions

2.10 Porosity Determinations from Commercial Well Logs

The determination of porosity from well logs is a vast subject and cannot be adequately dealt with in the short space available here. The interested reader is referred to Pirson (1963), Schlumberger (1972), and Campbell (1973) for fuller general discussions.

Porosity values were determined from six different types of logs in this study. They were the microlog (ML) microlaterolog (MLL), sonic log (CSL), thermal neutron log (GNT), epithermal neutron log (SNP), and the density log (CDL). In general, only two or three of these logs would be available for any one well.

The determination of porosity from the microresistivity logs, ML and MLL, is based on experimental results indicating that the resistivity of a 'clean' formation, that is one containing little or no clay, is proportional to the resistivity of the brine with which it is fully saturated. The constant of proportionality is referred to as the formation factor, F. Thus where R_o is the formation resistivity and R_w that of the brine,

$$F = R_o/R_w \tag{2.24}$$

The ML tool itself consists of three small electrodes spaced 25 mm. apart which are inserted into the face of a rubber pad which in turn is held against the well face by means of an arm and springs. Two resistivity readings are made, one of relatively shallow penetration ($R_{1\times1}$), and another of greater depth (R_2). The $R_{1\times1}$ value is significantly lowered by the presence of a mud cake, the residue left on the well face after mud filtrate enters a porous zone, while the R_2 value responds to the higher resistivity of the invaded zone, the area which mud filtrate permeates. A positive separation of R_2 from $R_{1\times1}$ is thus a qualitative indication of porosity and may be quantified by the following procedure. The $R_{1\times1}$ and R_2 values are first divided by the resistivity of the mudcake, R_{mc}. The R_{mc} value was typically available from

log headings although occasionally it had to be estimated from type curves where the drilling mud resistivity, R_m, formation temperature, and mud weight were known. The chart, Fig. 2.9, was used to estimate the ratio R_{xo}/R_{mc} where R_{xo} is the resistivity of the flushed zone. The ratio, R_{xo}/R_{mc}, was then multiplied by R_{mc} and the value of R_{xo} determined divided by R_{mf}, the resistivity of the mud filtrate, that fluid entering the flushed zone. Again, as in the case of R_{mc}, R_{mf} was typically available from log headings although occasionally it was obtained from type curves in a manner similar to R_{mc}. Both R_{mc} and R_{mf} are temperature dependent and were adjusted to their in-situ values.

The value of F, the formation factor in (2.24) is then computed from the R_{xo}/R_{mf} ratio by the formula,

$$F = R_{xo}/R_w = (R_{xo}/R_{mf}) \cdot (1-RHS) \tag{2.25}$$

where RHS is the residual hydrocarbon saturation factor. Archie (1942) proposed the empirical relation,

$$F = a/\phi_n^m \tag{2.26}$$

where m is the cementation factor, a is a constant, and ϕ_n is the porosity. Satisfactory results have been obtained from

$$F = .81/\phi_n^2 \quad \text{(sands)} \tag{2.27}$$

and

$$F = 1.0/\phi_n^2 \quad \text{(compacted sediments)} \tag{2.28}$$

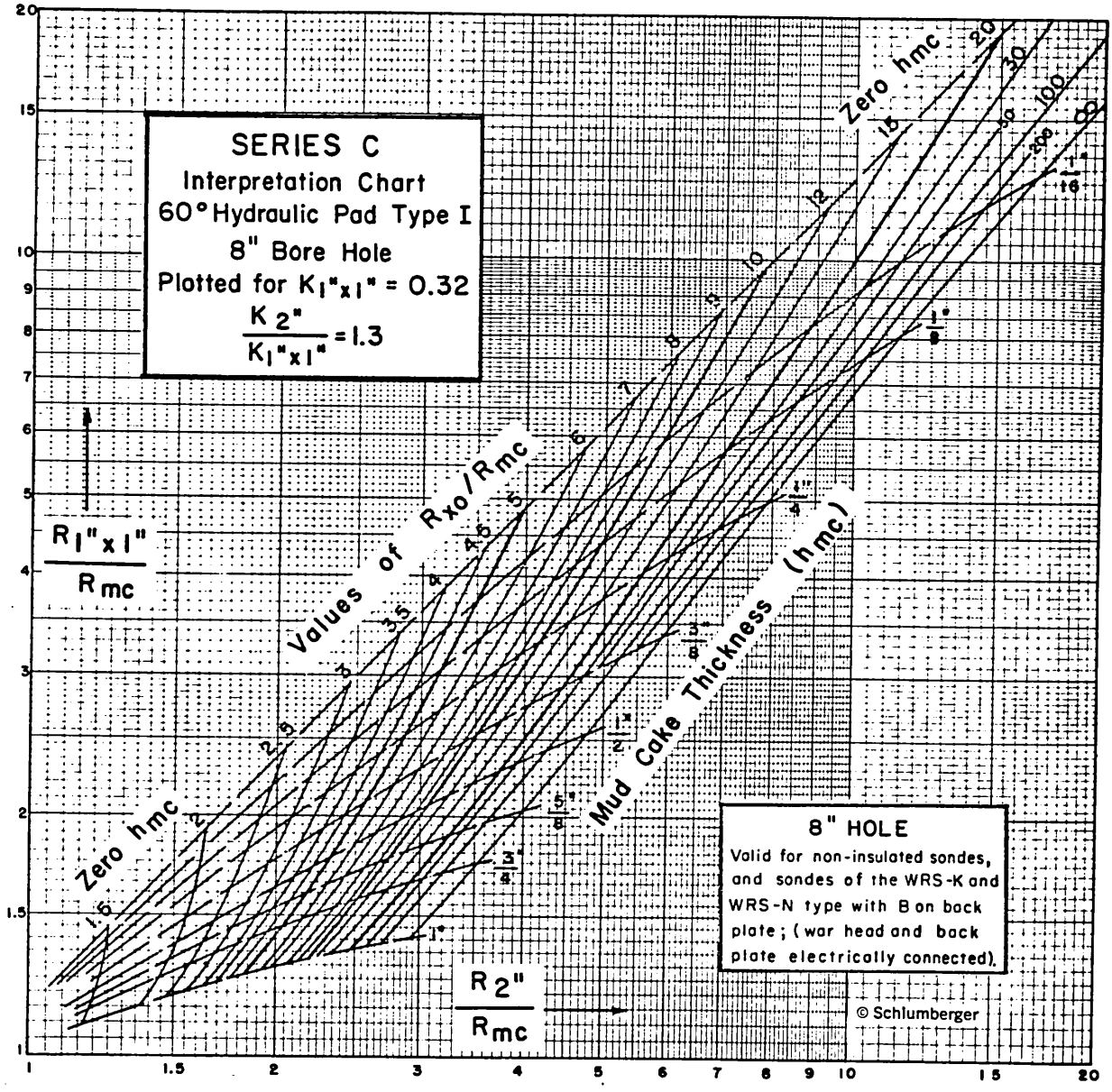
These results differ little over normal ranges of application from the so called 'Humble' formula,

$$F = .62/\phi_n^{2.15} \tag{2.29}$$

which was used for all determinations of porosity from MLs and MLLs in this study.

The MLL, while operating on the basic principle of the ML, has a different electrode configuration resulting in more current passing into

MICROLOG INTERPRETATION CHART



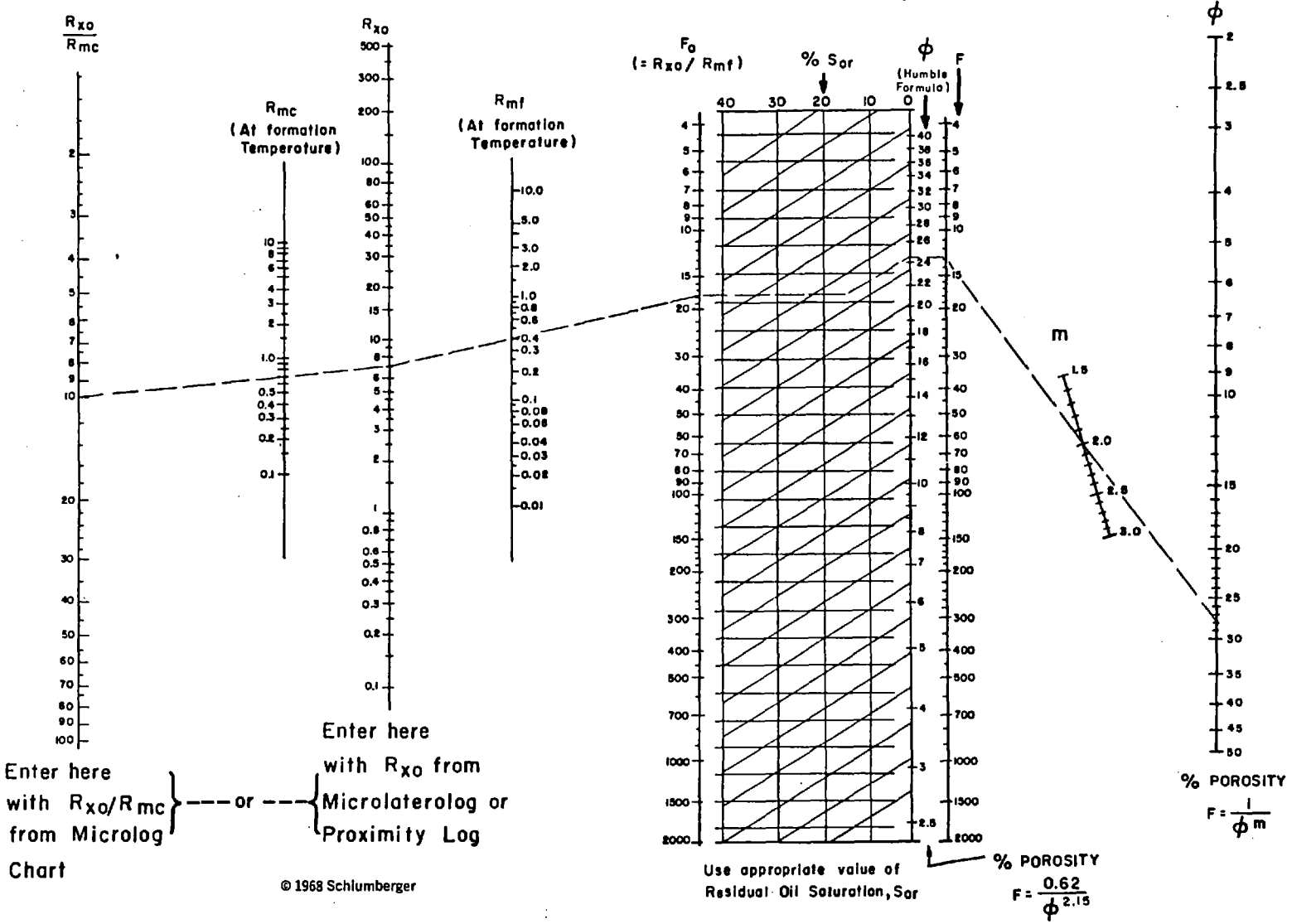
For hole sizes other than 8", multiply $R_{1"x1"}/R_{mc}$ by the following factors before entering the chart:

1.15 for 4¾-inch hole, 1.05 for 6-inch hole, 0.93 for 10-inch hole.

NOTE: An incorrect R_{mc} will displace the points in the chart along a 45° line. In certain cases this can be recognized when the mud cake thickness is different from direct measurement by the microcaliper. To correct, move the plotted point at 45° to intersect the known h_{mc}. For this new point read R_{xo}/R_{mc} from the chart and $R_{2"}/R_{mc}$ from the bottom scale of the chart. R_{xo}/R_{mc} times R_{mc} equals R_{xo}.

FIG. 2.9

POROSITY AND FORMATION FACTOR NOMOGRAM (CLEAN FORMATIONS)



© 1968 Schlumberger

FIG.2.10

the formation. This in turn results in a more accurate determination of R_{xo} which may be obtained directly from the log reading.

Fig. 2.10 is a nomogram illustrating the procedure to obtain porosity values from the micro-resistivity tools. Doll (1950) and Doll (1953) are the papers for reference for the ML and MLL respectively.

The sonic log (CSL) is a continuous recording of the time, Δt_{log}, required for a compressional wave to traverse one foot (.3048 metres) of formation, where Δt_{log} is referred to as the interval transit time.

The tool consists of one sonic transmitter located above two pairs of sonic receivers. The logging operation consists of pulsing the transmitter and recording arrivals on alternate pairs of receivers with results being automatically averaged.

Where the lithology is known the sonic log may be used to compute porosity. Wyllie et al. (1956) and Wyllie et al. (1958) have determined that given certain favorable conditions (a clean formation, uniformly distributed porosity) there exists a relation,

$$\phi_n = \frac{\Delta t_{log} - \Delta t_{ma}}{\Delta t_f - \Delta t_{ma}} \qquad (2.30)$$

where Δt_{ma} is the transit time of the rock matrix and Δt_f is the interstitial fluid transit time. Table 2.7, column two, gives values of Δt_{ma} commonly used for different lithologies; a Δt_f value of 189 μsec/ft. (Schlumberger, 1972) was used throughout. Equation (2.30) was used in conjunction with table 2.7 to compute ϕ_n's from sonic logs in this study. Further discussion of the sonic log may be found in Tixier et al. (1960) and Kokesh et al. (1965).

Neutron logging tools continuously emit high energy neutrons which collide with the nuclei of the adjacent formation and lose energy. The maximum loss per collision arises when the neutron strikes a nucleus most nearly equal to its own mass - the hydrogen atom. When the neutron has

sufficiently decreased in energy, to a level of about .025 eV, it is captured by a nucleus such as that of chlorine, hydrogen, silicon, etc. The capturing nucleus in turn emits a high energy gamma ray which is counted by a detector in the logging tool. Some neutron logging devices also measure the 'thermal neutrons'; those which have been sufficiently slowed so that they lose no further energy but have yet to be captured.

Clearly where the hydrogen concentration is large the neutrons will travel only a short distance into the formation and vice versa. The spacing of the detector and source is such that the count rate varies inversely with the hydrogen concentration.

The various types of neutron tools are laboratory and field calibrated against rocks of very accurately determined porosity. In general, the following relation holds for thermal (GNT) neutron tools,

$$ND = A - B \cdot \log \eta_n \tag{2.31}$$

where A and B are constants, determined by the calibration, and ND is the neutron log reading.

The newer epithermal (SNP) sidewall neutron tool is recorded such that porosity is displayed directly on the log, calibration and borehole corrections being automatically applied. However a correction for lithology is required.

Fig. 2.11 is an example departure curve for porosity determination from a GNT type log while Fig. 2.12 is a lithology correction chart for a SNP log. Several different charts were, in fact, used in this study for neutron prosity determinations as neutron source, detector spacing and counting units varied from log to log. The SNP log is discussed in Tittman et al. (1966).

The formation density log (CDL) is also a radioactive tool emitting medium-energy gamma rays into the formation. The gamma rays collide with

NEUTRON DEPARTURE CURVES
GNT F, G, or H

Pu-Be or Am-Be Source, 19½" Spacing

FRESH MUD, UNCASED HOLES, LIMESTONE

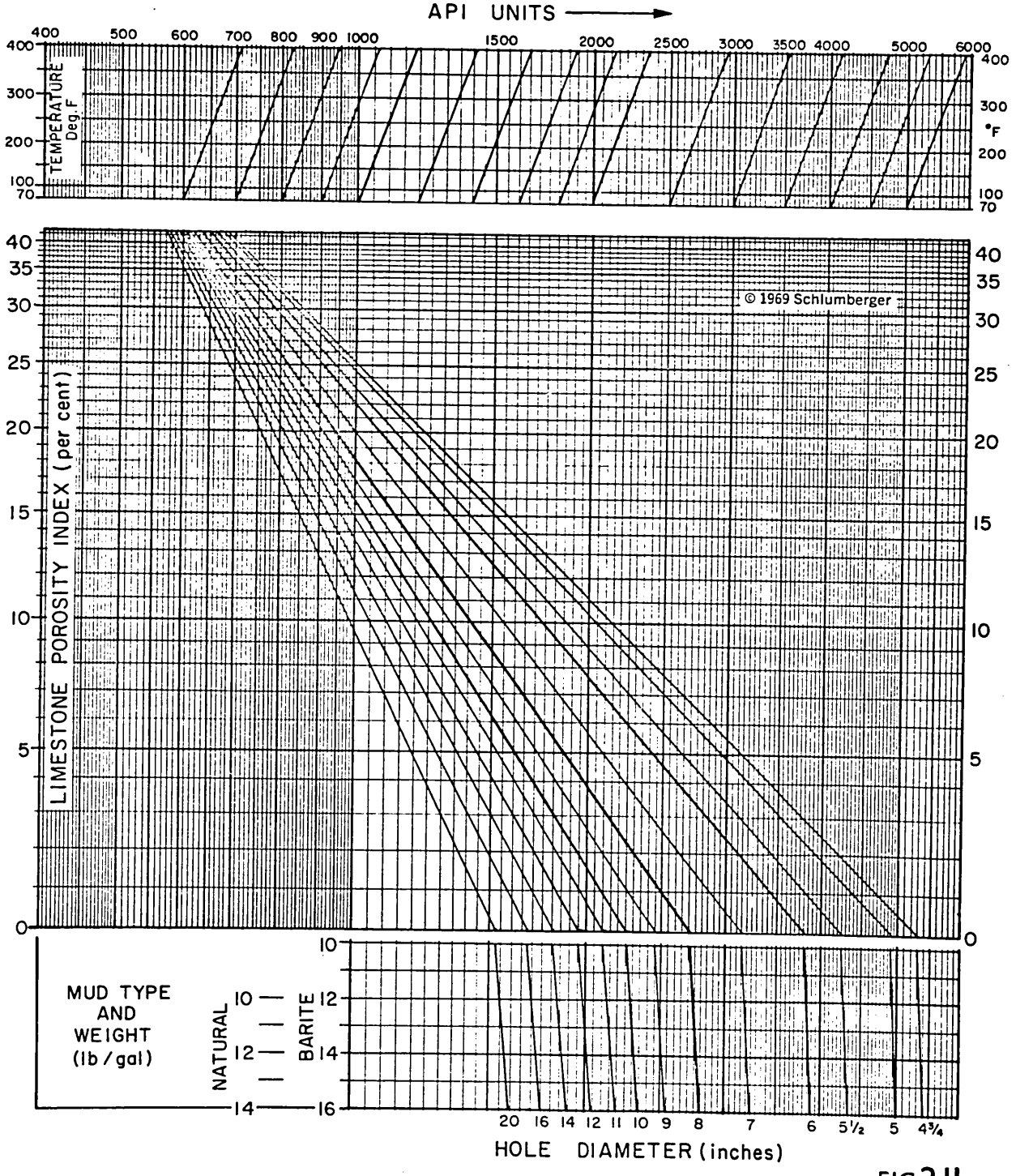
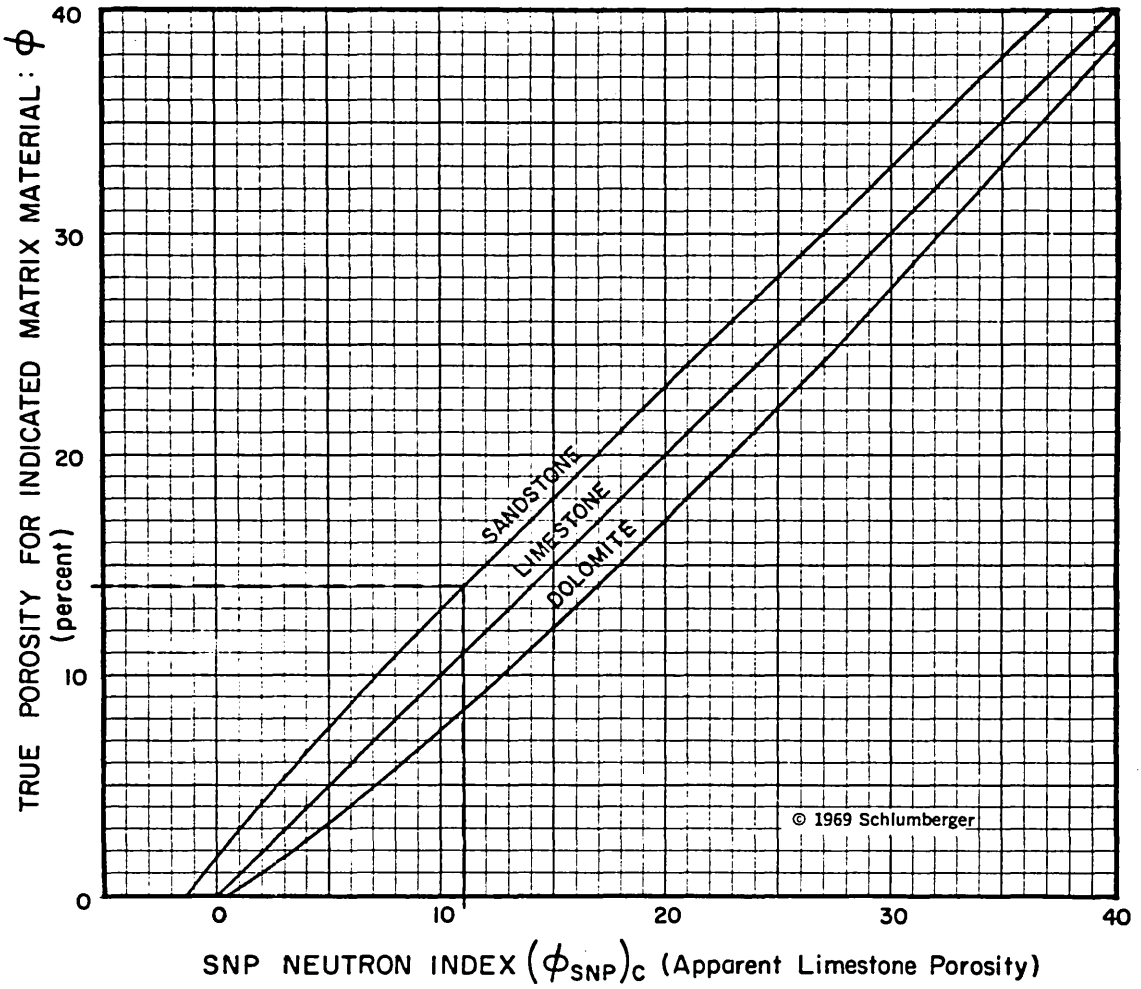


FIG.2.11

NEUTRON POROSITY EQUIVALENCE CURVES

SIDEWALL NEUTRON POROSITY LOG (SNP)

MAY ALSO BE USED FOR GNT NEUTRON LOGS



When the SNP is recorded in limestone porosity units, the above chart is used to find true porosities in sandstones or dolomites. First, correct the SNP for mud cake thickness using the small chart below. For mud cake thickness value use the full hole-diameter reduction shown on SNP caliper (since the backup shoe usually cuts through the mud cake). Then the corrected porosity value is entered on the abscissa of the chart above and carried to the appropriate matrix line. Read ordinate for true porosity. The chart can also be used to find limestone porosity (needed for entering Charts CP-1 and CP-2) if recording is in sandstone or dolomite porosity units. Always correct for mud cake *before* entering equivalence chart.

EXAMPLE: SANDSTONE BED: The SNP reads 13 porosity units (limestone). Bit size is 7⅞. Caliper reads 7⅝", so h_{mc} = ¼ inch. Corrected limestone porosity is 11%. Sandstone porosity equals 14%.

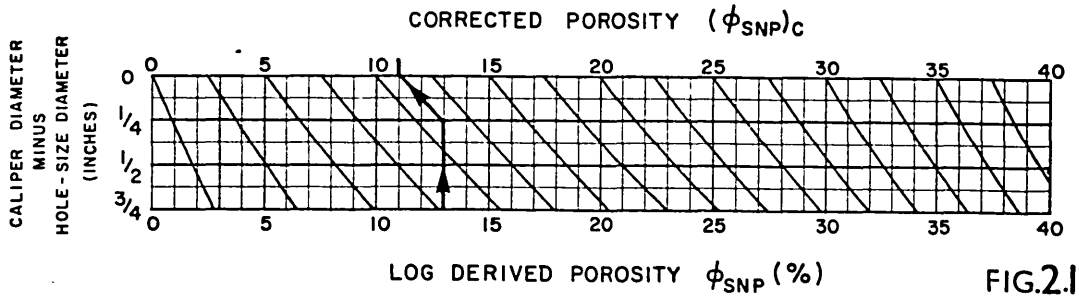


FIG.2.12

formation electrons, losing energy, the interaction being referred to as Compton-scattering. The scattered gamma rays are counted at the detector, the total response being essentially a measure of the electron density of the formation. Electron density is related to bulk density, ρ_b, which in turn depends on the rock matrix density, ρ_{ma}, the porosity and the density of the interstitial fluids, ρ_f.

The log value of density is practically identical with true bulk density (Schlumberger, 1972) with all borehole corrections being automatically compensated for. The porosity, ϕ_n, is thus determined by the relation,

$$\phi_n = \frac{\rho_{ma} - \rho_b}{\rho_{ma} - \rho_f} \tag{2.32}$$

Schlumberger (1972) gives values of ρ_{ma} and ρ_f for different lithologies and interstitial fluids. However, in this study the matrix density was determined from the weight differences made during the water saturation and conductivity measurement of the chips (section 2.9). Clearly,

$$\rho_{ma} = (WD - WC) / (V - WW + WD) \tag{2.33}$$

where WD, WW, and WC are the weights of the cell; filled with dry sample, saturated sample and empty respectively and V is the cell volume. A fuller discussion of the CDL is given by Tittman and Wahl (1965).

Table 2.7

Sonic Log Parameter, Δt_{ma}, for Various Lithologies

Lithology	Range Δt_{ma} (μsec./ft.)	Δt_{ma} used (μsec./ft.)
sandstone	51–55.5	51.0 consolidated 55.5 semiconsolidated
limestone	43.5–47.6	47.5
dolomite	43.5	43.5
anhydrite	50.0	50.0
halite	66.0–68.0	67.0
shale	variable	92.0*
marl	no standard	71.5 (chalk + shale)
sandy shale	no standard	74.0 (sand + shale)
limey shale	no standard	71.5 (as marl)
evaporitic shale	no standard	71.0 (anhydrite + shale)
chalk	no standard	51.0 (low limestone)
marly sand	no standard	66.0 (chalk + shale + sand)

* From Schlumberger Synergetic logs (North Sea)

2.11 Comparison of Porosity Determinations from Various Logs

Each of the six porosity logs discussed in section 2.10 has limitations, the most common of which is uncertain applicability in shaly formations. In general only neutron or density log determined porosities are reliable in formations where there is a significant clay content. Table 2.8, after Campbell (1973), summarizes the porosity log limitations.

The six porosity logs were evaluated by an analogous method to that employed in section 2.9 to determine the preferred method of computing porous rock conductivities. Using the geometric mean model, porous rock conductivities were calculated from individual log porosities and compared to the equivalent disc conductivity. The same criterion for computing K_d as was given in section 2.9 was applied. Table 2.9 gives the results for each of the six logs for both mean of differences and mean of absolute differences as previously defined.

With the possible exception of SNP, no single log is demonstrably better or worse than any other in terms of comparable disc-porous chip conductivities from log derived porosities. Relatively small, less than ten percent, average differences were observed.

Graphs of porous rock versus disc conductivity for those logs (GNT and MLL) having the largest comparison sample sets are given in Figs. 2.13a and 2.13b, the K_d coding convention being the same as that for Fig. 2.8, section 2.9.

The calculation of a porous rock conductivity, for the computing of a heat flow value, where more than one log porosity was available, was by using an arithmetic average of those porosities. This procedure was followed for two reasons; no single log was obviously better for the purpose at hand than any other log, and secondly the mean of absolute differences, as defined in section 2.9, was, for the $K_{pr} - K_d$ comparison discussed above, found to show a modest decrease where the porous rock conductivity was computed

POROUS ROCK CONDUCTIVITY, K_{pr}
versus
DISC CONDUCTIVITY, K_d

NEUTRON LOG POROSITY CORRECTED ONLY
(GEOMETRIC MEAN MODEL)

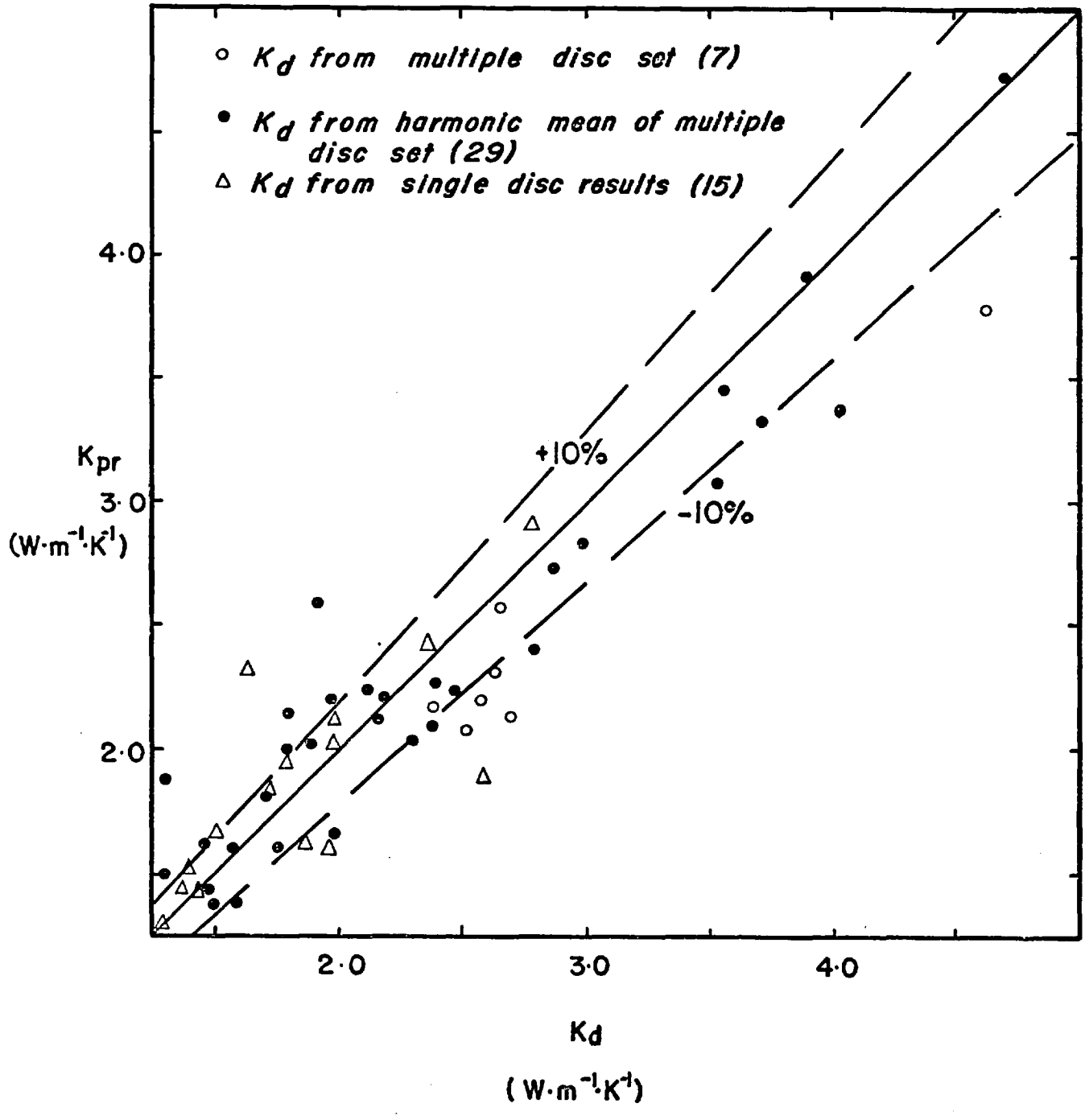


FIG. 2.13a

POROUS ROCK CONDUCTIVITY, K_{pr} versus DISC CONDUCTIVITY, K_d

MICROLATEROLOG POROSITY CORRECTED ONLY (GEOMETRIC MEAN MODEL)

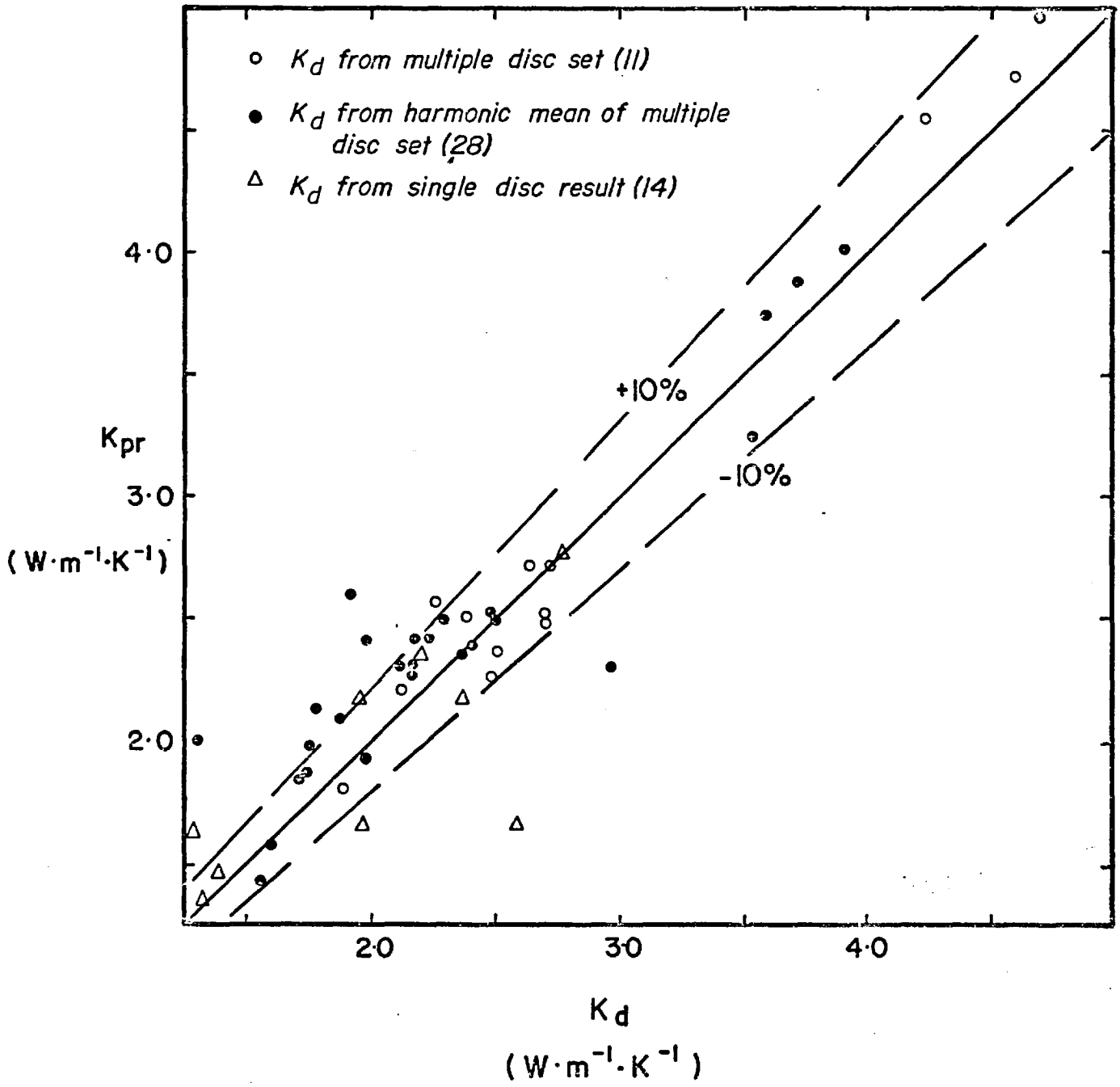


FIG 2.13 b

from an average of an increasing number of log derived porosities (see table 2.10).

Values of K_{pr} plotted on Fig. 2.8 were, in fact, determined from porosities averaged from all available logs.

Table 2.8

Porosity Determination Methods

Log	Log Response Equation	Optimum ϕ_n range	Optimum Formation Type	Other Variables
Sonic	$t = t_m + B\phi_n$	10 - 20%	consolidated	lithology, pore size distribution
GNT (Neutron)	$ND = C + D\log\phi_n$	1 - 10%	nonshaly	hole size, gas
SNP (Neutron)	$\phi_n = \phi SNP$	30%	nonshaly	hole size, gas
Density	$\phi_n = \frac{P_g - P_b}{P_g - P_f}$	20 - 40%	unconsolidated	grain density, borehole condition
ML, MLL (resistivity)	$F = a/\phi_n^m$	20 - 30%	nonshaly	shaliness, temperature

Table 2.9

Comparison of K_{pr} and K_d Where α_n Determined from Various Porosity Logs (Geometric Mean Model)

$W \cdot m^{-1} \cdot K^{-1}$

Porosity Log	Mean of Differences	Mean of Absolute Differences	Number of Comparisons
Sonic	$0.00 \pm .13$	$0.27 \pm .05$	28
GNT (Neutron)	$-0.08 \pm .10$	$0.25 \pm .04$	51
ML	$-0.04 \pm .19$	$0.33 \pm .08$	23
MLL	$0.07 \pm .08$	$0.22 \pm .04$	53
SNP (Neutron)	$0.14 \pm .08$	$0.25 \pm .03$	22
Density	$-0.17 \pm .02$	$0.18 \pm .01$	4

Table 2.10

Comparison of K_{pr} and K_d for α_n Computed From an Increasing Number of Logs (Geometric Mean Model)

$W \cdot m^{-1} \cdot K^{-1}$

Number of Logs	Mean of Differences	Mean of Absolute Differences	Number of Comparisons
1 or more	$.01 \pm .10$	$0.24 \pm .04$	90
2 or more	$.01 \pm .08$	$0.21 \pm .03$	68
3 or more	$-.10 \pm .17$	$0.25 \pm .06$	14
4 or more	$-.02 \pm .03$	$0.14 \pm .01$	7
5 or more	.09	.16	2

2.12 Measurement of Soluble Rock Chips

A practical problem encountered in this study involved the measurement of halite cuttings which are, of course, soluble in water. If the halite is measured in a cell (section 2.8) with fresh water, then the computed volume fraction of water, equation (2.19), is, as expected, far too low leading to erroneously low values of K_r in equation (2.20).

The seventy halite chip conductivity measurements made in this study used a saturated salt solution (brine) as the second phase component. The density of this brine was determined by pipetting exactly equal volumes of distilled water (m^{-3} ensity 1.000 $gm.cc^{-1}$) and brine, weighing both, and taking the ratio. The result, based on eight such measurements, was 1.202 $gm.cc^{-1}$ for the brine. The volume fraction of brine, η, is now computed from,

$$\eta = (WW - WD) / (V \cdot \rho_b) \tag{2.34}$$

this equation now replacing (2.19) with WW, WD and V as previously defined and ρ_b the brine density. A similar change is required to equation (2.33) for the calculation of the salt matrix density.

Schlumberger (1972) show that such a brine density at 20°C and atmospheric pressure implies a dissolved concentration of sodium chloride of 250,000 ppm; quite sufficient to prevent any dissolving of the halite chips.

The thermal conductivity of the brine was also measured, simply by filling several cells with the degassed brine. A value of .591 $W \cdot m^{-1} \cdot K^{-1}$ from five measurements was computed, approximately two percent less than that of fresh water at the same (24°C) temperature. This result is virtually identical with that obtained for a similar brine by Jamieson and Tudhope (1970). The value of brine conductivity replaces K_r in equation (2.20) for the computation of K_r.

As a final check, five nonsoluble samples with conductivities comparable to that of halite were measured both with brine and water. The results, table 2.11, suggest that little additional error is introduced into the conductivity computation by the use of brine as the second phase component in cell measurements.

Table 2.11

Nonporous Chip Measurements of Thermal Conductivity

A comparison of brine and water as second phase components with nonsoluble chips.

$W \cdot m^{-1} \cdot K^{-1}$

Sample	K_r (brine)	K_r (water)	% Diff.
1. WL2 - 005	5.14	5.97	-13.9
2. DD_1 - 001	3.58	3.70	- 3.2
3. DD_1 - 023	6.36	6.41	- 0.8
4. DD_1 - 024	4.60	4.50	2.2
5. DD_1 - 026	4.81	4.77	0.8

2.13 The Repeatibility of Disc and Chip Conductivity Measurements

An obvious criterion to be satisfied in any measurement of a physical quantity is that of repeatibility. Where good repeatibility is observed one may, with confidence, attach significance to comparisons made with other workers' results.

In order to investigate the repeatibility of the divided bar apparatus used in this study, seventy-six chips and sixty disc samples were remeasured. The results are graphed in Fig. 2.14 as histograms of frequency versus percentage difference of observed conductivity for both chips and discs.

The results indicate that there was little systematic bias in the second set of measurements, ie. approximate normal distributions with near zero means, and that individual disc determinations are about a factor of three more reliable than those of chips as evidenced by their respective standard deviations of 2.1 and 5.8 percent (table 2.12). Such a difference in repeatibility is not unexpected given the more complex measuring procedure of chips and the obvious fact that it is impossible to remeasure precisely the same chip sample.

These results will be dealt with in conjunction with estimates of error in measurement in section 2.15.

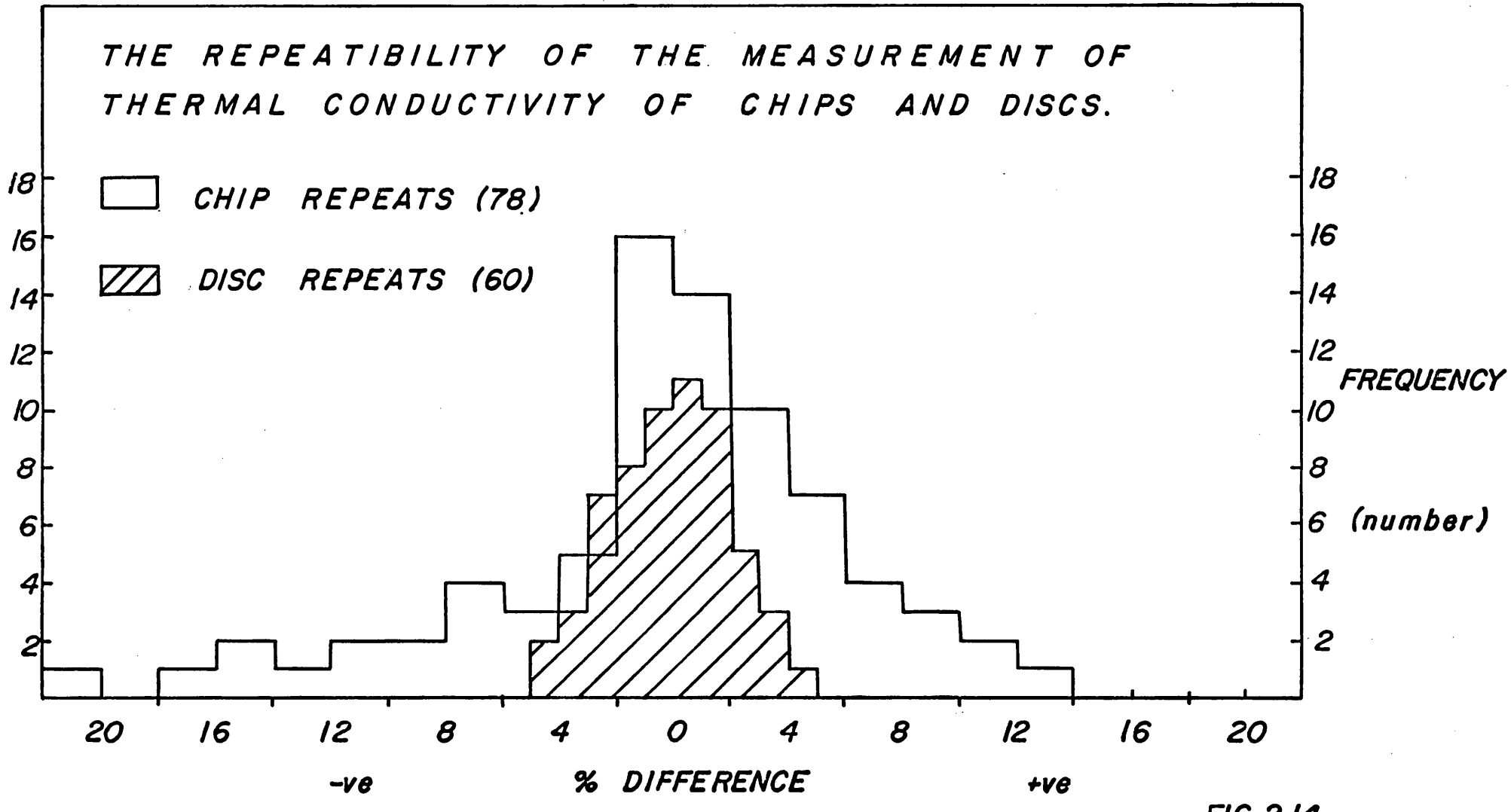

THE REPEATIBILITY OF THE MEASUREMENT OF
THERMAL CONDUCTIVITY OF CHIPS AND DISCS.
CHIP REPEATS (78)
DISC REPEATS (60)
18
16
14
12
10
8
6
4
2
FREQUENCY
(number)
20
16
12
8
4
0
4
8
12
16
20
-ve
% DIFFERENCE
+ve

FIG.2.14

Table 2.12

Repeatibility of Chip and Disc Measurements

Sample	% Difference	Number of Samples
Discs	$-.1 \pm 2.1$	60
Chips	$-.5 \pm 5.8$	76

2.14 Interlab Checks and Fluid Comparisons

The divided bar is a comparative measuring instrument and as such results from the apparatus used in this study might exhibit very real systematic differences when compared with those of other workers.

Having obtained an estimate of measurement repeatibility in section 2.13, a selection of multiple disc set samples of widely varying composition, thermal resistance and conductivity, was sent to other institutes for comparison. The results, given in table 2.13, indicate very good agreement apart from two comparisons, samples GAR 1020 and T 9348, which were made with the Department of Geology and Mineralogy, University of Oxford (UK). Richardson (1974, pers comm.) has commented that these particular Oxford results will probably have an uncertainty of about ten percent as a result of technical difficulties involving the inconvenient dimensions of the Imperial College discs. This would, perhaps, explain the T 9348 result but the GAR 1020 difference is still too large. GAR 1020 was by far the most porous sample included in the comparison study (about thirty-five percent) and with the Oxford apparatus operating at much higher axial pressures than that of Imperial College the discs may have been significantly compressed, lowering the natural porosity and thus increasing their effective conductivity.

It was felt that these comparisons indicated that the Imperial College divided bar was not introducing any systematic error in relation to other institutes' conductivity measurements. The differences observed are comparable with those obtained by Judge (1971) who conducted a similar survey.

A useful second check of system accuracy as well as the determination of the cell aggregate conductivity, K_a (section 2.8), may be made by the measurement of various fluids. The thermal conductivity of many fluids is known to a precision similar to that of fused and crystalline quartz (cf. Tsederberg, 1965, or Ziebland, 1969).

Three such fluids, water, glycerol ($CH_2OH.CHOH.CH_2OH$), and aniline ($C_6H_5.NH_2$), were measured. No significant difference in thermal conductivity was found between distilled and tap water, both of which were measured; the aniline and glycerol were chemically pure. The water was degassed prior to measurement in the cells; this was not possible with the glycerol and aniline for technical reasons.

The computed fluid conductivities, table 2.14, further suggest that the divided bar is relatively well calibrated and that the constants in the determination of the cell aggregate conductivity, equation (2.14) - (2.17), are reasonably correct.

We will return to these results in section 2.15 in connection with a small, about two percent, correction factor applied to the fluid conductivities in table 2.14.

Table 2.13

Interlab Conductivity Checks

$W \cdot m^{-1} \cdot K^{-1}$

Sample	Material/ Rock	USGS	Oxford	Dominion Obs.	SMU	Imperial College
Lexan	plastic	.222(5)	.224(2)	.212(6)	-	.218(25)
GAR 1020	marl	-	2.22*	-	1.81*	1.66*
WM1-006	siltstone	-	2.68*	-	2.70*	2.57*
T 9348	sandstone	-	3.43*	-	4.36*	3.83*
MAN-9332-A	shale	-	-	-	1.80(2)	1.75
MAN-9332-B	shale	-	-	-	1.86(2)	1.82
MAN-9332-C	shale	-	-	-	1.78	1.77
MAN-9332	shale	-	-	-	1.85*	1.79*
AS1-001-A	limestone	-	-	-	3.55(2)	3.58
AS1-001-B	limestone	-	-	-	3.62(2)	3.56
AS1-001-C	limestone	-	-	-	3.47	3.52
AS1-001-D	limestone	-	-	-	3.38	3.42
AS1-001	limestone	-	-	-	3.67*	3.64*
DR1-019-A	sandstone	-	-	-	6.11(4)	6.03
DR1-019-B	sandstone	-	-	-	6.00(4)	5.86
DR1-019-C	sandstone	-	-	-	5.52	5.76
DR1-019	sandstone	-	-	-	6.47*	6.11*

values in brackets are number of measurements

* Whole set determination

Comparison data supplied by:

USGS - Dr. R. Munroe, Menlo Park, Calif.

Oxford - Dr. S. Richardson, Oxford, UK.

Dominion Observatory - Dr. A. Jessop, Ottawa, Canada.

Southern Methodist U. - Dr. P. Morgan, Dallas, Texas.

Table 2.14

Thermal Conductivity of Fluids (24°C)

$W \cdot m^{-1} \cdot K^{-1}$

Reference	Water	Glycerol	Analine
This study*	.612 ± .010(40)	.302(4)	.194(3)
Schneider (1973)	.603	.285	-
Weast & Selby (1968)	.597	.294	.177*
Clark (1966)	.605	-	-
Powell (1958)	.608	-	-
Lawson et al. (1958)	.604	-	-

* Values in brackets are number of measurements

* A single determination at 16°C

2.15 Errors in the Determination of Thermal Conductivity - an Assessment

Obviously disc and chip measurements must be considered separately in estimating reasonable limits of error in the determination of their thermal conductivities (see section 2.13).

In the case of discs the estimation of error is quite straightforward, the uncertainty being composed of two principal parts. The first is that contributed by error in the bar calibration, which, from section 2.4, is of the order of two percent. This value has been arrived at as the inferred fused and crystalline quartz conductivities, table 2.3, differ by approximately this amount from those determined by other workers, table 2.2. In addition, the three fused quartz calibration sets, columns one, two and three, table 2.3, exhibited a range of inferred conductivities of two percent indicating real variations in supposed 'standard' material. No such variations were observed for the different crystalline quartz sets.

The second factor influencing accuracy in disc measurements is the random element observed in variations of repeated measurements, section 2.13. This incorporates a variety of sources of error including; variations in degree of water saturation, variations in bar environment, changes in contact resistance, and measurement errors. Repeated disc measurements indicate that, at the one standard deviation level, the random error is of the order of two percent (section 2.13, Fig. 2.14).

Equation (2.7) indicates a direct correspondence of error in bar calibration carrying over into disc measurement. Thus a simple sum of the two sources of error, in this instance four percent, is a reasonable estimate of the error in the determination of thermal conductivity of a single measurement on a single disc. Obviously this could be improved on, by remeasuring a single disc or making a multiple set measurement, reducing the error, in the limit, to the calibration uncertainty.

The error associated with a cell measurement is much less straight-

forward. Considering first those of a systematic nature, a two percent error in bar calibration will not, as with a disc, result in a two percent error in nonporous rock conductivity as a nonlinear equation (2.20), is involved. If we simplify the exact treatment of the calculation of the aggregate conductivity, K_a, in equations (2.14) - (2.17), and ignore the very small terms involving the conductivity of copper, K_c, we obtain (Sass et al., 1971),

$$(2.35) \qquad K_a = \frac{D_o^2 \cdot K_s}{d^2} - \frac{D_o^2 - d^2}{d^2} \cdot K_p$$

where D_o, d, K_a, K_s and K_p are as previously defined in section 2.8. Clearly if D_o, d, and K_p have no error then K_s, the apparent cell conductivity, which is determined in a linear manner from the bar calibration, equation (2.15), will be about two percent in error as will K_a, the K_p term being much smaller than the K_s term (2.35). It is emphasized that the error in bar calibration is the only uncertainty considered for the moment.

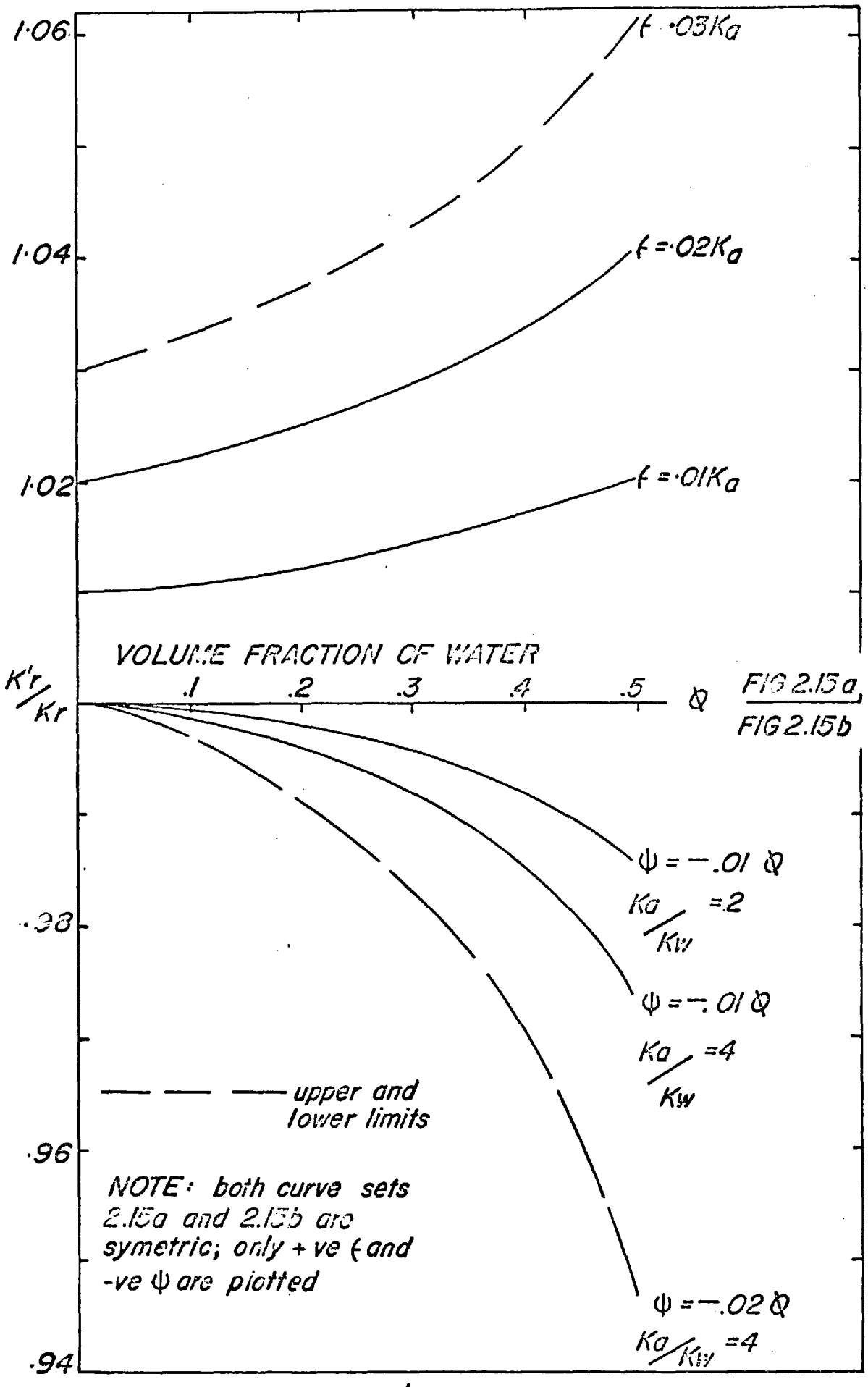
We may now alter equation (2.20) to,

$$(2.36) \qquad K_r' = e^{\left[\log (K_a \pm \epsilon / K_w^{\eta}) \,/\, 1 - \eta\right]}$$

where ϵ is the fractional error in K_a and remaining terms are as previously defined, section 2.9. Equation (2.36) indicates that a nonlinear error results in K_r from a given fractional error in aggregate conductivity. A trivial transformation leads to,

$$(2.37) \qquad K'_r/K_r = \left[\frac{K_a \pm \epsilon}{K_a}\right]^{1/1 - \eta}$$

which has been plotted, Fig. 2.15a, as K'_r/K_r versus η for reasonable values of ϵ expressed as a fraction of K_a. In general the volume fraction of water, η, varied from .3 to .4 for most measurements so that K_r was about three percent in error due to the bar calibration uncertainty alone.



FRACTIONAL ERROR($\frac{K'r}{Kr}$) IN NONPOROUS CONDUCTIVITY

FIG 2.15(a) from fractional error(f) in bar calibration

FIG 2.15(b) from fractional error(ψ) in volume fraction of water

Uncertainties in the conductivity terms K_w, K_p and K_c (section 2.8 - 2.9) are thought unlikely to contribute more than a further two percent error to the nonporous rock conductivity, K_r. The copper conductivity, K_c, terms in equation (2.17) are virtually negligible and were added only for completeness. The water conductivity term, K_w, is probably no more than one percent in error (section 2.14, table 2.14) which would change K_r in equation (2.20) by about .5% for a typical, .35, volume fraction of water. The plastic conductivity term, K_p, is only of the order of five to ten percent of K_a, equation (2.35), so that an error in K_p of four percent will only alter K_a by .4 percent at most. The plastic conductivity has been determined by several measurements on single discs of the same material hence the error quoted above. For typical values of η this additional error in K_a leads to a further .6% error in K_r.

The volume fraction of water, η, was probably in error by less than one percent as the cell dimensions and weights were very accurately determined (sections 2.8 - 2.9). In a manner similar to the derivation of (2.36) and (2.37) from equation (2.20) we may write,

$$\frac{K'_r}{K_r} = \frac{(K_a/K_w^{\eta \pm \psi})^{1/(1 - \eta \pm \psi)}}{(K_a/K_w^{\eta})^{1/(1 - \eta)}} \tag{2.38}$$

where ψ is the fractional error in η and K_r, K_a and K_w are as previously defined. Where only error in the volume fraction of water is considered the K'_r/K_r ratio of error term depends on the K_a/K_w ratio as one would intuitively expect. Fig. 2.15b graphically illustrates the error for reasonable η, ψ, and K_a/K_w; a one percent error in η results in about a 1.5 percent error in K_r for $.3 < \eta < .4$ and a reasonable K_a/K_w ratio.

It should be pointed out that in order to maintain accurate determinations of the volume fraction of water it was necessary to remeasure the cell dimensions and weights at regular intervals during the study.

Progressive wear due to abrasive minerals (quartz?) typically altered cell dimensions by .4 mm. in the case of plastic dimensions such as d, .02 mm. for copper values such as D_2, and .1 gram for the cell weights (Fig. 2.6 and table 2.4).

Another source of error in cell measurements arises as a result of their deformation due to loading during measurement. It was found necessary to apply a light, about .9 $MN \cdot m^{-2}$, axial pressure to the cells to establish good thermal contact with the bars. However, the plastic walls of the cell were then subject to a mild deformation with the result that the effective cell area changed. In addition, it was observed that a small, typically .1 gram, water loss occurred on compression. It was found that this loss only occurred during the initial part of the loading. The outside diameter of the cell, D_o, was found to have increased by .01 mm. at the end of compression. Thus we might expect the cell thermal resistance, R_c, to change from,

$$R_c = \frac{D_1}{A \cdot K_b} \tag{2.39}$$

to,

$$R_c = \frac{D_1 + dD_1}{(A + dA) \cdot K_b} \tag{2.40}$$

where A is the cell area, D_1 and K_b are as previously defined (sections 2.8 and 2.4 respectively), dD_1 is the change in cell length (negative) while dA is the change in cell area and is positive. The implicit assumption is that the cell must shorten to account for the areal expansion. Further, from first order theory,

$$dA = \frac{-V \cdot dD_1}{D_1^2} \tag{2.41}$$

where V is the cell volume and thus,

$$(2.42) \qquad R_c'/R_c = \frac{D_1 + dD_1}{D_1 - dD_1}$$

Now the previously mentioned cell expansion would correspond to a shortening of about .008 cm. or about one percent of the effective cell thickness. The loss of water was not thought to represent a volume change but rather was due to the lid 'seating' itself as the water was only lost at very low axial pressures. The weight of the saturated cell, WW, equation (2.19) was, therefore, determined after the cell had been removed from the bars. The one percent shortening leads to,

$$(2.43) \qquad R_c'/R_c \simeq 1.02$$

and results in values of the cell aggregate conductivity being two percent high.

In order to investigate the possible manifestation of this effect the forty cell conductivity determinations of water discussed in section 2.14 were recomputed incorporating this correction. The results, table 2.15, support the hypothesis that the cell does deform as predicted. However, despite several attempts to measure the shortening with a suitably precise travelling microscope, no conclusive change in cell length was observed. For this reason no correction was applied to the cell conductivity results presented here, though clearly a small systematic error may thus have been incorporated.

Nonsystematic, or random error, in cell measurements was inferred from scatter in repeated measurements, section 2.13, where a standard deviation of six percent was observed for nonporous rock conductivity. The sources of the random error are thought to be similar to those for discs the error being larger due to the greater number of individual measurements in a single determination.

Table 2.16 summarizes the sources and magnitudes of error in the determination of a value of nonporous rock conductivity from a single measurement. The sum of the individual errors is twelve percent.

The determination of a porous rock conductivity, K_{pr}, equation (2.21), has two principal sources of error; the above mentioned nonporous rock conductivity uncertainty and error in the term η_n, the natural rock porosity. The estimation of an average error in porosity can be little more than an educated guess as each log has its limitations and ranges of applicability.

In a manner similar to the previous error discussion we may modify (2.21) to,

$$K'_{pr}/K_{pr} = K_r^{\gamma} K_w^{-\gamma} \tag{2.44}$$

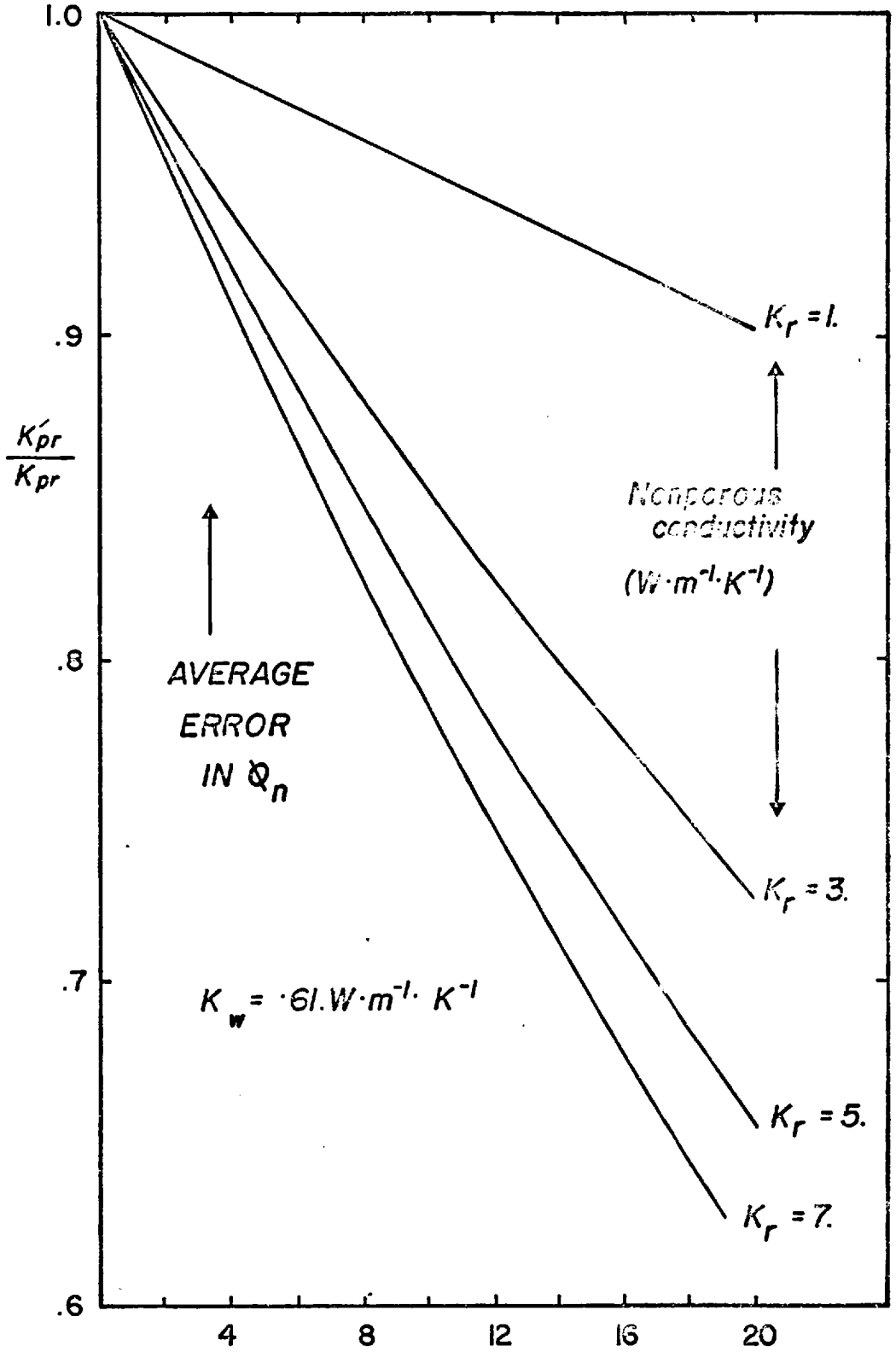
where γ is the absolute error in the fractional natural porosity, η_n. A plot of K'_{pr}/K_{pr} versus γ for reasonable K_r and fixed K_w is given in Fig. 2.15c. An estimation of average absolute error for log derived porosities would be of the order of one to three percent. It is emphasized though, that porosity determinations made where particularly unfavourable hole or formation conditions existed, for example from a sonic log in an unconsolidated sand or from a microlog where the ratio R_{xo}/R_{mc} exceeded fifteen, could result in significantly greater porosity errors, perhaps of the order of five to ten percent absolute. Whenever possible such situations were avoided by using a log or logs unaffected by any existing adverse conditions although this was not always possible. A typical average absolute porosity error of three percent is thus thought to be not unreasonable. Such an error, would for a typical value of $K_r = 3.0\ W \cdot m^{-1} \cdot K^{-1}$, result in an error of about five percent in K_{pr} due to the porosity uncertainty alone.

The estimation of the total error in K_{pr}, considering both error in porosity and nonporous rock conductivity, may be expressed as,

ERROR IN POROUS ROCK CONDUCTIVITY(K_{pr})

versus

ABSOLUTE ERROR IN POROSITY(ϕ_n)



(Take reciprocal of K'_{pr}/K_{pr})
values for negative error in ϕ_n

FIG. 2.15 c

$$(2.45) \qquad \frac{K'_{pr}}{K_{pr}} = \frac{K_w^{\pm\gamma} \cdot (K_r \pm \delta)^{1-\eta\pm\gamma}}{K_r^{1-\eta}}$$

Fig. 2.16 has been constructed from (2.45) where $\delta = .12\ K_r$ and $\gamma = .03$ absolute. Quite obviously where the signs of the errors are the same, there is, depending on the magnitude of K_r and η_n, a partial cancelling out of error in K_{pr} as one would expect. The effect of decreasing error with increasing porosity is due partly to choosing a fixed absolute error in porosity and partly in assuming negligible error in the K_w term (see above discussion). For typical values of K_r, of the order of 2.5 - 3.5 $W \cdot m^{-1} \cdot K^{-1}$, and with porosity in the range ten to thirty percent, the error in porous rock conductivity will typically be about ten percent and will rarely exceed seventeen percent. This is in good agreement with the disc-chip comparison discussed in section 2.9 and illustrated in Fig. 2.8.

ERROR IN POROUS ROCK CONDUCTIVITY AS A FUNCTION OF NONPOROUS (K_r) CONDUCTIVITY AND POROSITY (ϕ_n)

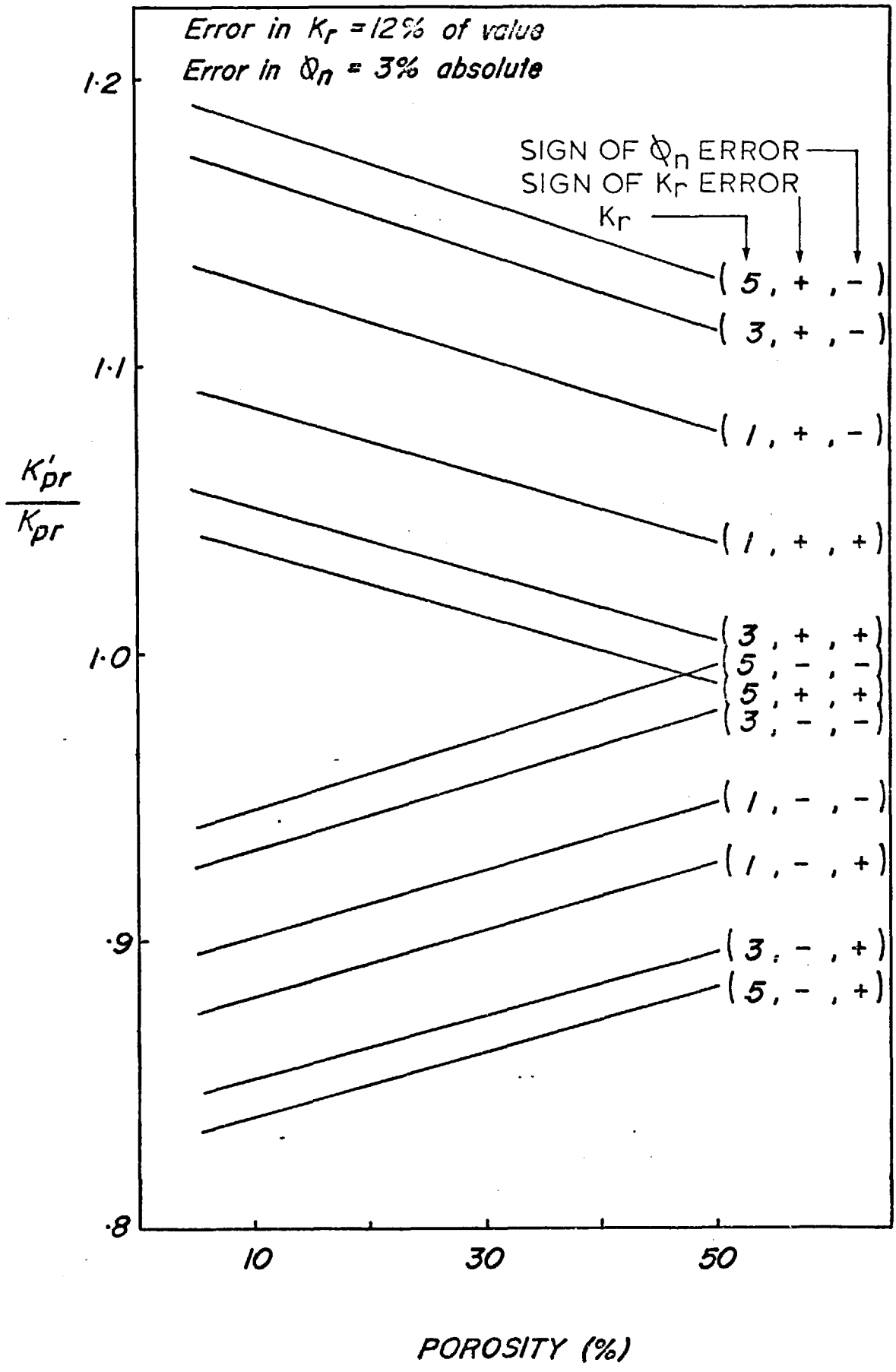


FIG 2.16

Table 2.15

Fluid Conductivities and the Effect of Cell Shortening

$W \cdot m^{-1} \cdot K^{-1}$

Fluid	Uncorrected for cell shortening	Corrected for cell shortening	Average values* for other workers
water	.630 ± .005	.612 ± .101	.603
glycerol	.312	.302	.290
aniline	.199	.194	.177

*see table 2.4

Table 2.16

Summary of Error in Nonporous Rock Conductivity, K_r

Source of error	% error in source	% error in K_r
Bar calibration	2%	3%
K_c	?	negligible
K_w	1%	.5%
K_p	4%	.6%
[illegible]	1%	1.5%
cell deformation	1%	(2%)
repeatibility	6%	6%
Total (omitting ( ) value)		~12%

2.16 Predicting Thermal Conductivities from Other Known Rock Properties

The discussion of sections 2.1 - 2.15 has clearly shown that the measurement of thermal conductivity of large numbers of rock samples is an arduous task particularly where those samples are but rock fragments. Many researchers, Ziefuss and Van der Vliet (1956), Beck and Beck (1958), Diment and Robertson (1963), Anand et al. (1973), to name but a few, have attempted to correlate thermal conductivity with other more readily available physical properties.

In theory the conductivity of porous rocks (those of most interest to this study) could be calculated if size, shape, conductivity, distribution, and cementation of the constituent grains were known - obviously an impractical approach. However, many other physical properties, such as sonic velocity, grain and bulk density and electrical resistivity may be obtained, as was shown in section 2.10, with little effort from conventional well logs.

The most detailed multivariate analysis of the above mentioned type of data is that of Anand et al. (1973) who, on the basis of fifty-two sample sets, proposed empirical relations for dry and saturated rock conductivity. However, when the Anand et al. relations were tested on data from this study their general applicability was found to be rather poor with both dry and porous conductivities being overestimated, typically by twenty to thirty percent.

In another study, that of Zierfuss and Van der Vliet (1956), the authors proposed the following relation,

$$\log (F \cdot K_{pr}) = A + B\phi_n + C\phi_n^2 + D\phi_n^3 \qquad (2.46)$$

where F is the formation resistivity factor, K_{pr} is the porous rock conductivity, ϕ_n is the porosity and A, B, C and D are constants. The constants were determined from multiple nonlinear regression analysis on thirty-eight samples.

Fig. 2.17 is a graph of log ($F \cdot K_{pr}$) versus η_n for ninety-eight samples from this study where F and η_n were determined from microlaterologs, the more reliable of the microresistivity tools. The Zierfuss and Van der Vliet 'sandstone line', which has been included for comparison, shows reasonable qualitative agreement although it is obviously slightly shifted, in a positive sense, on the porosity axis.

Where detailed lithologic logs are available, the method of Joyner (1960) offers an alternative for the estimation of conductivity. The procedure is to first classify various lithologic types into groups such as shales, limestones, calcareous shales, sandy shales, quartzose sandstones, and impure sandstones. A set of 'type samples' is measured for thermal conductivity (Joyner measured but twenty-five samples) and a mean value is assigned to each group. Conductivity values are then assigned directly where the lithologic log description matches that of a group; where a log description is intermediate between the groups, for example a 'slightly sandy shale' then the harmonic mean of the two closest matching groups, in this case sand and shale, is used. In addition Joyner had several further refinements such as using weighted harmonic means where percentages of various interbedded rock types were known. We will return to Joyner's method in connection with estimation of parameters for the calculation of heat flow in Chapter 3.

Judge (1971) has pointed out that where three well logs, such as SNP, CDL and CSL, are available complex combinations of three lithologies may be solved for percentages of constituent rock types. A typical lithologic breakdown, such as percentages of dolomite, limestone and anhydrite, can readily be accomplished by standard cross-plot techniques (Schlumberger, 1972). The implications for use with Joyner's method are obvious.

EXAMPLE OF AN EMPIRICAL CONDUCTIVITY RELATION

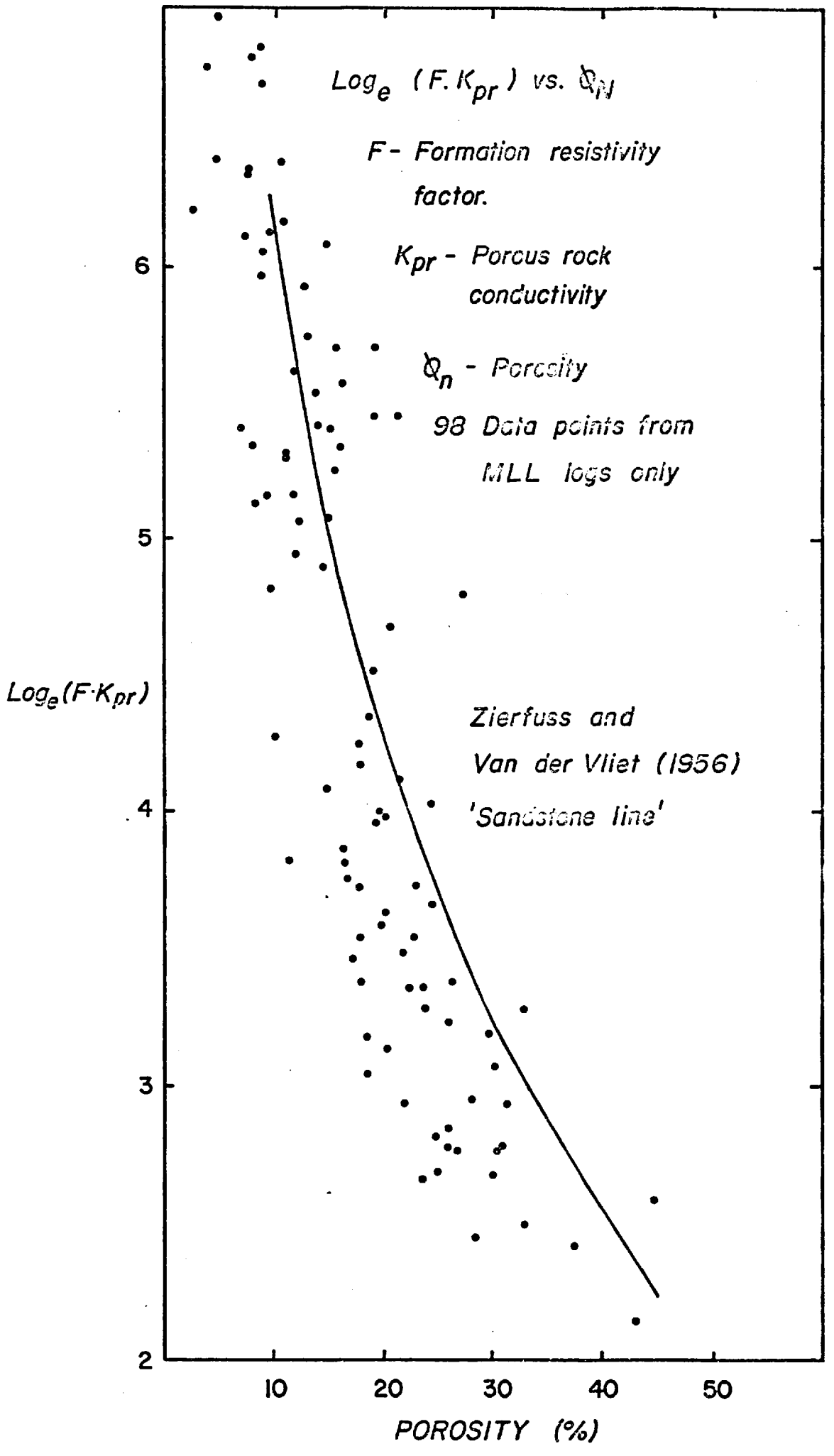


FIG 2.17

2.17 Suggestions for Further Research

The most pressing need, if oil well data is to be used for future heat flow calculations, is to shorten the length of time required for thermal conductivity measurements. The thirteen hundred conductivity determinations in this study required some two years to obtain, prepare, measure and computer process; a clearly disproportionate length of time in a supposed three year study. If heat flow researchers intend to use the vast, virtually unresearched, accumulation of oil exploration well temperature data, then they must concentrate development on a model to predict thermal conductivity from conventional well log parameters and lithologic descriptions. The data presented in this study would provide an excellent starting point for such a study.

One point not dealt with regarding chip or disc measurements was conductivity anisotropy which, for many rocks, is of the order of ten to twenty percent (Kappelmeyer and Haenel, 1974). Obviously the chip measurement gives a result somewhere between the two extreme conductivites; however, direct comparisons of anisotropic discs and chips are few. This is principally due to the difficulty in obtaining a disc parallel to the bedding planes, the source of anisotropy in most rocks. Sass et al. (1971) have found that for very highly anisotropic material the geometric mean model breaks down. There is obviously scope for limited research in this field.

The time of measurement of chips might be considerably reduced if a new transient technique could be developed. Such a technique would, ideally be quicker, more reliable and require a smaller sample than the needle probe method. Recent developments in this direction by Cull (1974) are promising although still in the prototype stage.

In-situ measurements are impractical at this time for two reasons; the current methods have largely been failures (Beck et al., 1971), and there are rarely opportunities to carry out such logging in oil exploration wells. The latter difficulty may be about to be resolved with the advent of

production platforms and static observation wells in the North Sea. A useful line of approach might be to abandon the ubiquitous line source method and develop a downhole conductivity tool similar to the resistivity pad of the microlog. Essentially it would consist of small circular, concentric electrical elements alternating with concentric rings of small time constant thermistors, all of which are held in a soft rubber pad which could be held firmly against the boreface. Measurements could be made relatively quickly, perhaps in ten to twenty seconds, if the heaters were close to the thermistors.

Finally instrumentation in the present divided bar used at Imperial College could be usefully improved on by modifying the thermocouple potential measuring system, Fig. 2.2. This could be accomplished by replacing the vernier potentiometer and galvonometer with a dc null voltmeter (ie. a Hewlett-Packard 419A) and a digital voltmeter (ie. a Hewlett-Packard 3430A). The null voltmeter would be used as an amplifier while the DVM would provide direct readings of the thermocouple potentials. If two null voltmeters were used then the sample and average reference potentials could be fed to separate amplifiers and the DVM used as ratiometer. With suitable scaling and a small offset, disc conductivity values could be displayed directly. This modification would significantly speed measurements although it would not improve either accuracy or repeatibility. The system described is, in fact, in use at Southern Methodist University, Dallas, Texas (Morgan, 1974, pers. comm.).

Chapter 3

The Calculation of and the Corrections Applied to the Heat Flow Values

3.1 Introduction

Heat flow is the product of the geothermal gradient (Chapter 1) and the thermal conductivity (Chapter 2) and has units of energy · length^{-2}. time^{-1}. In common with other geophysical measurements the 'raw' data heat flow value is subject to certain corrections. Local topography, uplift and erosion, downwarp and sedimentation, and past climatic changes may significantly alter the geothermal gradient; thermal conductivity values determined in the laboratory must be corrected for the effects of in-situ temperature and pressure. The basic theory of these corrections together with examples of their application are set out in Jaeger (1965) and Keppelmeyer and Haenel (1974).

Local topography apart, the correction of the geothermal gradient is invariably uncertain as a result of poorly defined parameters such as rates of uplift or sedimentation and times and magnitudes of past climatic variations. Often the uncertainty approaches the size of the correction itself; in many instances the correction does not significantly improve the estimate of error in the heat flow calculation.

Thermal conductivity 'in-situ' conditions corrections are probably less uncertain though far from exact. Where samples are of crystalline structure or are glasses, adequate theory on the temperature dependence of thermal conductivity exists. Porous sedimentary rocks are obviously of an indeterminate intermediate mixture and thus less predictable, in terms of thermal conductivity, at high temperatures.

A common problem encountered in the use of oil exploration well data for the calculation of heat flow is that of incomplete information. This may result from data either still regarded as confidential and unsuitable for release or may simply be that it is no longer available, ie. well samples that have been lost or destroyed. Where temperature data is missing, the hole is obviously of no use; however where samples only are missing, suitable conductivity estimates may be made if a detailed lithologic log is available (Joyner, 1969, Judge, 1971). Such an estimated heat flow value, while obviously less satisfactory than a result calculated from measured conductivities may still be sufficiently accurate to be of some use in a regional study such as this.

3.2 The Calculation of Heat Flow - Methods

There are two basic methods for the calculation of heat flow. That which is more expedient is to divide the borehole into its lithological units, to compute the harmonic mean of the thermal conductivity for each section, and to multiply this by the least squares determined gradient in the respective interval. (cf. Gough, 1963). The result is a mean flux for each section; these values may, in turn, be averaged to produce a single heat flow value for the hole. Arithmetic as opposed to harmonic means may be used in the calculation of the mean lithologic conductivity which usually results in only a slightly higher value (Sass and La Marne, 1963), although much higher results may occasionally arise (Diment and Robertson, 1963). Where detailed temperature logs are available this method will clearly show any variation of heat flow with depth as well as facilitate an estimate of error. However, this criterion is almost never met in oil exploration wells where temperature data are relatively few, irregularly spaced in depth, and only accidently recorded at lithologic boundaries.

In the absence of numerous evenly spaced temperature measurements the second method, the resistance integral procedure of Bullard (1939), is

preferred. The method is based on the linear relation,

$$(3.1) \qquad T(z) = T(o) + q \cdot \sum_i (z_i/K_i)$$

where $T(z)$ is the temperature at depth $z = \sum_i z_i$, $T(o)$ is the temperature where $\sum_i z_i/K_i = o$, q is the heat flow, and K_i is thermal conductivity of the i^{th} homogeneous lithogic unit of thickness z_i. The temperature terms, $T(z)$, are fitted by least squares to the terms $\sum_i (z_i/K_i)$ to determine values of q and $T(o)$.

The choice of the division of the depth units, z_i, and the corresponding conductivities assigned, K_i, are fundamental in determining heat flow from equation (3.1). Obviously it is impractical to measure the conductivity of the entire section, $\sum_i z_i$, which in the case of an oil well might amount to several kilometers of samples. Thus it is necessary to extrapolate measured conductivity results. The following procedure was used in the calculation of the depths, z_i; where a major lithologic boundary occurred a z_i value was assigned; where no lithologic boundary occurred between two measured conductivity values the midpoint of the two adjacent samples was assigned a z_i value. Conductivities were designated and extrapolated to that depth, where no lithologic boundaries occurred between two samples the sample conductivities were assumed to extend to the intervening midpoint. In those instances where a lithologic unit was without a measured conductivity a value was assigned from an equivalent sample in a nearby hole or, failing that, was given a value based on a lithologic description of the interval (see section 3.8).

In many instances it was possible to measure conductivity samples above the shallowest temperature point. In these cases a surface temperature was computed assuming that the conducted heat flow determined over the temperature depth range could be extrapolated to the surface using equation (3.1) with the same rules as given above for the assignment of values of z_i and K_i. Such values serve as a useful guide to the validity of the computed

heat flow, particularly where the shallowest temperature point occurs at depths of the order of one kilometre.

Two terms, defined for the purpose of this study and to be used in connection with the Bullard method, are the weighted harmonic mean thermal conductivity, K_h,

$$(3.2) \qquad K_h = \left[\sum_{i=1}^{n} z_i/K_i \right]^{-1} \cdot \left[\sum_{i=1}^{n} z_i \right]$$

and the weighted harmonic mean geothermal gradient, G_h,

$$(3.3) \qquad G_h = q \cdot K_h^{-1}$$

where the heat flow q is determined over the conductivity intervals z_i to z_n by equation (3.1).

Values of q computed from the Bullard method were calculated over various numbers of consecutive temperature points in this study to attempt to estimate the uncertainty in any given value. Typically, where three or more temperatures were available, three values of q were calculated; one over the entire temperature range, and one each over the upper and lower halves. Quoted values of G_h and K_h will, unless otherwise specified, refer to those values computed over the entire range of temperature.

An error of fit of equation (3.1) was also computed. The standard deviation, S of the fit of (3.1) is defined as, (cf. Kreysig, 1968),

$$(3.4) \qquad S = \left[1/(n-1) \cdot \sum_{j=1}^{n} \left(x_j - \bar{x} \right)^2 \right]^{\frac{1}{2}}$$

where

$$(3.5) \qquad x_j = \sum_{i=1}^{n} z_i/K_i$$

and,

$$(3.6) \qquad \bar{x} = \left[\sum_{j=1}^{n} \left(\sum_{i=1}^{j} z_i/K_i \right) \right] / n$$

All values of the error of such fits quoted in this study are at the two standard deviations or ninety-five percent confidence level. The reader should not interpret these values as realistic estimates of error in heat flow as other sources of uncertainty in the parameters T(z) and K_i in equation (3.1) will affect the computed q but not the degree of linearity of the relation. A separate estimate of total error will be given.

These calculations were all performed with a computer. Further discussion of technique of computation of (3.1) will be given in Section 3.9.

3.3 The Topographic Correction

The departure of the surface of the earth from a flat plane results in a nonuniform flow of heat in the near surface strata in proximity to the topographic relief. Several methods to correct for this effect have been formulated including models for idealized geometric shapes, (Lees, 1910; Van Orstrand, 1934, Sbrana and Bossolasco, 1952, Andrea, 1958, Lachenbruch, 1969) electrical analogues (Bullard, 1939, Guyod, 1946, Coster, 1947), analytical three dimensional treatments (Jeffreys, 1940, Bullard, 1940) and various numerical techniques such as finite difference modelling (cf. Haenel, 1970). Basic assumptions to all of the treatments are that the Laplace equation holds, that the region below the surface is homogeneous, isotropic and free of heat sources, the geothermal gradient is undisturbed as the depth tends to infinity and that the adiabatic lapse rate is linear.

As the bulk of the temperature data considered in this study falls in the depth range of one to four kilometres, it is useful to first consider if such a correction is necessary. This is most readily accomplished by analyzing the effect of an idealized geometric shape, for both realistic and extreme examples of topographic relief, on the geothermal gradient. Lees (1910) has given a solution for the variation of temperature with depth within a longitudinally extended monocline,

$$T = T_0 + g \cdot z + B \cdot (z + a) \cdot \left[x^2 + (z + a)^2\right]^{-1} \qquad (3.7)$$

where T is the temperature at depth z, g is the geothermal gradient, T_o is the surface temperature, x is the distance perpendicular to the monocline axis and B and a are constants. Differentiating (3.7) w.r.t. z we obtain,

$$(3.8) \qquad \frac{\partial T}{\partial z} = g + \frac{B \cdot \left[x^2 - (z+a)^2\right]}{\left[x^2 + (z+a)^2\right]^2}$$

where the constants B and a are,

$$(3.9) \qquad B = (g-g') \cdot H \cdot (\tfrac{1}{4} H^2 + b^2)^{\frac{1}{2}}$$

$$(3.10) \qquad a = H + (\tfrac{1}{4} H^2 + b^2)^{\frac{1}{2}}$$

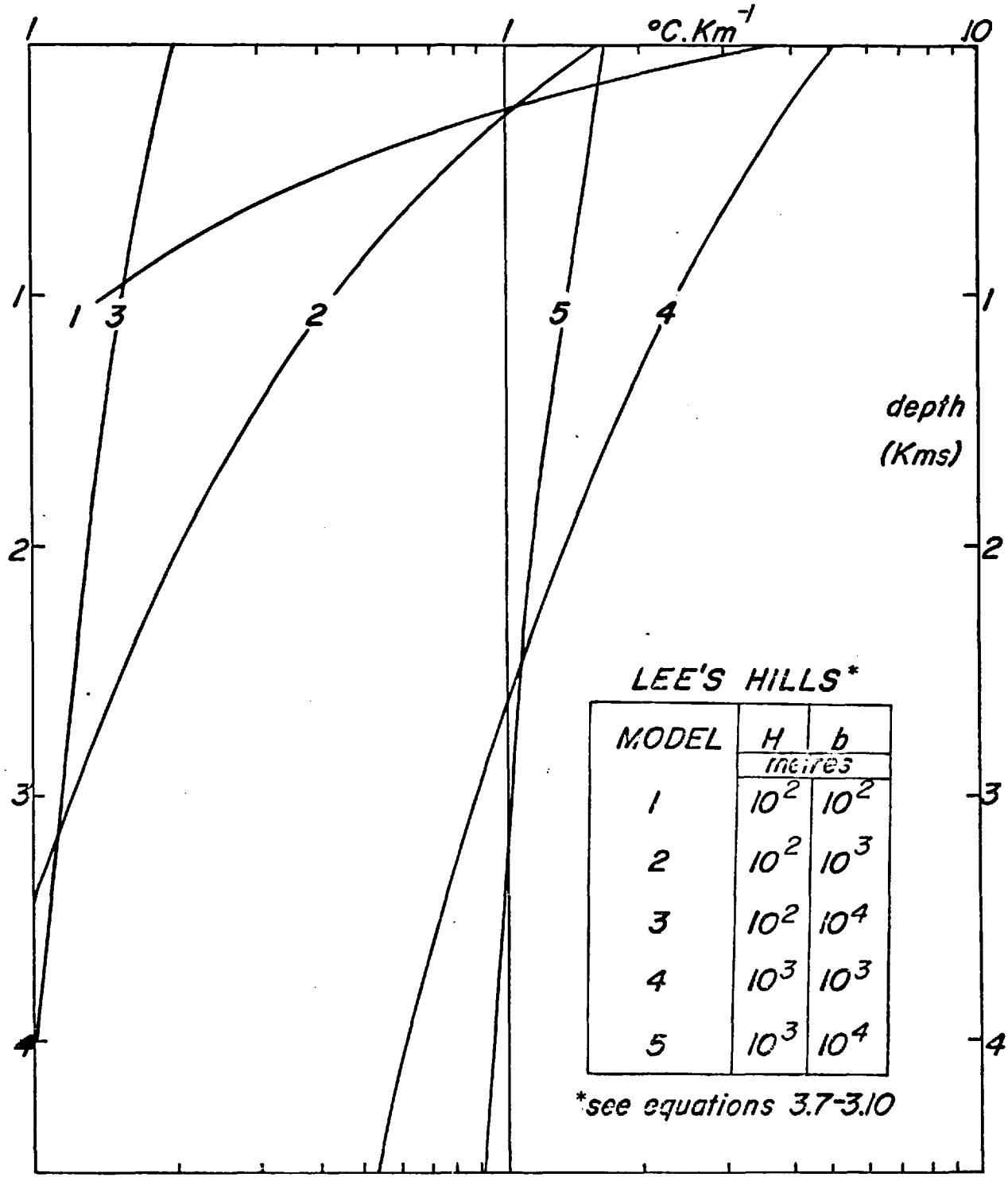
and g' is the adiabatic lapse rate while H and $2b$ are the monocline height and width at $H/2$ respectively. The surface defined by such a monocline conforms to the linear adiabatic lapse rate relation while (3.7) may be shown to satisfy the other condition given above (Jaeger, 1965).

If we take the extreme location, or position of the maximum gradient disturbance, of the borehole on the monocline, ie. x = o, and compute that disturbance as a function of depth for $g = 30.0^{o}C \cdot km^{-1}$ and $g' = 9.8^{o}C \cdot km^{-1}$ (Berry et al., 1945) we obtain curves of the type shown in Fig. 3.1 for various realistic and extreme combinations of H and b. In all instances where the topography is of the order of $H = 10^2$ metres and $b = 10^2 - 10^4$ metres (curves 1,2,3) we find that the gradient disturbance is less than $.5^{o}C \cdot km^{-1}$ at depths of one kilometre or more. Curves 4 and 5 of Fig. 3.1, for $H = 10^3$ metres and $b = 10^3$ and 10^4 metres do indicate significant gradient disturbances, especially at depths less than two kilometres.

Local topographic relief is relatively modest over virtually all of the regions considered here and would rarely exceed 100 metres within several kilometres of any of the boreholes, (cf. Addis Ababa and Nairobi sheets, Int. World Map Series, 1:2.5 million, 1969). It was thus considered unnecessary to correct any of the boreholes for topographic relief.

TOPOGRAPHIC GRADIENT CORRECTION VERSUS DEPTH

(for axis of various Lee's Hills)



LEE'S HILLS*

MODEL	H	b
	metres	
1	10^2	10^2
2	10^2	10^3
3	10^2	10^4
4	10^3	10^3
5	10^3	10^4

*see equations 3.7-3.10

NOTE [geothermal gradient = 30.°C. Km^{-1}
adiabatic lapse rate = 9·8 °C. Km^{-1}

FIG. 3.1

3.4 The Climatic Correction

It has long been recognized that the effect of large amplitude long period climatic events were a potential source of disturbance to the geothermal gradient. Lane (1923) was the first to attempt to correct his subsurface temperature data for the effect of the Pleistocene Ice-Ages.

The mathematical treatment is relatively simple. Equation (1.2), the source solution for one dimensional time dependent heat flow, equation (1.1), has a particular integral,

$$(3.11) \qquad (4\pi kt)^{-\frac{1}{2}} \, e^{-(x - x')^2/4kt}$$

where k is thermal diffusivity, t is time, and x is depth. Where an initial temperature, f(x), is present Carslaw and Jaeger (1959) show,

$$(3.12) \qquad T(x,t) = (4\pi kt)^{-\frac{1}{2}} \int_{-\infty}^{\infty} f(x') \, e^{-(x - x')^2/4kt} \, dx'$$

satisfies equation (1.1). This solution is of course for an infinite solid; the semi-infinite solid condition may be simulated if we introduce, at x = 0, a region with a -f(x) temperature such that,

$$(3.13) \qquad T(x,t) = (4\pi kt)^{-\frac{1}{2}} \int_{0}^{\infty} f(x') \cdot \left[e^{-(x-x')^2/4kt} - e^{-(x + x')^2/4kt} \right] dx'$$

where the plane x = o is held at a zero temperature. Where the initial temperature is a constant, T_o, (3.13) may be written,

$$(3.14) \qquad T(x,t) = \frac{2T_o}{\sqrt{\pi}} \cdot \int_{0}^{x/2\sqrt{kt}} e^{-\varepsilon^2} \, d\varepsilon$$

where

$$(3.15) \qquad x' = \pm x + 2 \cdot \varepsilon\sqrt{kt}$$

with the sign depending on whether the substitution was above or below the x plane. The integral term of (3.14) is defined as the error function,

$$(3.16) \qquad \operatorname{erf}\left(x/2\sqrt{kt}\right) = \frac{2}{\sqrt{\pi}} \cdot \int_0^{x/2\sqrt{kt}} e^{-\varepsilon^2}\, d\varepsilon$$

so that (3.14) may be substituted,

$$(3.17) \qquad T(x,t) = T_o \cdot \operatorname{erf}\left(x/2\sqrt{kt}\right)$$

where $T(x,t)$ is the temperature distribution in a semi-infinite solid initially at a uniform value, T_o, and with the surface $x = o$, at zero temperature. We may now interchange the boundary and initial conditions such that,

$$T(o,t) = T_o$$

$$T(x,o) = 0$$

and modify (3.17) to,

$$(3.18) \qquad T(x,t) = T_o \cdot \left[1 - \operatorname{erf}\left(x/2\sqrt{kt}\right)\right]$$

or,

$$= T_o \cdot \operatorname{erfc}\left(x/2\sqrt{kt}\right)$$

In the case where the surface temperature is maintained at a constant value for n discreet intervals of time,

ie.,

$$T(o,t) = T_1 \qquad t_1 < t < t_2$$

$$T(o,t) = 0 \qquad t_2 < t < t_3$$

$$(3.19) \qquad T(o,t) = T_2 \qquad t_3 < t < t_4$$

$$\cdots\cdots\cdots\cdots$$

$$T(o,t) = T_n \qquad t_{2n-1} < t < t_{2n}$$

then by Duhamel's superposition theorem we may write,

$$(3.20) \qquad T(x,t) = \sum_{i=1}^{n} T_i \cdot \left[\operatorname{erf}\left(x/2\sqrt{kt_{2i-1}} - \operatorname{erf}\left(x/2\sqrt{kt_{2i}}\right)\right)\right]$$

The gradient disturbance, G(x,t), may be obtained from (3.20) by differentiating w.r.t. x such that,

$$(3.21) \quad G(x,t) = \sum_{i=1}^{n} T_i \cdot \left[(\pi k t_{2i-1})^{-\frac{1}{2}} \; e^{-(x^2/4kt_{2i-1})} - (\pi k t_{2i})^{\frac{1}{2}} \; e^{-(x^2/4kt_{2i})} \right]$$

It is thus necessary to obtain data for the boundary conditions given by equations (3.19). It is convenient to consider three periods of time; the Holocene (0-10,000 years B.P.), the Pleistocene (10,000-1.5 million years B.P.) and the Pliocene and older ($<$ 1.5 million years B.P.) in connection with past climatic events.

Holocene temperature variations are relatively well known in Northern Europe, (cf. Fairbridge, 1961 and Lamb, 1965), such that a North Sea climatic correction would be calculable. A similar correction for Eastern Africa would be a good deal less certain as details of the Holocene climatic pattern are as yet to be resolved, Flint (1959), although some recent progress has been reported, Olausson and Olsson (1969), and Shackleton (1972). However, it is useful to compute some models for extreme Holocene temperature variations to establish whether a detailed correction would be justified at the typical minimum depths for which temperature data is considered here. Equation (3.21) has been evaluated for a single step function model for various values of t_1, t_2 and diffusivity, where T_1 has been taken as $1.0^{o}C$. The results are presented in tables 3.1 and 3.2 for depths of .1 and 1 kilometre respectively. The case of $t_2 = 10^4$ years, the entire Holocene up to the present being climatically disturbed, which is patently extreme, is the only instance of any appreciable gradient disturbance occurring at one kilometre.

Fairbridge (1961) estimates a maximum Holocene disturbance of $2.5^{o}C$ for Northern Europe while Flint believes changes of up to $5^{o}C$ may have occurred in Eastern Africa. Obviously since only unrealistic Holocene climatic models with these magnitudes would significantly alter the geothermal gradient at one

kilometre, no correction will be applied in this study. Table 3.1 emphasizes that, in case of shallow boreholes of depth one hundred metres, such a correction may well be necessary.

Birch (1948) clearly demonstrated the necessity of applying a correction in regions affected by Pleistocene glaciations. He (Birch) indicated that the correction would be significant in the depth range of one to five kilometres although he thought that it was unlikely to exceed $3^{o}C \cdot km^{-1}$.

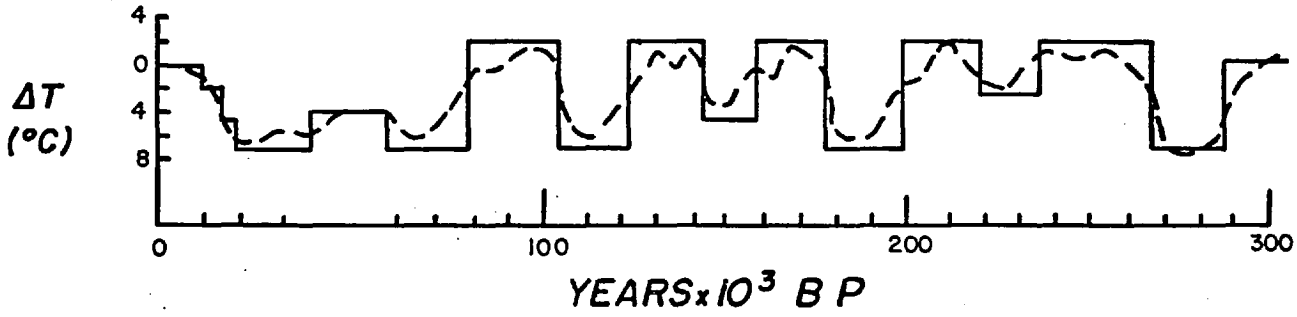
Urey (1947) was the first to suggest that the temperature dependence of the isotopic $^{18}O/^{16}O$ fractionization factor of oxygen in water and calcium carbonate might be used as a geologic thermometer. Emiliani (1955, 1961 and 1966) successfully exploited this technique to produce Pleistocene paleotemperature records from deep-sea carbonate oozes age-dated by carbon-14 techniques. Calibration of the technique, to establish the absolute scale of temperature variation, is made by comparing the $^{18}O/^{16}O$ ratios with similar ratios obtained from living forams existing at known temperatures. The most impressive result of the technique has been the uniformity of the paleotemperature curves obtained from world-wide measurements.

The correction of the North Sea temperature data is thought to be justified in view of the seeming consistency of oceanic paleotemperature data and the fact that this shelf sea was glaciated in Pleistocene times (Strakhov, 1967). During such an ice age the sea bottom temperature would have been lowered to the ice-point. The paleotemperature curve, Fig. 3.2, of Emiliana (1955), for times more recent than 3×10^{5} years, was used as the basis for the North Sea climatic correction. This curve has recently been modified (Emiliani and Shackleton, 1974) although the changes may be considered negligible for this study.

A step function model has been fitted to this curve, Fig. 3.2, to provide the boundary conditions, equations (3.19). Fig. 3.3 illustrates the results obtained from this step function model using equations (3.20)

NORTH SEA BOTTOM TEMPERATURE MODEL

ΔT (Temperature) vs TIME



——— Square wave model

_____ Oxygen isotope paleotemperatures after Emilliani (1955)

FIG. 3.2

NORTH SEA CLIMATIC MODEL TEMPERATURE AND GEOTHERMAL GRADIENT DISTURBANCES

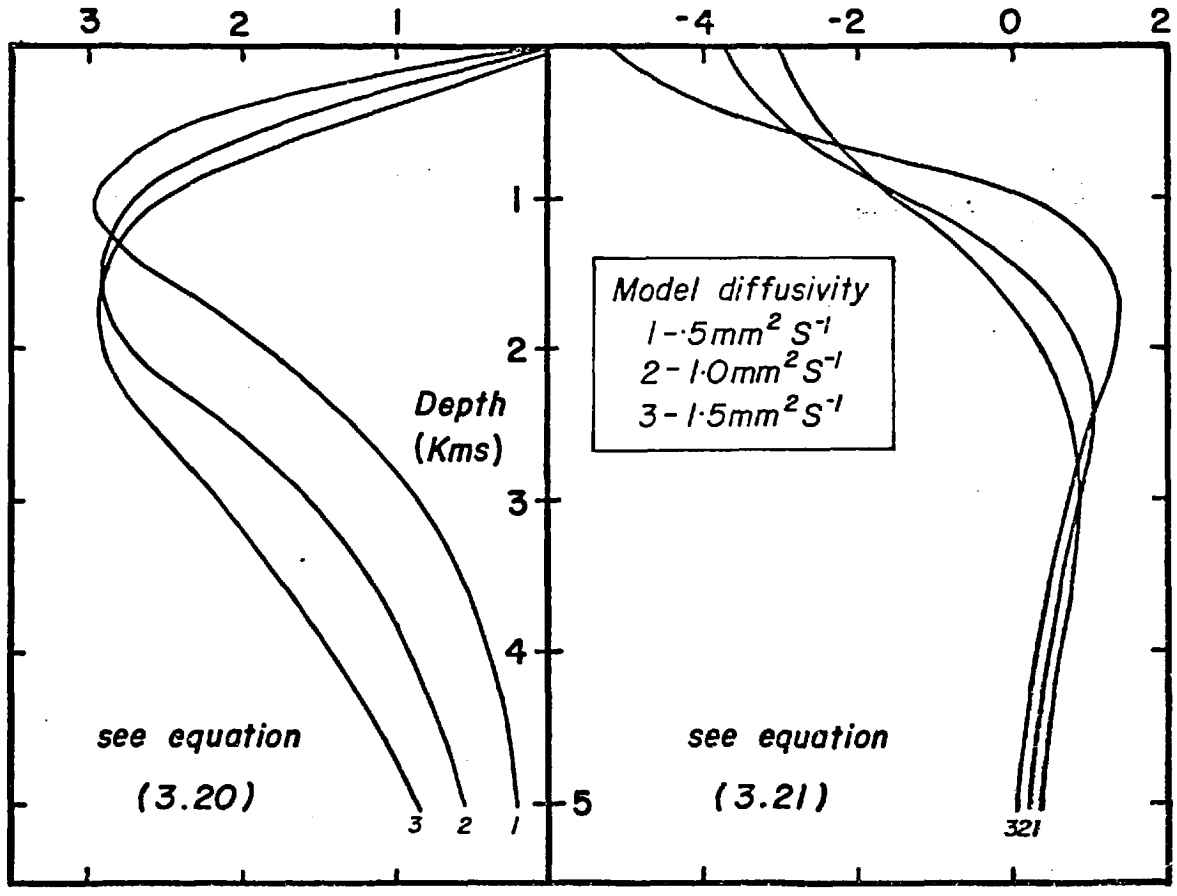


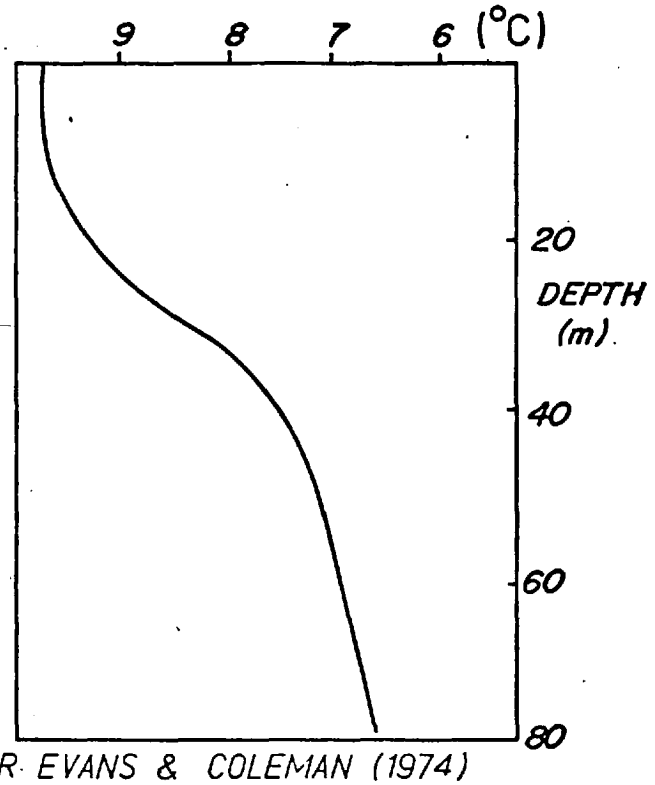
FIG. 3.3

and (3.21) to estimate temperature and gradient corrections as functions of depth. The magnitude of the temperature variations, Fig. 3.2, was assigned by computing a present mean annual sea bottom temperature of $7^{o}C$ from Fig. 3.4 after Evans and Coleman (1974) and assuming this value represented the difference between present day and glacial Pleistocene temperatures. Note that the interglacials are about $2^{o}C$ warmer than present day temperatures. The glacial value of $7^{o}C$ lower than present day is reasonable when compared with the range of $6-10^{o}C$ quoted by Flohn (1952) for West Central Europe and with those obtained from paleobotony by Fairbridge (1961).

A similar correction for Eastern Africa would be a good deal less justified in view of the less precise knowledge of its past climate. Flint (1959) has found that Pleistocene glacial advances have occurred on the equatorial mountains in East Africa. Glacier levels were as much as 1,000 metres lower on Mounts Kenya, Kilimanjaro, Elgon and Ruwenzori, implying a temperature drop of perhaps $5^{o}C$. Moreau (1952) has postulated Pleistocene temperature changes in Central Africa based on forest biogeography. Bishop (1971) has correlated late Pleistocene changes in the levels of the rift valley lakes with temperature variations. Olausson (1972) has found some correlation in Pleistocene paleotemperatures determined by the oxygen isotope method on Somali basin and Arabian Sea cores with those of Emiliani's Atlantic, Pacific and Caribbean work, though the results are far from complete. Shackleton (1972) reports that initial studies of paleotemperatures have begun on Western Indian Ocean cores. However, the climatic curve is still fragmentary for Africa when compared with Europe, Fig. 3.5, after Clark (1965). For this reason no attempt was made to correct the Eastern Africa temperature data for climate. The error introduced in the gradient by omitting such a correction is thought unlikely to exceed $3^{o}C \cdot km^{-1}$, (See Fig. 3.3).

Birch (1948) has suggested that Pliocene climatic events might be significant in boreholes of depths of a few kilometres. However, no detailed model of Pliocene climate has yet been produced, the dated record extending back only some 7×10^{5} years (Emiliani and Shackleton, 1974).

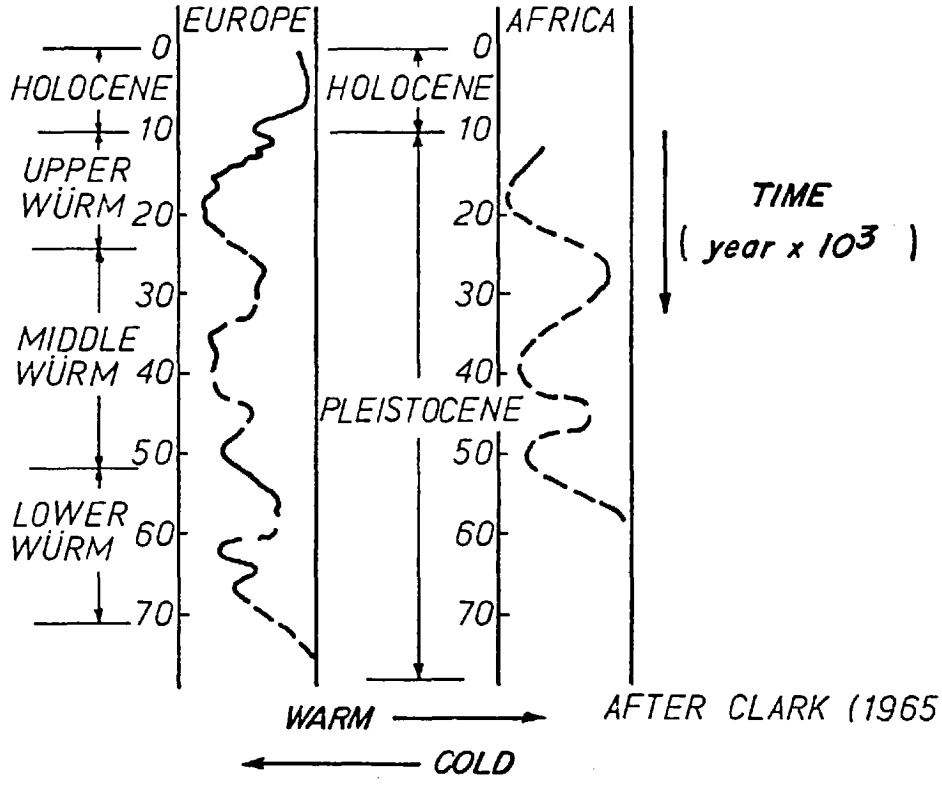
CENTRAL NORTH SEA
MEAN ANNUAL SEA
BOTTOM TEMPERATURE



AFTER EVANS & COLEMAN (1974)

FIG.3.4

EUROPEAN & AFRICAN PLEISTOCENE CLIMATES



AFTER CLARK (1965)

FIG.3.5.

The corrections applied to the North Sea borehole temperatures were computed from a model extending back 3×10^5 years; climatic events further back in time with variations of $10^{\circ}C$ and periods of 5×10^4 years, the typical Pleistocene maximums, will change the gradient by less than $.1^{\circ}C \cdot km^{-1}$. The maximum magnitude of the North Sea gradient correction is similar to that estimated by Birch (1948) and Horai (1969) although less than Crain (1968) and Ciaranei et al. (1973) have proposed. Sass et al. (1971b) have suggested, on the basis of uniform heat flow at all depths in a deep Canadian borehole, that in the absence of a consistent variation of heat flow to a particular model, the Pleistocene climatic correction uncertainty approaches the magnitude of the correction itself.

The method of the computation of the diffusivity for equation (3.20) will be discussed in section 3.9; an assessment of the results of the correction is given in Chapter 5.

Table 3.1

Holocene Climatic Model

Geothermal Gradient Disturbance

Depth = 100 meters

T_i °C	t_1 years	t_2 years	Diffusivity($mm^2 \cdot s^{-1}$)		
			.5	1.0	1.5
			°C · km^{-1}		
1.0	1	10^2	-2.91	-4.55	-4.84
1.0	1	10^3	-3.83	-2.93	-2.46
1.0	1	10^4	-1.40	-1.00	-0.82

Table 3.2

Holocene Climatic Model

Geothermal Gradient Disturbance

Depth = 1000 meters

T_i °C	t_1 years	t_2 years	Diffusivity($mm^2 \cdot s^{-1}$)		
			.5	.1	1.5
			°C · km^{-1}		
1.0	1	10^2	< .01	<.01	<.01
1.0	1	10^3	< .01	<.01	-.01
1.0	1	10^4	-.29	-.45	-.48

computed from equation (3.21)

for a single interval (n = 1).

3.5 The Uplift and Erosion or Downwarp and Sedimentation Correction

The great thickness of sediments, perhaps as much as twelve kilometres in some area of coastal Eastern Africa, is by the nature of its accumulation, another perturbing source of the geothermal regime. The sedimentation in both the North Sea and coastal Eastern Africa has been associated with contemporaneous downwarp of underlying rocks as will be discussed in Chapters 4 and 5. Only minor episodes of uplift and/or erosion have occurred during post-Paleozoic times in these two areas.

The thermal effects of sedimentation or erosion may be simulated by using the equation of one dimensional time dependent heat conduction for a moving medium (Benfield, 1949a, 1949b). Carslaw and Jaeger (1959) demonstrate that a 'convective' flux component, pcTu, is added to the heat equation (1.1) to simulate a moving body, which, with no heat production is described by,

$$(3.22) \qquad \frac{\partial^2 T}{\partial x^2} - \frac{u}{k} \cdot \frac{\partial T}{\partial x} - \frac{1}{k}\frac{\partial T}{\partial t} = 0$$

where T is temperature, x is depth, t is time, k is diffusivity, p is density, c is specific heat, and u is the velocity of the medium.

If we consider heat production at rate A_0 and the initial and boundary conditions,

$$(3.23) \qquad T = T_0 + ax \qquad x > 0, \quad t = 0$$

$$(3.24) \qquad T = T_1 + bx \qquad x = 0, \quad t > 0$$

we may modify (3.22) to,

$$(3.25) \qquad \frac{\partial^2 T}{\partial x^2} - \frac{u}{k} \cdot \frac{\partial T}{\partial x} - \frac{1}{k} \cdot \frac{\partial T}{\partial t} = \frac{-A_0}{K}$$

where K is thermal conductivity (Carslaw and Jaeger, 1959). Solution by Laplace transforms is, as in equation (1.16), most expedient here. Introducing the initial condition (3.23) we obtain the subsidiary equation,

$$(3.26)\qquad \frac{d^2\bar{T}}{dx^2} - \frac{u}{k}\cdot\frac{d\bar{T}}{dx} - \frac{p}{k}\cdot\bar{T} = \frac{A_o}{Kp} - \frac{T_o + ax}{k}$$

where p is the Laplace operator. Equation (3.26) is thus to be solved with the transform of the boundary condition (3.24),

$$(3.27)\qquad \bar{T} = T_1/p + b/p^2, \text{ at } x = o$$

The solution, which is rather involved and is detailed in Appendix 4, is,

$$(3.28)\qquad \bar{T} = \left[\frac{T_1 - T_o}{p} + \frac{b + au - (kA_o/K)}{p^2}\right] \cdot e^{\left\{\frac{ux}{2k} - x\left(\frac{u^2}{4k^2} - \frac{p}{k}\right)^{\frac{1}{2}}\right\}}$$

$$+ \left(\frac{kA_o}{K} - aU\right)\cdot\frac{1}{p^2} + \frac{V_o + ax}{p}$$

and using standard Laplace inversions,

$$(3.29)\qquad T = T_o + ax + (kA_o t/K) - aut$$

$$+ \frac{(T_1 - T_o)}{2}\cdot\left\{\operatorname{erfc}\left(\frac{x - ut}{2(kt)^{\frac{1}{2}}}\right) + e^{ux/k}\cdot\operatorname{erfc}\left(\frac{x + ut}{2(kt)^{\frac{1}{2}}}\right)\right\}$$

$$+\frac{1}{2u}\left(b + au - \frac{kA_o}{K}\right)\cdot\left\{(x + ut)\cdot e^{ux/k}\cdot\operatorname{erfc}\left(\frac{x + ut}{2(kt)^{\frac{1}{2}}}\right) + (ut - x)\cdot\operatorname{erfc}\left(\frac{x - ut}{2(kt)^{\frac{1}{2}}}\right)\right\}$$

where the function erfc is defined in (3.18). Differentiating (3.29) w.r.t. x, we obtain,

$$(3.30)\qquad \frac{\partial T}{\partial x} = a + \tfrac{1}{2}(T_1 - T_0)\cdot\left[(\pi kt)^{-\frac{1}{2}}\cdot e^{-\left(\frac{x-ut}{2(kt)^{\frac{1}{2}}}\right)^2} + e^{ux/k}\cdot(u/k)\cdot \operatorname{erfc}\left(\frac{x+ut}{2(kt)^{\frac{1}{2}}}\right) - (\pi kt)^{-\frac{1}{2}}\cdot e^{-\left(\frac{x+ut}{2(kt)^{\frac{1}{2}}}\right)^2}\right]$$

$$+ 1/2u\cdot\left[b + au - kA_0/K\right]\cdot\left\{(1 + ux/k + u^2t/k)\cdot e^{ux/k}\cdot\operatorname{erfc}\left(\frac{x+ut}{2(kt)^{\frac{1}{2}}}\right) - \frac{(x+ut)}{(\pi kt)^{\frac{1}{2}}}\cdot e^{ux/k}\cdot e^{-\left(\frac{x+ut}{2(kt)^{\frac{1}{2}}}\right)} - \operatorname{erfc}\left(\frac{x-ut}{2(kt)^{\frac{1}{2}}}\right) - \frac{(ut-x)}{(\pi kt)^{\frac{1}{2}}}\cdot e^{-\left(\frac{x-ut}{2(kt)^{\frac{1}{2}}}\right)^2}\right\}$$

which gives the gradient at any depth x in terms of the original gradient a.

It is useful to consider the physical situation in which the sedimentation takes place. Figs. 3.6 a, b, c, schematically illustrate the thermal perturbation resulting from sedimentation and/or downwarp. As was previously mentioned the sedimentation and downwarp have been largely contemporaneous in both the North Sea and Eastern Africa (Fig. 3.6, b). This leads to certain simplifications in (3.30) resulting from changes in the boundary conditions (3.24), namely (3.30a),

$$(3.30a)\qquad T = T_0 \quad \text{at} \quad x = o,\ t > o$$

implying $T_1 = T_0$ and $b = o$. The condition given by (3.30a) is that of sediment accumulating at a constant temperature at the ground surface, the equivalent of contemporaneous downwarp. Further, heat production in most sediments, apart from shales, is quite low (Sass, 1972) so that for our purpose $A_0 = o$. The effect of heat production in the accreting sediments is to lower the gradient disturbance although the effect is small (Von Herzen and Uyeda, 1963). The result of such simplifications reduces (3.29) to,

SCHEMATIC ILLUSTRATION OF TEMPERATURE REGIME DISTURBED BY DOWNWARP AND SEDIMENTATION

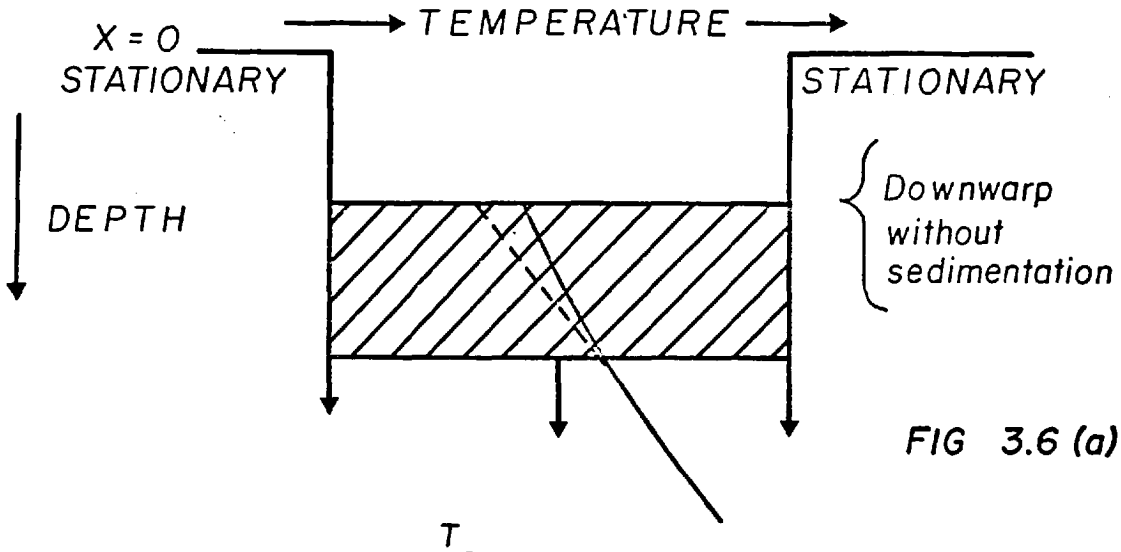


FIG 3.6 (a)

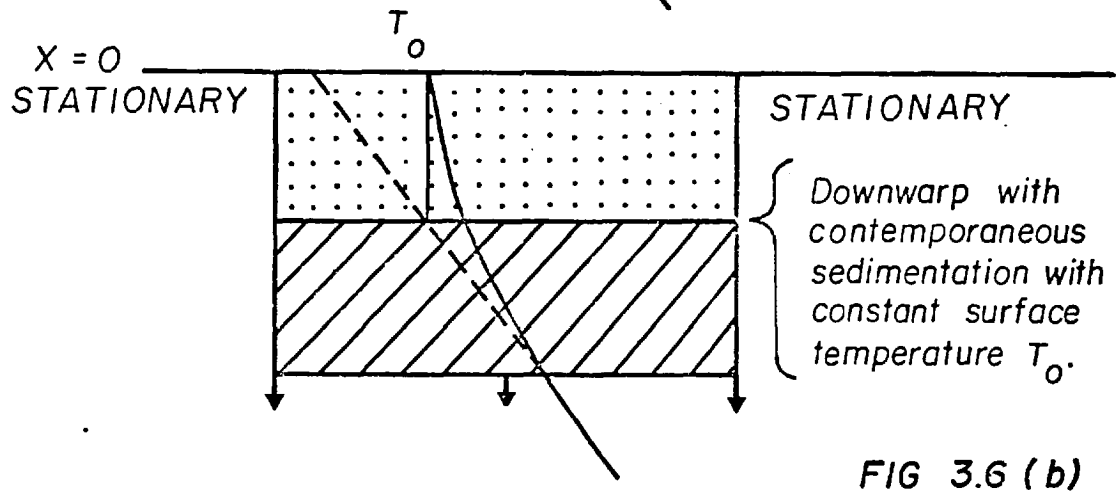


FIG 3.6 (b)

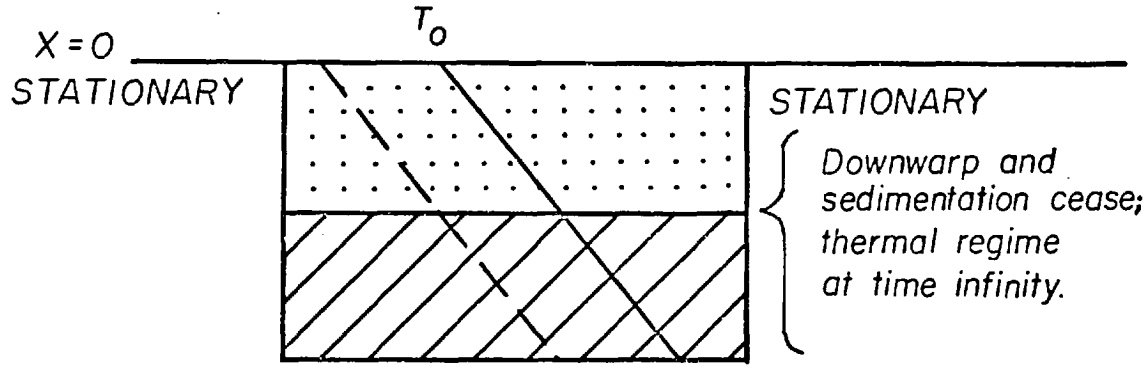


FIG 3.6 (c)

SEDIMENTS

DOWN FAULTED BLOCK

Undisturbed geothermal gradient

Measured geothermal gradient.

$$(3.31)\quad T = T_o + a\,(x - ut) + \frac{a}{2} \cdot \left\{ (x + ut)\, e^{ux/k}\, \operatorname{erfc}\left(\frac{x + ut}{2(kt)^{\frac{1}{2}}}\right) + (ut - x) \cdot \operatorname{erfc}\left(\frac{x - ut}{2(kt)^{\frac{1}{2}}}\right) \right\}$$

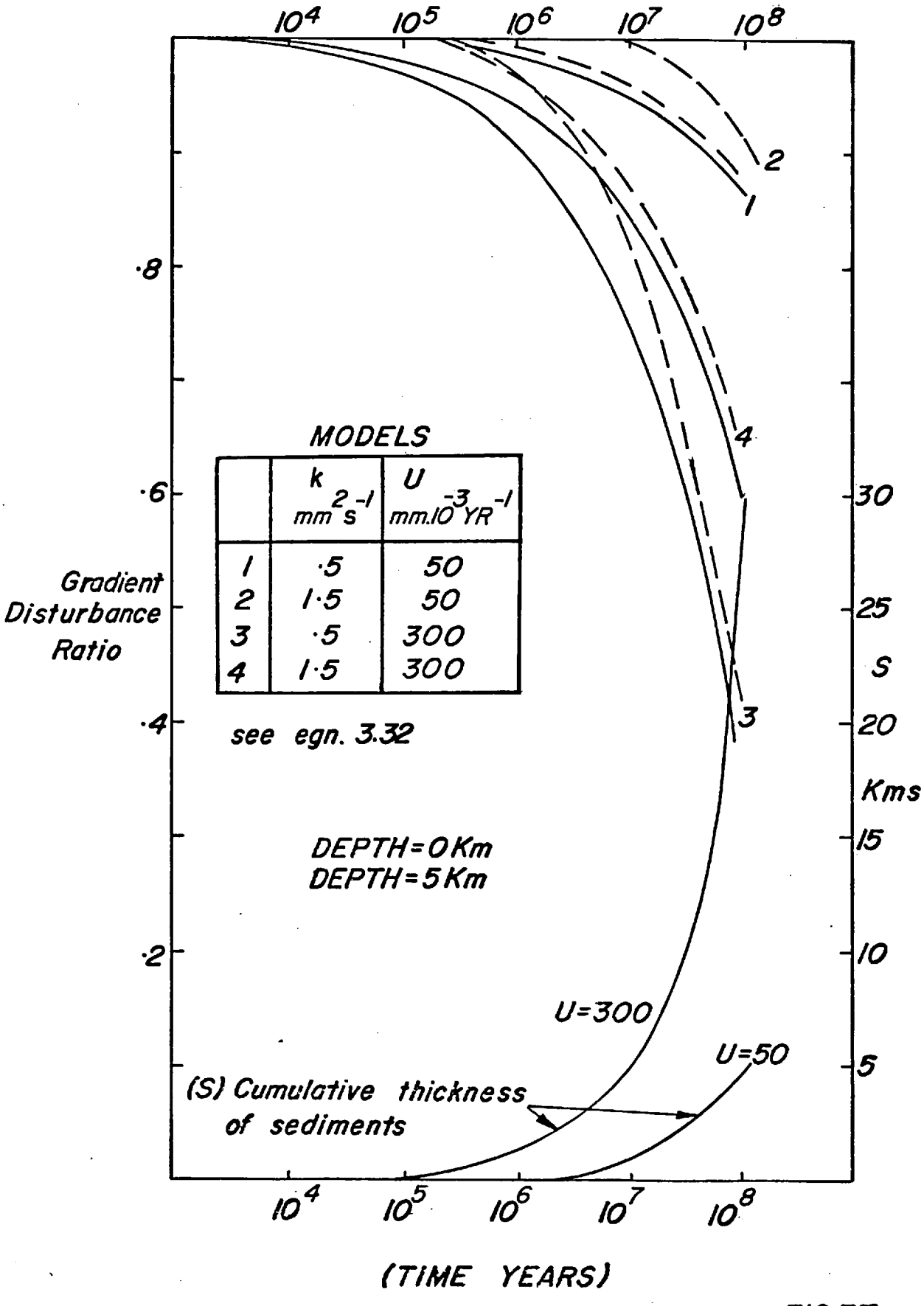
and (3.30) is modified to,

$$(3.32)\quad \frac{\partial T}{\partial x} = a + \tfrac{1}{2}a \cdot \left[(1 + xu/k + tu^2/k) \cdot e^{xu/k} \cdot \operatorname{erfc}\left(\frac{x + ut}{2(kt)^{\frac{1}{2}}}\right) - \operatorname{erfc}\left(\frac{x - ut}{2(kt)^{\frac{1}{2}}}\right) - \frac{x + ut}{(\pi kt)^{\frac{1}{2}}} \cdot e^{ux/k}\, e^{-\left(\frac{x - ut}{2(kt)^{\frac{1}{2}}}\right)^2} - \frac{ut - x}{(\pi kt)^{\frac{1}{2}}} \cdot e^{-\left(\frac{x - ut}{2(kt)^{\frac{1}{2}}}\right)^2} \right].$$

Fig. 3.7 illustrates the term $(\partial T/\partial x)/a$, the gradient disturbance ratio, as a function of duration of sedimentation/downwarp, for various values of diffusivity, depth and rates of sedimentation/downwarp. Clearly for long periods and high rates of sedimentation/downwarp the disturbance may be large; diffusivity and depth are correspondingly less important over reasonable ranges likely to be encountered in this study.

Values of velocity, u, and duration t, were estimated from lithologic logs, where available, for the boreholes considered here. The duration was assumed to be the time from the present to the age of the oldest dated sedimentary rocks penetrated. Dating of the rocks was, in all cases, by paleontology carried out by oil company geologists. The rate of sedimentation/downwarp was simply the total thickness of sediments penetrated divided by the duration. Further comments on the values of the sedimentation rates and durations as well as the estimation of diffusivity will be given in the discussion of results, Chapters 4 and 5 and in section 3.9.

THE EFFECT OF VARIOUS SEDIMENTATION/DOWNWARP MODELS ON THE GEOTHERMAL GRADIENT



	k $mm^2 s^{-1}$	U $mm.10^{-3} YR^{-1}$
1	·5	50
2	1·5	50
3	·5	300
4	1·5	300

FIG.3.7.

3.6 The Correction of Thermal Conductivity Data for In-Situ Pressure

The effect of pressure at depths of a few kilometres on thermal conductivity was, for many years, thought to be insignificant (Beck, 1965). However, recent studies, though far from definitive, suggest a small but significant increase in conductivity due to pressure for porous sedimentary rocks (cf. Kappelmeyer and Haenel, 1974).

Most of the research concerned with this effect (Bridgman, 1924, Clark, 1941, Clark, 1966) has suggested a linear relation of the form,

$$K = K_0 (1 + \gamma P) \qquad (3.33)$$

where K is the conductivity at pressure P, K_0 is the uncompressed conductivity and γ is a constant. While relation (3.33) appears to adequately describe the conductivity variation with pressure, no common opinion exists on the value of γ; Kappelmeyer and Haenel (1974) indicate that it most probably is of an order resulting in a one or two percent increase in conductivity per kilometre.

Hurtig and Brugger (1970) compressed several types of sedimentary rocks and found a distinctly nonlinear conductivity increase at low pressures (less than 4 $MN \cdot m^{-2}$) although at higher pressures, of up to 40 $MN \cdot m^{-2}$, they did observe an approximate linear increase in conductivity. The increase in conductivity, which they attributed to a reduction in crack porosity, was relatively large for anhydrite, dolomite and sandstone, and significantly less for limestone, conglomerates, and porphyries. Hurtig and Brugger proposed no empirical relation such as (3.33) to describe their results.

Anand et al. (1973), in a similar study based principally on measurements of porous sandstones, obtained by a multivariate nonlinear least squares analysis, the relation,

$$(3.34) \qquad K = .587p - 5.53\,\phi + .916L^{.10} + .025F - .054$$

where K is the thermal conductivity in $W \cdot m^{-1} \cdot K^{-1}$, p is density ($gm.cm^{-3}$), ϕ is fractional porosity, L is permeability (millidarcies), and F is the formation resistivity factor (section 2.10). The relation (3.34) is of the type discussed in section 2.16. Differentiating (3.34) w.r.t. pressure, P, we find,

$$(3.35) \qquad \frac{\partial K}{\partial P} = .587 \cdot \frac{\partial p}{\partial P} - 5.53 \cdot \frac{\partial \phi}{\partial P} + .916\, L^{-.9} \frac{\partial L}{\partial P} + .0225 \cdot \frac{\partial F}{\partial P}$$

Dobrynin (1962) has evaluated the derivative expressions in the right hand side of (3.35) in terms of rock compressibilities,

$$(3.36) \qquad \frac{1}{p}\frac{\partial p}{\partial P} = f_1\phi$$

$$\frac{1}{\phi}\frac{\partial \phi}{\partial P} = f_2$$

$$\frac{1}{L}\frac{\partial L}{\partial P} = f_3$$

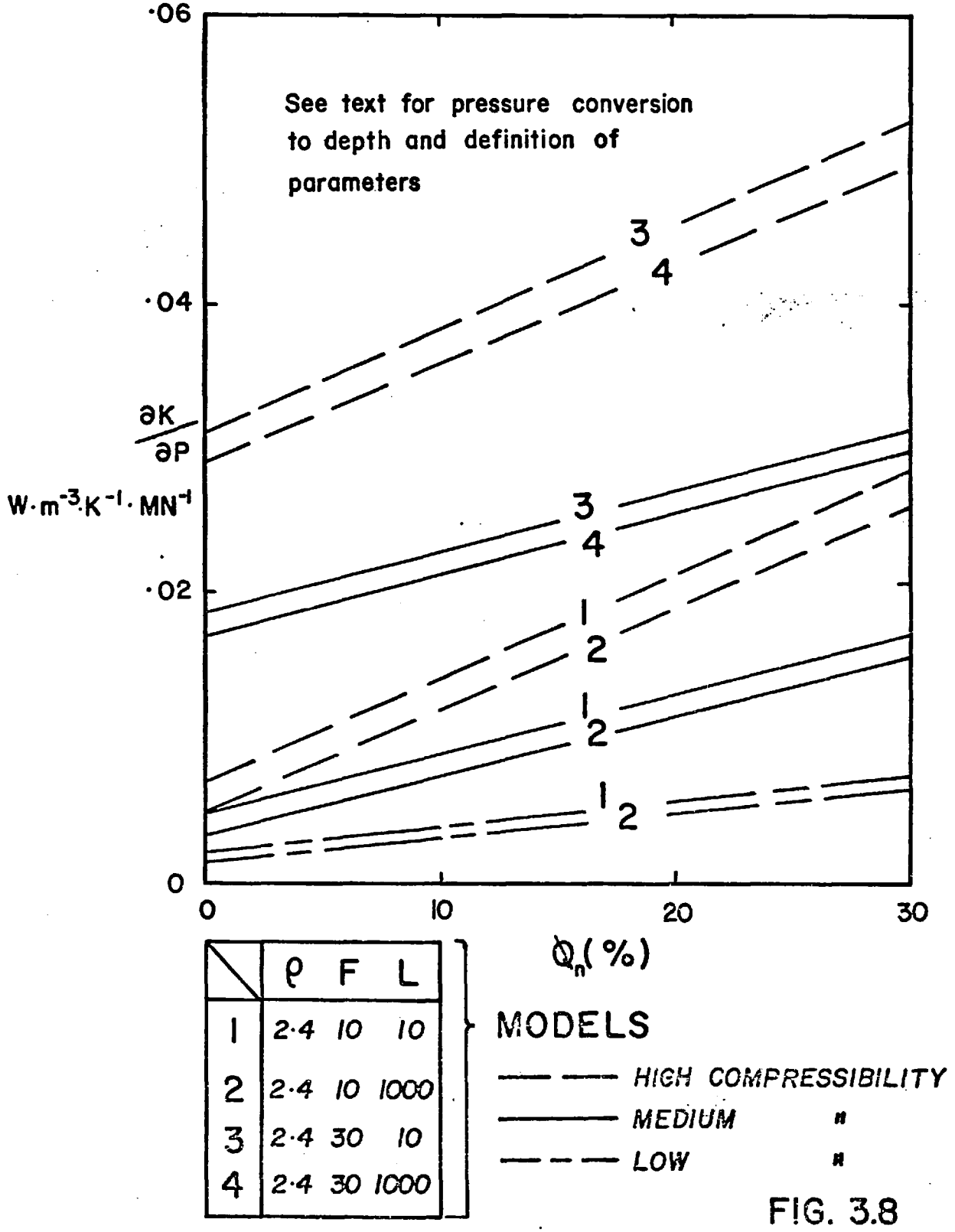
$$\frac{1}{F}\frac{\partial F}{\partial P} = f_4$$

where $f_{1, 2, 3, 4}$ are functions of compressibility. Anand et al. (1973) state that, in general, individual rock compressiblities are not known and thus a reasonable estimate can only be made by assigning values for high, medium and low compressilibity,

$$(3.37) \qquad \frac{\partial K}{\partial P} = 10^{-5} \cdot \left(Ap\phi + B\phi - CL^{.1} + DF\right)$$

Values of A, B, C, and D for high, medium and low compressibility are given in table 3.3. Fig. 3.8 graphically illustrates the conductivity/pressure relation (3.37) for typical p, ϕ, L, and F over the pressure range of interest

ABSOLUTE CHANGE IN CONDUCTIVITY (K) DUE TO PRESSURE (P) VERSUS % POROSITY. CONSTRUCTED FROM Eqn. (3.37), TABLE 3.3 AND MODELS BELOW



	ρ	F	L
1	2·4	10	10
2	2·4	10	1000
3	2·4	30	10
4	2·4	30	1000

FIG. 3.8

to this study. However, only two measurements, both on sandstones, were reported by Anand et al. to check the validity of (3.37). Results were in reasonable agreement but further experimental work is necessary.

The previously mentioned studies of Bridgman (1924), Clark (1941), Hurtig and Brugger (1970) and Anand et al. (1973) represent the sum total of published research on this subject. Although there is some evidence to suggest that (3.33) represents an over simplification of the problem it is still, to a first approximation, the most reasonable of models.

Table 3.4 is a compilation of the results of the four above mentioned studies for values of γ, the constant in equation (3.33). The pressure term, P, is in units of pressure increase per kilometre of depth while γ is given as a percentage. Values of γ from Hurtig and Brugger (1970) were obtained from the values of conductivity between the 4 and 40 $MN \cdot m^{-2}$ measurements. Timko and Fertl (1972) indicate that the lithostatic pressure within sedimentary basins increases at the rate of 22.6 $MN \cdot m^{-2}$ per kilometre, implying on average bulk density of $2.31\ gm \cdot cm^{-3}$. Thus we arrive at an 'average' conductivity increase of 2.5 percent per kilometre (table 3.4).

Conductivity values were thus modified by the relation,

$$K = K_0 \cdot (1 + .025 \cdot Z) \qquad (3.38)$$

where Z is the sample depth in kilometres and remaining terms are as defined in (3.33). The typical correction applied in this study was in the range three to seven percent.

Further discussion of the details of the computing of this correction will be given in section 3.9. Comments on further research into the effect are found in section 3.10.

Table 3.3

Coefficients for Equation (3.37)

(After Anand et al., 1973)

Compressibility	A	B	C	D
HIGH	.88	9.94	.64	.21
MEDIUM	.43	6.07	.31	.12
LOW	.22	2.49	.16	.059

Table 3.4

Percentage Increase of Conductivity

Due to a Pressure Increase Equivalent

To One Kilometre of Sediments

Rock Type	References *				Averages
	1	2	3	4	
Limestone	1.8 (3)	.3	.2	-	.8
Sandstone	5.5 (6)	1.7 (2)	-	3.9 (2)	3.7
Dolomite	4.4 (2)	1.2 (4)	-	-	2.6
Anhydrite	4.8 (6)	-	-	-	4.8
Halite	-	-	.8	-	.8
AVERAGES	4.2	1.1	.5	3.9	2.5

(6) number of measurements

* 1 - Hurtig and Brugger (1970), 2 - Clark (1941),

3 - Bridgman (1924), 4 - Anand et al. (1973)

3.7 The Correction of Thermal Conductivity Data for In-Situ Temperature

The transport of heat by lattice waves in solids is governed by anharmonicities of the lattice forces, imperfections and external boundaries. These travelling lattice waves, or phonons, transmit energy down a thermal gradient. At the molecular level the transfer of heat occurs during interaction of two thermally vibrating particles with differing amounts of energy. Where the thermal gradient is constant the energy flow is also constant and its magnitude is dependent on the lattice wave velocity, the heat capacity of the medium and the degree of wave scattering, all of which are temperature dependent.

At very low temperatures conduction by lattice waves is limited, in crystalline material, by the grain boundaries. This is due to the fact that the mean free path of the lattice waves can not exceed the crystal dimensions (Casmir, 1938). At higher temperatures, but still low in an absolute sense, heat transmission is more effective as the lattice wavelength decreases. At such temperatures the effects of wave scattering, which result from local velocity fluctuations and tend to reduce heat transfer, are not significant. At intermediate temperatures scattering becomes effective and thermal conductivity ceases to increase with increasing temperature. The conductivity may be further reduced in this temperature range by impurities which increase wave scattering. Finally at high temperatures the conductivity decreases due to increased lattice motion which leads to smaller mean free paths and still greater wave scatter.

The variation of thermal conductivity with temperature is known to be considerable and is thus of great importance to a study such as this where in-situ temperature may be as much as 150^{o}C greater than that at which the laboratory determination was made. What is required is a general theory which will relate the in-situ conductivity to the in-situ temperature and the laboratory conductivity value.

Debye (1914) proposed the relation, for crystalline materials, of,

$$(3.39) \qquad K = \frac{3\, p v^5 c}{16\pi^3 (3\alpha^2 + 1)\, x_0\, \gamma^4\, B_k T}$$

where K is thermal conductivity at temperature T (^oK), p is density, v is the velocity of the lattice waves, c is specific heat, B_k is Boltzmann's constant, x_0 is the compressibility at T = 0^oK, and α is the ratio $(x/p)T/(x/p)_0$ where the subscribts refer to temperature T and zero. At temperatures where the heat capacity is a constant, K varies as 1/T but at low temperatures the heat capacity varies as T^3 and thus K varies as T^2 (Kingery and MacQuarie, 1954).

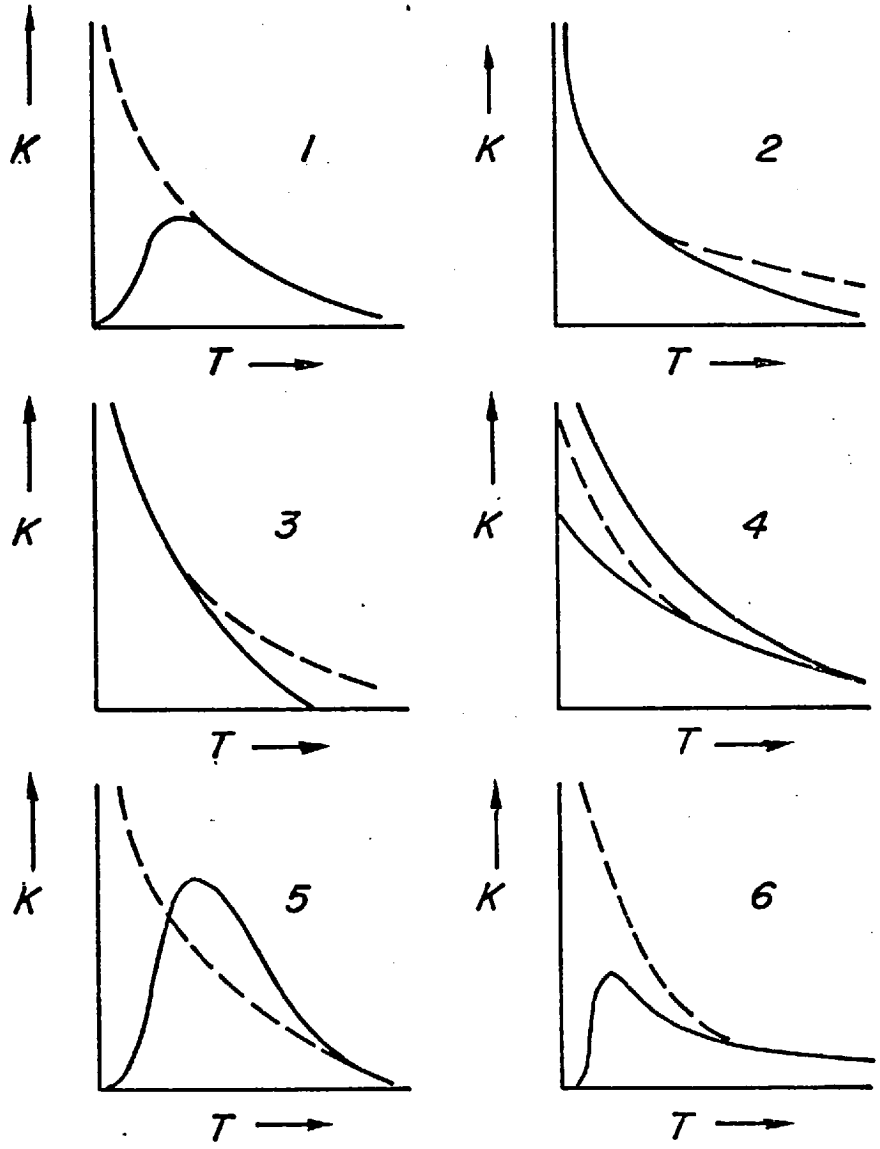
Several other theoretical studies have been made (Compton, 1916, Endo, 1922, Peierls, 1929, Papaetru, 1934, Makinson, 1938) on the dependence of conductivity with temperature for crystalline material. All of these relations are, at high temperatures, of the form,

$$(3.40) \qquad K = (a + b \cdot T)^{-1}$$

where a and b are constants and T is greater than a particular low value of temperature near absolute zero. These various relations are schematically illustrated in Fig. 3.9 (after Kingery and MacQuarie, 1954).

The only other class of nonmetallic solids to have been studied in detail for conductivity dependence of temperature are glasses which include many ceramics and plastics. Glasses have no structural symmetry or periodicity and as such the thermal vibration interaction of their atoms differs from those of crystals although heat transmission may still be resolved in terms of waves, (Klemens, 1958). Above room temperature their mean free path is effectively constant, although very small, and the thermal conductivity increases in proportion to the heat capacity (Kittel, 1949).

GENERAL RELATIONS PROPOSED FOR VARIATION OF THERMAL CONDUCTIVITY (K) WITH TEMPERATURE (T)



1 Debye (1914)

2 Peierls (1929)

3 Compton (1916)

4 Papapetru (1934)

5 Endo (1922)

6 Makinson (1938)

——— Various relationships

– – – – – – Relation -3.40 (inverse temp.)

FIG. 3.9.

This may be represented by a relation,

$$K = c \cdot T + d \tag{3.41}$$

where c and d are constants.

Crystalline and glass materials are the only groups of nonmetallic solids for which adequate theory exists to describe their conductivity temperature relations. Obviously neither represents, in general, a realistic approximation of a porous sedimentary rock - the bulk of the material measured for thermal conductivity in this study.

To date there have been only three major studies of the temperature dependence of conductivity on typical sedimentary rocks; those of Birch and Clark (1940), Tikhomirov (1968), and Anand et al. (1973). Bridgman (1924) and Sommerton and Boozer (1960), have conducted similar though much less extensive studies; Clark (1966) and Viloria and Ali (1968) have compiled thorough summaries of the research.

Birch and Clark (1940) found that results of most of their measurements, for a variety of rocks, conformed to relation (3.40), the crystalline model. The notable exceptions were dolomite, limestone and calcite for which conductivity decreased less rapidly than relation (3.40) and feldspar aggregates which exhibited behavior not unlike glasses, relation (3.41). They dismiss grain size and impurities as unimportant factors influencing the temperature dependence of rock conductivity.

Of the sedimentary rocks studied by Birch and Clark, quartzitic sandstone, limestone, and dolomite, only the sandstone, in this case a most untypical sample, conforms to crystalline theory. Important sedimentary rocks such as shales and more typical limestones and sandstones were, as Birch and Clark admitted, not studied though they did indicate a similar research project of these materials had been initiated. Results, if obtained, were never published.

Tikhomirov (1968) was the first to determine an empirical relationship between the thermal conductivity of a rock at any temperature and its conductivity at room temperature. He measured twenty-one igneous and metamorphic samples and obtained, by multiple regression analysis, the linear relation,

$$(3.42) \qquad \frac{d \log K_T}{d \log T} = .34 \cdot \log T - 1.61 \cdot \log K_{293} + .12$$

The coefficients in (3.42) were determined from sixty-eight measurements in the temperature range 293 - 1500°K, where K_T is the conductivity (cgs) at temperature T(°K), and K_{293} is the laboratory determined conductivity at temperature T = 293°K = 20°C. Rewriting (3.42) we obtain,

$$(3.43) \qquad K_T = .047 \cdot K_{293}^{4.98} \cdot T^{\left[.17 \log T - 1.61 \log K_{293} + .12\right]}$$

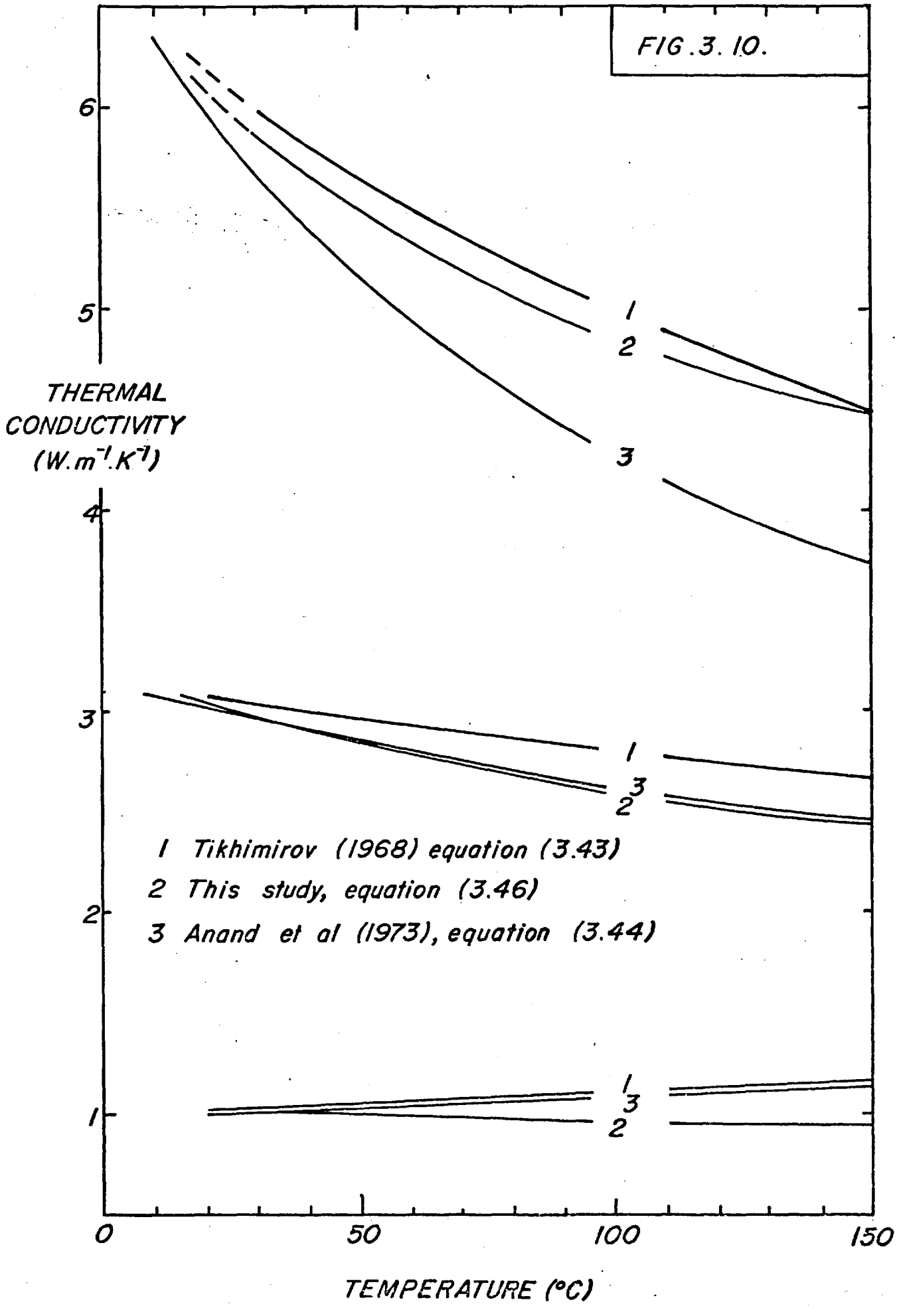
which is an extremely convenient form for the correction of conductivity for in-situ temperature. The predicted decrease in K_T with increasing temperature is less than that predicted by relation (3.40); at low values of K_{293}, K_T increases with increasing T. The relation (3.43) is illustrated, in S.I. units, for the temperature range of interest to this study in Fig. 3.10.

Anand et al. (1973) extended Tikhomirov's work by measuring water saturated sedimentary materials and obtaining the empirical relation,

$$(3.44) \qquad K_T = K_{293} - .00071 \cdot (T-528) \cdot (K_{293} - .80) \cdot \left[K_{293} \ (T \times 10^{-3}) - .55K_{293} + .74\right] \cdot K_{293}^{-.637}$$

with a correction provided by Sommerton (1974, personal communication), where K_T and K_{293} are as in (3.44) but in BTU · hr^{-1} · ft^{-1} · $^oF^{-1}$, and T is the temperature in °R, where °R = °F + 460. The measurements of Anand et al. have been in the range 20° - 260°C on sandstones with values of K_{293}

THERMAL CONDUCTIVITY AS A FUNCTION OF TEMPERATURE FOR 3 EMPIRICAL RELATIONS



in the range 1.3 to 5.1 $W \cdot m^{-1} \cdot k^{-1}$. Computation of coefficients in (3.44) was by nonlinear multiple regression analysis. The relation (3.44) is illustrated, in S.I. units, for the temperature range of interest to this study (Fig. 3.10). Note the close correspondence with Tikhomirov's relation except at high K_{293}.

The results of Tikhomirov and Anand et al. suggest that thermal conductivity decreases with temperature in a manner intermediate between that of relations (3.40) and (3.41) as was first noticed by Birch and Clark (1940) for three sedimentary samples.

In an attempt to verify the conductivity temperature dependence suggested by relations (3.43) and (3.44) a similar study on twenty-four selected samples was made. The divided bar apparatus described in section 2.3 was used to measure disc specimens, section 2.5, at five different temperatures. The variation of bar mid-point temperature was effected by raising or lowering the hot and cold reservoirs, Fig. 2.2, to $5^{o}C$ above and below the required value respectively. An exact determination of the midpoint temperature was then made with an absolute thermocouple, section 2.4.

Measurements were made at $10.22^{o}C$, $23.92^{o}C$, $49.26^{o}C$, $68.95^{o}C$, and $88.06^{o}C$; values higher than about $90^{o}C$ were not attempted as significant design modifications to the divided bar apparatus would have been necessary.

At each temperature it was necessary to recalibrate the divided bar (section 2.4) using fused and crystalline quartz as standards. These two materials, the former a glass, the latter crystalline, conform to relations (3.41) and (3.40) respectively where equations (2.6.1) and (2.6.2), after Ratcliffe (1959), describe their conductivity as a function of temperature.

The results of these calibrations are given in table 3.5. The larger error associated with the $88.06^{o}C$ calibration is undoubtedly due to heat losses, despite thick lagging, through the sides of the quartz discs and the upper and lower bar stacks. Calibration uncertainty at other temperatures

is uniform; no obvious change in contact resistance was observed (section 2.6).

Before attaching any significance to the sample results it is necessary to examine measurements made on 'control material' for which there is well documented data on its conductivity temperature dependence. Halite (NaCl) and Lexan were chosen as control material. The former, a crystalline material, has been measured by several workers and conforms to relation (3.40) with a large temperature coefficient. Lexan has been less well studied but should, in theory, behave as a glass (relation 3.41); it is also the material used as the reference in the divided bar.

Fig. 3.11(a) illustrates the conductivity results obtained for the halite, with values obtained by Birch and Clark (1940) added for comparison. Clark (1969) has computed the a and b constants, equation (3.40), for the Birch and Clark halite results; a and b values have also been determined by least squares for the measurements presented here, table 3.6. The halite values are in close agreement, particularly the temperature coefficient, with the classic Birch and Clark study and suggest that results obtained here on other samples will be quantitatively reliable.

The Lexan results gave a very consistent linear increase, Fig 3.11(b),with temperature, in agreement with expectations and with the bar calibrations, table 3.5. Munroe (1972) measured Lexan over a much smaller temperature range, Fig. 3.11(b), and obtained similar though less definitive results. Results for other polymers, after Kline (1961), are included in Fig. 3.11(b) for comparison. The Lexan data tends to support the halite results indicating that the divided bar is operating satisfactorily at the different temperature levels.

In order to detect if any permanent change occurred during these measurements in the thermal properties of the bar reference material measurements were not made in order of ascending or descending temperature but rather at 23.92°C, 49.26°C, 88.06°C, 10.22°C, 68.95°C and again at 23.92°C

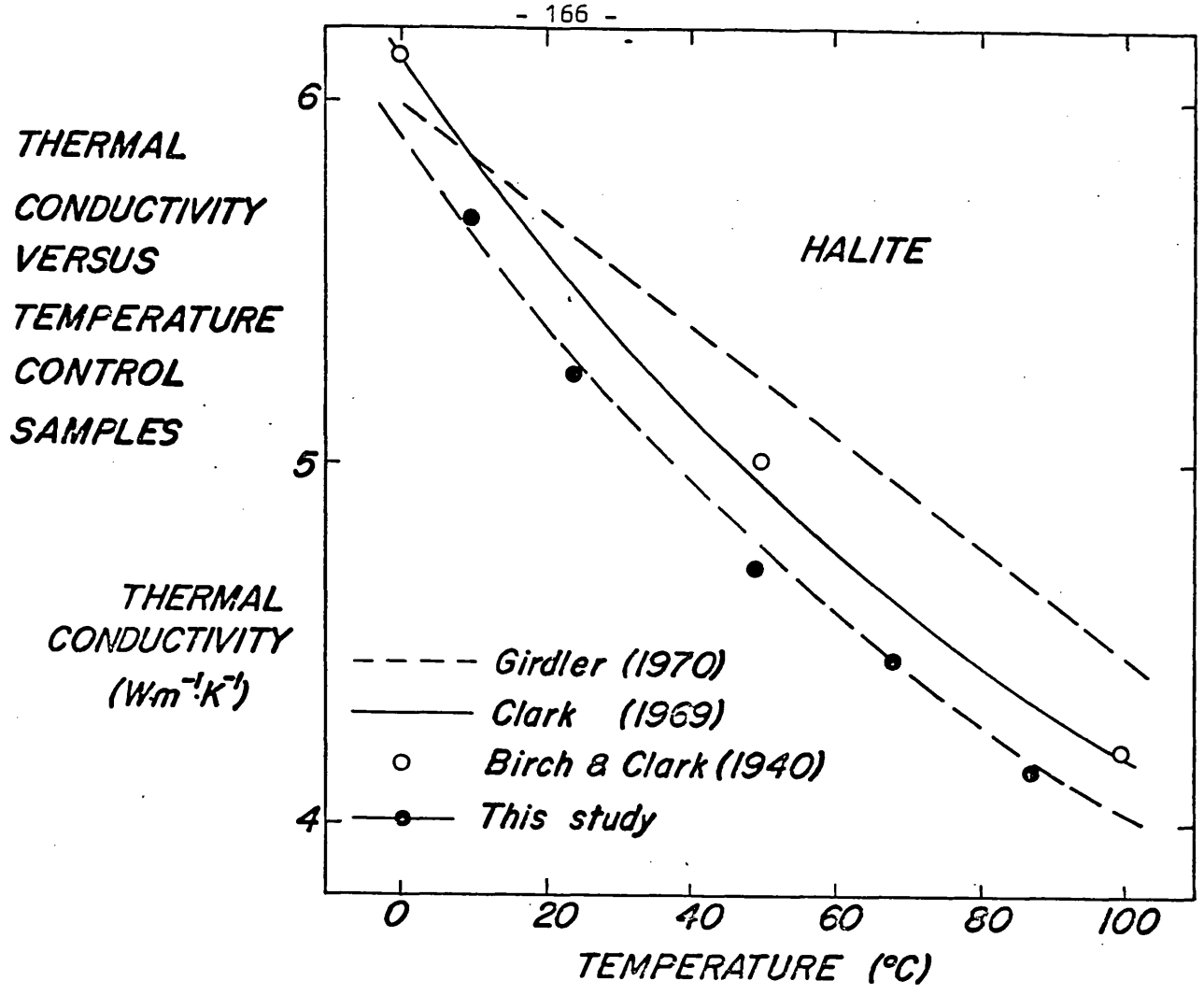


FIG.3.11(a)

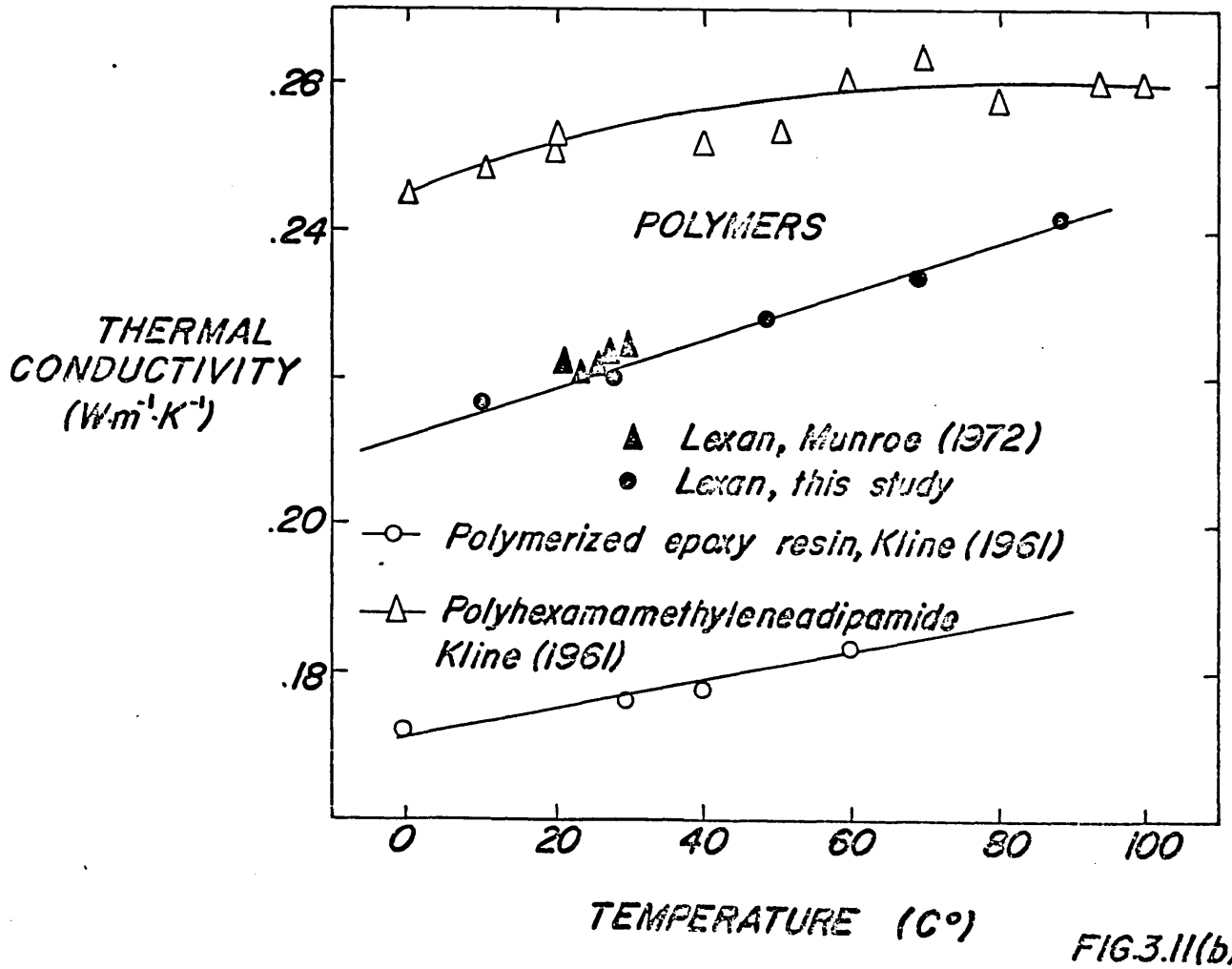


FIG.3.11(b)

with several repeat runs at each temperature. This allowed several internal checks and, as calibrations were also repeated, a check against fused and crystalline quartz which are known to not suffer any permanent change of thermal properties in this temperature range (Ratcliffe, 1959). No permanent change in either sample or bar reference material (Lexan) conductivity was observed.

The twenty-four samples analyzed are described in table 3.7 and conductivity results are given in table 3.8. In total one hundred and fifteen measurements were made. Measurements at the higher temperatures required up to forty minutes as the bar came to equilibrium much more slowly.

The data from table 3.8 was input to the multiple linear regression program MULTR described by Davis (1973). A linear equation of the form (3.42), Tikhomirov (1968), was solved for regression coefficients. Data from the 88.06°C was not used as it was probably less accurate than the remainder due to the poorer calibration. Ninety-two data values for twenty-three samples were thus used (sample DR1-001-A, table 3.8, had incomplete results) and gave the relation,

$$(3.45) \qquad \frac{d \log K_T}{d \log T} = -.0747 \log T - .0661 \cdot \log K_{23.92} + 3.199$$

where K_T and $K_{23.92}$ are the thermal conductivities in $mcal \cdot cm^{-1} \cdot s^{-1} \cdot {}^{o}c^{-1}$ at temperatures T°C and 23.92°C respectively. The formulation of (3.45) in cgs. units of conductivity will be explained in section 3.9. The multiple regression correlation coefficient (cf. Davies, 1973, pg. 198) was .63, comparable with that obtained by Tikhomirov.

Integrating (3.45) w.r.t. T from 23.92°C we obtain,

$$(3.46) \qquad K_T = .528 \cdot K_{23.92}^{1.21} \cdot T \left[-.0374 \log T - .0661 \log K_{23.92} + .320 \right]$$

which is shown in S.I. conductivity units in Fig. 3.10. At high $K_{23.92}$ the

relation (3.46) approximates that of Tikhomirov while for intermediate $K_{23.92}$ it is virtually identical to that of Anand et al. over the temperature range of interest to this study. At low $K_{23.92}$ (3.46) diverges from the Tikhomirov and Anand et al. relations as expected. This is due to the fact that none of the low $K_{23.92}$ samples, table 3.8, showed a significant increase in conductivity with increasing temperature.

Figs. 3.12, 3.13, and 3.14 graphically show the results of table 3.8 with various curves of the form (3.46) superimposed. The qualitative agreement is obvious.

Relation (3.46) was used to reduce all laboratory measured conductivities, $K_{23.92}$, to values at in-situ temperature T. Details of computation and assessment of results will be given in section 3.9 and Chapters 4 and 5 respectively. Further comments on conductivity temperature dependence are made in section 3.10.

THERMAL CONDUCTIVITY OF VARIOUS ROCKS MEASURED IN THE TEMPERATURE RANGE 10-90°C

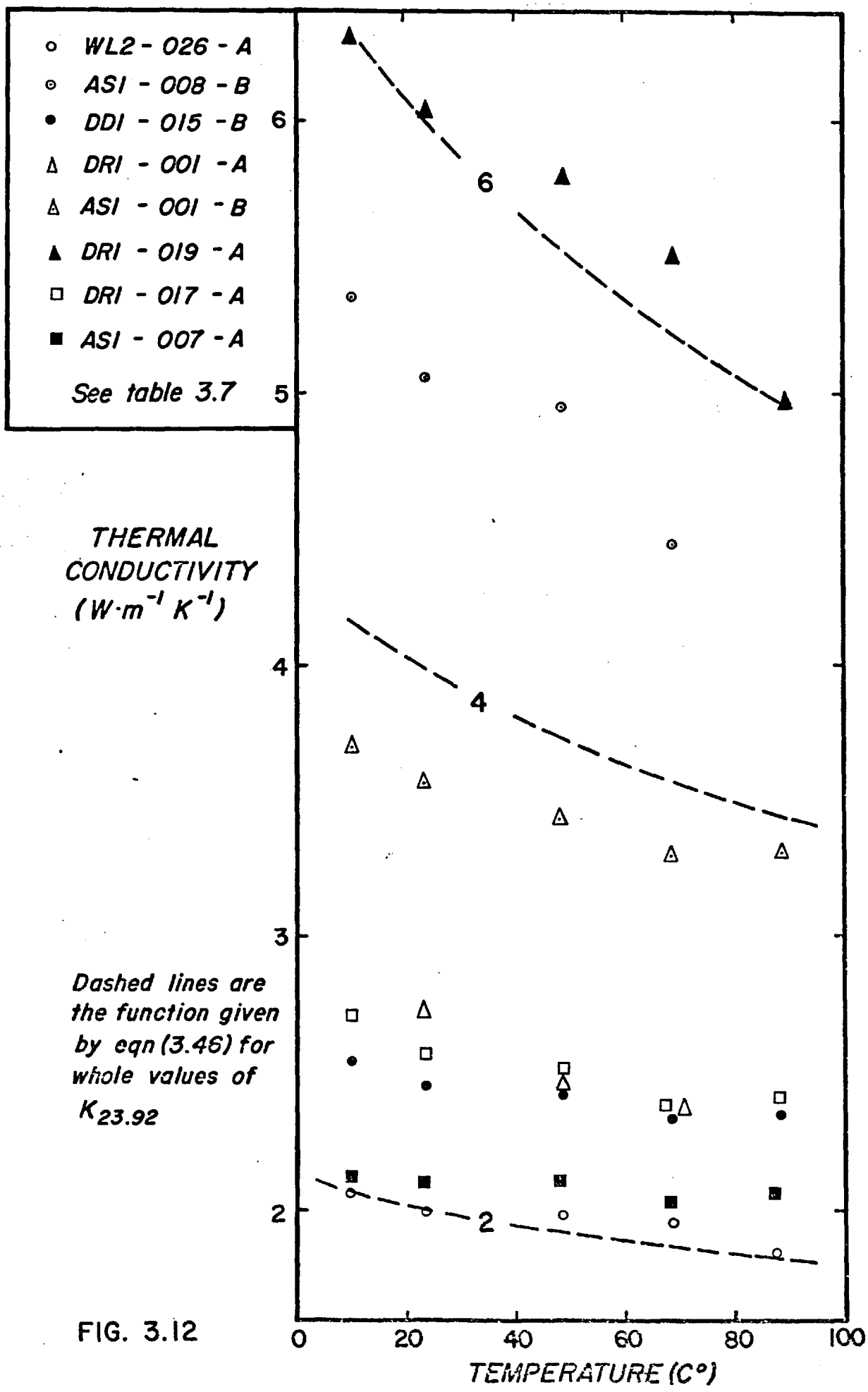
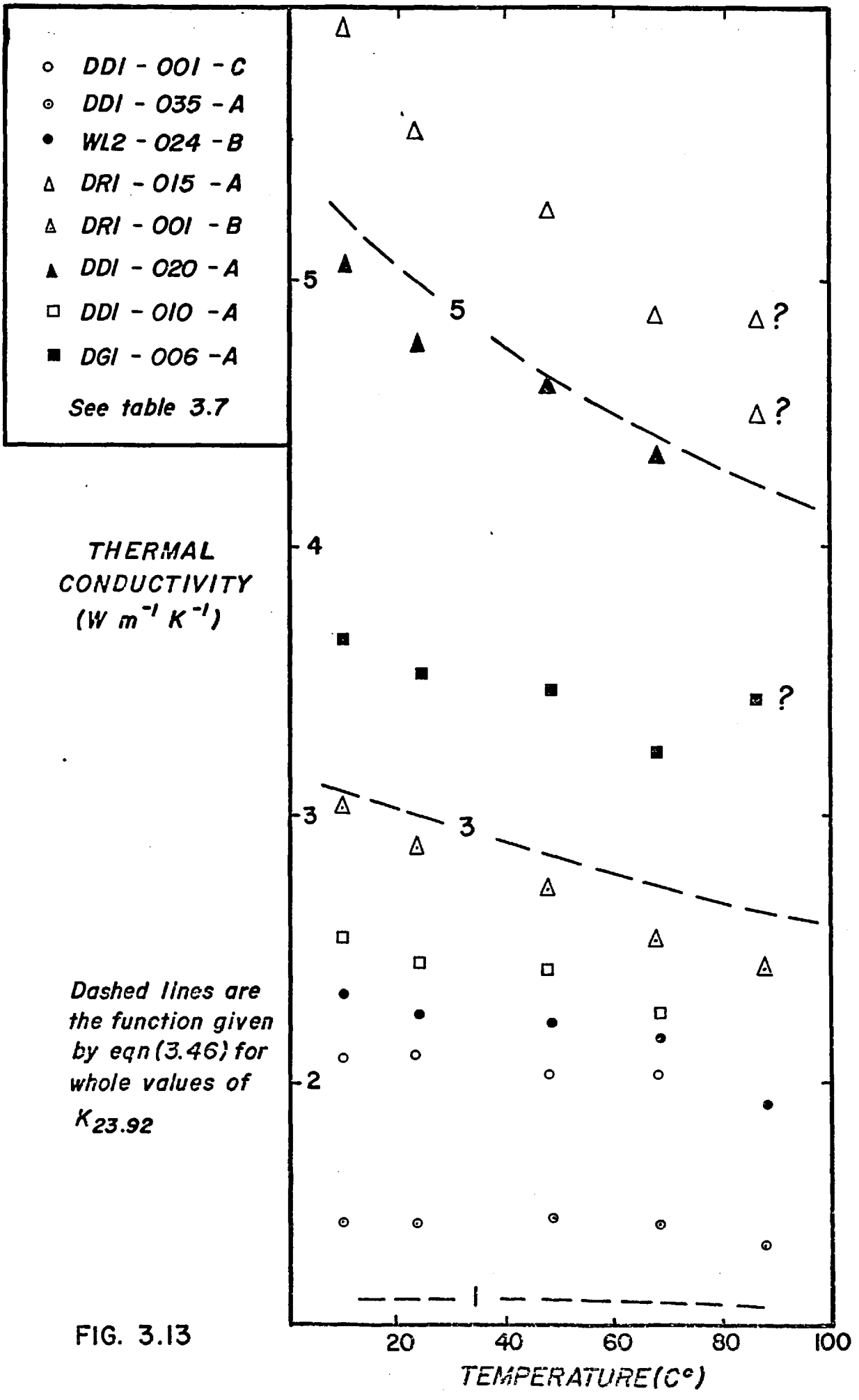


FIG. 3.12

THERMAL CONDUCTIVITY OF VARIOUS ROCKS MEASURED IN THE TEMPERATURE RANGE 10-90°C



Dashed lines are the function given by eqn (3.46) for whole values of $K_{23.92}$

FIG. 3.13

THERMAL CONDUCTIVITY OF VARIOUS ROCKS MEASURED IN THE TEMPERATURE RANGE 10-90°C

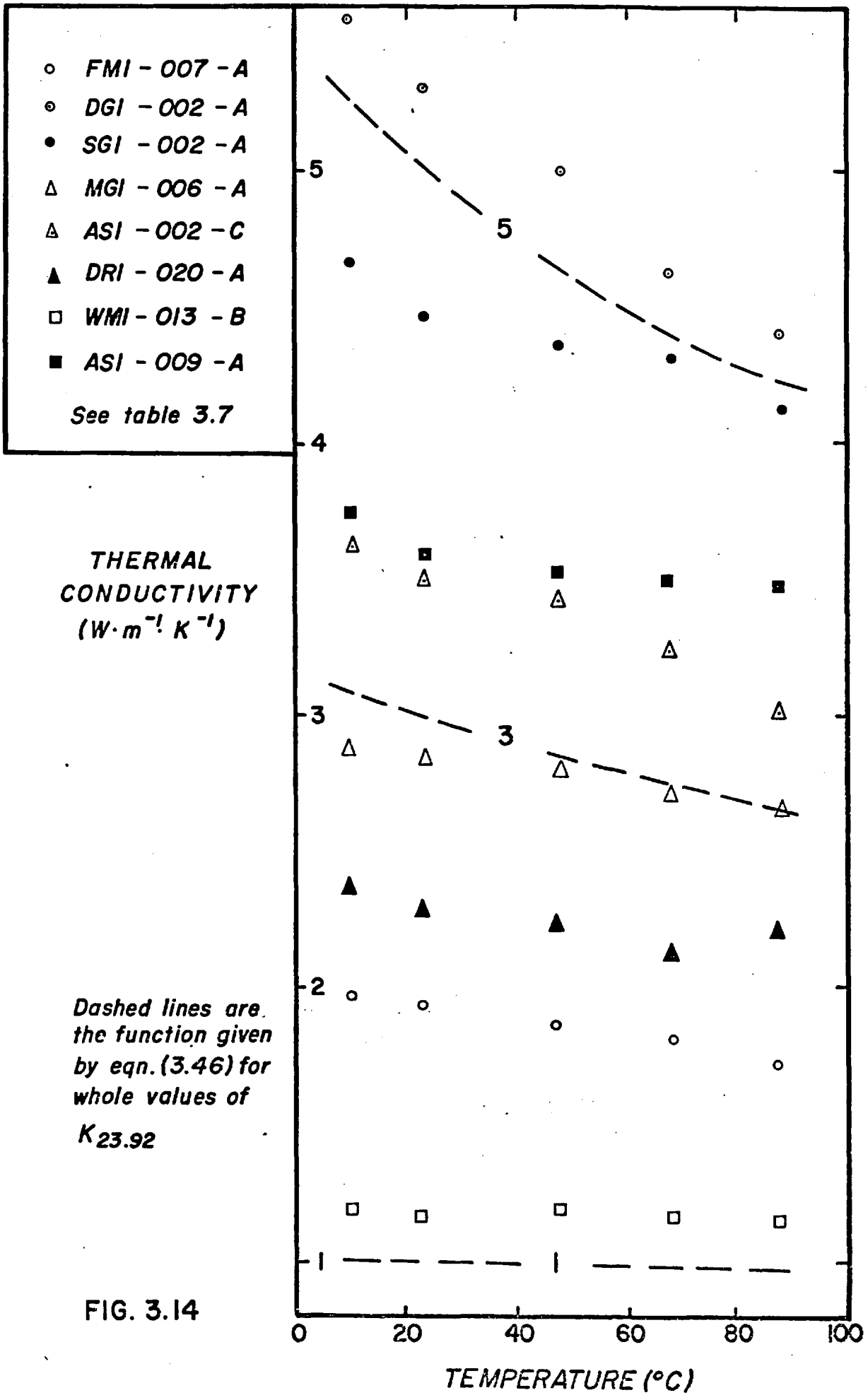


FIG. 3.14

Table 3.5

Divided Bar Calibrations At

Various Mid-Point Temperatures

$W \cdot m^{-1} \cdot K^{-1}$

Bar Temperature °C	Fused Quartz[1] K_{fq}	Crystalline Quartz[2] K_{cq}	Bar Calibrations $(K_b)^3$		
			Fused Qtz.	Cryst. Qtz.	Mean
10.22	1.342	6.626	.222 ± .001	.218 ± .001	.221
23.92	1.369	6.199	.226 ± .000	.219 ± .001	.222
49.26	1.401	5.764	.229 ± .001	.220 ± .000	.225
68.95	1.424	5.409	.236 ± .001	.228 ± .003	.232
88.06	1.440	5.104	.239 ± .004	.229 ± .007	.235

1, 2, 3 - See equations (2.6.1),(2.6.2)and (2.7) respectively.

Table 3.6

Coefficients a and b in the

Equation $K = (a + bT)^{-1}$, (3.40)

For Halite (NaCl)

Reference	a	b
Clark* (1969)	-22	.330
This study	-19.3	.331

* Clark (1969) used the Birch and Clark (1940) data.

Table 3.7

Descriptions of Samples Measured for Thermal Conductivity in the Range 10^{o} - 90^{o}C

Sample	Description	Well Name	Depth Metres	Age	Country
DD1-001-C	Gy., sft., f.g., s.c., arg., sst.	Dodori-1	2119	M. Eocene	Kenya
DD1-035-A	Gy., blk., silty shale	Dodori-1	4129	U. Cret.	Kenya
WL2-024-B	Siltstone	Walu-2	3086	L. Cret.	Kenya
WL2-026-A	Claystone	Walu-2	3225	L. Cret.	Kenya
FM1-007-A	Chalk, porous	Fetcham Mill	?	U. Cret.	U.K.
DD1-010-A	Grey oolitic limestone	Dodori-1	2878	L. Eocene	Kenya
DD1-015-B	Dense, n.p., micritic limestone	Dodori-1	3172	Paleocene	Kenya
DR1-015-A	Nodular anhydrite	Darin-1	2255	U. Jurassic	Somalia
DD1-020-A	Gy., f.g., n.p., calc. sst.	Dodori-1	3529	Paleocene	Kenya
AS1-008-B	n.p., c.g., qtz., sandstone	Abu Shagara-1	2202	?	Sudan
DR1-001-B	c.g., soft, calcarenite	Darin-1	193	U. Eocene	Somalia
DR1-001-A	c.g., soft, calcarenite	Darin-1	193	U. Eocene	Somalia
DR1-019-A	c.g., qtz., mic., sandstone	Darin-1	2840	L. Jurassic	Somalia
SG1-002-A	n.p., massive dolomite	Sagaleh-1	664	M. Eocene	Somalia
DG1-002-A	Gy., massive anhydrite	Dungunab-1	568	M. Miocene	Sudan
AS1-001-B	Gy., grn., dense, reefal, lst.	Abu Shagara-1	885	M. Miocene	Sudan
MG1-006-A	Altered rhyolite	Maghersum-1	1778	?	Sudan
AS1-007-A	Basalt	Abu Shagara-1	2001	?	Sudan
DR1-020-A	Biotitic schist	Darin-1	2971	?	Somalia
DG1-006-B	Granite	Dungunab-1	1463	Pre-Camb?	Sudan
DR1-017-A	Dense, n.p., argil., limestone	Darin-1	2648	M. Jurassic	Somalia
AS1-002-C	Breccia, ign., ang., frags.	Abu Shagara-1	1163	M. Miocene	Sudan
WM1-013-B	Pyritiferous, mudstone	Wal Merer-1	3760	L. Cret.	Kenya
AS1-009-C	Grn./White, marble	Abu Shagara-1	2254	?	Sudan

Table 3.8

Thermal Conductivity of Various Sedimentary, Igneous and Metamorphic Rocks in the Temperature Range 10^{o} - 90^{o}C

Sample	Thermal Conductivity ($W \cdot m^{-1} \cdot K^{-1}$)				
	10.22	23.92	49.26	68.95	88.06 ^{o}C
DD1-001-C	2.08(2)	2.11(2)	2.01	2.03	-
DD1-035-A	1.48	1.49(2)	1.50(2)	1.48	1.39
WL2-024-B	2.33	2.25(2)	2.23(2)	2.17	1.92
WL2-026-A	2.06	1.99	1.98	1.95	1.84
FM1-007-A	1.96	1.93	1.87(2)	1.81	1.71
DD1-010-A	2.54(2)	2.45	2.42	2.27	-
DD1-015-B	2.54(2)	2.45	2.44	2.33	2.35
DR1-015-A	5.93	5.55(2)	5.29	4.83	4.89
DD1-020-A	5.05(2)	4.76	4.60	4.34	4.51
AS1-008-B	5.34(2)	5.06(2)	4.97	4.42	-
DR1-001-B	3.02	2.88	2.71	2.53	2.42
DR1-001-A	-	2.71	2.39	-	2.32
DR1-019-A	6.32	6.04(2)	5.82	5.51	4.96
SG1-002-A	4.66	4.47(2)	4.37	4.31	4.13
DG1-002-A	5.54	5.30(2)	5.02	4.64	4.41
AS1-001-B	3.70	3.58(2)	3.49(2)	3.29	3.31
MG1-006-A	2.88	2.85	2.80(2)	2.72	2.66
AS1-007-A	2.13	2.12(2)	2.13(2)	2.01	2.07
DR1-020-A	2.37(2)	2.28(2)	2.24	2.11	2.21
DG1-006-B	3.65(2)	3.53	3.49	3.22	3.42
DR1-017-A	2.69(2)	2.57	2.49	2.38	2.44
AS1-002-C	3.61	3.47(2)	3.44	3.27	3.01
WM1-013-B	1.19	1.15(2)	1.21(2)	1.16	1.15
AS1-009-A	3.71	3.59	3.53	3.50	3.49

(2) mean of two measurements

3.8 Estimation of Parameters in the Calculation of Heat Flow

A common difficulty encountered in the use of oil exploration borehole data for heat flow calculations is incomplete information.

Of the sixty-eight boreholes from Eastern Africa, nine had only a single BHT while a further twelve had but two. In addition eleven other holes, with between three and six BHTs each, were adjudged to have an inadequate coverage of temperature with depth; ie. a three kilometre borehole with four BHTs all below 2.2 Km. A single North Sea well, for which conductivity data was available, had but one BHT.

Obviously some estimate of mean annual surface temperature is required to augment the BHT data in these three cases. The use of mean annual surface temperatures is accepted as a method of computing geothermal gradients from single BHTs in the oil industry, (cf. Moses, 1961), although results obtained will be less satisfactory.

Table 3.9 is a compilation of mean annual surface temperatures from Eastern Africa. The bulk of the data are from Griffiths (1972); single values from Clift (1956) and Brewer and Spencer (1969) are also included. These values were applied, where necessary, to the nearest borehole; heat flow values computed from such data will be clearly labelled. Mean annual bottom temperature in the North Sea is a function of depth (Defant, 1961). Fig. 3.4, after Evans and Coleman (1974) was used to estimate the single North Sea value.

In one instance a group of five boreholes with one or two BHTs were located between two stations of widely differing elevation, table 3.9. In this instance borehole elevations were known and, since the lapse rate is approximately constant, direct interpolation was used to obtain surface temperatures.

It was possible to obtain and measure core and/or chips for conductivity for only twenty-five of the sixty-eight Eastern Africe boreholes.

Of these twenty-five, several lacked samples for one or two major lithologic units. Some estimate of thermal conductivity was therefore required. Joyner (1961) and Judge (1971) have convincingly demonstrated that where adequate lithologic descriptions of major formations are available, reasonable estimates of conductivity may be made.

Table 3.10 formed the basis for such estimations in this study. Fifteen lithologic classes, largely sedimentary, are summarized for conductivity measurements made by or tabulated by Birch and Clark (1940), Zierfuss and van der Vliet (1956), Sommerton (1958), Clark (1966) and Kappelmayer and Haenel (1974). In addition, a review of seventy disc measurements made during this study is also incorporated. This was thought to be particularly relevant data as most of the samples tabulated were assigned lithologies by well-site geologists. As the eventual estimation of conductivity will be also based on well-site geologists' evaluation of rock type, this study has obvious advantages. Averages are tabulated, column 8, table 3.10, for the fifteen basic lithologies and were assigned to corresponding depth intervals where such data was lacking. Where two or more of the basic lithologies were mentioned in a given interval, ie. interbedded sandstones and shales, the harmonic mean of the revelant values was assigned. In a few instances where conductivity measurements were made on an equivalent lithology in a nearby well, these values were assigned; conductivities estimated in this manner are thought to provide a better result.

Estimation of conductivity for North Sea boreholes was less involved; again only one borehole required such values. Suitable equivalent samples had been measured in the other two wells and were assigned. The North Sea conductivity data is particularly useful to check the hypothesis of Judge (1971) who states that where the major lithologic units are well mapped and described, conductivity data may be extrapolated for considerable distance from a borehole within a sedimentary basin. We will

return to these considerations in Chapter 5.

Computation of heat flow, the effects on errors, and the classification of conductivity, both estimated and measured, will be discussed in section 3.9.

Table 3.9

Mean Annual Surface Temperatures

For Eastern Africa

Country	Locality	Lat.	Long.	Mean Temp. °C	Years Record	Elevation metres	Ref.*
Kenya	Garissa	0°29'S	39°38'E	28.5	23	128	1
Somalia	Mogadiscio	2°02'N	45°21'E	27.0	48	17	1
Somalia	Lugh Ferrandi	3°45'N	42°35'E	30.5	36	198	1
Kenya	Mandera	3°57'N	41°52'E	29.0	27	331	1
Somalia	Galcaio	6°46'N	47°25'E	27.5	26	240	1
Somalia	Berbera	10°26'N	45°02'E	30.0	30	8	1
Somalia	Erigavo	10°37'N	47°22'E	17.0	14	1730	1
Sudan	Port Sudan	19°35'N	37°13'E	29.0	30	5	1
Kenya	Mombasa	4°02'S	39°37'E	26.5	17	55	1
Tanzania	Dar-es-Salem	6°50'S	39°18'E	26.0	14	14	1
Tanzania	Mitwara	10°16'S	40°11'E	26.0	6	113	1
Somalia	Bender Casim	11°17'N	49°11'E	29.5	12	6	1
Ethiopia	Ogaden	-	-	26.3	-	-	2
Ethiopia	Red Sea	-	-	26.0	-	-	3

* References: 1 - Griffiths (1972)
2 - Clift (1956)
3 - Brewer et al. (1969)

Table 3.10

Summary of Thermal Conductivity

For Various Rock Types

Rock Type	References *						$W \cdot m^{-1} \cdot K^{-1}$ Average
	1	2	3	4	5+	6	
Anhydrite	5.26(7)	-	5.61(3)	-	-	-	5.44
Clay	2.22(3)	-	-	-	-	-	2.22
Clay Marl	2.04(7)	-	1.47(5)	-	-	-	1.76
Claystone	2.38(15)	-	-	-	-	1.87(4)	2.13
Dolomite	4.54	-	5.06(15)	-	4.65	-	4.75
Limestone	2.83(6)	2.22(9)	2.60(31)	3.55	2.63(2)	2.52(9)	2.72
Limestone Marl	2.12(8)	-	2.19(5)	-	-	1.57(5)	1.96
Halite	5.52(14)	-	6.03(10)	-	5.57	-	5.71
Sandstone	3.24(54)	3.41(37)	2.82(29)	2.75	-	2.90(7)	3.03
Siltstone	-	-	-	1.79	-	2.54(13)	2.17
Mudstone	-	-	-	-	-	1.78(20)	1.78
Shale	-	-	1.72(54)	1.69	-	2.03(11)	1.81
Sandy Marl	-	3.16(3)	-	-	-	1.62	2.39
Basalt	1.67(30)	-	-	-	-	-	1.67
Gabbro	2.21(7)	-	-	-	2.14(2)	-	2.18
Total measmnt.	146	49	152	4	6	70	427

* References:
1 - Kappelmeyer and Haenel (1974)
2 - Zierfuss and van der Vliet (1956)
3 - Clark (1966)
4 - Sommerton (1958)
5 - Birch and Clark (1940)
6 - This study

+ values interpolated from 0^{o} and $50^{o}C$ results.

3.9 The Computation and Correction of Heat Flow Values - Computer Use, Data Presentation and Errors

The heat flow values were calculated with the aid of a digital computer. A main data reduction and correction program was written incorporating the Bullard method, as described in section 3.2, and the correction techniques discussed in sections 3.4 - 3.7 inclusive. The program is schematicized in Fig. 3.15.

The basic data, temperature and conductivity values and their depths, were input for each borehole. The depth values were corrected to ground level or, in the case of an offshore well, to sea bed.

All conductivity data measured was input; selection and assignment of depth intervals was automatic. Selection of a single conductivity value, for a given depth, was made by first checking for a multiple disc result with an error, at the one standard deviation level, of two percent of its value or better. If there was a multiple set disc which failed this criterion, or if the multiple set contain only two discs, a harmonic mean of the single values was assigned. If only a single disc was available this result was assigned. At the next level, if chip results only were measured then the value was used; results corrected for porosity were assigned in preference to those without. Where no measurements were made then estimates (see section 3.8) were used; lithologically equivalent values being preferred to results obtained from lithologic comparison. Thus there are seven levels of conductivity data quality. These are summarized in table 3.11 and assigned to the individual results, in brackets following the conductivity value, in the data listing, Appendices 5 and 6 for Eastern Africa and the North Sea respectively. Depth intervals for the conductivity values were assigned as described in section 3.2

Having 'preprocessed' the basic data and produced the listings given in Appendices 5 and 6, it is straightforward to reduce the conductivity

SCHEMATIC PROCESSING FLOW CHART FOR HEAT FLOW DATA

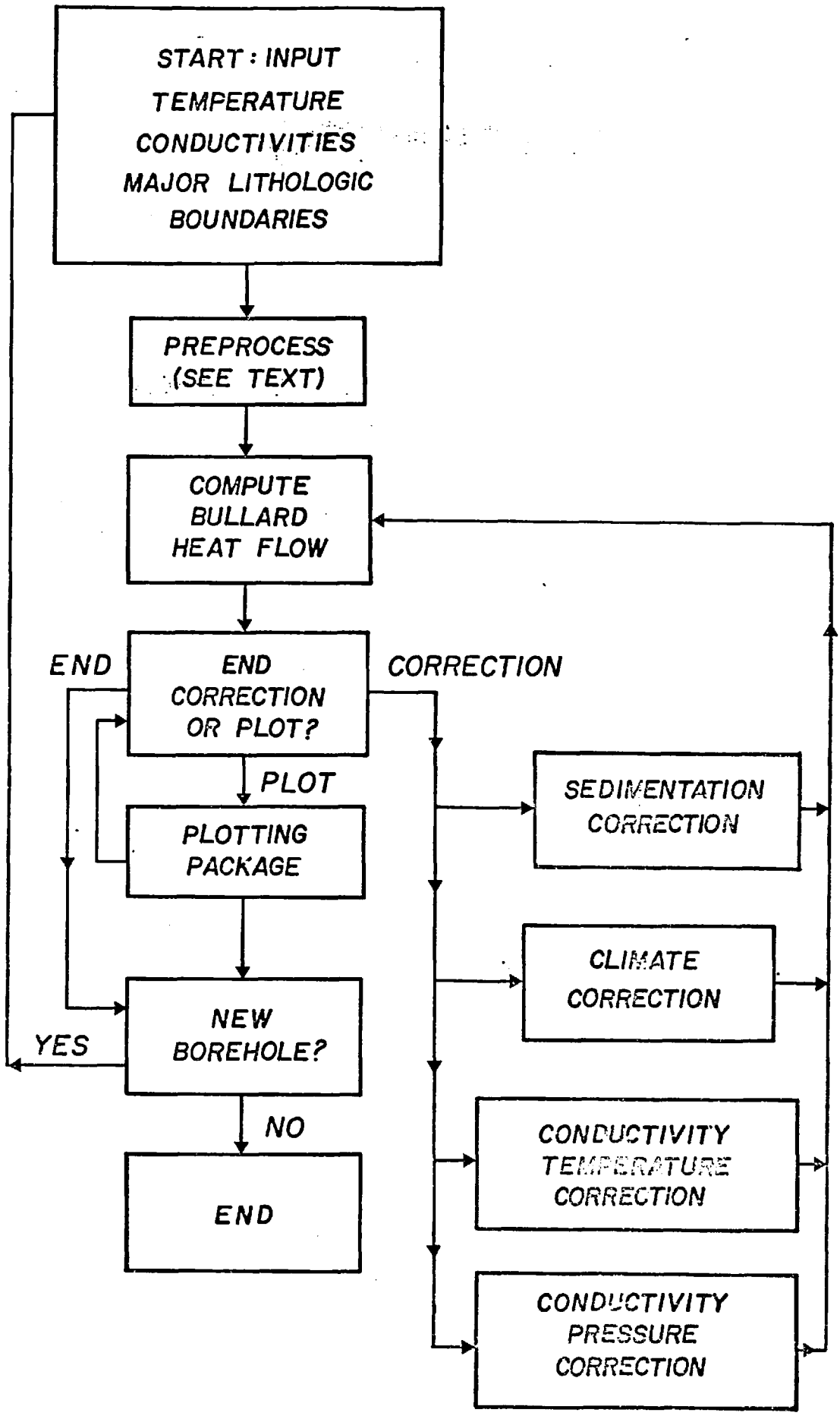


FIG. 3. 15.

and temperature values to heat flow results. First a 'raw data' uncorrected heat flow value was computed by the Bullard method. Then the conductivity temperature dependence, conductivity pressure dependence, sedimentation (where parameters known) and climatic (North Sea only) corrections were applied. Following each individual correction a new heat flow value was computed by the Bullard method. In the case of the climatic and sedimentation corrections equations (3.20) and (3.31) respectively were used to modify the temperature arrays; for the pressure and temperature conductivity corrections equations (3.38) and (3.46) respectively were applied. Diffusivity values were computed for climatic and sedimentation corrections by using a single value for the hole; this was implicit in the derivation of equations (3.20) and (3.31). Diffusivity values were calculated from the overall weighted harmonic mean conductivity, equation (3.2), divided by the product of the average porous sedimentary density, 2400 $kg \cdot m^{-3}$, and mean specific heat, 840 $J \cdot kg^{-1} \cdot K^{-1}$, (Kessler, 1927). C.g.s. units were used throughout for calculations and S.I. equivalents displayed only for final values. This facilitated comparison with literature values which are almost entirely in the older units.

A second program to produce composite computer-drawn plots of the 'raw' data together with the heat flow computation was also written. These plots, incorporated into the text of Chapters 4 and 5, display temperature values, conductivity as incremental steps each representing a measurement or estimate, and heat flow values. A geologic column with lithologic and age descriptions, where available, together with basic well data (name, company drilled by, latitude, longitude, and country) were also displayed. A dashed line along the temperature depth trend is the predicted temperature profile for constant heat flux as determined by the Bullard method for all temperature data. The corresponding weighted harmonic mean gradient, equation (3.3), is also plotted near this line. The heat flow value determined by the Bullard method using all the temperature data, is

shown as a solid line; the error bars correspond to plus and minus two standard deviations (95% confidence) of fit, equation (3.4). Where sufficient temperature data existed, ie. three of more BHTs, two further Bullard heat flow values were calculated and displayed as dashed lines. These correspond, in general, to depth intervals ranging from the shallowest to middle and middle to deepest temperature points.

At present, the internal consistency of the data is the only available basis for the estimation of reliability of a heat flow value (King and Simmons, 1972). Thus the error of fit in the Bullard method, equations (3.1) and (3.4), has little meaning as a realistic estimate of error. However, the two subsidiary calculations of heat flow, as described above, will be better indicators of the degree of confidence which may be placed in the result. The assignment of some estimate of error to heat flow values is fraught with difficulties; the error in the gradient and conductivity may be ten and fifteen percent respectively, sections 1.8 and 2.15. The total, twenty-five percent, while probably a reasonable 'average' for this study, is thought to be unrealistic for many values. It was, therefore, necessary to evaluate each hole individually assigning four quality grades, A, B, C, and D corresponding to 0 - 15%, 15 - 30%, 30 - 50%, >50% estimated error. The grade was assigned by consideration of data consistency, quality and quantity and must be regarded as much as a qualitative assessment as opposed to quantitative estimate of error.

The computation of intermediate heat flow values following each correction of data (see above) facilitated an evaluation of the correction. Results and comments on the heat flow values follow in Chapters 4 and 5.

Table 3.11

Classification of Thermal

Conductivity Data

Classification Number *	Description
1	multiple disc set, error <2%
2	multiple disc set, error >2%
3	single disc
4	chip measurement with porosity
5	chip measurement without porosity
6	estimated conductivity (equivalent)
7	estimated conductivity (Table 3.10)

* These numbers are found in brackets following every conductivity value listed in Appendices 5 (Eastern Africa) and 6 (North Sea).

3.10 Recommendations for Future Research

The effect of pressure on thermal conductivity is very poorly understood. This is especially true of porous sedimentary rocks where only a few controlled compression measurements have been made. It is obviously of some importance to initiate a detailed study of this effect although the design and building of a suitable system will be both expensive and time-consuming.

The effect of temperature is better understood though it would be useful to extend the range of the measurements presented in section 3.7 above 100°C. As was stated extensive modifications of the divided bar apparatus would be necessary though in this instance it should prove less expensive. It would be particularly interesting to further study the anhydrite samples measured in section 3.7 in view of the relatively small temperature coefficients so far obtained. A combined experimental high pressure high temperature conductivity apparatus would be ideal.

Finally, there were several aspects not touched on in consideration of corrections to be applied to the data (cf. Jaeger, 1965) though most or all were thought to be insignificant here. However, the interstitial fluids of the sediments themselves have pressure and temperature dependent conductivities, ie. water conductivity increases with both parameters (Powell, 1958, and Lawson et al., 1959). Preliminary calculations indicate that the effect would be small though perhaps worth considering in future detailed heat flow studies.

Chapter 4

Eastern Africa Heat Flow Results And Interpretation

4.1 Introduction

Eastern Africa, as considered here, extends from the Egypt/Sudan border south to the Tanzania/Mozambique boundary and includes the countries of Sudan, Ethiopia, Somalia, Kenya and Tanzania. The heat flow results presented are all from boreholes in the virtually continuous, often narrow, sedimentary basin fringing some five thousand kilometres of coastline from the central Red Sea to the northern approaches of the Mozambique Channel.

The boreholes themselves were drilled by nine different oil companies during the period 1954-1972. These wells, shown in Fig. 4.1, represent all of the temperature logged oil exploration holes in Eastern Africa up to the end of 1972.

Tectonically the area is considered an Atlantic type continental margin or as LePichon et al. (1973) have described it, 'a fossil accreting plate boundary' where the transition of continental rift to open-ocean accretion occurred. However, the Red Sea is generally held to be in the proto-ocean phase and so for convenience of discussion will be dealt with in a separate section of this chapter. Regional discussions will, thus, be divided by a line of latitude, in this case 15^{o}N.

The regional discussions will include geology, tectonics, geophysical surveys and an assessment of heat flow new and old; subregions will be considered individually with analyses of local structure, heat sources, etc. A series of interpretation sections concludes the chapter.

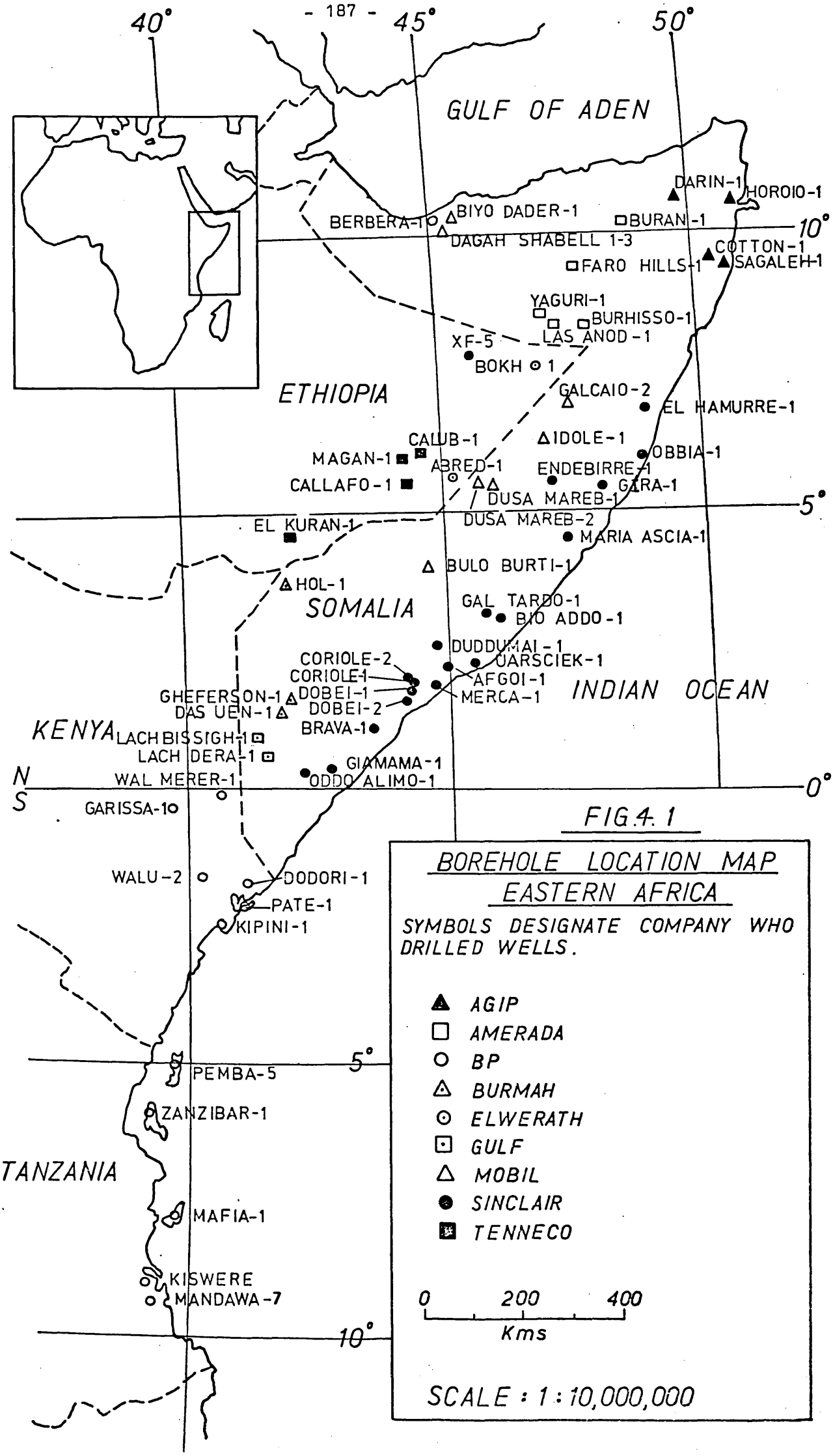


FIG.4.1

BOREHOLE LOCATION MAP EASTERN AFRICA

SYMBOLS DESIGNATE COMPANY WHO DRILLED WELLS.

- ▲ AGIP
- □ AMERADA
- ○ BP
- △ BURMAH
- ⊙ ELWERATH
- ⊡ GULF
- △ MOBIL
- ● SINCLAIR
- ■ TENNECO

While every attempt has been made to incorporate all previous pertinent research it is, of course, quite impossible to give a thorough review or treatment to all such work when dealing with so vast an area.

4.2 The Regional Geology of Eastern Africa (South of 15°N)

The African continent, apart from the Atlas Mountains which comprise an uplifted Cenozoic geosyncline, is a platform and is largely underlain by a folded Precambrian basement. The Precambrian basement system is composed of a number of shields, or cratonic nucleii, comprising rocks older than 2200 m.y. which are separated by younger mobile belts. These belts, which are characterised by a migmatitic type intermediate P-T metamorphism (Saggerson, 1973) are, in general, the foundation on which the transgressive deposition of the Paleozoic and post Paleozoic sedimentary basins took place.

In Eastern Africa the metamorphic basement described above is generally referred to as the Mozambique belt. Holmes (1951) states that these rocks represent the uplifted and eroded deep interior of an orogenic belt; its origin was most probably that of a late Precambrian Tethysian dimensioned geosyncline (Holmes, 1965). The Mozambique belt is characterised by a well defined meridional trend and may be traced for over one thousand kilometres through Eastern Africa. It is principally composed of migmitites, biotite gneisses, with minor amphibolites, schists, younger granites, syenites and recent pegmatites. Geochronological evidence suggests an age of 400-700 m.y. (Cahen and Snelling, 1966) throughout most of its exent; its striking uniformity and vast area bear testimony to the magnitude of the late Precambrian Pan African thermal event (Kennedy, 1965).

Within Kenya and Tanzania the Mozambique belt abuts, to the west, the Tanganykan shield (1900-3100 m.y.) comprising, in part, the Nyanzian and Dodoman orogenic belts, or it is overlain by Tertiary volcanics. To the east it dips beneath the Mesozoic through recent sediments. In northern

Kenya older radiometric dates of 800-900 m.y. (Cahen and Snelling, 1966) and lower grade metamorphism within the Mozambique belt have prompted Saggerson (1973) to propose a possible relic early (Archean?) Precambrian Shield extending north into Ethiopia.

The Mozambique belt has a postulated extension into Ethiopia and South-West and Northern Somalia. High grade metamorphism and intrusive granites occur in large inliers south and south-east of Addis Ababa and in the Hargeisa-Borama region of Somalia. In Ethiopia gneisses predominate (Cahen and Snelling, 1966) while in Northern Somalia granodiorites, granite gneisses and metaarkoses are most common (Warden and Daniels, 1965). Daniels et al. (1965) demonstrate that two phases of metamorphism, the first reaching granulite to amphibolite facies, occurred in Northern Somalia with an intervening series of intrusions comprising gabbros and later granites (500 m.y.) penetrating the lower Paleozoic sedimentary Inda Ad series (Greenwood, 1961).

In the Bur region of South-West Somalia an oval outcrop composed of gneisses, granites, mica schists and amphibolites occurs (United Nations Development Program, 1970). The metamorphics have been intruded by a series of granite and granodiorite stocks and pegmatite dykes; the former have been dated at 615 m.y. (Beltrandi and Pyre, 1973).

Lower Paleozoic (Cambrian through Devonian) sediments are restricted, in outcrop, in Eastern Africa to the Inda Ad formation of Northern Somalia (Greenwood, 1961). In many areas these sediments have been metamorphosed, to unfoliated greywackes and slates, presumably by the later phases of the Pan African thermal event (Azzaroli and Fois, 1964).

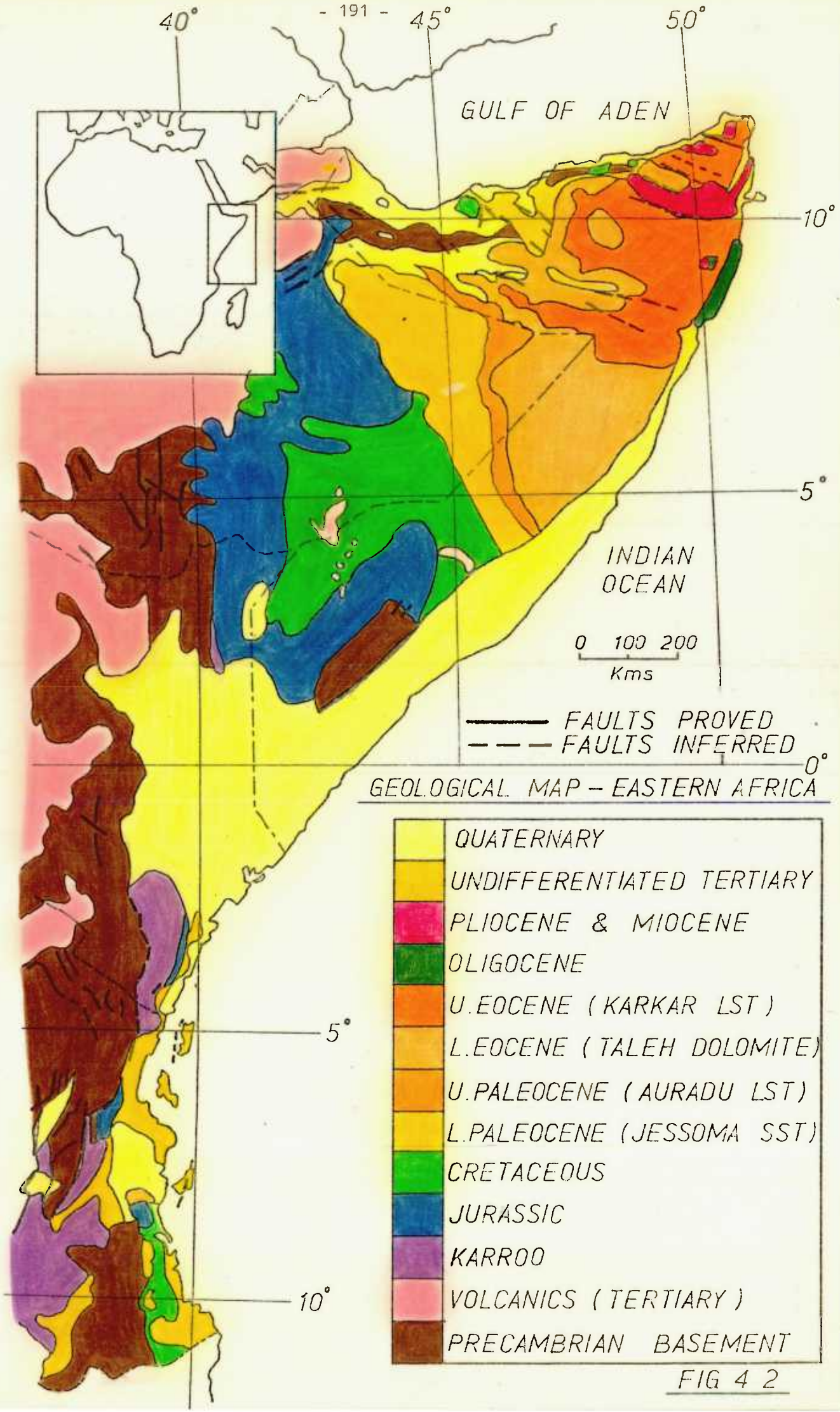
In early Karroo times (Carboniferous) a period of intense erosion led to a virtual complete peneplanation of the entire Eastern African platform (Pallister, 1971). By the Permian the crustal plates of Eastern Africa were being deformed by epeirogenic movements (Walters and Linton, 1973, Beltrandi and Pyre, 1973, Kent, 1974a). Tectonics of a diastrophic nature produced

large dislocations following Phaneorozoic lines of weakness (McConnell, 1974). A series of grabens bounded by large normal faults evolved; the faults, with throws of up to 6 kilometres, show no evidence to support regional crustal extension (Kent et al., 1971). Beltrandi and Pyre (1973) have suggested that these pre-Jurassic grabens may have been linked in a single rift or trough extending from coastal Tanzania north to the Afar. They also propose, as do Walters and Linton (1973), that the grabens or troughs or single rift were associated with the major initial fractures which broke the Gondwanaland continent.

Sedimentation was entirely continental and predominantly clastic though minor evaporites of Permo-Trias age have been reported for both Tanzania (Kent, 1965) and South-West Somalia (Burmah Oil, pers. comm., 1974). Outcrops of Karroo are limited to south coastal Kenya, North-East Kenya and central Tanzania, Fig. 4.2; locally thicknesses may exceed 4 kilometres. Paleozoic volcanism appears to have been limited to Mozambique, Malawi and possibly Northern Somalia.

The earliest established marine ingression began in the lower Jurassic (Liassic) with the proto-Indian Ocean advancing in a south-westerly direction across the Horn of Africa (Somaliland Oil Exploration Co., 1954, Kent, 1972). The subsidence continued into the upper Jurassic with a widespread carbonate sequence passing up into open water shales as the marine transgression reached a maximum in the Kimmeridgian.

Throughout most of Eastern Africa the end of Jurassic and early Cretaceous marked a major uplift of the region west of the coastal basin and a marine regression. Shallow water conditions returned; the sea completely withdrew from the Ogaden resulting in large sabka (evaporitic) type deposits (Clift, 1956, Beltrandi and Pyre, 1973, Mobil Oil, pers. comm., 1974). In Northern Somalia extensive uplift and erosion occurred, in many places removing the entire Jurassic sequence (Somaliland Oil Exploration Co., 1954).



GEOLOGICAL MAP – EASTERN AFRICA

FIG 4 2

By Barremian times subsidence was again active on a regional scale with a maximum ingression of the Cretaceous Sea in the Cenomanian (Somalialand Exploration Oil Co., 1954, Azzaroli and Fois, 1964). Widespread clastic deposition was followed by yet another period of regional warping, uplift, and marine regression during the upper Cretaceous.

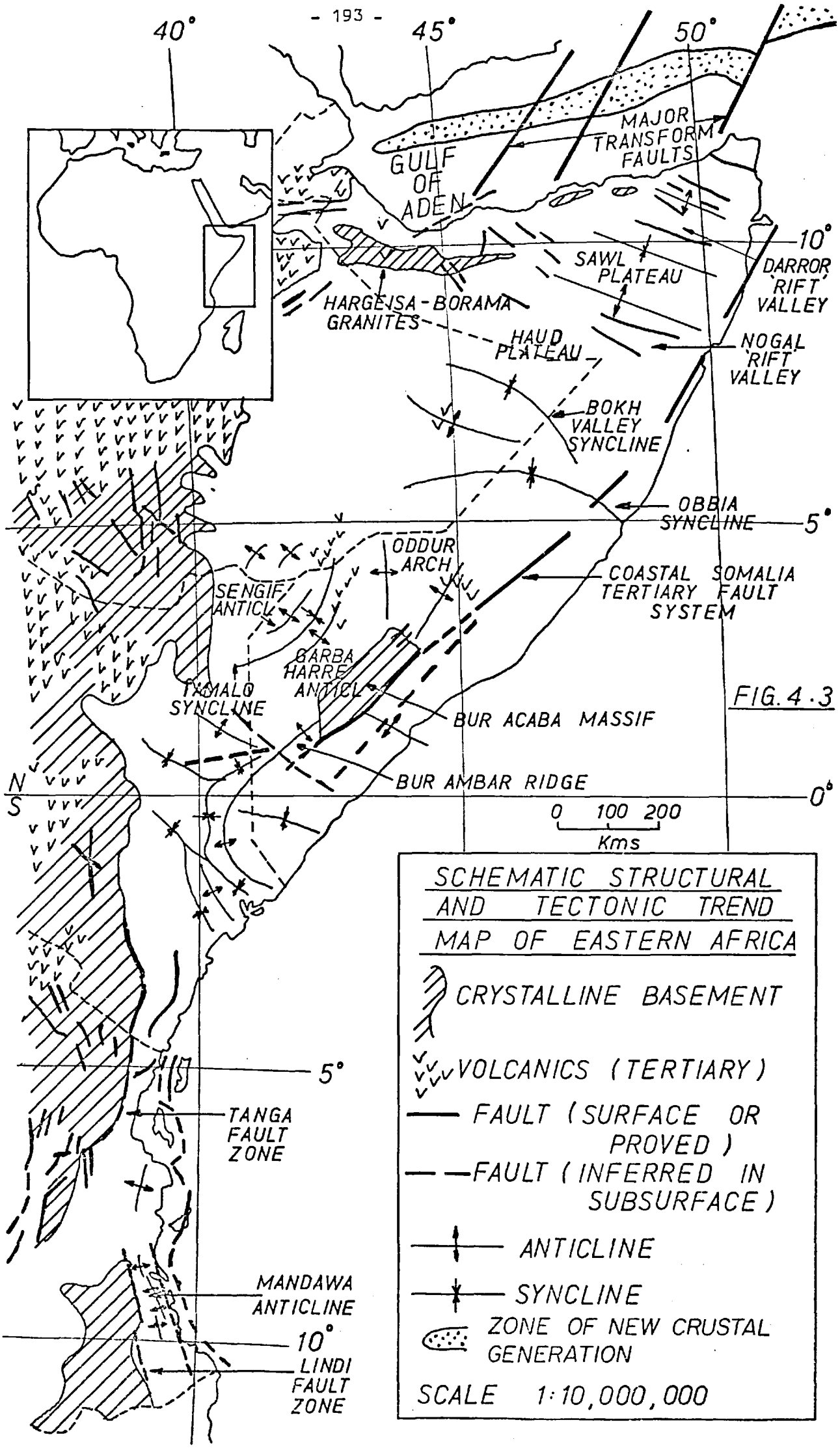
Mesozoic volcanism appears to have been restricted to the extensive lower Cretaceous basalts of Mozambique and Madagascar (Kent, 1974b). Two minor nephaline-syenite intrusions at Jombo and Sabaki in coastal Kenya are probably of late Cretaceous age (Harrison and Haw, 1964).

In the Paleocene and lower Eocene the warping of the western basement resulted in rejuvenation of the Eastern Africa coastal fault system. This phase of tectonism is often regarded as contemporaneous with the initiation of the Red Sea, Gulf of Aden, East Africa rift systems. (Laughton et al., 1970, Beltrandi and Pyre, 1973, Girdler and Styles, 1974). The migeosynclinal development of the southern coast continued through the lower Tertiary (Kent et al., 1971). Deposition ranged from outer shelf to deltaic facies.

The third major marine transgression of Eastern Africa occurred during the Eocene, probably as a result of subsidence or downwarp in response to the uplift of the Afro-Arabian shield. Enormous amounts of clastic deposition in coastal Tanzania, Kenya and Somalia record the rapid degradation of this dome.

The Oligocene of Eastern Africa is largely absent (cf. Azzaroli and Fois, 1964, Walters and Linton, 1973); it is generally attributed to a period of uplift and erosion although Davies et al. (1975) have found that it exists in virtually all of the Indian Ocean DSDP holes.

By the Miocene marine sedimentation returned but only along the margins of the present coast. The renewed subsidence may have been linked with the intense volcanicity in the East African rift (Baker et al., 1972)


40°
45°
50°
MAJOR TRANSFORM FAULTS
GULF OF ADEN
10°
SAWL PLATEAU
DARROR RIFT VALLEY
HARGEISA - BORAMA GRANITES
HAUD PLATEAU
NOGAL RIFT VALLEY
BOKH VALLEY SYNCLINE
OBBIA SYNCLINE
5°
ODDUR ARCH
COASTAL SOMALIA TERTIARY FAULT SYSTEM
SENGIF ANTICL
GARBA HARRE ANTICL
TXMALO SYNCLINE
BUR ACABA MASSIF
BUR AMBAR RIDGE
N
S
0°
0 100 200
Kms
FIG. 4.3
SCHEMATIC STRUCTURAL AND TECTONIC TREND MAP OF EASTERN AFRICA
CRYSTALLINE BASEMENT
VOLCANICS (TERTIARY)
FAULT (SURFACE OR PROVED)
FAULT (INFERRED IN SUBSURFACE)
ANTICLINE
SYNCLINE
ZONE OF NEW CRUSTAL GENERATION
SCALE 1:10,000,000
5°
TANGA FAULT ZONE
MANDAWA ANTICLINE
10°
LINDI FAULT ZONE

MESOZOIC/CENOZOIC STRUCTURAL AND DEPOSITIONAL HISTORY:

EASTERN AFRICA

			Coastal Tanzania	Coastal Kenya	Mandera-Lugh Basin	Ogaden Region	North-East Somalia	Guban Region
	Quaternary		Uplift, Regression	Quiescene			Eolian & alluvial sands	Eolian & alluvial sands
Neogene	Pliocene	U		Regional Uplift				Volcanism
		L	Limestones	Limestones, shales		Eolian & alluvial sands	Minor volcanism	Minor Uplift?
	Miocene	U M L	Uplift to West Basin Subsid.	Marine Transgr.			Minor Uplift?	Pebble beds
			Subareal Erosion?	Uplift to West Basin Subsid.			Coastal Subsidence	Coastal Subs.
Palaeogene	Oligocene		Regression	sst. & mudst.	Volcanism	Uplift Basin Emergent	Basin Emergent Regression	Uplift, Basin Emergent
	Eocene	U	Uplift to West	Basin Subsid. Uplift to West			Basin Uplift	Evaporites limestones
		M			Post Depositional Uplift & Faulting	Limestone	limestone	Subsidence
		L	Shallow Water Deposition	Basinal Basement Warping		Subsidence	Subsidence	Minor Regression
	Paleocene					Nubian sst.	Regression	limestones sandstones
L.Cretaceous U.Cretaceous	Senonian	M	Claystones	limestones & shales		Basin Uplift Regression	Uplift	Subsidence
		C	Transgression				Nubian sst.	Minor Regression
		S		Subsidence	Emergence	shales Limestones	maximum ingression	Subsidence
		C	Minor Regression					
	Turonian			sandstones & siltstones	Continental Deposition	Transgression Subsidence	Limestone shale	Subareal Erosion
	Cenomanian		Transgression		Evaporites	evaporites	Subsidence?	
	Albian				Regression	Regression	Regression	Basin Uplifted
	Aptian						limestone	Regression
	Necomian	B	Clastic deposition	Basin downwarp	Basin Warped & Uplifted	Basin Uplifted	basal sst.	limestones
		H						
		V	Regression, Uplift to West	Uplift to West				
		B		sandstones & shales	carbonates	limestones shales		
Jurassic	Upper		Marine Transgression		Subsidence	Subsidence		Marine Transgression
	Middle			Graben Formation	Marine Transgression	Transgression	Transgression	
	Lower		Intense Faulting					

Structural and Depositional History - Eastern Africa

Table 4.0

or the second phase of the Gulf of Aden/Red Sea spreading (Laughton et al., 1970). In the Guban thick pebble beds testify to the intense earth movements which resulted in the present coastal scarp and the uplift of the Golis Plateau.

Middle Pliocene uplift initiated minor dislocations and, later, further differential subsidence of individual fault blocks in the coastal plain. The Quaternary has been a period of quiescence with widespread fluvial alluvium deposition.

Tertiary volcanism occurred in two periods; Eocene and Plio-Pleistocene. The former is broadly equivalent to the 'Trap' series, the dominant flood in Ethiopia and Arabia (Mohr, 1962). Several outcrops are mapped in the Ogaden (Fig. 4.2) region of Somalia and Ethiopia. Flows are invariably intercalated in the Auradu (Eocene) limestone (Beltrandi and Pyre, 1973, Mobil Oil, pers. comm., 1974). Harrison and Haw (1964) reported a Paleocene/Eocene radiometrically determined age for an dolerite intrusion encountered at 3.5 kilometres in the exploration well Coriole-1 (Fig. 4.1). The more recent volcanism, the Aden series, has several outcrops in Northern Somalia (Somaliland Oil Exploration Co., 1954, Azzaroli and Fois, 1964).

4.3 Regional Geophysical Studies of Eastern Africa (South of 15°N)

Regional geophysical surveys or compilations of data in coastal Eastern Africa are few with the bulk of the information still held in oil company or survey reports.

Slettene et al. (1973) have compiled a regional Bouguer anomaly map of Africa, the relevant portion of which has been reproduced here as Fig. 4.4. Before discussing this gravity map it is prudent to bear in mind that its accuracy is of the order of $\pm$ 12 milligals and may, in certain instances, be misleading in terms of small, local anomalies. Nevertheless certain correlations are evident.

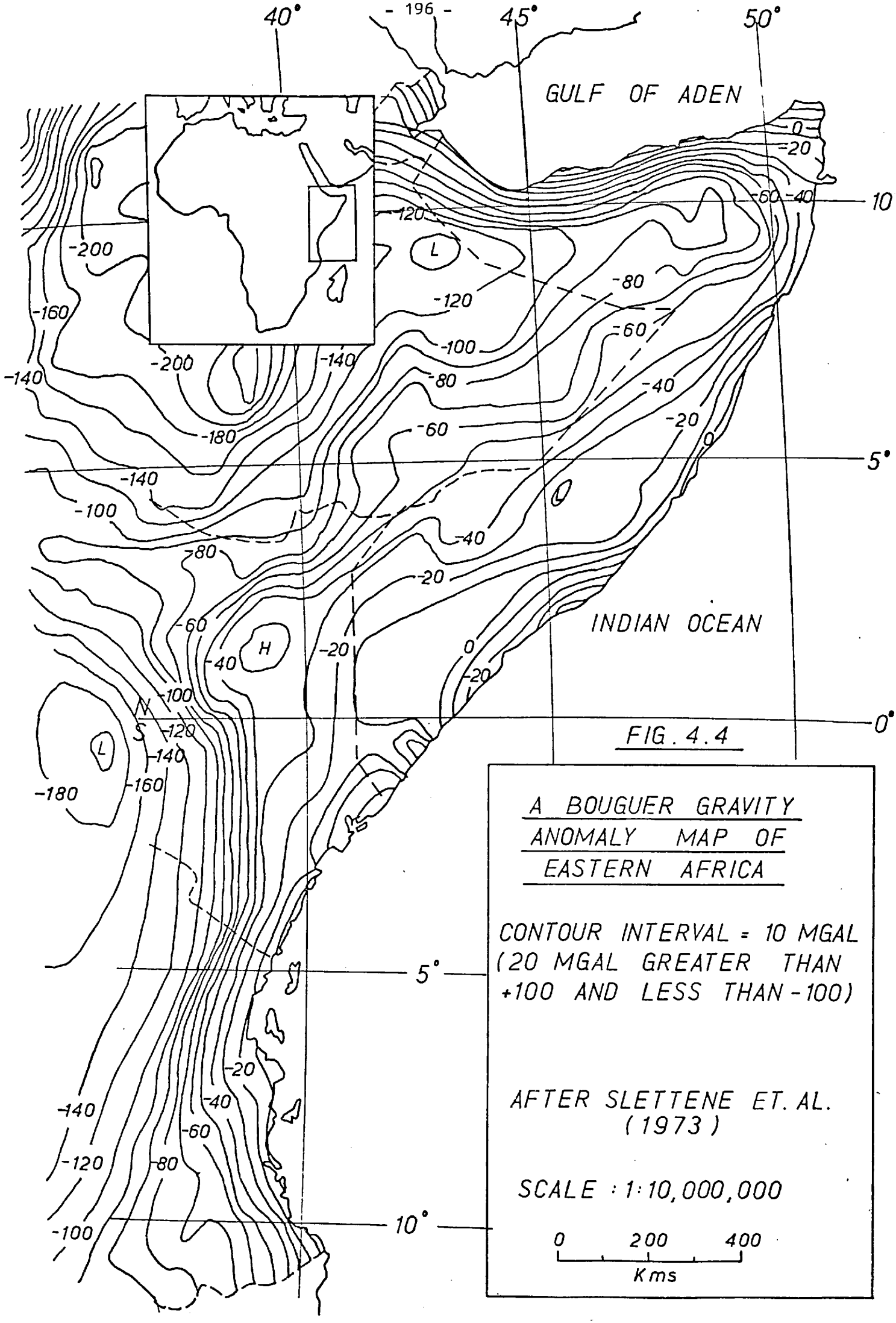


FIG. 4.4

A BOUGUER GRAVITY ANOMALY MAP OF EASTERN AFRICA

CONTOUR INTERVAL = 10 MGAL (20 MGAL GREATER THAN +100 AND LESS THAN -100)

AFTER SLETTENE ET. AL. (1973)

SCALE : 1:10,000,000

0 200 400
Kms

An increasing (less negative) Bouguer anomaly is observed as the continental margin is approached. As virtually all of the sedimentary basins thicken seaward this might imply crustal thinning or a transition to a higher density basement. There is very little reliable data on thickness of crust or sediments over most of this region and as such it is not possible to uniquely determine whether the margin is in isostatic equilibrium from Fig 4.4. However Kent et al. (1971) have computed isostatic anomaly maps over Pemba, Zanzibar and Mafia Islands off Tanzania and found positive (ie. undercompensated) values. Fig. 4.4 does not contradict this result as positive (about 20 mgal.) Bouguer anomalies are found along the Somalia coast though Bott (1971a) has pointed out that free-air anomalies (equal to Bouguer at sea level) give only a rough guide to isostasy and then only near the centre of the feature in question. Similar positive Bouguer values have been observed off the Kenya coast by Admirality (1963) and Harrison and Haw (1964).

The extreme gradient near the Gulf of Aden coast may simply mirror rapid crustal thinning towards the axial ridge. The regional low over the Kenya Rift Valley has been attributed by various authors (cf. Baker and Wohlenberg, 1971) to a low density high temperature discontinuity in the upper mantle. A gravity high, of about 20 mgals., in North-East Kenya has been shown to be correlated with a large basement ridge extending west from the Bur Acaba Massif, Fig. 4.3 (Harrison and Haw, 1964). A gravity high in Northern Somalia appears roughly coincident with the Hargeissa-Borama gabbro-granite complex. Widespread Tertiary flood basalts in the Eastern Ogaden (see section 4.2) outcrop in the vicinity of that region's gravity low.

The Bouguer anomaly map, Fig. 4.4, is too speculative to allow any quantitative modelling. Flavelle and Yoshimura (1974) discuss some of the problems of interpreting Bouguer anomaly maps at a continental margin.

Seismicity has been studied in Africa for many years, the first

compilations being produced by Montessus de Ballore (1906), Struck (1909) and Krenkel (1926); the historical record of African earthquakes and their study is well summarised in Gorshkov (1963).

Continental margins are divided into two categories; seismic or Pacific-type, and aseismic or Atlantic-type. Fig. 4.5, after Baker et al., (1972) readily confirms Heezen and Tharp's (1964) morphological interpretation that Eastern Africa is indeed an Atlantic-type margin. Within the area of interest to this study only the coastal region of Tanzania is seismically active. Seismicity in Eastern Africa is elsewhere concentrated within the Gulf of Aden, Red Sea and Western Rift - the Eastern Rift being strangely aseismic (Gouin, 1970, Baker et al., 1972, Maasha and Molnar, 1972).

Oliver et al. (1974) have commented that the aseismicity of a margin such as Eastern Africa may be more apparent than real. They argue that effect of margin structure on wave attenuation and phase transformation (ie. S_n to L_g) may give a false impression of seismic quiescence. The total lack of seismicity is indeed puzzling in a margin which, subjected to intense deformation from the Karroo-Mesozoic, is intuitively a zone of significant weakness. Further Bott and Dean (1972) and Artyshkov (1973) have pointed out that the juxtaposition of oceanic and continental crust at such a margin leads to a significant nonhydrostatic stress field in the lithosphere.

Gumper and Pomeroy (1970) studied phase and group velocities for Rayleigh waves, group velocities for Love waves, body-wave (direct P_n and S_n) velocities, and Love channel waves for the granitic layer (L_g); results indicate that the structure of the African continent is that of a shield. They, together with Searle and Gouin (1971) also demonstrate that attenuation of the S_n phase, the low Q condition of Oliver and Isacks (1967), is observed only for paths through the northern East Africa rift; it is attributed to a discontinuity in the mantle lithosphere. Travel time studies of well located events (cf. Wohlenberg, 1969) together with the observed late (ie. slow)

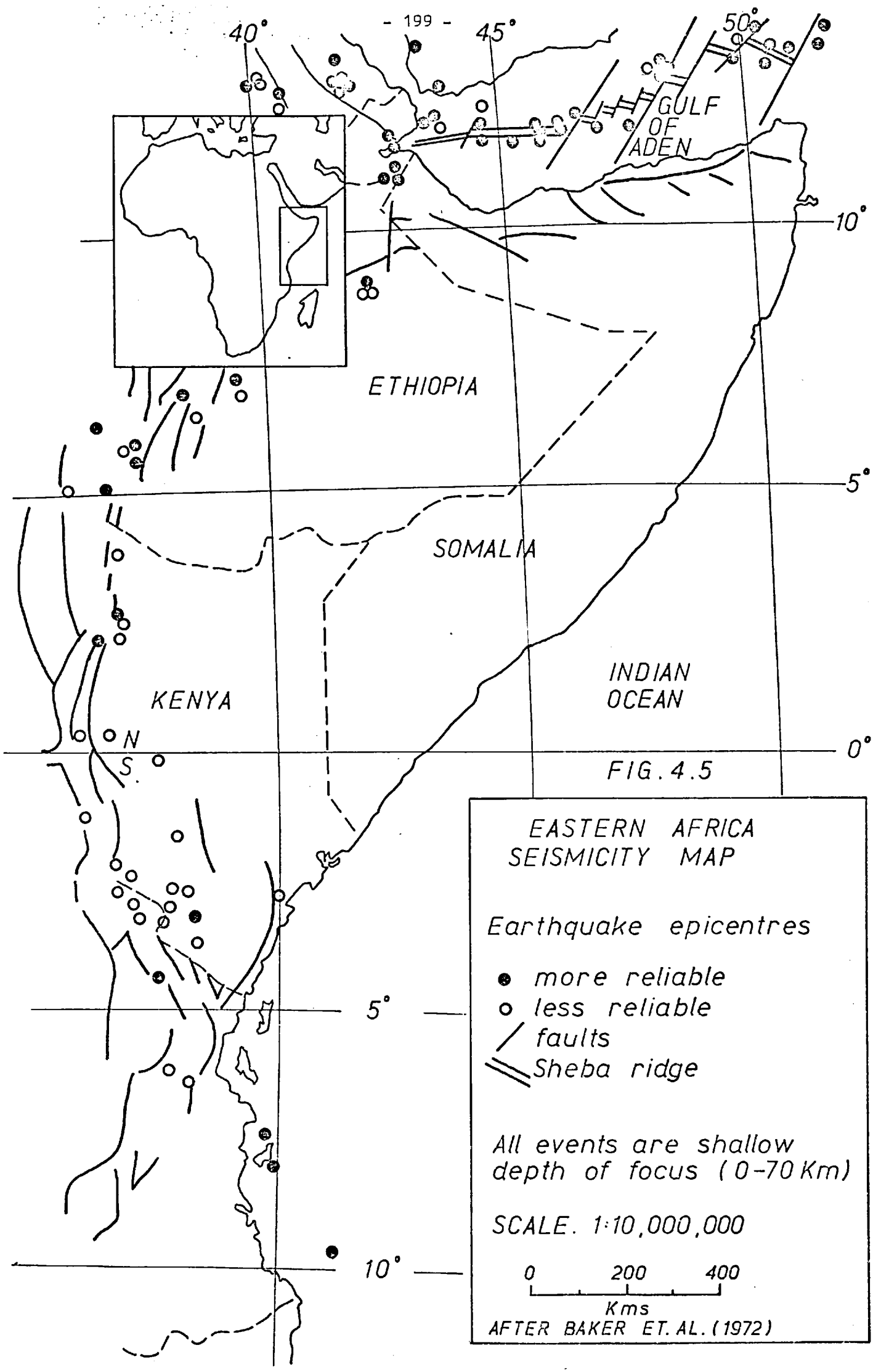

40°
45°
50°
GULF OF ADEN
10°
ETHIOPIA
5°
SOMALIA
INDIAN OCEAN
KENYA
N
S
0°
5°
10°
EASTERN AFRICA
SEISMICITY MAP
Earthquake epicentres
more reliable
less reliable
faults
Sheba ridge
All events are shallow depth of focus (0-70 Km)
SCALE. 1:10,000,000
0
200
400
Kms
AFTER BAKER ET. AL. (1972)

FIG. 4.5

teleseismic P wave residuals for stations near this part of the rift (Fairhead and Girdler, 1971) further support the view that anomalous low velocity upper mantle is restricted to the region beneath the East Africa Rift.

Fault plane solutions of several Eastern Africa events have been compiled by Fairhead and Girdler (1972) and Maasha and Molnar (1972). The solution planes correspond to extension along the Red Sea and Gulf of Aden transforms, while rift results indicate an ESE stress field. No results have been published for those few epicentres in coastal Tanzania, though normal NS faulting, (ie. the old Karroo trend) might be expected.

Griffiths et al. (1971) share the view that anomalous upper mantle is limited to the Eastern Rift on the basis of seismic refraction studies indicating a low, 7.5 $km \cdot s^{-1}$, P velocity and a thin, 20 km., thick crust beneath the Kenyan rift. A marine refraction survey reported by Francis et al. (1966) indicates thick consolidated sediments extending some 300-400 km. off the Kenya coast; they are interpreted to be a continuation of the Mesozoic-Karroo sequence found onshore. Crustal thicknesses varied from 19 km. near the Kenya coast to only 8.5 km. west of the Seychelles Bank, the latter region being a possible scar of the southward drift of Madagascar (Fisher et al., 1968). Gulf of Aden seismic refraction data, consistent with an oceanic ridge-rift structure has been reviewed by Laughton and Trammontini (1969).

Bunce et al. (1967) and Schlich et al. (1972) have carried out seismic reflection studies within the Somali Basin, Fig. 4.6; results show about a kilometre of flat lying sediments in the region south of Socotra, west of the Chain Ridge and north of $3^{o}N$. The area south of this latitude is underlain by a rough basement topography partially buried in faulted, stratified, ponded sediments. Deeper sediments in both regions are probably

pre-mid Cretaceous, a view put forward by Francis et al. (1966) and now proved by the Deep Sea Drilling Project at site 241 (Geotimes, 1972).

A limited number of oil exploration geophysical surveys (seismic reflection, gravity and aeromagnetics) have been published or were obtained in the course of this research. Discussion of these investigations is deferred to the sections 4.9 - 4.18 dealing with specific regions of Eastern Africa.

Marine magnetic surveys have been carried out over much of the North-West Indian Ocean and Gulf of Aden (cf. Matthews, 1966, Bunce et al., 1967, Fisher et al., 1968, Laughton et al., 1970); results have been interpreted in terms of magnetic lineations produced during seafloor spreading (McKenzie and Sclater, 1971) and are reviewed in section 4.5. No linear magnetic anomalies have been recognised in the Somali Basin.

Eastern Africa paleomagnetic studies have been reviewed by Tarling (1970). Previous work by Irving and Tarling (1961), Tarling et al. (1967), and Brock et al. (1970) suggest a 6-7^{o} anticlockwise rotation of Arabia about a pole near the Dead Sea during the past 5-10 m.y. while Africa has remained essentially fixed (ie. late Tertiary declinations in Africa are essentially that of the geocentric dipole). Girdler (1968) and Brock (1968) have further suggested that Africa was also rotating in an anticlockwise direction during the Paleozoic through late Cenozoic when its motion ceased (Piper and Richardson, 1972).

4.4 The Central and Southern Red Sea Regions

Discussion of the Red Sea geology and geophysics was omitted from sections (4.2) and 4.3) respectively as the region differs so fundamentally from the Somalian-Kenyan-Tanzanian coastal margin. While the latter represents a mature Atlantic-type continental margin, the Red Sea is generally held to be in the proto-ocean stage of development (Girdler, 1958, Drake and Girdler,

1964, Vine, 1966, Trammontini and Davies, 1969).

The North African, Sinai and Arabian shields were, until the late Precambrian, a single unit (Dubertret, 1970). The Pan African orogeny resulted in large regional dislocations, plutonic intrusions, volcanism and the incorporation of this area into the Mozambique belt (Schurmann, 1966).

The pre-upper Cretaceous history is poorly known though clearly the Jurassic sea spread west across the Horn of Africa to at least as far as Massawa with an east-west shoreline at about 17°N (Somaliland Oil Exploration Ltd., 1954). By the end of the Cretaceous the Tethys reached south to 21°N. However, no firm evidence for a pre-Tertiary Red Sea rift or even depression exists, (Coleman, 1973).

In the early Tertiary (Eocene) vast quantities of alkalic basalts flooded the Mesozoic sediments and adjacent crystalline basement, (Gass, 1970), during which the Red Sea region was uplifted to form the Afro-Arabian dome. By the late Oligocene, a central depression formed, perhaps as the result of isostatic compensation due to erosion of the dome and/or thermal metamorphism of the lower crust (Falvey, 1974). A series of large en echelon normal faults resulted along the western margin with a monoclinal flexure to the east.

Pre-Oligocene marine sediments are known only in a few locations in the Red Sea region. Lowell and Genik (1972) have assigned an Oligocene age to an evaporitic and clastic sequence in the B-1 borehole on the basis of radiometric age determinations of interlayered basalts. By mid-Miocene times a marine connection with the Mediterranean was established through the Gulf of Suez (Heybrook, 1965). Thick sequences of evaporites and clastics, the latter near the margins, accumulated with a second phase of intense volcanism occuring on the flanks.

The Pliocene marks the end of the Mediterranean connection with the uplift of the Isthmus of Suez. The Indian Ocean flooded in with marine

oozes and clastics being deposited on the Miocene evaporites. During this period the axial trough formed as a major rift - a marked departure from the Eocene-Miocene development of the Red Sea depression.

Gass (1970) has attributed this initiation of rifting to a progressive heating of the lithosphere by a sequence of upward injection of magma, distortion of isotherms and equilibrium of magma at progressively shallower depths. Repeated basaltic injections will separate the sialic crust and eventually allow the primary magma source to equilibrate within ten kilometres of the surface. Such a process should lead to progressively less alkalic, more tholeitic, type basalts toward the centre of the axial trough. This has been largely born out by the work of Gass et al. (1973). The Plio-Pleistocene history of the Red Sea has been characterised by progressive gentle subsidence of the graben together with further volcanicity on the flanks, particularly in Ethiopia and Arabia (Gass, 1973).

Magnetic surveys have been carried out by a number of researchers (Drake and Girdler, 1964, Phillips et al., 1969, Allan, 1970, Kabbani, 1970, Girdler and Styles, 1974). The results, when correlated with the Heirtzler magnetic time scale, all indicate a period of continuous axial spreading at a rate of one to two $cm \cdot y^{-1}$ for the past three to five million years, (Vine, 1966). Girdler and Styles (1974) have found a tentative correlation of lower amplitude shelf anomalies with the late Eocene - early Oligiocene geomagnetic polarity history.

Gravity results (Girdler, 1958, Drake and Girdler, 1964, Phillips et al., 1969) suggest that the Red Sea is in isostatic equilibrium. A central positive Bouguer anomaly is thought to result from a high density axial intrusion at a depth of only a few kilometres. The gravity data also tend to indicate thinned or necked continental crust on the Red Sea margins and shelf.

Fairhead and Girdler (1970) have demonstrated that most of the

seismicity originates as shallow (< 100 km.) events within the axial trough with a noticeable decrease in activity to the north. Fault plane solutions (McKenzie et al., 1970, Fairhead and Girdler, 1972) indicate NE-SW motion consistent with the orientation of the Red Sea transforms (Le Pichon et al., 1973).

Seismic refraction studies (Drake and Girdler, 1964, Trammontini and Davies, 1969) indicate oceanic crust (layer 3) with a seismic velocity of 6.6-7.0 $km \cdot s^{-1}$ at a depth of less than 5 kilometres within the axial trough. Beneath a shelf sedimentary layer, of velocity 3.5-4.5 $km \cdot s^{-1}$ with a thickness 2.5 kms., is a layer with velocity 5.8-7.0 $km \cdot s^{-1}$. This unit is now thought to be Precambrian basement (Coleman, 1973) though considerable controversy has raged over the subject.

Continuous reflection seismic surveys clearly indicate the top of the Miocene evaporite layer (Ross and Schlee, 1973) at depths of 0-500 metres beneath the surface of the Red Sea shelf. A gap of 48-74 kms. exists, in these otherwise continuous evaporites, across the axial trough.

4.5 Plate Tectonics of Eastern Africa and the Surrounding Seas

No discussion such as this would be complete without mentioning the role plate tectonics has played in shaping the Eastern Africa continental margin. Fig. 4.6 diagramatically illustrates the principal features associated with plate tectonics in the region of Eastern Africa and its surrounding seas. Four major plates, Africa or Nubia, Somalia, Arabia and India are evident (McKenzie et al., 1970), together with three minor fragments, Danikil, Dubious (not shown) and Sinai (Le Pichon et al., 1973).

The Somalia plate, on which the bulk of the heat flow data presented here was gathered, is bounded to the east and south by the Indian Ocean ridges, to the north by the Gulf of Aden spreading centre, and to the west by the Ethiopian and Kenyan rift systems. The south-western boundary

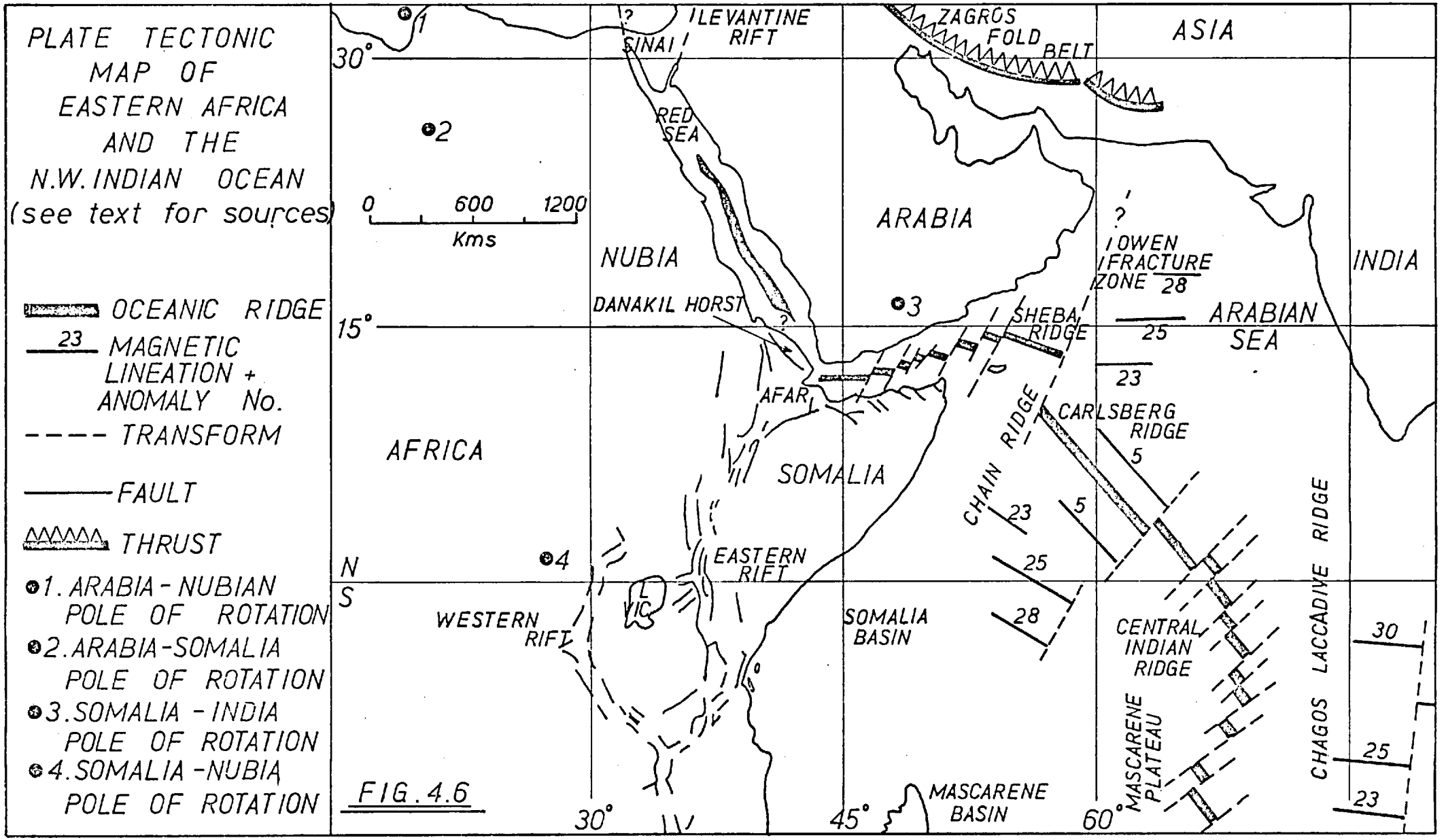

PLATE TECTONIC MAP OF EASTERN AFRICA AND THE N.W. INDIAN OCEAN
(see text for sources)
OCEANIC RIDGE
23 MAGNETIC LINEATION + ANOMALY No.
TRANSFORM
FAULT
THRUST
1. ARABIA - NUBIAN POLE OF ROTATION
2. ARABIA - SOMALIA POLE OF ROTATION
3. SOMALIA - INDIA POLE OF ROTATION
4. SOMALIA - NUBIA POLE OF ROTATION
0 600 1200
Kms
ASIA
ZAGROS FOLD BELT
ILEVANTINE RIFT
SINAI
RED SEA
ARABIA
NUBIA
INDIA
OWEN FRACTURE ZONE
28
DANAKIL HORST
SHEBA RIDGE
25
ARABIAN SEA
23
AFAR
CARLSBERG RIDGE
CHAIN RIDGE
5
AFRICA
SOMALIA
23
5
25
EASTERN RIFT
N
S
WESTERN RIFT
L VIC
SOMALIA BASIN
28
CENTRAL INDIAN RIDGE
MASCARENE PLATEAU
CHAGOS LACCADIVE RIDGE
30
25
23
MASCARENE BASIN
30°
45°
60°
15°
30°

FIG. 4.6

is not well defined (Le Pichon et al., 1973).

The north-west Indian Ocean ridges are divided into two principal sections, the Carlsberg Ridge to the north and the Central Indian Ridge to the south. The Carlsberg Ridge has been actively spreading for the past ten million years with magnetic lineations mapped out to anomaly number five on the Heirtzler time scale (Fisher et al., 1968). This ridge, which is seismically active and divides the Indian and Somalian plates, is terminated to the north by the Owen Fracture Zone, a large, weakly seismic, slowly moving transform separating the Arabian and Indian plates (McKenzie and Sclater, 1971).

The Central Indian Ridge, trending NNE/SSW with many transform offsets, is also actively spreading, again with no magnetic lineations older than anomaly five (Schlich, 1974). McKenzie and Sclater (1971) have suggested that the adjacent aseismic ridges, the Chagos-Laccadive and Mascarene Plateau, were once part of a very large fracture zone dividing the Carlsberg Ridge from the present south-east Indian Ridge. During this period, the upper Cretaceous through lower Eocene, the now isolated and divergent magnetic anomalies 23-29 in the Arabian Sea and north of the Seychelles were produced (Matthews, 1966, and Fisher et al., 1968). This was followed by a period of quiescence or very slow spreading on the Carlsberg Ridge during the period 55-10 m.y. B.P., or until about the time of anomaly number five, mid-upper Miocene, when it was suddenly regenerated in a new orientation (NE/SW) with spreading also starting on the fossil Chagos Fracture Zone.

West of the Carlsberg Ridge radiometric dating of dredge samples from the Chain Ridge (Bunce et al., 1967) and Admirante Plateau (Fisher et al., 1968) give ages of 90 and 82 m.y. respectively and probably represent an upper limit to the age of the Somalia basin basement. Recent Deep Sea Drilling, Leg 25, site 241, (Geotimes, 1972) tends to support such a statement.

North of the Owen Fracture Zone the mid-ocean ridge system is continued through the Gulf of Aden by the Sheba Ridge where again magnetic lineations are not mapped beyond anomaly five (Laughton et al., 1970). Thus the Gulf of Aden, which is thought to be a tensional feature (Laughton, 1966), is supposedly younger than mid-Miocene. However, Le Pichon et al. (1973) have shown that the most suitable single rotation reconstruction of Somalia/Arabia plate motion would only close about 70 percent of the Gulf of Aden between the 500 fathom contour lines. As with the mid-Indian ridges a two phase spreading history appears to be required; Azzaroli (1968) favouring a Jurassic through Cretaceous period of rifting while Girdler (1975, pers. comm.) is investigating a late Eocene through lower Oligocene analogy with the Red Sea.

The Gulf of Aden ridge/rift extends west to bifurcate in the region of the Afar which has been widely regarded as a triple junction (cf. McKenzie and Morgan, 1969) though the explanation as to its fracture geometry is still in dispute (Morgan, 1972, Bhattacharji and Koide, 1975). The Red Sea trough, which is the northward continuation of the ridge/rift, extends for some 1700 km. to be truncated against the left lateral transcurrent Jordan shear.

The central trough is seismically active (Girdler, 1969) and has been spreading at between 1 and 2 $cm \cdot y^{-1}$ for some 4 m.y. (Vine, 1966). Once again an earlier stage of spreading is suggested (Girdler and Styles, 1974).

The rotation of the Arabian plate away from Africa appears well supported, both by paleomagnetic data (section 4.3) as well as plate reconstructions (cf. Le Pichon et al., 1973). The northern end of the Red Sea is yet another possible triple junction with the Jordan shear (Gulf of Aqaba) and the Gulf of Suez extending north to surround Cyprus along the western extension of the Zagros thrust zone, the Bitlis thrust-Ionian trench, and define the microplate of Sinai (Picard, 1970, Le Pichon et al., 1973).

The remaining major tectonic lineament is the East Africa rift system extending south from the Afar. While plate tectonics confirms the genetic link between the oceanic ridge/rift system and this continental rift, ie. the compatibility of the pole of Somalie/Arabia rotation with observed crustal extension in the Ethiopian Rift, (Le Pichon et al., 1973) the rift, as a unit, is atypical of a proto-ocean spreading centre (Baker et al., 1972). This is inferred from the very slow spreading rate as well as fundamental differences in the composition of their volcanic products (Murray, 1970).

4.6 Previous Heat Flow Studies in Eastern Africa and the Surrounding Seas

During the past decade a great deal of effort has gone into obtaining heat flow data from the Indian Ocean. This is particularly true of the north-west sector, defined, for the purposes of this study, from $70^{o}E$ to the Eastern Africa continental margin and from $10^{o}S$ to $15^{o}N$, excluding the Gulf of Aden. Some ninety-seven determinations have been made in this region by various workers (Sclater, 1966, Von Herzen and Vacquier, 1966, Von Herzen and Langseth, 1966, Birch and Halunen, 1966 and Popova, 1968). Seven of these results were rejected from the following analysis as they fell in the range 0-17 $mW \cdot m^{-2}$; Birch (1967) has demonstrated that such low values are most likely to result from a gradient disturbance due to nearby sea floor topographic relief.

A total of sixteen Gulf of Aden values have been reported by Von Herzen (1963), Sclater (1966), and Haenel (1972). The results are uniformly high with thirteen of the values exceeding 100 $mW \cdot m^{-2}$.

Continental heat flow results in Eastern Africa have been limited to the rift valley lake values of Von Herzen and Vacquier (1967), Degens et al. (1970) and Von Herzen (1972) together with twenty-three recent determinations in boreholes in Kenya by Morgan (1973). For the purposes

of a regional interpretation values west of $35^{o}E$ will not be considered here; this eliminates the lake values. Four of Morgan's values are also not considered as the author (Morgan) indicated the results to be dubious.

No less than eighty heat flow measurements have been reported for the Red Sea (Sclater, 1966, Birch and Halunen, 1966, Langseth and Taylor, 1967, Erickson and Simmons, 1969, Girdler, 1970, Haenel, 1972, Scheuch, 1973 and Girdler et al., 1974). The results of Scheuch are not included in this study as his publication indicated that the results were only preliminary and would be followed by a more detailed (revised?) discussion. In addition three of the remaining values are not considered as the authors (Birch and Halunen, 1966, Erickson and Simmons, 1969 and Girdler et al., 1974) thought them unreliable. Finally the Girdler (1970) result for the deep oil exploration well Amber-1 is also omitted as it has been recomputed in this study.

Seven recent determinations by the author (Evans and Tammemagi, 1974) are also not included as they have been recomputed for this study. Borehole results by Williamson (1975) for Kenya will also be discussed with the new heat flow data, sections 4.7 and 4.17.

Fig. 4.7 summarizes in histogram form, all of the above mentioned pre-1975 heat flow data less the dubious values. The one hundred and sixty-four values, from the area bound by $35^{o}E$ to $70^{o}E$ and $10^{o}S$ to $15^{o}N$, plus the Red Sea, are grouped for each of the above mentioned four regions.

The North-West Indian Ocean average of 63.2 ± 39.6 $mW \cdot m^{-2}$ differs insignificantly from the world oceanic mean of 69.9 ± 48.1 $mW \cdot m^{-2}$ or the Indian ocean average of 56.9 ± 39.8 (Lee, 1970) where all results are means of individual values. Averages for 5 x 5 degree squares will be considered in section 4.7.

The higher heat flow means of 75.9 ± 47.6, 147.6 ± 70.2 and 125.9 ± 65.8 $mW \cdot m^{-2}$ for Kenya (several rift valley results), the Gulf of

SUMMARY OF HEAT FLOW VALUES FOR EASTERN AFRICA & THE SURROUNDING SEAS

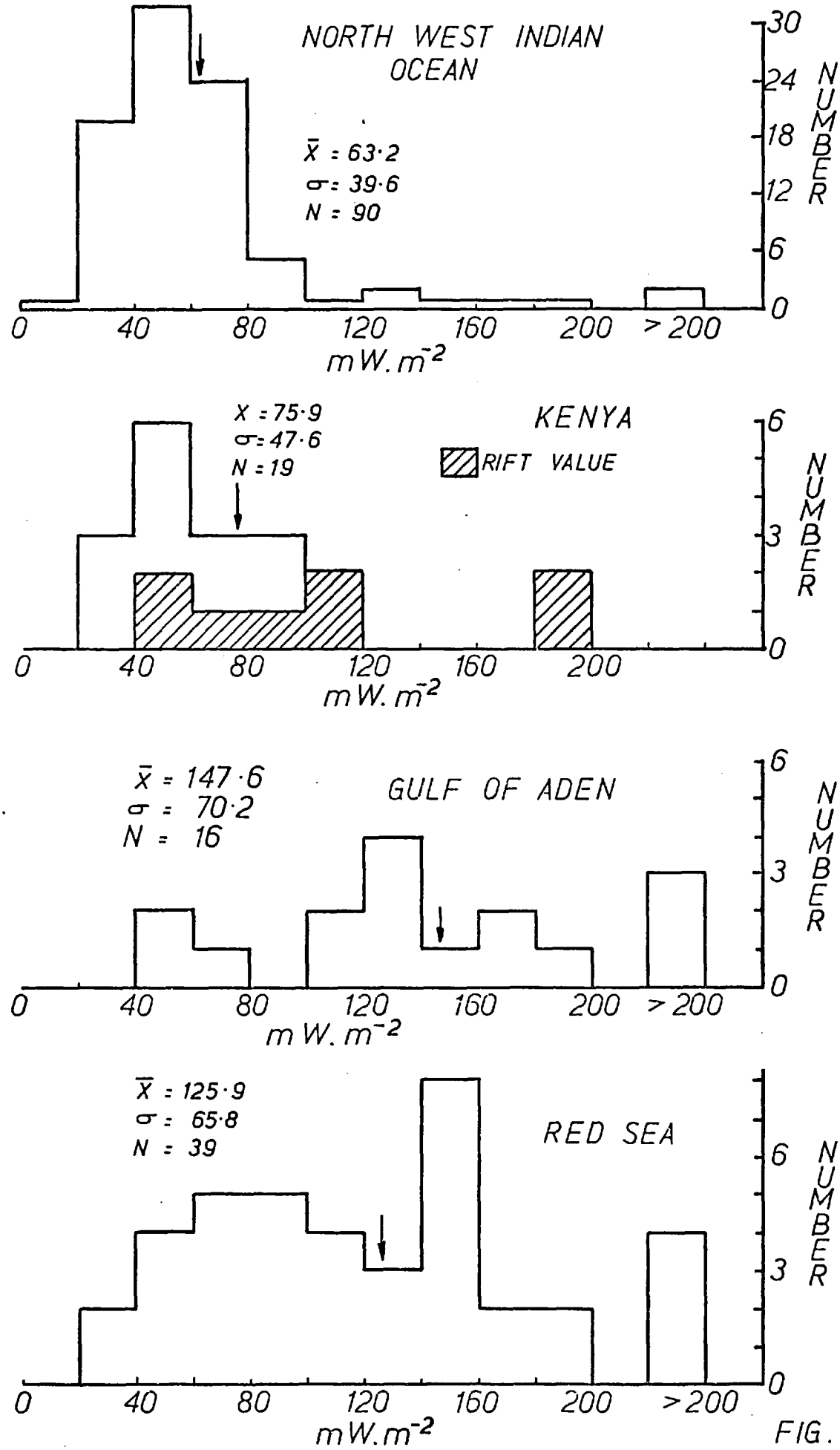


FIG. 4.7

NOTE; $\bar{X}$, mean; σ standard deviation; N, number values.

Aden, and the Red Sea region respectively are consistent with other geophysical and the geological evidence (sections 4.2 - 4.5) of a genetic link of the ridge/rift pattern of these three areas with that of the world oceanic system.

We will return to these published results in connection with the new data discussion, section 4.7, and the significance of regional variations of heat flow, section 4.19.

4.7 New Heat Flow Data From Eastern Africa

Sixty-eight new values of heat flow, all computed from oil exploration borehole data (see chapters 1, 2, and 3), are presented in tables 4.1, 4.2, and 4.3. For convenience of discussion, the data has been grouped into ten regions; Coastal Red Sea, The Guban, The Nogal and Darror Valleys, Obbia Embayment, Eastern Ogaden Basin, Benadir Coast, Mandera-Lugh Basin, The South-West Somalia Basin, The Lamu Embayment, and Coastal Tanzania. With the exception of the Benadir Coast all of these areas have been recognised as distinct regions by various authors on the basis of diverse criteria such as morphology, structural evolution, structural boundaries, etc. The regional division boundaries are shown in Fig. 4.11.

Table 4.1 gives the basic data pertaining to each borehole; name, location, depth, etc. Table 4.2 lists the initial or 'raw' data Bullard heat flow values (section 3.2 and 3.9) for each of the sixty-eight wells. Table 4.3 gives the heat flow values corrected for conductivity at in-situ temperatures (section 3.7), conductivity at in-situ pressures (section 3.6), and the effect of sedimentation on the geothermal gradient (section 3.5).

Uncertainties listed are at the one standard deviation level, equation (3.4), section 3.2.

In table 4.2 a data grade of A, B, C or D has been assigned to each heat flow value. These grades were assigned by an individual assessment

of each borehole taking into consideration the quantity of BHT and conductivity data available. Boreholes graded A were those with both good BHT data, generally more than three, together with a sufficient number, typically about thirty, measured conductivity results. Results graded B comprised those values computed from a borehole lacking one of the primary factors necessary for an A grade. Typically this would be a borehole with several BHTs and perhaps only six measured conductivities, or a borehole with two BHTs and twenty-five conductivities. This class also includes boreholes which might normally be classed A but were thought less reliable due to poor internal consistency of data or were relatively shallow, of the order of two kilometres. In addition, class B includes a few results where there was excellent BHT data and a very detailed lithologic log from which reasonable conductivity estimates might be made. Class C were those results where only several BHTs were available, together with, in a few instances, a brief lithologic log. It also includes some better quality B-type data from shallower holes. Class D were those results where only one or two BHTs were obtained with but a schematic well log with which to estimate conductivity.

The error in heat flow for these various grades A, B, C and D is thought to be less than fifteen, fifteen to thirty, thirty to fifty and greater than fifty percent, respectively. These estimates are based partly on the quantitative results of sections 1.8, 2.15 and 3.9 together with a subjective analysis of the individual values.

The uncorrected heat flow results from table 4.2 have been compiled in histogram form for figures 4.8(a) and 4.8(b). The mean of the individual values is 66.4 $\pm$ 26.5 $mW \cdot m^{-2}$, or, where the ABCD graded results are weighted 8:4:2:1 respectively, an average of 64.4 $\pm$ 26.1 $mW \cdot m^{-2}$ is obtained. A similar weighting technique was used by Lee (1970) who obtained a mean of 60.7 $\pm$ 23.9 $mW \cdot m^{-2}$ for the then total of 597 continental heat flow measurements. The weighted and unweighted individual value means for the ten regions are given in table 4.4. Individual uncorrected heat flow values are indicated on the

EASTERN AFRICA HEAT FLOW
(BY RELIABILITY)

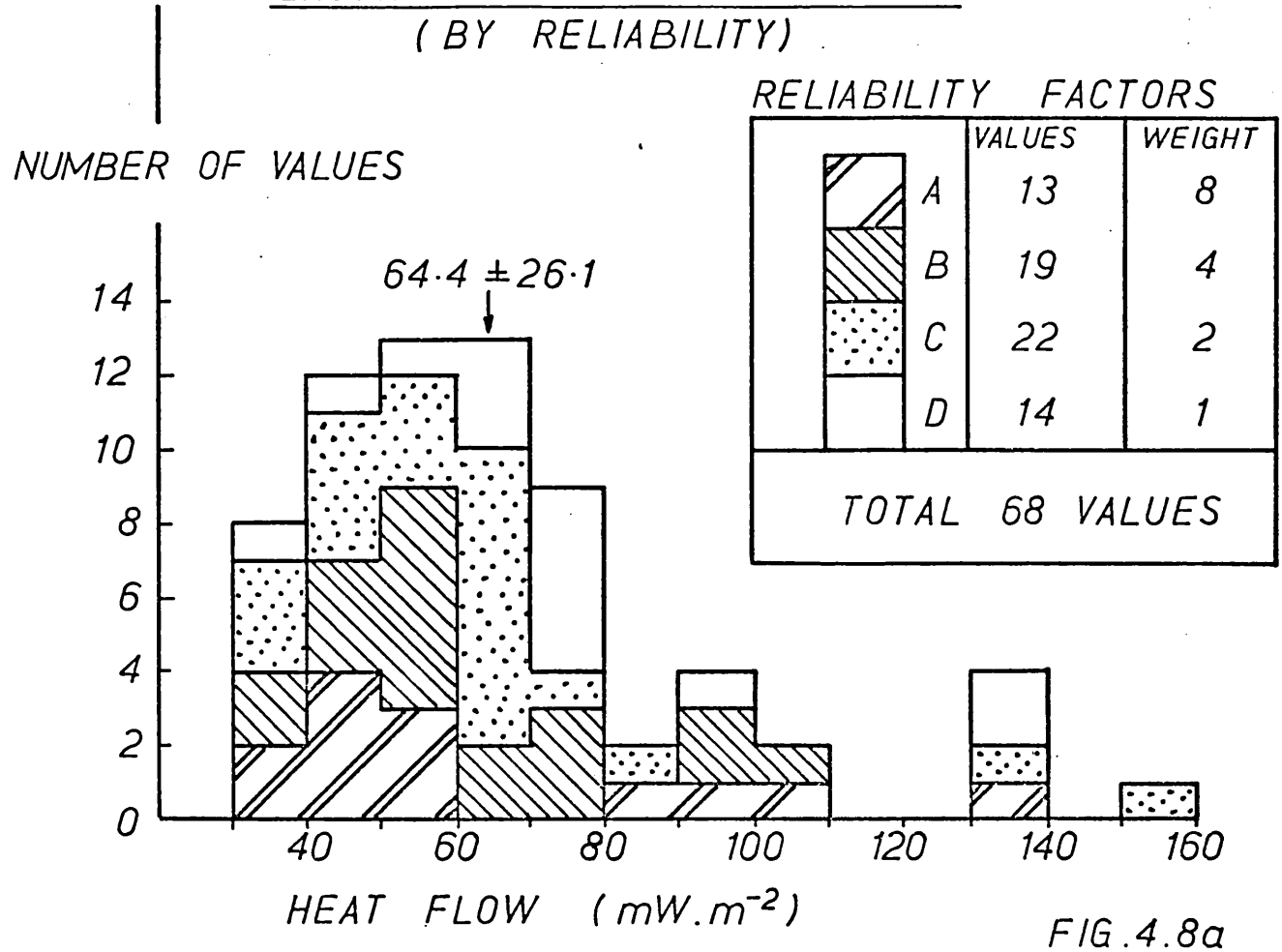


FIG.4.8a

EASTERN AFRICA HEAT FLOW
(BY REGION)

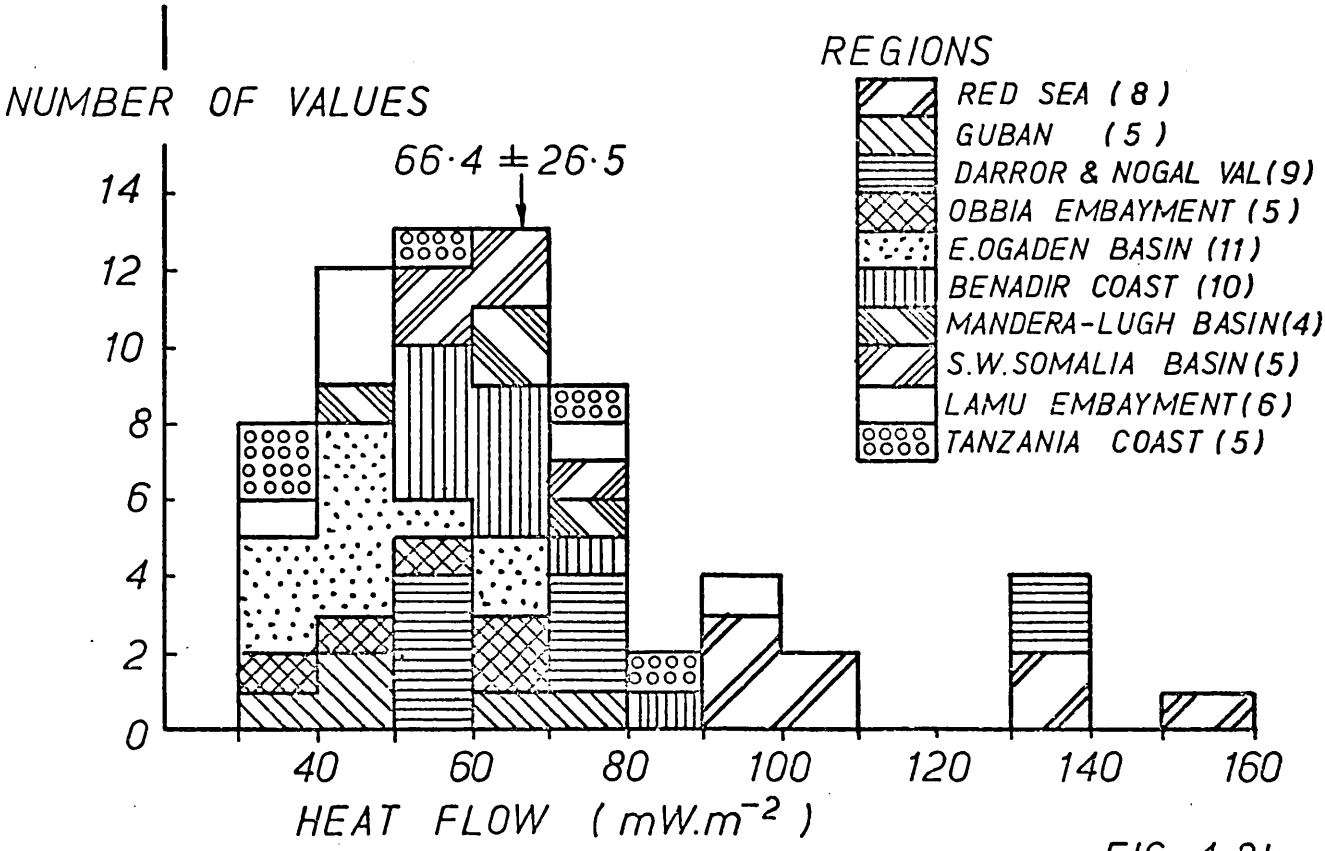


FIG.4·8b

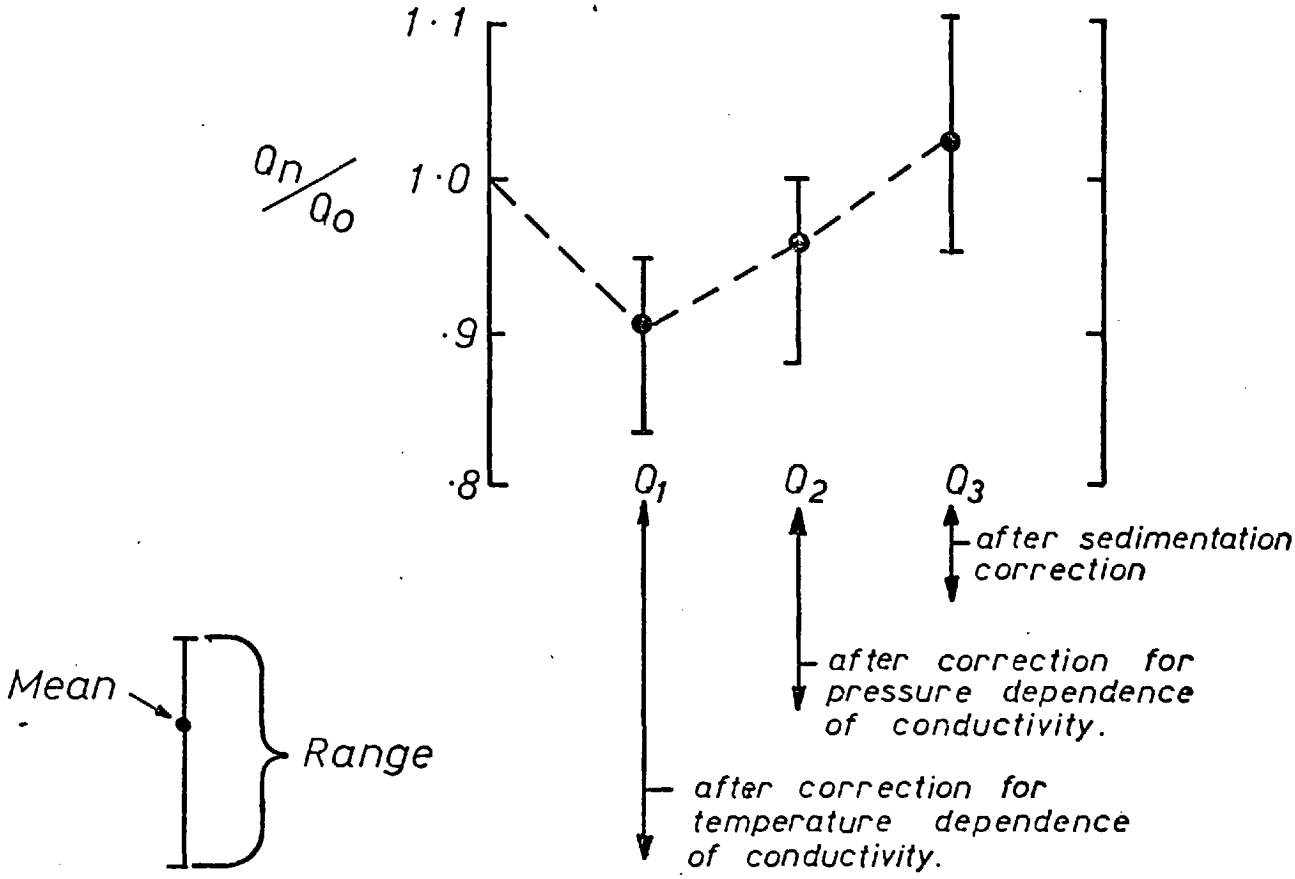
regional Eastern Africa map, Fig. 4.11.

The net result of correcting the heat flow values for temperature and pressure dependence of conductivity and sedimentation (table 4.3) was, in general, to produce a heat flow value, Q_n, little different from the uncorrected, Q_o, result. This is clearly indicated in Fig. 4.9 where the ratio Q_n/Q_o, for n = 1, 2, 3, from table 4.3, has been plotted for the range and mean for the thirteen grade A results, table 4.2. The first correction, Q_1, for the temperature dependence of conductivity, lowered the computed heat flow by as much as 17% and 9% on average. However, the remaining two corrections, for pressure dependence of conductivity, Q_2, and the sedimentation factor, Q_3, both increase the computed heat flow and effectively cancel the Q_1 decrease. The average Q_n/Q_o ratio is 1.02 after the three corrections.

The correction of the temperature and conductivity data does in fact produce a modest improvement in the percentage error of fit, ϵ_n, of equation (3.1) for the computation of heat flow, Q_n. The average is a .4% improvement although values approaching 1% were obtained, Fig. 4.9. However, is was thought that despite this small improvement, the net change in heat flow was so small that the discussion to follow will be concerned only with the uncorrected heat flow values.

A useful summary of heat flow data for large areas may be made by grid averaging results over equal areas. This was demonstrated by Lee (1970), who chose an area equivalent to a 5 x 5 degree square at the equator. In section 4.6 previous heat flow surveys in the region bounded by 10^oS to 15^oN and 35^oE to 70^oE were reviewed. As this region is bisected by the equator and is of limited north south extent 5 x 5 degree squares within it differ little in area. Fig. 4.10 is a plot showing the positions of all available heat flow data, some one hundred and ninety-three values, for the region. Mean values of heat flow with the number of determinations in brackets are shown for all the 5 x 5 degree squares with data.

CHANGE IN HEAT FLOW FROM UNCORRECTED Q_o. TO CORRECTED, Q_n, VALUE.
(for class A heat flow values, Tables 4.1 - 4.3)



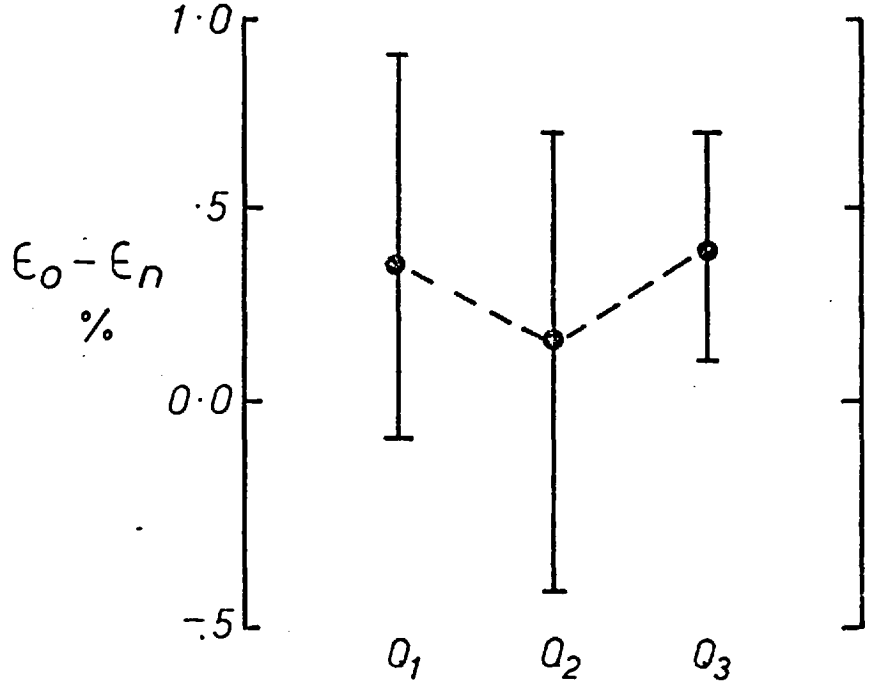
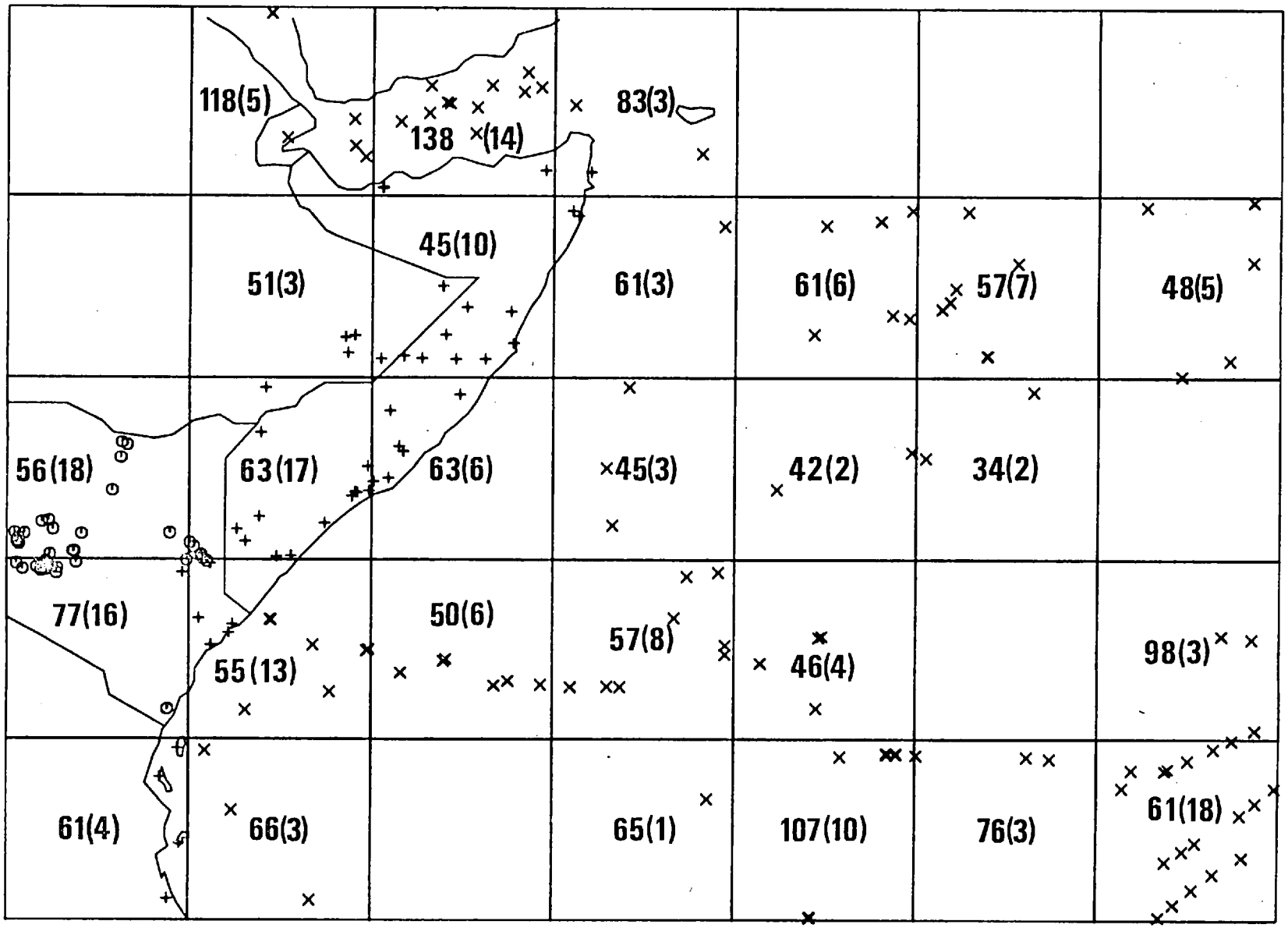


FIG. 4.9

IMPROVEMENT IN PERCENTAGE ERROR, ϵ, OF FIT OF EQUATION (3.1) FOR CORRECTED HEAT FLOW VALUES, Q_n.



NUMBER OF HEAT FLOW OBSERVATIONS = 193
LAT AND LONG IN 5 DEGREE SQUARES
LOWER LEFT CORNER = 10 DEG.S., 35 DEG.E.

o -MORGAN (1973) AND WILLIAMSON (1975), + -THIS STUDY, × -OTHERS
HEAT FLOW VALUES ARE MEANS OF 5 DEGREE SQUARE DATA

EASTERN AFRICA AND SURROUNDING SEAS HEAT FLOW DATA

Fig.4.10

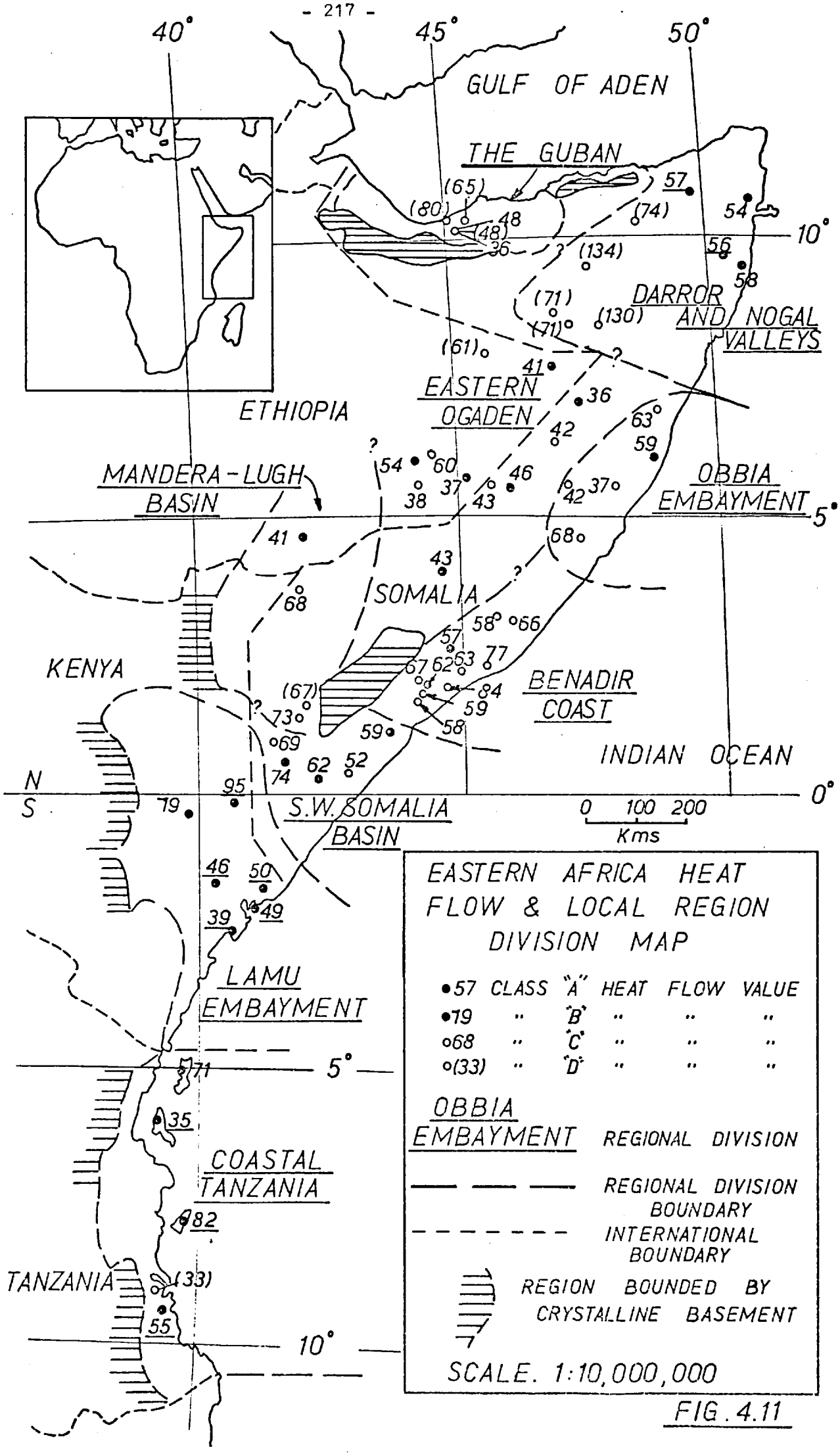

40°
45°
50°
GULF OF ADEN
THE GUBAN
ETHIOPIA
EASTERN OGADEN
DARROR AND NOGAL VALLEYS
MANDERA-LUGH BASIN
OBBIA EMBAYMENT
SOMALIA
KENYA
BENADIR COAST
INDIAN OCEAN
S.W. SOMALIA BASIN
LAMU EMBAYMENT
COASTAL TANZANIA
TANZANIA
10°
5°
0°
N
S
0 100 200
Kms
EASTERN AFRICA HEAT FLOW & LOCAL REGION DIVISION MAP
•57 CLASS "A" HEAT FLOW VALUE
•79 " "B" " " "
○68 " "C" " " "
○(33) " "D" " " "
OBBIA EMBAYMENT REGIONAL DIVISION
REGIONAL DIVISION BOUNDARY
INTERNATIONAL BOUNDARY
REGION BOUNDED BY CRYSTALLINE BASEMENT
SCALE. 1:10,000,000

FIG. 4.11

In addition to the relevant data from section 4.6 this summary includes nineteen unpublished heat flow values for Kenya (Williamson, 1975). A further seven values given by Williamson (1975) were rejected as dubious or west of 35^{o}E. Finally, Fig. 4.10 also incorporates forty-eight values from table 4.2 of this thesis; class D results and the coastal Red Sea values were omitted.

A salient feature of Fig. 4.10 is the east-west low trend between 5^{o}N and 5^{o}S. We will return to this observation in section 4.19. The map, Fig. 4.10, represents a significant improvement in coverage, for this region, on those summaries of Langseth and Taylor (1967) and Lee (1970).

Table 4.1

Eastern Africa - Borehole Descriptions

Well	Country	Company	Lat (N)	Long (E)	Depth (m)	Rte (m)
Coastal Red Sea (Sudan And Ethiopia)						
Dungunab-1	Sudan	AGIP	21° 08'	37° 05'	1567	-
Maghersum-1	Sudan	AGIP	20° 49'	37° 17'	2254	-
Abu Shagara-1	Sudan	AGIP	21° 03'	37° 17'	2293	-
Marafit-1	Sudan	AGIP	18° 19'	37° 54'	2256	-
Amber-1	Ethiopia	Mobil	16° 21'	40° 01'	3526	-25.3
B-1	Ethiopia	Mobil	16° 35'	40° 25'	2881	-85.0
C-1	Ethiopia	Mobil	16° 49'	39° 13'	2831	-75.6
C-1A	Ethiopia	Mobil	16° 49'	39° 13'	1906	-75.6
The Guban (North Coast Of Somalia)						
Berbera-1	Somalia	BP	10° 25'	44° 59'	770	-
Dagah Shabell-1	Somalia	Mobil	10° 11'	45° 17'	1367	4.3
Dagah Shabell-2	Somalia	Mobil	10° 11'	45° 17'	1451	4.0
Dagah Shabell-3	Somalia	Mobil	10° 11'	45° 17'	1505	4.3
Biyo Dader-1	Somalia	Mobil	10° 15'	45° 26'	1475	-
The Nogal And Darror Valleys (NE Somalia)						
Buran-1	Somalia	Amerada	10° 14'	48° 54'	2432	4.3
Burhisso-1	Somalia	Amerada	08° 19'	47° 54'	1545	4.3
Faro Hills-1	Somalia	Amerado	09° 38'	47° 47'	1632	4.3
Las Anod-1	Somalia	Amerada	08° 28'	47° 12'	1659	4.3
Yaguri-1	Somalia	Amerada	08° 39'	47° 01'	1437	4.3
Darin-1	Somalia	AGIP	10° 40'	49° 45'	2963	-
Sagaleh-1	Somalia	AGIP	09° 25'	50° 40'	3264	4.1
Hordio-1	Somalia	AGIP	10° 37'	51° 00'	3405	3.7
Cotton-1	Somalia	AGIP	09° 33'	50° 31'	3306	4.0
Obbia Embayment (Central Coastal Somalia)						
El Hammure-1	Somalia	Sinclair	06° 48'	48° 50'	3567	-
Obbia-1	Somalia	Sinclair	05° 56'	48° 54'	4874	-
Endibere-1	Somalia	Sinclair	05° 30'	47° 18'	3341	-
Gira-1	Somalia	Sinclair	05° 30'	48° 07'	3253	-
Maria Ascia-1	Somalia	Sinclair	04° 31'	47° 26'	4111	-
Eastern Ogaden Basin (Somalia And Ethiopia)						
XF-5	Ethiopia	Sinclair	07° 49'	45° 37'	1329	-

Table 4.1 (Cont'd)

Well	Country	Company	Lat (N)	Long (E)	Depth (m)	Rte (m)
Bokh-1	Ethiopia	Elwerath	07° 30'	46° 57'	3060	-
Galcaio-2	Somalia	Mobil	06° 55'	47° 36'	2131	3.0
Idole-1	Somalia	Mobil	06° 10'	47° 02'	2132	3.0
Dusa Mareb-1	Somalia	Mobil	05° 31'	46° 22'	2066	2.7
Dusa Mareb-2	Somalia	Mobil	05° 35'	45° 53'	2114	2.7
Bulo Burti-1	Somalia	Mobil	04° 04'	45° 30'	2134	3.0
Abred-1	Ethiopia	Elwerath	05° 30'	45° 15'	3103	-
Gallafo-1	Ethiopia	Tenneco	05° 40'	44° 21'	3237	-
Magan-1	Ethiopia	Tenneco	06° 06'	44° 17'	3574	-
Calub-1	Ethiopia	Tenneco	06° 09'	44° 32'	3700	-
Benadir Coast (South Coastal Somalia)						
Gal Tardo-1	Somalia	Sinclair	03° 05'	45° 45'	2432	-
Bio Addo-1	Somalia	Sinclair	02° 57'	45° 52'	2602	-
Duddumai-1	Somalia	Sinclair	02° 32'	44° 54'	3378	-
Uarsciek-1	Somalia	Sinclair	02° 13'	45° 27'	4101	-
Merca-1	Somalia	Sinclair	01° 52'	44° 56'	3957	-
Afgoi-1	Somalia	Sinclair	02° 07'	45° 03'	4148	-
Dobei-1	Somalia	Sinclair	01° 49'	44° 31'	2126	-
Dobei-2	Somalia	Sinclair	01° 43'	44° 28'	3825	-
Coriole-1	Somalia	Sinclair	01° 50'	44° 33'	3516	-
Coriole-2	Somalia	Sinclair	01° 49'	44° 36'	4064	-
Mandera - Lugh Basin (Ethiopia And Somalia)						
El Kuran-1	Ethiopia	Tenneco	04° 42'	42° 05'	3189	-
Hol-1	Somalia	Burmah	03° 28'	41° 57'	4039	-
Gheferson-1	Somalia	Burmah	01° 21'	42° 08'	2183	-
Das Uen-1	Somalia	Burmah	01° 09'	41° 55'	3250	-
S.W. Somalia Basin						
Lach Bissigh-1	Somalia	Gulf	00° 49'	41° 19'	3086	-
Lach Dera-1	Somalia	Gulf	00° 29'	41° 32'	2868	-
Brava-1	Somalia	Sinclair	00° 59'	43° 43'	3581	-
Giamama-1	Somalia	Sinclair	00° 05'	42° 48'	4126	-
Oddo Alimo-1	Somalia	Sinclair	00° 04'	42° 24'	4460	-

Table 4.1 (Cont'd)

Well	Country	Company	Lat (S)	Long (E)	Depth (m)	Rte (m)
			Lamu Embayment (Kenya)			
Wal Merer-1	Kenya	BP	00° 07'	40° 35'	3789	6.1
Garissa-1	Kenya	BP	00° 22'	39° 49'	1214	6.1
Walu-2	Kenya	BP	01° 38'	40° 15'	3722	5.8
Dodori-1	Kenya	BP	01° 49'	41° 11'	4282	5.5
Pate-1	Kenya	BP	02° 04'	41° 05'	3741	5.9
Kipini-1	Kenya	BP	02° 24'	40° 36'	3639	6.5
			Coastal Tanzania			
Pemba-5	Tanzania	BP	05° 16'	39° 42'	3758	6.1
Zanzibar-1	Tanzania	BP	06° 03'	39° 13'	3837	-
Mafia-1	Tanzania	BP	07° 53'	39° 45'	3000	-
Mandawa-7	Tanzania	BP	09° 25'	39° 25'	4058	5.8
Kiswere	Tanzania	BP	09° 27'	39° 31'	784	-

Rte - Rotary turnable elevation (above ground level).

- negative values are subsea.

- Values used to correct borehole depths to sub ground or sub seabed level.

Table 4.2

Eastern Africa - Raw Data Results

Well	NT	NC	Q_o	T_o	G_o	K_o	R
Coastal Red Sea (Sudan And Ethiopia)							
Dungunab-1	3	6(11)	93.3 ± 2.1	(29.0)	30.0 ± .7	3.08	B
Maghersum-1	4	9(11)	100.8 ± 2.7	29.5 ± 1.5	31.0 ± .8	3.25	A
Abu Shagara-1	3	9(11)	95.1 ± .6	27.5 ± .4	29.4 ± .2	3.24	B
Marafit-1	3	0(1)	99.6 ± 5.5	(29.0)	28.7 ± 1.6	3.47	D
Amber-1	3	22(22)	134.2 ± 1.5	26.5 ± .8	29.2 ± .3	4.59	A
B-1	5	0(9)	105.5 ± 6.0	50.0 ± 4.4	43.6 ± 2.5	2.42	B
C-1	3	0(4)	152.3 ± 18.7	(26.0)	46.9 ± 5.8	3.25	C
C-1A	3	0(3)	134.3 ± 3.1	(26.0)	54.5 ± 1.2	2.47	C
The Guban (North Coast Of Somalia)							
Berbera-1	2	0(6)	79.7	(30.0)	35.3	2.26	D
Dagah Shabell-1	7	0(9)	47.6 ± 4.5	(30.0)	18.6 ± 1.8	2.56	C
Dagah Shabell-2	4	0(9)	47.9 ± 10.0	(30.0)	18.9 ± 3.9	2.54	D
Dagah Shabell-3	4	0(6)	35.6 ± 7.6	(30.0)	15.9 ± 3.4	2.23	C
Biyo Dader-1	3	0(9)	65.2 ± 3.2	(30.0)	25.7	2.53	D
The Nogal And Darror Valleys (NE Somalia)							
Buran-1	2	0(6)	74.2	(23.9)	28.1	2.64	D
Burhisso-1	2	0(6)	130.4	(23.9)	47.8	2.73	D
Faro Hills-1	3	0(6)	133.8	(23.9)	49.4	2.71	D
Las Anod-1	3	0(6)	70.8	(23.9)	26.6	2.66	D
Yaguri-1	2	0(6)	70.8	(23.9)	26.7	2.66	D
Darin-1	6	20(21)	57.0 ± 6.6	29.0 ± 4.9	20.1 ± 2.3	2.83	A
Sagaleh-1	5	10(11)	57.6 ± 6.1	20.7 ± 5.3	22.1 ± 2.4	2.60	B
Hordio-1	5	32(32)	54.3 ± 7.3	29.8 ± 7.2	23.8 ± 3.2	2.28	B
Cotton-1	4	28(30)	56.1 ± 4.7	21.3 ± 4.3	24.4 ± 2.0	2.30	A
Obbia Embayment (Central Coastal Somalia)							
El Hammure-1	5	0(4)	62.7 ± 4.2	24.1 ± 3.1	18.6 ± 1.3	3.37	C
Obbia-1	10	0(6)	59.2 ± 3.7	22.0 ± 5.1	76.5 ± 1.6	2.23	B
Endibere-1	4	0(5)	41.9 ± 6.4	36.1 ± 8.8	20.61 ± 3.2	2.03	C
Gira-1	5	0(6)	36.9 ± 3.1	44.3 ± 3.5	17.6 ± 1.5	2.10	C
Maria Ascia-1	4	0(6)	68.0 ± 7.4	28.5 ± 9.4	31.2 ± 3.4	2.18	C

Table 4.2 (Cont'd)

Well	NT	NC	Q_o	T_o	G_o	K_o	R
Eastern Ogaden Basin (Somalia And Ethiopia)							
XF-5	2	0(6)	62.5	(26.3)	22.9	2.73	D
Bokh-1	7	30(30)	41.4 ± 1.3	32.9 ± .9	16.6	2.49	A
Galcaio-2	3	23(23)	35.6 ± 7.0	(27.5)	19.1 ± 3.8	1.86	B
Idole-1	2	13(14)	41.7	(27.5)	22.6	1.85	C
Dusa Mareb-1	3	25(24)	46.1 ± 3.4	(27.5)	18.7 ± 1.4	2.47	B
Dusa Mareb-2	2	13(14)	42.9	(27.5)	18.3	2.24	C
Bulo Burti-1	3	25(25)	43.0 ± 5.6	(27.5)	20.1 ± 2.6	2.13	B
Abred-1	5	0(5)	37.0 ± 1.6	30.3 ± 1.3	16.6 ± .7	2.24	B
Gallafo-1	3	0(3)	38.2 ± 5.2	39.5 ± 4.4	14.9 ± 2.0	2.57	C
Magan-1	9	0(7)	54.3 ± 3.2	39.6 ± 2.7	20.5 ± 1.2	2.65	B
Calub-1	6	0(7)	60.0 ± 4.4	33.6 ± 1.7	22.9 ± 1.7	2.62	C
Benadir Coast (South Coastal Somalia)							
Gal Tardo-1	4	0(6)	58.3 ± 6.6	45.1 ± 5.3	26.5 ± 2.9	2.21	C
Bio Addo-1	3	0(6)	66.2 ± .0	29.3 ± .0	29.8 ± .0	2.23	C
Duddumai-1	5	0(6)	57.0 ± 2.0	23.6 ± 2.0	24.9 ± .9	2.29	B
Uarsciek-1	4	0(8)	77.3 ± 1.2	(27.0)	30.5 ± .5	2.53	C
Merca-1	7	0(11)	83.8 ± 2.8	(27.0)	36.5 ± 1.2	2.31	C
Afgoi-1	4	0(10)	63.3 ± 2.4	(27.0)	26.6 ± 1.0	2.38	C
Dobei-1	3	0(5)	58.7 ± 3.0	(27.0)	22.5 ± 1.1	2.61	D
Dobei-2	7	0(7)	57.8 ± 3.1	(27.0)	23.5 ± 3.1	2.46	C
Coriole-1	8	0(11)	61.7 ± 2.6	36.4 ± 2.4	25.8 ± 1.1	2.39	B
Coriole-2	5	0(9)	67.2 ± 1.7	(27.0)	27.6 ± .7	2.44	C
Mandera - Lugh Basin (Ethiopia And Somalia)							
El Kuran-1	5	4(4)	40.8 ± 1.5	54.0 ± 1.4	15.6 ± .6	2.64	B
Hol-1	20	0(9)	67.5 ± 4.7	37.6 ± 6.1	28.2 ± 2.0	2.39	C
Gheferson-1	2	0(1)	67.2	(29.5)	24.7	2.72	D
Das Uen-1	4	0(1)	73.2 ± 2.9	(29.5)	26.9 ± 1.1	2.72	D
S.W. Somalia Basin							
Lach Bissigh-1	3	0(5)	68.5 ± 1.3	(29.5)	31.7 ± .6	2.16	C
Lach Dera-1	3	0(4)	73.8 ± .4	25.6 ± .4	33.4 ± .2	2.21	B
Brava-1	11	0(9)	59.1 ± 3.1	33.7 ± 3.6	29.5 ± 3.6	2.01	B
Giamama-1	4	0(6)	52.3 ± 1.7	35.9 ± 2.3	25.0 ± .8	2.10	C
Oddo Alimo-1	6	0(7)	61.8 ± 1.5	27.3 ± 2.0	26.5 ± .6	2.33	B

Table 4.2 (Cont'd)

Well	NT	NC	Q_o	T_o	G_o	K_o	R
			Lamu Embayment (Kenya)				
Wal Merer-1	6	55(55)	94.9 ± 4.4	11.7 ± 5.5	40.2 ± 1.9	2.36	A
Garissa-1	2	16(16)	79.0	(28.5)	35.1	2.25	B
Walu-2	5	52(52)	46.2 ± 1.6	49.7 ± 2.6	26.6 ± .9	1.75	A
Dodori-1	8	66(66)	49.8 ± 1.1	33.8 ± 1.8	25.3 ± .6	1.97	A
Pate-1	3	50(50)	49.0 ± 1.7	18.9 ± 2.7	27.8 ± 1.0	1.76	A
Kipini-1	3	48(48)	37.2 ± .4	42.7 ± .6	22.0 ± .2	1.69	A
			Coastal Tanzania				
Pemba-5	4	57(57)	70.6 ± .9	(26.5)	41.5 ± .5	1.70	B
Zanzibar-1	5	44(44)	35.0 ± 1.9	41.5 ± 2.9	19.3 ± 1.1	1.82	A
Mafia-1	7	38(38)	81.9 ± 3.7	17.7 ± 3.6	40.7 ± 1.9	2.01	A
Mandawa-7	7	38(38)	55.2 ± 1.6	18.8 ± 1.7	20.5 ± .6	2.69	A
Kiswere	6	0(2)	33.0 ± 7.9	(26.0)	17.7 ± 4.2	1.87	D

NT - Number of BHTs

NC - Number of conductivity values;
First number - measured values
Bracketed number - measured and assumed values.

Q_o - Uncorrected heat flow values. $(mW \cdot m^{-2})$

T_o - Extrapolated surface temperature; bracketed values had surface temperature input. (^oC)

G_o - Weighted harmonic mean geothermal gradient. $(^oC \cdot Km^{-1})$

K_o - Weighted harmonic mean thermal conductivity. $(W \cdot m^{-1} \cdot K^{-1})$

R - Data grade.

See text for fuller description of terms.

Table 4.3

Eastern Africa - Corrected Heat Flow Values

Well	Q_o	Q_1	Q_2	Q_3	Sed. Rate	Sed. Dur.
Coastal Red Sea (Sudan And Ethiopia)						
Dungunab-1	93.3 ± 2.1	88.2 ± 2.3	89.8 ± 2.1	93.4 ± 2.2	50	25
Maghersum-1	100.8 ± 2.7	91.2 ± 2.0	94.9 ± 2.2	98.4 ± 2.2	40	45
Abu Shagara-1	95.1 ± .6	85.2 ± .4	89.0 ± .5	91.4 ± .5	20	80
Marafit-1	99.6 ± 5.5	91.5 ± 5.1	94.1 ± 5.2	-	?	?
Amber-1	134.2 ± 1.5	112.3 ± .2	118.5 ± .8	129.3 ± .6	120	30
B-1	105.5 ± 6.0	92.1 ± 5.2	97.0 ± 5.3	105.0 ± 5.8	100	30
C-1	152.3 ± 18.7	135.8 ± 13.3	139.9 ± 14.5	-	?	?
C-1A	134.3 ± 3.1	123.0 ± 1.6	126.2 ± 2.0	-	?	?
The Guban (North Coast Of Somalia)						
Berbera-1	79.7	77.4	78.2	-	?	?
Dagah Shabell-1	47.6 ± 4.5	45.9 ± 4.4	46.7 ± 4.4	47.7 ± 4.4	10	175
Dagah Shabell-2	47.9 ± 10.0	46.0 ± 9.5	46.8 ± 9.7	-	?	?
Dagah Shabell-3	35.6 ± 7.6	34.3 ± 7.4	35.0 ± 7.5	35.9 ± 7.5	10	175
Biyo Dader-1	65.2 ± 3.2	62.4 ± 3.4	63.6 ± 3.3	-	?	?
The Nogal And Darror Valleys (NE Somalia)						
Buran-1	74.2	69.7	71.8	73.5	10	175
Burhisso-1	130.4	121.6	124.0	126.8	10	175
Faro Hills-1	133.8	124.1	126.6	129.6	10	175
Las Anod-1	70.8	67.7	69.2	70.8	10	175
Yaguri-1	70.8	68.4	69.6	-	?	?
Darin-1	57.0 ± 6.6	52.9 ± 5.8	55.0 ± 6.2	56.4 ± 6.3	10	210
Sagaleh-1	57.6 ± 6.1	53.8 ± 5.7	56.1 ± 5.9	58.9 ± 6.0	20	210
Hordio-1	54.3 ± 7.3	50.1 ± 6.7	52.5 ± 7.1	55.4 ± 7.1	30	100
Cotton-1	56.1 ± 4.7	52.6 ± 4.1	54.9 ± 4.4	57.7 ± 4.5	20	210
Obbia Embayment (Central Coastal Somalia)						
El Hammure-1	62.7 ± 4.2	56.4 ± 3.8	59.8 ± 4.0	64.0 ± 4.0	60	55
Obbia-1	59.2 ± 3.7	53.0 ± 2.9	56.5 ± 3.3	60.4 ± 3.3	30	155
Endibere-1	41.9 ± 6.4	39.1 ± 5.8	40.9 ± 6.2	43.6 ± 6.2	30	140
Gira-1	36.9 ± 3.1	34.2 ± 2.8	35.8 ± 3.0	37.4 ± 3.0	20	155
Maria Ascia-1	68.0 ± 7.4	60.9 ± 5.7	64.2 ± 6.4	68.6 ± 6.5	30	155

Table 4.3 (Cont'd)

Well	Q_o	Q_1	Q_2	Q_3	Sed. Rate	Sed. Dur.
Eastern Ogaden Basin (Somalia And Ethiopia)						
XF-5	62.5	60.4	61.5	63.0	10	210
Bokh-1	41.4 ± 1.3	39.0 ± 1.0	40.6 ± 1.2	41.6 ± 1.2	10	210
Galcaio-2	35.6 ± 7.0	34.3 ± 6.8	35.4 ± 6.9	37.0 ± 7.0	20	120
Idole-1	41.7	40.2	41.3	43.1	20	120
Dusa Mareb-1	46.1 ± 3.4	44.0 ± 3.4	45.2 ± 3.4	46.8 ± 3.4	20	100
Dusa Mareb-2	42.9	40.9	41.9	43.6	20	120
Bulo Burti-1	43.0 ± 5.6	41.2 ± 5.4	42.4 ± 5.5	44.2 ± 5.5	20	120
Abred-1	37.0 ± 1.6	35.0 ± 1.6	36.6 ± 1.6	37.6 ± 1.6	10	210
Gallafo-1	38.2 ± 5.2	35.3 ± 4.5	37.0 ± 4.9	-	?	?
Magan-1	54.3 ± 3.2	48.8 ± 2.6	51.5 ± 3.0	-	?	?
Calub-1	60.0 ± 4.4	53.0 ± 3.9	56.9 ± 4.2	-	?	?
Benadir Coast (South Coastal Somalia)						
Gal Tardo-1	58.3 ± 6.6	53.4 ± 5.9	55.4 ± 6.2	58.0 ± 6.2	20	155
Bio Addo-1	66.2 ± .0	61.4 ± .4	63.8 ± .1	66.7 ± .2	20	155
Duddumai-1	57.0 ± 2.0	52.3 ± 2.1	55.2 ± 2.1	57.6 ± 2.1	20	155
Uarsciek-1	77.3 ± 1.2	69.4 ± 2.0	73.0 ± 1.6	79.8 ± 1.7	70	60
Merca-1	83.8 ± 2.8	75.4 ± 2.1	79.7 ± 2.4	86.0 ± 2.3	50	80
Afgoi-1	63.3 ± 2.4	57.8 ± 2.5	60.9 ± 2.4	65.8 ± 2.5	50	80
Dobei-1	58.7 ± 3.0	55.9 ± 3.1	57.4 ± 3.1	60.7 ± 3.1	50	45
Dobei-2	57.8 ± 3.1	53.0 ± 3.1	55.9 ± 3.1	60.2 ± 3.1	50	80
Coriole-1	61.7 ± 2.6	55.6 ± 2.4	58.7 ± 2.5	62.4 ± 2.5	40	80
Coriole-2	67.2 ± 1.7	61.0 ± 1.7	64.4 ± 1.6	70.4 ± 1.7	40	60
Mandera - Lugh Basin (Ethiopia And Somalia)						
El Kuran-1	40.8 ± 1.5	36.6 ± 1.3	38.6 ± 1.4	-	?	?
Hol-1	67.5 ± 4.7	58.2 ± 4.0	62.0 ± 4.3	65.2 ± 4.3	20	175
Gheferson-1	67.2	63.1	64.8	-	?	?
Das Uen-1	73.2 ± 2.9	66.6 ± 2.7	69.3 ± 2.8	-	?	?
S.W. Somalia Basin						
Lach Bissigh-1	68.5 ± 1.3	62.9 ± .5	65.5 ± .8	70.2 ± .8	50	60
Lach Dera-1	73.8 ± .4	67.5 ± .4	70.4 ± .4	75.4 ± .4	60	45
Brava-1	59.1 ± 3.1	53.8 ± 2.8	56.6 ± 3.0	60.0 ± 3.0	20	250
Giamama-1	52.3 ± 1.7	47.5 ± 1.6	50.3 ± 1.7	55.7 ± 1.6	90	45
Oddo Alimo-1	61.8 ± 1.5	55.3 ± 1.0	58.6 ± 1.2	64.0 ± 1.2	60	80

Table 4.3 (Cont'd)

Well	Q_o	Q_1	Q_2	Q_3	Sed. Rate	Sed. Dur.
			Lamu Embayment (Kenya)			
Wal Merer-1	94.9 ± 4.4	82.1 ± 3.0	87.4 ± 3.4	92.5 ± 3.6	30	120
Garissa-1	79.0	76.0	77.2	79.0	10	155
Walu-2	46.2 ± 1.6	42.1 ± 1.4	44.7 ± 1.5	48.2 ± 1.5	40	100
Dodori-1	49.8 ± 1.1	45.6 ± 1.0	48.3 ± 1.1	52.3 ± 1.1	50	80
Pate-1	49.0 ± 1.7	45.9 ± 1.6	48.8 ± 1.9	54.3 ± 1.6	80	55
Kipini-1	37.2 ± .4	34.2 ± .2	36.3 ± .3	39.6 ± .3	50	80
			Coastal Tanzania			
Pemba-5	70.6 ± .9	65.4 ± 1.0	67.7 ± .9	73.9 ± .9	50	80
Zanzibar-1	35.0 ± 1.9	33.0 ± 1.8	35.0 ± 1.9	37.5 ± 1.9	50	80
Mafia-1	81.9 ± 3.7	75.6 ± 3.4	79.2 ± 3.6	84.1 ± 3.5	40	80
Mandawa-7	55.2 ± 1.6	50.1 ± 1.4	53.3 ± 1.6	56.3 ± 1.5	20	210
Kiswere	33.0 ± 7.9	32.5 ± 7.8	32.8 ± 7.8	33.5 ± 7.8	10	100

Q_o - Uncorrected heat flow value.

Q_1 - Temperature effect on conductivity corrected heat flow value.

Q_2 - Pressure effect on conductivity corrected heat flow value.

Q_3 - Sedimentation corrected heat flow value. $(\overline{mW \cdot m^{-2}})$

Sed. Rate - Sedimentation rate $(mm \cdot 10^{-3} \cdot yr^{-1})$.

Sed. Dur. - Sedimentation duration $(10^6 yr)$.

Table 4.4

Mean Heat Flow Values for the

Individual Regions; Eastern Africa

Area	Values	Mean[1] ($mW \cdot m^{-2}$)	Mean[2] ($mW \cdot m^{-2}$)
1 Coastal Red Sea	8	114 ± 22	113 ± 19
2 The Guban	5	55 ± 17	51 ± 16
3 Darror and Nogal Valleys	9	78 ± 31	63 ± 20
4 Obbia Embayment	5	54 ± 14	55 ± 11
5 Eastern Ogaden Basin	11	46 ± 9	44 ± 7
6 Benadir Coast	10	65 ± 9	64 ± 8
7 Mandera-Lugh Basin	4	62 ± 15	55 ± 15
8 S.W. Somalia Basin	5	63 ± 8	64 ± 7
9 Lamu Embayment	6	59 ± 22	58 ± 21
10 Tanzania Coast	5	55 ± 22	58 ± 19
Overall Averages	68	66 ± 27	64 ± 26

Note: 1 - unweighted mean

2 - weighted mean (A:B:C:D, 8:4:2:1)

4.8 Heat Production Measurements

The natural heat production of seventeen Eastern Africa igneous and sedimentary rocks was measured. A gamma ray spectrometer, located at the Imperial College Silwood Park Reactor Centre, was used.

The spectrometer is essentially a 7.6 cm. diameter, 7.6 cm. long sodium iodide crystal. Impinging gamma rays, from natural radioactive isotopes, result in crystal scintillations. An attached photomultiplier converts each scintillation to a voltage which is amplified and fed to a multi-channel pulse height analyser. The pulse height or voltage is a measure of the gamma ray energy which is, in turn, indicative of a particular radioactive decay in the decay scheme of an isotope. The pulses were stored in the multi-channel analyser such that at the end of the measurement a spectrum of count rate versus energy was obtained.

Sample preparation consisted of crushing the rock to a fine powder and packing a weighed amount, about 1 kilogram, into a plastic container which fitted over the sodium iodide crystal. The sample, crystal, and photomultiplier were effectively shielded by a ten centimetre lead barrier to minimize unwanted background count. Each measurement lasted six hours to insure sufficient counts to obtain a reliable result.

The only isotopes which contribute significantly to heat production in rocks are U_{238}, U_{235}, Th_{232}, and K_{40}, where U, Th, and K are uranium, thorium and potassium respectively. Computation of their concentrations from the sample count rate energy spectrum was made by comparison with similar spectra obtained from measurements on standard samples of precisely known concentrations of U, Th, and K. Birch (1954) has calculated the heat produced per unit mass per unit time for the relevant isotopes. Thus, by assuming a density, in this case 2.68 $gm \cdot cm^{-3}$, we may calculate heat production per unit volume where the time of measurement was precisely recorded. Further details of the Imperial College Silwood Park gamma ray spectrometer and the analysis

of count rate energy spectra may be found in Strachan (1973).

The results are presented in table 4.5 and will be incorporated into the discussions of the Kenya and Sudan heat flow. Morgan (1974, pers. comm.) has rerun two of the samples on the gamma ray spectrometer of Southern Methodist University, Dallas, Texas. No significant differences were obtained. Morgan also measured a single sample from the bottom of Darin-1 well at 2971 metres (Fig. 4.1). The sample is from the metamorphic basement of the Somalia Horn, the Inda Ad formation discussed in section 4.2.

Table 4.5

Heat Production Measurements

Of Eastern Africa Samples

	Sample Number	Description	U ppm	Th ppm	K %	A $W \cdot m^{-3}$
	Sudan Samples					
1	S-5	Biotite granite	1.68	3.28	2.41	.90
2	S-13	Gneissose biot. granite	.88	1.11	2.21	.52
3	S-92	Biotite granodiorite	.58	.69	1.31	.33
4	S-97	Hornblende syenite	2.48	11.87	3.20	1.80
5	S-14399	C.g. hble. granite	.50	2.94	1.19	.45
6	S-14406	Biot. hble. granite	.98	3.42	1.59	.65
7	S-15081	Biotite granite	.65	3.52	1.70	.58
8	DG1-006	Biotite granite	.37	.58	1.63	.29
		MEANS	1.02	3.43	1.91	.69 ± .49
	Kenya Samples					
9	WM1-CR-1	Limestone, brn., sndy.	3.51	.63	.23	.98
10	WM1-CR-2	Red sandstone	1.07	4.17	.96	.67
11	WM1-CR-3	argill. limestone	1.85	5.29	.90	.94
12	WM1-CR-4	argill. limestone	1.76	4.84	2.03	1.00
13	WM1-CR-5	f.g. calc. sandstone	1.14	4.30	1.42	.74
14	WM1-CR-6	calcareous siltstone	2.88	10.93	4.07	1.92
15	WM1-CR-8	gry. shale, silty	2.38	10.13	4.61	1.78
16	WM1-CR-9	gry. shale, silty	3.14	11.93	2.64	1.92
17	WM1-CR-10	black shale	2.71	10.56	2.72	1.72
		MEANS	2.27	6.98	2.18	1.30 ± .53
	Samples rerun at SMU					
8*	DG1-006	Biotite granite	.75	.8	1.4	.4
16*	WM1-CR-9	gry. shale, silty	3.1	11.9	2.3	1.8
	Somalia Sample - SMU					
18	DR1-020	Biotite schist	2.5	11.9	2.5	1.72

U, Th, K, A : Uranium, Thorium, Potassium, Heat Production, respectively.

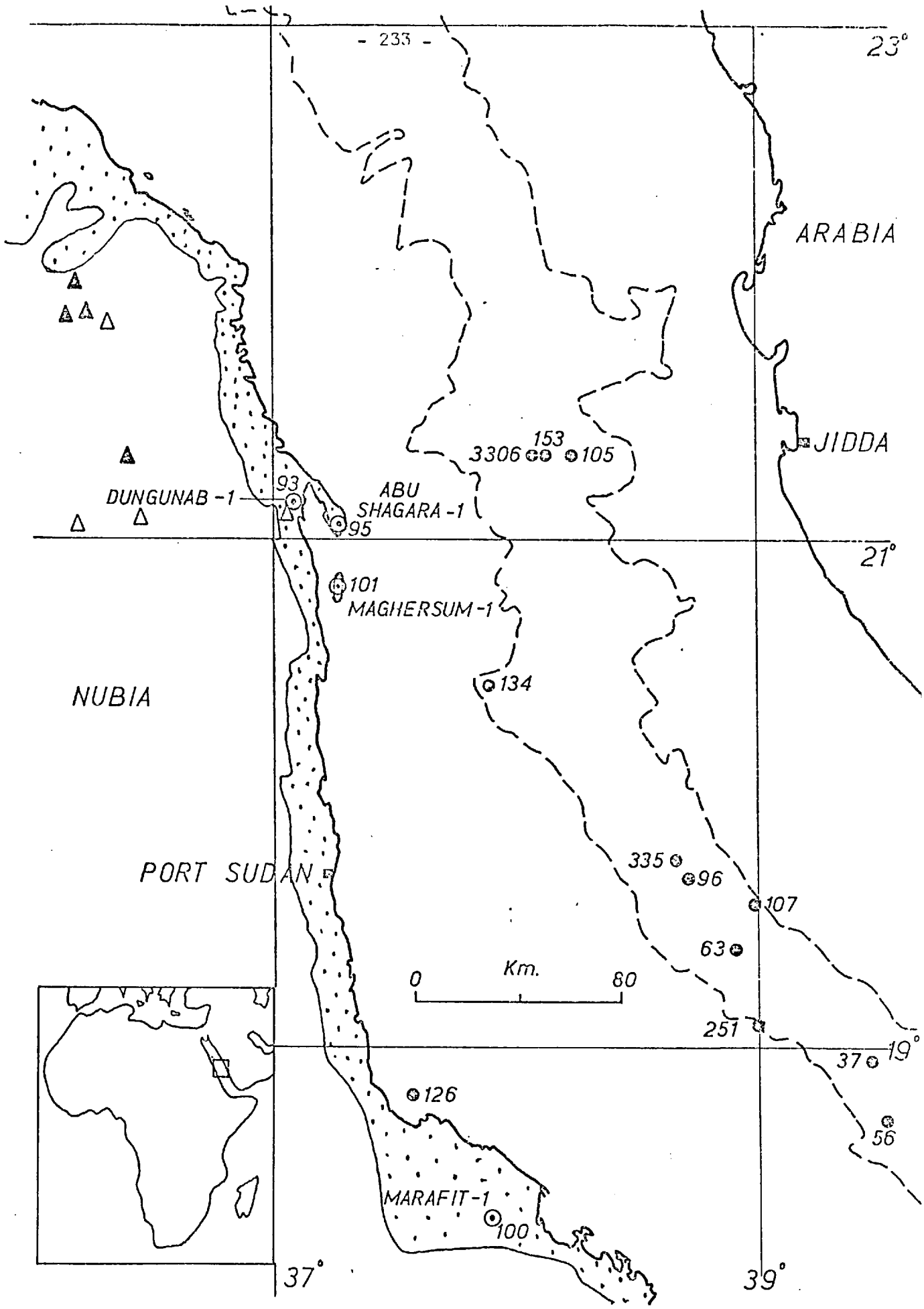
4.9 Coastal Red Sea Heat Flow

Eight values of heat flow, four each from the coastal plain/shelf areas of the Sudan and Ethiopia, are presented for the Red Sea region. Three of the four Sudan results have previously been given by Evans and Tammemagi (1974); Girdler (1970) has also published one of the Ethiopian values. These data were incorporated here as minor modifications were made to the former results while significantly more data was available for the latter.

The Sudan coastal plain results are shown on Fig. 4.12 together with all published data, apart from that of Scheuch (1973) for this area (see section 4.7). Three of the values, Dungunab-1, Abu Shagara-1, and Maghersum-1 are grouped closely together at about 37°E, 21'N, on a narrow coastal strip of Tertiary sediments and volcanics unconformably overlying crystalline basement (Carella and Scarpa, 1962, Sestini, 1965). The basement is composed of a Precambrian metamorphic complex into which granites have been intruded in two major phases. These two granites, which have been dated at 554 ± 54 and 394 ± 9 m.y. (Gass and Neary, 1975) are referred to as the Batholithic and Younger series respectively. Gamma-ray spectrometry of four samples each of the two granites, table 4.5, reveals that both are remarkably depleted in the radioactive elements U, Th, K and hence low in heat production when compared with 'average' values (Sass, 1972).

The fourth Sudan result is from the deeper Tertiary basin of Southern Sudan (Baldarassi, 1968) near the previously reported oil well heat flow result Durwara - 1/2 of Girdler (1970).

The composite heat flow plots, Figs. 4.13 - 4.15, indicate the north-east coastal Sudan results to be internally consistent with small Bullard temperature residuals (uniform heat flow with depth) and reasonable extrapolated surface temperatures; the southern result, Fig. 4.16, is poor by comparison due to the lack of conductivity samples.



COASTAL SUDAN & RED SEA HEAT FLOW

● OTHER WORKERS
⊙ THIS STUDY
▲, △, HEAT PRODUCTION RESULT.

COASTAL SEDIMENTS
500 FATHOMS

FIG. 4.12

DUNGUNAB-1

COUNTRY-SUDAN
COMPANY-AGIP

LAT-21D 08M N.
LONG-37D 05M E.

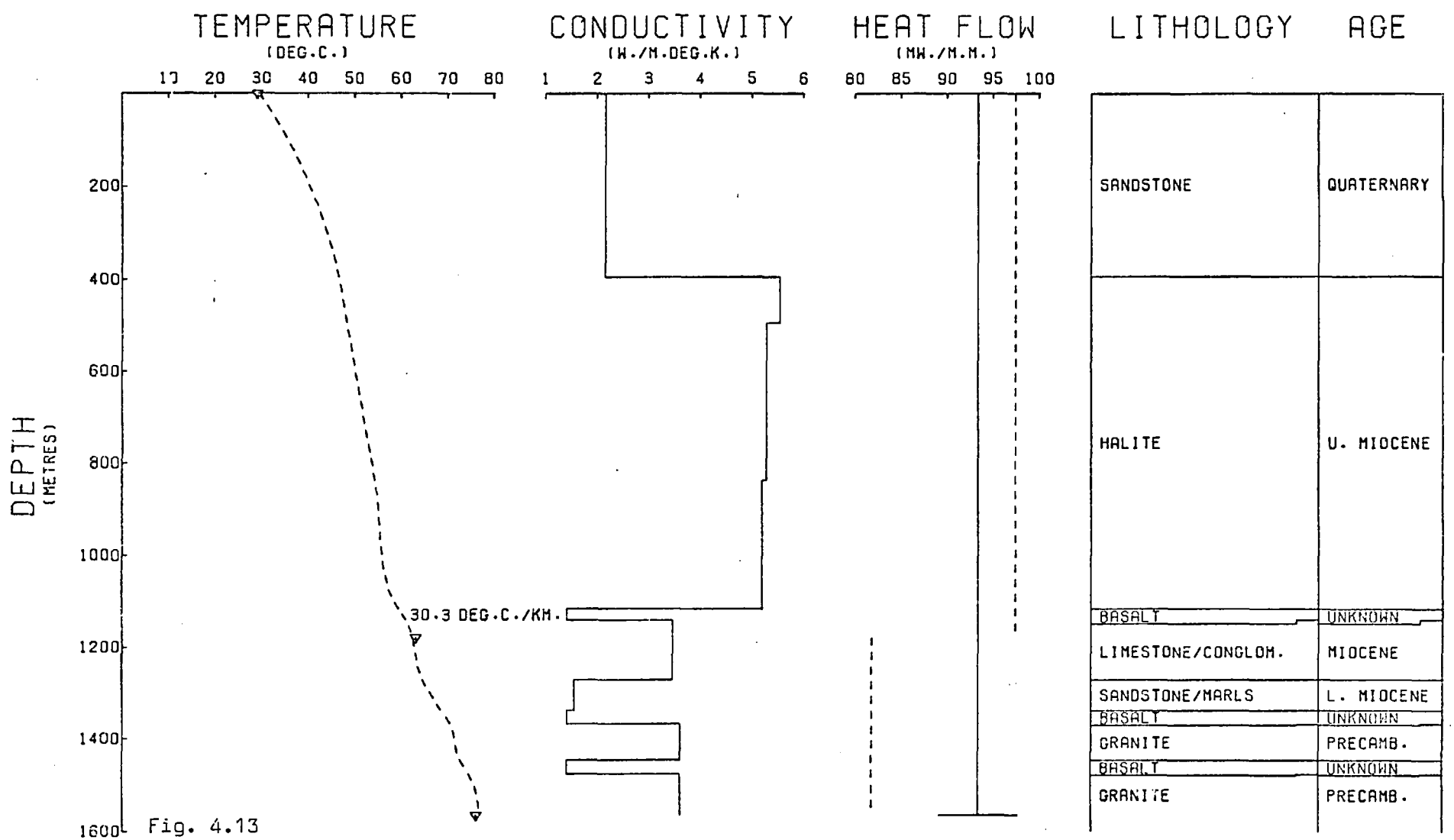


Fig. 4.13

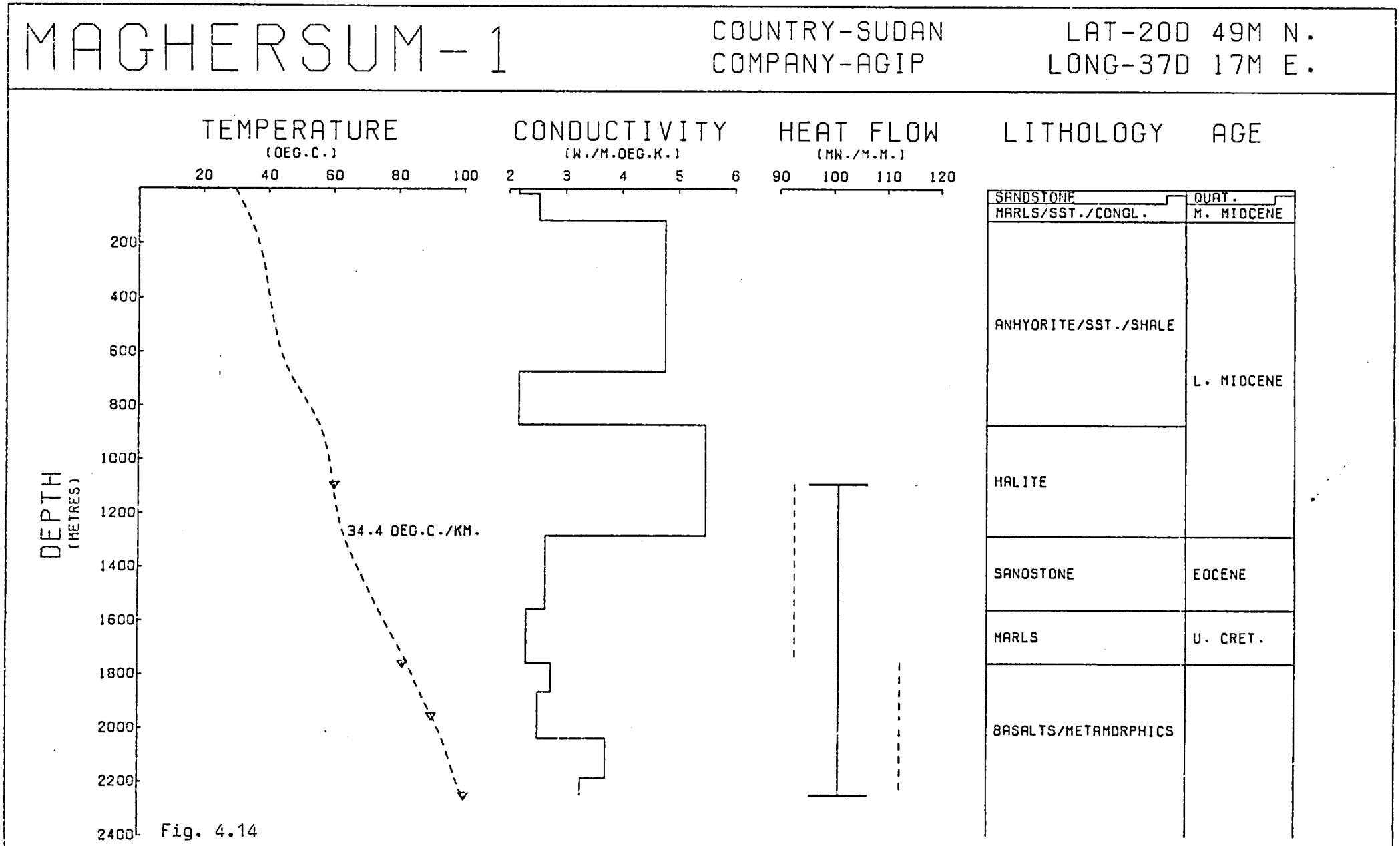

MAGHERSUM-1
COUNTRY-SUDAN
COMPANY-AGIP
LAT-20D 49M N.
LONG-37D 17M E.
TEMPERATURE
(DEG.C.)
20
40
60
80
100
CONDUCTIVITY
(W./M.DEG.K.)
2
3
4
5
6
HEAT FLOW
(MW./M.M.)
90
100
110
120
LITHOLOGY
AGE
DEPTH
(METRES)
200
400
600
800
1000
1200
1400
1600
1800
2000
2200
2400
34.4 DEG.C./KM.
SANDSTONE
MARLS/SST./CONGL.
QUAT.
M. MIOCENE
ANHYDRITE/SST./SHALE
L. MIOCENE
HALITE
SANDSTONE
EOCENE
MARLS
U. CRET.
BASALTS/METAMORPHICS

Fig. 4.14

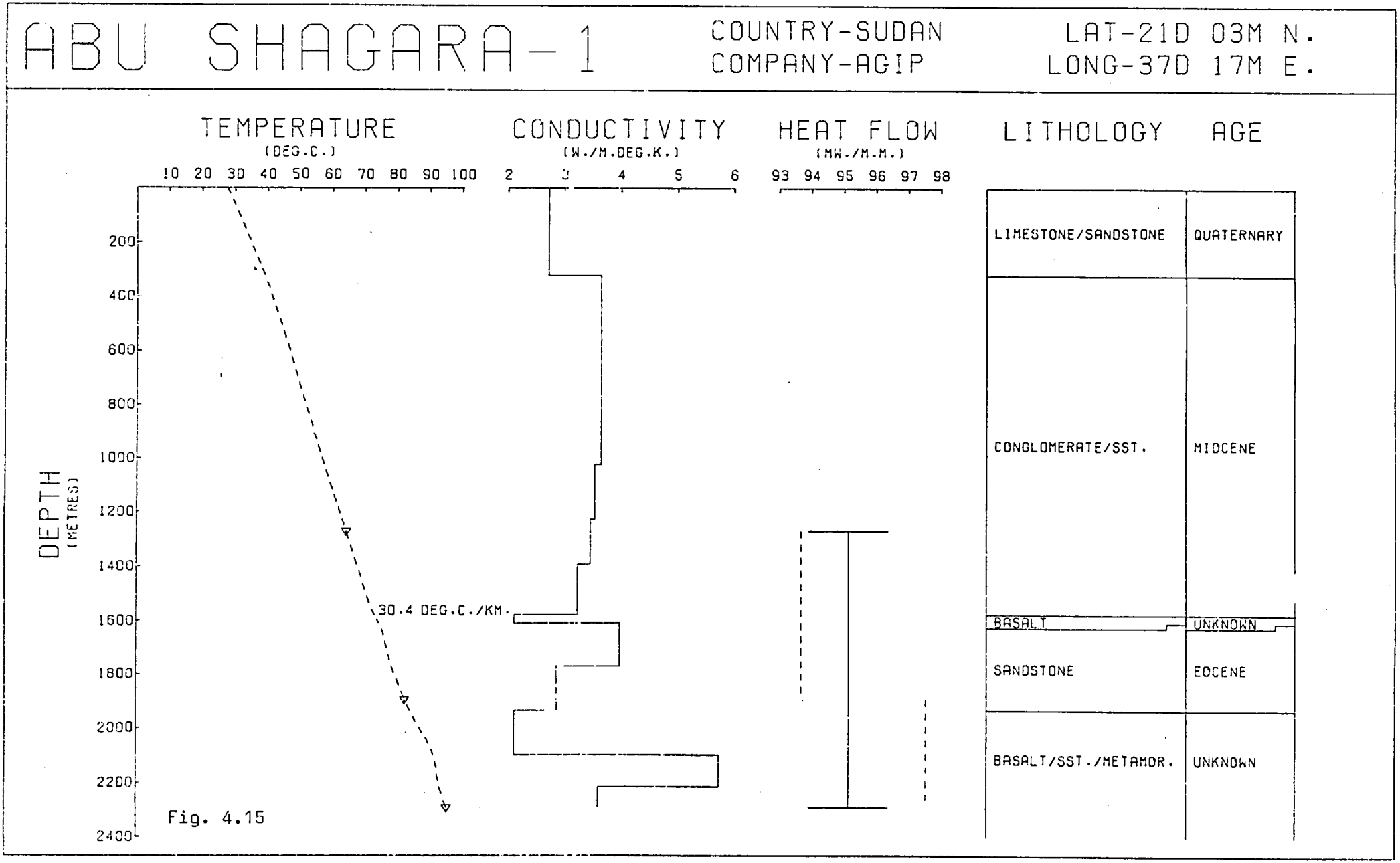

ABU SHAGARA-1
COUNTRY-SUDAN
COMPANY-AGIP
LAT-21D 03M N.
LONG-37D 17M E.
TEMPERATURE
(DEG.C.)
10 20 30 40 50 60 70 80 90 100
CONDUCTIVITY
(W./M.DEG.K.)
2 3 4 5 6
HEAT FLOW
(MW./M.M.)
93 94 95 96 97 98
LITHOLOGY
AGE
DEPTH
(METRES)
200
400
600
800
1000
1200
1400
1600
1800
2000
2200
2400
30.4 DEG.C./KM.
LIMESTONE/SANDSTONE
QUATERNARY
CONGLOMERATE/SST.
MIOCENE
BASALT
UNKNOWN
SANDSTONE
EOCENE
BASALT/SST./METAMOR.
UNKNOWN

Fig. 4.15

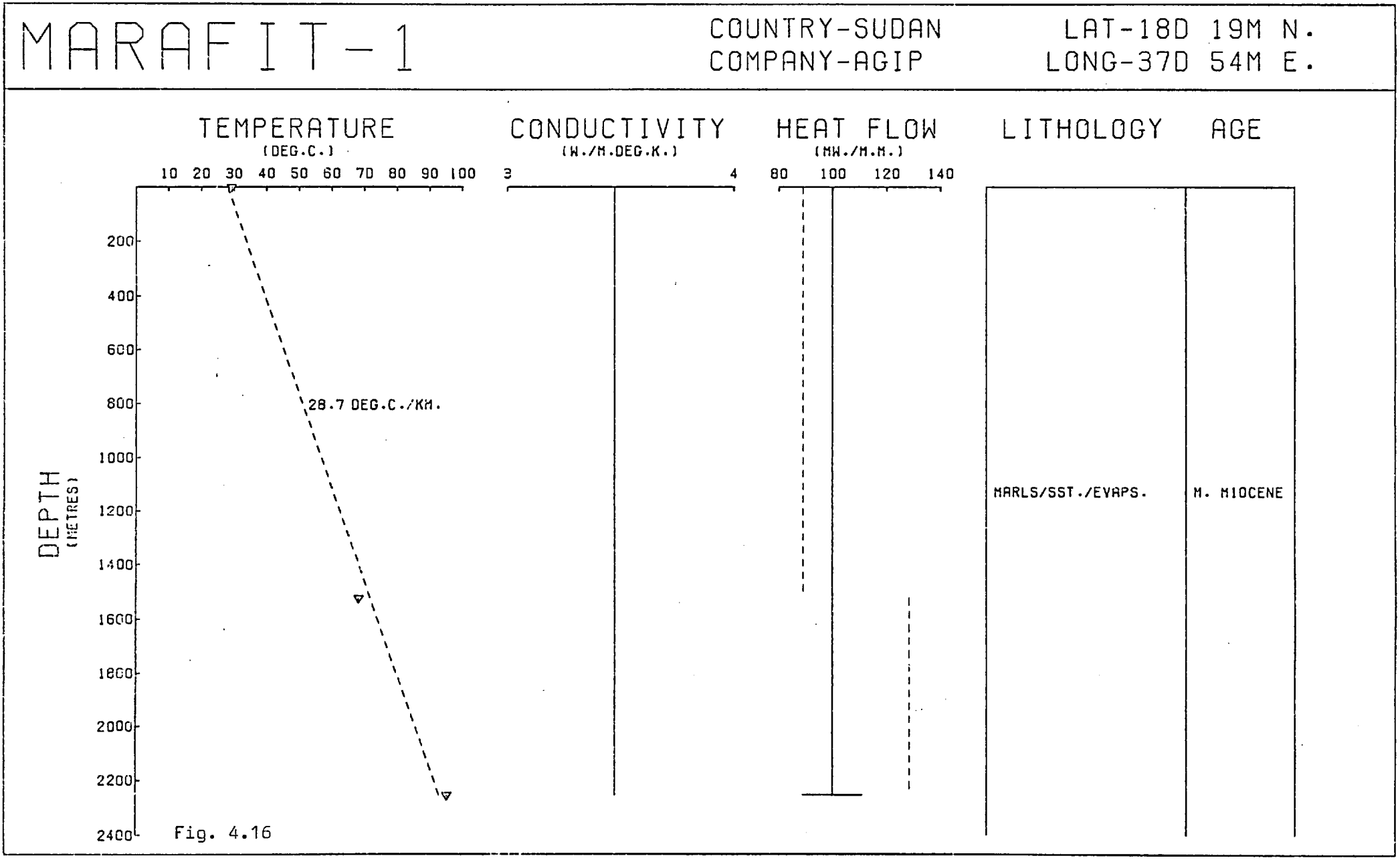

MARAFIT-1
COUNTRY-SUDAN
COMPANY-AGIP
LAT-18D 19M N.
LONG-37D 54M E.
TEMPERATURE
(DEG.C.)
10 20 30 40 50 60 70 80 90 100
CONDUCTIVITY
(W./M.DEG.K.)
3 4
HEAT FLOW
(MW./M.M.)
80 100 120 140
LITHOLOGY
AGE
DEPTH
(METRES)
200 400 600 800 1000 1200 1400 1600 1800 2000 2200 2400
28.7 DEG.C./KM.
MARLS/SST./EVAPS.
M. MIOCENE

Fig. 4.16

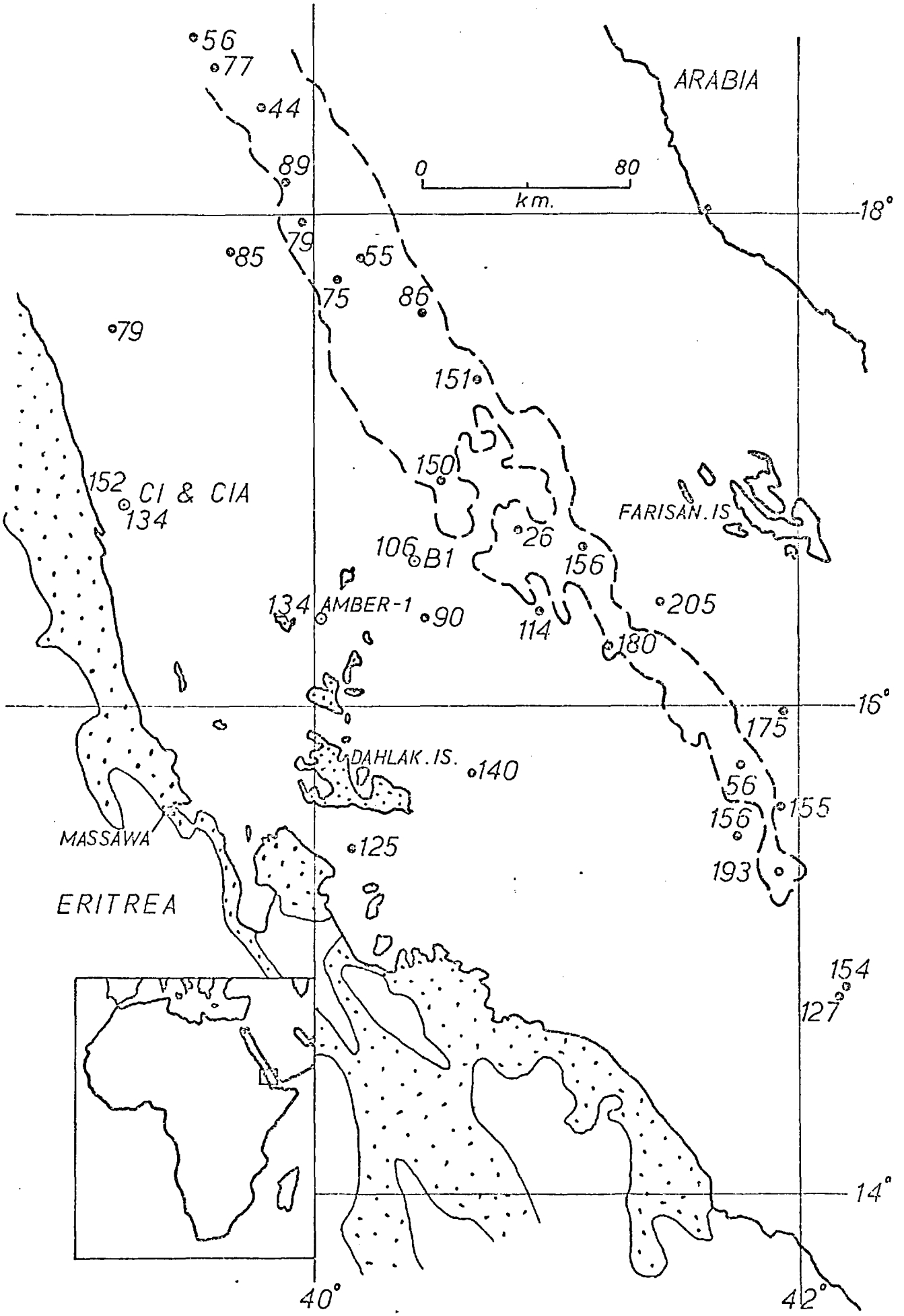
The four Ethiopian shelf results are mapped in Fig. 4.17, again with all previously published heat flow values (section 4.6). The Red Sea shelf in this region is overlain by a remarkably thick upper Tertiary carbonate-evaporite sequence (cf. Lowell and Genik, 1972). The basement rocks in this region have been the subject of considerable dispute (section 4.4) though the bulk of the evidence tends to suggest a drastically thinned Precambrian crust.

The composite heat flow plots, Figs. 4.18 - 4.21, reveal the Amber-1 result to be internally consistent and, at 134 $mW \cdot m^{-2}$, table 4.2, slightly higher than the estimated value of 122 $mW \cdot m^{-2}$ of Girdler (1970). The remaining three values, B-1, C-1, and C-1A, are uniformly high though less well determined due to a lack of conductivity samples.

The mean value of heat flow of all eight results is 114 ± 22 $mW \cdot m^{-2}$, table 4.4, which, while considerably greater than any other region in this study, is slightly less than the average of the 39 published values of 126 ± 66 $mW \cdot m^{-2}$, Fig. 4.7.

McKenzie (1967) has obtained solutions for the heat flow over a lithospheric plate of constant thickness moving at a constant velocity with a 'dyke intrusion' of constant temperature at one margin. Fig. 4.22 illustrates the computed heat flow for a 50 kilometre thick lithospheric plate moving with velocities of 1 and 2 $cm \cdot y^{-1}$, consistent with the geophysical data (section 4.4). All available data including the eight values presented here are superimposed; the qualitative agreement is obvious. A similar plot of the Gulf of Aden data (see section 4.6) is shown for comparison, Fig. 4.22. While more elaborate models have been proposed (cf. Bottinga and Allegre, 1973, Lubimova and Nikitina, 1975) the McKenzie model is still thought to represent a reasonable approximation to the physical situation (Le Pichon et al., 1973).

We will return to these new heat flow values in connection with one dimensional temperature models of the crust and upper mantle, section 4.21.



COASTAL ETHIOPIA AND RED SEA HEAT FLOW

• OTHER WORKERS
⊙ THIS STUDY
COASTAL SEDIMENTS
500 FATHOMS

FIG. 4.17

AMBER-1

COUNTRY-ETHIOPIA LAT-16D 21M N.
COMPANY-MOBIL LONG-40D 01M E.

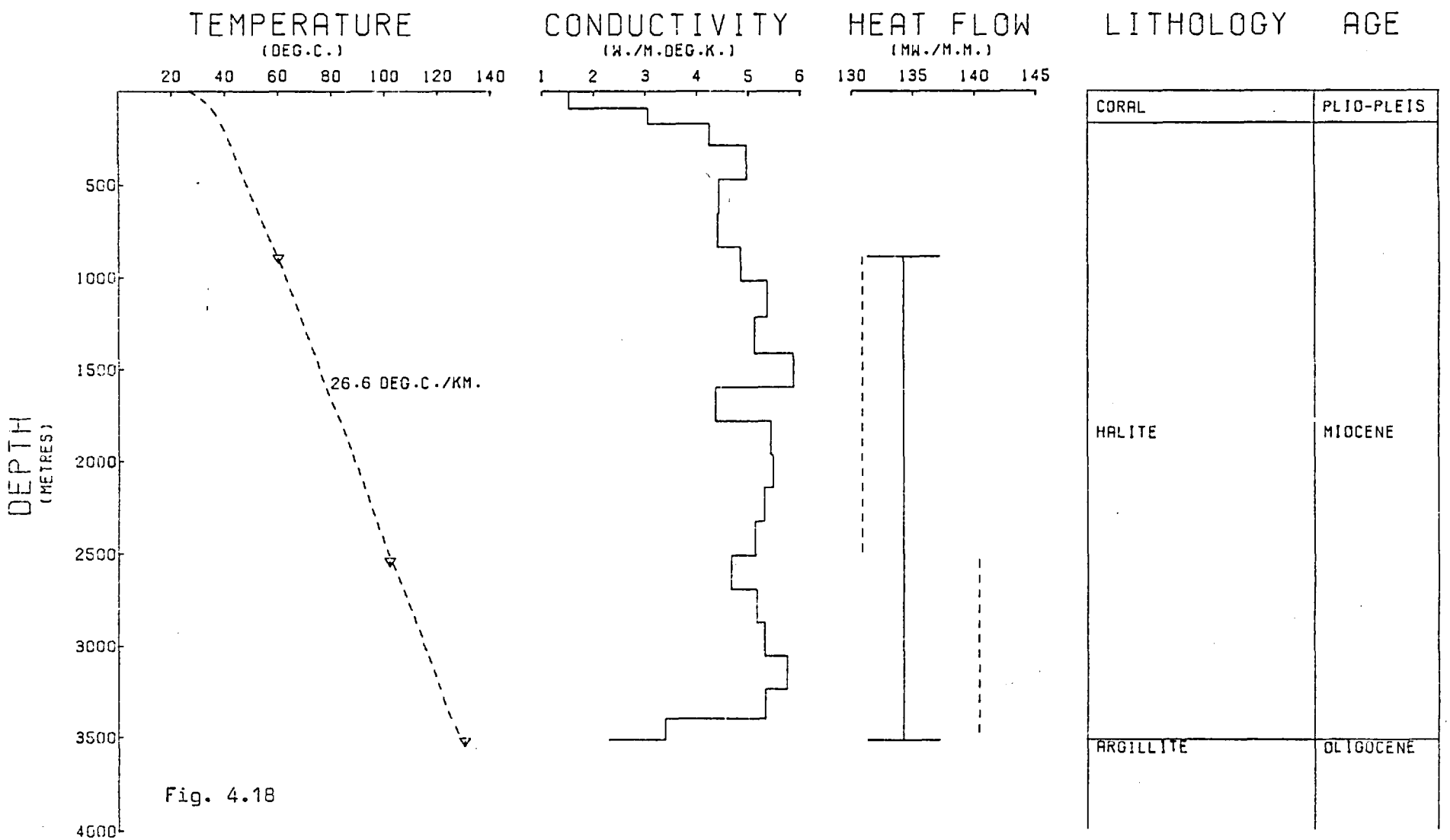


Fig. 4.18

B - 1

COUNTRY-ETHIOPIA LAT-16D 35M N.
COMPANY-MOBIL LONG-40D 25M E.

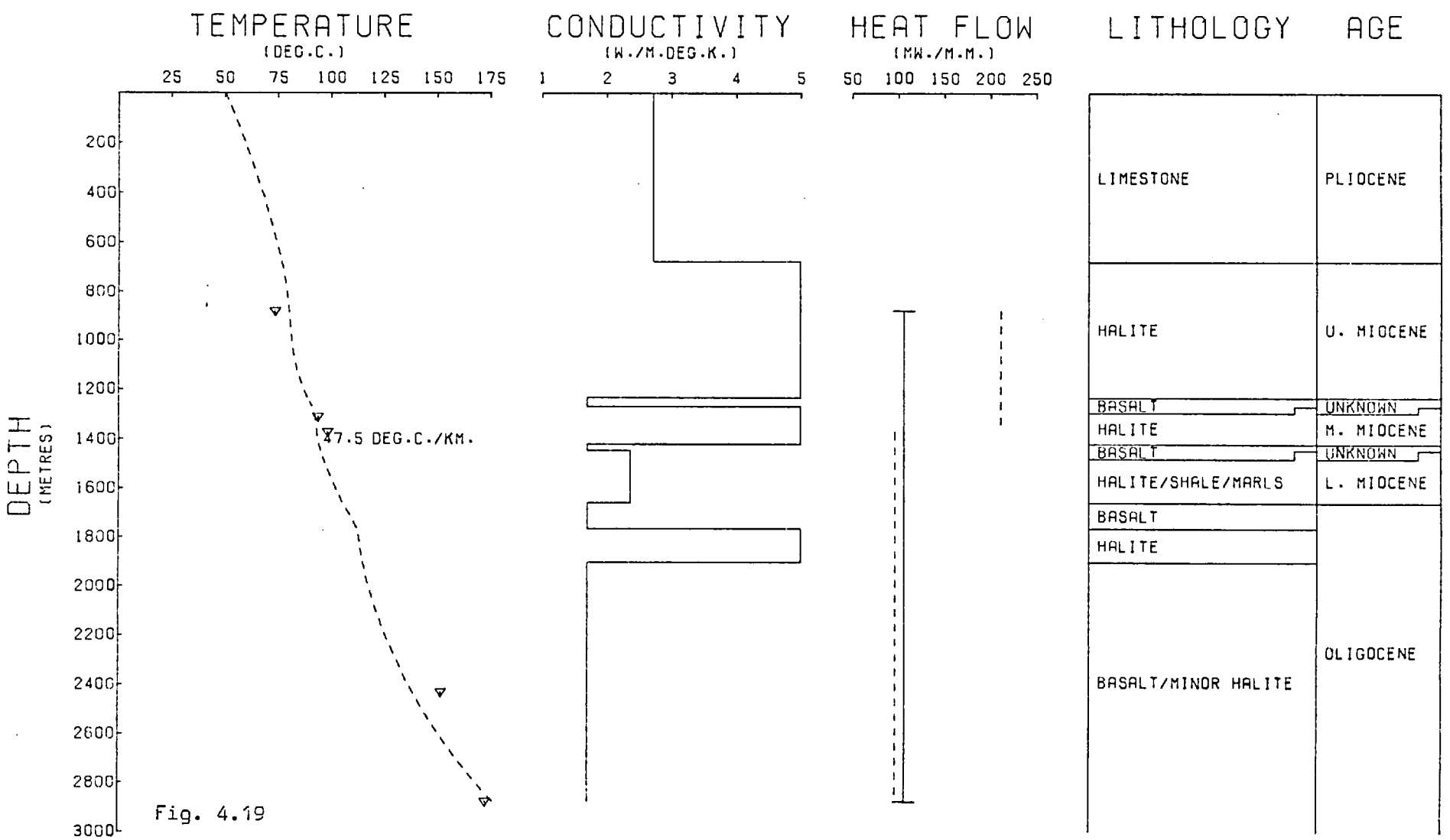


Fig. 4.19

C - 1

COUNTRY-ETHIOPIA LAT-16D 49M N.
COMPANY-MOBIL LONG-39D 13M E.

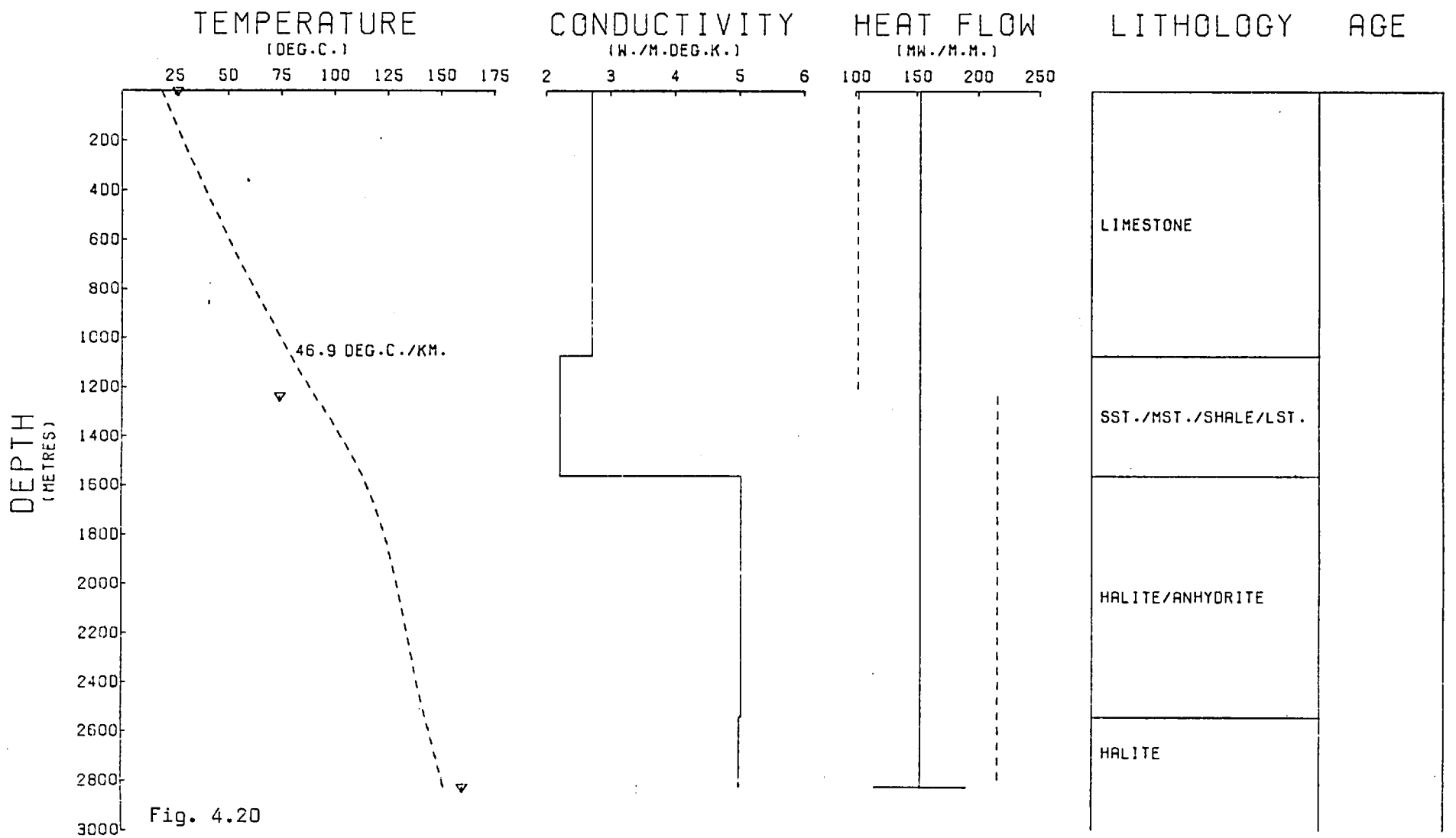


Fig. 4.20

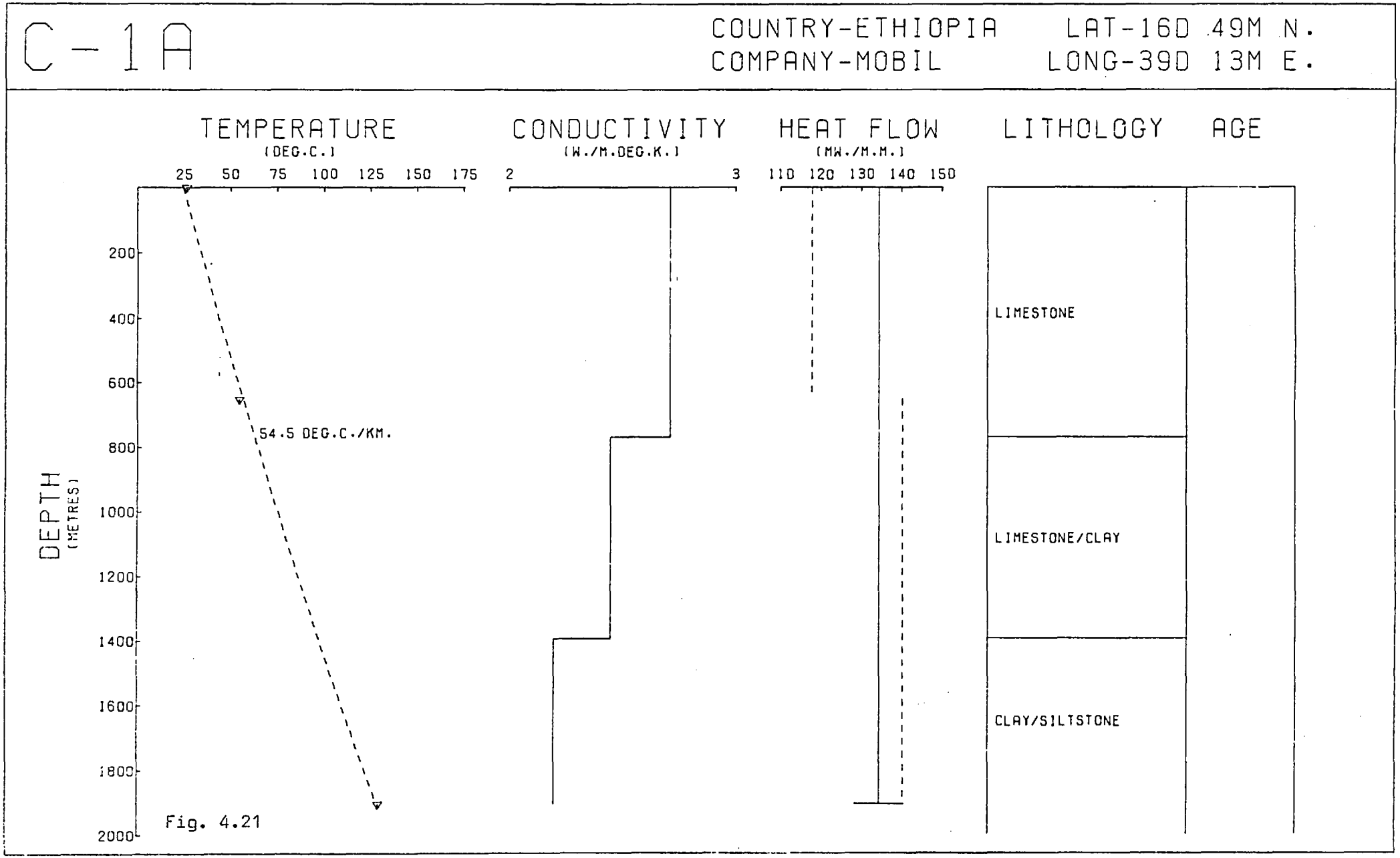
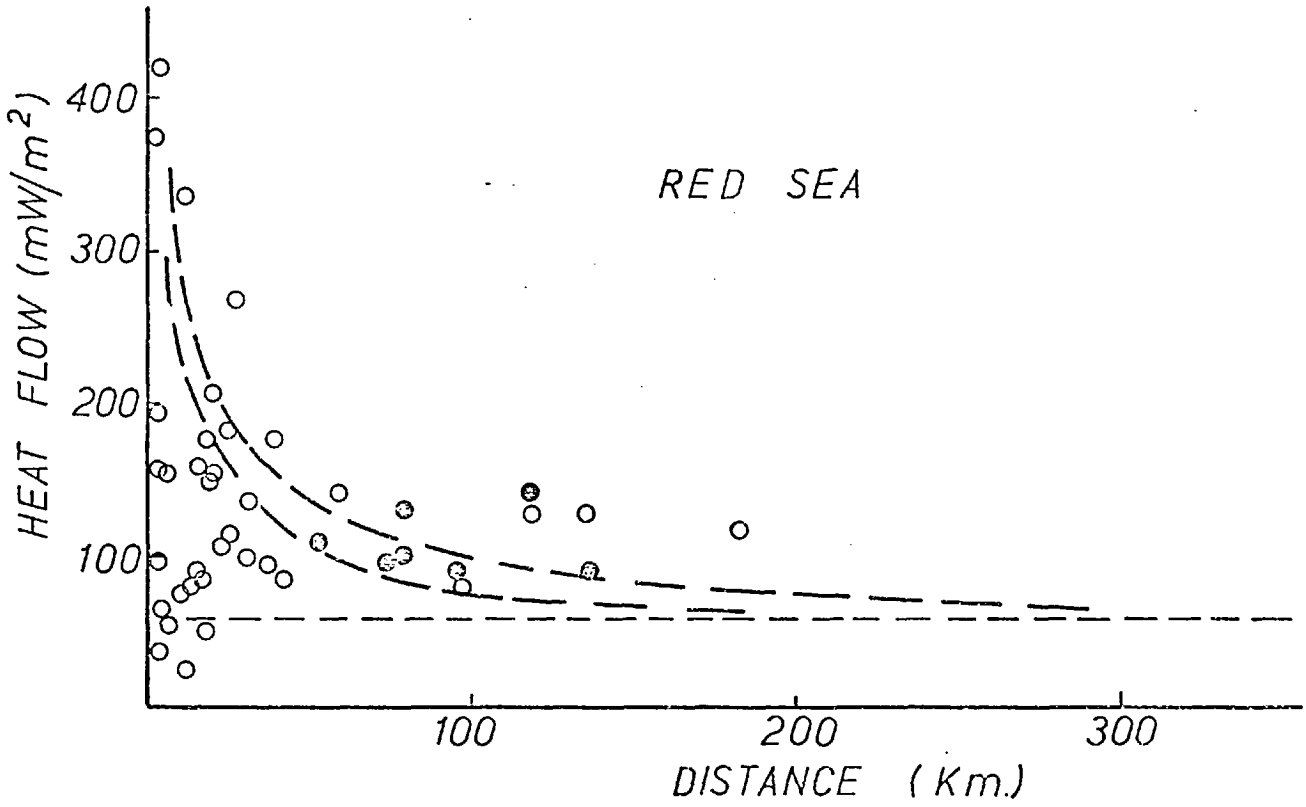
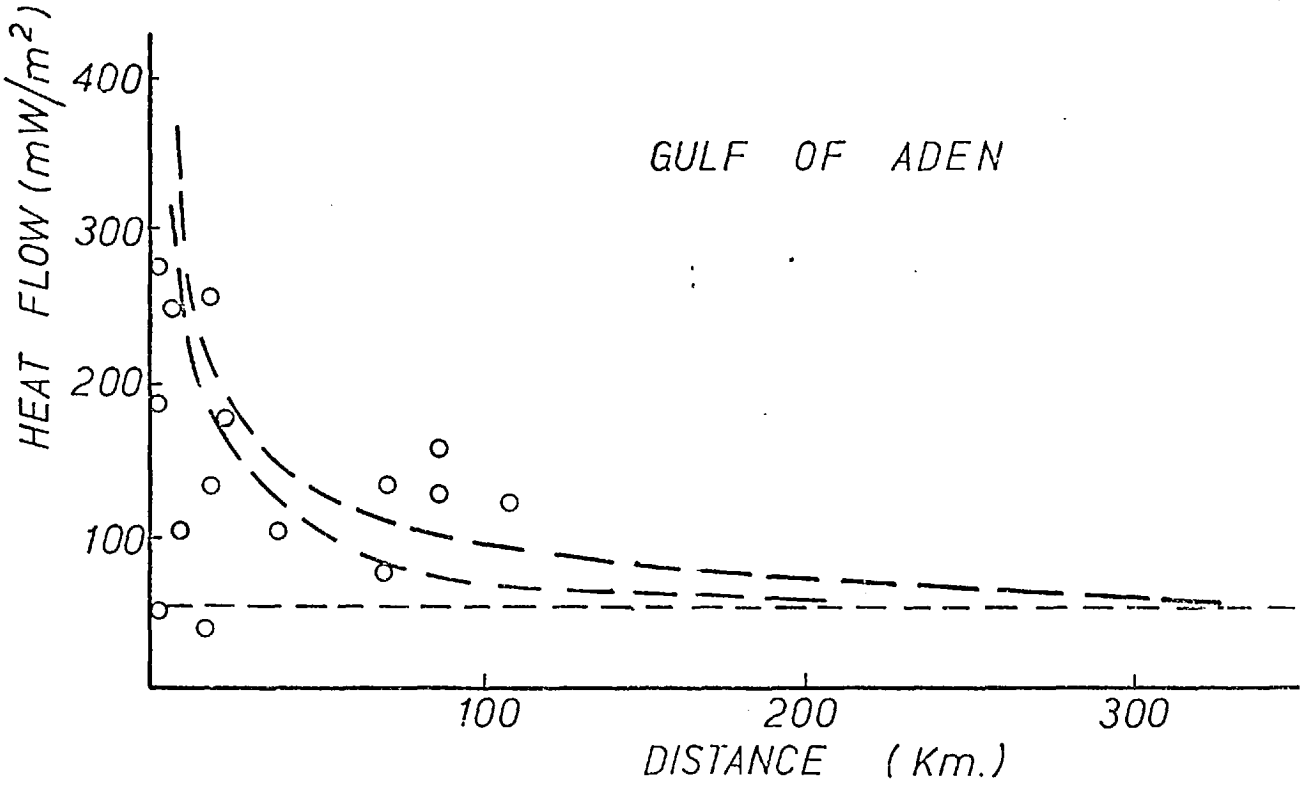

C-1A
COUNTRY-ETHIOPIA
COMPANY-MOBIL
LAT-16D 49M N.
LONG-39D 13M E.
TEMPERATURE
(DEG.C.)
25 50 75 100 125 150 175
CONDUCTIVITY
(W./M.DEG.K.)
2 3
HEAT FLOW
(MW./M.M.)
110 120 130 140 150
LITHOLOGY
AGE
DEPTH
(METRES)
200 400 600 800 1000 1200 1400 1600 1800 2000
54.5 DEG.C./KM.
LIMESTONE
LIMESTONE/CLAY
CLAY/SILTSTONE

Fig. 4.21

HEAT FLOW MODELS FOR A SPREADING LITHOSPHERE





UPPER CURVE SPREADING RATE = 2 cm·a^{-1}
LOWER CURVE SPREADING RATE = 1 cm·a^{-1}
ALL AVAILABLE DATA INCORPORATED

● THIS STUDY

FIG. 4.22

4.10 The Guban Region Heat Flow

The Guban is that low lying plain in northern Somalia on the down-thrown side of the Golis fault which forms the southern boundary of the Gulf of Aden graben. Five heat flow values have been computed for this region, Fig. 4.28.

The area is geologically complex with a highly faulted basement overlain by Mesozoic and Cenozoic sediments. Hunt (1960) has proposed that the gneissose basement is of Archean age with several younger granitic intrusions. The distribution of the sediments is strongly controlled by basement fault blocks with variations of a few thousand metres occurring over similar lateral distances (Pallister, 1959, Hunt, 1960). Most of the Guban faulting follows the NW/SE Red Sea trend (Azzaroli and Fois, 1964). The marine Jurassic rocks are overlain, by coarse Cretaceous continental clastics and, in turn, near the coast, by Paleocene-Eocene limestones and Oligocene-Pliocene boulder beds (Mobil Oil, pers. comm., 1974). The basalt in which Berbera-1, Fig. 4.23, bottomed is most probably of the Aden (Pliocene) series (British Petroleum, pers. comm., 1974).

The five determinations, Figs. 4.23 - 4.27, are uniformly poor; the shallow depths and lack of conductivity samples are the principal problems. The mean heat flow of 55 $\pm$ 17 $mW \cdot m^{-2}$ would seem low in a region of Pliocene volcanism (Sclater and Francheteau, 1970). Further there are several known hot springs in the general area (Somaliland Oil Exploration Co., 1954) which might also suggest higher heat flow.

The three boreholes Dagah Shabell-1, 2, 3, which were drilled within a few kilometres of each other, yielded the lowest results, 36 - 48 $mW \cdot m^{-2}$. The Shabell area is a well known oil seep, Pallister (1959), and thus the possibility of a borehole disturbance cannot be ruled out. The Dagah Shabell-1 well penetrated some sixty metres of crystalline basement which when logged gave a very low gamma ray count compared to the overlying sedimentary rocks

indicating low heat production. A basement heat production contrast is thus another, though less plausible, explanation of the low heat flow.

These data illustrate some of the severe limitations encountered in the use of oil borehole data for heat flow purposes. The Berbera-1 value, of 80 $mW \cdot m^{-2}$, is, perhaps, the only significant result. The data are plotted on the map, Fig. 4.28, which also incorporates the Gulf of Aden heat flow values, section 4.6.

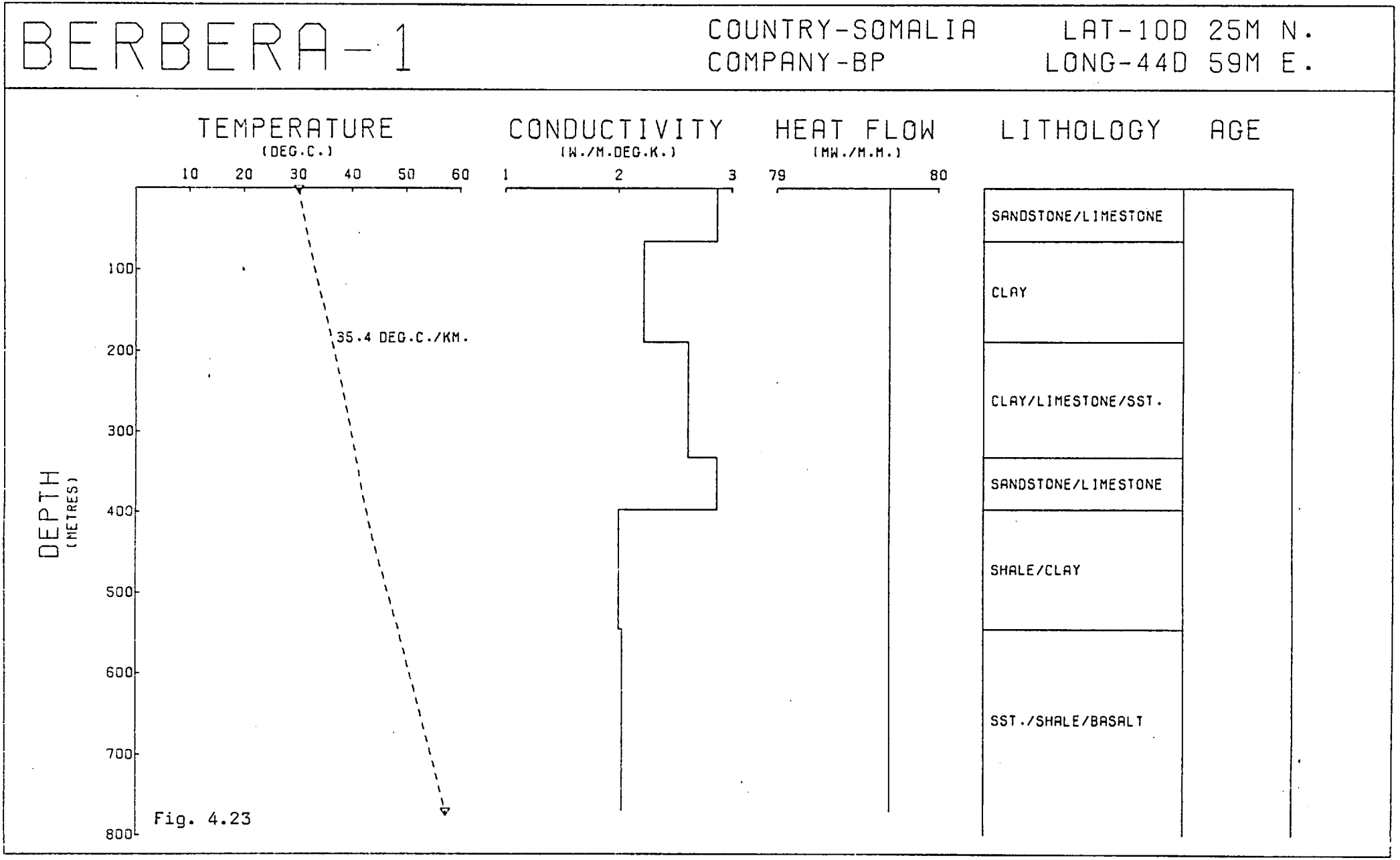

BERBERA-1
COUNTRY-SOMALIA
COMPANY-BP
LAT-10D 25M N.
LONG-44D 59M E.
TEMPERATURE
(DEG.C.)
10
20
30
40
50
60
CONDUCTIVITY
(W./M.DEG.K.)
1
2
3
HEAT FLOW
(MW./M.M.)
79
80
LITHOLOGY
AGE
SANDSTONE/LIMESTONE
CLAY
CLAY/LIMESTONE/SST.
SANDSTONE/LIMESTONE
SHALE/CLAY
SST./SHALE/BASALT
35.4 DEG.C./KM.
DEPTH
(METRES)
100
200
300
400
500
600
700
800

Fig. 4.23

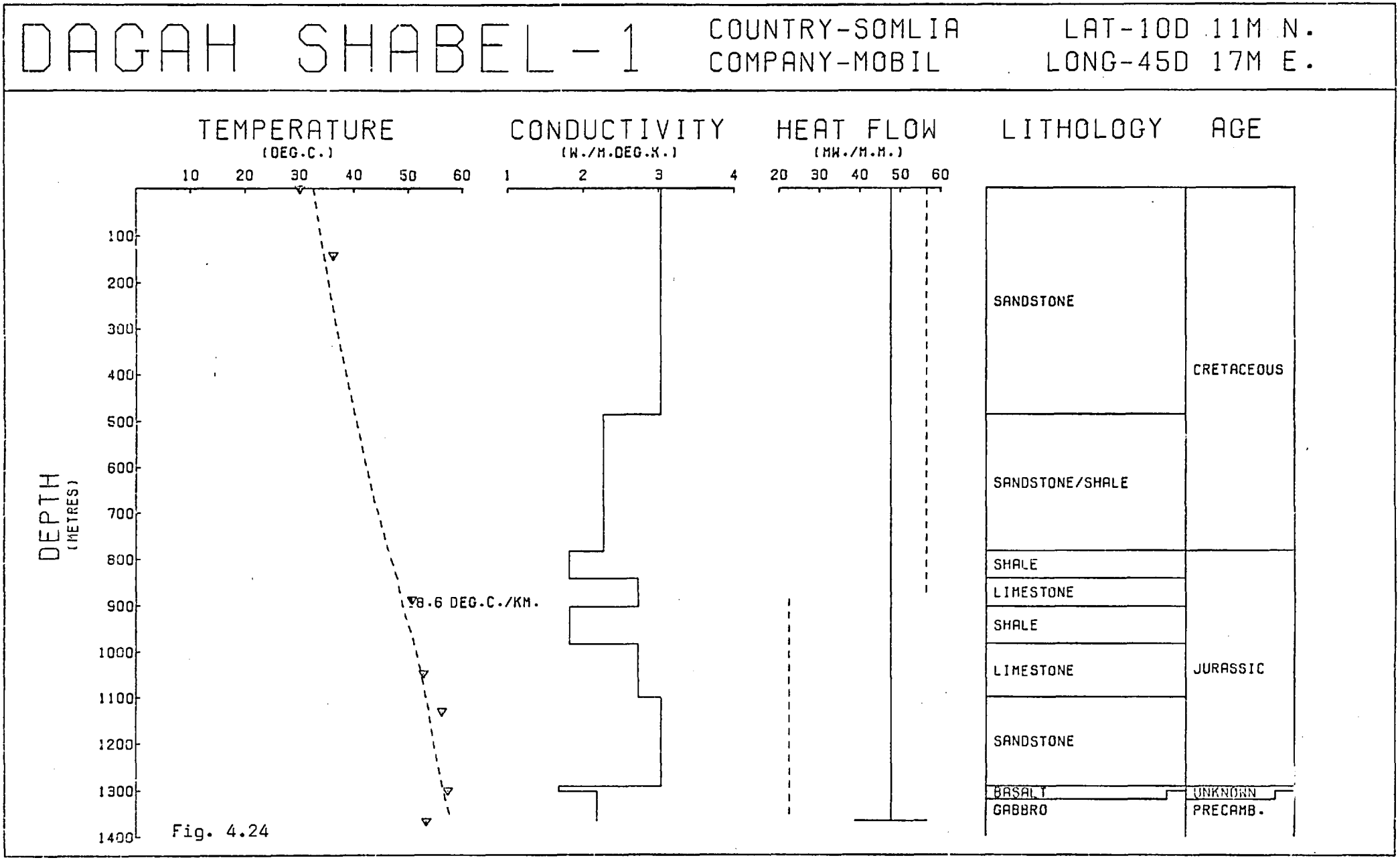

DAGAH SHABEL-1
COUNTRY-SOMLIA
COMPANY-MOBIL
LAT-10D 11M N.
LONG-45D 17M E.
TEMPERATURE
(DEG.C.)
10 20 30 40 50 60
CONDUCTIVITY
(W./M.DEG.K.)
1 2 3 4
HEAT FLOW
(MW./M.M.)
20 30 40 50 60
LITHOLOGY
AGE
DEPTH
(METRES)
100 200 300 400 500 600 700 800 900 1000 1100 1200 1300 1400
8.6 DEG.C./KM.
SANDSTONE
SANDSTONE/SHALE
SHALE
LIMESTONE
SHALE
LIMESTONE
SANDSTONE
BASALT
GABBRO
CRETACEOUS
JURASSIC
UNKNOWN
PRECAMB.

Fig. 4.24

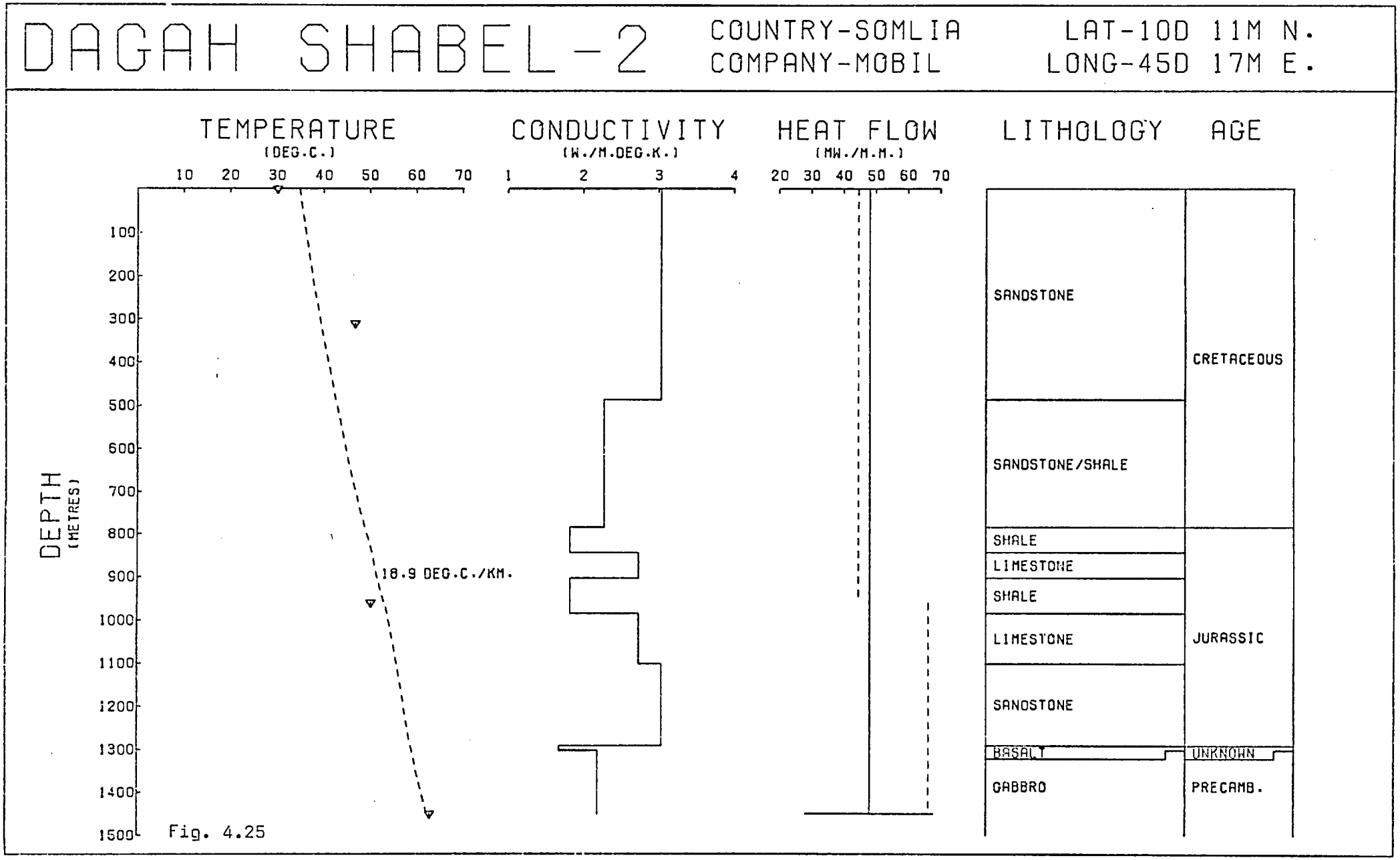

DAGAH SHABEL-2
COUNTRY-SOMLIA
COMPANY-MOBIL
LAT-10D 11M N.
LONG-45D 17M E.
TEMPERATURE
(DEG.C.)
10 20 30 40 50 60 70
CONDUCTIVITY
(W./M.DEG.K.)
1 2 3 4
HEAT FLOW
(MW./M.M.)
20 30 40 50 60 70
LITHOLOGY
AGE
DEPTH
(METRES)
100 200 300 400 500 600 700 800 900 1000 1100 1200 1300 1400 1500
18.9 DEG.C./KM.
SANDSTONE
SANDSTONE/SHALE
SHALE
LIMESTONE
SHALE
LIMESTONE
SANDSTONE
BASALT
GABBRO
CRETACEOUS
JURASSIC
UNKNOWN
PRECAMB.

Fig. 4.25

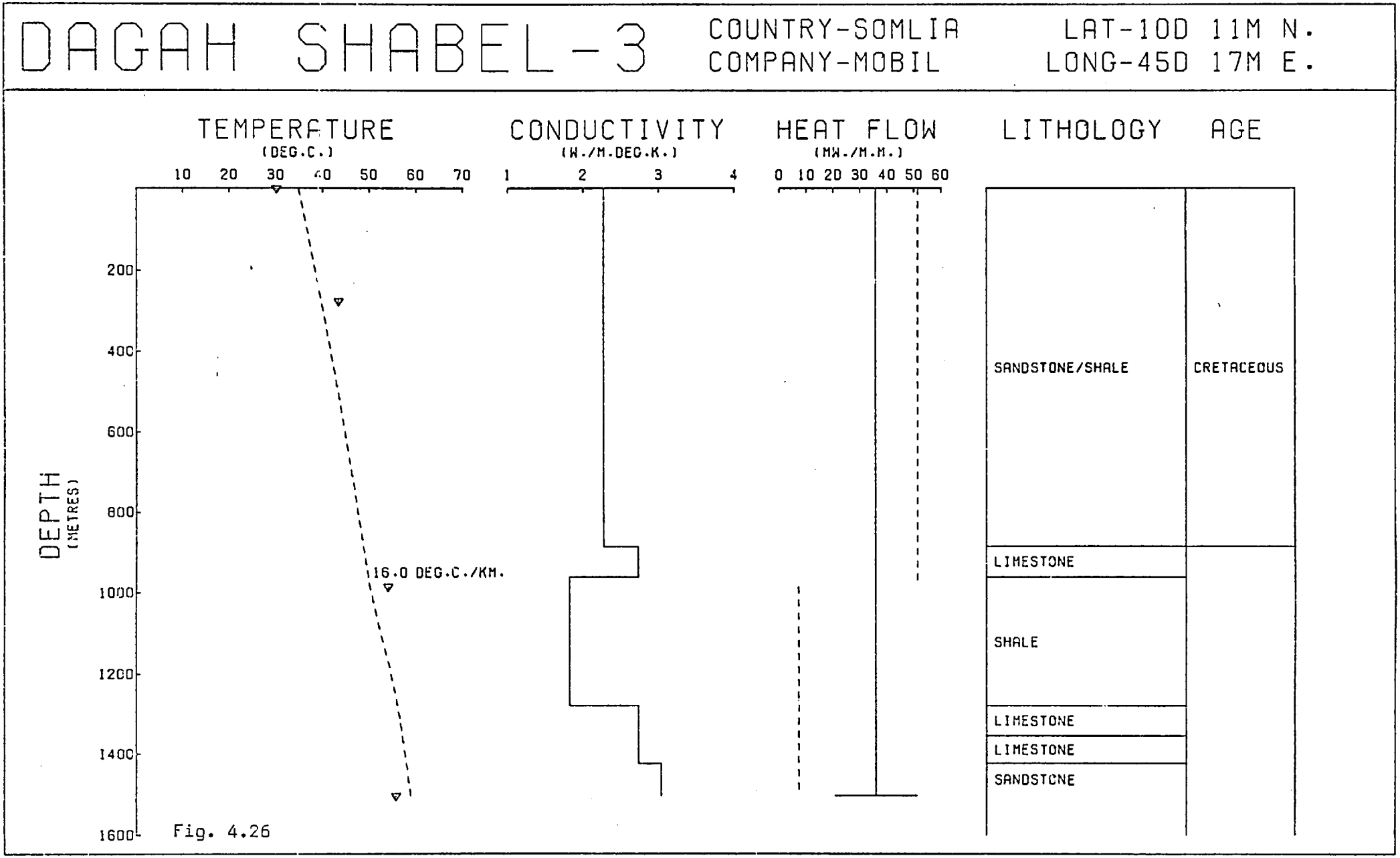

DAGAH SHABEL-3
COUNTRY-SOMLIA
COMPANY-MOBIL
LAT-10D 11M N.
LONG-45D 17M E.
TEMPERATURE
(DEG.C.)
10 20 30 40 50 60 70
CONDUCTIVITY
(W./M.DEG.K.)
1 2 3 4
HEAT FLOW
(MW./M.M.)
0 10 20 30 40 50 60
LITHOLOGY
AGE
DEPTH
(METRES)
200
400
600
800
1000
1200
1400
1600
16.0 DEG.C./KM.
SANDSTONE/SHALE
CRETACEOUS
LIMESTONE
SHALE
LIMESTONE
LIMESTONE
SANDSTONE

Fig. 4.26

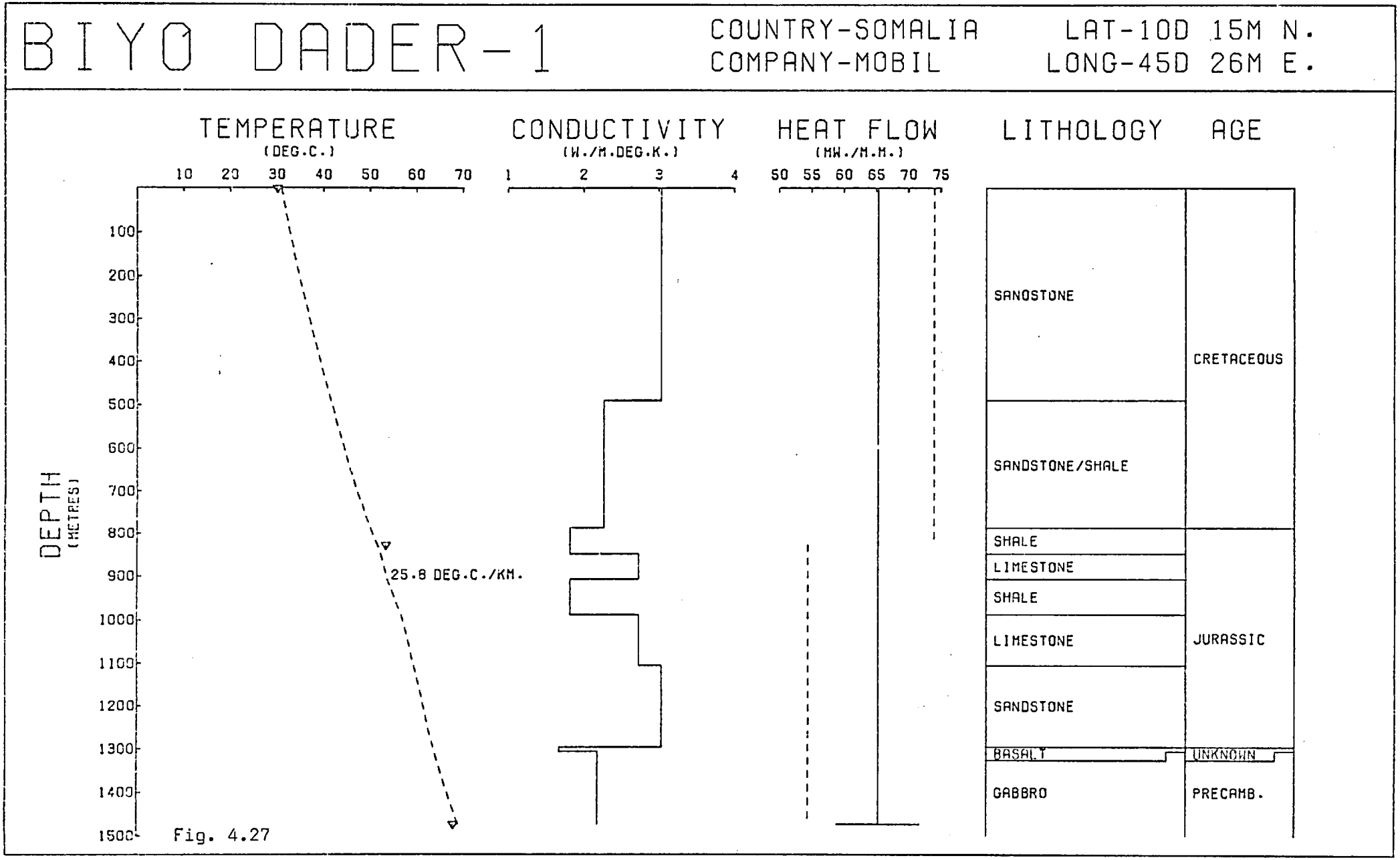

BIYO DADER-1
COUNTRY-SOMALIA
COMPANY-MOBIL
LAT-10D 15M N.
LONG-45D 26M E.
TEMPERATURE
(DEG.C.)
10 20 30 40 50 60 70
CONDUCTIVITY
(W./M.DEG.K.)
1 2 3 4
HEAT FLOW
(MW./M.M.)
50 55 60 65 70 75
LITHOLOGY
AGE
DEPTH
(METRES)
100 200 300 400 500 600 700 800 900 1000 1100 1200 1300 1400 1500
25.8 DEG.C./KM.
SANOSTONE
SANDSTONE/SHALE
CRETACEOUS
SHALE
LIMESTONE
SHALE
LIMESTONE
SANDSTONE
JURASSIC
BASALT
UNKNOWN
GABBRO
PRECAMB.

Fig. 4.27

4.11 The Darror and Nogal Valley Region Heat Flow

The Horn of Somalia is bisected, in a NW/SE direction, by two prominent parallel structures, the Darror (or Asseh) and Nogal Valleys, Fig. 4.28. Nine heat flow values have been determined within or on the flanks of these two depressions.

The Somaliland Oil and Exploration Co. (1954) report indicates a horst and graben basement structure in North-East Somalia. The Darror and Nogal valleys are controlled by this basement structure which is clearly oriented along the Red Sea fault trend. Both valleys have been loosely termed 'rifts' by various authors (Azzaroli and Fois, 1964, McConnell, 1974). The two valleys are separated by the Sawl Plateau (horst) and bounded west, north and south by the Golis Plateau, the Al Medo Mountains and the Haud Arch, respectively.

The basement rocks, penetrated by six of the nine wells, have been, with a single exception, the Lower Paleozoic-Precambrian Inda Ad metamorphic sequence of schists, greywackes and slates. The Faro Hills-1 borehole, Fig. 4.31, on the northern flank of the Nogal Valley, bottomed in granite which may be related to the nearby quartz-syenite intrusion at Gorei described by Mason (1957). Mason proposed that the granitic basement is Archean though the evidence is not conclusive.

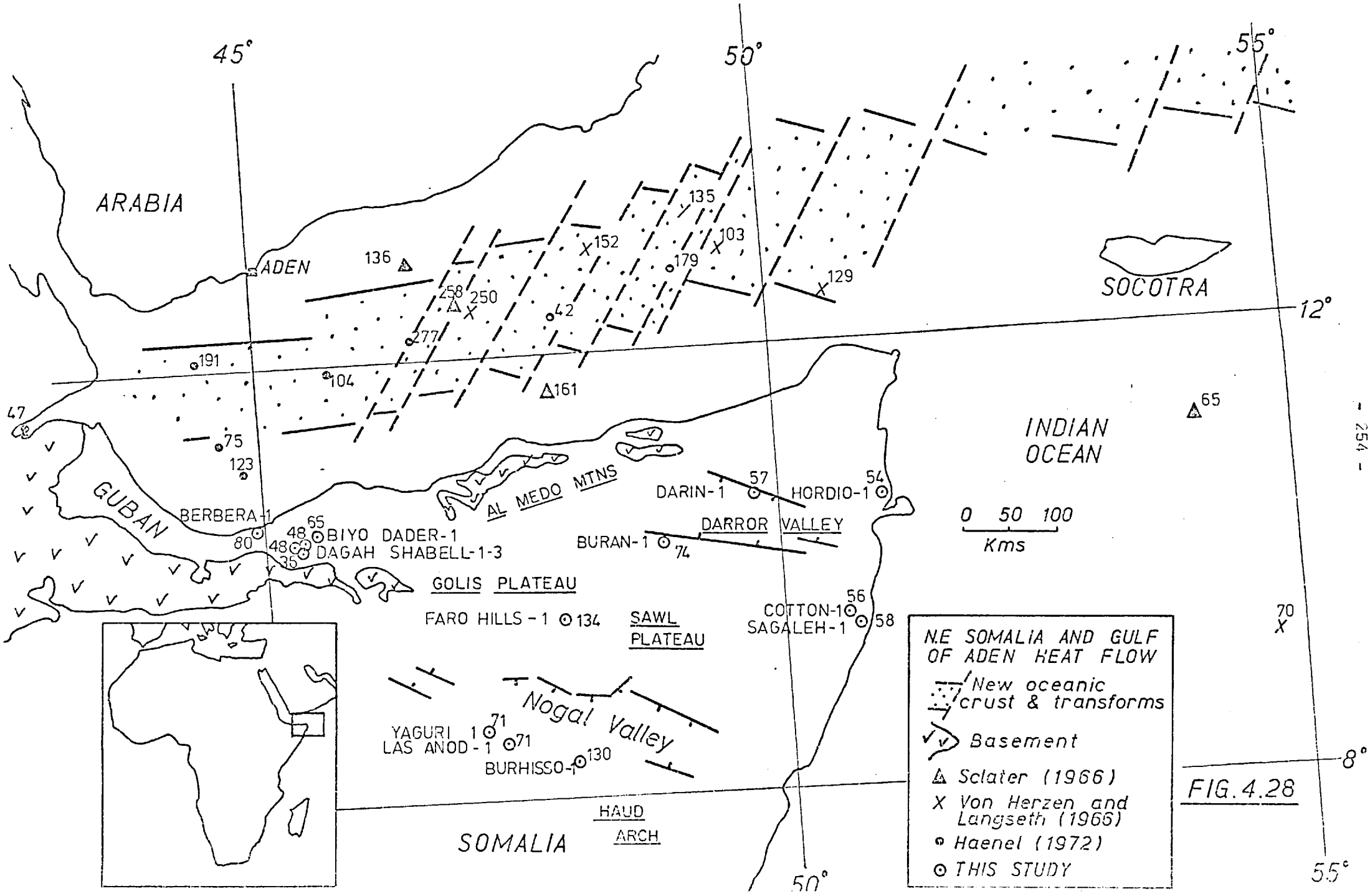
The sediments, which unconformably overlie the basement, are a continuous Jurassic-Lower Tertiary marine sequence thickening towards the coast (Azzaroli and Fois, 1964, Marathon Oil, pers. comm., 1974). The surface expression of the Darror and Nogal valleys is lost in the region of the Indian Ocean coastal plain.

The mean heat flow for this area is 78 ± 31 mW$\cdot$m^{-2}. However, as five of the nine wells are graded D, table 4.2, the weighted mean of 63 ± 20 mW$\cdot$m^{-2} is probably more appropriate. Only a few BHTs and the lithologic logs (brief) were available for those boreholes graded D; Buran-1, Burhisso-1,

Faro Hills-1, Las Anod-1, and Yaguri-1, Figs. 4.29 - 4.33, inclusive. The high values at Faro Hills-1 and Burhisso-1, 130-140 $mW \cdot m^{-2}$, while interesting, are suspect.

Much better data was available for the four coastal wells, Darin-1, Sagaleh-1, Hordio-1, and Cotton-1, Figs. 4.34 - 4.37, inclusive. These boreholes, which were previously discussed by Evans and Tammemagi (1974), gave consistent results, 54-58 $mW \cdot m^{-2}$, despite a number of somewhat large Bullard residuals.

Fig. 4.28 shows these nine boreholes in relation to the Darror and Nogal Valley faults and the heat flow data values measured in the Gulf of Aden, section 4.6.



N.E SOMALIA AND GULF OF ADEN HEAT FLOW

- New oceanic crust & transforms
- Basement
- Sclater (1966)
- X Von Herzen and Langseth (1966)
- Haenel (1972)
- THIS STUDY

FIG. 4.28

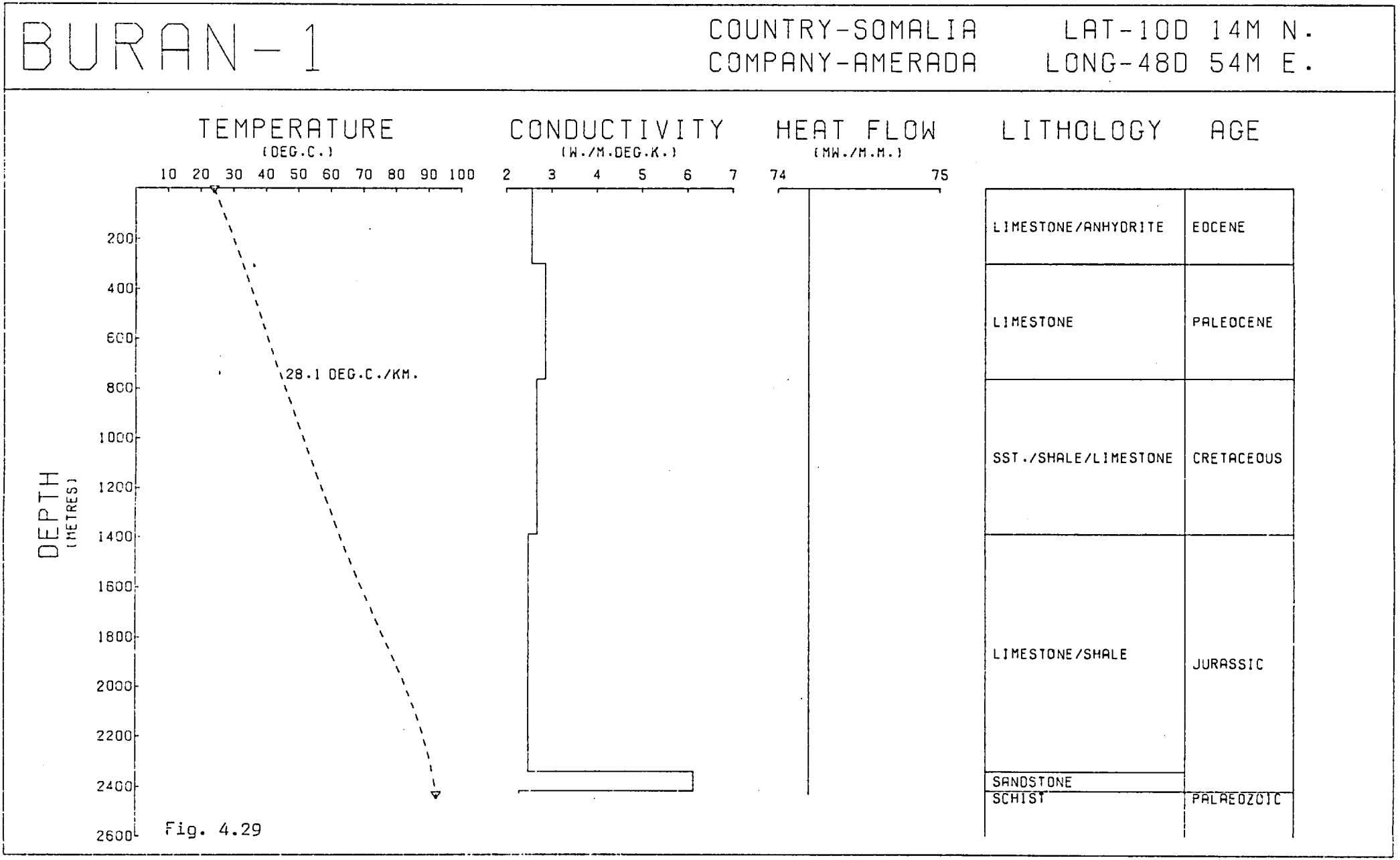

BURAN-1
COUNTRY-SOMALIA
COMPANY-AMERADA
LAT-10D 14M N.
LONG-48D 54M E.
TEMPERATURE
(DEG.C.)
10 20 30 40 50 60 70 80 90 100
CONDUCTIVITY
(W./M.DEG.K.)
2 3 4 5 6 7
HEAT FLOW
(MW./M.M.)
74 75
LITHOLOGY
AGE
28.1 DEG.C./KM.
DEPTH
(METRES)
200
400
600
800
1000
1200
1400
1600
1800
2000
2200
2400
2600
LIMESTONE/ANHYDRITE
EOCENE
LIMESTONE
PALEOCENE
SST./SHALE/LIMESTONE
CRETACEOUS
LIMESTONE/SHALE
JURASSIC
SANDSTONE
SCHIST
PALAEOZOIC

Fig. 4.29

BURHISSO-1

COUNTRY-SOMALIA LAT-08D 19M N.
COMPANY-AMERADA LONG-47D 54M E.

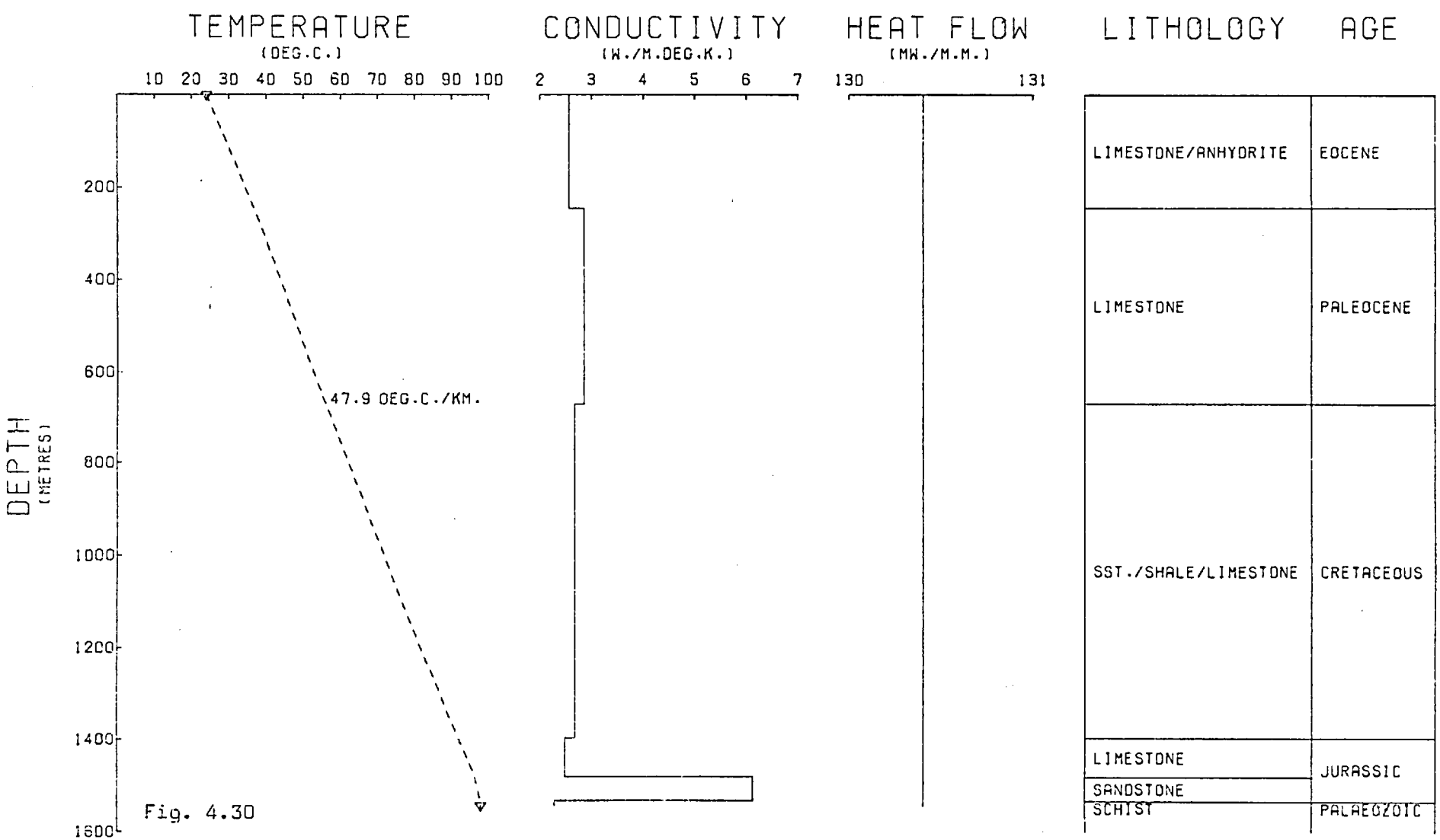


Fig. 4.30

FARO HILLS-1

COUNTRY-SOMALIA LAT-09D 38M N.
COMPANY-AMERADA LONG-47D 47M E.

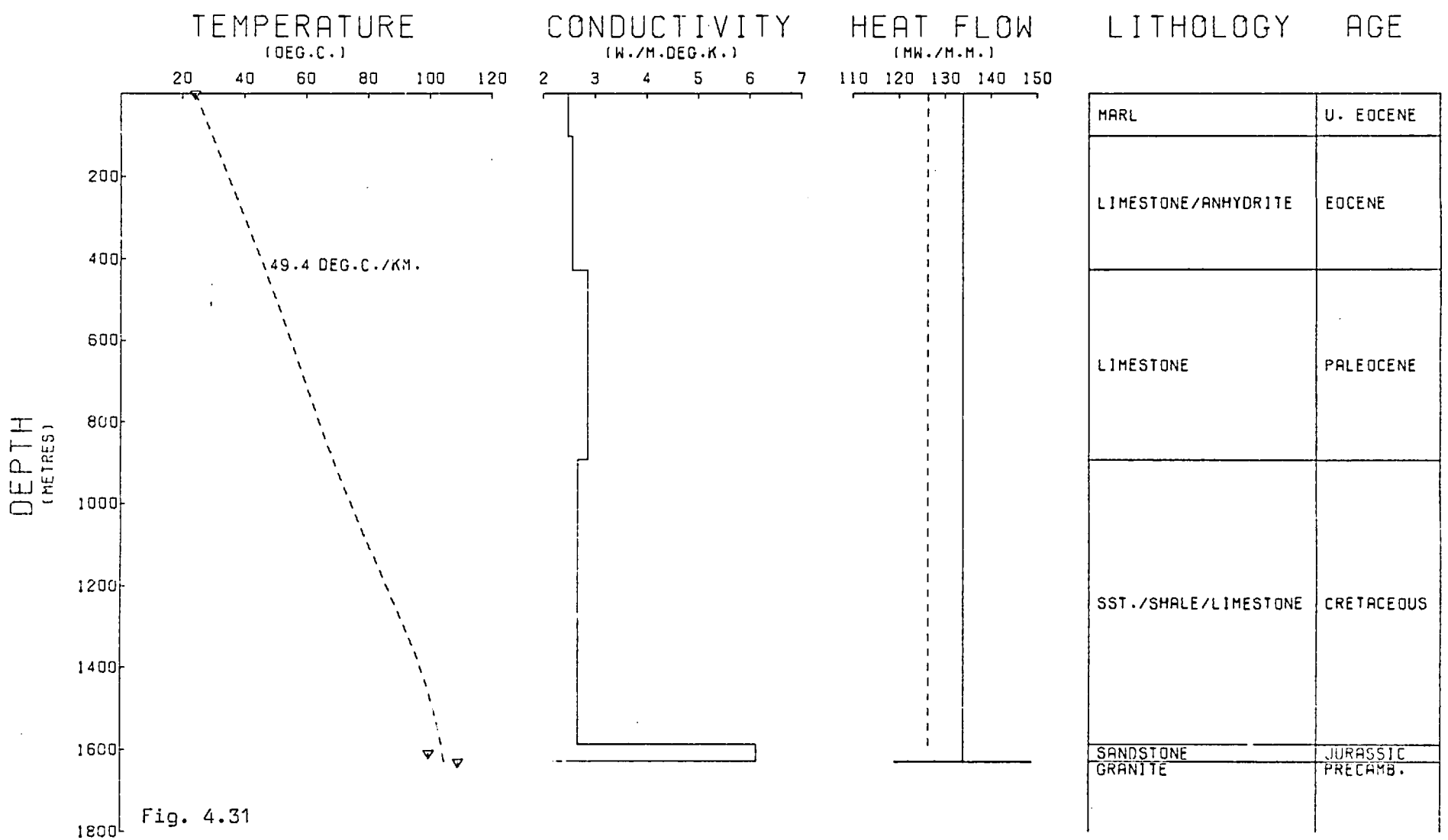


Fig. 4.31

LAS ANOD-1

COUNTRY-SOMALIA LAT-08D 28M N.
COMPANY-AMERADA LONG-47D 12M E.

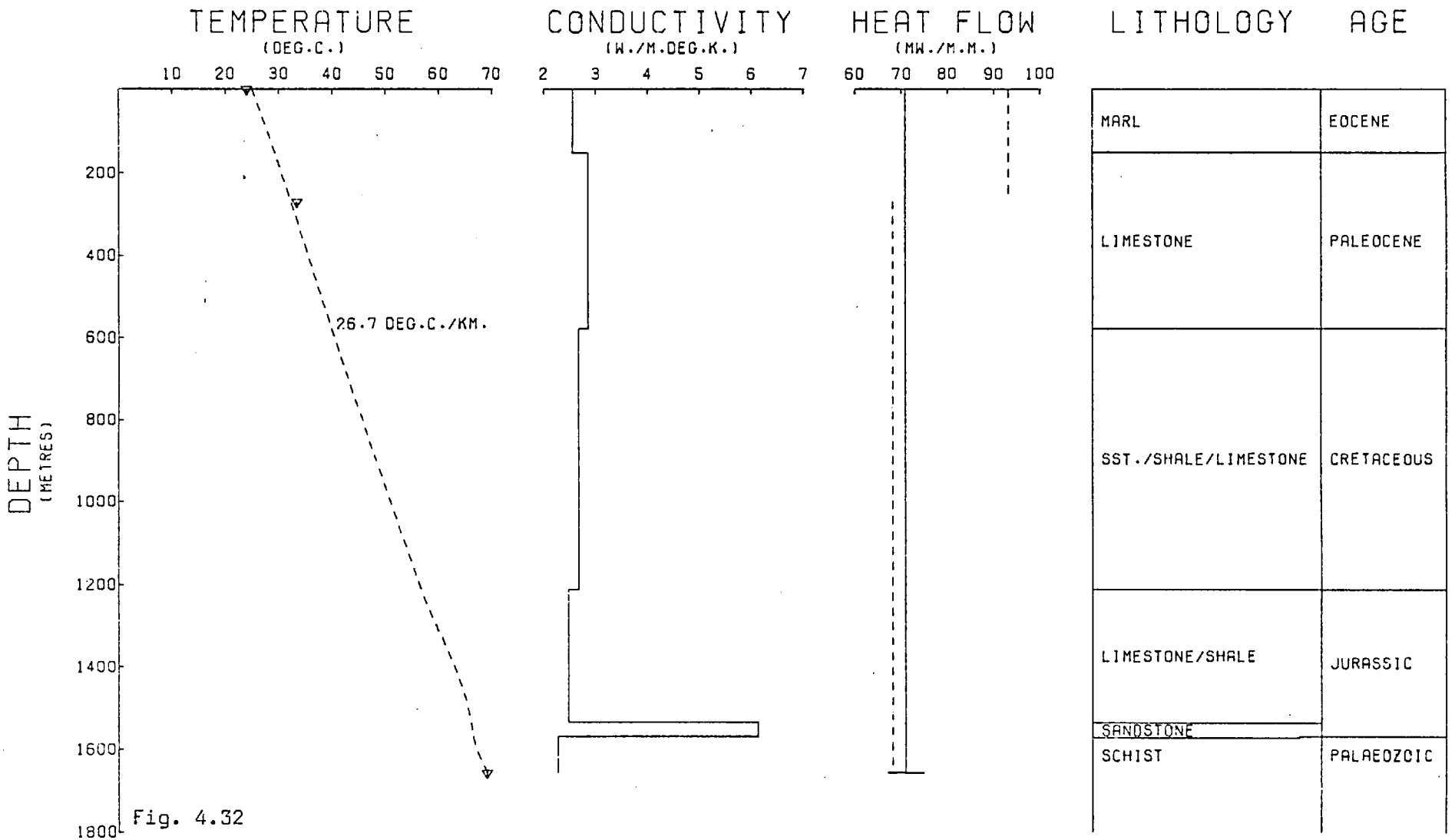


Fig. 4.32

YAGURI-1

COUNTRY-SOMALIA LAT-08D 39M N.
COMPANY-AMERADA LONG-47D 01M E.

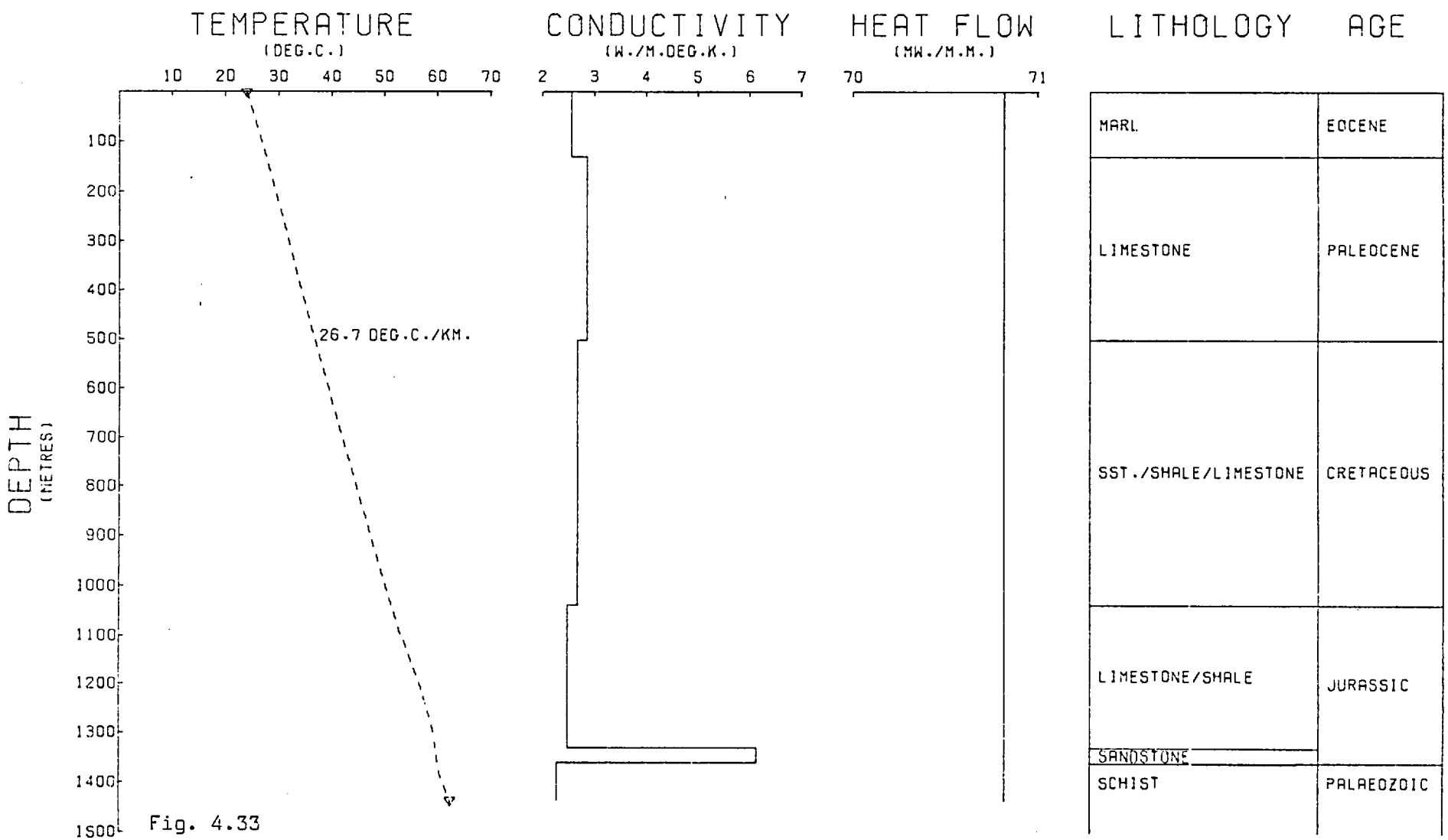


Fig. 4.33

DARIN-1

COUNTRY-SOMALIA LAT-10D 40M N.
COMPANY-AGIP LONG-49D 45M E.

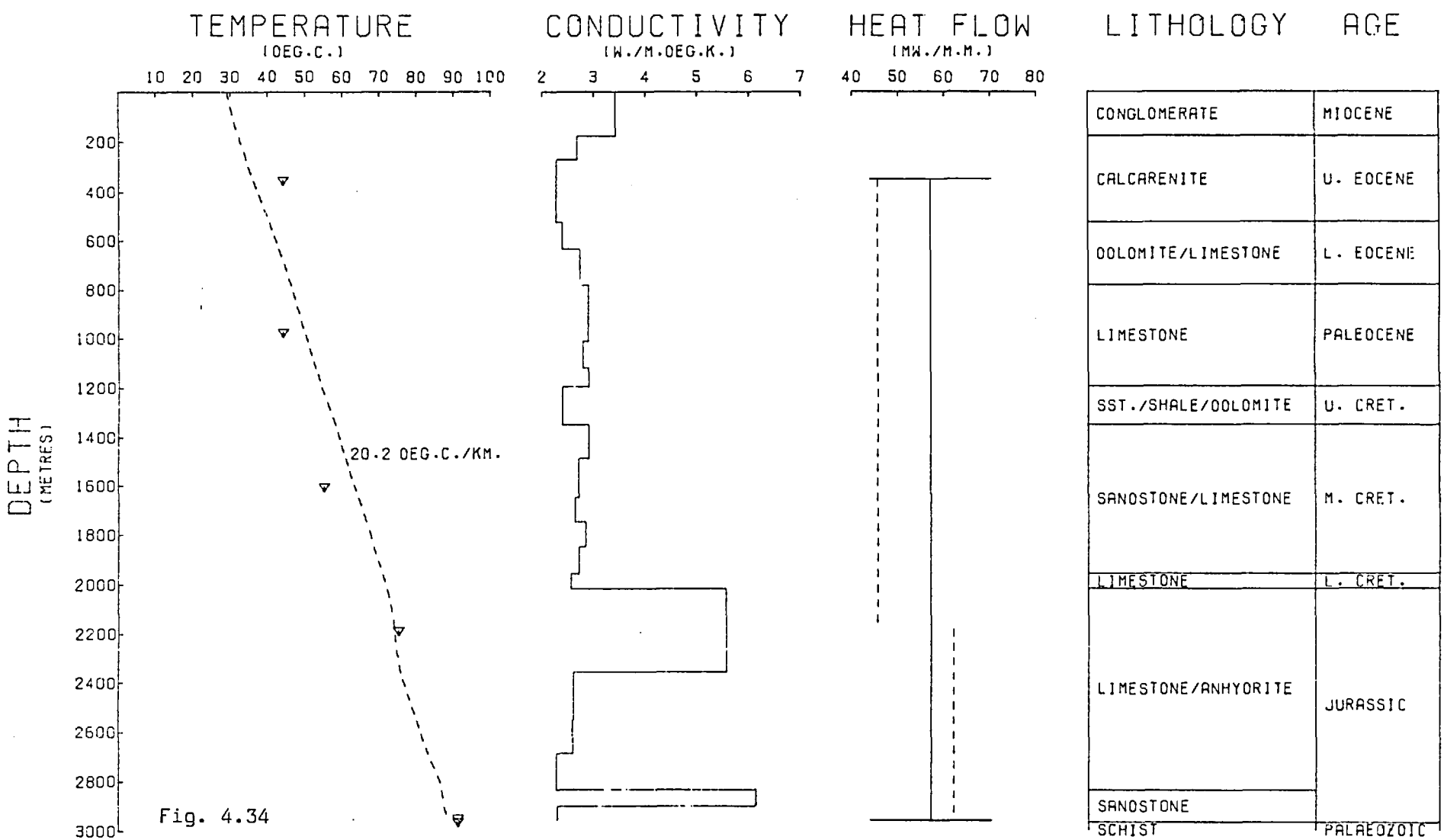


Fig. 4.34

SAGALEH-1

COUNTRY-SOMALIA LAT-09D 25M N.
COMPANY-AGIP LONG-50D 40M E.

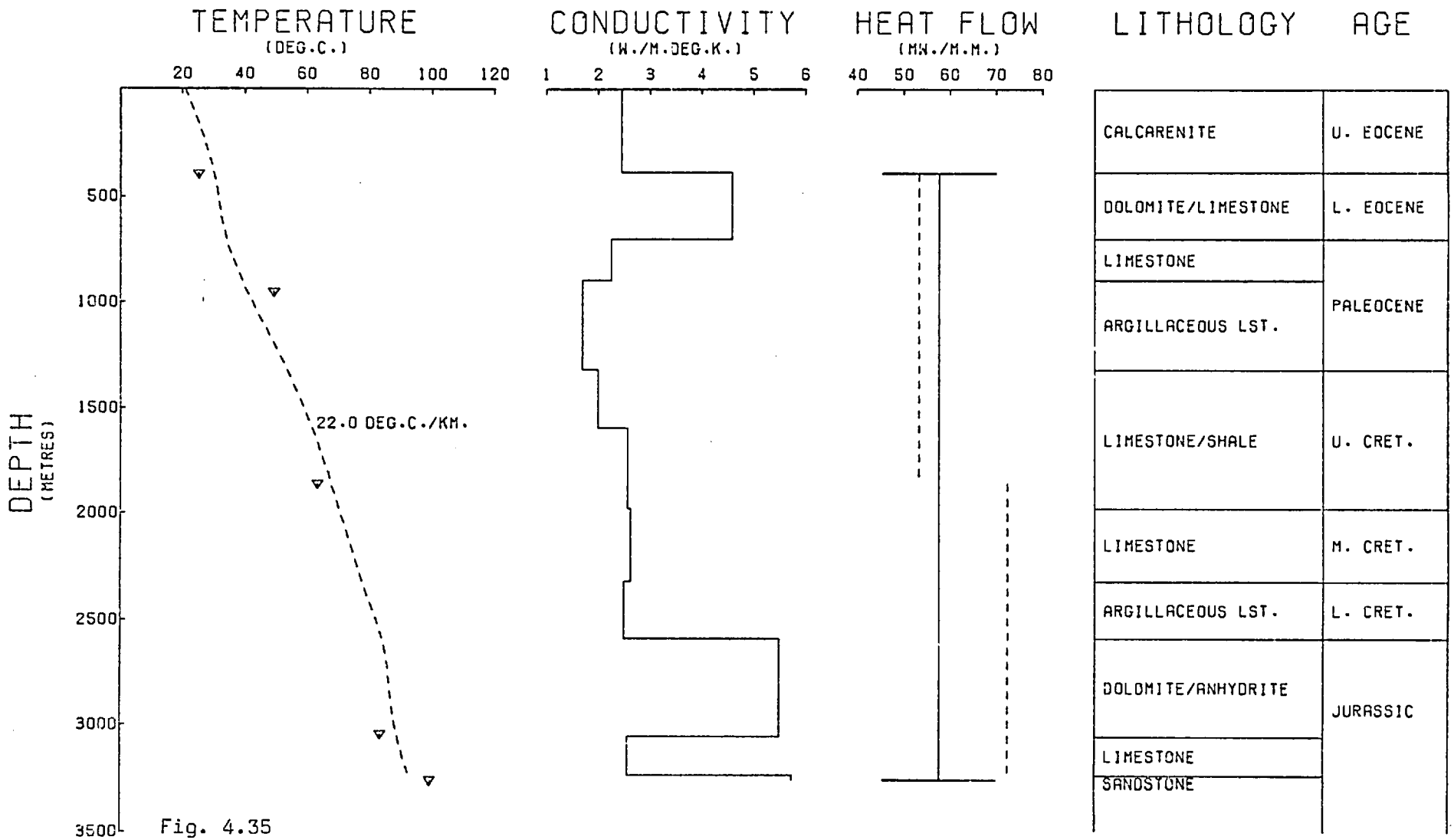


Fig. 4.35

HORDIO-1

COUNTRY-SOMALIA LAT-10D 37M N.
COMPANY-AGIP LONG-51D 00M E.

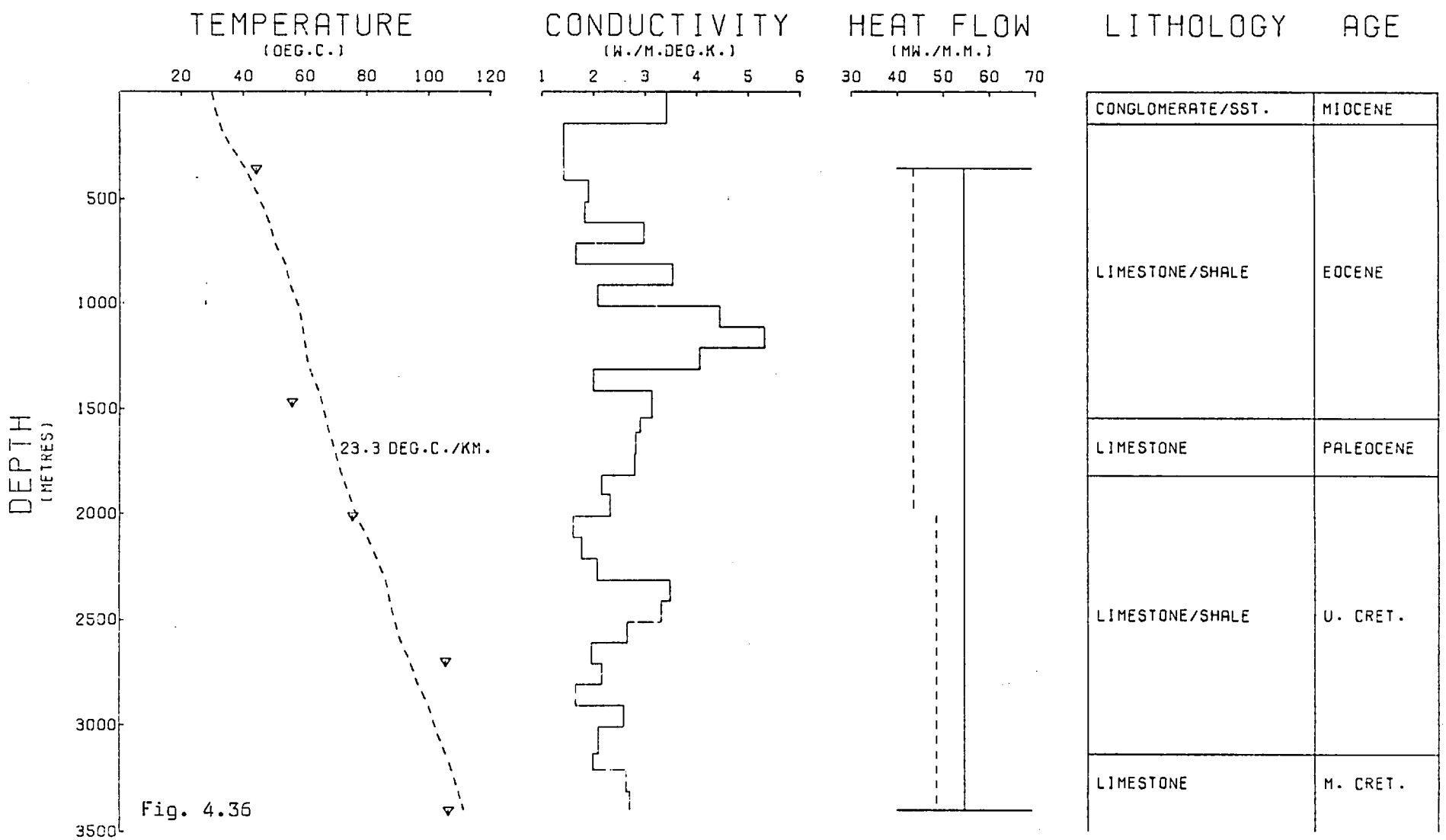


Fig. 4.36

COTTON-1

COUNTRY-SOMALIA LAT-09D 33M N.
COMPANY-AGIP LONG-50D 31M E.

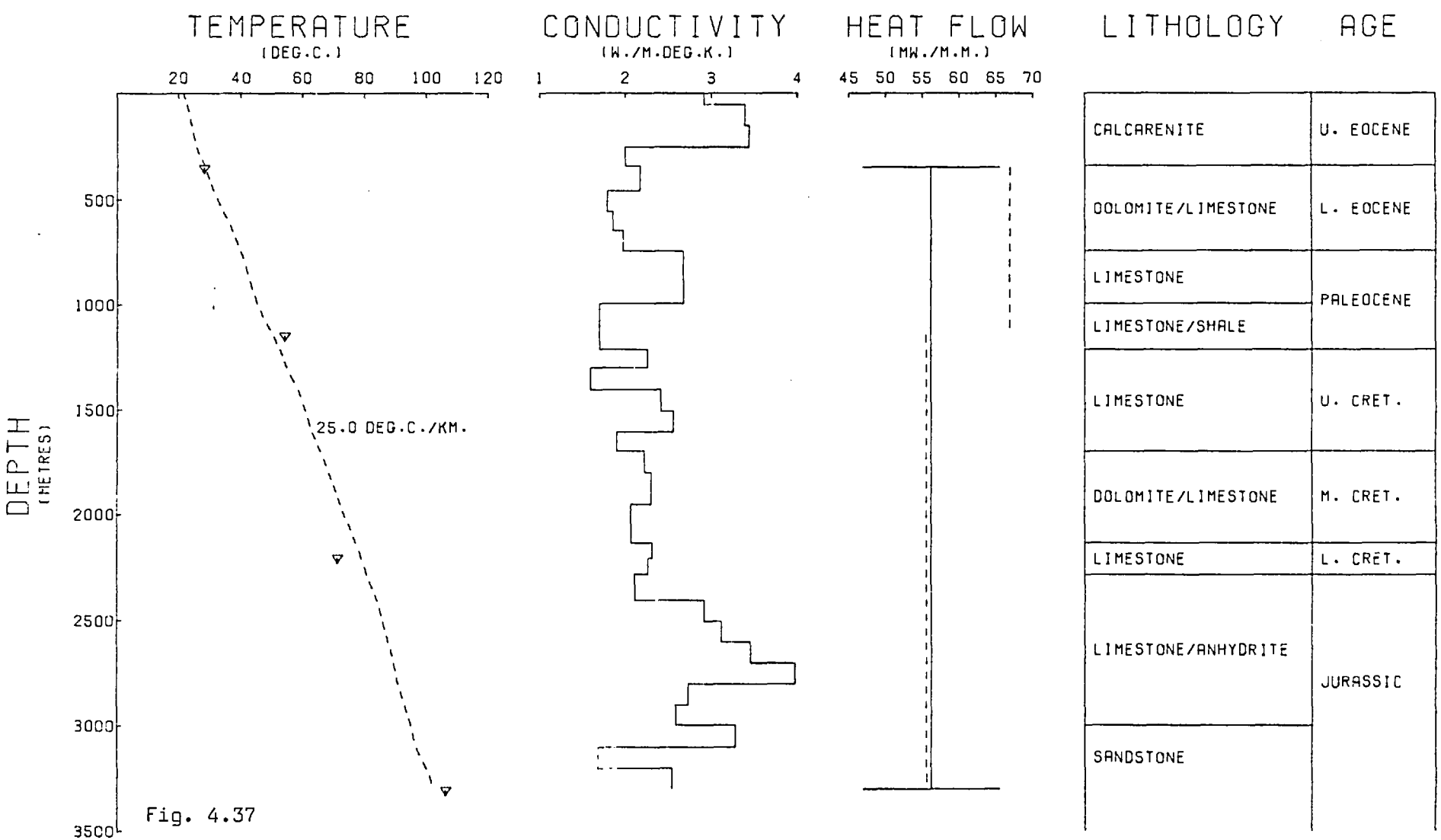


Fig. 4.37

4.12 The Obbia Embayment Region Heat Flow

Five values of heat flow, with a mean of 54 ± 15 $mW \cdot m^{-2}$, were computed for the Obbia Embayment. The region is a poorly defined depression in the crystalline basement at about $5^{o}N$, $48^{o}E$, on the Indian Ocean coastal plain of Somalia, Fig. 4.11. It is bounded to the north by the Haud Arch and to the south it funnels into the narrow, fault bounded, Benadir Coast region, section 4.14. To the west the basement depression bifurcates into the Ogaden Basin and the Bokh syncline (section 4.13). The Tectonic Map of Africa (UNESCO, 1968) indicates a maximum depth to basement of 7 kilometres in this region. There has been, to the author's knowledge, no previous discussion of the geology of this area.

The data quality was fair to poor in this region with a reasonable number of BHTs available but no conductivity data. A detailed lithologic log for the Obbia well facilitated conductivity estimates; only schematic or total depth lithologies were obtained for the remaining holes. As might be expected, the heat flow composite plots, Figs. 4.39 - 4.42, for the Obbia region wells indicate poor internal consistency apart from the El-Hammure-1 and possibly Gira-1 holes.

An interesting aspect to emerge from the Obbia-1 lithologic log is a major unconformity with several hundred metres of Pliocene sands and clays resting on Eocene clay. The remarkably thick Mesozoic carbonate sequence is consistent with Kent's (1972) view of a proto-Indian Ocean existing in earliest Jurassic times.

EL HAMURRE-1

COUNTRY-SOMALIA LAT-06D 48M N.
COMPANY-SINCLAIR LONG-48D 50M E.

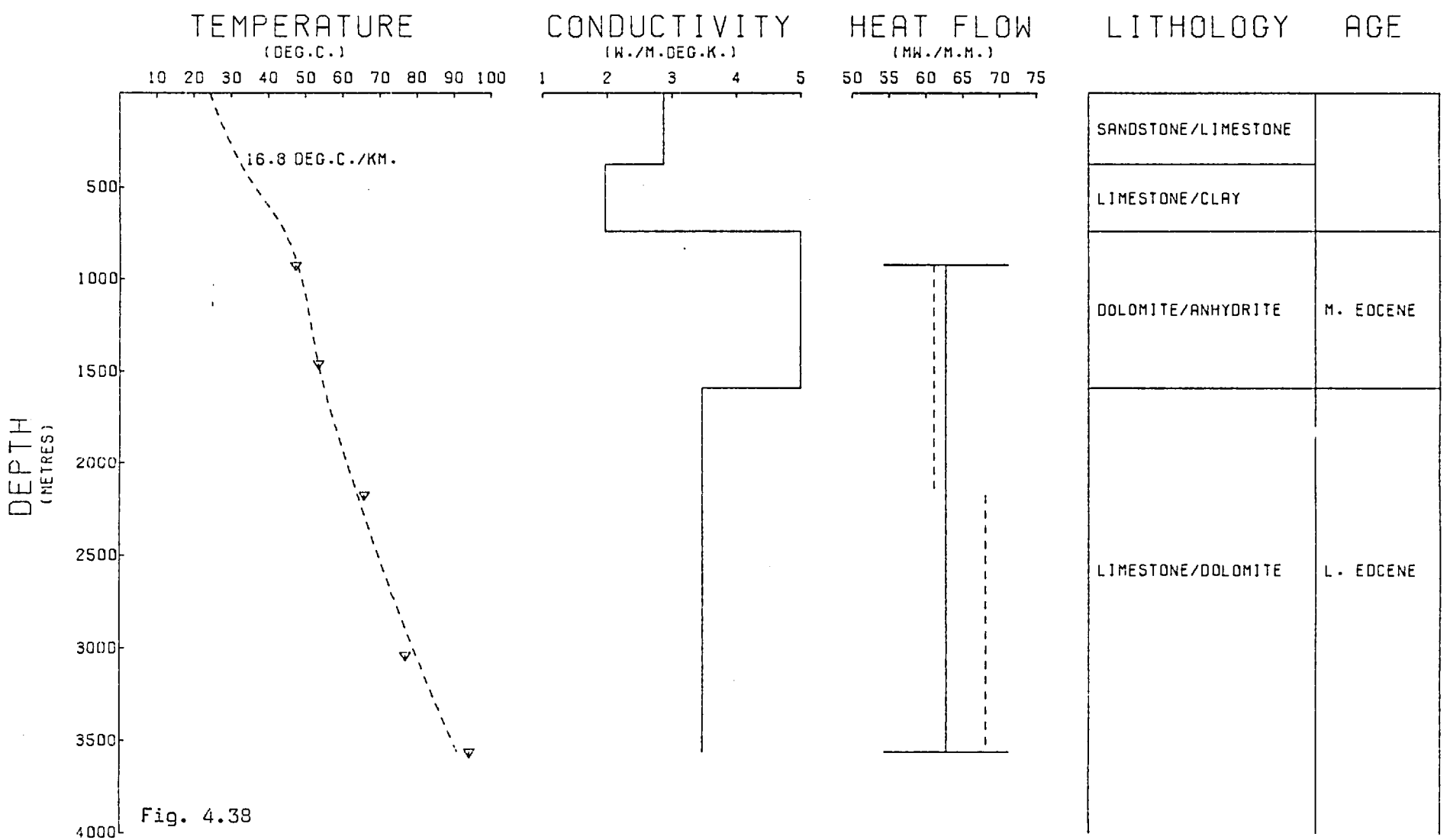


Fig. 4.38

OBBIA-1

COUNTRY-SOMALIA LAT-05D 56M N.
COMPANY-SINCLAIR LONG-48D 54M E.

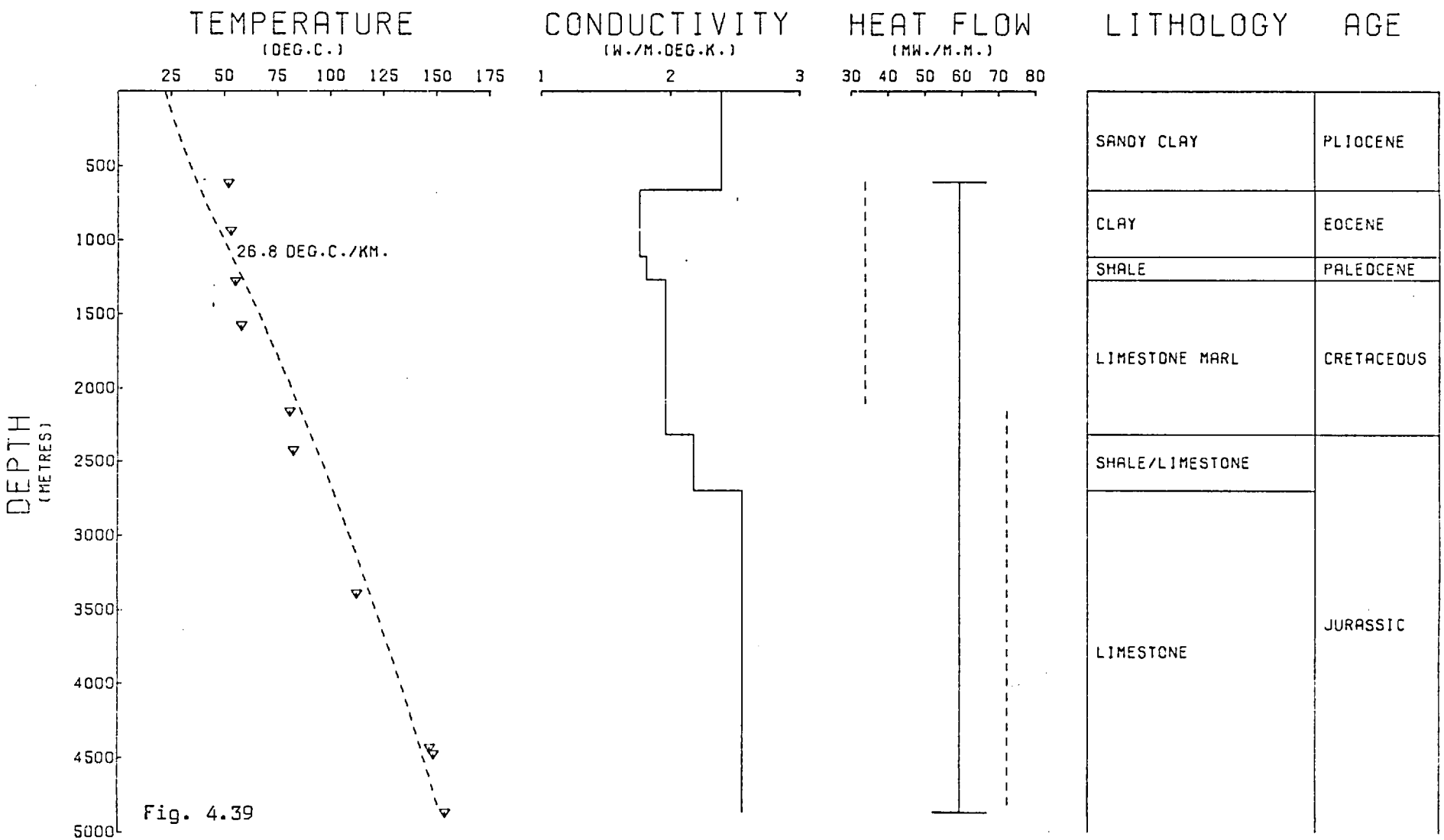


Fig. 4.39

ENDEBIRRE-1

COUNTRY-SOMALIA LAT-05D 30M N.
COMPANY-SINCLAIR LONG-47D 18M E.

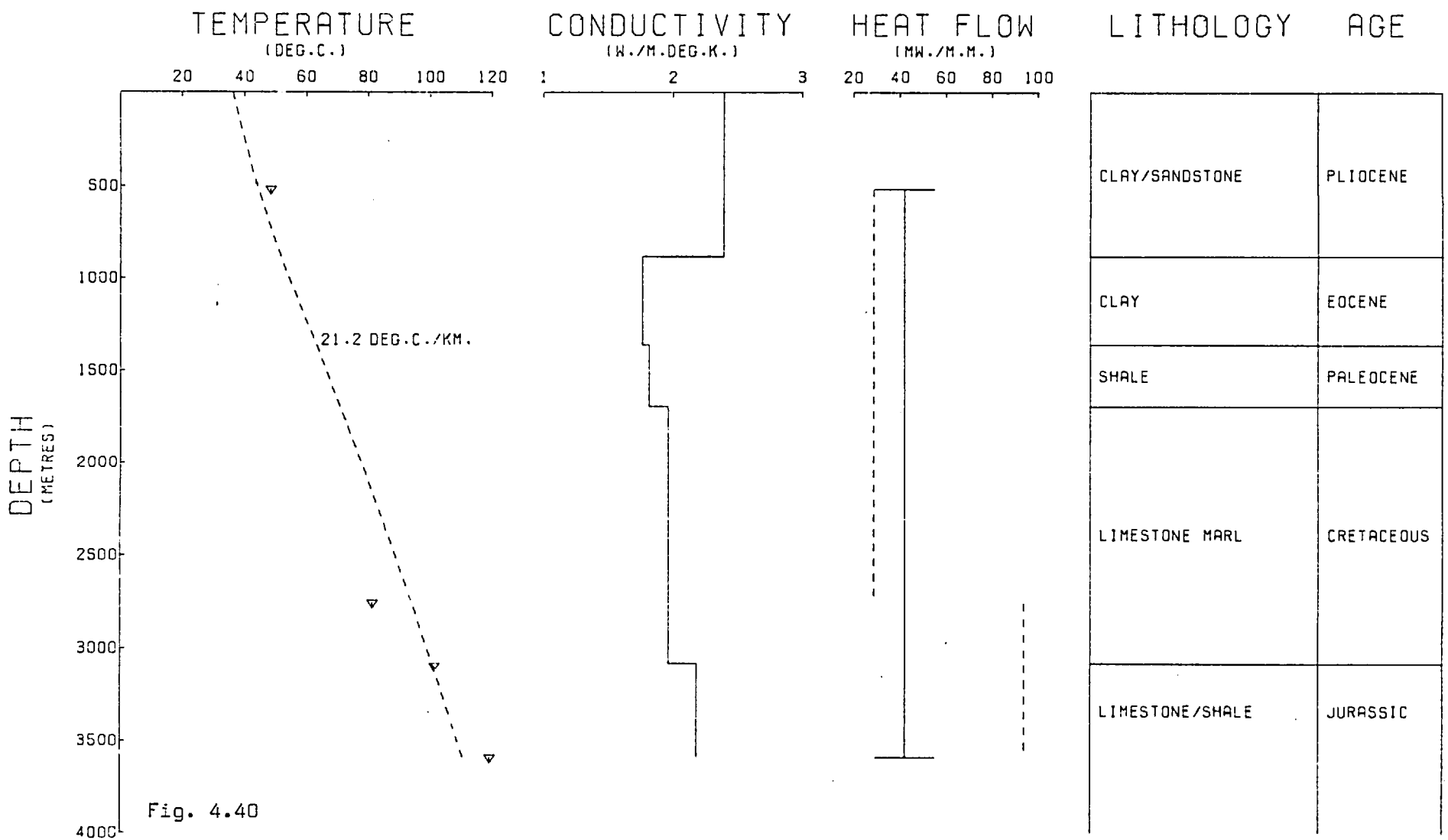


Fig. 4.40

GIRA-1

COUNTRY-SOMALIA LAT-05D 30M N.
COMPANY-SINCLAIR LONG-48D 07M E.

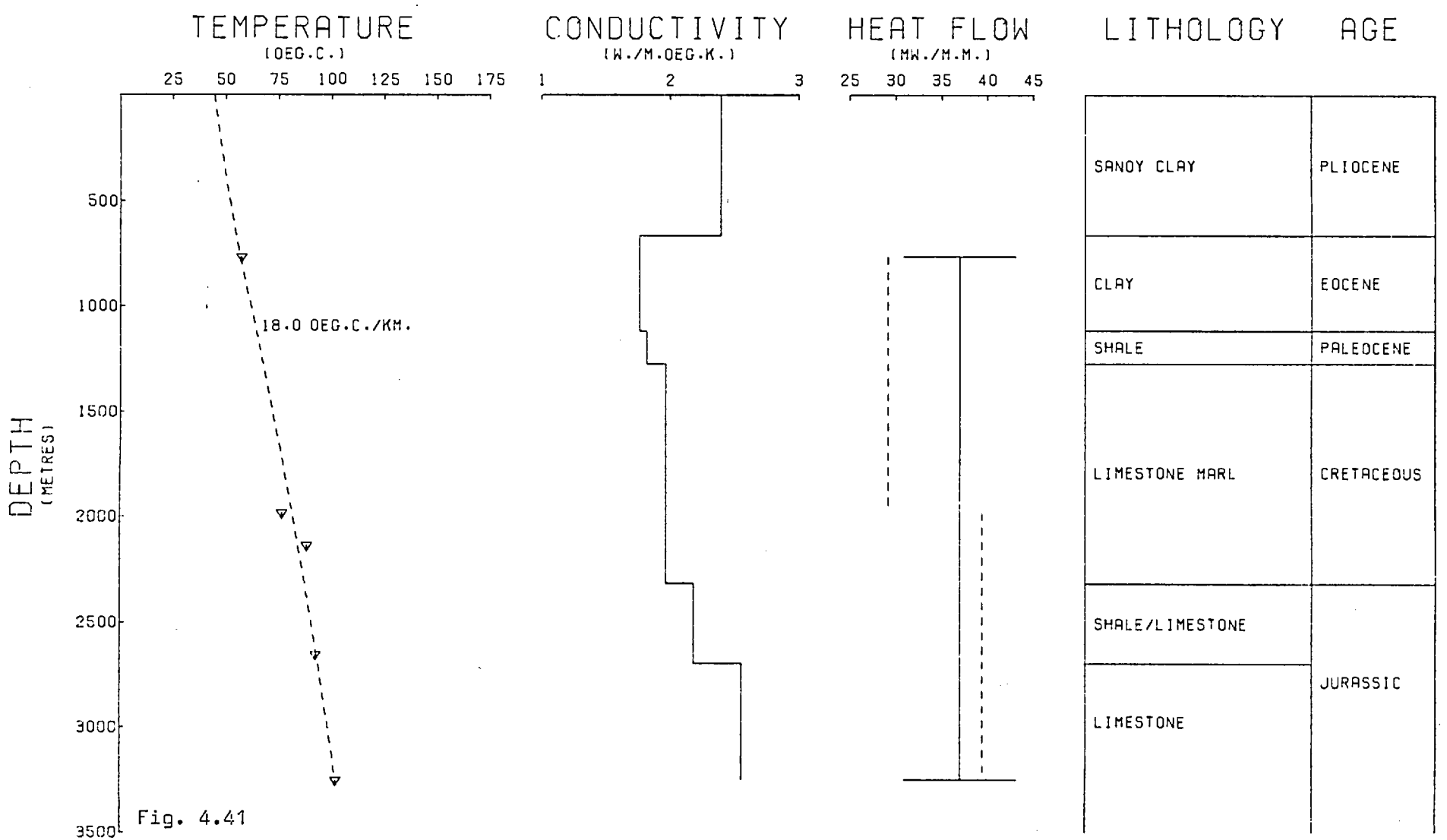


Fig. 4.41

MARIA ASCIA-1

COUNTRY-SOMALIA LAT-04D 31M N.
COMPANY-SINCLAIR LONG-47D 26M E.

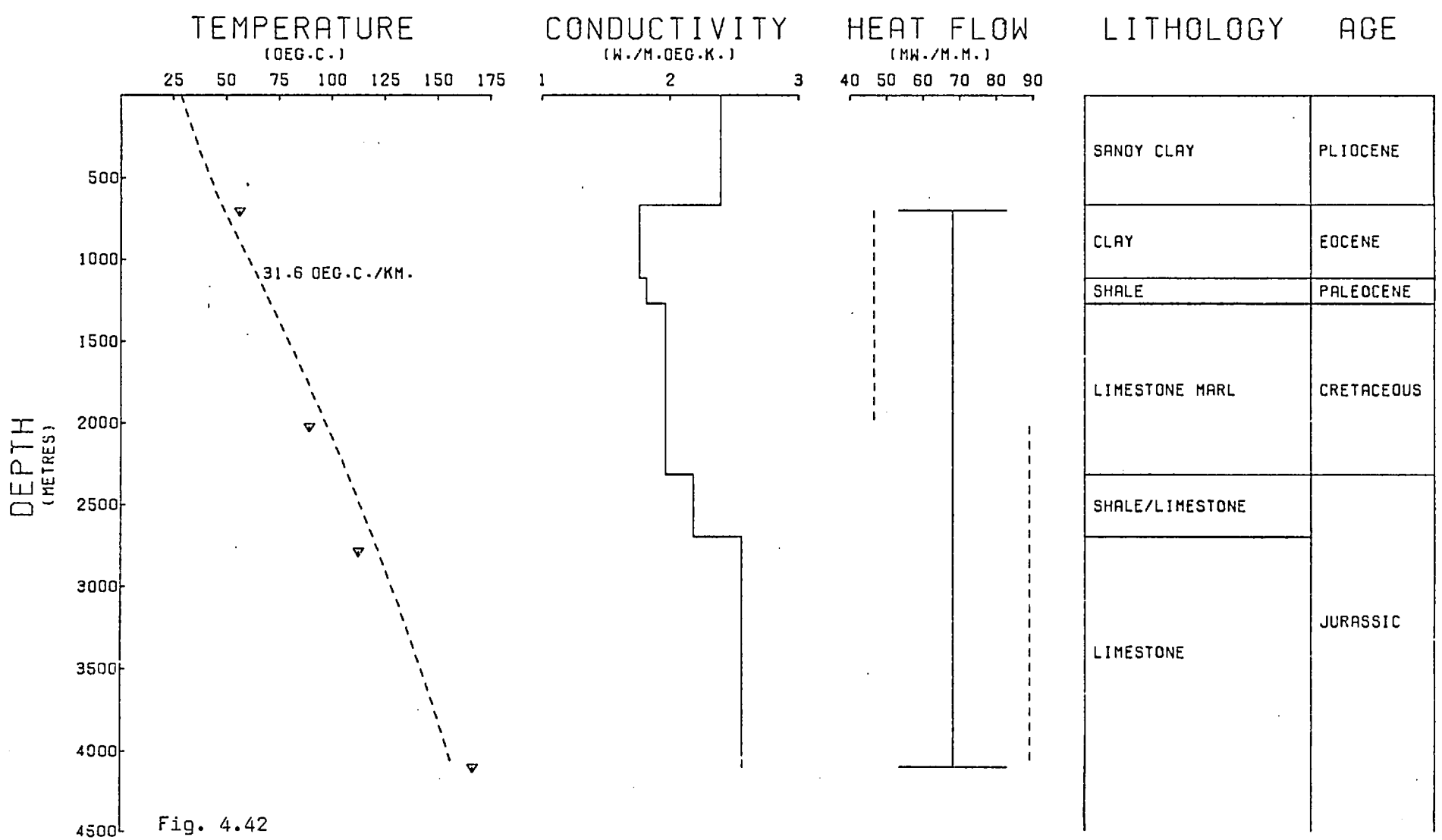


Fig. 4.42

4.13 The Eastern Ogaden Region Heat Flow

The Eastern Ogaden Basin is the western extension of the Obbia Embayment and incorporates two sedimentary troughs with an intervening basement ridge, Figs. 4.3 and 4.11. It sits astride the Ethiopian-Somalian border at about $5^{o}N$, $45^{o}E$ and is distinct from the Obbia Embayment with a thinner sedimentary cover and a markedly different facies. To the west it onlaps the Precambrian basement of Ethiopia while to the south it is bounded by the Oddur Arch, the north-eastern subsurface continuation of the Bur Acaba Massif, Fig. 4.3.

The near surface sediments are Lower Eocene limestones through Cretaceous continental sandstones which are underlain by an extensive Jurassic carbonate-evaporate sequence (Clift, 1956). The base of Jurassic is marked by an extensive eolian sand formation, which according to Clift, passes directly into metamorphic basement. However, more recent deep drilling, specifically the Bokh-1 and Abred-1 wells (Figs. 4.44 and 4.50 respectively), has revealed an extensive Cambrian sequence of sediments and metasediments (Gewerschaft Elwerath, pers. comm., 1973).

This sequence, which may be equivalent to the Inda Ad formation of Northern Somalia (section 4.2), has considerable significance with regard to the Pan-African thermal event and the Mozambique belt. Clearly the Eastern Ogaden region may be underlain by basement much older than the typical Mozambiquan age of 500 m.y., a conclusion reached independently by Cahen and Snelling (1966) and Saggerson (1973). This view is also supported by Kazmin (1971) who believes the Eastern Ogaden region to have been part of a major Proterozoic geosyncline.

Eleven values of heat flow were obtained from this region; the mean of 46 $\pm$ 9 $mW \cdot m^{-2}$ (weighted mean 44 $\pm$ 7 $mW \cdot m^{-2}$) was the lowest regional average obtained in this study (table 4.5). Such a low value might well be expected if the Eastern Ogaden basement is indeed significantly older than Mozambiquan. Polyak and Smirnov (1968) and Sclater and Francheteau (1970)

have demonstrated a world wide correlation of heat flow with tectonic provinces, the older ones having lower heat flow. Sclater and Francheteau indicate average heat flows of 45.6 and 54.8 $mW \cdot m^{-2}$ for provinces of Precambrian folding and Caledonian tectonism respectively. This is consistent with the observed heat flow variation of this area, Fig. 4.11, assuming the surrounding regions, Darror and Nogal Valleys, Obbia Embayment, Benadir Coast, and Mandera Lugh Basin, to be underlain by the Mozambique (Caledonide equivalent) belt.

The individual results, Figs. 4.43 - 4.53, span the entire range of reliability, A-D, table 4.2. The Bokh-1 value of 41 $mW \cdot m^{-2}$ is thought to be relatively well determined with small Bullard temperature residuals (Fig. 4.44).

Two of the boreholes, Idole-1 and Dusa Mareb-1, penetrated basalt flows of post Paleocene-Pre Miocene? age (Figs. 4.46 and 4.47). The flows, which are only tens of metres thick, are thought to be equivalent to the Oligocene 'Trap' series described by Mohr (1962) and evident in outcrop within the Eastern Ogaden Basin, Fig. 4.2.

We will return to the Eastern Ogaden region heat flow results in connection with steady state crust and mantle temperature profiles (section 4.21) and two dimensional crustal temperature models (section 4.22).

XF-5

COUNTRY-ETHIOPIA LAT-07D 49M N.
COMPANY-SINCLAIR LONG-45D 37M E.

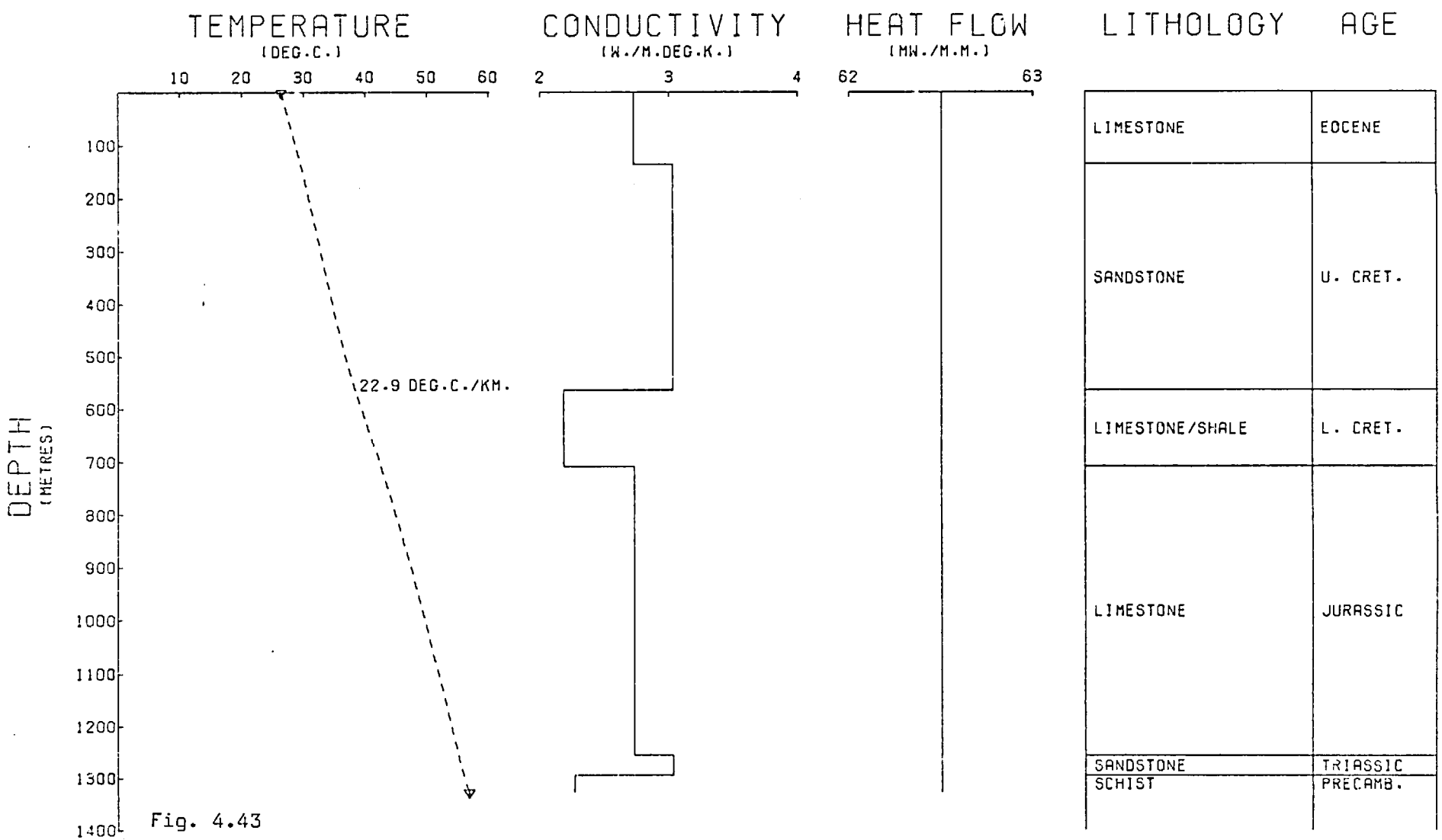


Fig. 4.43

BOKH-1

COUNTRY-ETHIOPIA LAT-07D 30M N.
COMPANY-ELWERATH LONG-46D 57M E.

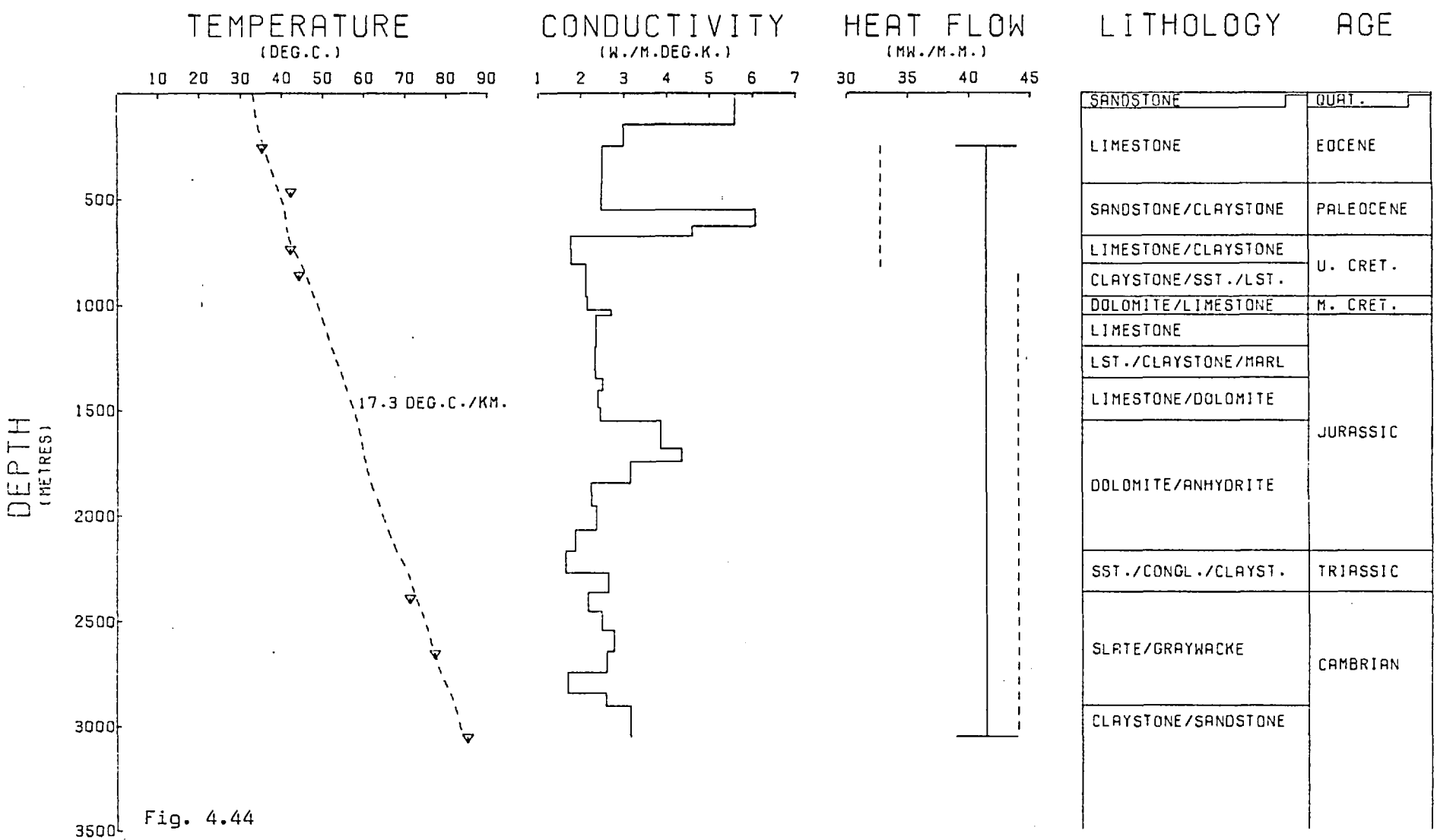


Fig. 4.44

GALCAIO-2

COUNTRY-SOMALIA LAT-06D 55M N.
COMPANY-MOBIL LONG-47D 36M E.

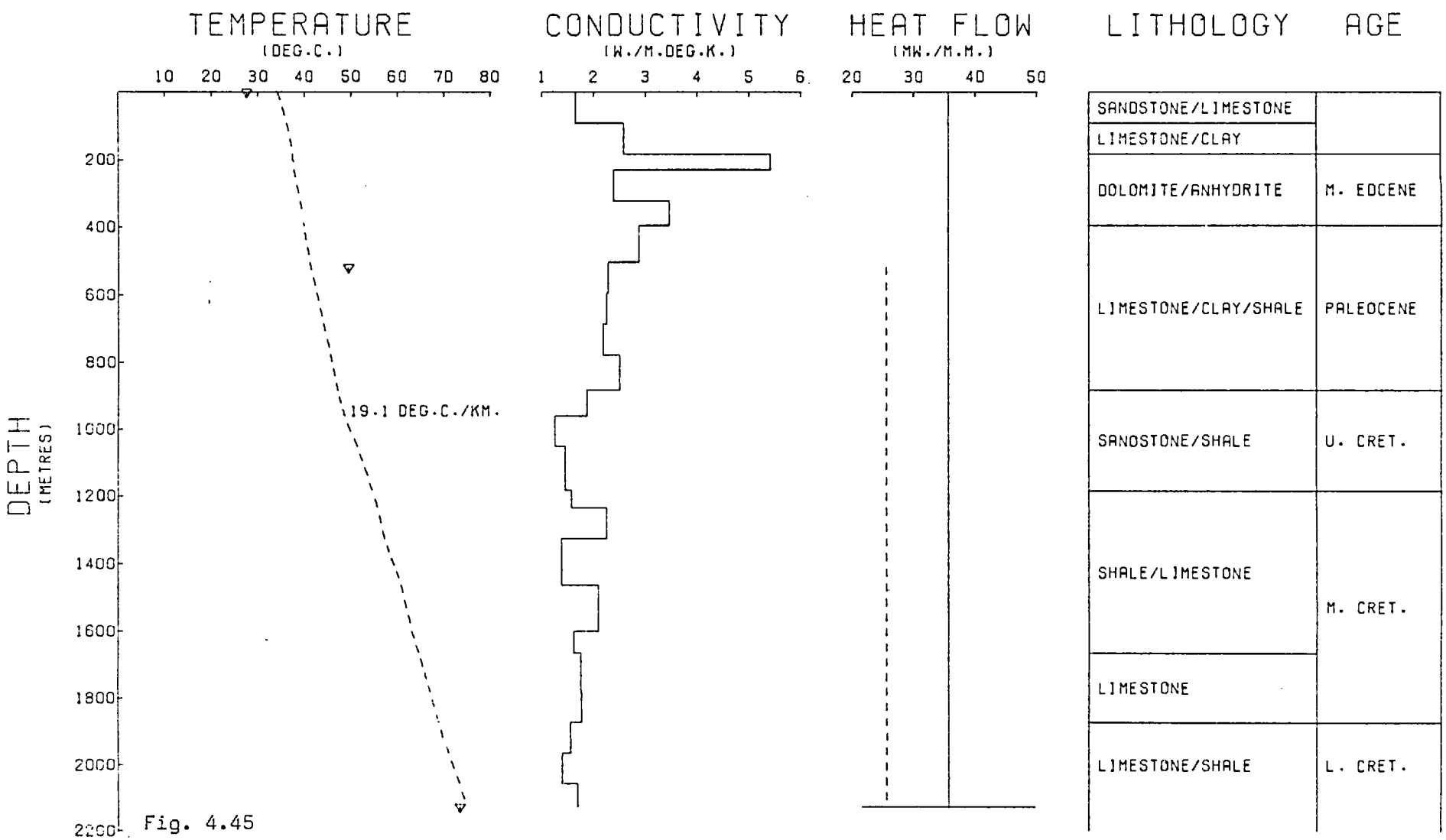


Fig. 4.45

IDOLE-1

COUNTRY-SOMALIA LAT-06D 10M N.
COMPANY-MOBIL LONG-47D 02M E.

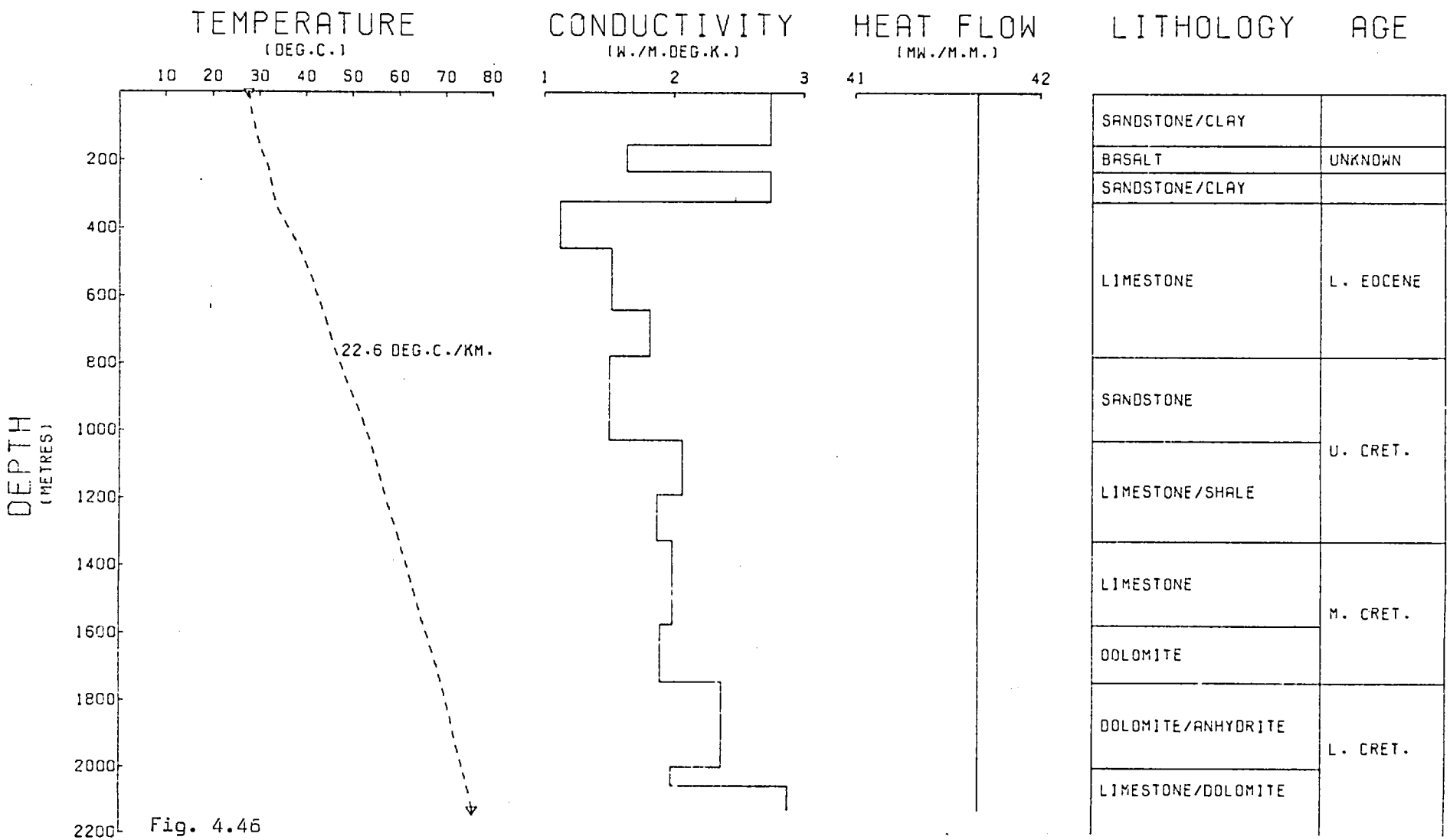


Fig. 4.46

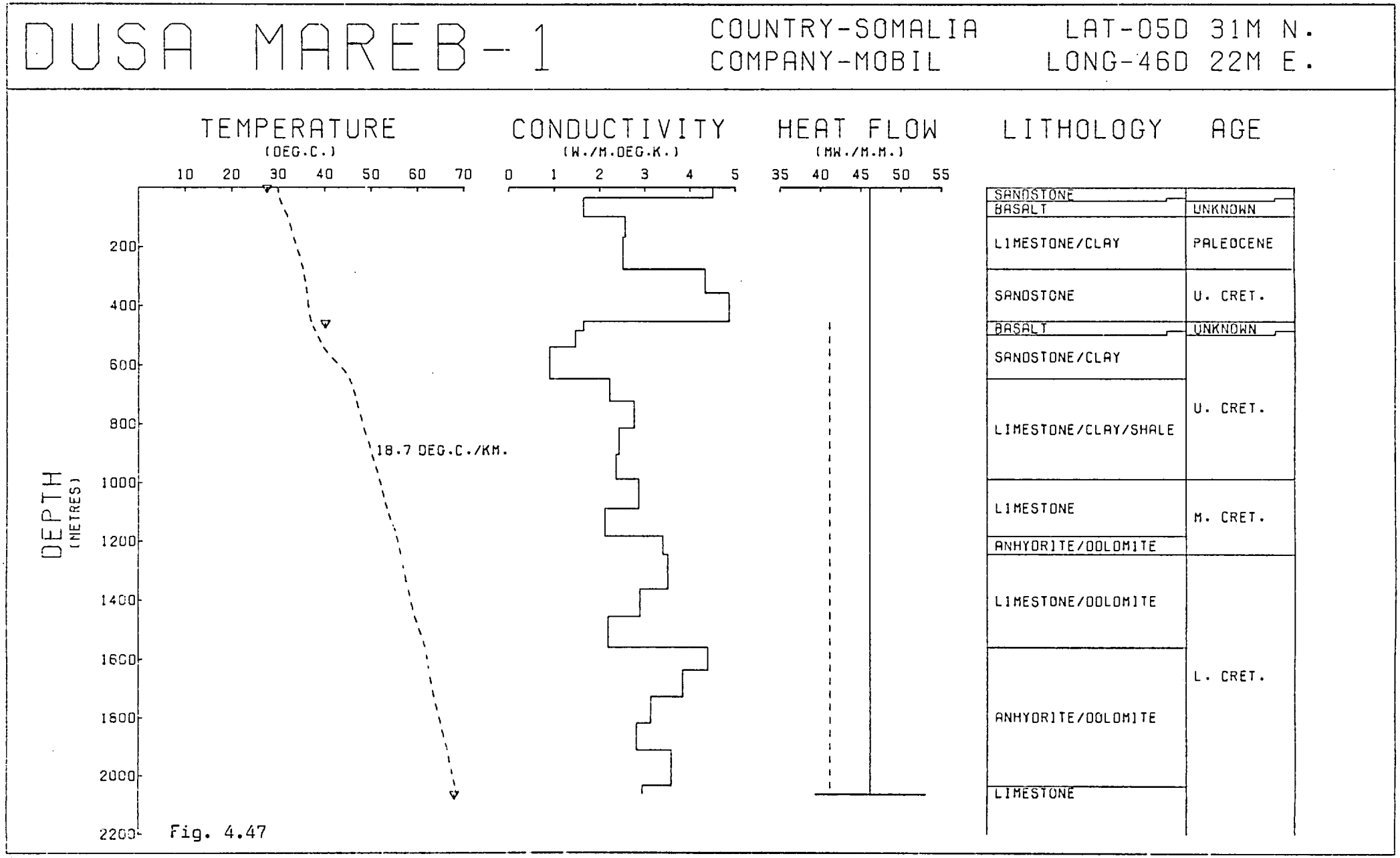

DUSA MAREB-1
COUNTRY-SOMALIA
COMPANY-MOBIL
LAT-05D 31M N.
LONG-46D 22M E.
TEMPERATURE
(DEG.C.)
10 20 30 40 50 60 70
CONDUCTIVITY
(W./M.DEG.K.)
0 1 2 3 4 5
HEAT FLOW
(MW./M.M.)
35 40 45 50 55
LITHOLOGY
AGE
DEPTH
(METRES)
200
400
600
800
1000
1200
1400
1600
1800
2000
2200
18.7 DEG.C./KM.
SANDSTONE
BASALT
UNKNOWN
LIMESTONE/CLAY
PALEOCENE
SANDSTONE
U. CRET.
BASALT
UNKNOWN
SANDSTONE/CLAY
LIMESTONE/CLAY/SHALE
U. CRET.
LIMESTONE
M. CRET.
ANHYDRITE/DOLOMITE
LIMESTONE/DOLOMITE
ANHYDRITE/DOLOMITE
L. CRET.
LIMESTONE

Fig. 4.47

DUSA MAREB-2

COUNTRY-SOMALIA
COMPANY-MOBIL

LAT-05D 35M N.
LONG-45D 53M E.

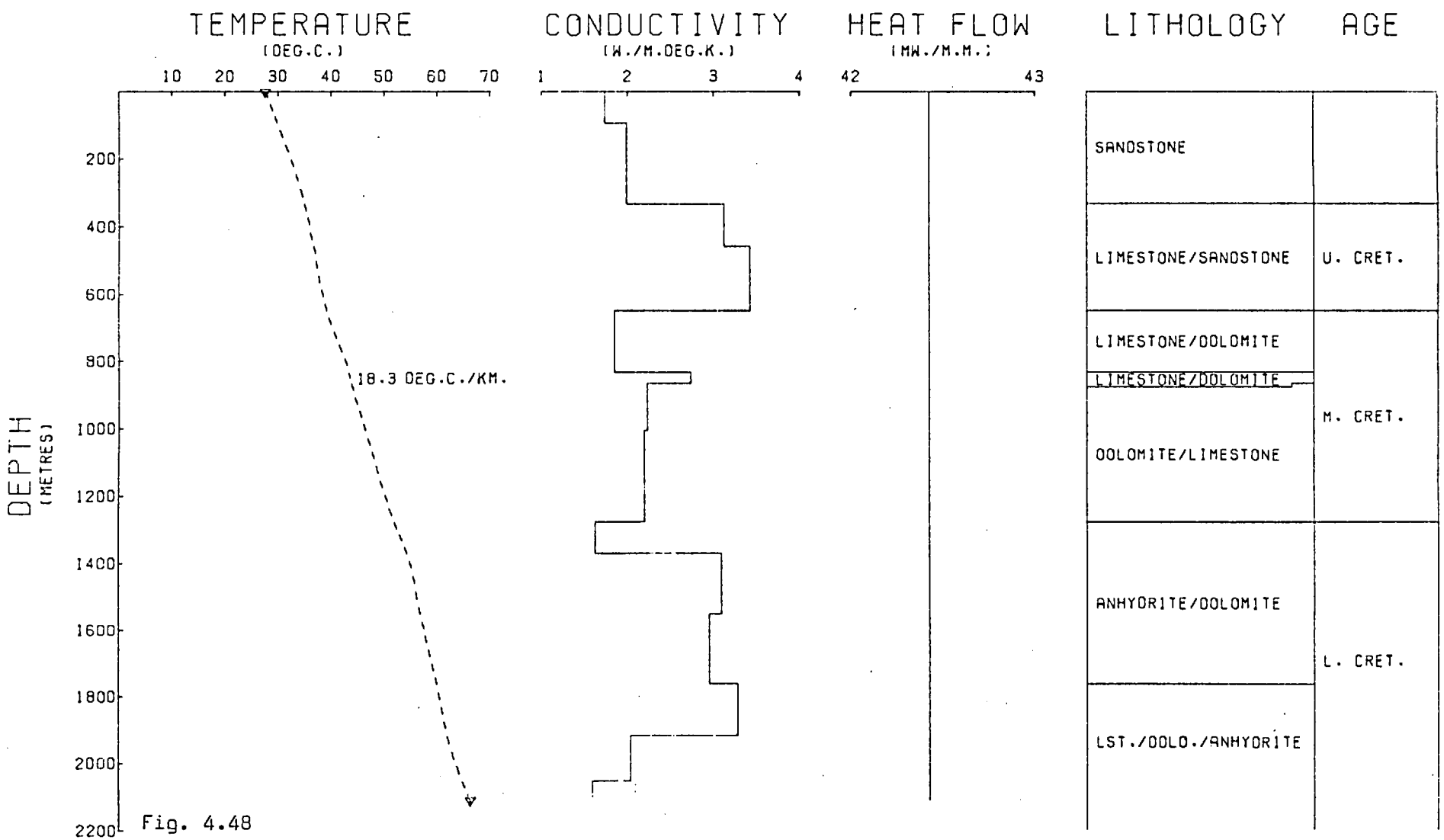


Fig. 4.48

BULO BURTI-1

COUNTRY-SOMALIA
COMPANY-MOBIL

LAT-04D 04M N.
LONG-45D 30M E.

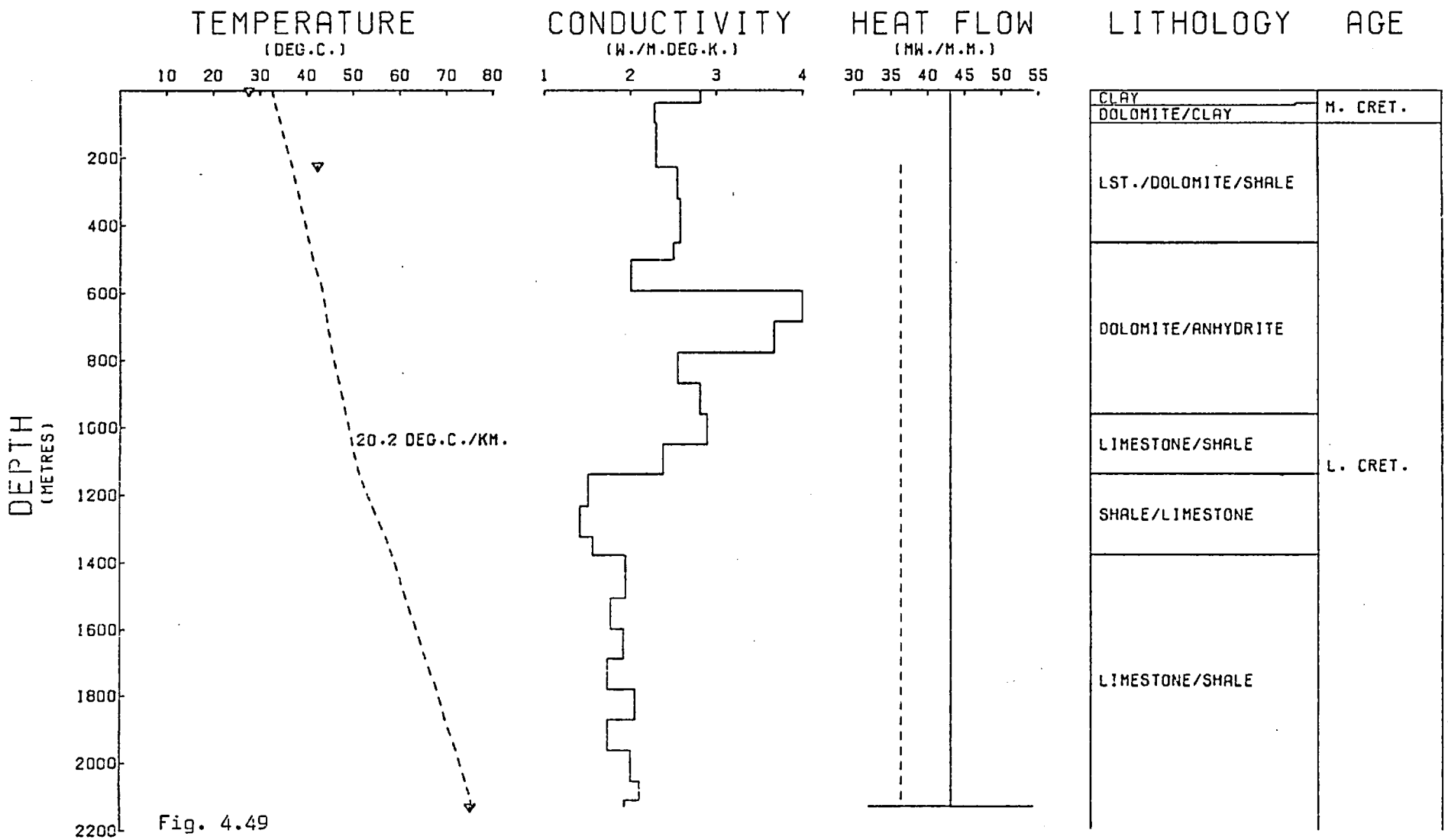


Fig. 4.49

ABRED-1

COUNTRY-ETHIOPIA LAT-05D 30M N.
COMPANY-ELWERATH LONG-45D 15M E.

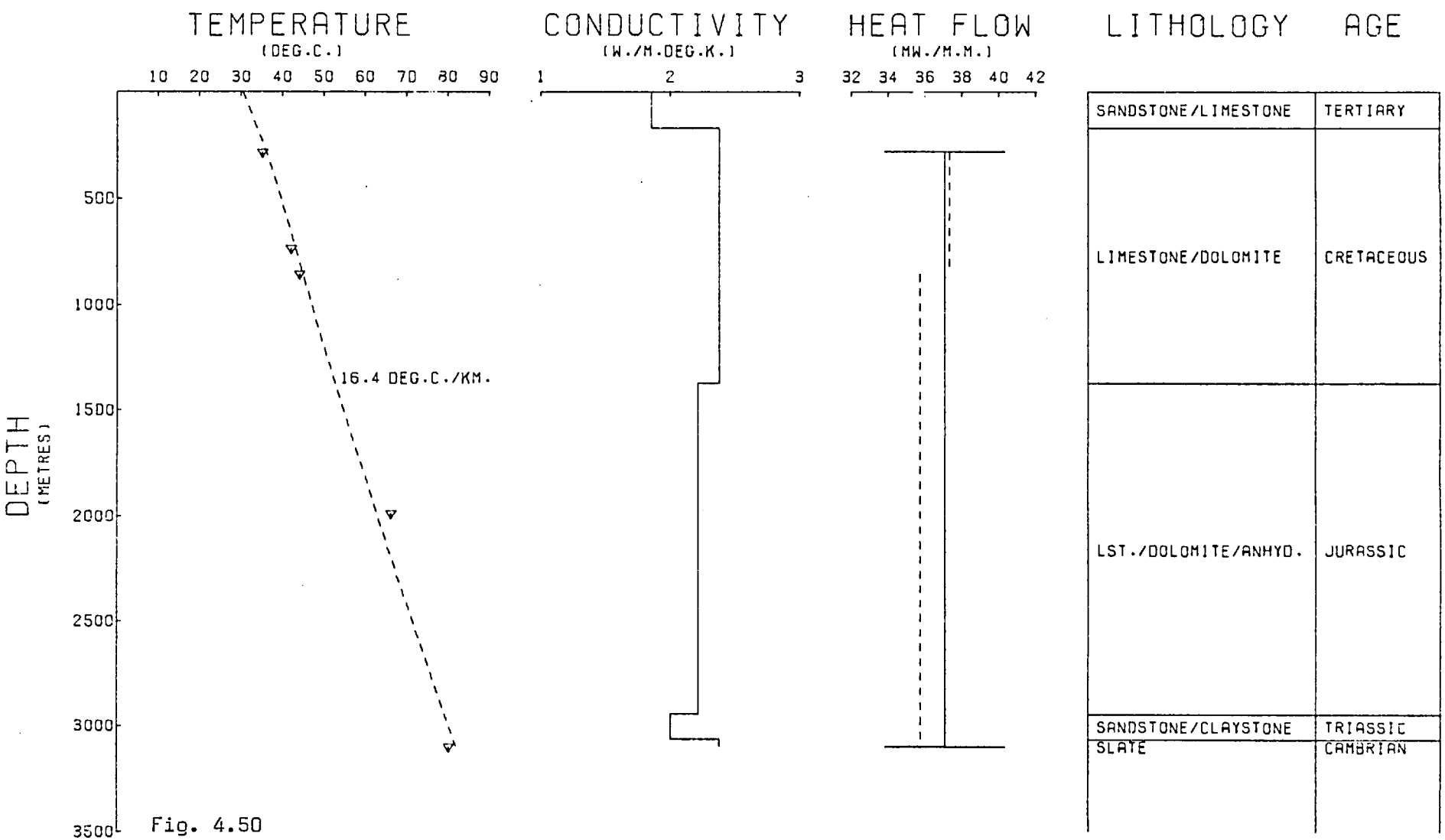


Fig. 4.50

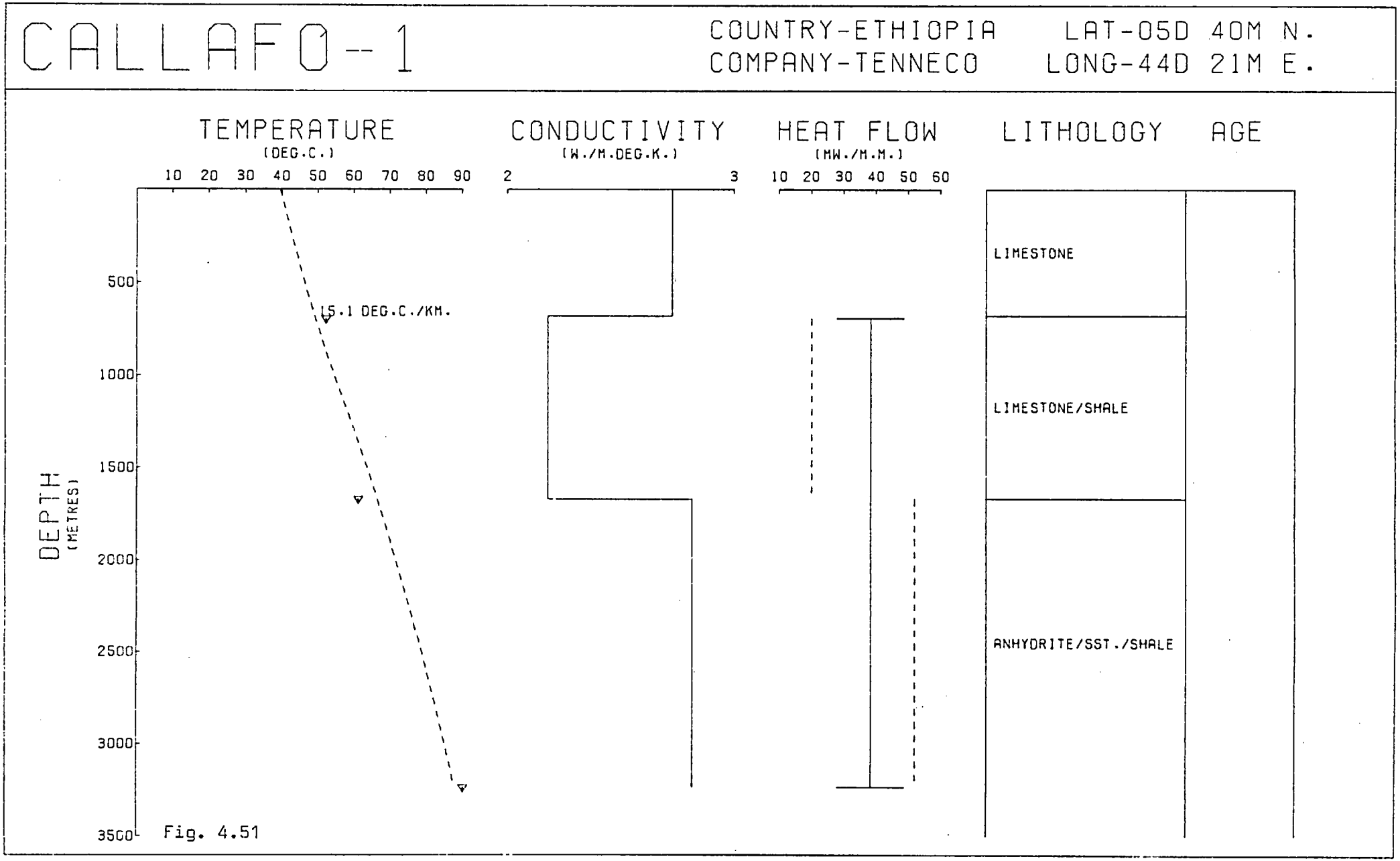

CALLAFO-1
COUNTRY-ETHIOPIA
COMPANY-TENNECO
LAT-05D 40M N.
LONG-44D 21M E.
TEMPERATURE
(DEG.C.)
10 20 30 40 50 60 70 80 90
CONDUCTIVITY
(W./M.DEG.K.)
2 3
HEAT FLOW
(MW./M.M.)
10 20 30 40 50 60
LITHOLOGY
AGE
DEPTH
(METRES)
500
1000
1500
2000
2500
3000
3500
45.1 DEG.C./KM.
LIMESTONE
LIMESTONE/SHALE
ANHYDRITE/SST./SHALE

Fig. 4.51

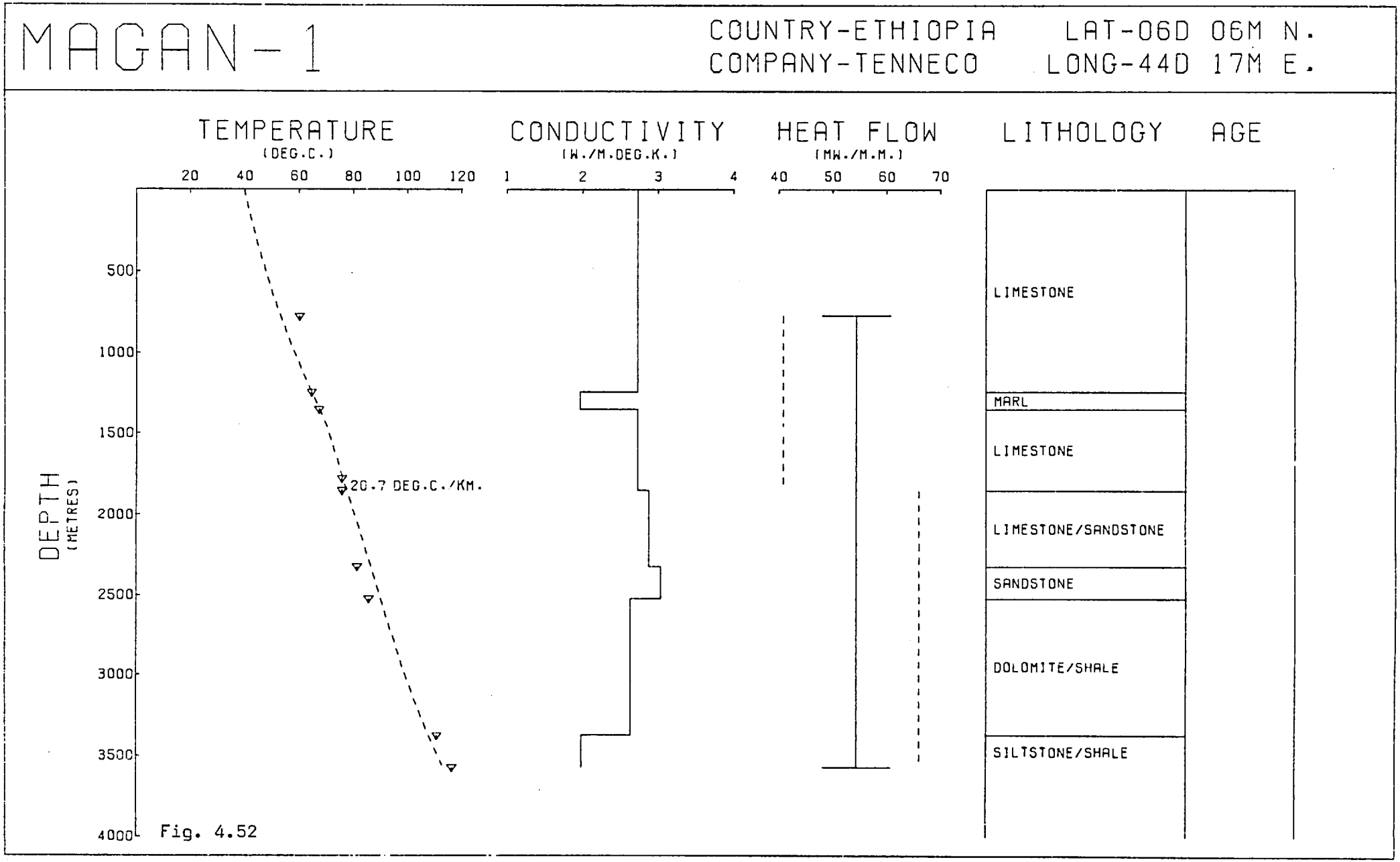

MAGAN-1
COUNTRY-ETHIOPIA
COMPANY-TENNECO
LAT-06D 06M N.
LONG-44D 17M E.
TEMPERATURE
(DEG.C.)
20
40
60
80
100
120
CONDUCTIVITY
(W./M.DEG.K.)
1
2
3
4
HEAT FLOW
(MW./M.M.)
40
50
60
70
LITHOLOGY
AGE
DEPTH
(METRES)
500
1000
1500
2000
2500
3000
3500
4000
20.7 DEG.C./KM.
LIMESTONE
MARL
LIMESTONE
LIMESTONE/SANDSTONE
SANDSTONE
DOLOMITE/SHALE
SILTSTONE/SHALE

Fig. 4.52

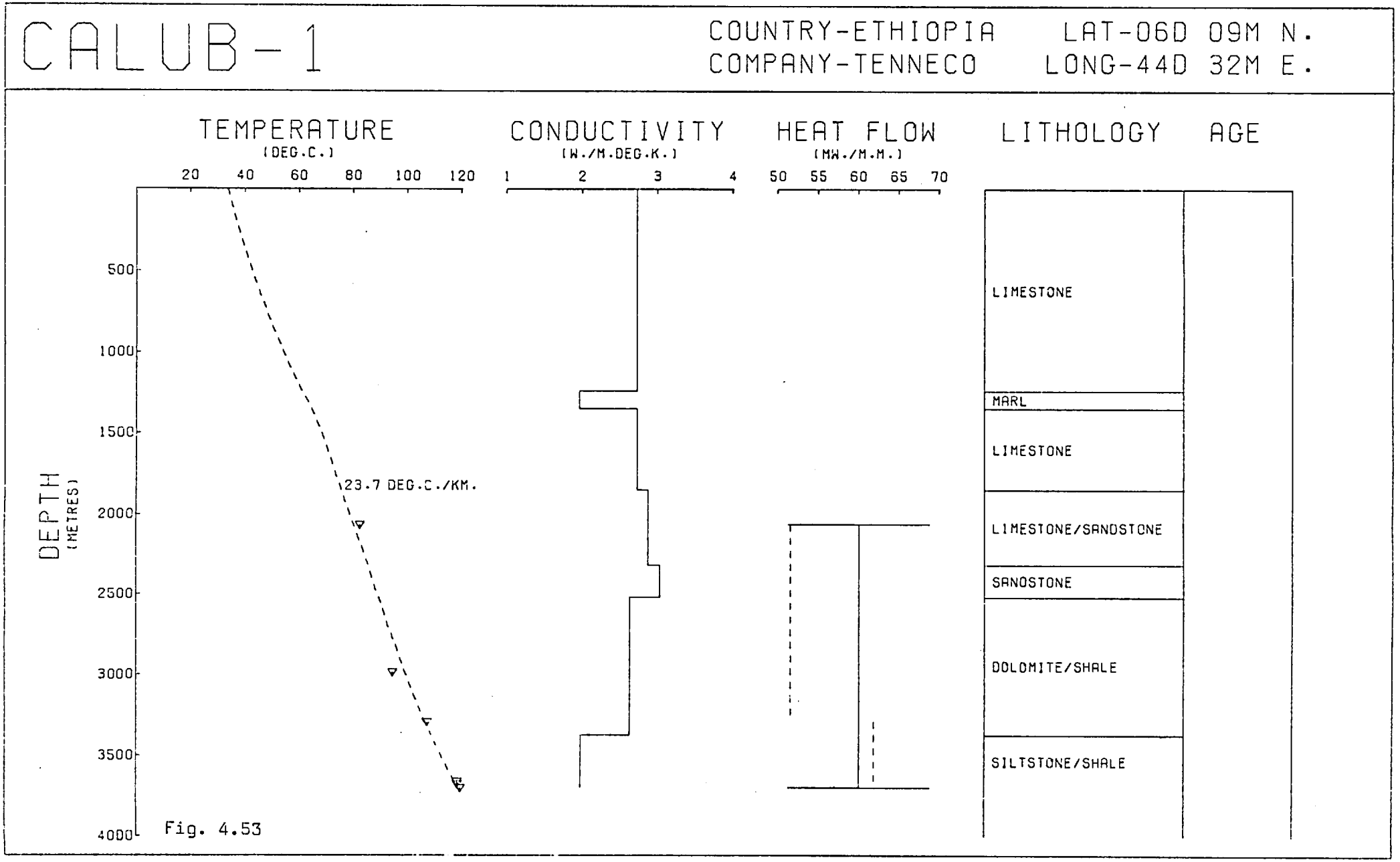

CALUB-1
COUNTRY-ETHIOPIA
COMPANY-TENNECO
LAT-06D 09M N.
LONG-44D 32M E.
TEMPERATURE
(DEG.C.)
20 40 60 80 100 120
CONDUCTIVITY
(W./M.DEG.K.)
1 2 3 4
HEAT FLOW
(MW./M.M.)
50 55 60 65 70
LITHOLOGY
AGE
DEPTH
(METRES)
500
1000
1500
2000
2500
3000
3500
4000
23.7 DEG.C./KM.
LIMESTONE
MARL
LIMESTONE
LIMESTONE/SANDSTONE
SANDSTONE
DOLOMITE/SHALE
SILTSTONE/SHALE

Fig. 4.53

4.14 The Benadir Coast Region Heat Flow

The Benadir Coast is that narrow plain between the eastern boundary of the Bur Acaba Massif and the Indian Ocean (Fig. 4.3). As with the Obbia Embayment there are no previous publications dealing specifically with the geology or geophysics of this region.

The eastern boundary of the Bur Acaba Massif is faulted, with a throw of several thousand metres, against Jurassic sediments; a second major fault subparallels this basement contact at some 50 kilometres to the east (Beltrandi and Pyre, 1973). Beltrandi and Pyre believe that this coastal fault system resulted from early Tertiary crustal deformation associated with the initial rifting of the Gulf of Aden.

The Tectonic Map of Africa (UNESCO, 1968) indicates some six to seven kilometres of sediment in this region. Harrison and Haw (1964) describe a thick, three to four kilometre, complete Tertiary sequence of largely shallow marine limestones and shales with occasional thick deltaic sands overlying a mainly carbonate Mesozoic sequence. Local unconformities are present as at Duddumai-1, Fig. 4.56, where Pliocene sands pass directly into Paleocene or Upper Cretaceous limestones. This is undoubtedly due to the well being located on the up thrown edge of a basement fault block.

Ten heat flow determinations were made with a mean value of 65 ± 9 $mW \cdot m^{-2}$ (table 4.4). Data quality was fair to poor; BHT data being fair to good but with no conductivity samples available. Two detailed lithologic logs, Duddumai-1 and Coriole-1, were used to estimate thermal conductivities. The composite plots, Figs. 4.54 - 4.63, indicate, that for several holes, the estimated conductivities resulted in computed heat flow values with apparent low error. The effect is almost certainly illusory as without measured conductivity data and lithologic logs for most of the holes, the internal consistency must be regarded as more fortuitous than real.

Two of the wells, Uarschiek-1 and Merca-1, Figs. 4.57 and 4.58, yielded higher heat flows, 77 and 84 $mW \cdot m^{-2}$, than the other wells. The

results for Coriole-1 and Duddumai-1, of 62 and 57 $mW \cdot m^{-2}$ respectively, are thought to be the best determined for this region (Figs. 4.62 and 4.56).

Both Coriole-1 and Merca-1 bottomed in dolerite intrusions; Harrison and Haw (1964) report that the former was of Paleocene-Eocene age; the latter is unknown.

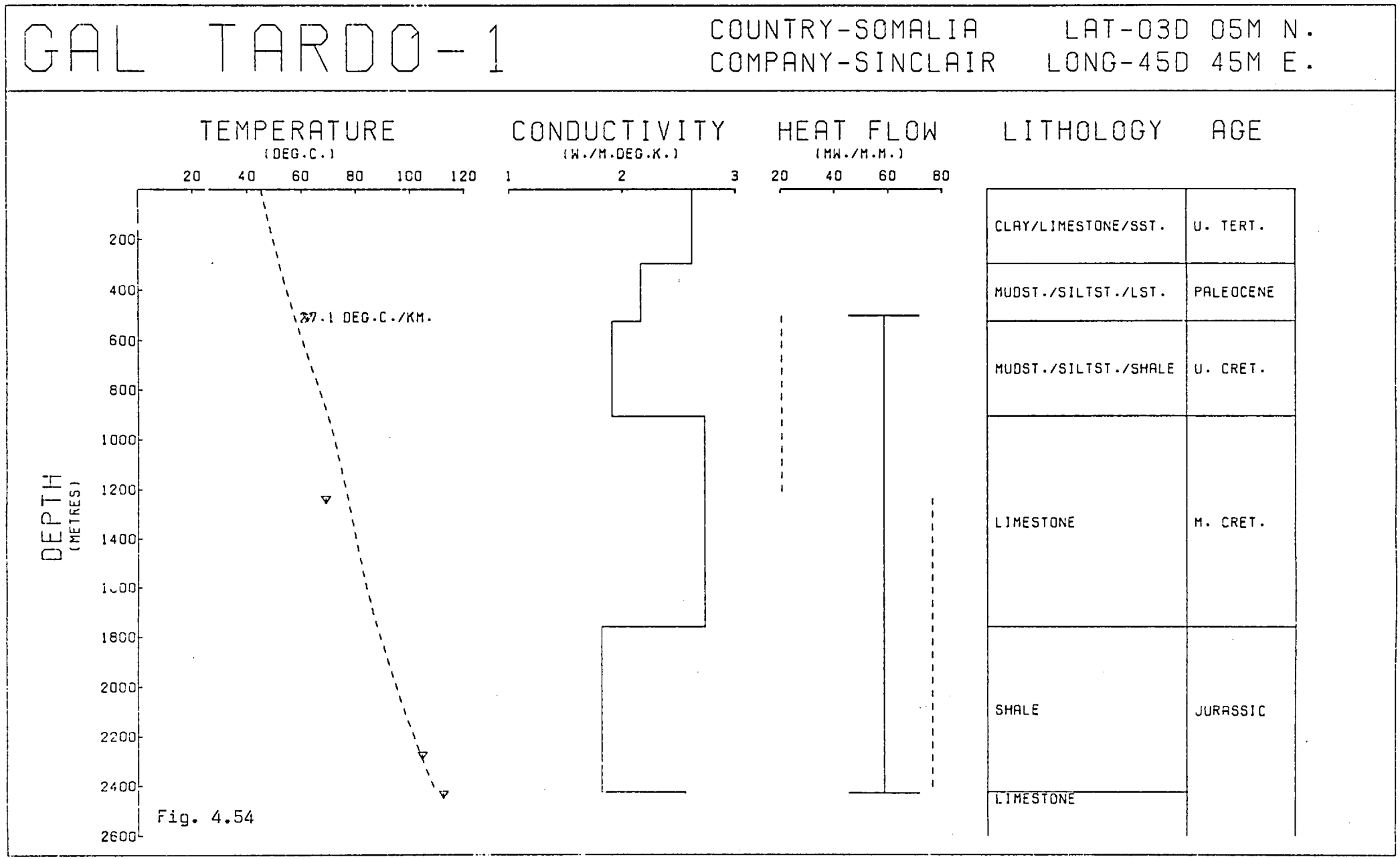

GAL TARDO-1
COUNTRY-SOMALIA
COMPANY-SINCLAIR
LAT-03D 05M N.
LONG-45D 45M E.
TEMPERATURE
(DEG.C.)
20 40 60 80 100 120
CONDUCTIVITY
(W./M.DEG.K.)
1 2 3
HEAT FLOW
(MW./M.M.)
20 40 60 80
LITHOLOGY
AGE
DEPTH
(METRES)
200 400 600 800 1000 1200 1400 1600 1800 2000 2200 2400 2600
37.1 DEG.C./KM.
CLAY/LIMESTONE/SST.
U. TERT.
MUDST./SILTST./LST.
PALEOCENE
MUDST./SILTST./SHALE
U. CRET.
LIMESTONE
M. CRET.
SHALE
JURASSIC
LIMESTONE

Fig. 4.54

BIO ADDO-1

COUNTRY-SOMALIA LAT-02D 57M N.
COMPANY-SINCLAIR LONG-45D 52M E.

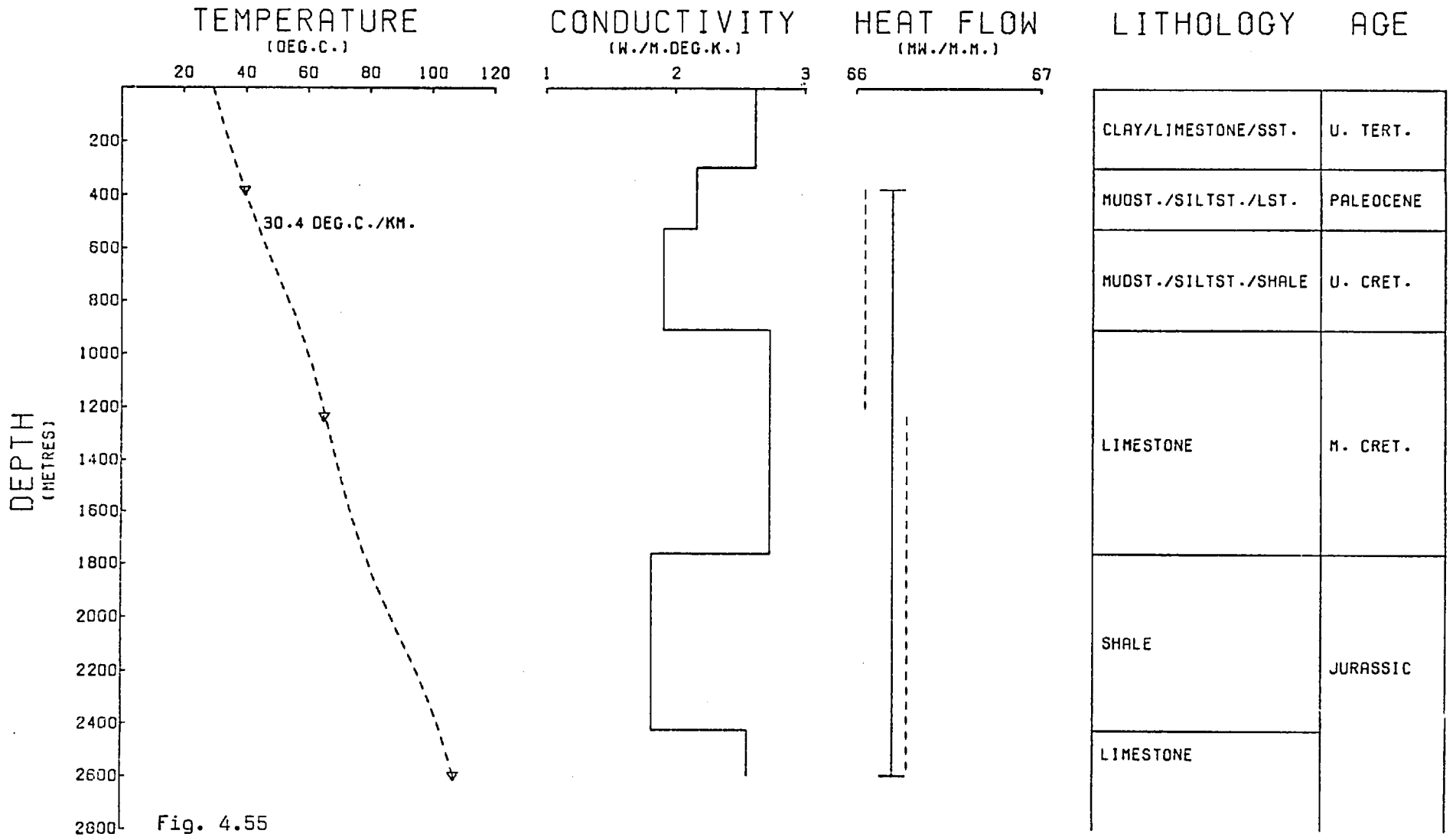


Fig. 4.55

DUDDUMAI-1

COUNTRY-SOMALIA LAT-02D 32M N.
COMPANY-SINCLAIR LONG-44D 54M E.

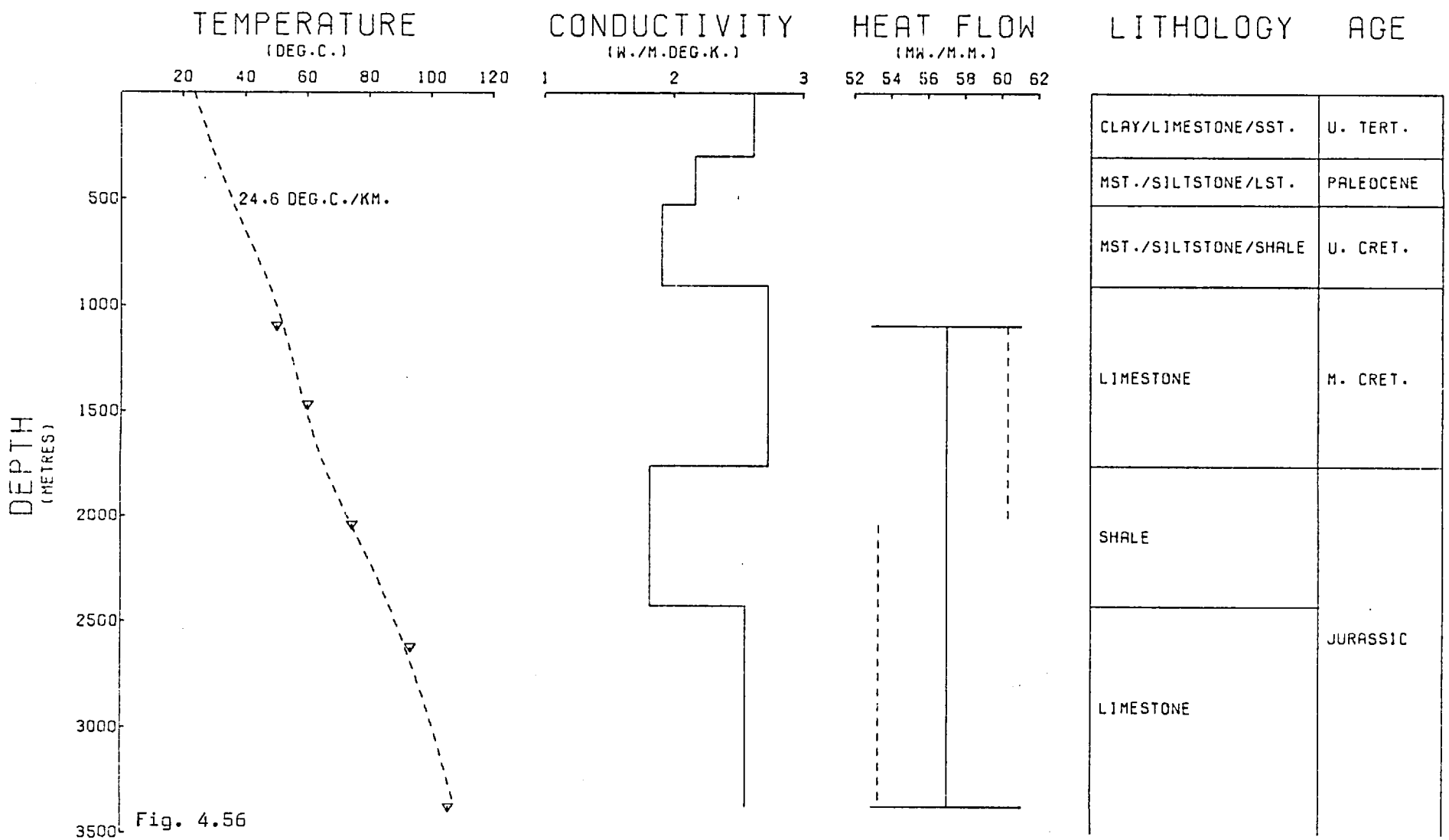


Fig. 4.56

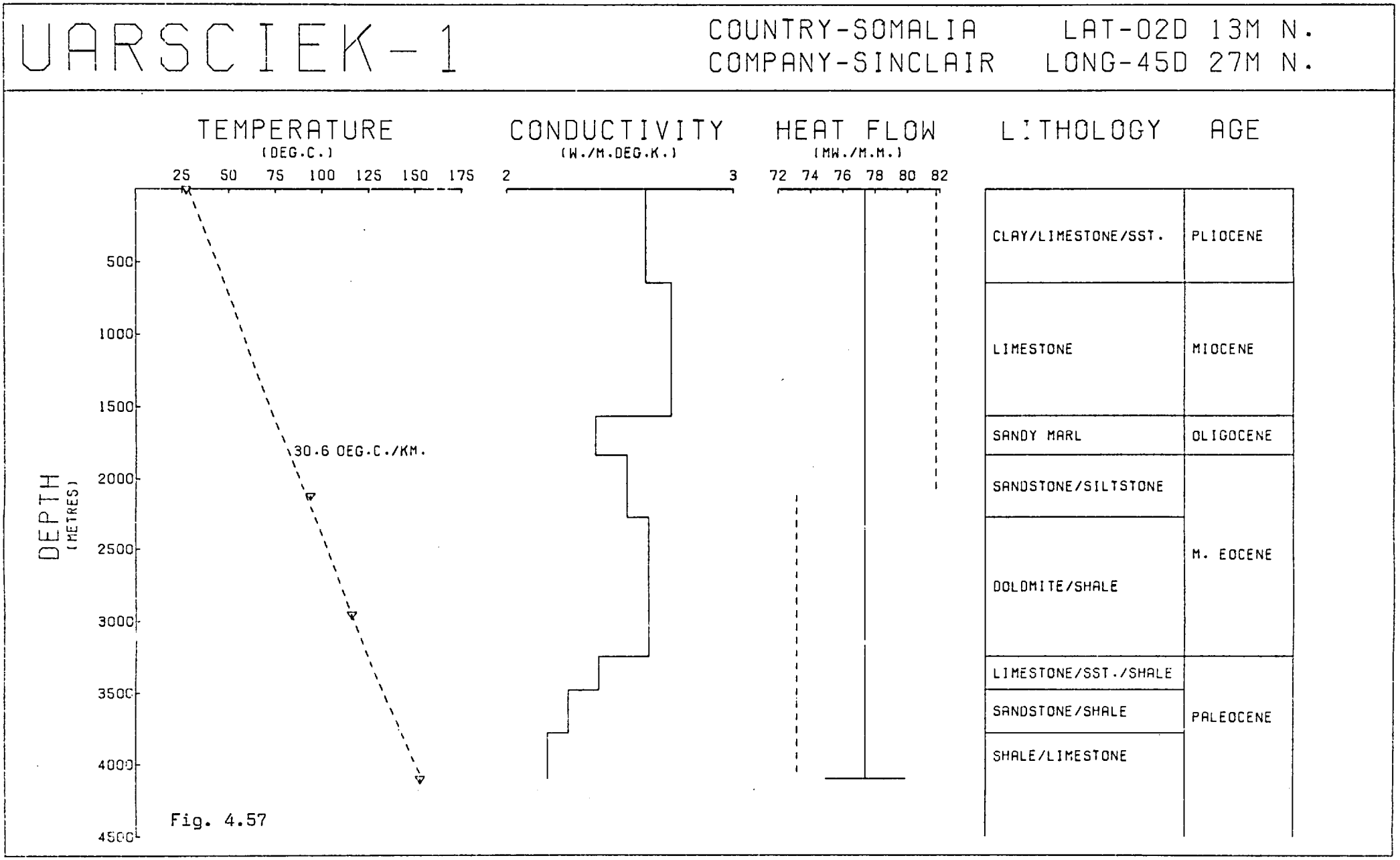

UARSCIEK-1
COUNTRY-SOMALIA
COMPANY-SINCLAIR
LAT-02D 13M N.
LONG-45D 27M N.
TEMPERATURE
(DEG.C.)
25 50 75 100 125 150 175
CONDUCTIVITY
(W./M.DEG.K.)
2 3
HEAT FLOW
(MW./M.M.)
72 74 76 78 80 82
LITHOLOGY
AGE
DEPTH
(METRES)
500
1000
1500
2000
2500
3000
3500
4000
4500
30.6 DEG.C./KM.
CLAY/LIMESTONE/SST.
PLIOCENE
LIMESTONE
MIOCENE
SANDY MARL
OLIGOCENE
SANDSTONE/SILTSTONE
DOLOMITE/SHALE
M. EOCENE
LIMESTONE/SST./SHALE
SANDSTONE/SHALE
SHALE/LIMESTONE
PALEOCENE

Fig. 4.57

MERCA-1

COUNTRY-SOMALIA LAT-01D 52M N.
COMPANY-SINCLAIR LONG-44D 56M E.

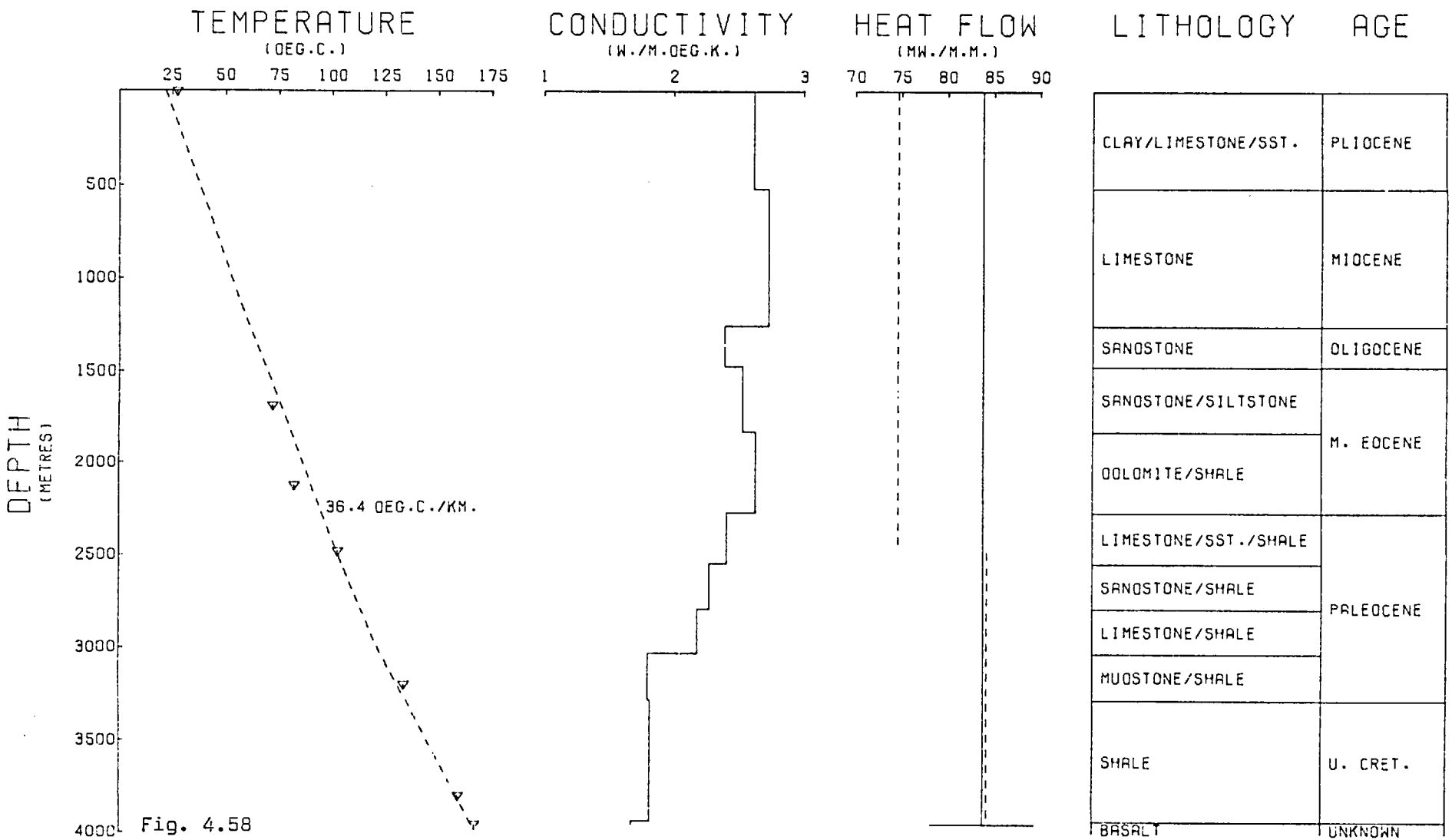


Fig. 4.58

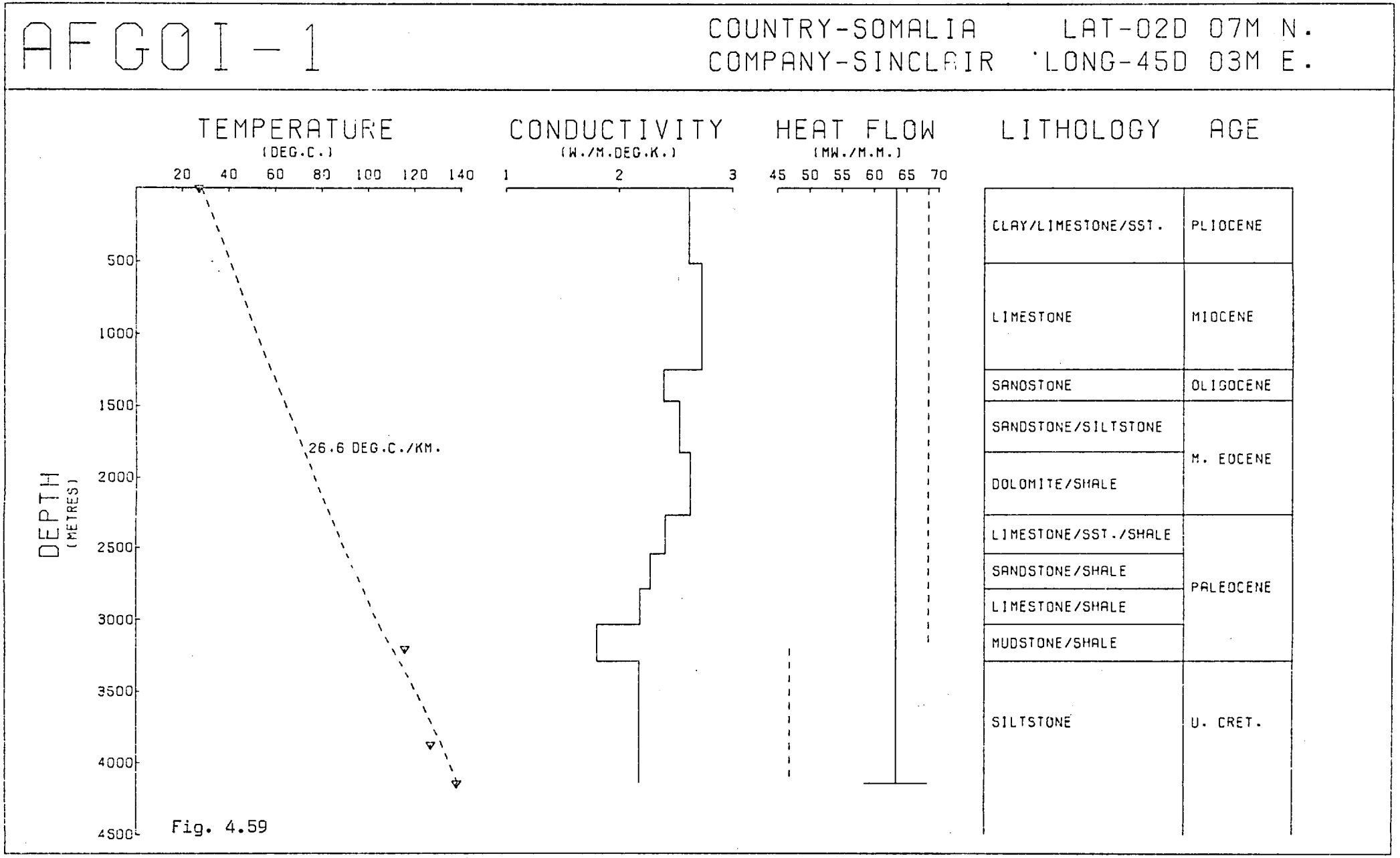

AFGOI-1
COUNTRY-SOMALIA
COMPANY-SINCLAIR
LAT-02D 07M N.
LONG-45D 03M E.
TEMPERATURE
(DEG.C.)
20 40 60 80 100 120 140
CONDUCTIVITY
(W./M.DEG.K.)
1 2 3
HEAT FLOW
(MW./M.M.)
45 50 55 60 65 70
LITHOLOGY
AGE
DEPTH
(METRES)
500
1000
1500
2000
2500
3000
3500
4000
4500
26.6 DEG.C./KM.
CLAY/LIMESTONE/SST.
PLIOCENE
LIMESTONE
MIOCENE
SANDSTONE
OLIGOCENE
SANDSTONE/SILTSTONE
DOLOMITE/SHALE
M. EOCENE
LIMESTONE/SST./SHALE
SANDSTONE/SHALE
LIMESTONE/SHALE
MUDSTONE/SHALE
PALEOCENE
SILTSTONE
U. CRET.

Fig. 4.59

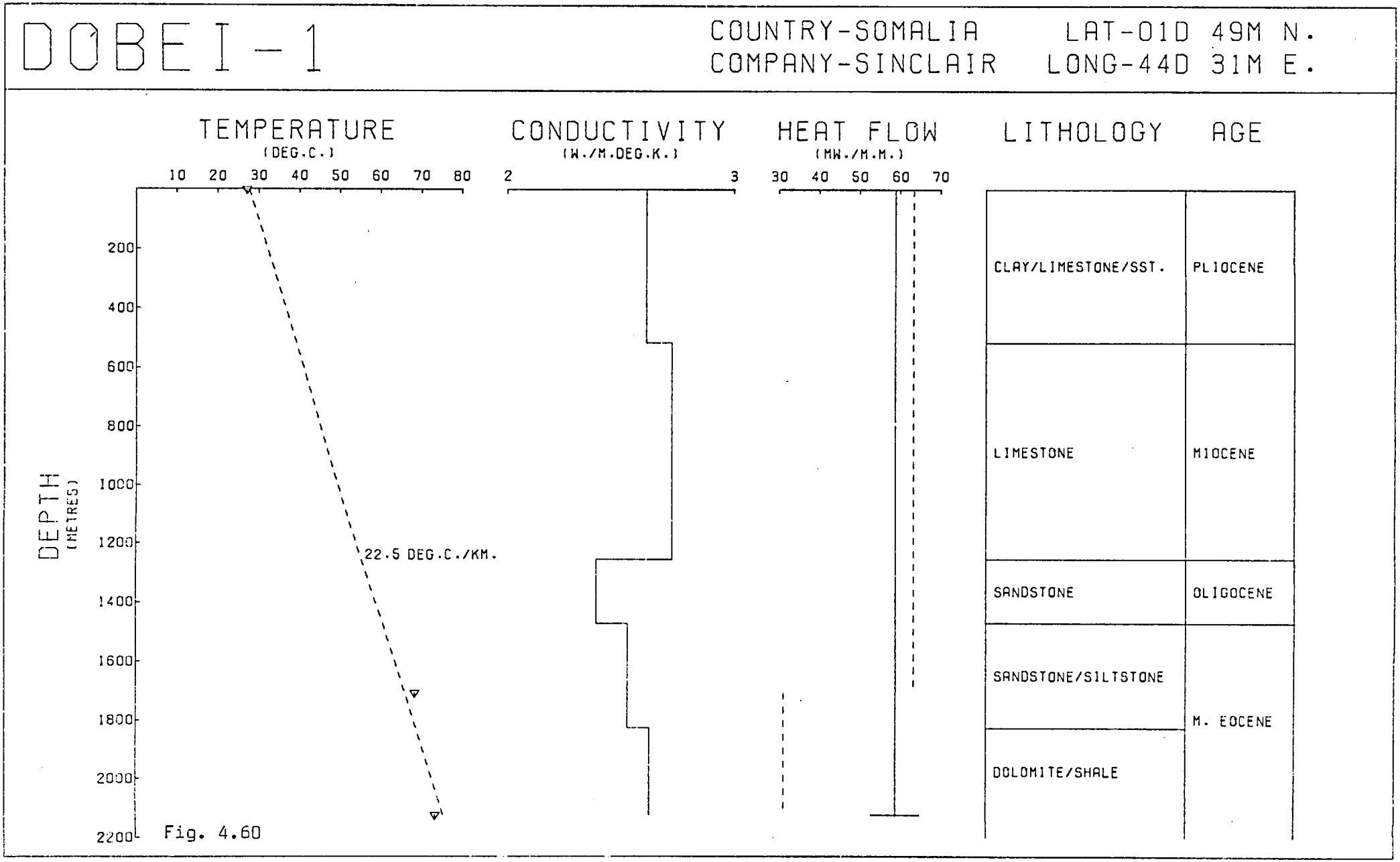

DOBEI-1
COUNTRY-SOMALIA
COMPANY-SINCLAIR
LAT-01D 49M N.
LONG-44D 31M E.
TEMPERATURE
(DEG.C.)
10 20 30 40 50 60 70 80
CONDUCTIVITY
(W./M.DEG.K.)
2 3
HEAT FLOW
(MW./M.M.)
30 40 50 60 70
LITHOLOGY
AGE
DEPTH
(METRES)
200
400
600
800
1000
1200
1400
1600
1800
2000
2200
22.5 DEG.C./KM.
CLAY/LIMESTONE/SST.
PLIOCENE
LIMESTONE
MIOCENE
SANDSTONE
OLIGOCENE
SANDSTONE/SILTSTONE
M. EOCENE
DOLOMITE/SHALE

Fig. 4.60

DOBEI-2

COUNTRY-SOMALIA LAT-01D 43M N.
COMPANY-SINCLAIR LONG-44D 28M E.

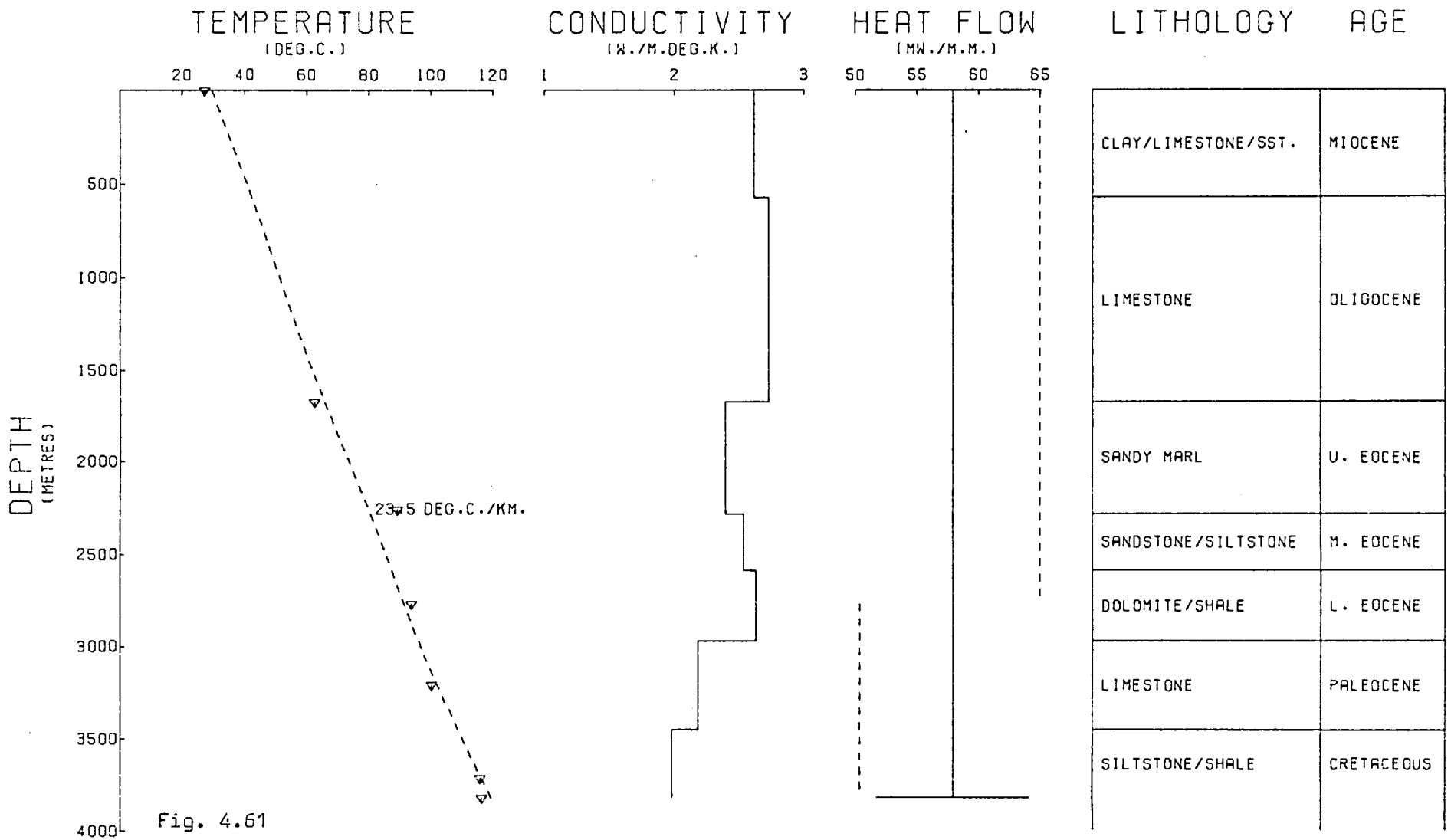


Fig. 4.61

CORIOLE-1

COUNTRY-SOMALIA LAT-01D 50M N.
COMPANY-SINCLAIR LONG-44D 33M E.

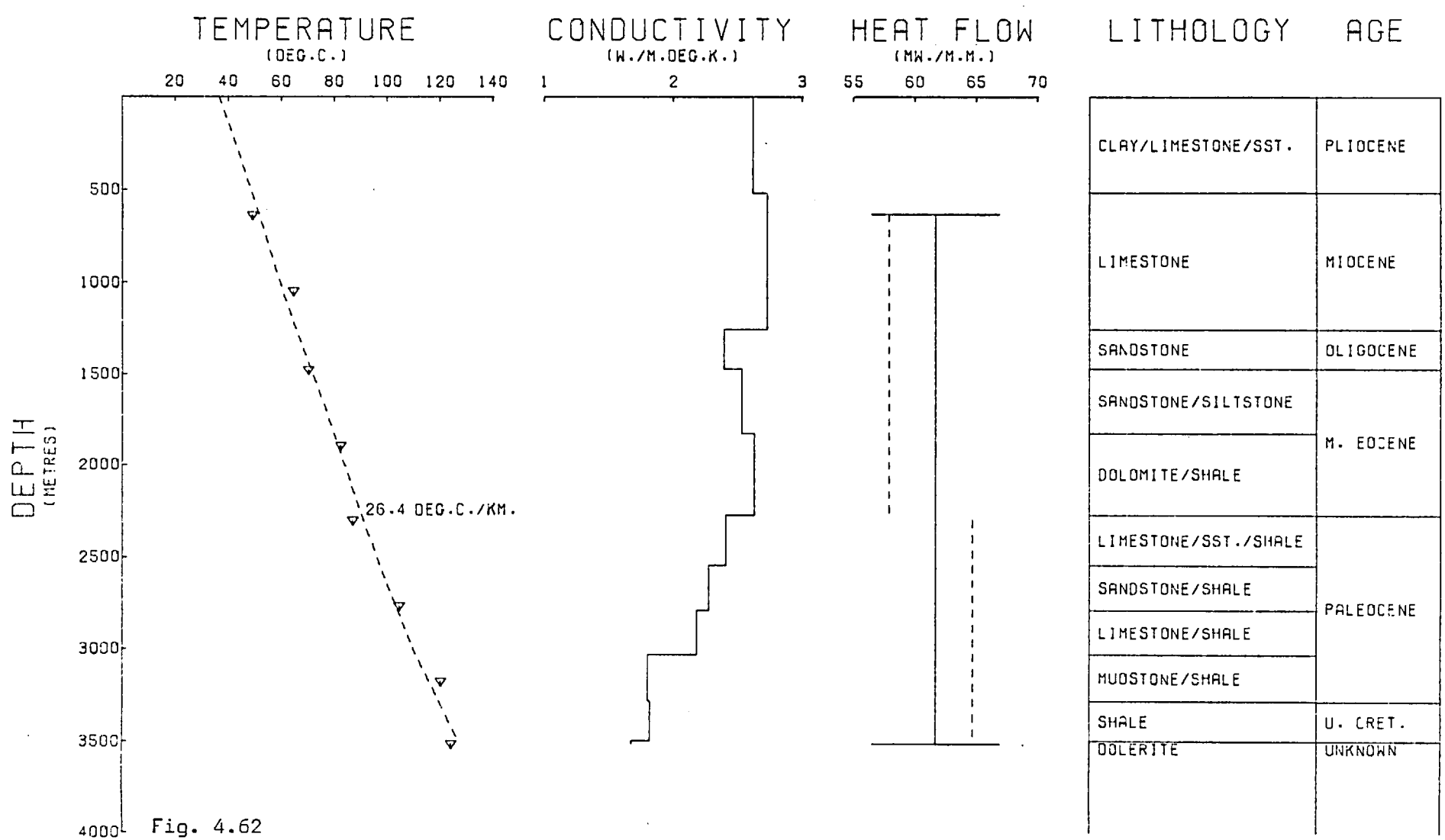


Fig. 4.62

CORIOLE-2

COUNTRY-SOMALIA LAT-01D 49M N.
COMPANY-SINCLAIR LONG-44D 36M E.

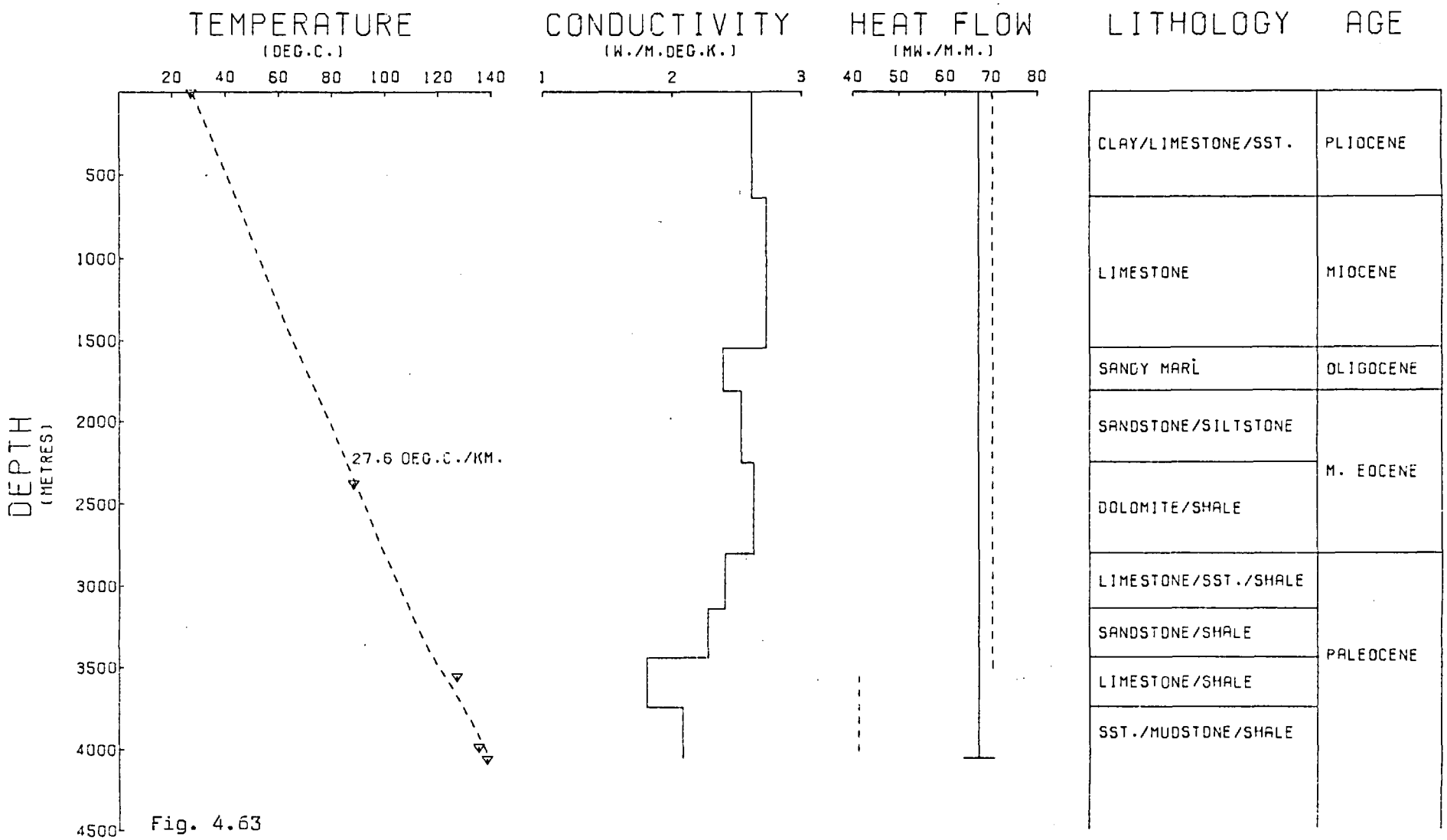


Fig. 4.63

4.15 The Mandera-Lugh Basin Region Heat Flow

The Mandera-Lugh Basin is the only true intracratonic basin examined in this study of Eastern Africa. It is bounded to the south by the Bur Acaba Massif and Bur Ambar Ridge, to the east by the Oddur Arch and to the west and north it terminates against the Precambrian basement of Kenya and Ethiopia.

Beltrandi and Pyre (1973) have proposed that the Mandera-Lugh Basin is part of a large fossil graben or rift of Pre-Jurassic age which extended from coastal Tanzania to the Afar. The basement rocks were dissected into a series of horsts and grabens. Uplift of the basin and the adjacent Bur Acaba Massif together with the regression of the Jurassic sea in the early Cretaceous effectively ended the basin's development. During this final phase of tectonism the basin's internal structure of several parallel anticlines evolved (Fig. 4.3).

The sedimentary sequence consists largely of lower Mesozoic limestones, claystones and shales with minor evaporites and sands, (Tenneco, pers. comm., 1974, Burmah Oil, pers. comm., 1974). Extensive Eocene-Oligocene volcanism, contemporaneous with that in the Eastern Ogaden, has been reported by Beltrandi and Pyre (1973).

Four heat flow values with a mean of 62 $\pm$ 15 $mW \cdot m^{-2}$ were obtained, Figs. 4.64 - 4.67. BHT data was poor to good; conductivity samples were available for El Kuran-1 only. A lithologic summary was used to estimate conductivities for Hol-1. Das Uen-1 and Gherferson-1 were, in fact, drilled on the Bur Ambar Ridge which is covered with a comparitively thin layer of Mesozoic limestones.

The heat flow value at El Kuran-1 is, at 41 $mW \cdot m^{-2}$, considerably less than that at the nearest well, Hol-1, 68 $mW \cdot m^{-2}$. The El Kuran-1 value is more typical of the Eastern Ogaden heat flow (section 4.13). The Hol-1 value is thought to represent a lower limit as the higher than predicted temperatures at total depth, Fig. 4.65, may well be correct. A heat flow of

80 $mW \cdot m^{-2}$ could, conceivably be a more appropriate value. The heat flow at Das Uen-1, 73 $mW \cdot m^{-2}$, and Gheferson-1, 67 $mW \cdot m^{-2}$, while consistent with the nearby Lach Dera-1 and Lach Bissigh-1 results (section 4.16), are considered highly suspect. The data are shown on Fig. 4.73.

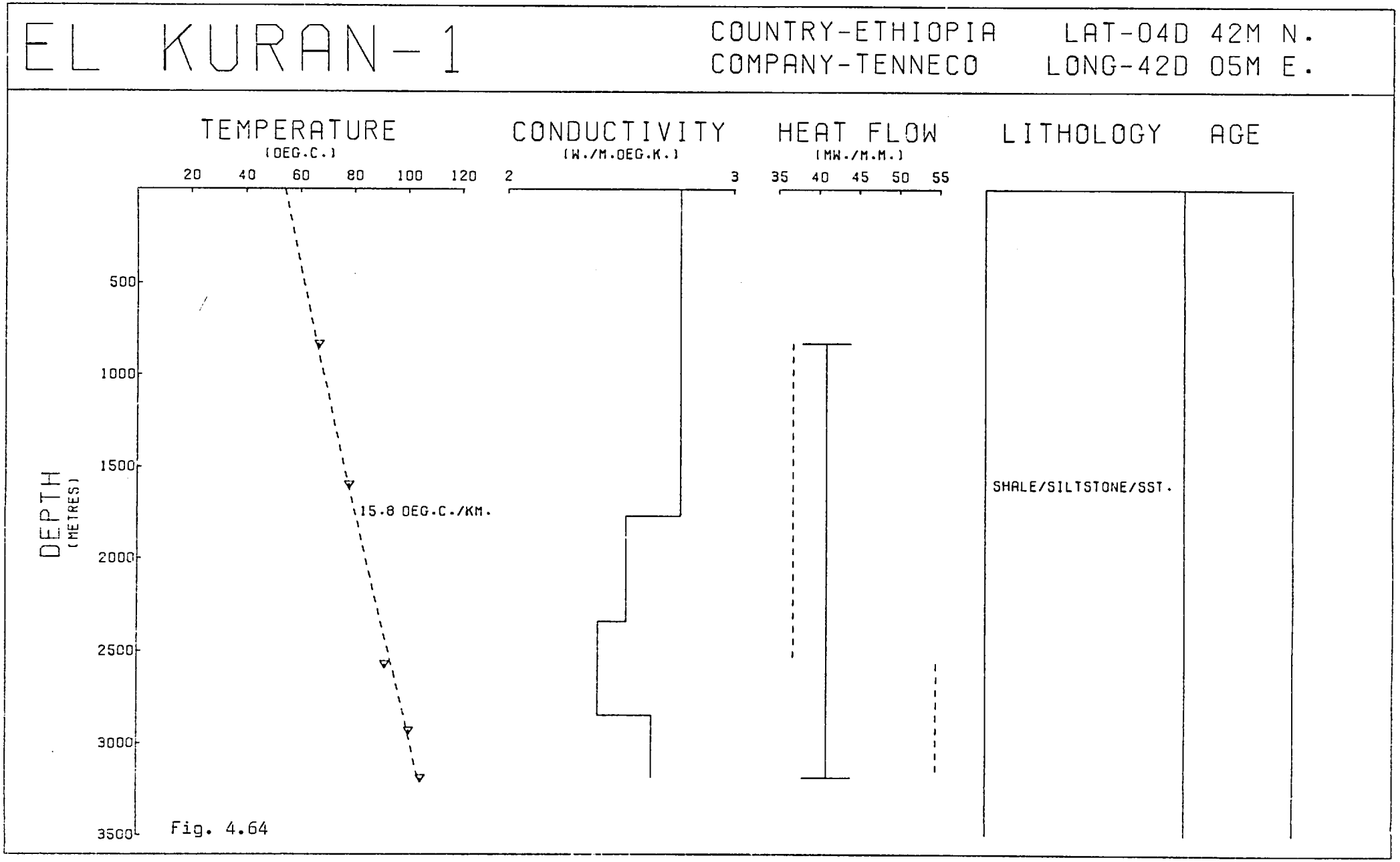

EL KURAN-1
COUNTRY-ETHIOPIA
COMPANY-TENNECO
LAT-04D 42M N.
LONG-42D 05M E.
TEMPERATURE
(DEG.C.)
20 40 60 80 100 120
CONDUCTIVITY
(W./M.DEG.K.)
2 3
HEAT FLOW
(MW./M.M.)
35 40 45 50 55
LITHOLOGY
AGE
DEPTH
(METRES)
500
1000
1500
2000
2500
3000
3500
15.8 DEG.C./KM.
SHALE/SILTSTONE/SST.

Fig. 4.64

HOL-1

COUNTRY-SOMALIA LAT-03D 28M N.
COMPANY-BURMAH LONG-41D 57M E.

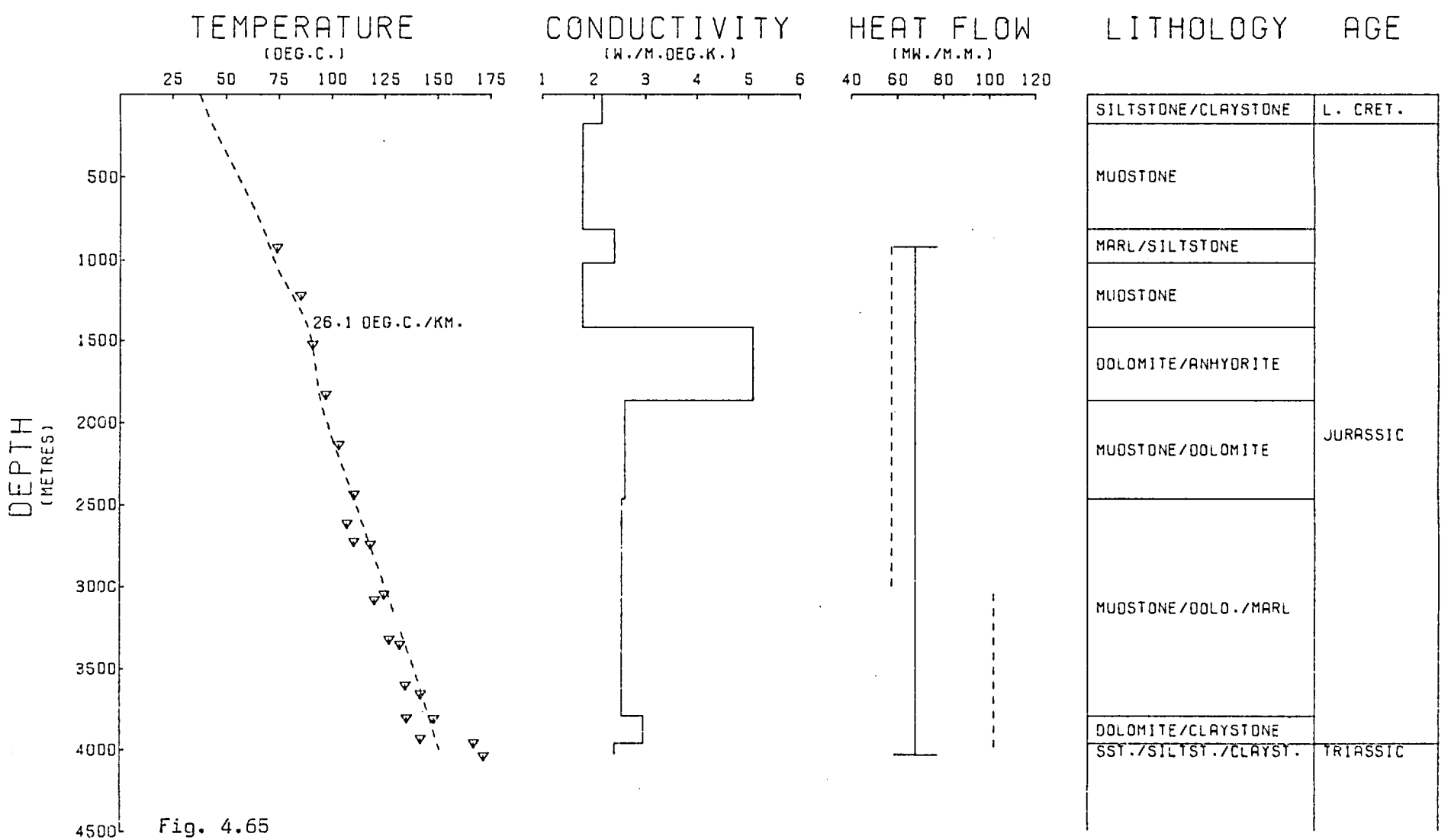


Fig. 4.65

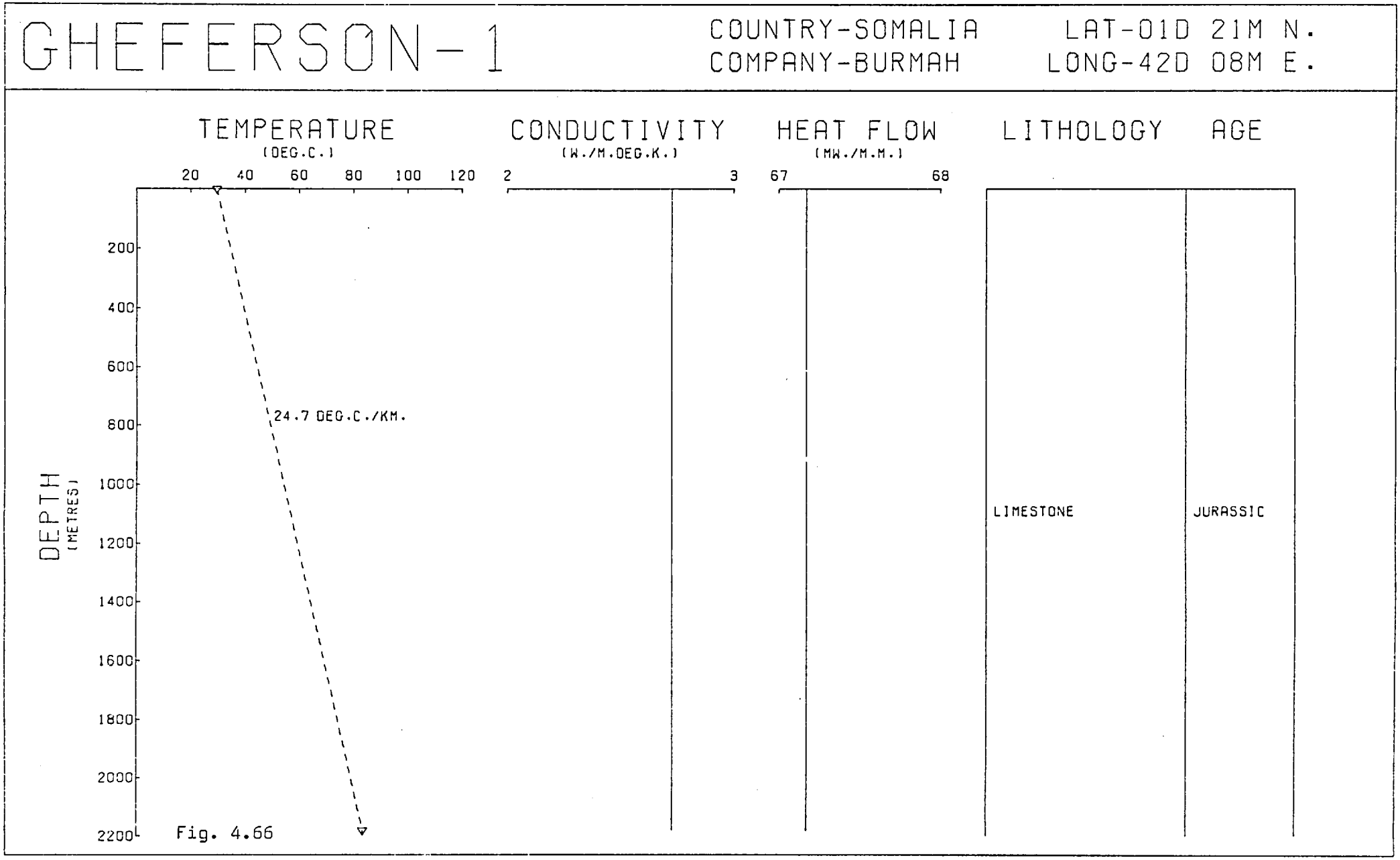

GHEFERSON-1
COUNTRY-SOMALIA
COMPANY-BURMAH
LAT-01D 21M N.
LONG-42D 08M E.
TEMPERATURE
(DEG.C.)
20
40
60
80
100
120
CONDUCTIVITY
(W./M.DEG.K.)
2
3
HEAT FLOW
(MW./M.M.)
67
68
LITHOLOGY
AGE
DEPTH
(METRES)
200
400
600
800
1000
1200
1400
1600
1800
2000
2200
24.7 DEG.C./KM.
LIMESTONE
JURASSIC

Fig. 4.66

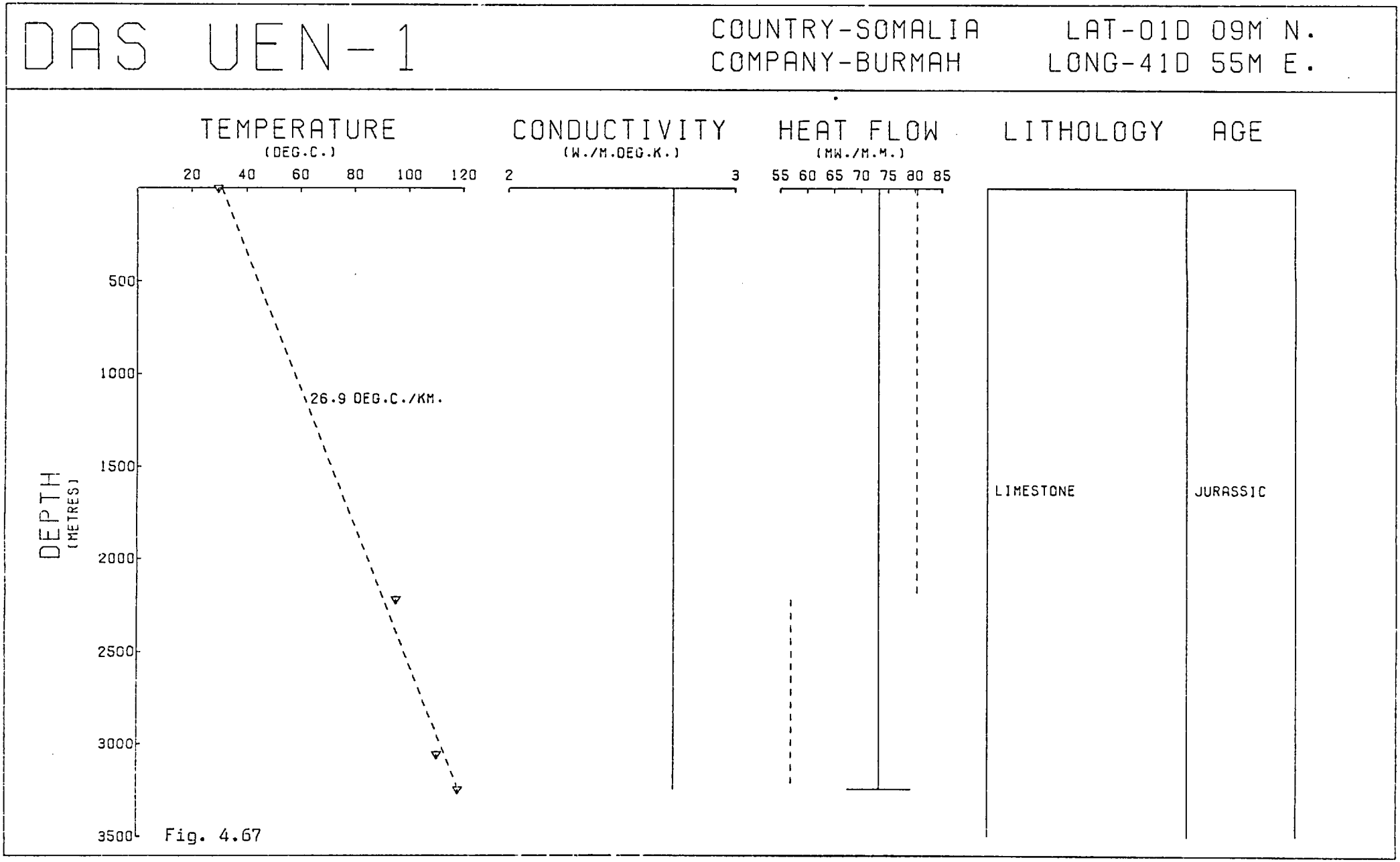

DAS UEN-1
COUNTRY-SOMALIA
COMPANY-BURMAH
LAT-01D 09M N.
LONG-41D 55M E.
TEMPERATURE
(DEG.C.)
20 40 60 80 100 120
CONDUCTIVITY
(W./M.DEG.K.)
2 3
HEAT FLOW
(MW./M.M.)
55 60 65 70 75 80 85
LITHOLOGY
AGE
DEPTH
(METRES)
500
1000
1500
2000
2500
3000
3500
26.9 DEG.C./KM.
LIMESTONE
JURASSIC

Fig. 4.67

4.16 The South-West Somalia Basin Region Heat Flow

The South-West Somalia Basin is located south of the Bur Ambar Ridge, a western subsurface continuation of the Bur Acaba Massif. It is separated from the adjacent Lamu Embayment and Benadir Coast regions by smaller basement anticlines (Fig. 4.3).

A flat plain of Quaternary sediments conceals a thick upper Tertiary carbonate/shale sequence unconformably overlying early Tertiary continental through deltaic sands and Mesozoic shales (Gulf Oil, pers. comm., 1972, Beltrandi and Pyre, 1973).

Five heat flow values were calculated for the area; an average result of 63 ± 8 mW·m^{-2} was obtained (table 4.4). Once again good BHT data was obtained but no conductivity samples. However, detailed lithologic logs were available for all the wells apart from Giamama-1. The heat flow values, Figs. 4.68 - 4.72, particularly that for Oddo Alimo-1, are thought to be as good as can be obtained from oil exploration wells where conductivity data is lacking.

The Brava-1 borehole, located on a basement anticline, is most interesting as it is one of the few wells in Eastern Africa to penetrate a proven upper Paleozoic sequence. The sandstone encountered near total depth was an orthoquartzite (Carboniferous?) which, according to Pettijohn (1957) represents the final products of intense and profound erosion. This is consistent with the widely held opinion that all of Eastern Africa was peneplained during the Karroo (cf. Azzaroli and Fois, 1964).

The higher heat flow at Lach Dera (74 mW·m^{-2}) and Lach Bissigh (69 mW·m^{-2}) is consistent, as we shall see in section 4.17, with values from holes in proximity to the Bur Ambar Ridge.

The South-West Somalia Basin data are shown on Fig. 4.73.

LACH BISSIGH-1

COUNTRY-SOMALIA
COMPANY-GULF

LAT-00D 49M N.
LONG-41D 19M E.

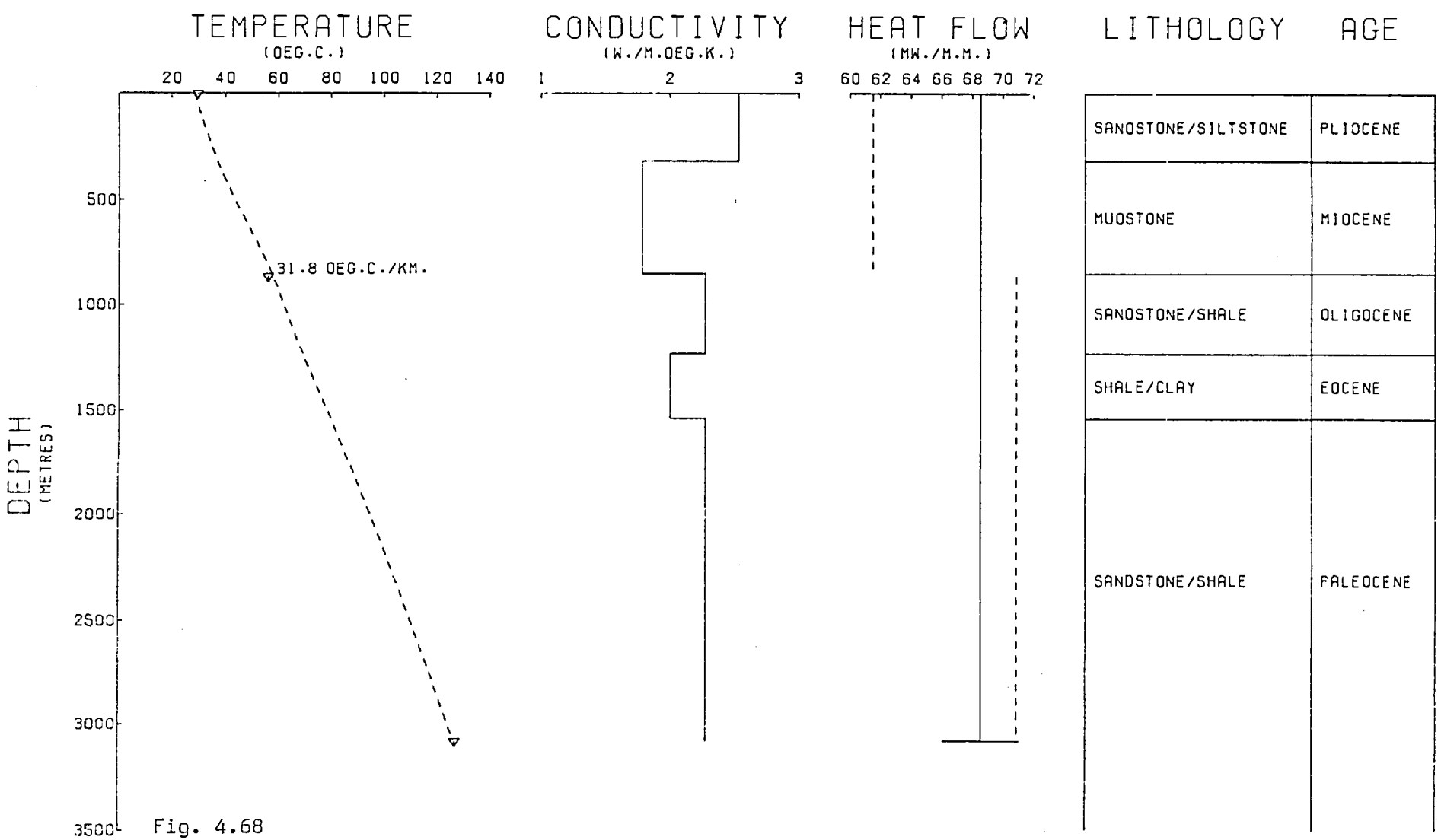


Fig. 4.68

LACH DERA-1

COUNTRY-SOMALIA
COMPANY-GULF

LAT-00D 29M N.
LONG-41D 32M E.

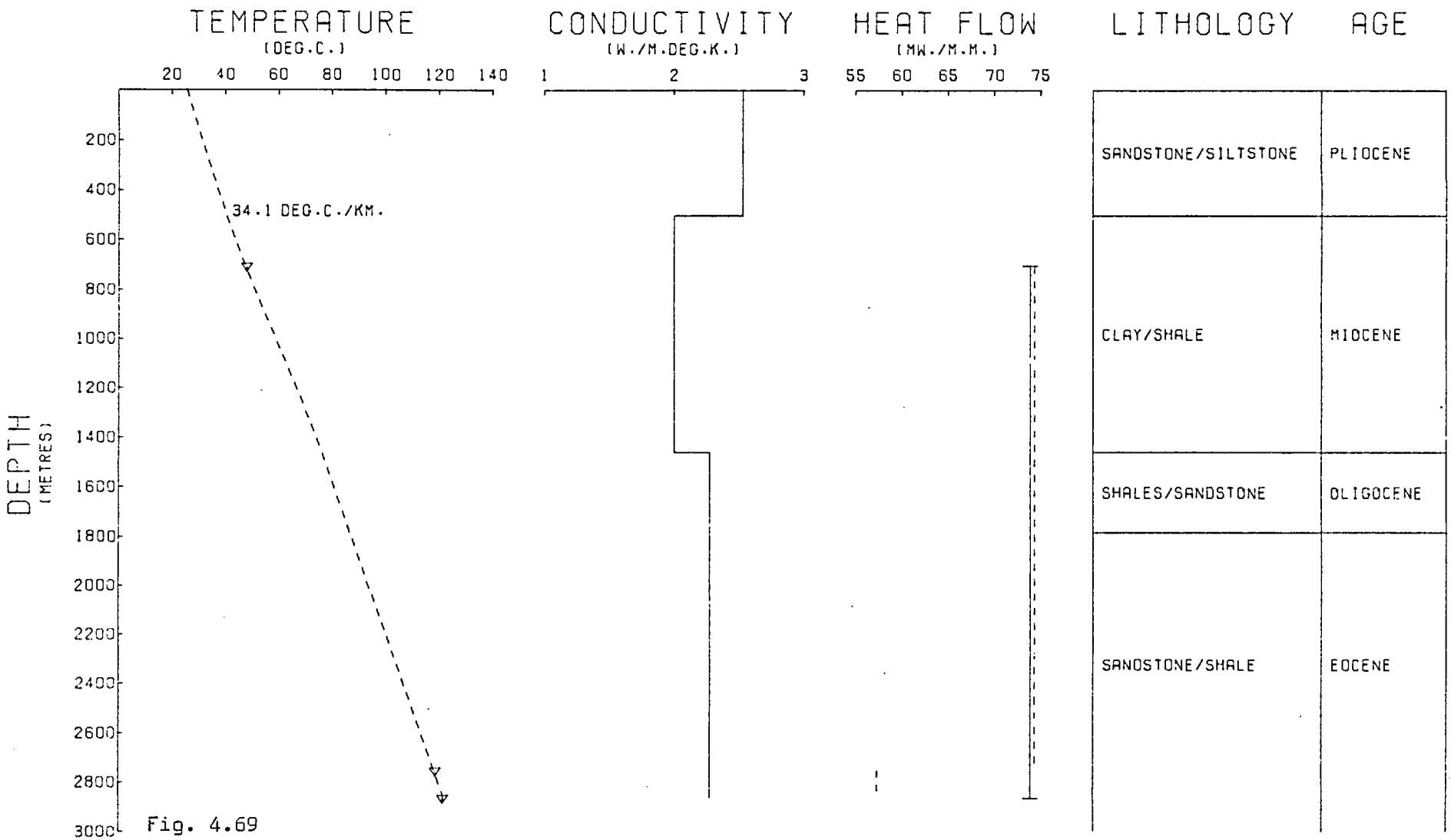


Fig. 4.69

BRAVA-1

COUNTRY-SOMALIA LAT-00D 59M N.
COMPANY-SINCLAIR LONG-43D 43M E.

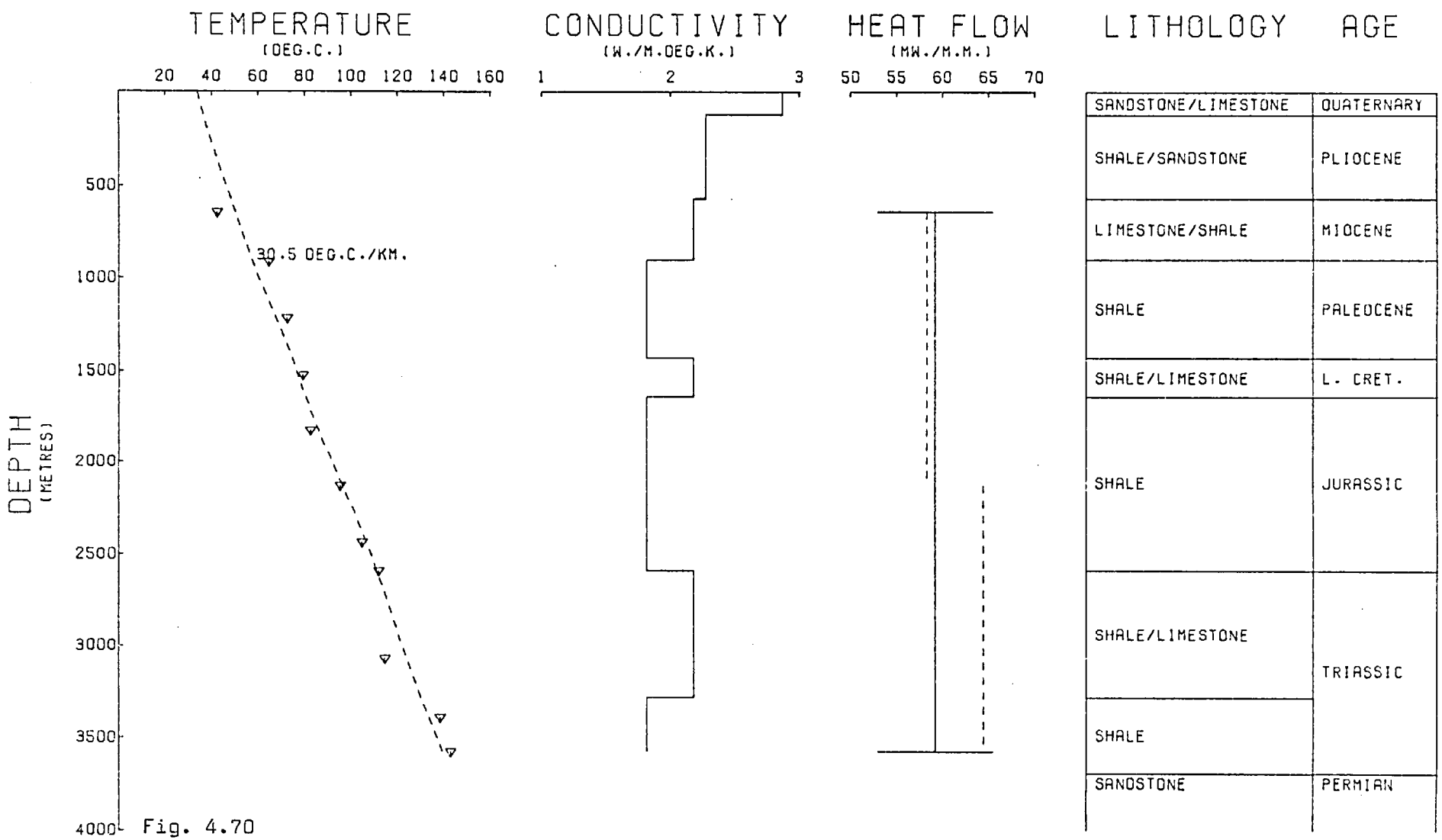


Fig. 4.70

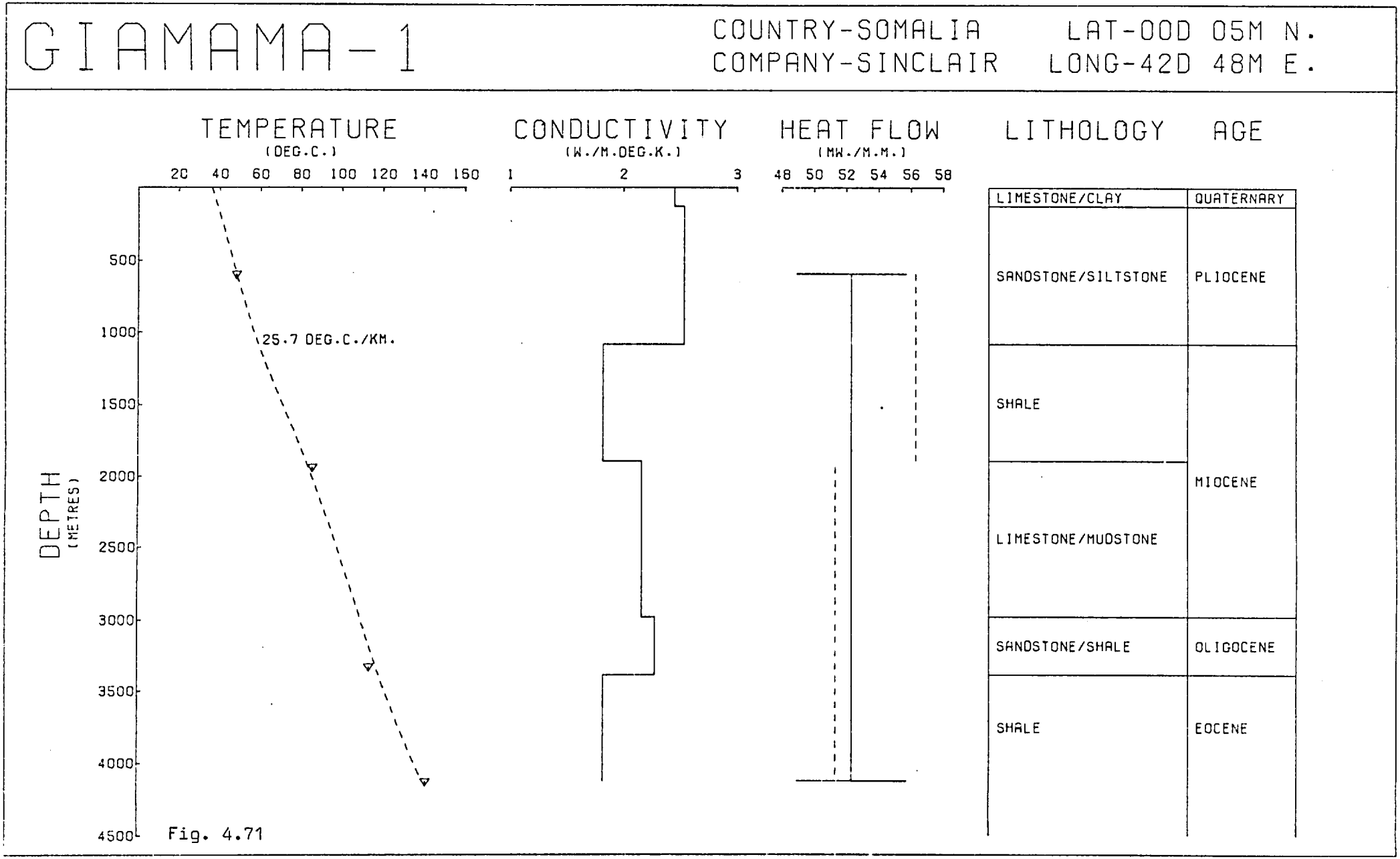

GIAMAMA-1
COUNTRY-SOMALIA
COMPANY-SINCLAIR
LAT-00D 05M N.
LONG-42D 48M E.
TEMPERATURE
(DEG.C.)
20 40 60 80 100 120 140 150
CONDUCTIVITY
(W./M.DEG.K.)
1 2 3
HEAT FLOW
(MW./M.M.)
48 50 52 54 56 58
LITHOLOGY
AGE
DEPTH
(METRES)
500
1000
1500
2000
2500
3000
3500
4000
4500
25.7 DEG.C./KM.
LIMESTONE/CLAY
QUATERNARY
SANDSTONE/SILTSTONE
PLIOCENE
SHALE
LIMESTONE/MUDSTONE
MIOCENE
SANDSTONE/SHALE
OLIGOCENE
SHALE
EOCENE

Fig. 4.71

ODDO ALIMO-1

COUNTRY-SOMALIA LAT-00D 04M N.
COMPANY-SINCLAIR LONG-42D 24M E.

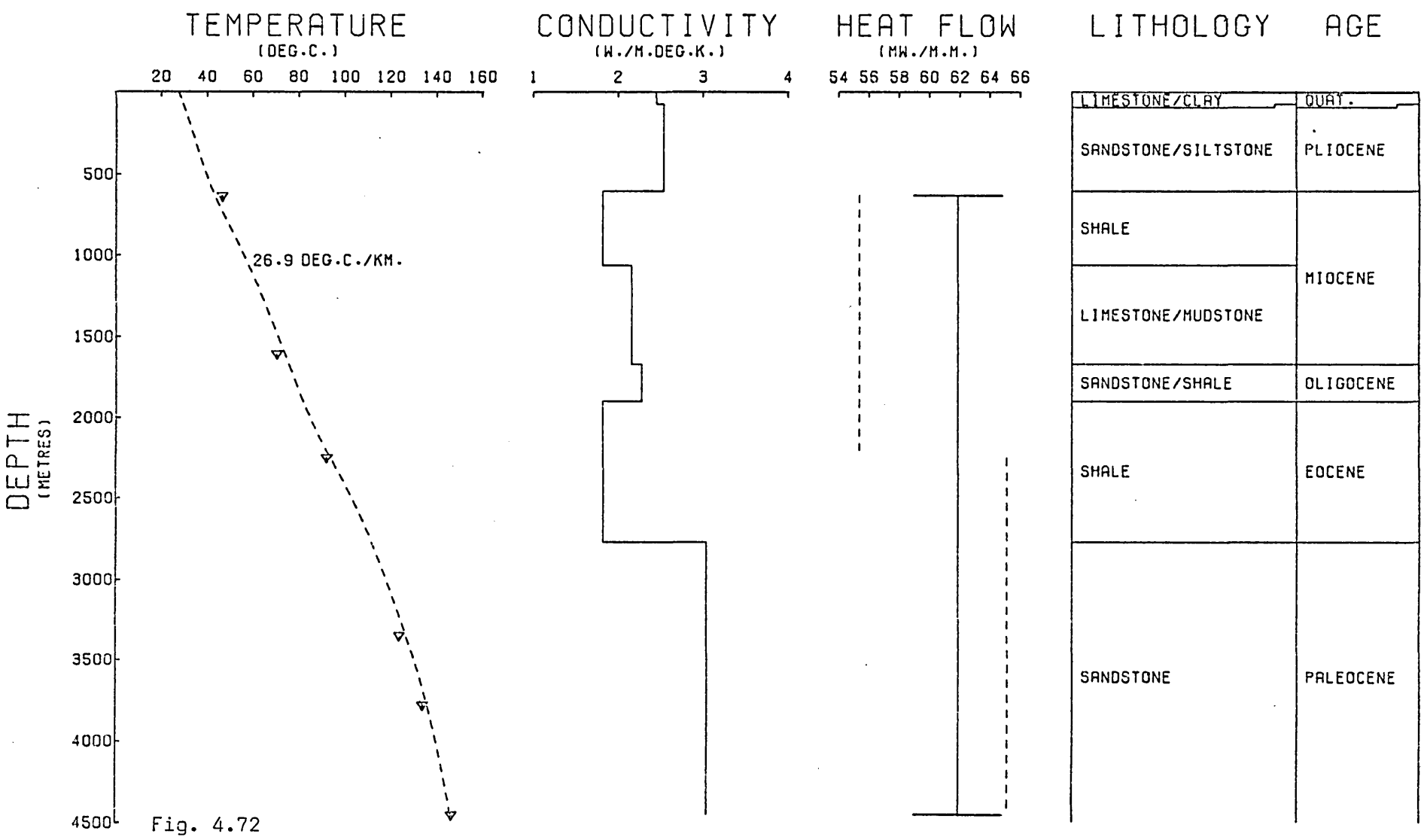


Fig. 4.72

4.17 The Lamu Embayment Region Heat Flow

The Lamu Embayment is a broad north-south elongate basement depression in Eastern Kenya and is filled with Paleozoic through Quaternary sediments (Walters and Linton, 1973). To the west it onlaps Precambrian basement and Tertiary volcanics while in the north it is bounded by the Bur Ambar Ridge (Fig. 4.3). The Lamu Embayment, which cuts across a continental platform and fringes a shield, may be termed an epeirogenic or peri-cratonic basin; it is characterised by gentle warping, normal faulting and the absence of geosynclinal orogenic folding (Harrison and Haw, 1964).

Thick basal Karroo (Carboniferous) clastics were deposited on the Precambrian metamorphic basement within a NNE-SSW trough or graben, roughly coincident with the present continental margin, and predating the formation of the Lamu Embayment. Since the early Jurassic the Lamu Embayment region, and indeed virtually all of coastal Eastern Africa, has been slowly subsiding (Kent, 1972). Mesozoic sedimentation was largely clastic with Jurassic shales passing upwards into Cretaceous and Lower Tertiary deltaics; deeper water conditions prevailed during the Eocene when clays and mudstones were deposited. By the Neogene the west and possibly north basin margins were acting as hinge lines, with monoclinal flexure and further downwarp. A widespread Miocene carbonate sequence was followed by a Pliocene regressive facies, uplift, and emergence, beginning in the northwest and progressing south. The entire basin has subsequently been blanketed with Plio-Pleistocene fluvial sands (Walters and Linton, 1973).

Extensive seismic, gravity and aeromagnetic results have been compiled by Harrison and Haw (1964) and the British Petroleum Co. (pers. comm., 1974). Seismic reflection and refraction results indicate in excess of twelve kilometres of sediments along the present day coast; several important basement highs or ridges have also been defined (gravity highs). The aeromagnetic data indicate shallow volcanic plugs along the supposed

northern hinge line of the basin. Francis et al. (1966) found four to five kilometres of sediments and a crustal thickness of nineteen kilometres at two seismic refraction stations forty kilometres from the North Kenya coast. The gravity maps and profiles of Admirality (1963), Harrison and Haw (1964) and Slettene et al. (1973) all indicate a rapid coastward and offshore increase in the Bouguer anomaly consistent with sediment and/or crustal thinning (Flavelle and Yoshimura, 1974). The gross basin structure, largely defined by British Petroleum's geophysical surveys, is incorporated into Fig. 4.3.

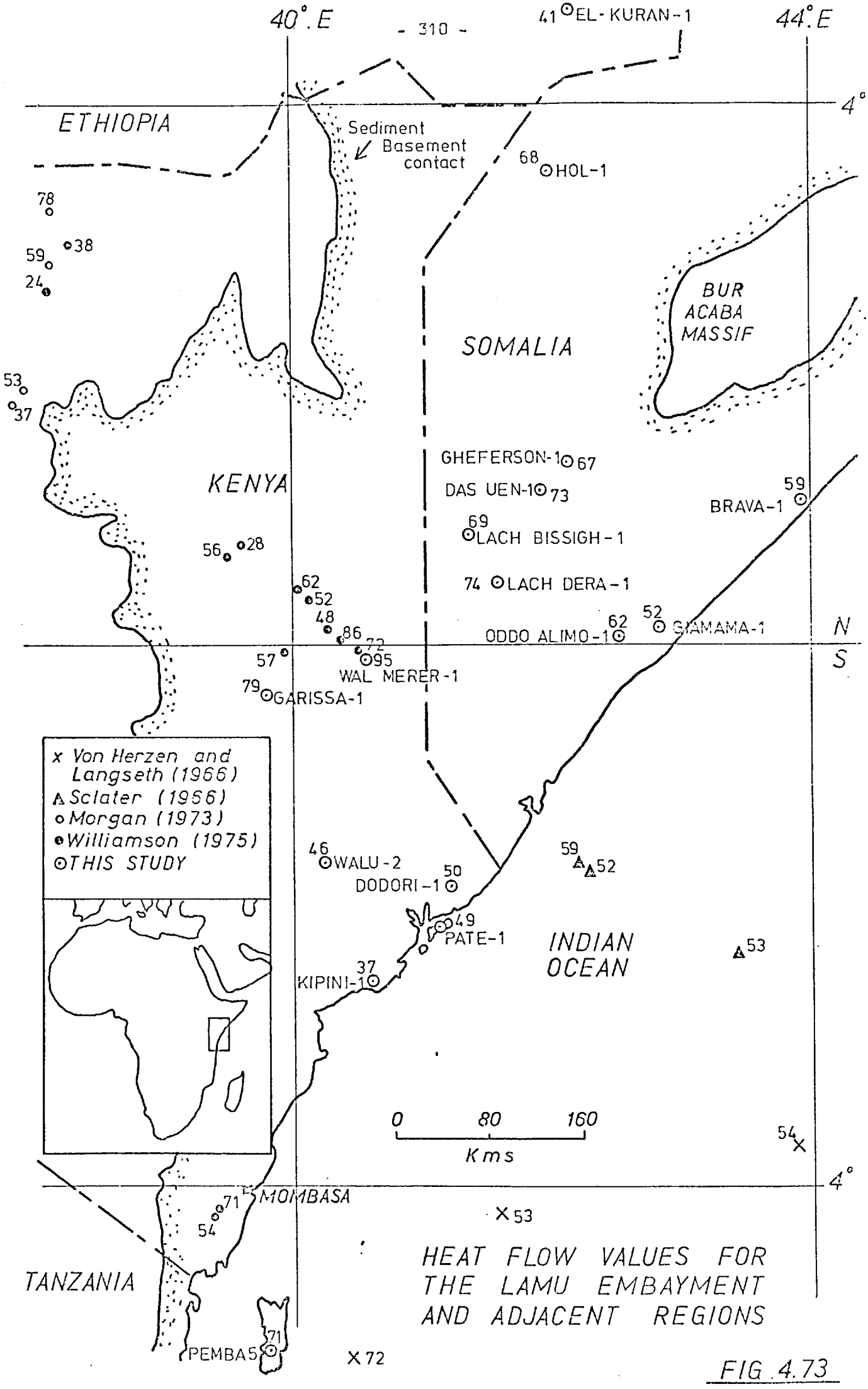
Six heat flow values, with a mean of 59 $\pm$ 22 $mW \cdot m^{-2}$, were computed for this basin. Data quality was good with five of the six results graded A, ie. estimated error less than 15 percent. Four of the results, Walu-2, Dodori-1, Pate-1, and Kipini-1 (composite plots Figs. 4.76 - 4.79, inclusive) were obtained from the southern coastal region of the embayment. Small Bullard residuals indicate a high internal consistency for these results. In particular one should note the result for Pate-1 (Fig. 4.78) where the gradient doubled over the lower pair of three BHTs but the measured conductivity (on 50 samples) compensated for most of this increase. The four coastal values are in close agreement, with a range of 37 - 50 $mW \cdot m^{-2}$, and are comparable to the results reported by Sclater (1966) of 52 - 59 $mW \cdot m^{-2}$ obtained some 100 kilometres off the coast on the continental rise (Fig. 4.73).

In the northern or Garissa region of the embayment the two results, Wal Merer-1 and Garissa-1 (Figs. 4.74 and 4.75) are, at 95 and 79 $mW \cdot m^{-2}$ respectively, significantly higher than the coastal values. Williamson (1975) has measured eight shallow boreholes by conventional heat flow techniques in the Garissa region. His results, incorporated into Fig. 4.73, together with the previously discussed values at Gheferson-1, Das Uen-1, Lach Bissigh-1 and Lach Dera-1 (sections 4.15 and 4.16) indicate that the Bur Ambar Ridge region (Fig. 4.3) is an area of above normal heat flow (70 - 90 $mW \cdot m^{-2}$). Williamson's (1975) data together with that of Morgan (1973) also indicate that this region of high heat flow is most likely of limited areal extent,

both authors having found low to normal heat flow in the Northern Frontier District of Kenya, on the eastern rift flank, and along the western margin of the Lamu Embayment.

A geomagnetic depth sounding survey of Banks and Ottey (1974) has suggested that a region of high electrical conductivity may underlie the Garissa region. The inferred conductivity, of .05 $ohm^{-1} \cdot m^{-1}$ at a depth of 50 kilometres, would, for an olivine, imply a temperature of the order of 1100-1300^{o}C (cf. Duba and Lilley, 1972). Blackwell (1971) has demonstrated that such a range of temperature would be consistent, in the case of the Basin and Range Province of the Western United States, with a surface heat flow of 80 $mW \cdot m^{-2}$ and various, equally plausible, thermal conductivity and heat production models. Gough (1974) shows that an electric conductivity structure such as that of Banks and Ottey (1974), would, if due to temperature, indicate a zone of partial melt between 50-100 kilometres. However, none of the seismic refraction or wave dispersion studies (see section 4.3) with the possible exception of that of Long et al. (1972) have indicated a shallow low velocity zone east of the Kenya rift.

We will return to the Lamu Embayment results in connection with steady state crust and mantle temperature profiles (section 4.21) and two dimensional crustal temperature models (section 4.22).



HEAT FLOW VALUES FOR THE LAMU EMBAYMENT AND ADJACENT REGIONS

FIG. 4.73

WAL MERER-1

COUNTRY-KENYA
COMPANY-BP

LAT-00D 07M S.
LONG-40D 35M E.

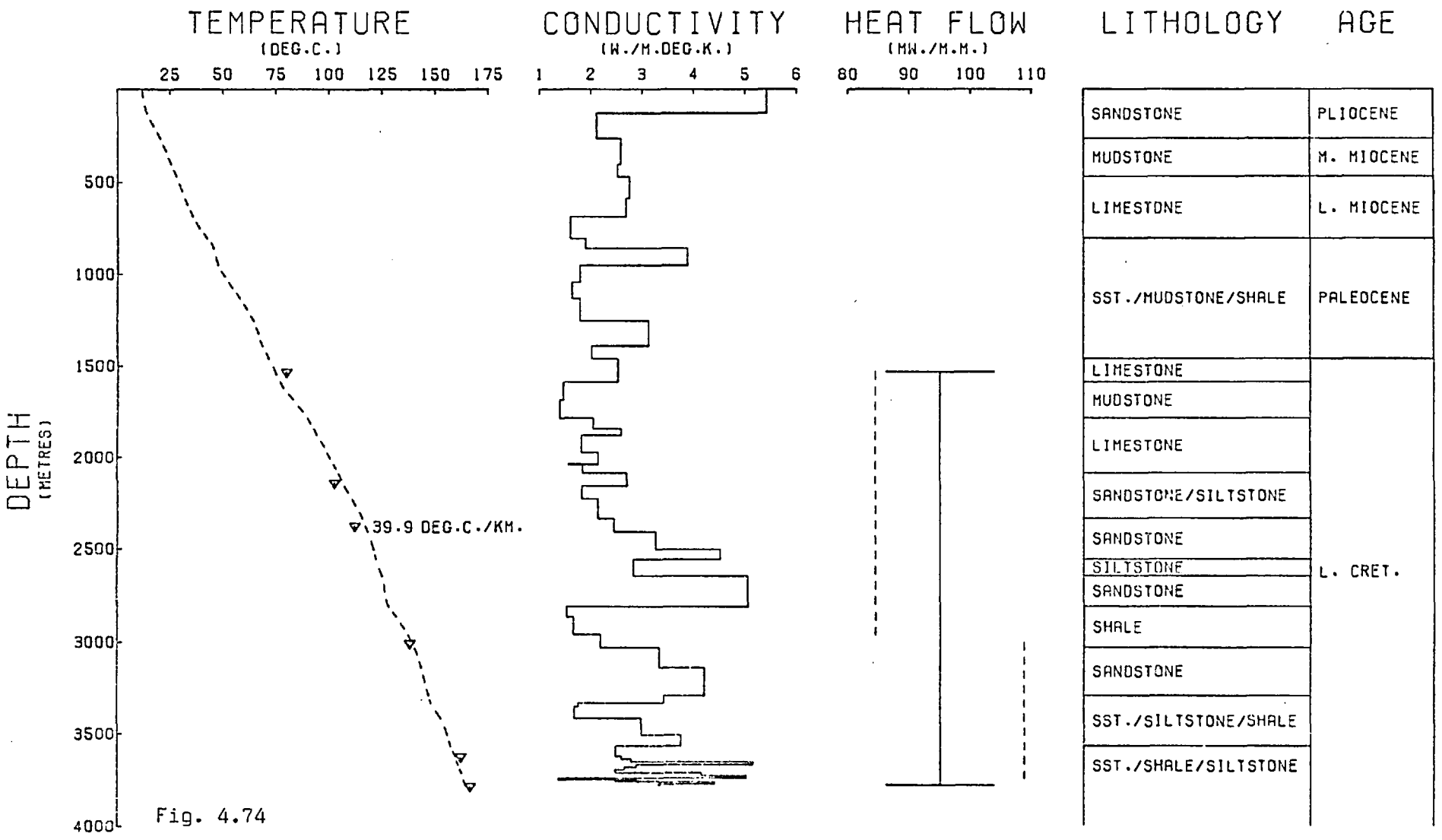


Fig. 4.74

GARISSA-1

COUNTRY-KENYA
COMPANY-BP

LAT-00D 22M S.
LONG-39D 49M E.

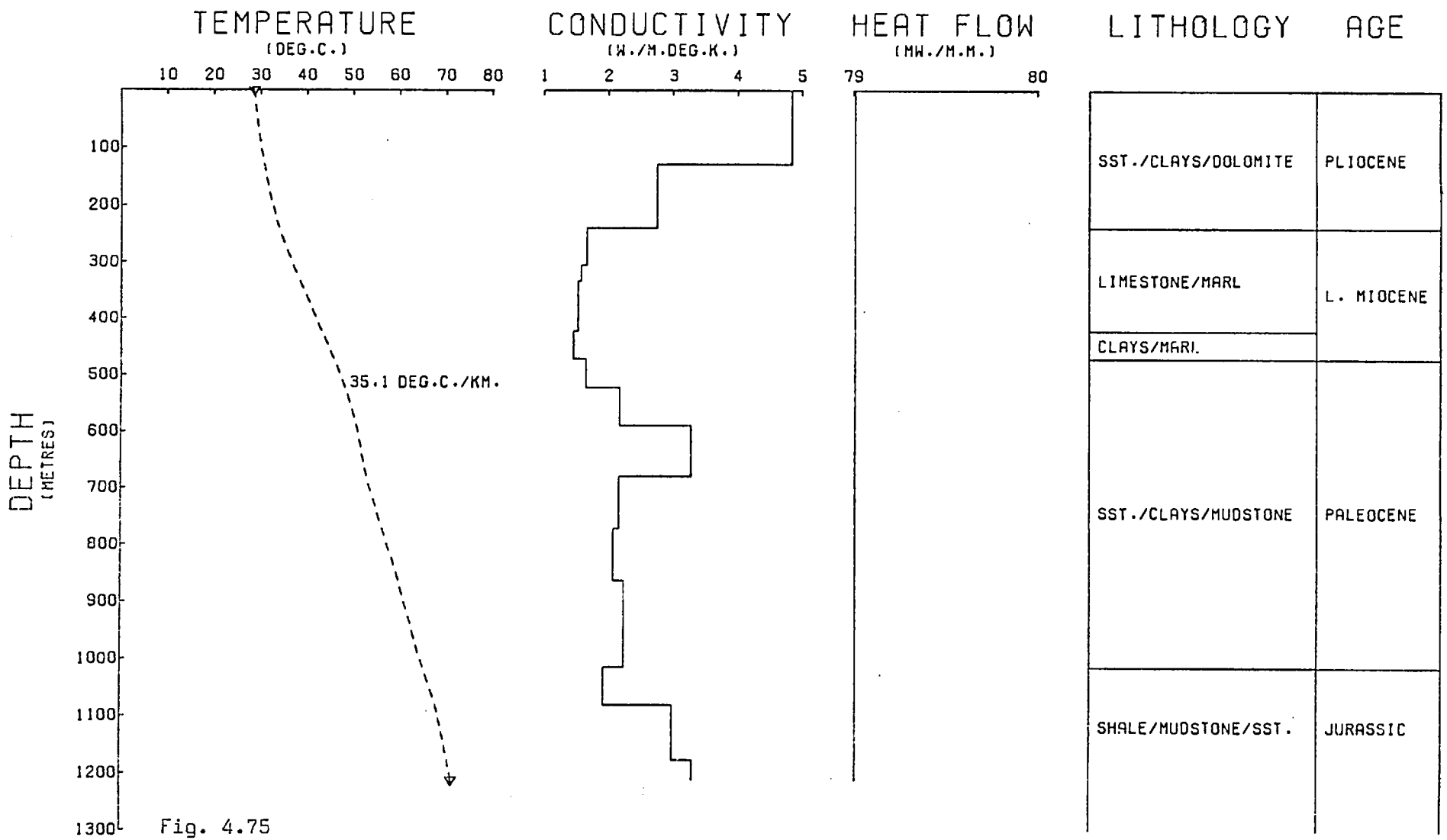


Fig. 4.75

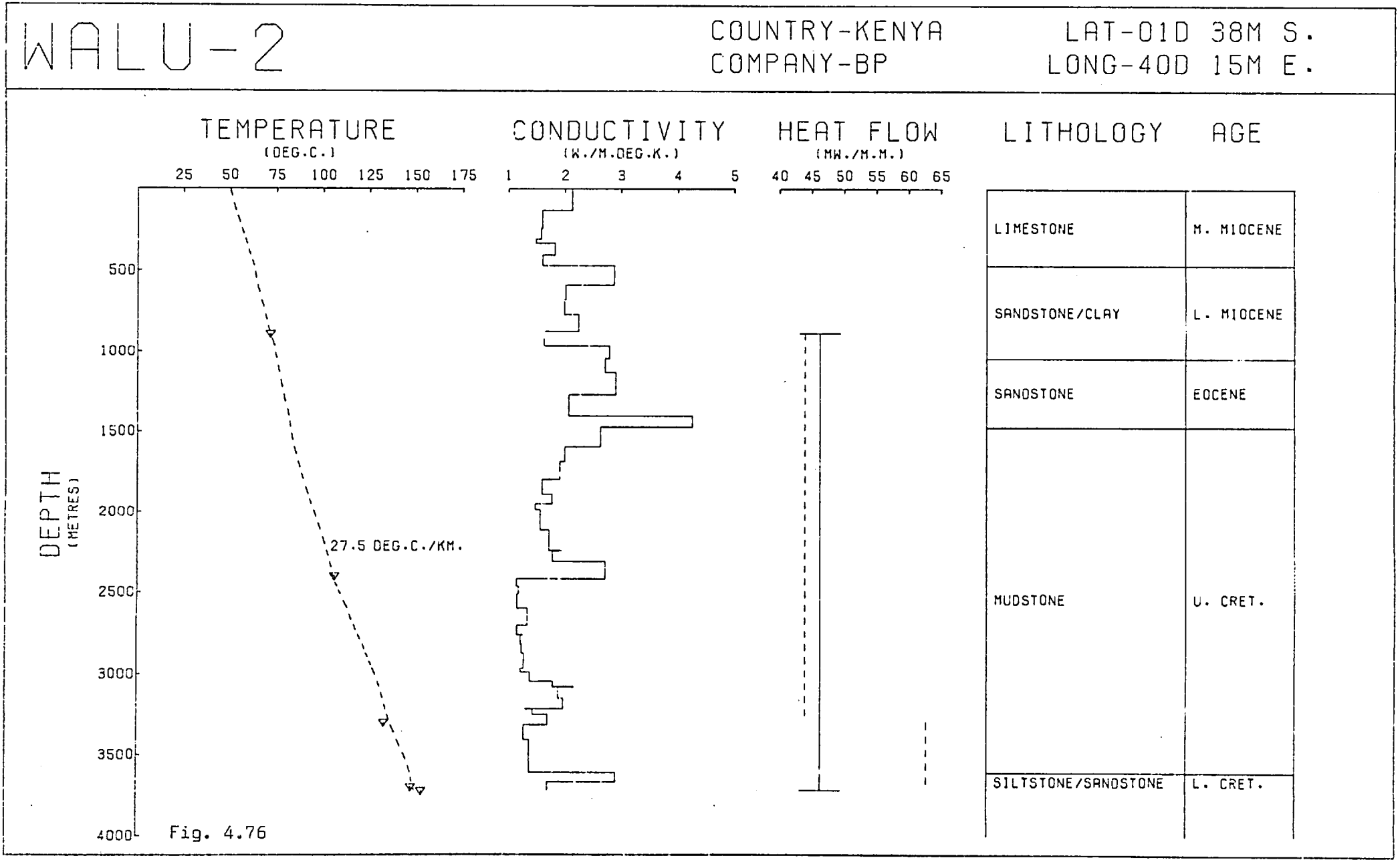

WALU-2
COUNTRY-KENYA
COMPANY-BP
LAT-01D 38M S.
LONG-40D 15M E.
TEMPERATURE
(DEG.C.)
25 50 75 100 125 150 175
CONDUCTIVITY
(W./M.DEG.K.)
1 2 3 4 5
HEAT FLOW
(MW./M.M.)
40 45 50 55 60 65
LITHOLOGY
AGE
DEPTH
(METRES)
500
1000
1500
2000
2500
3000
3500
4000
27.5 DEG.C./KM.
LIMESTONE
M. MIOCENE
SANDSTONE/CLAY
L. MIOCENE
SANDSTONE
EOCENE
MUDSTONE
U. CRET.
SILTSTONE/SANDSTONE
L. CRET.

Fig. 4.76

DODORI-1

COUNTRY-KENYA
COMPANY-BP

LAT-01D 49M S.
LONG-41D 11M E.

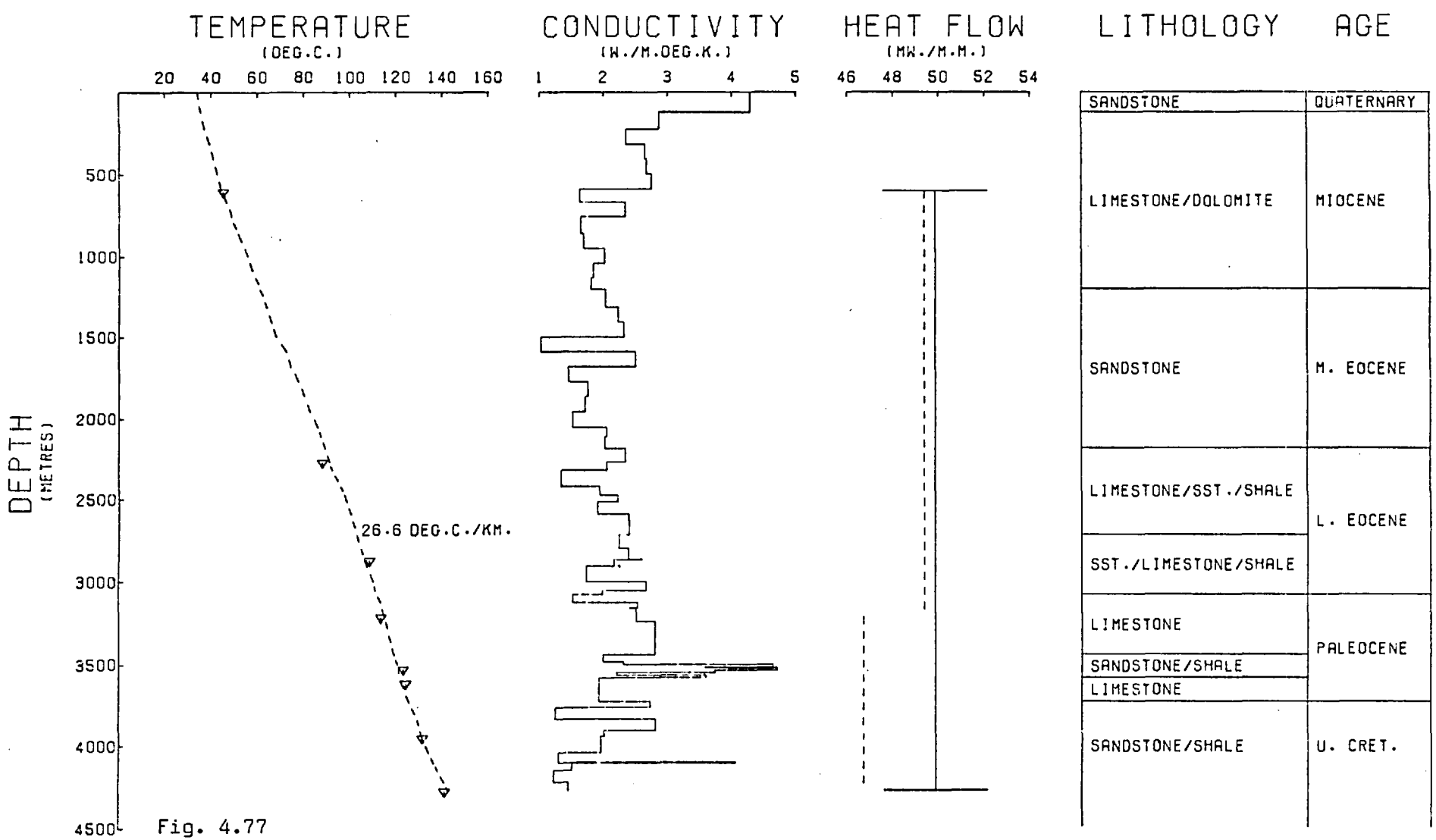


Fig. 4.77

PATE-1

COUNTRY-KENYA
COMPANY-BP

LAT-02D 04M S.
LONG-41D 05M E.

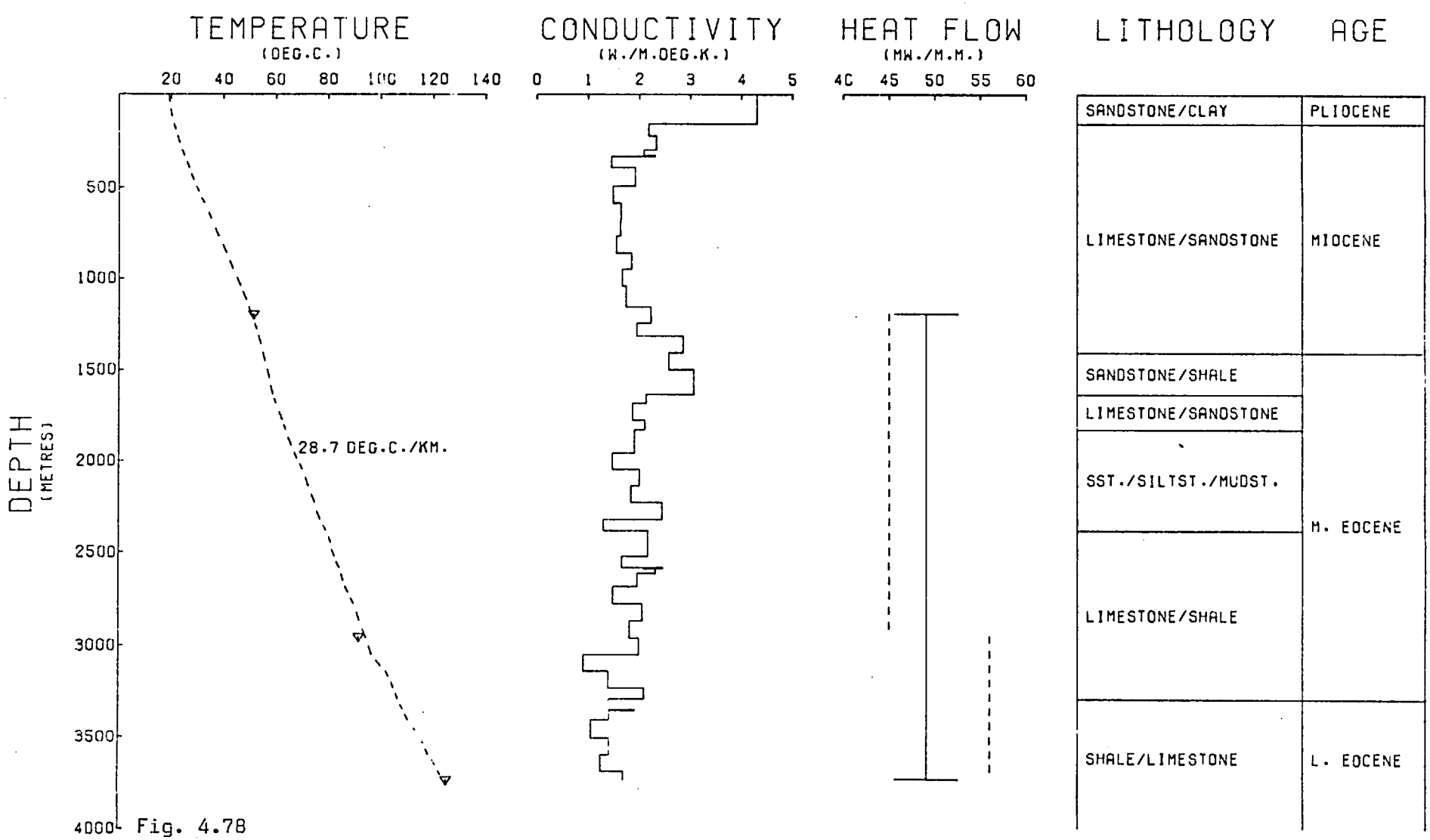


Fig. 4.78

KIPINI-1

COUNTRY-KENYA
COMPANY-BP

LAT-02D 24M S.
LONG-40D 36M E.

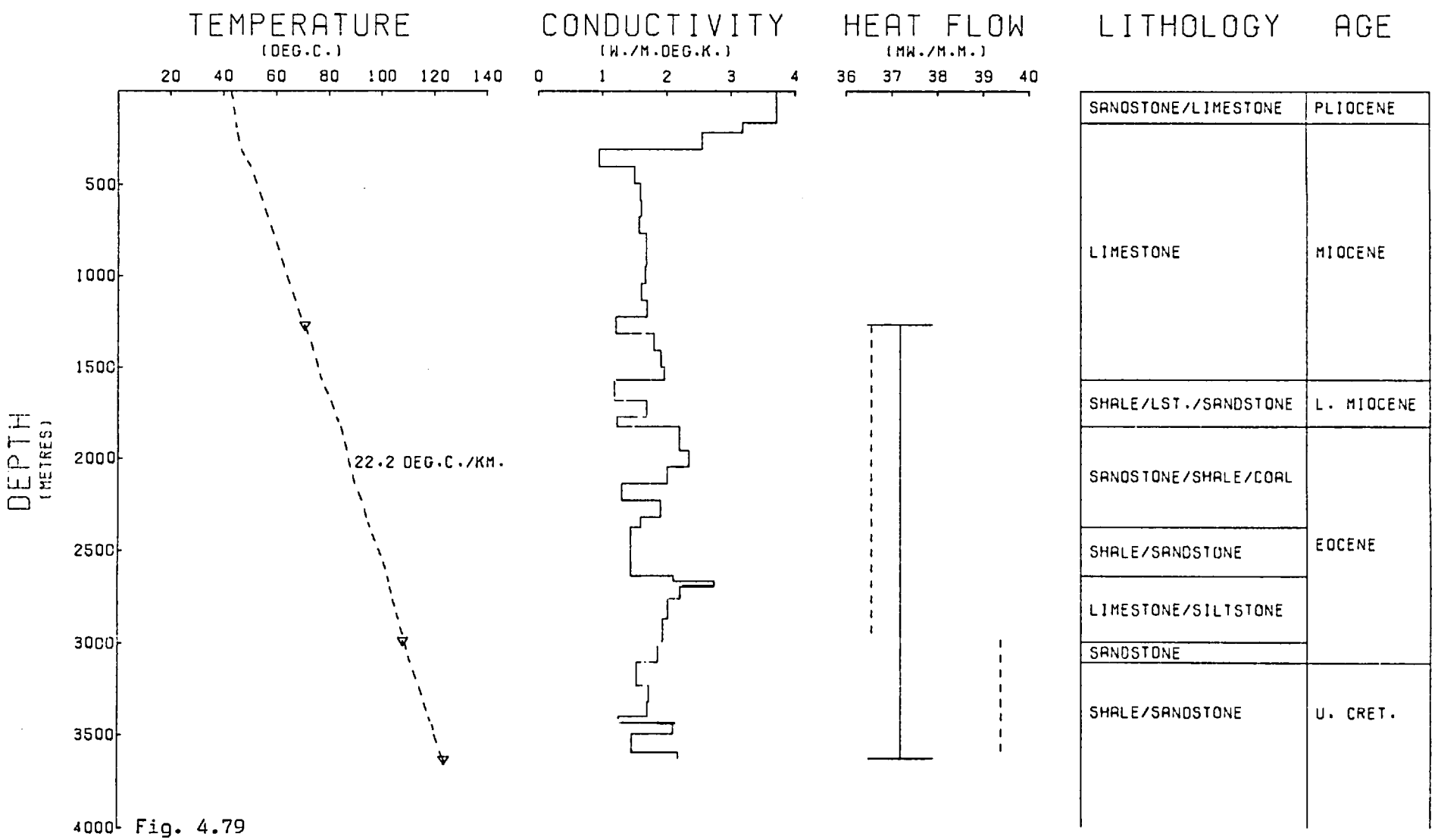


Fig. 4.79

4.18 The Coastal Tanzania Region Heat Flow

The coastal sedimentary basin of Tanzania is composed of a twenty to one hundred kilometre wide strip of Upper Paleozoic through recent sediments. The basin, which extends the length of the Tanzanian coast, is fault bounded to the east against the Mozambique belt (Figs. 4.2 and 4.3).

The basin, like the Lamu Embayment, originated in the Karroo as a major trough or graben which filled with predominantly clastic sediments (Kent and Perry, 1973). In southern Tanzania a Triassic evaporite sequence in the Mandawa region is described by Kent (1965). The Jurassic marine transgression flooded the Karroo clastic-evaporite basin; sedimentation was largely carbonate. The major fault trends, the Lindi in the south and the Tanga in the north, which were active in the Karroo, ceased to move in the Lower Mesozoic; vertical displacements of several kilometres are known (Kent et al., 1971). A lower Cretaceous regression was followed by a return to deep water conditions in the Upper Cretaceous through Eocene when thick clay and limestone sequences were laid down. The Oligocene is typically thin or absent but a renewed transgression in the Miocene brought extensive shelf carbonate and deltaic sedimentation. The post Miocene deposition has largely been fluviatile.

Kent et al. (1971) estimate the total sedimentary thickness to be in excess of ten kilometres. Kent and Perry (1973) have demonstrated that sedimentation has kept pace with subsidence since at least the Eocene.

Large epeirogenic movements beginning in the Paleogene, have produced the three major islands, Pemba, Zanzibar and Mafia. Structurally each of the islands is a horst as well as a stratigraphic culmination. Pemba and Mafia are separated from the mainland by well defined grabens; Zanzibar is located on a major delta.

Extensive geophysical studies are reported by Kent et al. (1971) and Kent and Perry (1973). Seismic reflection and refraction results sub-

stantiate the horst structure of the three islands. The gravity data show them to be positive features while the aeromagnetic data imply enormous depths to basement. Earthquake compilations (cf. Gorshkov, 1963) and microseismic studies (Porstendorfer and Kuhn, 1965) indicate relatively high activity and an unstable continental margin.

Five heat flow values have been obtained from coastal Tanzania; the mean is 55 ± 22 $mW \cdot m^{-2}$. Data quality was good for four of the five results including one each from the three islands. The data from Kiswere, Fig. 4.84, is in fact, from four separate holes drilled within a few kilometres of each other.

The Pemba-5 (Fig. 4.80) and Mafia-1 (Fig. 4.82) results are, at 71 and 82 $mW \cdot m^{-2}$ respectively, relatively high; however the 35 $mW \cdot m^{-2}$ result at Zanzibar-1 (Fig. 4.81) is puzzlingly low. Williamson (1975) has measured two shallow holes for heat flow in southern-most Kenya while Von Herzen and Langseth (1966) have made a single oceanic determination forty kilometres east of Pemba Island; their results, Fig. 4.73, are in good agreement with the Pemba-5 borehole. A single determination, Mandawa-7, Fig. 4.83, gave a value of 55 $mW \cdot m^{-2}$ for the Triassic evaporite basin of southern Tanzania.

The Mafia-1 borehole penetrated a trachyte of unknown age near total depth; Kent and Perry (1973) remark that this is only the second known occurance of volcanism in coastal Tanzania.

PEMBA-5

COUNTRY-TANZANIA LAT-05D 16M S.
COMPANY-BP LONG-39D 42M E.

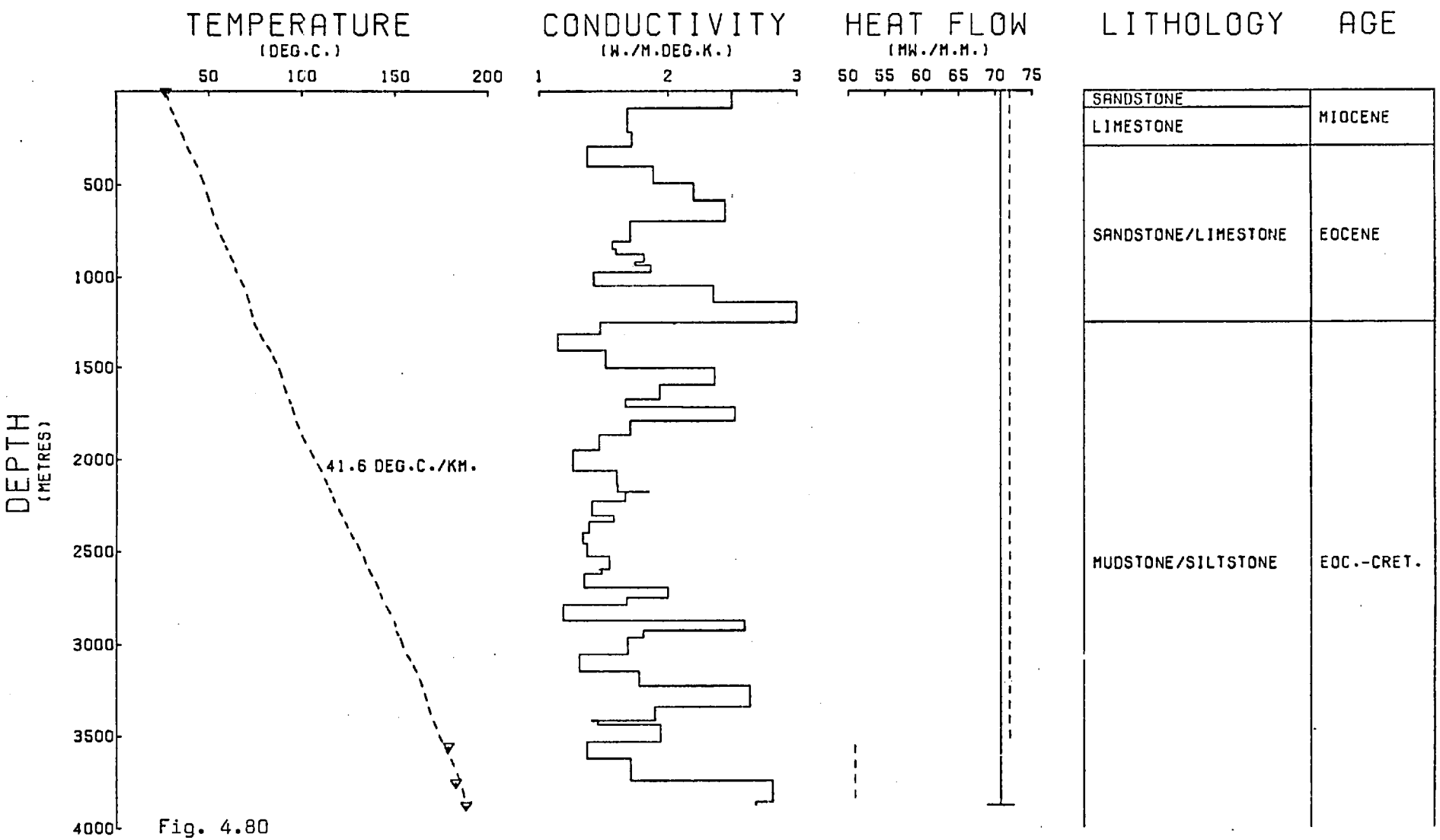


Fig. 4.80

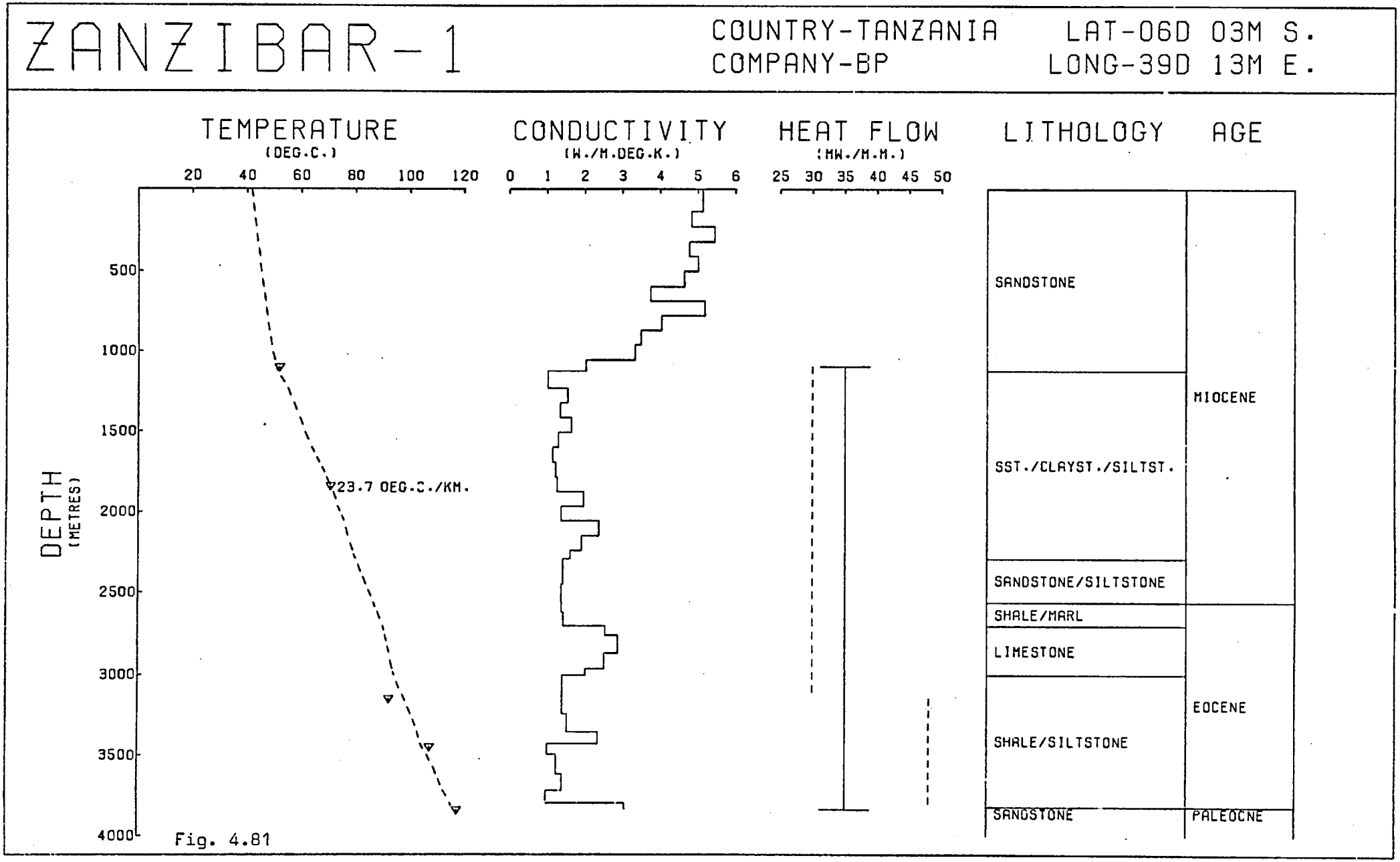

ZANZIBAR-1
COUNTRY-TANZANIA
COMPANY-BP
LAT-06D 03M S.
LONG-39D 13M E.
TEMPERATURE
(DEG.C.)
20 40 60 80 100 120
CONDUCTIVITY
(W./M.DEG.K.)
0 1 2 3 4 5 6
HEAT FLOW
(MW./M.M.)
25 30 35 40 45 50
LITHOLOGY
AGE
DEPTH
(METRES)
500
1000
1500
2000
2500
3000
3500
4000
23.7 DEG.C./KM.
SANDSTONE
SST./CLAYST./SILTST.
SANDSTONE/SILTSTONE
SHALE/MARL
LIMESTONE
SHALE/SILTSTONE
SANDSTONE
MIOCENE
EOCENE
PALEOCNE

Fig. 4.81

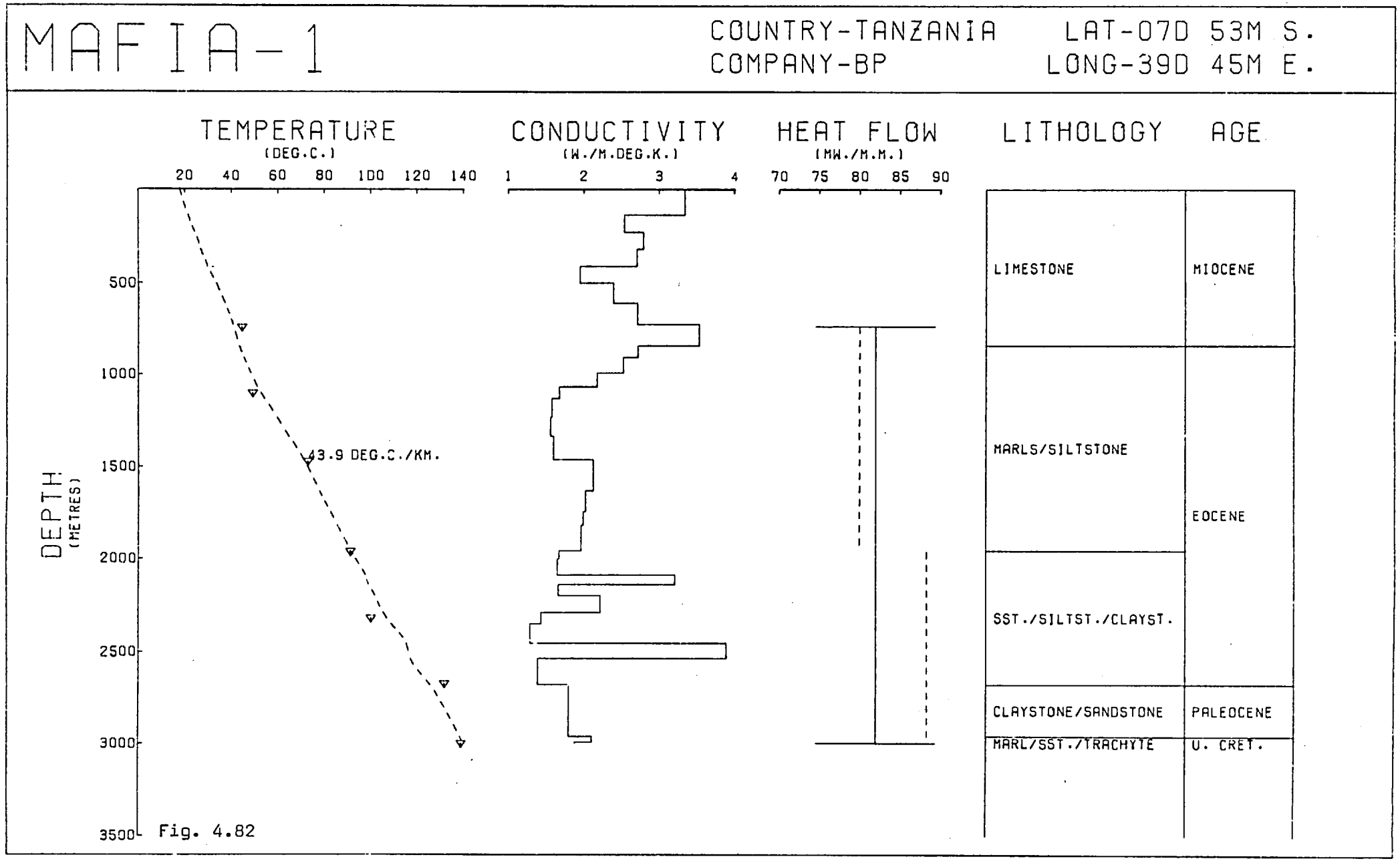

MAFIA-1
COUNTRY-TANZANIA
COMPANY-BP
LAT-07D 53M S.
LONG-39D 45M E.
TEMPERATURE
(DEG.C.)
20 40 60 80 100 120 140
CONDUCTIVITY
(W./M.DEG.K.)
1 2 3 4
HEAT FLOW
(MW./M.M.)
70 75 80 85 90
LITHOLOGY
AGE
DEPTH
(METRES)
500
1000
1500
2000
2500
3000
3500
43.9 DEG.C./KM.
LIMESTONE
MIOCENE
MARLS/SILTSTONE
EOCENE
SST./SILTST./CLAYST.
CLAYSTONE/SANDSTONE
PALEOCENE
MARL/SST./TRACHYTE
U. CRET.

Fig. 4.82

MANDAWA-7

COUNTRY-TANZANIA LAT-09D 25M S.
COMPANY-BP LONG-39D 25M E.

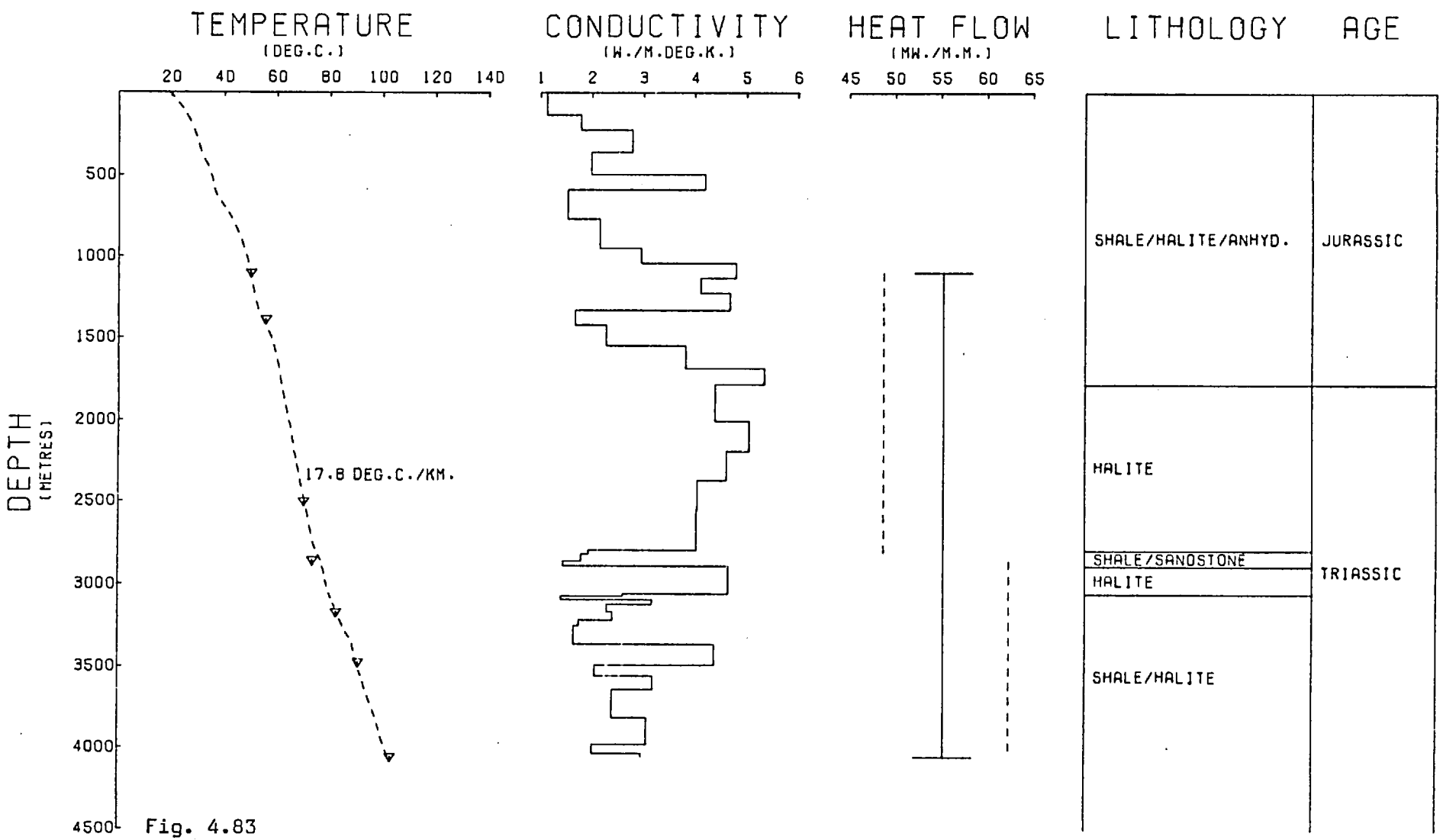


Fig. 4.83

KISWERE

COUNTRY-TANZANIA LAT-09D 27M S.
COMPANY-BP LONG-39D 31M E.

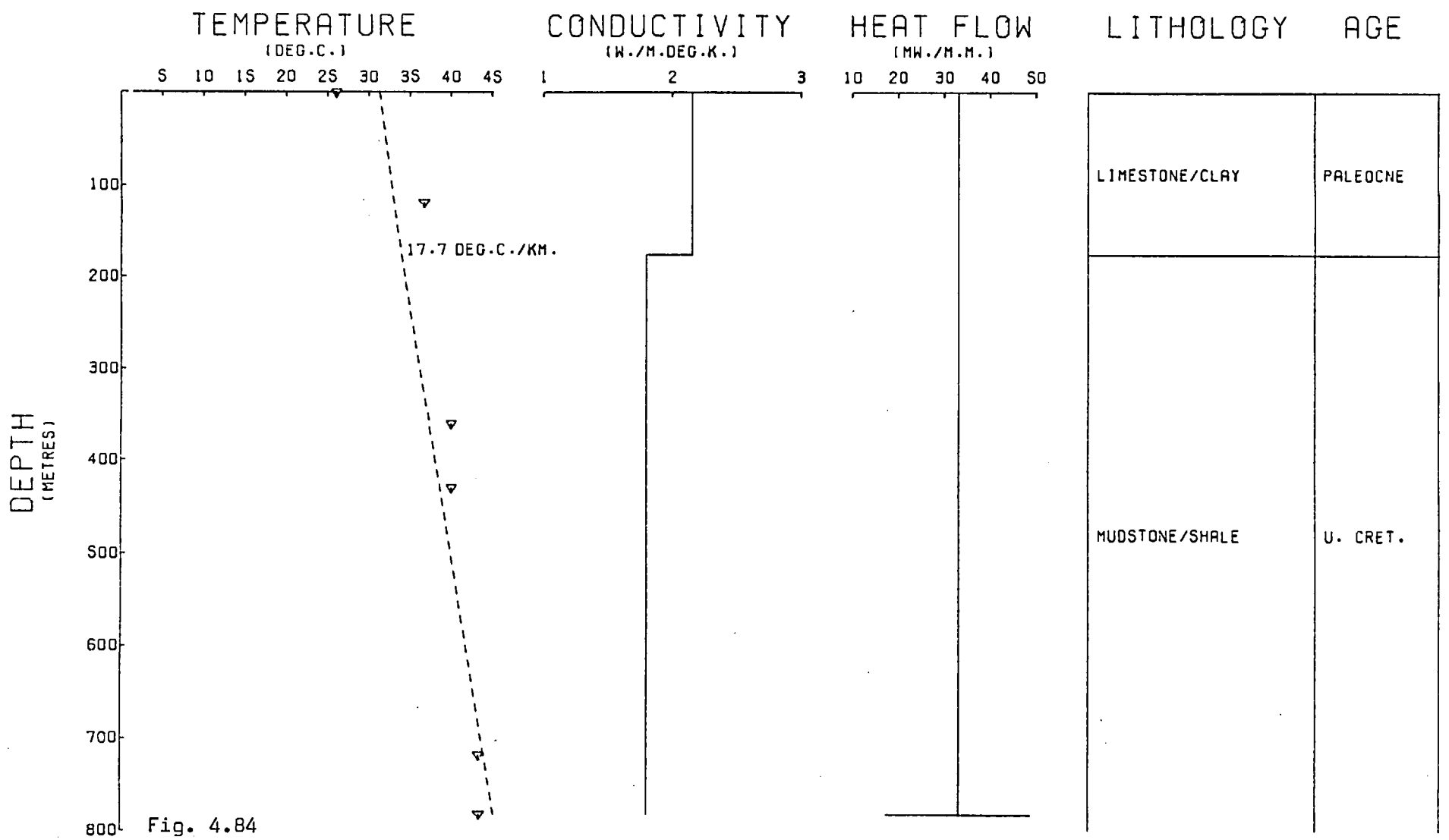


Fig. 4.84

4.19 Trend Surface Analysis of Heat Flow Data between 10°S, 15°N, and 35°E, 70°E

Having computed and reviewed the heat flow of Eastern Africa, it would be useful to obtain some quantitative representation of its spatial variation. Such a result, ideally in some form of a contour map with isolines of heat flow, may then be readily compared with other regional geological or geophysical maps.

The preparation of such a map may follow several procedures; contouring by 'eye' (Cermak, 1975), spherical harmonic analysis (Lee and Uyeda, 1965) or trend surface analysis (Haenel, 1971 and 1973). The third mentioned procedure, trend surface analysis, was followed here as it will yield a relatively unbiased representation of irregularly spaced data. As the region of interest is bisected by, and extends only a limited distance beyond, the equator, the representation of the data on an orthogonal grid is justified.

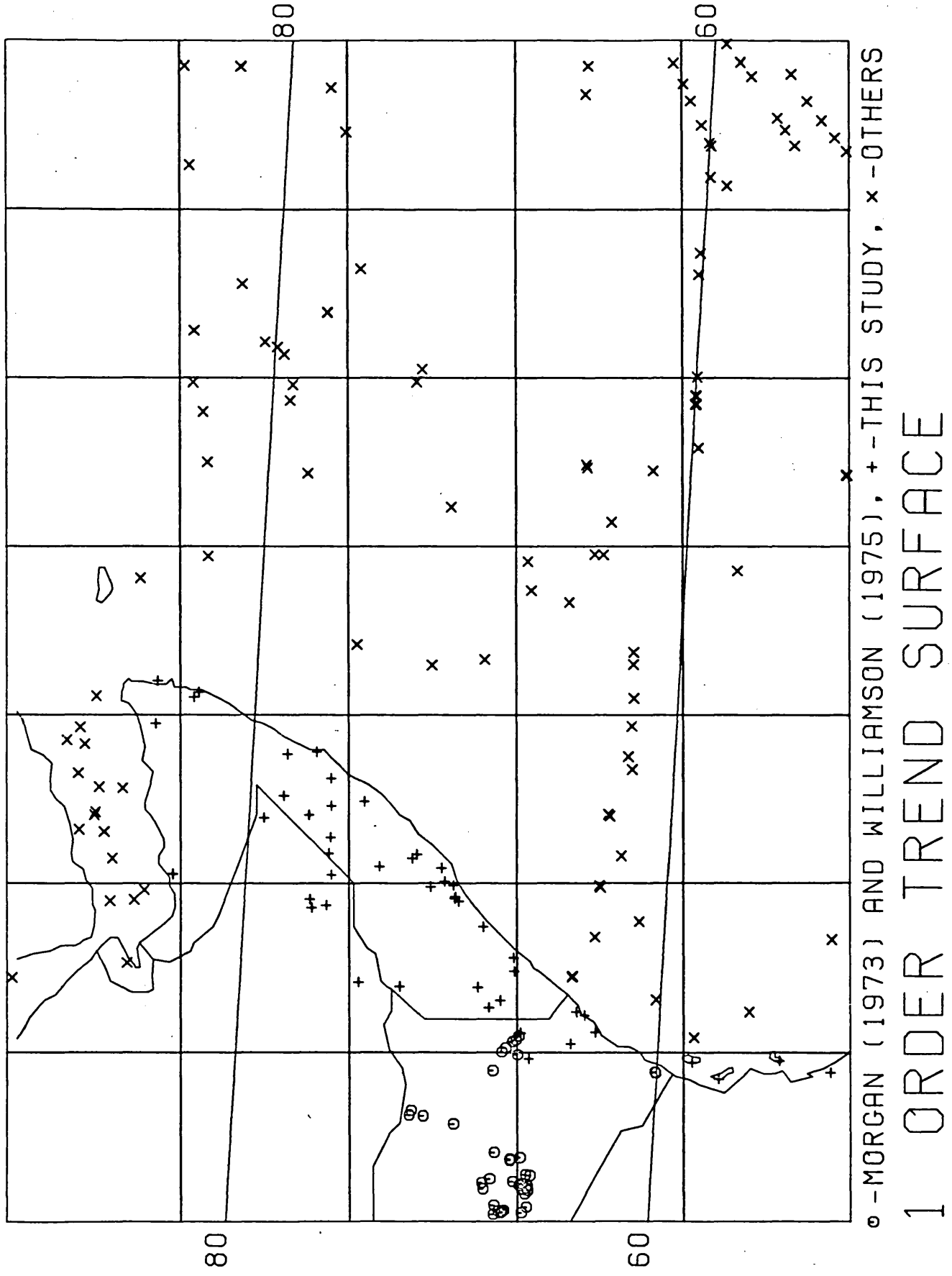
There exists a vast collection of literature on the meaning, computation technique and interpretation of trend surface maps; the reader is referred to Merriam and Cocke (1967) and Watson (1971). For the purposes of this study it suffices to say that the trend surface is that two dimensional polynomial of specified order which best 'fits' a given set of data; the criterion of fit being minimum variance. The computation was performed with a slightly modified version of the published program TREND of Davis (1973). The objective, and hence subject of interpretation, of such a mapping exercise is to identify anomalies of both regional (the trend) and local (the residuals) extent.

The one hundred and ninety-three heat flow values used to calculate the five degree square means (sections 4.7, Fig. 4.10) formed the basis of the trend analysis. Surfaces of up to sixth order were computed. Results, both for the surface and the residuals were machine plotted and contoured on a base

map similar to that shown in Fig. 4.10. Contouring of the residuals, of course, necessitated a regridding of the results.

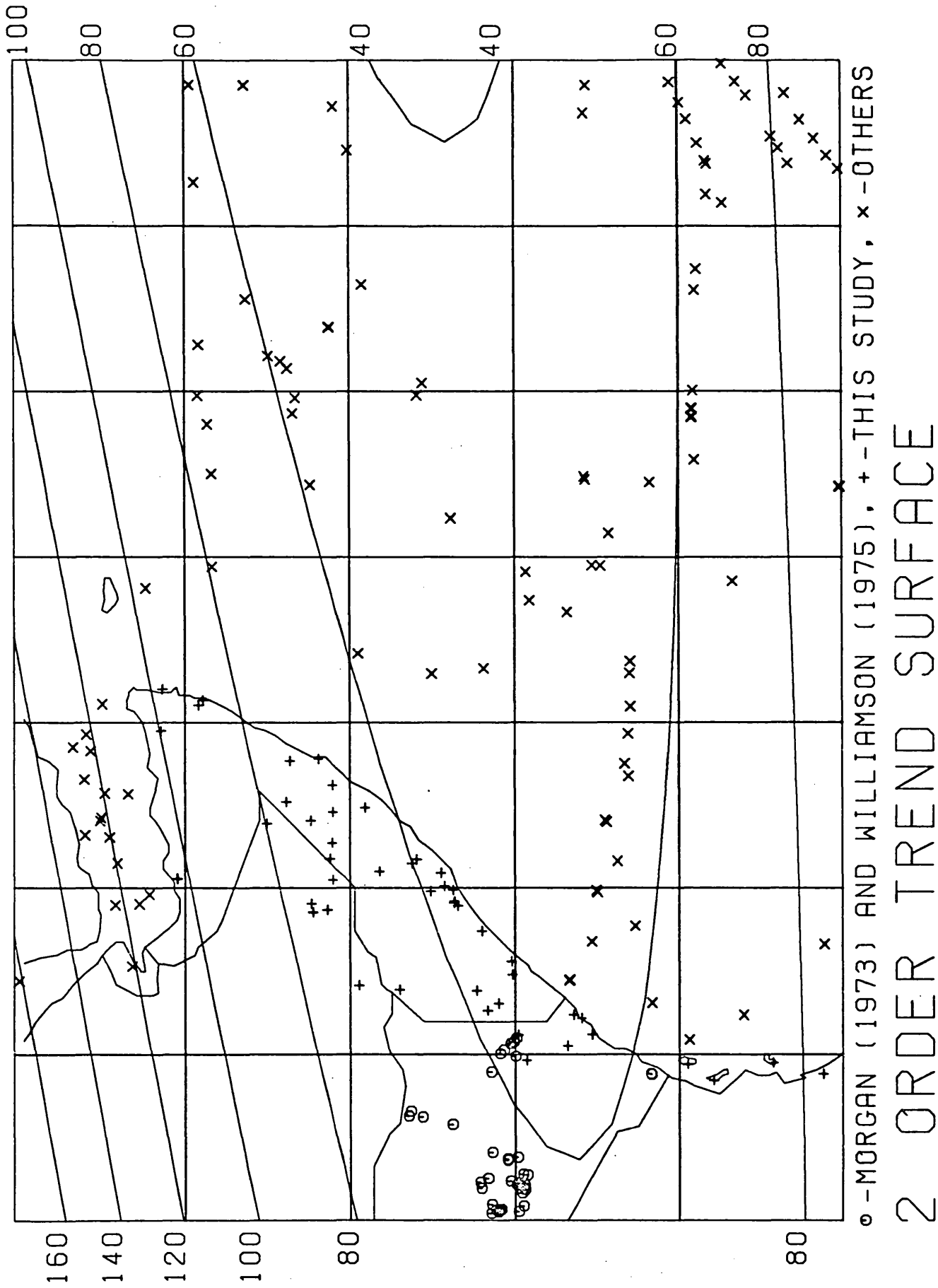
Table 4.6 lists the statistical results for the trend analysis. The multiple correlation coefficient (cf. Davis, 1973) indicates that the first order surface was not significant; this was confirmed by an analysis of variance, or F test, indicating no significant regression at the one per-cent level. Surface order two is clearly quite significant as are orders three and four; order five shows virtually no improvement in fit despite the addition of six coefficients; trend order six would be regarded as conforming closely to the original data. A detailed discussion of the statistical methods used to arrive at the above conclusions may be found in Chayes (1970).

Trend order one, Fig. 4.85, shows a modest northward increase in heat flow with contours of heat flow running almost due east-west. The second order surface indicates an elongate low with an equatorial axis, Fig. 4.86; the high heat flow to the north-east is largely an 'edge effect' - the surface being almost unconstrained along boundaries with little or no data (Davis, 1973). The third order surface, Fig. 4.87, is again dominated by an east-west grain. The north and north-east boundaries are, as in order two, unrealistic due to extrapolation of the surface in data poor regions. Trend surface order four, Fig. 4.88, breaks the east-west anomaly trend; three highs, the north, south-west and south boundaries are separated by a continuous low with a major saddle. The fifth order plot showed only minor changes and is omitted. The sixth order map (Fig. 4.89) is dominated by the high located over southern Arabia and the Gulf of Aden. The very high values of 200-280 $mW \cdot m^{-2}$ are 'edge effects' as are the large blank areas (suppressed negative contours) in the north-east and north-west. Note the highs also located over the Carlsberg Ridge, the Mascarene Plateau, Central Kenya - S.W. Somalia, and coastal Tanzania; the first two anomalies have been recognised by other researchers (see section 4.6), the last three have not.



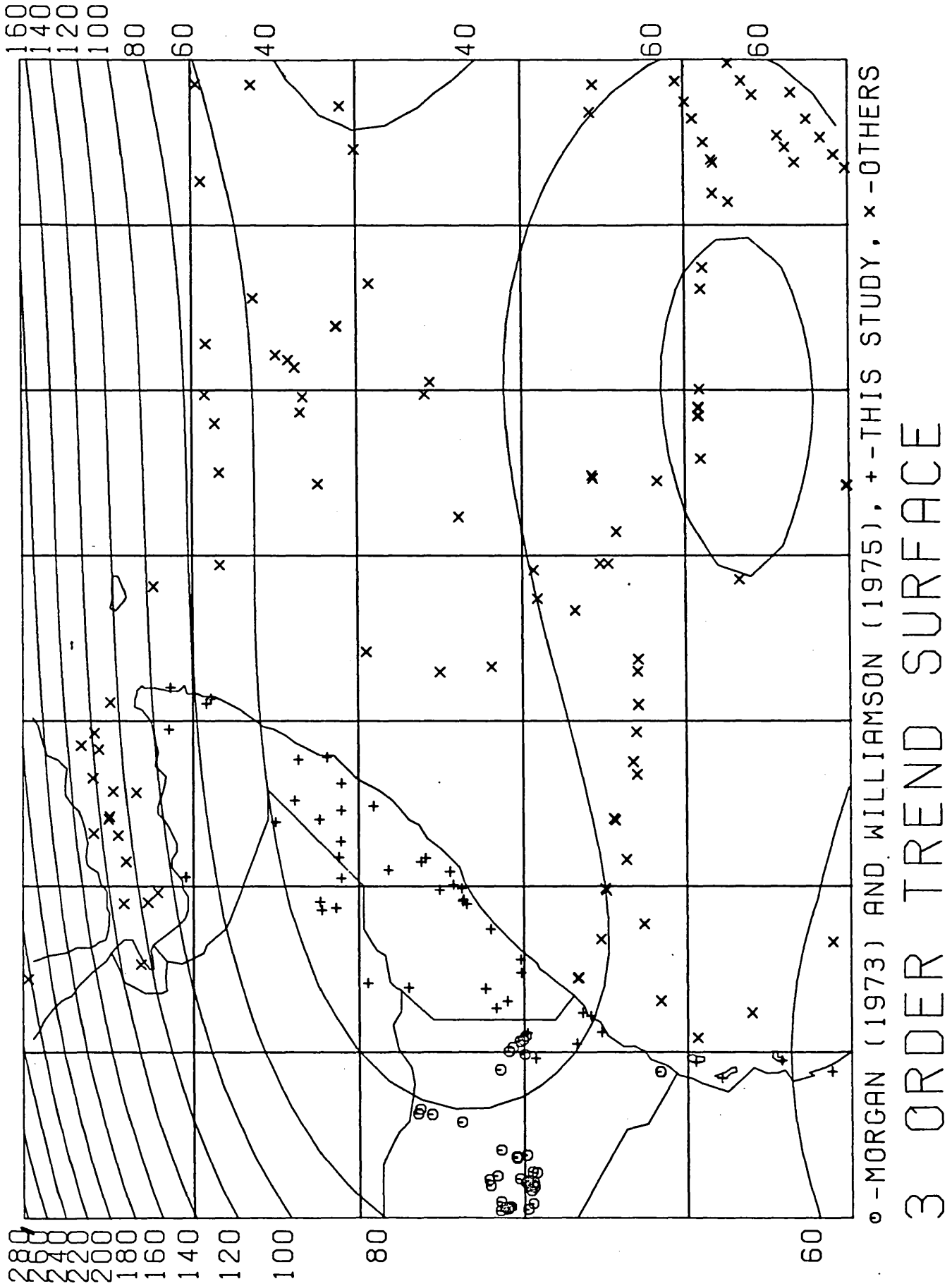
NUMBER OF HEAT FLOW OBSERVATIONS = 193
LAT AND LONG IN 5 DEGREE SQUARES
LOWER LEFT CORNER = 10 DEG.S., 35 DEG.E.
CONTOUR INTERVAL OF HEAT FLOW = 20 MW/M.M

Fig.4.85



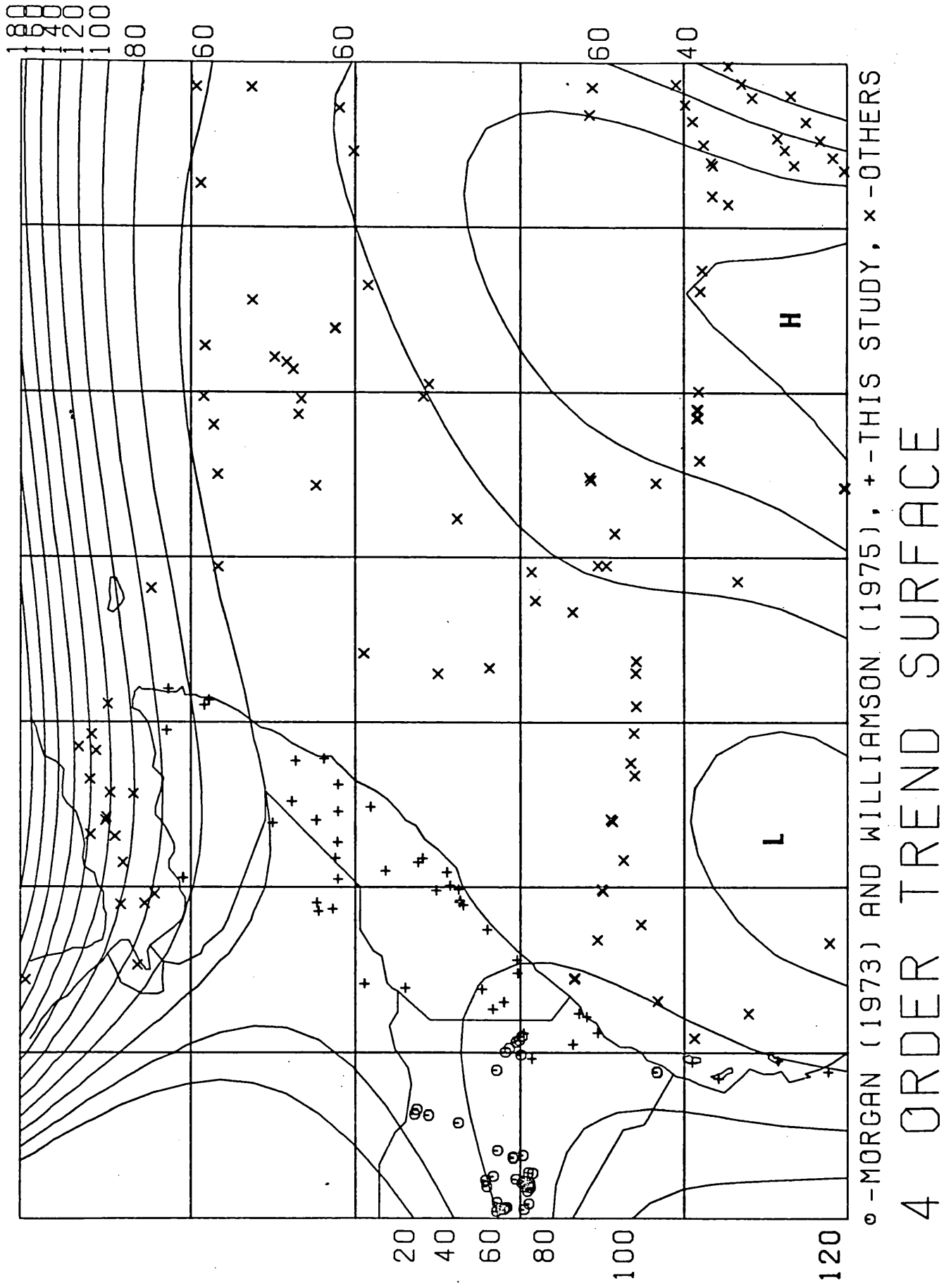
NUMBER OF HEAT FLOW OBSERVATIONS = 193
LAT AND LONG IN 5 DEGREE SQUARES
LOWER LEFT CORNER = 10 DEG.S., 35 DEG.E.
CONTOUR INTERVAL OF HEAT FLOW = 20 MW/M.M

Fig.4.86



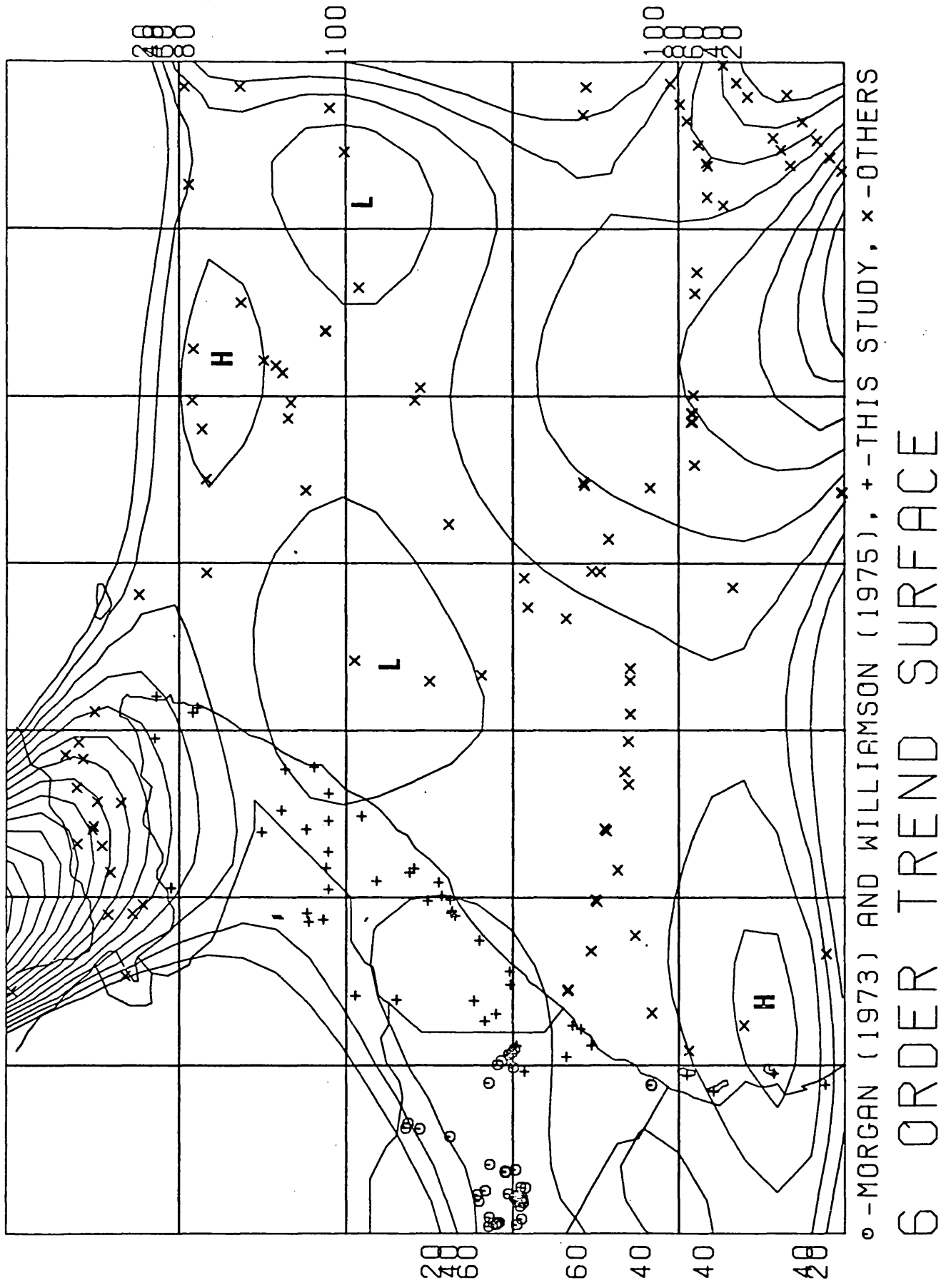
NUMBER OF HEAT FLOW OBSERVATIONS = 193
LAT AND LONG IN 5 DEGREE SQUARES
LOWER LEFT CORNER = 10 DEG.S., 35 DEG.E.
CONTOUR INTERVAL OF HEAT FLOW = 20 MW/M.M

Fig. 4.87



NUMBER OF HEAT FLOW OBSERVATIONS = 193
LAT AND LONG IN 5 DEGREE SQUARES
LOWER LEFT CORNER = 10 DEG.S., 35 DEG.E.
CONTOUR INTERVAL OF HEAT FLOW = 20 MW/M.M

Fig.4.88



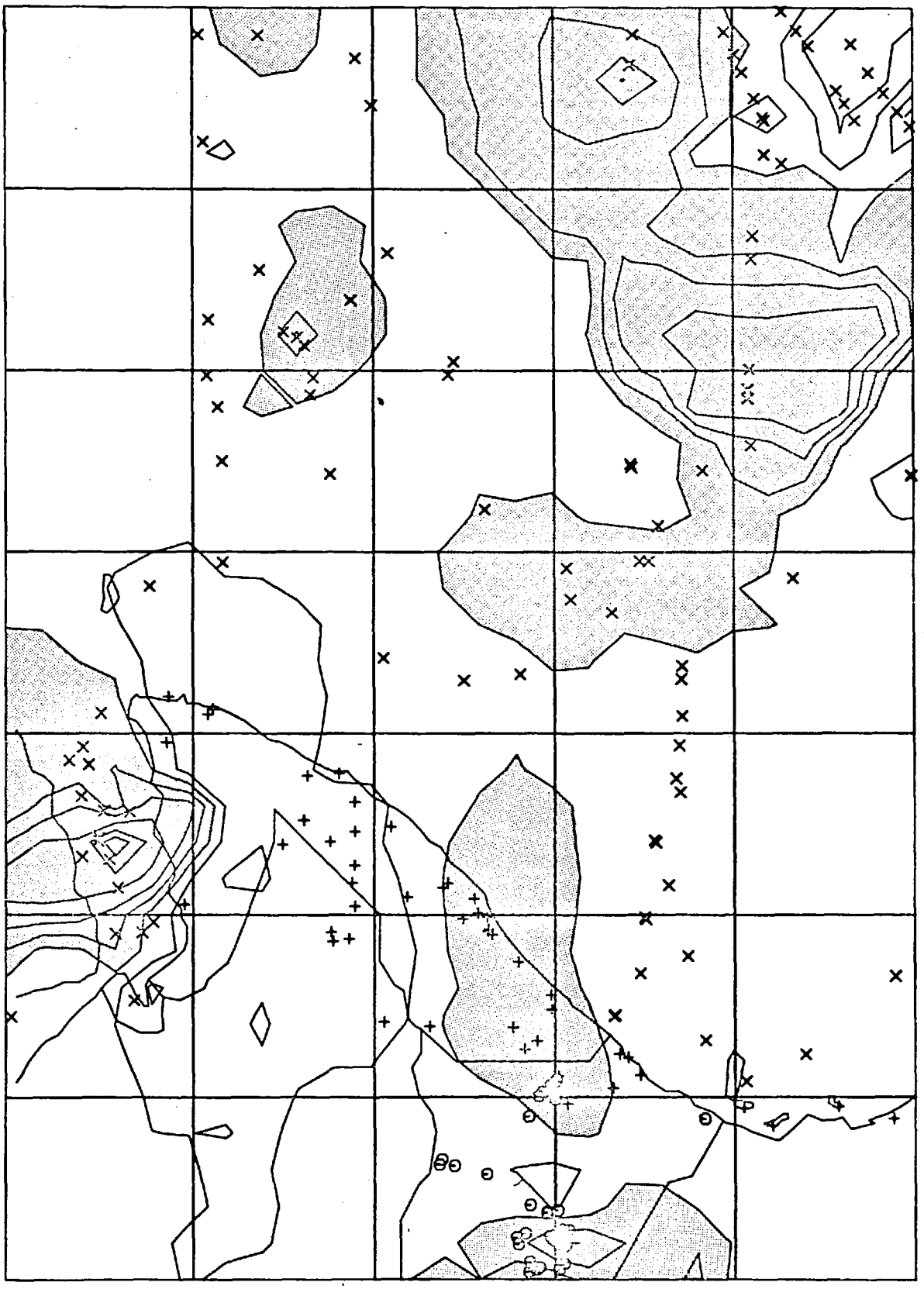
NUMBER OF HEAT FLOW OBSERVATIONS = 193
LAT AND LONG IN 5 DEGREE SQUARES
LOWER LEFT CORNER = 10 DEG.S., 35 DEG.E.
CONTOUR INTERVAL OF HEAT FLOW = 20 MW/M.M

Fig. 4.89

The Mascarene plateau (section 4.5) may have been part of the Indian Ocean ridge system (McKenzie and Sclater, 1971) as recently as the Oligocene or Miocene. Its shallow depth may indicate thermal expansion and a lithospheric temperature regime analogous with an active ridge. The Kenya-south-west Somalia anomaly is at least partly due to the high values in the Eastern Rift (Morgan, 1973). The Tanzanian anomaly has no obvious explanation. The Eastern Ogaden region appears as saddle in a major low; it represents a possible western extension of two oceanic lows.

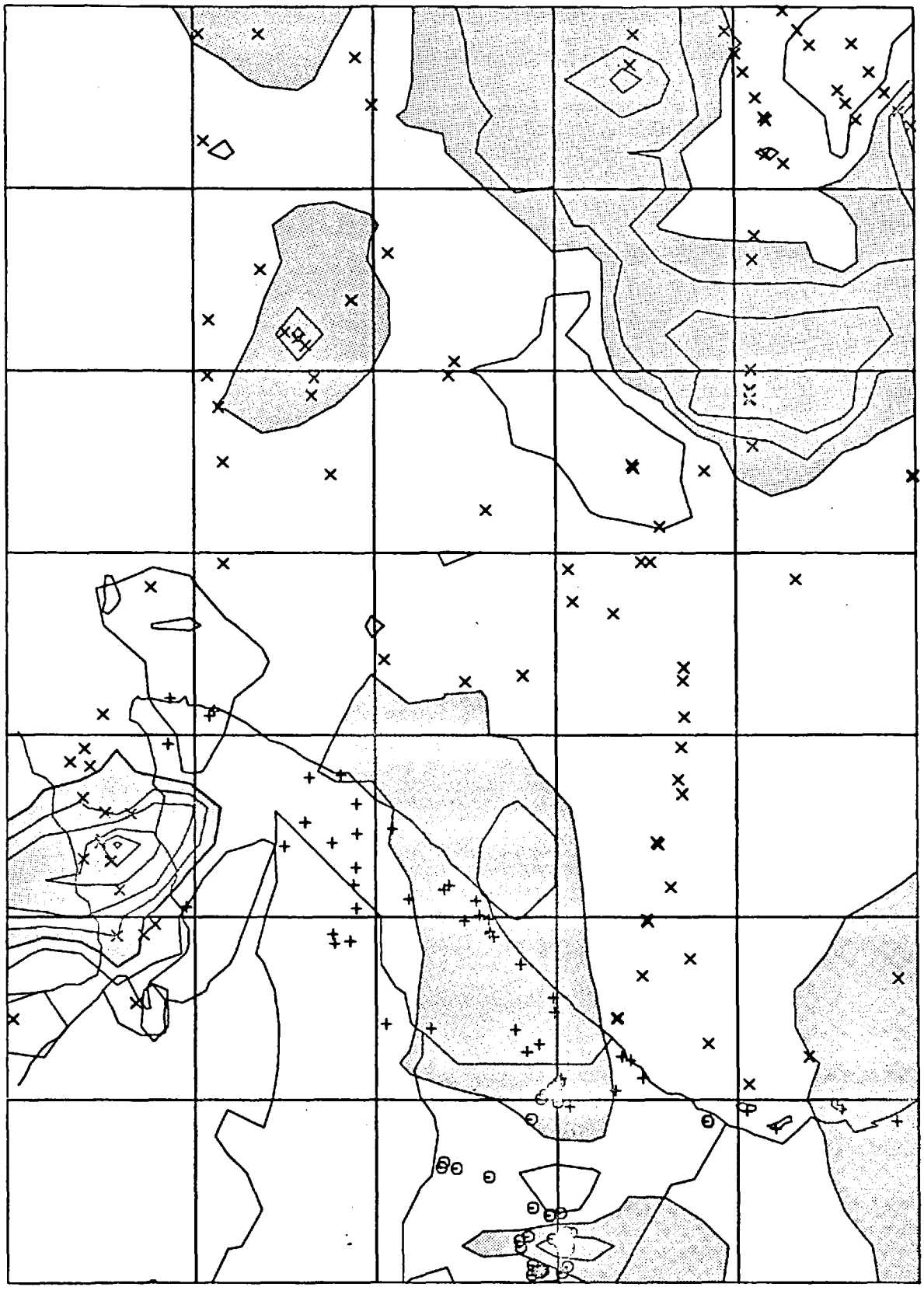
Contoured residual maps for the second and third order trends, Figs. 4.90 and 4.91 respectively, were also prepared. Positive residual regions (heat flow observed greater than heat flow calculated) are stippled. The second order residual map again shows that the Gulf of Aden and Carlsberg Ridge are high; the Central Indian ridge and Mascarene anomalies have coalesced and extend further west than in the sixth order trend. The eastern Kenya-south-west Somalia anomaly has separated into two and the coastal Tanzania anomaly has disappeared. The Ogaden region is again part of a major low. The third order residuals slightly modify the picture extending the eastern Kenya-south-west Somalia anomaly and shrinking that over the Mascarene plateau.

In order to investigate the relation of the trend surface heat flow to other geophysical parameters a composite gravity-magnetic map, Fig. 4.92, was prepared on the same base as the trend plots. The gravity data was taken from the Gaposchkin and Lambeck (1971) free air anomaly map computed from a 16th order spherical harmonic analysis of both terrestrial and satellite data. The magnetic contours were traced from the Regan et al. (1975) global anomaly map which was compiled from the 'Pogo' satellite magnetometer data. The most striking relationship is the magnetic low ($<$ - 4 gammas) roughly coincident with the E-W equatorial axis heat flow low of the 2nd and 3rd order trend surfaces. The gravity also shows a positive correlation with a +10 mgal. anomaly over the Gulf of Aden and lows ($<$ - 30 mgals.) near heat flow minima observed on trend orders 2, 3, and 4.



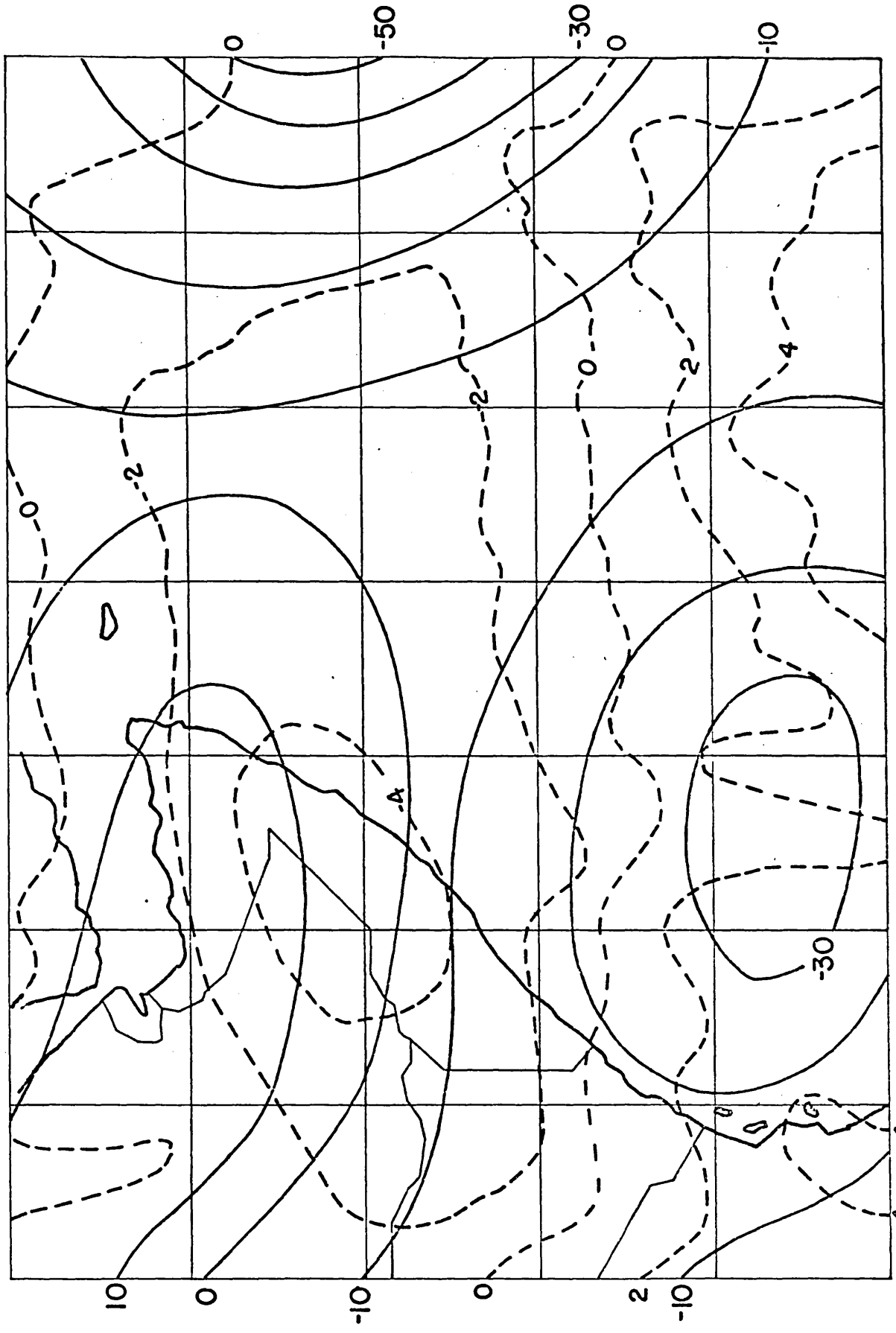
NUMBER OF HEAT FLOW OBSERVATIONS = 193
LAT AND LONG IN 5 DEGREE SQUARES
LOWER LEFT CORNER = 10 DEG.S., 35 DEG.E.
CONTOUR INTERVAL OF HEAT FLOW = 20 MW/M.M
POSITIVE RESIDUAL REGIONS STIPPLED

Fig. 4.90



NUMBER OF HEAT FLOW OBSERVATIONS = 193
LAT AND LONG IN 5 DEGREE SQUARES
LOWER LEFT CORNER = 10 DEG.S., 35 DEG.E.
CONTOUR INTERVAL OF HEAT FLOW = 20 MW/M.M
POSITIVE RESIDUAL REGIONS STIPPLED

Fig.4.91



Data from;

Magnetics - Regan et al. (1975)
Gravity - Gaposchkin and Lambeck (1971)

Lat. and Long. in 5 degree squares
Lower left corner = 10° S, 35° E

FIG 4.92

Heat flow-gravity-magnetic profiles were plotted along lines of latitude (7^{o}S, equator, 7^{o}N; Fig. 4.93) to further investigate the apparent positive correlation. The curves show a significant degree of similarity for the southern two profiles; the northern profile exhibits no distinct correlations.

A positive correlation between heat flow, gravity and magnetics is surprising in that previous researchers have found and/or postulated the reverse. Both Wang (1965) and Toskoz and Arkani-Hamed (1967) found negative correlation of heat flow with gravity; Zietz (1969) obtained a similar result with magnetics. The latter inverse correlation appears justified in that the isotherm should be sufficiently depressed in an area of low heat flow such that the lower crust and part of the upper mantle will be below the Curie temperature. The correlation with gravity has been linked with thermal expansion of the crust and upper mantle leading to density variations.

Bott (1971c) has suggested that long wavelength gravity anomalies may be due to the mantle phase transitions. The olivine-spinel (350-430 km.) and spinel-oxide (650-730 km.) transitions would produce negative and positive gravity anomalies respectively due to an increase in temperature. However, the temperature variation (50^{o}C) consistent with the gravity variations is too small to significantly alter the surface heat flow. Bott (1971c) also notes though that thermal convection in the asthenosphere between 60 and 350 km. would heat the lithosphere (positive heat flow anomaly) and cool the olivine-spinel transition zone (positive gravity anomaly). Bott further states that the long wavelength gravity anomaly may record a fossil mantle convection cell as the upward migration of the olivine-spinel transition will take 10-100 m.y. to dissipate while the lithosphere will continue to move over it at a few $cm \cdot y^{-1}$. Thus, by the time the fossil convection cell heat rises from the base of the lithosphere to the surface of the crust (10-100 m.y.) the associated gravity anomaly may be some 100-2000 km. distant.

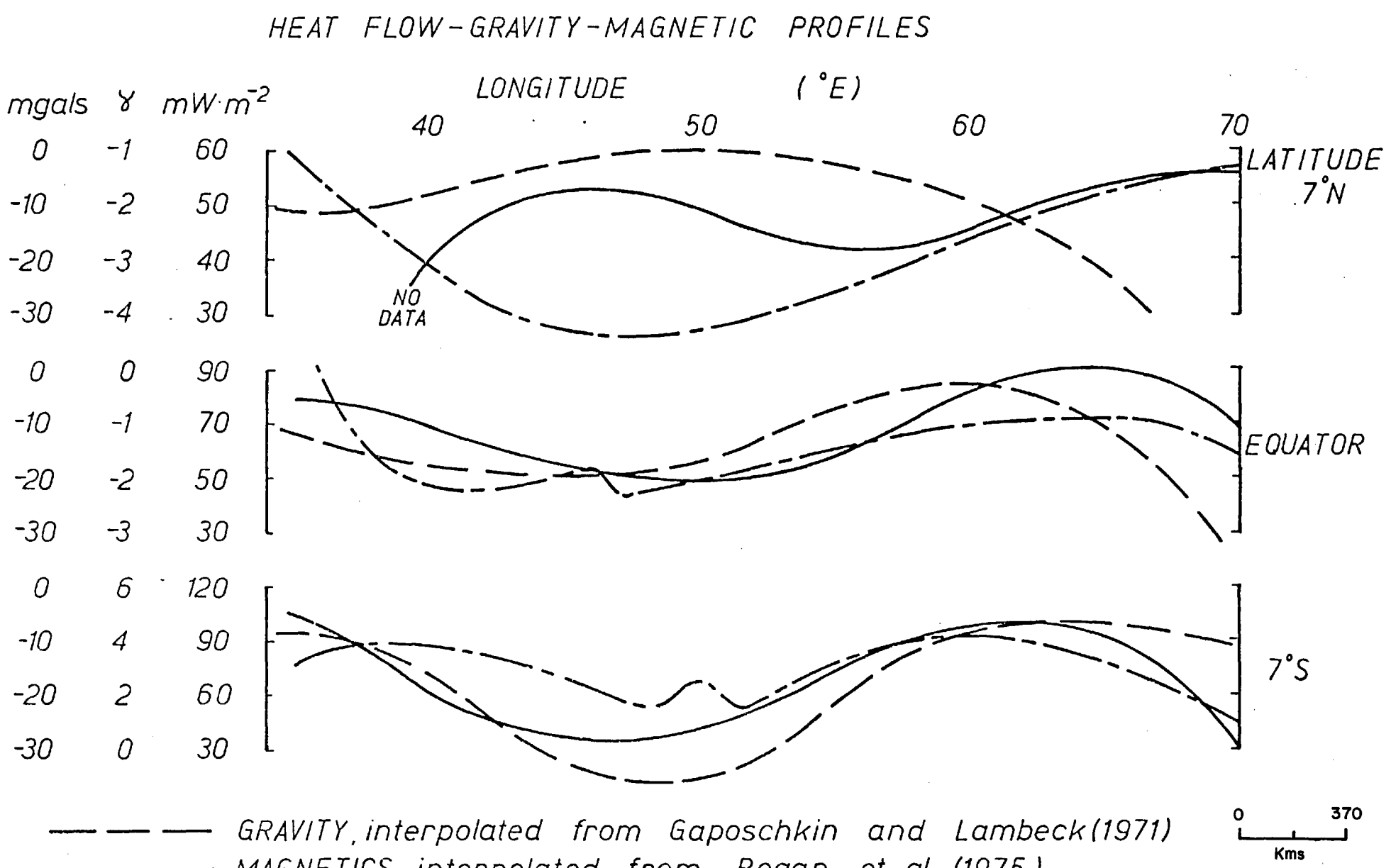

HEAT FLOW - GRAVITY - MAGNETIC PROFILES
mgals
γ
mW·m⁻²
LONGITUDE (°E)
40
50
60
70
0
-10
-20
-30
-1
-2
-3
-4
60
50
40
30
NO DATA
LATITUDE
7°N
0
-10
-20
-30
0
-1
-2
-3
90
70
50
30
EQUATOR
0
-10
-20
-30
6
4
2
0
120
90
60
30
7°S
GRAVITY, interpolated from Gaposchkin and Lambeck (1971)
MAGNETICS, interpolated from Regan et. al. (1975)
HEAT FLOW, from 4th order trend surface., fig. 4.88
0
370
Kms

FIG. 4.93

Table 4.6

Trend Surface Statistics

Order Of Trend	Number Of Coefficients	Degrees Of Freedom	Correlation Coefficient	F Test Term	Significant?	
					At 1% Leval	Over Previous Trend
1	2	190	.21	4.57	NO	-
2	5	187	.45	9.53	YES	YES
3	9	183	.53	8.13	YES	YES
4	14	178	.59	6.71	YES	YES
5	20	172	.60	4.81	JUST	JUST
6	27	165	.67	5.11	YES	YES

4.20 Heat Flow and the Subsidence of the Eastern Africa Continental Margin

The discussion of Eastern Africa geology, section 4.2, and in particular table 4.0, emphasized the considerable amount of crustal subsidence and contemperaneous sedimentation which has occurred on this continental margin. In several regions the basement has been downwarped some 6-12 kms.; the overlying sediment pile is regarded as one of the most formidable in the world (Heezen, 1974).

At least five independent continental margin subsidence models have been proposed. They are all a function, to varying degrees, of the lithospheric temperature regime. A discussion of the implications of the previously mentioned Eastern Africa heat flow values and temperature profiles (sections 4.7 - 4.19) to these models follows.

Sleep (1971) has proposed a thermally controlled evolution of an Atlantic type continental margin in which crustal thinning occurs as a result of subareal erosion of a region initially subjected to uplift due to thermal expansion during its early rift valley phase(s). Sleep considers the combined effects of isostatic compensation due to crustal thinning and thermal contraction of the lithosphere which result in an exponential decrease in elevation (initially positive) and, eventually, the sedimentation rate (assumed contemporaneous). The amount of erosion which occurs may be several times the initial uplift (Foucher and Le Pichon, 1972) due to isostatic adjustments (Sleep, 1973) though the exact value will depend on the erosion rate and the lithospheric thermal time constant. Sleep (1971) found that the sedimentary history of the eastern Atlantic margin was consistent with such a model with a thermal time constant of 50 m.y. and sediment thicknesses of the order of two kilometres. Such a study was not attempted on the well data presented in sections 4.9 - 4.18 as precise and consistent paleontological dating was not available. Moreover Bott (1973) and Le Pichon et al. (1973)

have demonstrated shortcomings in Sleep's model, implying that lithospheric contraction and subareal erosion may not be the principal cause of continental margin subsidence.

Walcott (1972) has discussed the subsidence at margins in terms of a monoclinal downwarp due to sediment loading at the base of and along the continental slope and rise. The flexural rigidity of the continental lithosphere would accommodate such a regional downwarp. There is some evidence for this 'hinge-line' type tectonics in Eastern Africa, particularly along the northern periphery of the Lamu Embayment and the south-west Somalia basin.

A number of researchers, among them MacDonald and Ness (1960), Wetherill (1961), Van de Lindt (1967), Joyner (1967) and O'Connell and Wasserburg (1967), have investigated subsidence induced by the movement of a crust-mantle phase boundary. The models, of varying degrees of sophistication, all consider the effect on the postulated basalt-eclogite boundary resulting from a sudden loading of the crust within a modest thickness of sediments. The resulting pressure pertubation, will, compared to the thermal effect, be virtually instantaneous, shifting the phase transition up, converting basalt to eclogite with concomitant contraction and crustal subsidence. Eventually, the temperature rise will permeate to the transition zone, reverse the process and induce uplift (see section 3.5). Those models which considered time dependent effects (Van de Lindt, 1967 and Joyner, 1967) give a maximum of 3-10 km. of sediments accumulating in 20-120 m.y. before the uplift and erosion cycle begins. The phase transition models have, however, fallen into disfavour recently (cf. Bott, 1971a) as a result of experimental petrology studies (cf. Ringwood and Green, 1964).

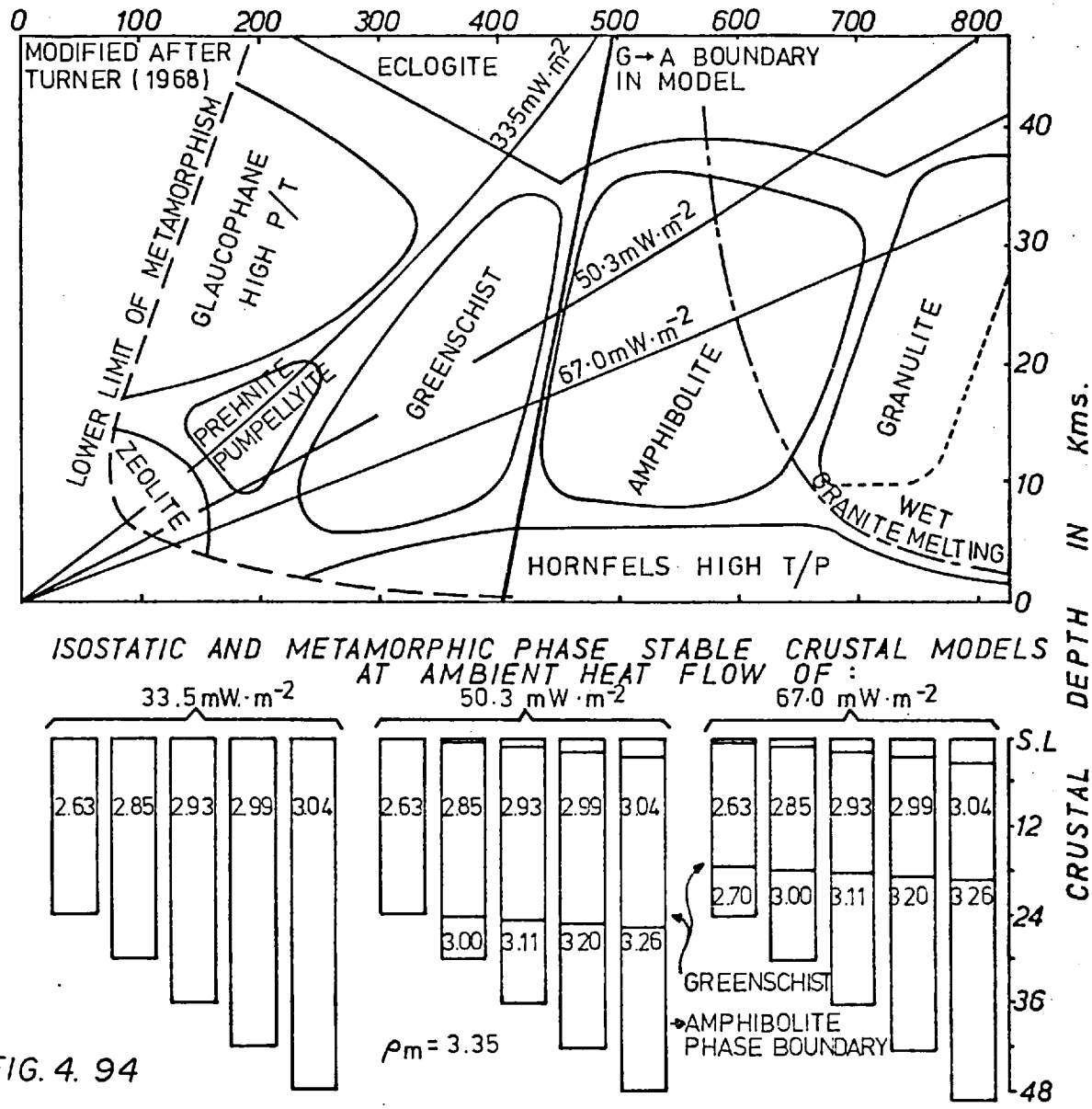
The fourth mechanism for margin subisdence is oceanward hot creep of lower continental crustal material (Bott, 1971a, 1973). The crust thins by ductile flow in response to the stress difference resulting from the juxtaposition of oceanic-continental lithospheres at young margins, (Bott and Dean,

1972). Misra and Murrell (1965) indicate that hot creep will be effective at about half the melting temperature, or for the Eastern Africa average geotherm (Fig. 4.96) at a depth of about 25 km. Bott envisages a return viscous counter flow near the base of the lithosphere. The model is particularly attractive for Eastern Africa in that the temperature and the stress differences would be high enough to support a creep subsidence mechanism which is one of the few models that, by itself, will produce major downwarps of several kilometres. Moreover the model predicts a series of normal faults perpendicular to the creep flow lines; Fig. 4.3 supports this. The schematic type crust profile resulting from creep subsidence presented by Bott (1971a, Fig.2) bears a striking resemblance to the coastal Tanzania profiles of Kent et al. (1971 , Fig. 44.7).

The final model of margin subsidence considered here is that of Falvey (1974). His mechanism is a rise in heat flow inducing crustal metamorphism, increasing crustal density and, where crustal mass is preserved, effecting isostatic subsidence. Fig. 4.94 (after Falvey, 1974) indicates the metamorphic phases, for the crust with 'average' geotherms for a range of surface heat flow superimposed. Clearly at low (30-40 $mW \cdot m^{-2}$) heat flow the entire crust may be at greenschist facies (low density) or lower. Any rise above such a level of heat flow would push the lower crust into the amphibolite-granulite field, raise the mean crustal density, thin the crust and produce subsidence. The crustal models illustrated below the metamorphic phase diagram (Fig. 4.94) indicate the density structure and isostatic subsidence for various ambient heat flow values, initial heat flow values, density and crustal depths. Fig. 4.95 illustrates the maximum subsidence effected for a given heat flow value where the computed crustal sections are balanced against a standard 30 km. column of density 2.85, (Falvey, 1974).

The mean Eastern Africa heat flow (64 $mW \cdot m^{-2}$) is sufficient to induce about 5 km. of subsidence (maximum) in terms of such a model. The mechanism is more attractive than that of Sleep (1971) in that it involves no

METAMORPIC PHASES , HEAT FLOW AND CRUSTAL STRUCTURE



ISOSTATIC AND METAMORPHIC PHASE STABLE CRUSTAL MODELS AT AMBIENT HEAT FLOW OF :

FIG. 4. 94

from Falvey (1974)

SUBSIDENCE IN RESPONSE TO A RISE IN HEAT FLOW ABOVE 33·5 mW.m⁻²

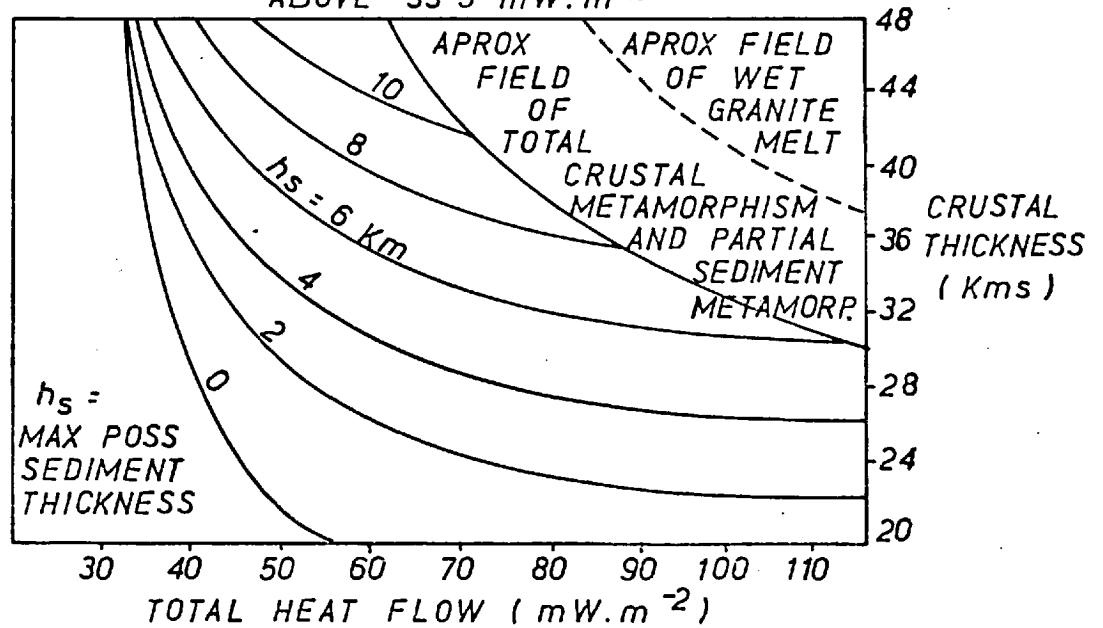


FIG. 4. 95

uplift or erosion and may continue at a relatively constant rate for some considerable period.

The source of the increase of crustal heat flow might be assigned to one or more of the periods of major tectonism in Eastern Africa; the Cambro-Ordovician Pan African event (500 m.y.), the Karroo Carboniferous-Permian graben/rift phase (280 m.y.) and the Cretaceous opening of the Indian Ocean (130 m.y.). Herein may be the clue to the relative continuity and thickness of the Eastern Africa sedimentary column. Sclater and Francheteau (1970) indicate that the additional heat flow from a major orogeny may be dissipated in a period of 200 m.y. The Eastern Africa continental margin has had three evenly spaced orogenies in the past 500 m.y. which may have been sufficient to maintain progressive crustal metamorphism, subsidence and the accumulation of sediments.

4.21 Crust and Upper Mantle Temperature Profiles

Crust and mantle temperature profiles may yield estimates of lithospheric structure, viscosity and depth to partial melting. The calculation of such a profile requires estimates of the surface heat flow, the concentration and distribution of radiogenic elements, and the magnitude and variation of thermal conductivity with depth.

Many crust and mantle temperature regimes have been proposed (cf. Lachenbruch, 1968, Sclater and Francheteau, 1970, Blackwell, 1971, Schatz and Simmons, 1972, Smithson and Decker, 1974); the models presented here incorporate aspects of much of this research.

The calculation of temperature for stationary one-dimensional heat flow is given by,

$$T = T_o + \frac{Q \cdot z}{K} - \frac{A \cdot z^2}{2K} \qquad (4.1)$$

where T is temperature, T_o is surface temperature, z is depth, K is thermal conductivity, Q is the heat flow at z = 0, and A is the natural heat production. Relation (4.1) is valid over a region where A and K are both constant. Lachenbruch (1970) has derived similar expressions for regions where A decreases exponentially and linearly with depth; such models will not be considered here.

Any model of the crust and upper mantle should consider four regions; the upper or granitic crust, the lower or gabbroic crust, and the upper and lower chemical zones of the upper mantle; the dunite-peridotite and pyrolite layers respectively. In addition we will consider a fifth layer, the sediments, for completeness.

The heat production of sediments has been measured only at the Wal Merer-1 borehole in Kenya (table 4.5). For all of the other areas the mean value of 1.0 $\mu W \cdot m^{-3}$ for carbonates, shales and sands (Sass, 1972) will be

used. Where thermal conductivities have been measured for the sediments in an area the mean result will be used; otherwise the value will be set to 2.5 $W \cdot m^{-1} \cdot K^{-1}$. The thickness of the layer will, where no geological or geophysical evidence is to the contrary, be set equal to 4 km.

The granitic layer heat production has been measured only in the north-east Sudan, table 4.5; a value of 2.1 $\mu W \cdot m^{-3}$ will be used as an average elsewhere. This value is consistent with that of Smithson and Decker (1974) as well as that for the continental platform model of Sclater and Francheteau (1970). The thermal conductivity assigned was 2.7 $W \cdot m^{-1} \cdot K^{-1}$ which is identical with virtually all of the above mentioned researchers. The choice of thickness for this layer is crucial to the temperature regime due to its high heat production. A value of 8 km. was arrived at as Sclater and Francheteau have demonstrated that variations of heat flow in Caledonian and older regions may be explained by variable heat production ($A = 2.1 \pm .8\ \mu W \cdot m^{-3}$) in a layer of such a thickness. This is the so called 'linear heat flow-heat production relation' first proposed by Birch et al. (1968) and Lachenbruch (1968) in which the slope and intercept of the plot of the above mentioned variables yield the depth and heat flow at depth of this radioactive layer. With the exception of the Red Sea none of the Eastern Africa regions discussed here has been subject to significant tectonism since the Caledonian.

The lower crust layer conductivity was set 2.1 $W \cdot m^{-1} \cdot K^{-1}$, consistent with the value obtained for gabbro between 200° and 300°C by Birch and Clark (1940). The heat production assigned was .4 $\mu W \cdot m^{-3}$ which is intermediate between the values assigned by Blackwell (1971) of 0.-.6 $\mu W \cdot m^{-3}$ and Smithson and Decker (1974) of .2-.6 $\mu W \cdot m^{-3}$. The thickness of the layer was computed from that crust remaining after the sediment and granitic layers had been subtracted, the crustal thickness being set to a standard 34 km. where no measurement had been made.

The dunite-peridotite layer heat production has been given by Holmes (1965) as .01 $\mu W \cdot m^{-3}$. The determination of thermal conductivity must

take into consideration radiative effects at temperatures above 500°K, i.e., in general below the lower crust or upper-most mantle. Schatz and Simmons (1972) have proposed, on the basis of considerable experimental data, the following empirical relations to describe the variation of thermal conductivity of olivine associated materials at elevated temperatures,

$$(4.2) \qquad K_L = (.074 + .0005 \cdot T)^{-1}$$

$$(4.3) \qquad K_r = 0 \qquad T \leq 500^{\circ}K$$

$$(4.4) \qquad K_r = .023 \cdot (T - 500) \qquad T > 500^{\circ}K$$

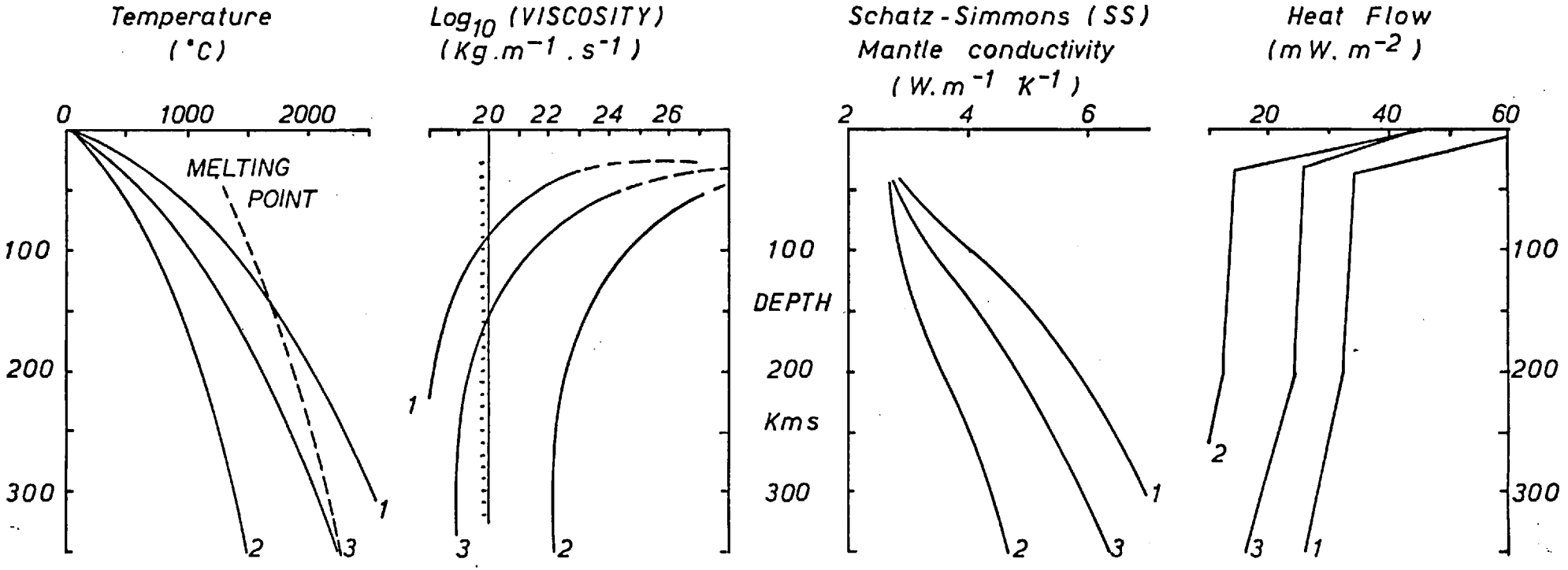
$$(4.5) \qquad K_{L\ min} = 1.26\ (1 + Z)$$

$$(4.6) \qquad K = K_L + K_r, \text{ or, } K_{L\ min} + K_r$$

where K_L, K_r, $K_{L\ min}$ and K are the lattice, radiative, minimum lattice and total thermal conductivities ($W \cdot m^{-1} \cdot K^{-1}$) respectively, T is temperature in degrees Kelvin and Z is the depth in thousands of kilometres. The total conductivity, K, at a given depth and temperature is determined from the sum of the radiative conductivity and the larger of K_L or $K_{L\ min}$ (4.6). This conductivity was used in both the dunite-peridotite and pyrolite zones of the mantle. The division between the zones was set at 200 km. to be consistent with Sclater and Francheteau (1970). The heat production of pyrolite was set to .04 $\mu W \cdot m^{-3}$ (Ringwood, 1958). Temperature calculations were carried out to 350 km., the approximate upper limit of the pyrolite-spinel phase transition.

Fig. 4.96 illustrates the results obtained for an average Eastern Africa model, the Eastern Ogaden region (section 4.13) and a standard continental shield (after Sclater and Francheteau, 1970). Heat flow values for the first two regions were taken from the weighted mean column of table 4.4,

THE VARIATION OF TEMPERATURE (T), VISCOSITY, Mantle Conductivity (K) AND HEAT FLOW (Q) with Depth (z) for an AVERAGE EASTERN AFRICA MODEL, The EASTERN OGADEN and a Typical Continental Shield



—MODELS—

1		2		3	
Q_o = 64 T_o = 25	z	Q_o = 44 T_o = 25	z	Q_o = 44 , T_o = 25	z
A = 1.0 , K = 2.5	4	A = 1.0 K = 2.7	4	A = ·6 , K = 2·5	30
A = 2·1 , K = 2·7	12	A = 2·1 , K = 2·7	12	A = ·01 , K = SS	200
A = ·4 , K = 2·1	34	A = ·4 , K = 2·1	34	A = ·04 , K = SS	
A = ·01 , K = SS	200	A = ·01 , K = SS	200		
A = ·04 , K = SS		A = ·04 , K = SS			
EASTERN AFRICA AVERAGE		EASTERN OGADEN		CONTINENTAL SHEILD	

FIG. 4.96

section 4.7. The melting point curve is for dry pyrolite (Ringwood, 1969). The variation of heat flow and mantle thermal conductivity (Schatz-Simmons) are graphed as well.

The isotherm at the base of the lithosphere is most probably coincident with the solidus (cf. Le Pichon et al., 1973). A partial melt, of the order of 1%, appears necessary to explain the now well established low velocity zone underlying both continental and oceanic regions (Anderson and Sammis, 1970). Such a partial melt will occur at temperatures significantly below ($\backsim 200^{o}C$) the dry solidus in the presence of trace amounts of water. Thus the average lithospheric plate thickness of Eastern Africa is of the order of 70-90 km. as opposed to the 200 km. thick shield plate; this latter value is consistent with the seismic data of Brune and Dorman (1963). Of course once the solidus is reached, the curves determined by (4.1) are invalid as the latent heat of melting and possible convection will decrease the gradient, probably to less than $4^{o}C \cdot km^{-1}$. Note that the Eastern Ogaden profile is never closer than $700^{o}C$ to the solidus.

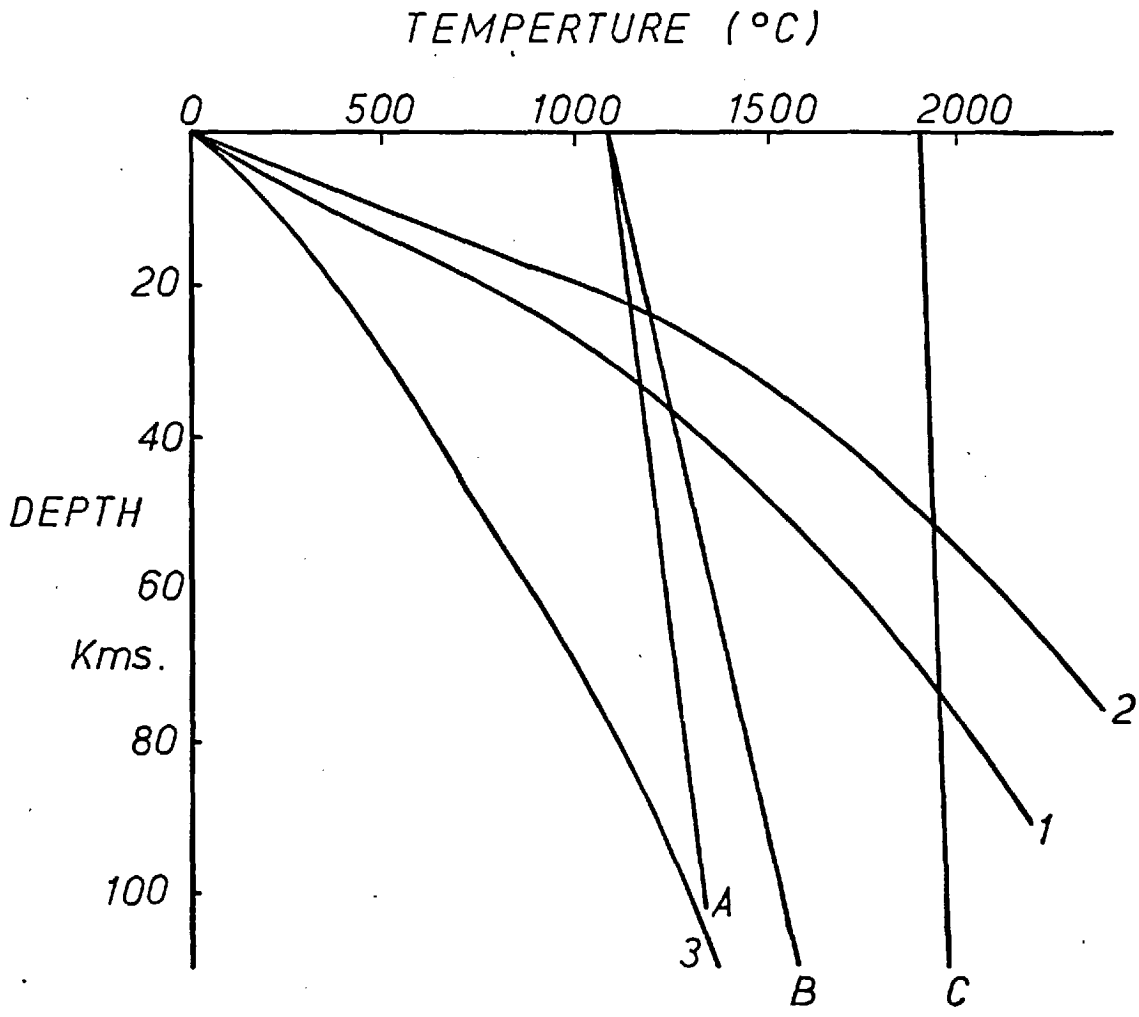
Chapman and Pollack (1974) have proposed a second definition for the lithosphere-asthenosphere boundary. They define it as that point at which the effective viscosity of the mantle is reduced to 10^{20} $kg \cdot m^{-1} \cdot s^{-1}$, a value supported by McConnell (1968) and Walcott (1972). Weertman (1970) has proposed an empirical relation for creep controlled by dislocation glide, the rate being a function of (amongst other things) temperature, pressure and applied stress. Assuming, as did Pollack and Chapman (1974), a stress of 10^{4} $N \cdot m^{-2}$ and employing equation (9) from Weertman (1970) we obtain the curves shown in Fig. 4.96. As expected, the Eastern Africa and continental shield viscosity values fall to 10^{20} $kg \cdot m^{-1} \cdot s^{-1}$ at about 85 and 150 km. respectively. However, the Eastern Ogaden model is never within two orders of magnitude of this viscosity. The plaussible explanations are; that the heat production within the Eastern Ogaden crust has been seriously overestimated, that the mantle conductivity has been overestimated, or that the

asthenosphere is thin or absent under this area of Africa. The implication of the third explanation is, as Chapman and Pollack have stated, that the lithospheric plate (Somalia) extends to the relatively viscous mantle transition zone, which in turn implies that plate motion should be impeded. Piper and Richardson (1972) and Briden and Gass (1974) have also suggested, on the basis of paleomagnetism and geochronological studies, that African plate movement ceased some thirty million years ago.

Fig. 4.97 illustrates crust and upper-most mantle temperature profiles for the Red Sea region. Curve one, modified after Evans and Tammemagi (1974), is for the Central Red Sea region of the Sudan coast; curve two is for the Southern Red Sea Eritrean coast. The crustal thickness and divisions are consistent with the gravity data of Phillips et al. (1969) and Qureshi (1971) and the seismic results of Tramontini and Davies (1969). The higher thermal conductivity of the crust is due to the thick accumulation of shelf carbonates and evaporites (Lowell and Cenik, 1972). The heat production for the NE Sudan profile was obtained from the mean of the eight measurements of granitic basement, table 4.5. The gabbro, pyrolite and forsterite solidii are after Wylie (1971), Ringwood (1969) and Davis and England (1964) respectively. The results indicate that partial melting may occur as shallow as the base of the crust (25 km.) and almost certainly no deeper than 40-50 kms. A standard oceanic geotherm (Schatz and Simmons, 1972) is included for comparison.

Three profiles have been computed for the Lamu Embayment region of Kenya (section 4.17). The curves, Fig. 4.98, for both the Garissa and coastal regions, indicate large variations in crustal and upper mantle temperature regimes for two regions separated by less than 200 km. The heat flows used in the models are the weighted means for the two Garissa region holes (Wal Merer-1 and Garissa-1) and the four coastal holes. The heat production for the sediments at Wal Merer was presented in table 4.5; the thickness of sediments is consistent with geophysical investigations of the region

RED SEA TEMPERATURE PROFILES



CENTRAL RED SEA

1 $Q_o = 97$, $T_o = 25$

$\frac{}{z}$

A = 1·0 , K = 3·0

---------- 3

A = ·7 , K = 2·7

---------- 10

A = ·4 , K = 2·1

---------- 25

A = ·01 , K = SS

SOUTHERN RED SEA

2 $Q_o = 133$, $T_o = 25$

$\frac{}{z}$

A = 1·0 , K = 3·0

---------- 3

A = 2·1 , K = 2·7

---------- 10

A = ·4 , K = 2·1

---------- 25

A = ·01 , K = SS

OCEANIC BASIN

3 $Q_o = 46$, $T_o = 0$

$\frac{}{z}$

A = ·6 , K = 2·5

---------- 10

A = ·01 , K = SS

---------- 100

A = ·04 , K = SS

A – Dry Gabbro Solidus

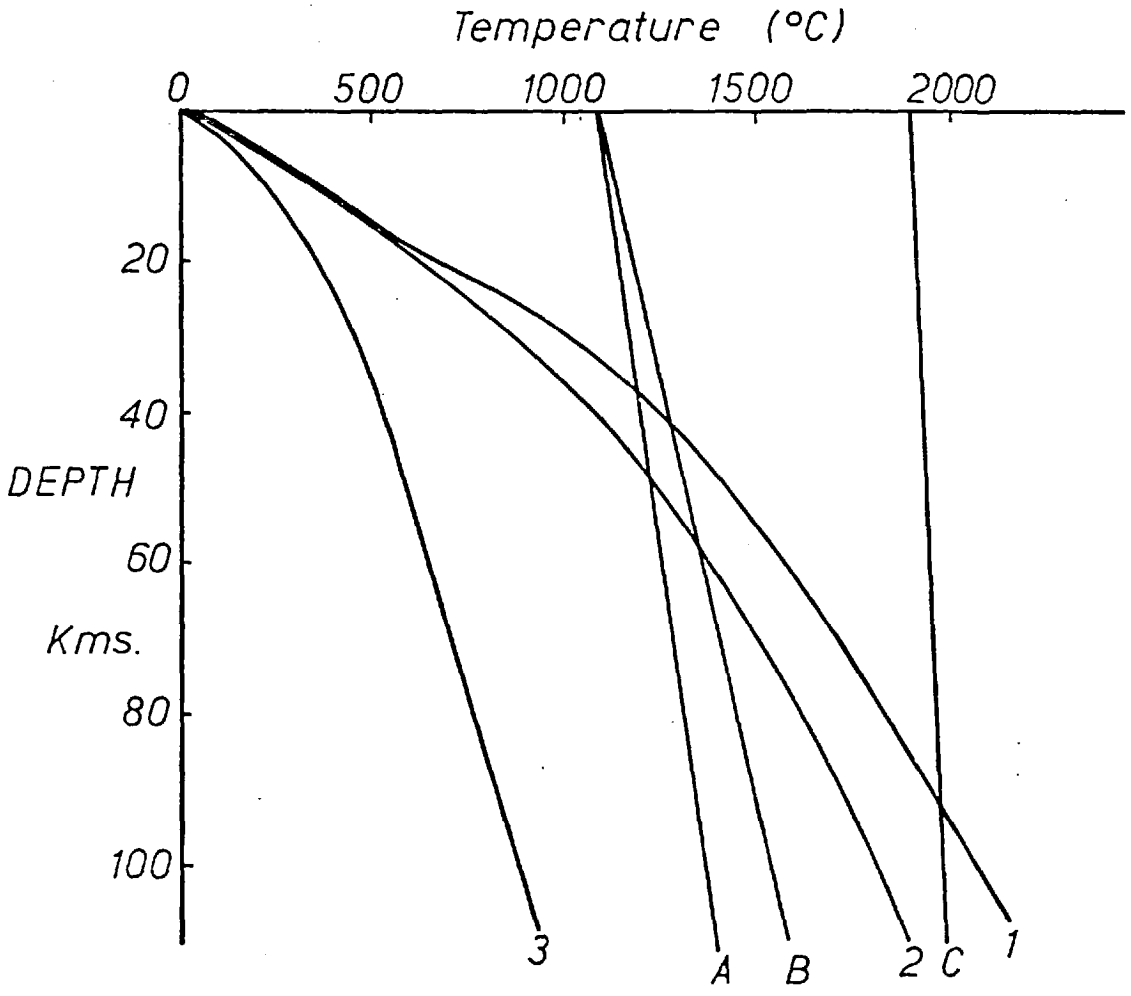
B – Pyrolite Solidus

C – Forsterite Solidus

K = SS, Schatz - Simmons conductivity

FIG. 4.97

KENYA TEMPERATURE PROFILES



GARISSA MODEL A

1	Q_o = 89 T_o = 25 z
	A = 1·3 , K = 2·3
	4
	A = 1·3 , K = 2·7
	12
	A = ·4 , K = 2·1
	34
	A = ·01 , K = SS

GARISSA MODEL B

2	Q_o = 89 T_o = 25 z
	A = 1·3 , K = 2·3
	4
	A = 3·0 , K = 2·7
	12
	A = ·4 , K = 2·1
	34
	A = ·01 , K = SS

KENYA COAST

3	Q_o = 46 T_o = 25 z
	A = 1·3 , K = 2·3
	8
	A = 1·3 , K = 2·7
	16
	A = ·4 , K = 2·1
	34
	A = ·01 , K = SS

A – Dry Gabbro Solidus

B – Pyrotite Solidus

C – Forsterite Solidus

K = SS, Schatz - Simmons conductivity

FIG. 4.98

(Harrison and Haw, 1964, BP pers. comm., 1974). The sediment thermal conductivities were assigned from the means of some 280 individual determinations.

The Garissa models A and B are thought to represent the reasonable limits of the possible temperature regime constructed from steady state heat flow assumptions. Only a single coastal model, equivalent to the upper limit case of the Garissa model B, was included. A Garissa model A coastal equivalent would result in a virtually isothermal upper mantle; an unlikely situation. The Garissa models indicate the possible presence of a partial melt zone in the range 40-60 km. This is in excellent agreement with the electrical conductivity models of Banks and Ottey (1974) who have defined a zone of enhanced conductivity (high temperature?) at a postulated depth of 50 km. Further discussion of the relation of heat flow to electrical conductivity may be found in Gough (1974).

4.22 Two Dimensional Crust and Upper Mantle Temperature Models

The crust and upper mantle profiles derived in section 4.21 assumed a flat layer model, that is an absence of structure involving units of varying conductivity and/or heat production. Two dimensional modelling of the thermal field may provide additional insight, particularly in those regions where the heat flow anomaly is of local rather than regional extent.

Various analytical and numerical approaches exist for two dimensional modelling of Laplace's equation. Conductivity contrasts involving very simple geometric shapes, such as an ellipsoid, have analytical solutions (Carslaw and Jaeger, 1959) while more complicated structures have been modelled by electrolytic tank analogues (Bullard, 1939). Simmons (1967) has developed a method analogous to that used in gravity for the calculation of heat flow anomalies due to contrasts in heat production (density). Formulae for simple geometric forms are given; the extension of the method to bodies of arbitrary shape is by the technique of Talwani and Ewing (1960). However, numerical methods, and in particular finite difference techniques, present the quickest and often only solution to many problems of this form.

As was the case with trend surface analysis (section 4.19) a great deal of literature has been written on the subject of finite difference methods for the solution of partial differential equations. A detailed discussion of the subject is beyond the scope of this thesis; the reader is referred to Forsythe and Wasow (1960) for an authorative account of finite difference techniques.

We will be concerned only with the solution of elliptic partial differential equations - either Poisson's or Laplace's equations. There are several finite difference schemes for dealing with elliptic equations; Jacobi method, Gauss-Seidal method, Young-Leibmann relaxation method, etc. all of which are reviewed in Smith (1965). The Young-Leibmann, or as it is sometimes known, Successive Over-Relaxation (SOR) method, was used here as

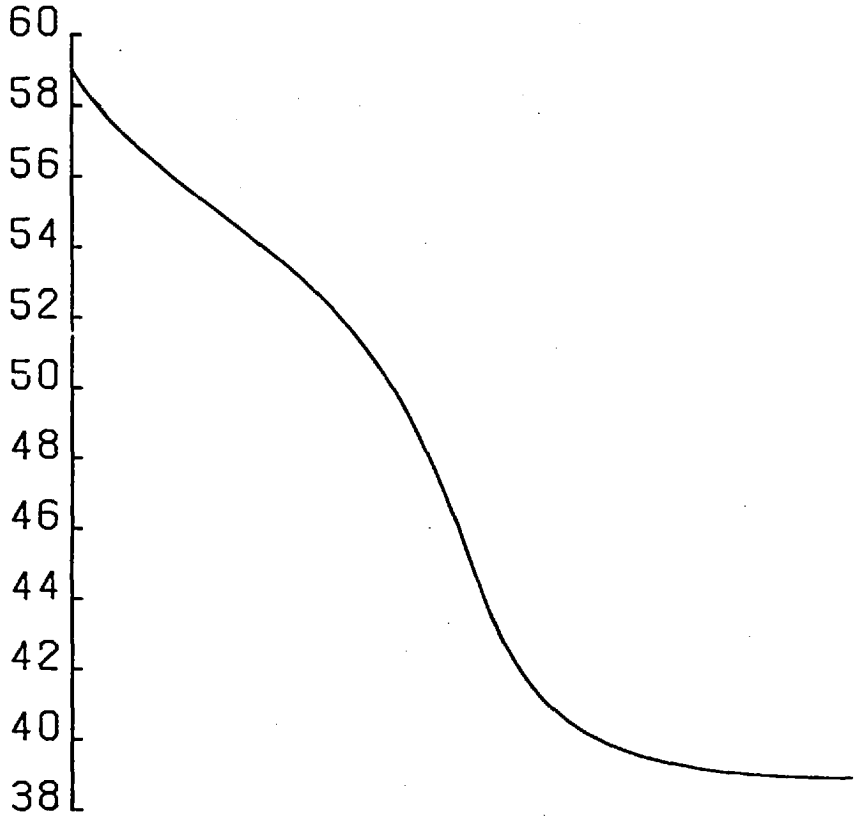
it is one of the more efficient schemes in terms of computing time. The programming of the method is relatively straight forward (cf. Mundry, 1966). However, the rate of convergence of the solution depends critically on the choice of the relaxation factor used (Carre, 1961). In general, a value of 1.3 to 1.7 was found to be satisfactory for most of the models presented here.

The computer program, which was of the interactive type and run from a remote terminal, itterated the temperature array until a preset convergence limit, typically .01^{o}C, was reached. Boundary conditions, (surface temperature, undisturbed surface heat flow), choice of symetry axis or base of grid at constant temperature, grid increment, as well as internal conductivity and heat production boundaries were all preset. Calculations were performed on a 31 x 31 grid although the option to extend it to a finer mesh was available with a concomitant rise in computation time.

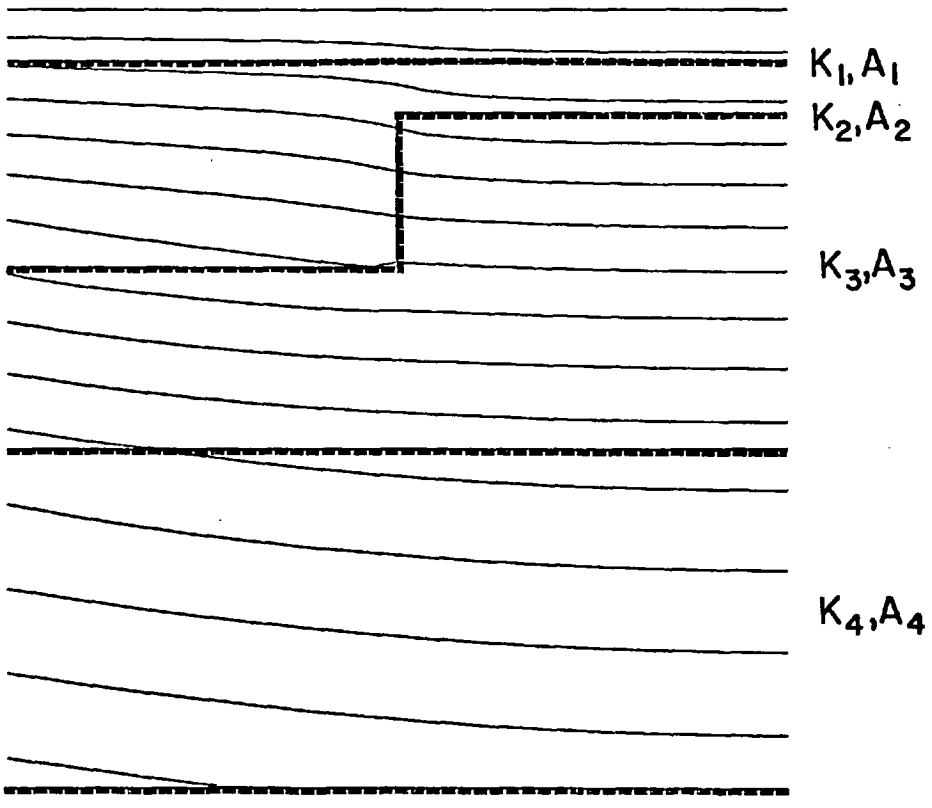
The output array of temperatures was fed to a second program where automatic machine contouring of the isotherms was done. A plot of the vertical component of heat flow, either at the surface or for the entire temperature array, was also made.

A glance at Fig. 4.11 reveals that there are two prominent heat flow anomalies; the Garissa region (North Lamu Embayment) geothermal high and the Eastern Ogaden low, both of which are supported by class A heat flow data. The Eastern Ogaden region, mean 44 mW$\cdot$m^{-2}, is clearly some 10-20 mW$\cdot$m^{-2} lower in surface heat flow than the adjacent Obbia Embayment (55 mW$\cdot$m^{-2}), the Benadir Coast (64 mW$\cdot$m^{-2}) and the Mandera-Lugh Basin (55 mW$\cdot$m^{-2}). A model consistent with a Smithson and Decker (1974) crust was used for the region (s) of undisturbed heat flow. A surface heat flow of 60 mW$\cdot$m^{-2} with 4 km. of sediment, 16 km. of high heat production metamorphic and/or granitic crust, underlain by 14 km. of gabbroic crust and a standard mantle was used for the left hand boundary of the Eastern Ogaden Model, Fig. 4.99. This model is

SURFACE HEAT FLOW
(MW/M.M)



ISOTHERM CONFIGURATION
CONTOUR INTERVAL = 50 DEG.C.



EASTERN OGADEN MODEL

CONDUCTIVITY, $K_1=2.50, K_2=2.70, K_3=2.10, K_4=3.00$

HEAT PRODUCTION, $A_1=1.00, A_2=1.70, A_3=0.40, A_4=0.01$

SCALE = 60 KM. SQUARE, STRUCTURE LINES DASHED

Fig 4.99

extended to the vertical midpoint of the grid where it is terminated with a step up of the gabbroic lower crust resulting in 4 km. of sediments, 4 km. of granitic and/or metamorphic crust, 26 km. of gabbroic crust, and a standard mantle; this structure is extended laterally to the right hand boundary. Conductivities and heat production values are also consistent with Smithson and Decker (1974). Presetting the left hand temperature regime and the surface temperature and invoking right hand rotational symetry of the indicated structure, a plot of isotherms and surface heat flow (0-2 km. nodal points), Fig. 4.99 was obtained. The negative heat production and conductivity contrast of the gabbroic crust relative to the metamorphic-granitic layer is quite sufficient, for such a structure, to explain the lateral variation (10-20 $mW \cdot m^{-2}$) of heat flow.

Two obvious questions are immediately asked; is such a model both geologically and geophysically plaussible? As was mentioned in section (4.2) both Cahen and Snelling (1966) and Saggerson (1973) have indicated that the Eastern Ogaden basement may be significantly older than the Mozambique Belt age of 400-700 m.y. If it were, in fact, to be Archean the erosion of some 12 km. of crust would not be at all unreasonable. However, one might argue plaussibly for a much more diffuse boundary than that indicated. The relatively thickening of the gabbroic crust would also lead to a regional positive in the Bouguer anomaly field. There is some indication of this in Fig. 4.4, though the evidence is certainly far from definitive.

The Garissa area, Fig. 4.73, is quite clearly a thermal anomaly region with values 20-40 $mW \cdot m^{-2}$ above the 50 $mW \cdot m^{-2}$ value found at the coast. This situation is also in evidence in the adjacent South-West Somalia Basin and southern extremity of the Mandera-Lugh Basin. The major structural element of this region is the south-western extension of the Bur Acaba Massif, Fig. 4.3. This lower most Paleozoic pluton is composed of gneisses and granites with interleaved schists and amphibolites (see also section 4.2).

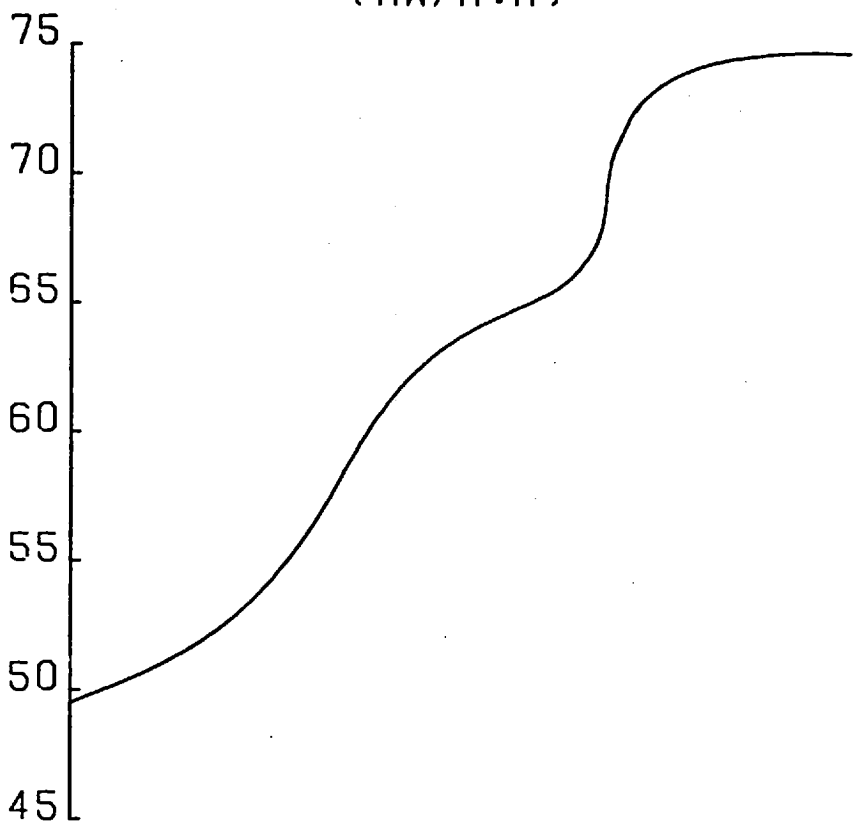
Recent geological and geophysical petroleum exploration surveys (Harrison and Haw, 1964, Walters and Linton, 1973 BP pers. comm., 1974) have confirmed that the concealed graben and horst province of the Garissa region is contiguous with the Bur Acaba Massif. Gravity, magnetics and seismic reflection data indicate about 4-5 km. of sediment draped over the ridge. At least one post emplacement epeirogenic movement of the ridge has occurred, most probably in the upper Cretaceous, isolating the Mandera-Lugh Basin (Beltrandi and Pyre, 1973) and resulting in crestal erosion in Kenya (Walters and Linton, 1973). Recent geophysical surveys in Somalia (United Nations Development Program, 1970) have proved marginal economic uranium and thorium orebodies within the Bur Acaba region.

To investigate the possible disturbance to the thermal field that such a concealed ridge might effect, two plaussible Garissa region models were computed. A somewhat different crustal model to that of the Eastern Ogaden was used for the undisturbed left hand boundary of Figs. 4.100 and 4.101. A heat production and conductivity consistent with the continental crust model of Schatz and Simmons (1972) was used; the values do not conflict significantly with measured heat production and conductivity (tables 4.5 and 4.2 respectively). A crustal thickness of 30 km. was assigned; the dimensions of the ridge, both horizontally and vertically, are consistent with the geological and geophysical evidence.

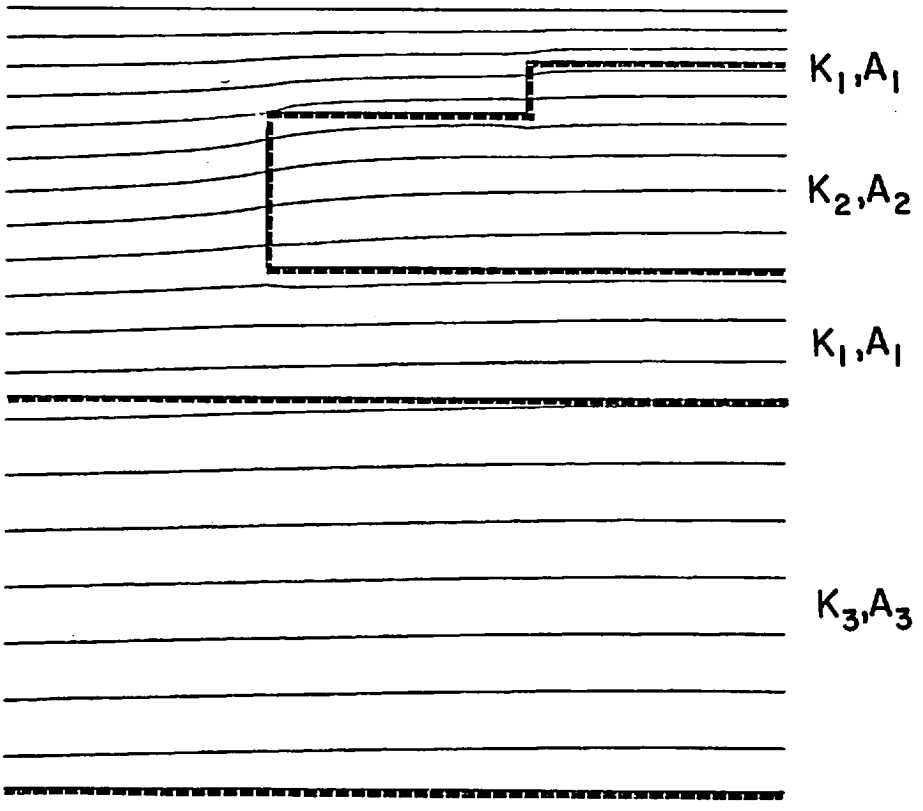
The first and possibly most plaussible model, Fig. 4.100, for the concealed Garissa region high heat production - conductivity ridge, indicates a peak disturbance of 24 $mW \cdot m^{-2}$ on the structure's crest. The second, and more extreme, model (Fig. 4.101) for such a concealed ridge raised the heat flow more rapidly to a crestal anomaly of 30 $mW \cdot m^{-2}$. Such values and the relatively short distances over which they occur ($\sim$40-60 km.) are consistent in a gross fashion with the data presented in Fig. 4.73.

It should be noted that the Wal Merer-1 borehole (Fig. 4.74) indicates an increase of heat flow with depth which is consistent with the

SURFACE HEAT FLOW
(MW/M.M)



ISOTHERM CONFIGURATION
CONTOUR INTERVAL = 50 DEG.C.



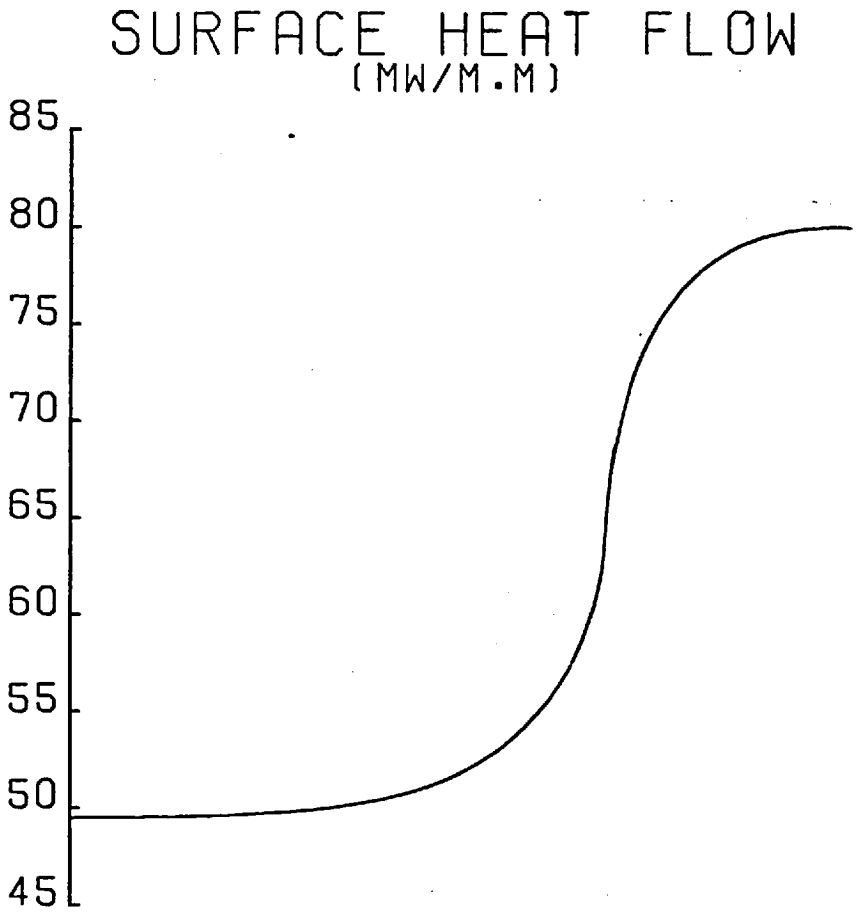
GARISSA REGION MODEL

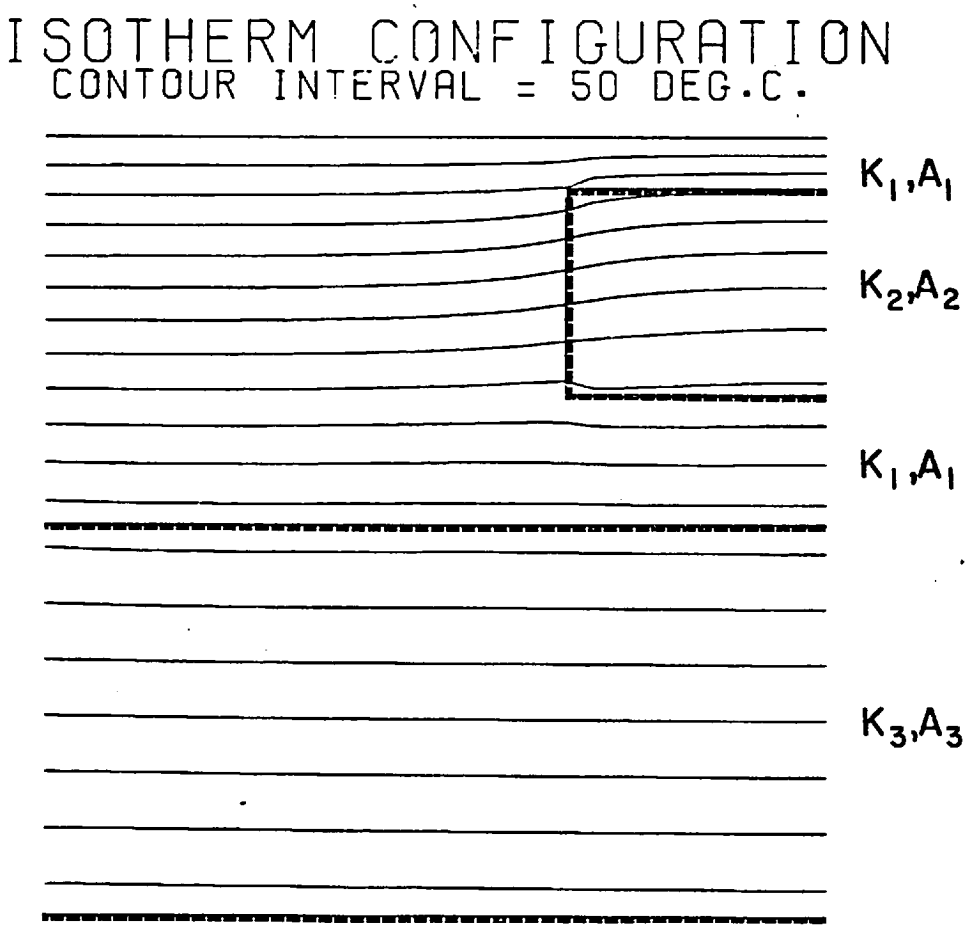
CONDUCTIVITY, $K_1 = 2.20, K_2 = 2.70, K_3 = 3.00$

HEAT PRODUCTION, $A_1 = 0.50, A_2 = 2.70, A_3 = 0.01$

SCALE = 60 KM. SQUARE, STRUCTURE LINES DASHED

Fig. 4.100





GARISSA REGION MODEL

CONDUCTIVITY, $K_1=2.20, K_2=3.20, K_3=3.00$

HEAT PRODUCTION, $A_1=0.50, A_2=3.20, A_3=0.01$

SCALE = 60 KM. SQUARE, STRUCTURE LINES DASHED

Fig. 4.101

prediction of a shallow positive heat production - conductivity contrast. However, the Garissa anomaly may also be due to thermal waters rising along the major faults on the periphery of the Lamu Embayment. Its limited areal extent would appear to rule out a mantle source as predicted by Banks and Ottey (1974) who obtained, on the basis of electrical conductivity data, a model of a possible partial melt zone in the depth region 50-100 km. beneath the Garissa area. The ridge model does not conflict with the gravity data which indicates a local maximum in the Garissa region (Fig. 4.4).

Chapter 5

Preliminary Heat Flow Studies In the North Sea

5.1 Introduction

The North Sea is that shallow marine region bounded by Norway, Denmark, the Netherlands and Great Britain. For the purposes of this thesis, discussion will be limited to that area south of 62°N, though clearly the North Sea sedimentary basin extends beyond this line (Talwani and Eldholm, 1972).

During the past ten years, the North Sea has been the scene of intense oil exploration activity with over eight hundred deep wells having been sunk. In addition to providing a wealth of structural and stratigraphic information, a great deal of BHT data has been obtained during the geophysical logging of these holes. Three previous publications (Harper, 1971, Evans and Coleman, 1974, Cornelius, 1975) have dealt with the BHT derived geothermal gradient field of this region. The purpose of this investigation was to augment these previous studies with extensive thermal conductivity measurements of the major lithologic units of the North Sea.

A brief review of the published literature dealing with the geology and geophysics is followed by a discussion of three new heat flow values. With such limited data the interpretation which follows must be regarded as strictly preliminary.

5.2 The Geology of the North Sea Basin

North West Europe is composed of three major structural elements; the Fenno-Scandia or Baltic Shield, the western margin of the Russian platform

and the northern edge of the Alpine geosyncline fold belt. The North Sea basin, at the intersection of the tectonic lineaments bounding these regions, has undergone a complex history of cratonic deformation since Cambro-Ordovician times.

P.A. Zeigler (1975) has divided the evolution of the North Sea region into five phases:-

1. Caledonide geosynclinal stage
   (Cambrian - Silurian)

2. Hercynian geosynclinal stage
   (Devonian - Carboniferous)

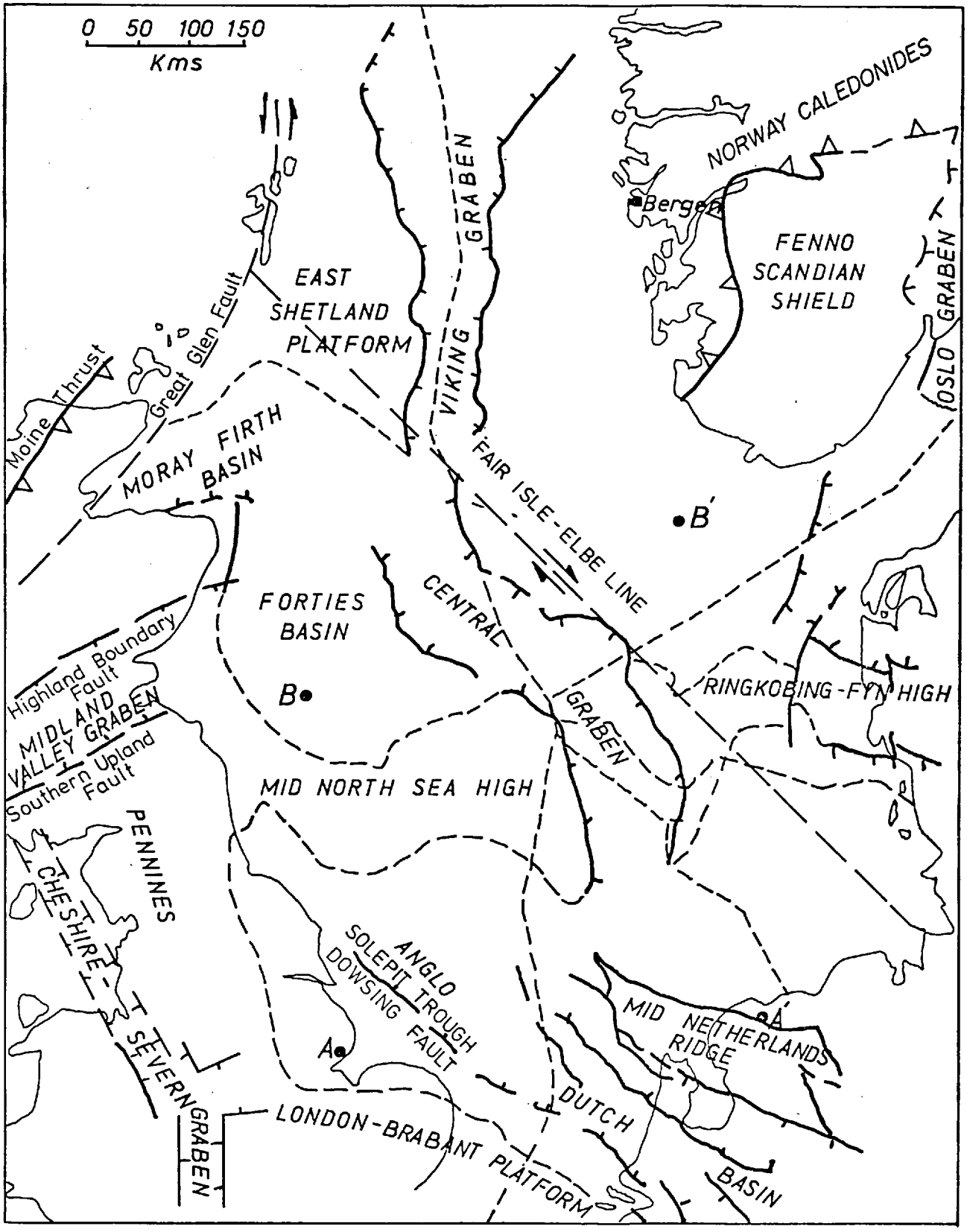
3. Permo - Triassic intracratonic stage

4. Taphrogenic rifting stage
   (Jurassic - Cretaceous)

5. Post-rifting intracratonic stage
   (Tertiary)

These stages, recognised in various forms by other authors (Armstrong, 1972, Kent, 1975, W.H. Zeigler, 1975, Whiteman et al., 1975), represent the fundamental periods of tectonism or intervening quiescence which have shaped the North Sea basin.

The Caledonian orogeny, a possible manifestation of an Asian-North American plate collision (Wilson, 1966) resulted in a major geanticline extending through Northern Ireland, the Scottish Highlands and Norway and across the northern reaches of the present day North Sea. South of this uplift, a major geosyncline evolved. The Great Glen fault and the en echelon equivalent of the Tornquist line, the Fair Isle-Elbe line, Fig. 5.1, were probably established as a conjugate shear couple with compression resulting from the Caledonian plate collision (W.H. Zeigler, 1975). The Tornquist line and its subsidiaries mark the boundary between the stable



MAJOR STRUCTURAL ELEMENTS OF THE NORTH SEA

CALEDONIDE FRONT

FAULT

FORM LINE

After Rhys (1974)

FIG. 5.1

Baltic Shield-Russion Platform and the more mobile north-west European craton.

The collision of the Asian-North American plates and the probable establishment of a subduction zone has been postulated as the driving mechanism of the second orogeny, the Hercynian diastrophic event, (W.H. Zeigler, 1975). The cycle, which lasted from the Devonian through the Carboniferous, further consolidated the North Sea craton. Geosynclinal development continued in the central North Sea, Ireland and the Netherlands. The major highs, the north-west Caledonian mountains and the Anglo Brabant Massif in the south, were rapidly eroded, reaching an advanced stage of peneplanation by the lower Carboniferous (Kent, 1975). The Devonian sediments (Old Red Sandstone) were largely continental; the Carboniferous was a marine period with a widespread carbonate (Waulsortian) sea extending from Ireland to Poland (P.A. Ziegler, 1975).

The Permo-Triassic intracratonic period is characterised by gentle subsidence with continental deposition followed by shallow water carbonates and evaporites. During the lower Permian (Rotliegende) the collapse of the Hercynian mountains was accompanied by considerable volcanism (Rasmussen, 1974). The mid North Sea and Ringkobing-Fyn high(s) emerged to bisect the North Sea basin; both the Oslo and Central North Sea grabens were initiated during the Rotliegendes (W.H. Zeigler, 1975). Aeolian deposition was followed by a catastrophic marine ingression during the middle Permian (Zechstein). A widespread cyclic carbonate-evaporite sabka facies was deposited during a tectonic quiet interval. The Triassic is marked by a return to clastic deposition (Bunter) followed by minor uplift and local erosion. The Middle and Upper Triassic is marked by regional subsidence with clastic muds and local evaporites being deposited. The Viking and Hessen grabens were also initiated in the Upper Trias.

Whiteman et al. (1975) interpret the emergence of these grabens (Viking, Central, Hessen, Oslo, West Sole, Netherlands, Moray Firth, Forties;

see Fig. 5.1) or troughs as the result of triple r (rrr) fracture geometry associated with the passage of the north-west European lithosphere over a mantle plume (cf. Morgan, 1972). These fractures, the geometry of which is consistent with the stress field over a dipping oblate intrusion (Bhattacharji and Koide, 1975) are postulated as failed arms in a lithospheric spreading system due to the speed with which the plate moved over the 'fixed' hot spot. However, whether this mechanism or that of crustal stretching, with the North Sea caught in an extensional quandrant of a regional stress field (the Great Glen Fault and Fair Isle Elbe line being rejuvenated as a conjugate couple, W.H. Zeigler, 1975) is invoked, a period of taphrogensis began in the lower Jurassic. Three phases of Kimmerian rifting are observed; the first of relative minor intensity, the second associated with strong vertical faulting, differential uplift of basement blocks and localized erosion and the third with uplift of the craton margins and rapid subsidence of the graben floors (P.A. Zeigler, 1975).

Howitt et al. (1975) have reported major occurrences of alkalic volcanics of probable Bathonian (2nd Kimmerian phase) age from the Forties Basin (Fig. 5.1). Rapid, primarily clastic, sedimentation kept pace with the subsidence of the grabens. Volcanism, faulting, rifting and wrenching continued through the Malm into the Lower Cretaceous with most of the tectonism now occurring south-west of the Fair Isle-Elbe line (W.H. Zeigler, 1975). The period of taphrogenesis in the North Sea is contemporaneous with the Pleinsbachian opening of the Arctic North Atlantic (Hallam, 1971) though it clearly predates that of the central North Atlantic (cf. Laughton, 1975).

The Lower Cretaceous tectonism abated and the shale and marl deposition passes up into a thick homogenous chalk unit as the Albo-Aptain sea spread out to cover most of north-west Europe. The Laramide event in the Senonian temporarily reversed the orientation of the regional stress field causing the inversion of the Wealden basins in the southern North Sea.

The final evolutionary phase, the post-rifting incrationic stage (Tertiary), is dominated by rapid subsidence of virtually the entire basin.

NORTH SEA . SUMMARY CHART

SYSTEM	TECTONISM		
	GLOBAL	NORTH SEA	MAIN EFFECT
NEOGENE	Alpine Subduction Zone in W.Tethys	ALPINE	Subsidence
PALEOGENE	Spreading & rifting of N.Atlantic	LARAMIDE	R/W/Inversion
U.CRETACEOUS			Subsidence
L.CRETACEOUS			
MALM	Subduction Tethys Plate below Asia Plate. Rifting in N.Atlantic and Insipient spreading	LATE	R/W/V
DOGGER		MAIN	Subsidence
			R/W/V
LIASSIC		EARLY	Subsidence
			R/W
TRIASSIC			Subsidence
BUNTER	Central Atlantic spreaing starts	Hardegsen movements	R/W
			Subsidence
ZECHSTEIN			R/W/V
			Subsidence
ROTLIEGENDE	Lt.Hercynian rifting	LT. HERCYNIAN MOVEMENTS	R/W/V
			Subsidence
PENNSYLVANIAN	Hercynian orogeny closing of a Proto Atlantic	HERCYNIAN OROGENY	R/W/V/S
MISSISSIPPIAN			
DEVONIAN	Post Caled. Rifts	Late Caled. rifts	R/W/V/S
SILURIAN	Caledonide Orogeny Closing of a Proto North Atlantic	CALEDONIDE OROGENY	R/W/V/S
ORDOVICIAN			
CAMBRIAN			
PRE-CAMBRIAN			

R = RIFTING , V = VOLCANISM
W = WRENCHING , S = SUBSIDENCE
AFTER ZIEGLER (1975)

FIG. 5.2

The main centre of volcanism shifted to the West Scotland-Northern Ireland-Greenland region in the Paleocene as oceanic spreading of the Central Atlantic began. Paleocene through Eocene sedimentation was rapid, clastic and from the north-west (Greenland?); by the Oligocene the source had disappeared and muds and clays filled the saucer shapped depression of the North Sea.

Fig. 5.2, after W.H. Zeigler (1975), is a summary chart of the tectonic evolution of the North Sea. The dominant pattern in the evolution of the North Sea basin is clearly one of repeated orogeny followed by subsidence.

5.3 Geophysical Studies of the North Sea

Despite the vast amount of data gathered and in marked contrast to the recent release of geologic information from deep drilling, few results of oil exploration geophysical surveys have been published for the North Sea region. Further, apart from the region north-west of Shetland (cf. Bott, 1975) and the Norwegian Sea (Talwani and Eldholm, 1972) both of which lie outside the area of interest, the North Sea has been largely ignored, geophysically, by university research.

The gravity field of the North Sea has been mapped by Collette (1960) and Fleischer (1963). Collette (1968) has reviewed his earlier work, an isostatic anomaly map, in terms of crustal structure. Within the southern Anglo Dutch basin (Fig. 5.1) he notes the close correspondence of negative isostatic anomalies, typically of the order of 10-20 mgals., with the post Hercynian depotcentres. Further north a similar axial low in the isostatic anomaly map delineates the northern Central Graben, the Forties Basin and the Southern Viking Graben. The two lows are divided by an area of positive isostatic anomalies coincident with the structural highs; Mid North Sea, Ringkobing-Fyn, East Shetland Platform, etc. Collette argues that such small anomalies are consistent with the sedimentary basins being filled with about 5000 metres of material with a mass deficiency of 0.3 $gm \cdot cm^{-3}$, the

significant implication being that the North Sea basins are roughly in isostatic equilibrium. The free air map of Fleischer (1963) tends to support the Collette (1968) interpretation.

An aeromagnetic survey of the entire North Sea region was flown in 1962-63; the full results have yet to be released. Howitt et al. (1975) have demonstrated the coincidence of some intense short wavelength anomalies within the region of Jurassic volcanism, section 5.2. Domzalski (1975) has presented, though avoided publishing, aeromagnetic data from the Viking Graben region.

Collette et al. (1965, 1967, 1970) and Sornes (1971) have reported seismic refraction studies from the southern and northern North Sea regions respectively. The Collette et al. surveys, which were made in the area of Flamborough Head (0^{o}E, 54^{o}N) and the Dogger Bank (3^{o}E, 55^{o}N), gave poor results due, in part, to the complex crustal structure of these two areas. They (Collette et al.) computed crustal models based on depths to the Moho of 31 km., with 5-8, 17 and 6-9 kilometres of sediment, granitic and/or metamorphic, and gabbroic crust respectively. However, the authors emphasized the uncertainty of their models. The Flamborough Head refraction profile was thought to indicate crustal thickening to the north, ie. onto the structurally high Mid North Sea basement ridge. Collette et al. (1970) interpreted this, in the context of a region of supposed isostatic equilibrium, (Collette, 1968) to indicate an Airy type compensation mechanism.

The survey of Sornes (1971) was carried out between the Northern U.K. and the Norwegian coast. He obtained more reliable results indicating relatively thin crust (28 km.) beneath the Norwegian Channel and near the western margin of the Viking graben with the intervening crust thickening to 35 km. In marked contrast to the Collette et al. models, Sornes obtained much more normal crustal divisions of about 10 and 20 kilometres of granitic and/or metamorphic (6.1 $km \cdot s^{-1}$) and gabbroic (6.8 $km \cdot s^{-1}$) material respectively. Further west Sornes obtained slightly thinner crustal thicknesses (25-30 km.)

on a profile Shetland-Fair Isle-Aberdeenshire.

Willmore (1973) has reviewed land refraction data in the U.K.; crustal thicknesses of 28-30 km. for northern Britain are indicated. Sellevoll (1973) has compiled a similar survey for the adjacent Fennoscandia region. Here crustal thickness rapidly increases from a value of 30 kilometres at the coast and within the Oslo graben to over 40 kilometres in central Norway and Sweden.

Seismic reflection studies are limited to those few isolated profiles (cf. Brunstrom and Walmsley, 1969, Hornabrook, 1975) which have been published. The results, together with the schematic sections of Kent and Walmsley (1970), indicate rapid lateral variations in the thickness of the Zechstein evaporite in the Southern North Sea. Halokinesis has resulted in numerous domes, usually elongated with a 2-8 km. wide plug and a vertical rise of a few kilometres.

Karnik (1971) has compiled a 50 year seismicity map of west and north Europe. Apart from some activity along the Norwegian Channel, there are only two events (both greater than $M = 4.7$) indicated for the North Sea region. Some seismicity is indicated along the Great Glen fault, in the Scottish Tertiary volcanic province, and beneath the Pennine block.

We will return to aspects of the preceeding discussion in connection with crustal temperature profiles and mechanisms of subsidence in the North Sea, sections 5.5 - 5.7.

5.4 North-West European Heat Flow

The previously published heat flow results for the North-West European region adjacent to the North Sea are indicated in Fig. 5.3. No previous heat flow determinations have been made for the North Sea basin.

The values plotted for the U.K. are from the works of Benfield (1939), Anderson (1940), Bullard and Niblett (1951), Chadwick (1956),

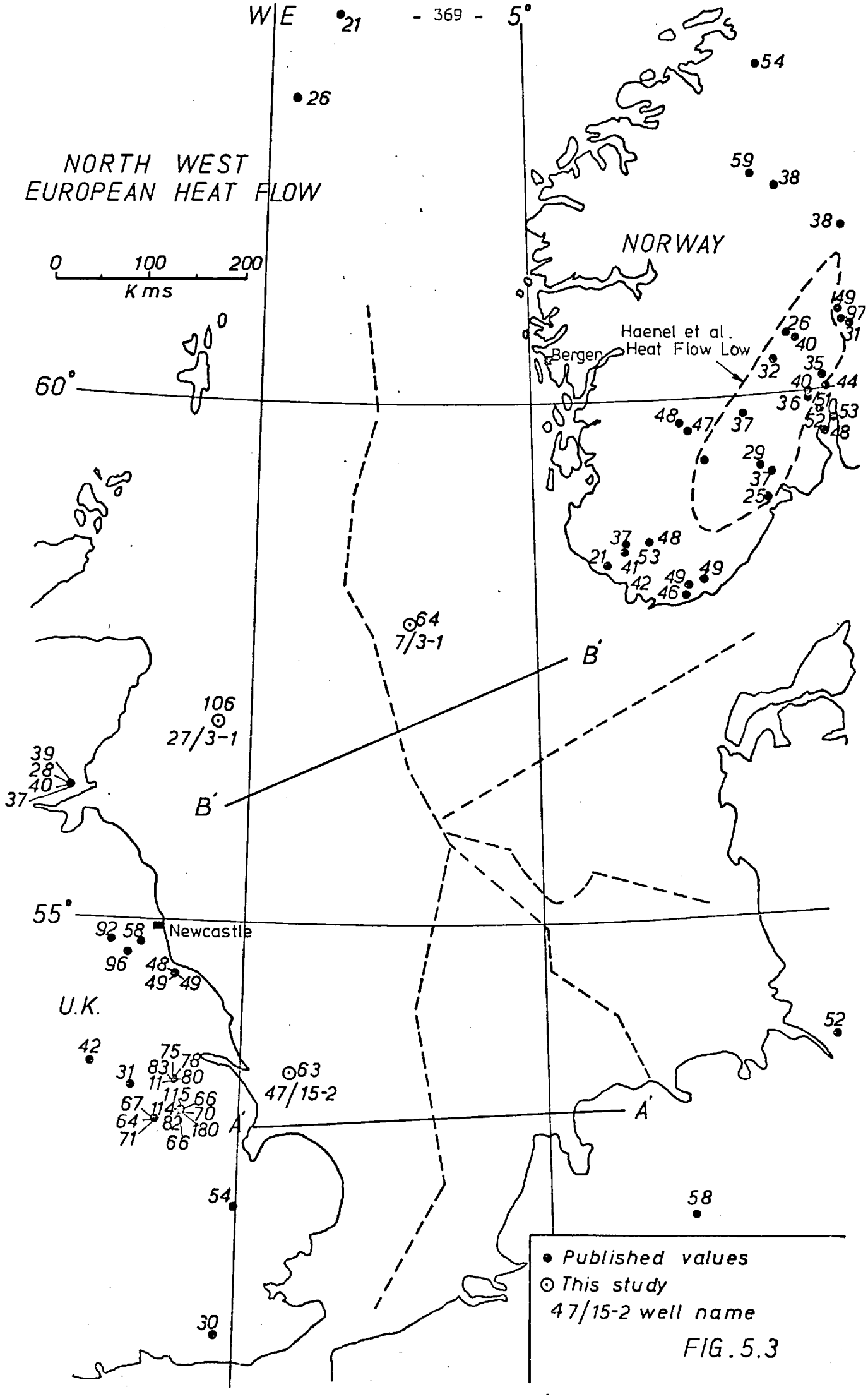

W
E
5°
NORTH WEST
EUROPEAN HEAT FLOW
0 100 200
Kms
NORWAY
Bergen
Haenel et al.
Heat Flow Low
60°
55°
Newcastle
U.K.
64
7/3-1
106
27/3-1
63
47/15-2
B
B'
A
A'
• Published values
⊙ This study
47/15-2 well name

FIG. 5.3

Mullins and Hinsley (1958), and Bott et al. (1972). The mean of the twenty-six values shown in Fig. 5.3 is 64.9 ± 26.4 $mW \cdot m^{-2}$. However, several of the high values (see Bullard and Niblett, 1951 and Bott et al., 1972), in Yorkshire and Nottinghamshire have been interpretted as water circulation anomalies; Lee and Uyeda (1965) have suggested that a U.K. heat flow mean of 54.8 ± 15.9 $mW \cdot m^{-2}$ from the seven most reliable values is a more representative average.

The two heat flow values from north-west Germany (Fig. 5.3) are from Haenel (1971). The more southerly of the two values is from a six kilometre deep borehole which Haenel believes to have been disturbed, possibly by a shallow heat source.

Swanberg et al. (1974) and Haenel et al. (1974) have obtained thirty-nine values from Norway of which thirty-four are shown in Fig. 5.3. The Norwegian mean is 41.9 ± 8.8 $mW \cdot m^{-2}$; this may be subdivided by tectonic regions into Fennoscandia (Baltic) Shield, 38.5 ± 9.2 (21 values), Caledonian Orogenic Zone, 44.4 ± 6.7 (12 values) and the Permian Oslo Graben, 46.9 ± 7.1 (6 values) with all heat flows in $mW \cdot m^{-2}$. Haenel et al. (1974) have delineated a region (Fig. 5.3) of low, mean 33.1 ± 5.4 $mW \cdot m^{-2}$, heat flow on the Fennoscandia Shield. They, as do Swanberg et al. (1974) attribute it to an anomalously low mantle heat flow.

Langseth and Zielinski (1974) have made a number of oceanic determinations in the Norwegian Sea, two of which plot on Fig. 5.3. The values, which lie near the foot of the Faeroe-Shetland escarpment, are, at 21 and 26 $mW \cdot m^{-2}$, very low. However, these two results are specifically discussed by the authors who consider them reliable. The values, which are as low or lower than those within the Haenel et al. (1974) anomaly form part of a broader trend within Langseth and Zielinski's work indicating decreasing heat flow as the Norwegian continental margin is approached.

Although there have been no previous heat flow determinations, per

se, for the North Sea basin proper, Harper (1971), Evans and Coleman (1974) and Cornelius (1975) have produced BHT derived geothermal gradient maps. Harper (1971) and Evans and Coleman (1974) estimated heat flows of 50-62 and 71-75 $mW \cdot m^{-2}$ respectively, on the basis of assumed 'average' values of conductivity. We will return to these gradient maps in section 5.5

Thermal conductivity samples were made available for three North Sea wells by Amoco Europe Inc. and Amoco U.K. Inc. (pers. comm., 1974). These wells, indicated on Fig. 5.3, were selected to provide as complete and representative a set of samples as possible of the entire North Sea sedimentary succession. Heat flow values, computed from the BHT, conductivity and lithologic data, are presented in tables 5.1, 5.2, and 5.3 and are analogous in layout with tables 4.1, 4.2, and 4.3, section 4.7. Details regarding the BHTs, conductivity data, and computation of heat flow were given in Chapters 1, 2, and 3 respectively. Table 5.3, the corrected heat flow values, contains an additional column compared with table 4.3. This is the column, headed Q_4, containing the heat flow values corrected for Pleistocene climatic variations, Figs. 3.2 and 3.3, section 3.4.

Figs. 5.4 - 5.6 are the composite heat flow plots, details of which were given in section 3.9. The northern-most well, 7/3-1, Fig. 5.4, was located along the western margin of the northern end of the Central Graben. The heat flow value, $Q_0 = 63.8\ mW \cdot m^{-2}$, table 5.2, was graded A (see section 3.9) and thought to be the most reliable of the three North Sea determinations. The second borehole, 47/15-2, was drilled along the western Dowsing fault margin of the Solepit Trough, a sub-basin of the Anglo-Dutch Basin. The heat flow value, $Q_0 = 62.7\ mW \cdot m^{-2}$, table 5.2, was graded B principally because of the rather large Bullard residual evident on the composite plot (Fig. 5.5) for the BHT at about 2000 metres. The final well, 27/3-1, Fig. 5.6, was drilled along the northern margin of the Mid North Sea high, a basement block of Lower Paleozoic sediments and metamorphics, which was uplifted during the lower Permian (P.A. Zeigler, 1975). The heat flow, $Q_0 = 106.1$

7/3-1

COUNTRY-NORTH SEA LAT-57D 51M N.
COMPANY-AMOCO LONG-02D 45M E.

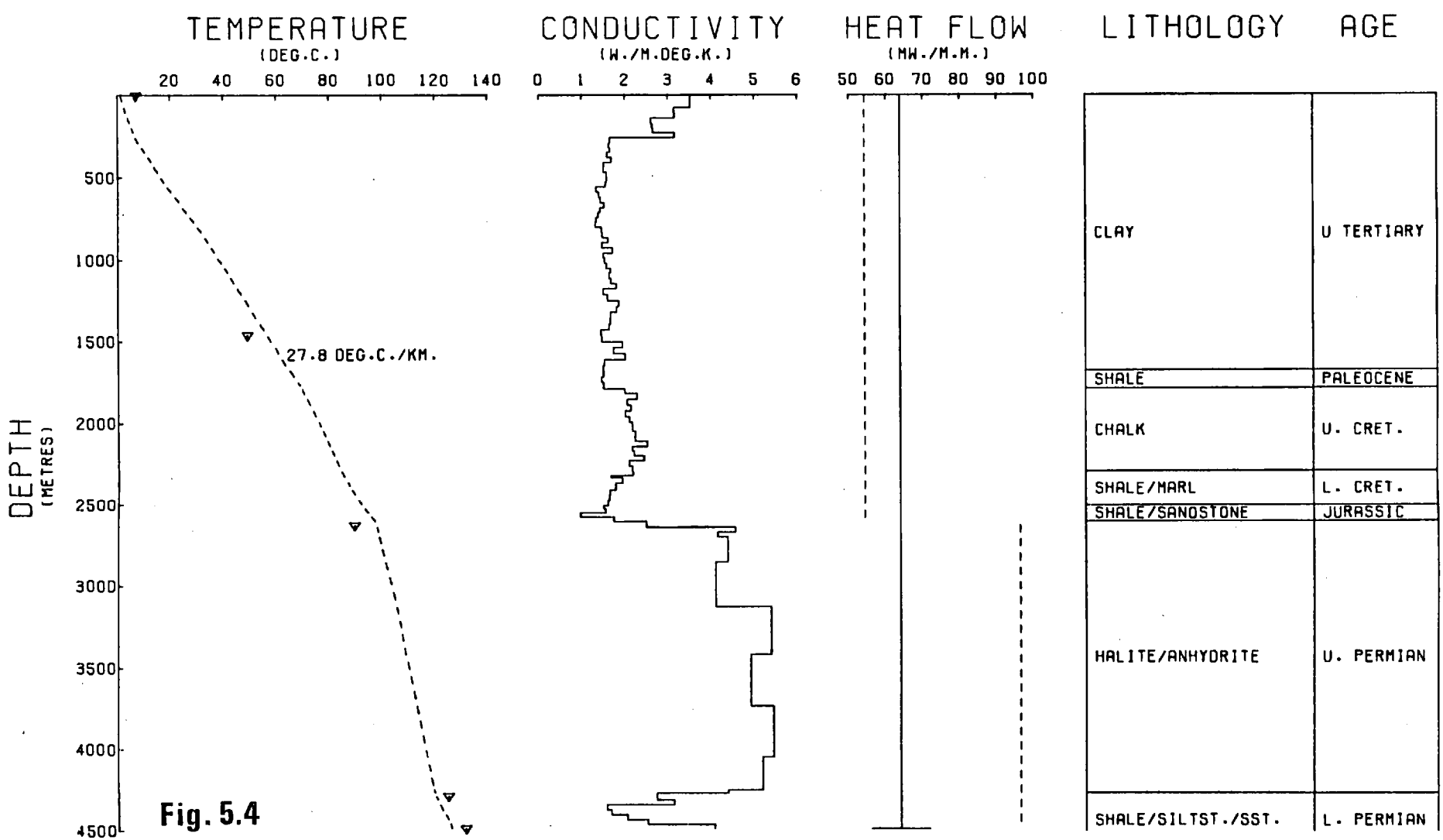


Fig. 5.4

47/15-2

COUNTRY-NORTH SEA LAT-53D 33M N.
COMPANY-AMOCO LONG-00D 54M E.

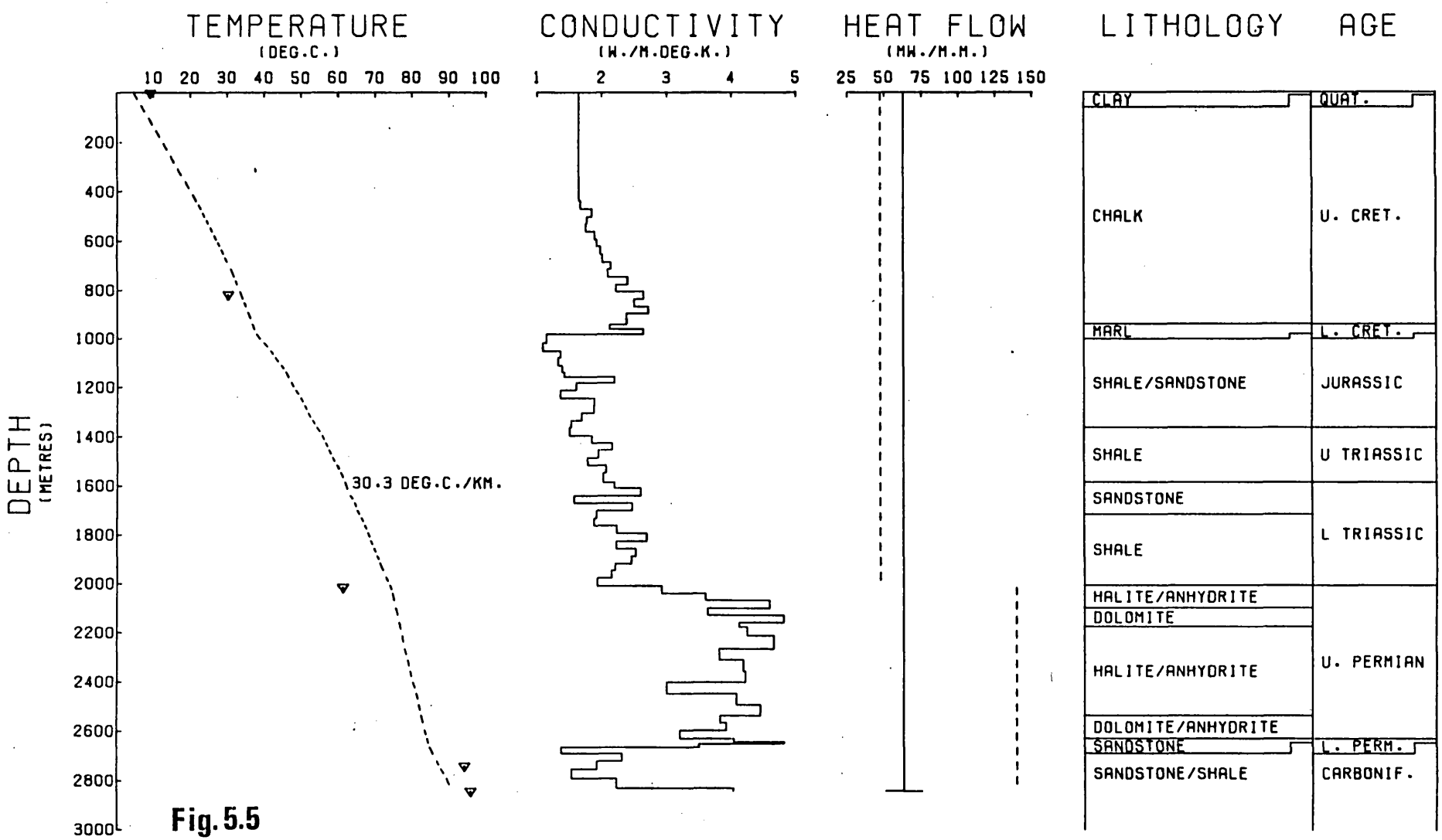


Fig. 5.5

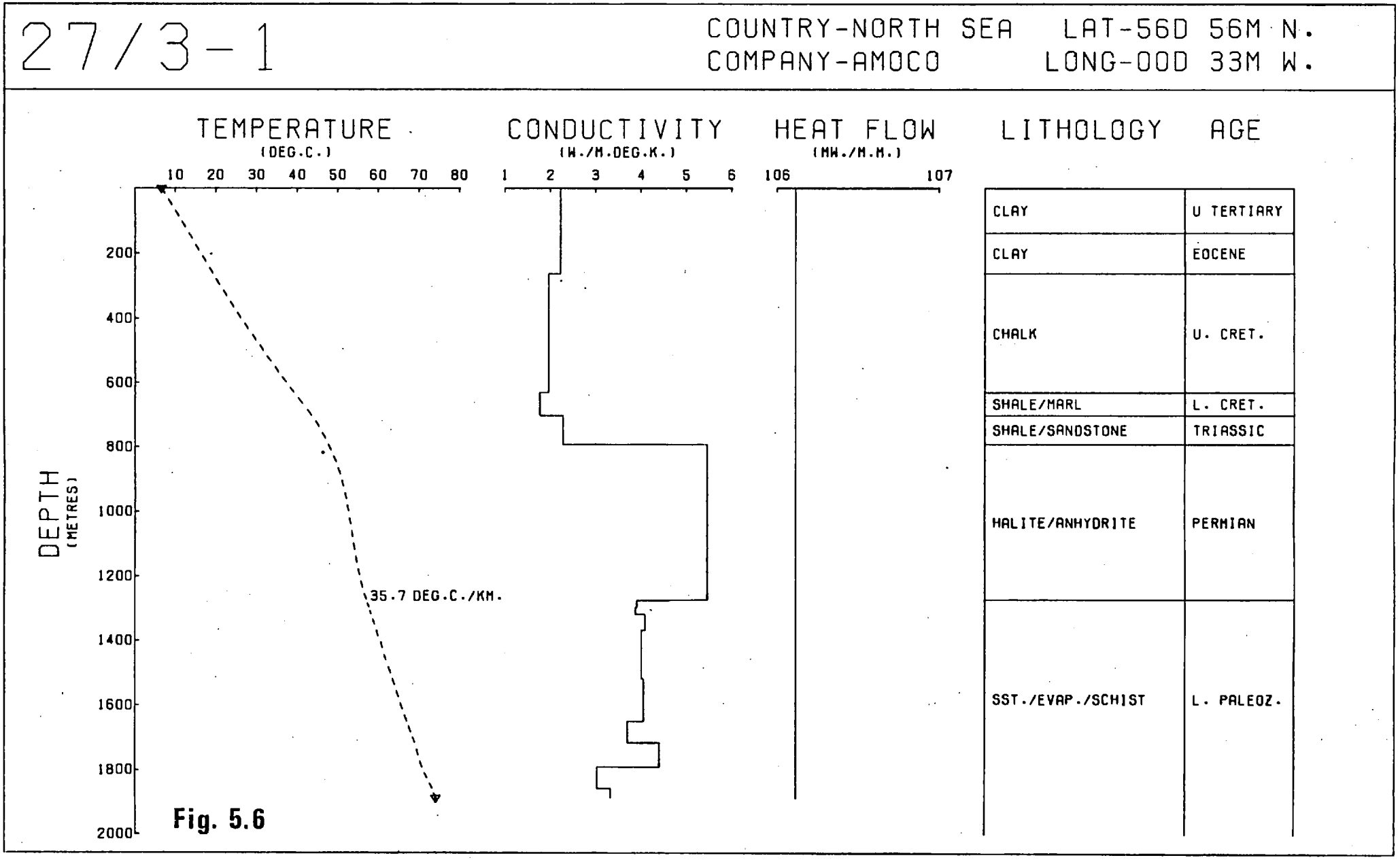

27/3-1
COUNTRY-NORTH SEA
COMPANY-AMOCO
LAT-56D 56M N.
LONG-00D 33M W.
TEMPERATURE
(DEG.C.)
10 20 30 40 50 60 70 80
CONDUCTIVITY
(W./M.DEG.K.)
1 2 3 4 5 6
HEAT FLOW
(MW./M.M.)
106 107
LITHOLOGY
AGE
DEPTH
(METRES)
200 400 600 800 1000 1200 1400 1600 1800 2000
35.7 DEG.C./KM.
CLAY
U TERTIARY
CLAY
EOCENE
CHALK
U. CRET.
SHALE/MARL
L. CRET.
SHALE/SANDSTONE
TRIASSIC
HALITE/ANHYDRITE
PERMIAN
SST./EVAP./SCHIST
L. PALEOZ.

Fig. 5.6

$mW \cdot m^{-2}$, table 5.2, was graded C as only a single BHT at 1889 metres was available.

The conductivity samples for both 7/3-1 and 47/15-2 were drill cuttings, core samples were available for the Zechstein and Lower Paleozoic sections of 27/3-1. Good well log porosity control (section 2.10) was available for the computation of porous rock conductivities for the chips. The unsampled 27/3-1 post-Zechstein section conductivities were estimated from lithologic log descriptions and the measured conductivities for similar units from 7/3-1 and 47/15-2. Appendix 6 gives a full listing of the raw data used in the heat flow computations for the three wells (see also section 3.9).

The values are clearly greater than the Norwegian and Faeroe-Shetland Escarpment results, Fig. 5.3, and marginally more than the North-West Germany values and the Lee and Uyeda (1965) preferred mean for the U.K. However, the 7/3-1 and 47/15-2 values are virtually identical with the mean U.K. value when all determinations are incorporated. Sclater and Francheteau (1970) indicate a mean heat flow of 64 $mW \cdot m^{-2}$ as characteristic of a tectonic province which last underwent folding and activation in the Mesozoic. Such a value is consistent with the two preferred North Sea results located, as they are, in an intracratonic basin last subjected to significant tectonism during the taphrogenic Kimmerian movements (Liassic-Malm).

The 27/3-1 value is clearly discordant. The high heat flow may be the result of rising thermal waters along an en echelon extension of the Highland Boundary Fault, the Mid North Sea high being widely interpreted as a fault bounded basement block (cf. Armstrong, 1972, Rhys, 1974). Alternatively the Permian uplift may have been associated with the emplacement of a relatively radioactive granite at shallow depth. Permian granites with high (3.5 - 4.0 $\mu W \cdot m^{-3}$) radioactivity are known in southern Norway (Swanberg et al., 1974) while Bott et al. (1972) give a value of 4.65 $\mu W \cdot m^{-3}$ for the Weardale granite (Devonian) in North Yorkshire. Further the 27/3-1 hole is relatively near the Jurassic volcanic province described by Howitt

et al. (1975). However, it is probably premature to speculate too deeply on the source of high heat flow in this region of the North Sea until the rather poorly determined 27/3-1 value is supported by more reliable results.

- HEAT FLOW RESULTS -

Table 5.1

North Sea - Borehole Descriptions

Well	Company	North Sea Sector	Latitude	Longitude	Depth (metres)	Rte (metres)
7/3-1	Amoco	Norway	57° 51' N.	02° 45' E.	4487	- 95
47/15-2	Amoco	U.K.	53° 33' N.	00° 54' E.	2843	- 53
27/3-1	Amoco	U.K.	56° 56' N.	00° 33' W.	1889	-101

Table 5.2

North Sea - Raw Data Results

Well	Number		Q_o	T_o	G_o	K_o	R
	BHTs	Conds.	m $W \cdot m^{-2}$	^oC	$^oC \cdot km^{-1}$	$W \cdot m^{-1} \cdot K^{-1}$	
7/3-1	4(5)	99	63.8 ± 4.0	1.2 ± 5.7	27.8 ± 1.7	2.30	A
47/15-2	4(5)	81	62.7 ± 6.2	4.5 ± 6.2	30.2 ± 3.0	2.07	B
27/3-1	1(2)	11(16)	106.1	6.5	35.7	2.97	C

Table 5.3

North Sea - Corrected Data Results

Well	Q_o $mW \cdot m^{-2}$	Q_1 $mW \cdot m^{-2}$	Q_2 $mW \cdot m^{-2}$	Q_3 $mW \cdot m^{-2}$	Q_4 $mW \cdot m^{-2}$	Sedimentation	
						Rate $cm \cdot 10^{-3} Yr^{-1}$	duratn $10^6 Yr.$
7/3-1	63.8 ± 4.0	59.6 ± 2.8	62.4 ± 3.2	66.3 ± 3.6	66.5 ± 3.0	2.0	300
47/15-2	62.7 ± 6.2	60.4 ± 5.5	62.3 ± 5.9	64.4 ± 6.0	65.5 ± 5.5	1.0	300
27/3-1	106.0	101.6	103.6	-	108.1	-	-

See text for definition of symbols; also tables 4.1, 4.2, 4.3, section 4.7.

5.5 Crust and Upper Mantle Thermal Profiles

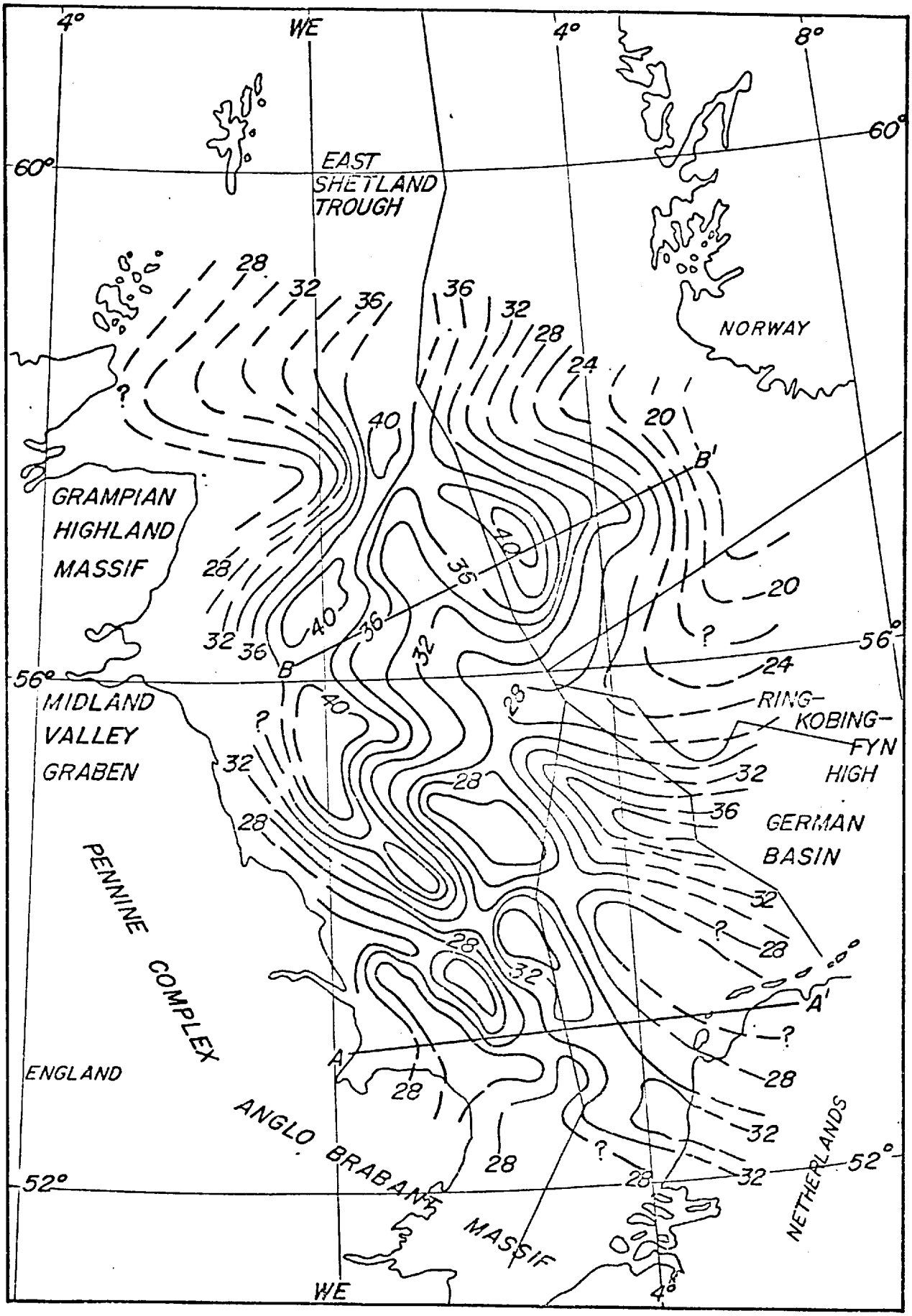
While useful in themselves, three values of heat flow in a region the size of the North Sea Basin do not convey any idea of possible lateral variations in the surface heat flow. Judge (1971) has demonstrated though, that where one is dealing with a single depositional environment, the thermal conductivity of the individual lithogic units is relatively constant. This would imply that where the regional sedimentary structure and geothermal gradient field are known, the surface heat flow might be computed provided a reasonable number of conductivity determinations have been made on each of the lithologic divisions.

Table 5.4 is such a compilation for 191 of the measured conductivity values for the three North Sea wells, Figs. 5.4 - 5.6, discussed in section 5.4. Most of the units show similar conductivity values despite the large distances between the wells.

Fig. 5.7, after Evans and Coleman (1974), is a geothermal gradient map of the North Sea. It was prepared from BHT data from 103 wells corrected, where possible, to equilibrium values (sections 1.4 - 1.6). Two profiles, A-A' and B-B', are indicated; they are also shown on Figs. 5.1 and 5.3. Evans and Coleman, with these profiles, obtained estimated heat flow profiles using thermal conductivities consistent with the published lithologic descriptions and the geologic structure sections of Armstrong (1972). These calculations have been repeated here using the conductivity values of table 5.4, column 7. The results, together with an interpolated isostatic anomaly profile from Collette (1960) are shown as Figs. 5.8a and 5.8b.

Evans and Coleman (1974) indicated that the mean heat flows on A-A' and B-B' were approximately equal (75 and 71 $mW \cdot m^{-2}$ respectively) despite the higher gradients to the north; the revised values (64 and 65 $mW \cdot m^{-2}$ respectively) do not alter this conclusion. Evans and Coleman also proposed, on the basis of their profiles, an apparent decrease in heat flow towards the European continent. The profile B-B' still supports such a view;

North Sea Geothermal Gradients

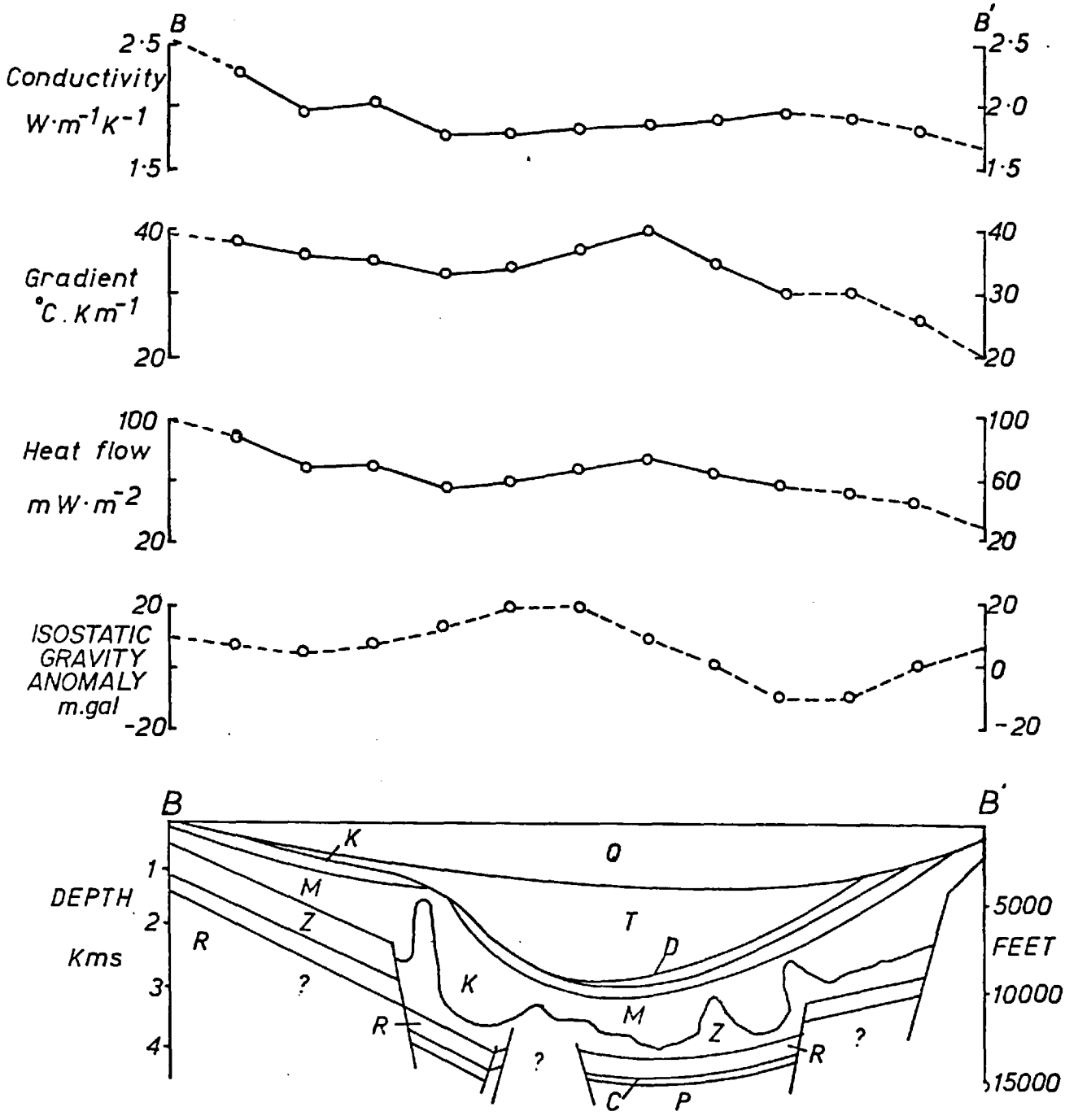


Contour Interval = 2°C Km

after Evans and Coleman (1974)

FIG. 5.7

CENTRAL NORTH SEA PROFILE

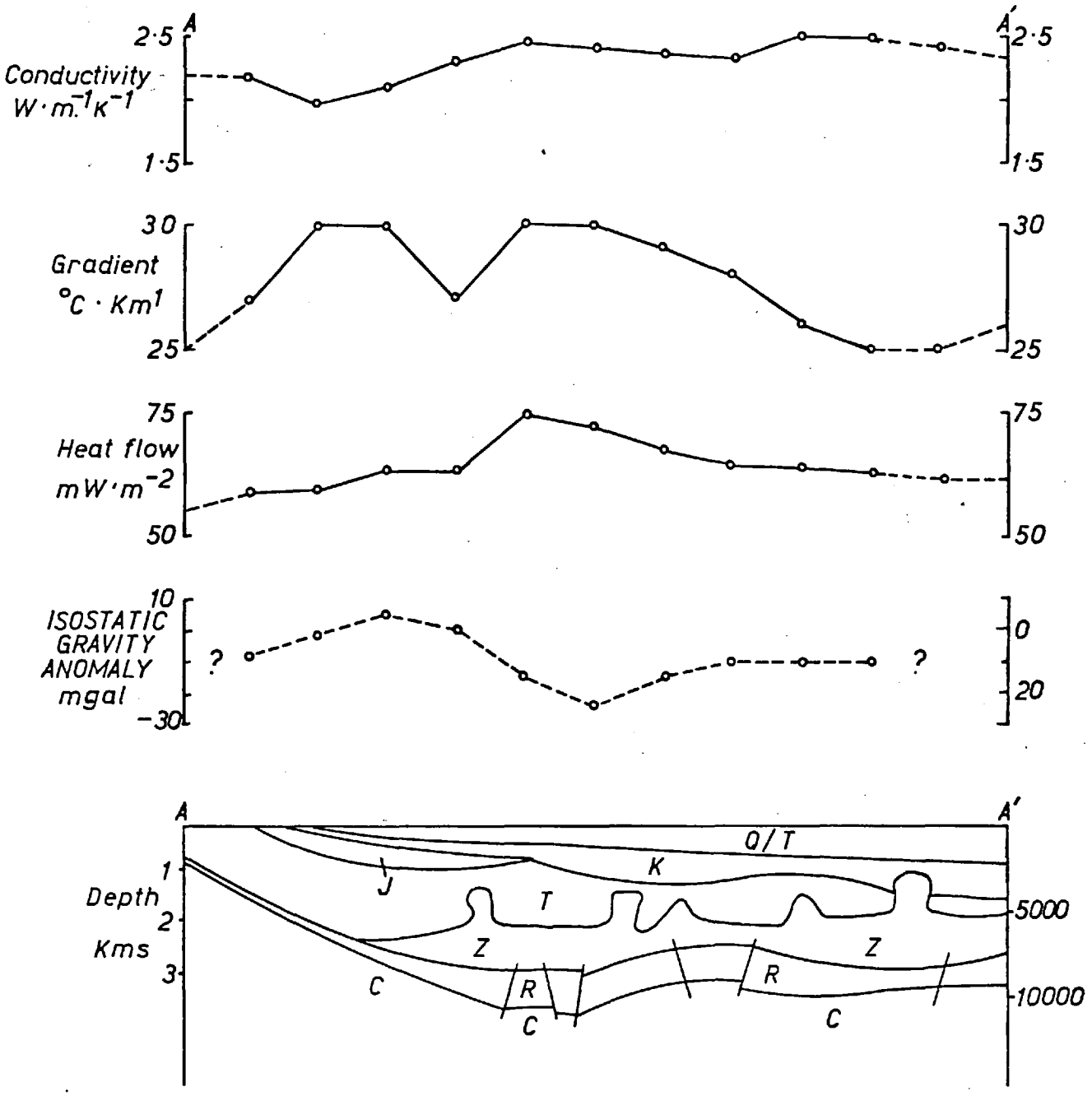


Q - Quaternary
T - Tertiary
D - Danian
K - Cretaceous
M - L. Cretaceous + Jurassic
Z - Zechstein
R - Rotleigendes
C - Carboniferous
P - Lower Paleozoics

Gravity interpolated from Collette (1960)
Geologic profile from Armstrong (1972)

FIG. 5.8a

SOUTHERN NORTH SEA PROFILE



Q/T Quaternary / Tertiary
K Cretaceous
J Jurassic
T Triassic
Z Zechstein
R Rotleigendes
C Carboniferous

Gravity interpolated from Collette (1960)
Geologic profile from Armstrong (1972)

FIG 5.8b.

A-A' now indicates a small, 10-15 $mW \cdot m^{-2}$, maximum in the central southern North Sea. The high heat flows to the west on profile B-B' are based on limited temperature data; if the region is indeed lower in heat flow than shown, the two profiles might show a similar small axial heat flow anomaly, roughly coincident with the centre of deposition and subsidence.

Precisely determined reservoir temperatures of 90°C at the Forties (57° 40' N, 1° 0' E) oil field (unpub. obs.) and 129°C at Ekofisk (56° 30' N, 3° 10' E) oil field (Dunn et al., 1973) yield gradients of 39 and $37°C \cdot km^{-1}$. These two reservoirs, the former in the Paleocene the latter in the Danian, directly underly a uniform upper and middle Tertiary clay and mudstone sequence. Table 5.4 indicates a conductivity of about 1.8 $W \cdot m^{-1} \cdot k^{-1}$ for this lithologic unit. The heat flows of 70 (Forties) and 67 $mW \cdot m^{-2}$ (Ekofisk) are consistent with the northern profile B-B'.

The geologic profiles, Figs. 8a and 8b, of Armstrong (1972) are, strictly, schematic representations only. The published isopach maps of Dunn et al. (1973) offer a more precise picture of the regional sedimentary structure. Recomputing a limited number of profile points from the isopach maps indicated that this further sophistication would not significantly alter either profile.

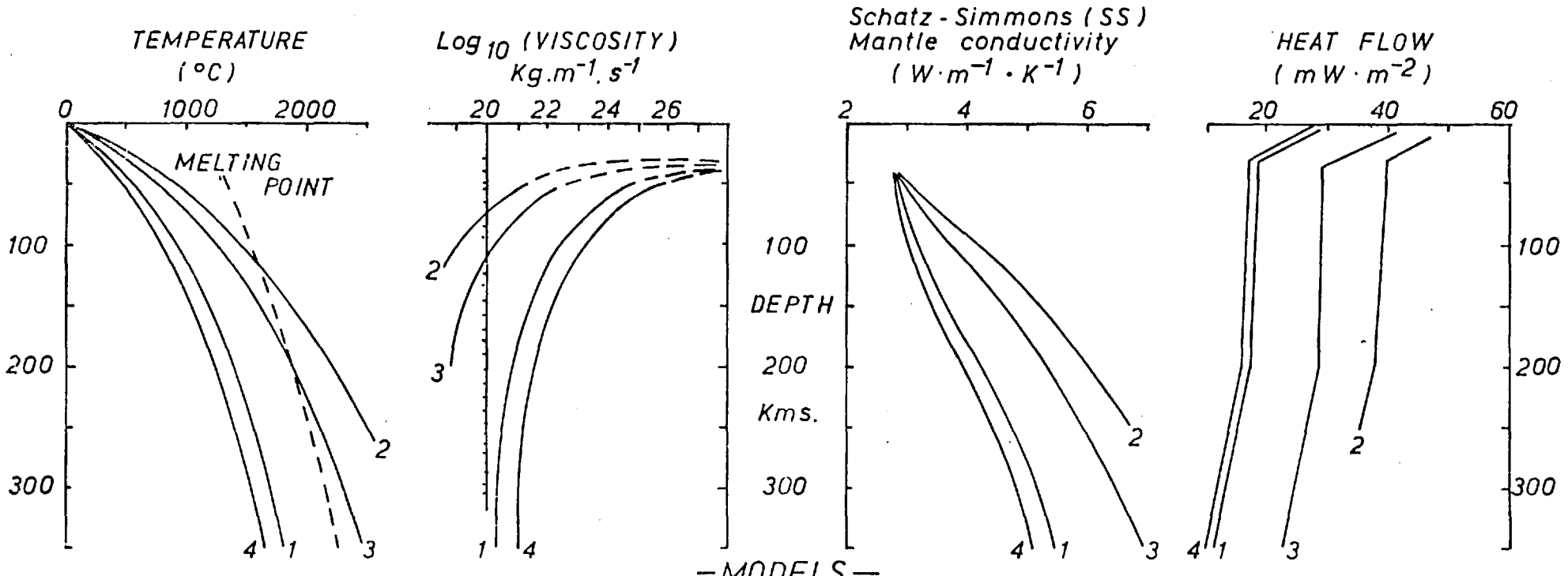
In section 4.21 a discussion of the computation of crust and upper mantle vertical temperature profiles was given. Four conductivity heat production models were calculated in a manner analogous to those shown in Fig. 4.96. Two North Sea models, A and B, are proposed, the former follows the Collette et al. (1970) refraction results, the latter the Sornes (1971) refraction results. Two further models, the United Kingdom and Southern (Fennoscandia Shield) Norway, are also incorporated. The crustal heat production and conductivity values for the North Sea follow Smithson and Decker (1974); the United Kingdom and Southern Norway values are consistent with the platform and shield models, respectively, of Sclater and Francheteau (1970).

The models and results are shown in Fig. 5.9. The North Sea A model (curve 1) is almost certainly unrealistic giving a temperature profile little different from that of Southern Norway (curve 4). This is due entirely to the unreasonable thickness of granitic/metamorphic 'velocity type' crust computed by Collette et al. (1970). The Sornes result, curve 2, North Sea B, is the preferred model. The temperature curve indicates a possible partial melt in the range 80-120 km; the viscosity is reduced to base of lithosphere values (10^{20} $kg \cdot m^{-1} \cdot s^{-1}$) at about 80 km. (Chapman and Pollack, 1974).

The United Kingdom model, curve 3, was computed using the mean heat flow incorporating all the data shown in Fig. 5.3. The temperature curve indicates a possible partial melt between 160-200 km; the viscosity drops to 10^{20} $kg \cdot s^{-1} \cdot m^{-1}$ at 120 km.

The South Norway shield curve does not indicate a probable partial melt at depth; the lithosphere is of the order of 400 km. thick in this region. These conclusions are consistent with those of Sellevoll and Pomeroy (1968) who, on the basis of a travel time study for Fennoscandia, propose a crust and upper mantle structure similar to that of the Canadian Shield. Brune and Dorman (1963) have demonstrated that the low velocity zone is deeper and less pronounced, or absent, beneath the Canadian Shield.

THE VARIATION OF TEMPERATURE (T), VISCOSITY, Mantle conductivity (K), and HEAT FLOW (Q), with Depth (Z), for the NORTH SEA and The surrounding Regions



—MODELS—

1	Q_o = 63 T_o = 6	Z
	A = 1·0 , K = 2·2	5
	A = 2·1 , K = 2·7	22
	A = ·4 , K = 2·1	31
	A = ·01 , K = SS	200
	A = ·04 , K = SS	

NORTH SEA 'A'

2	Q_o = 63 T_o = 6	Z
	A = 1·0 , K = 2·2	5
	A = 2·1 , K = 2·7	10
	A = ·4 , K = 2·1	30
	A = ·01 , K = SS	200
	A = ·04 , K = SS	

NORTH SEA 'B'

3	Q_o = 65 T_o = 10	Z
	A = 3·0 , K = 2·7	8
	A = ·4 , K = 2·1	36
	A = ·01 , K = SS	200
	A = ·04 , K = SS	

UNITED KINGDOM

4	Q_o = 39 T_o = 10	Z
	A = 1·3 , K = 2·7	8
	A = ·4 , K = 2·1	36
	A = ·01 , K = SS	200
	A = ·04 , K = SS	

SOUTHERN NORWAY

FIG 5.9

Table 5.4

Thermal Conductivity of North Sea Sedimentary Rocks

Age	Formation	Dominant Lithology	7/3-1	47/15-2	27/3-1	Weighted Mean ($W \cdot m^{-1} \cdot K^{-1}$)
Post Paleocene	-	clay	1.76 ± .52(51)	No Samples	No Samples	1.74
Paleocene	-	shale	1.47 ± .03(3)	Absent	Absent	
U. Cretaceous	-	chalk	2.16 ± .14(16)	2.08 ± .33(17)	No Samples	2.07
L. Cretaceous	-	shale/marl	1.76 ± .21(7)	2.37 ± .36(2)	No Samples	
Jurassic	-	shale/sst	1.41 ± .33(4)	1.51 ± .32(13)	Absent	1.49
U. Triassic	Keuper	shale/marl	Absent	1.84 ± .28(5)	No Samples	2.10
M. Triassic	Muschelkalk	evap./shale	Absent	2.05(1)	No Samples	
L. Triassic	Bunter	sst/shale	Absent	2.19 ± .31(15)	No Samples	
U. Permian	Zechstein	evap./carb.	4.53 ± .84(11)	3.94 ± .56(17)	5.45(1)	4.22
L. Permian	Rotleigendes	sandstone	2.50 ± .89(7)	4.41 ± .55(2)	Absent?	2.92
Carbonifer.	Coal Measures	shale/sst	-	2.82 ± 1.23(9)	Absent?	2.82
L. Paleozoic	-	lst./sst./ metamorph.	-	-	3.89 ± .47(10)	3.89

Number of samples measured in brackets

5.6 Heat Flow and the Subsidence of the North Sea Intracratonic Basin

The discussion of the geological evolution of the North Sea basin, section 5.2, emphasized the almost continuous post-Hercynian subsidence, Fig. 5.2, and the contemporaneous accumulation of some 5-10 kilometres of sediments. Possible mechanisms controlling such subsidence have been reviewed in section 4.20. Subsidence within an intracratonic region may well be more complex than at a continental margin (section 4.20); further, mechanisms of subsidence plausible in one region may not be relevant in the other. Sediment loading of the continental slope and rise and concomitant subsidence of the shelf due to lithospheric flexural rigidity (Walcott, 1972), while a possible Eastern Africa model of subsidence,is patently inconsistent with the tectonic setting of the North Sea.

Subsidence induced by oceanward hot creep (Bott, 1971a) would, at first glance, also appear unlikely as the mechanism is dependent on the presence of a stress field induced by the juxtaposition of oceanic and continental crust. However, Bott and Dean (1972) have, assuming an elastic lithosphere, demonstrated that the stress field at a young rifted continental margin does not decrease away from the margin in the direction of the continent. Further, the stress field may be induced by other mechanisms than a density contrast, ie. lateral variations in crustal temperature. Nevertheless it is, as Le Pichon et al. (1973) state, difficult to visualize hot creep induced subsidence of an intracratonic basin.

Collette (1968) has dealt directly with the subject of North Sea subsidence. He envisages a process of crustal thinning inducing subsidence to maintain an Airy type isostatic equilibrium (Collette, 1960, Collette et al., 1970). Collette invokes an upward migration of a postulated basalt-eclogite phase transition resulting from a pressure perturbation due to an initial loading of sediments (see section 4.20). Bott (1971a) has criticised the mechanism, principally on the lack of petrological evidence for a phase transition Moho. However, the crust may be thinned by regional extension.

W.H. Zeigler (1975) has postulated that the North Sea basin has been trapped in the extensional quadrant of a shear ellipse since the Caledonian orogeny.

P.A. Zeigler (1975) has proposed a subsidence model linked to the Jurassic taphrogenic stage in the evolution of the North Sea. Regional extension initially thins the crust to the extent of temporarily decoupling the crust and mantle and inducing fractional distillation in the upper mantle (Artemjev and Artyushkov, 1971). This results in a 'rift cushion', of low density (3.1), low P velocity (7.5 - 7.9 $km \cdot s^{-1}$) mantle material, and regional doming (Illies, 1970). Subsidence occurs within a central 'rift' valley while the uplifted margins are eroded. However, the major regional subsidence takes place in the post-rifting stage when the low density - low velocity cushion is reabsorbed into the mantle (Osmaston, 1971). P.A. Zeigler (1975) proposed such a model to account for the saucer shaped Tertiary basin of the North Sea (Dunn et al., 1973).

The thermal contraction continental subsidence model of Sleep (1971) was discussed in section 4.20. Suprisingly, Sleep found that his exponential decay subsidence model was also consistent with the sedimentological record of intracratonic basins in the central United States. Perhaps a thermal contraction of the North Sea lithosphere after the Jurassic rifting and volcanism was the mechanism of the Tertiary subsidence. Bott (1973) has pointed out, though, that the amount of isostatic subsidence induced by subareal erosion in Sleep's model is unlikely to amount to more than 2 kilometres; Dunn et al. (1972) indicate over 3 kilometres of sediments at the centre of the North Sea Tertiary depression. Further it is quite evident from the thick Quaternary sequence in the North Sea (ie. over 400 metres in the 7/3-1 well, Fig. 5.4) that subsidence and sedimentation rates are most probably not decreasing.

The thermal metamorphism model of Falvey (1974) was also reviewed in section 4.20. The North Sea mean heat flow of 63 $mW \cdot m^{-2}$ would indicate

a maximum subsidence of about 5 kilometres, Fig. 4.95. The source of increased heat flow may have been the Jurassic taphrogenic-volcanic period; the Upper Paleozoic subsidence may have been linked with the additional heat input of the Hercynian orogeny. However, the Falvey model, which is essentially a mechanism of increasing mean crustal density, would also predict a zone of high, 7.0 - 7.2 $km \cdot s^{-1}$, velocity material in the lower crust. The refraction studies of Collette et al. (1970) and Sornes (1971) do not support such a value.

Finally, it should be noted that the subsidence of the North Sea has involved a number of complex differential movements. These have included the uplift of the structural highs (Mid North Sea, Ringkobing-Fyn, Mid Netherlands, etc.). Collette (1968) has proposed eutectic melts, resulting from deep subsidence and burial, and with eventual recovery of thermal equilibrium, rising as ridges or diapiric structures. The geothermal gradient maps of Harper (1971), Evans and Coleman (1974) and Cornelius (1975) indicate low, 20-25 $^{o}C \cdot km^{-1}$, values over the positive structural elements. Such values would not tend to support Collette's theory of their origin.

5.7 The Effect of Local Structure on Heat Flow Determination

The selection of an oil exploration drilling site is, almost invariably, made on a structural high or a stratigraphic culmination; the classic petroleum traps. If the folded or faulted sedimentary units have significant lateral conductivity and/or heat production contrasts, the thermal field will be distorted in proximity to the discontinuity.

In section 4.22, the modelling of such two dimensional structures was reviewed. A finite difference program capable of such modelling was described and gross crustal structures were analysed. The program is also suitable for the modelling of small scale structures of the order of a few kilometres.

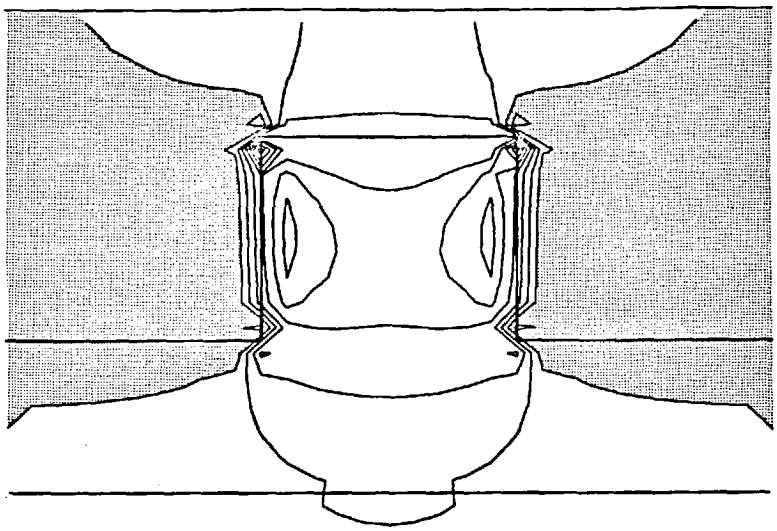
The principal mechanism for the formation of such small scale structure in the North Sea is halokinesis. The Zechstein halite has flowed to form many salt pillows (anticlines) and plugs (piercement structures) throughout the central and southern North Sea (Sorgenfrei, 1969, Brunstrom and Walmsley, 1969). The upward flow results from gravitational instability due to the low (2.0 - 2.2 $gm \cdot cm^{-3}$) density halite. The dimensions of the domes are typically 2-8 km. across and a few kilometres high.

A salt dome model is shown in Fig. 5.10 (structure lines dashed). The top of the dome is 2.0 km. beneath the ground level; it is 4 km. across and rises 3.2 kilometres from its source. The conductivity values have been assigned to represent Zechstein salt intruding a Tertiary clay with a base of Carboniferous rocks. The values are from table 5.4. No heat production contrasts were considered.

The isotherms in Fig. 5.10 clearly indicate non-uniform heat flow in and around the dome as one would intuitively expect. The isotherm plot is similar to that obtained by Mundry (1966) for a salt dome with somewhat larger conductivity contrasts. Above the isotherm configuration, Fig. 5.10, is a contoured display of the anomalous vertical heat flow, the stippled region being negative. Two symetrical highs, of 50 $mW \cdot m^{-2}$, indicate that such a dome is indeed an effective heat guide. The result is quite similar to that obtained by Giesal and Holtz (1970), (reproduced without details of computation in Kappelmeyer and Haenel, 1974), for a salt diapir in Germany.

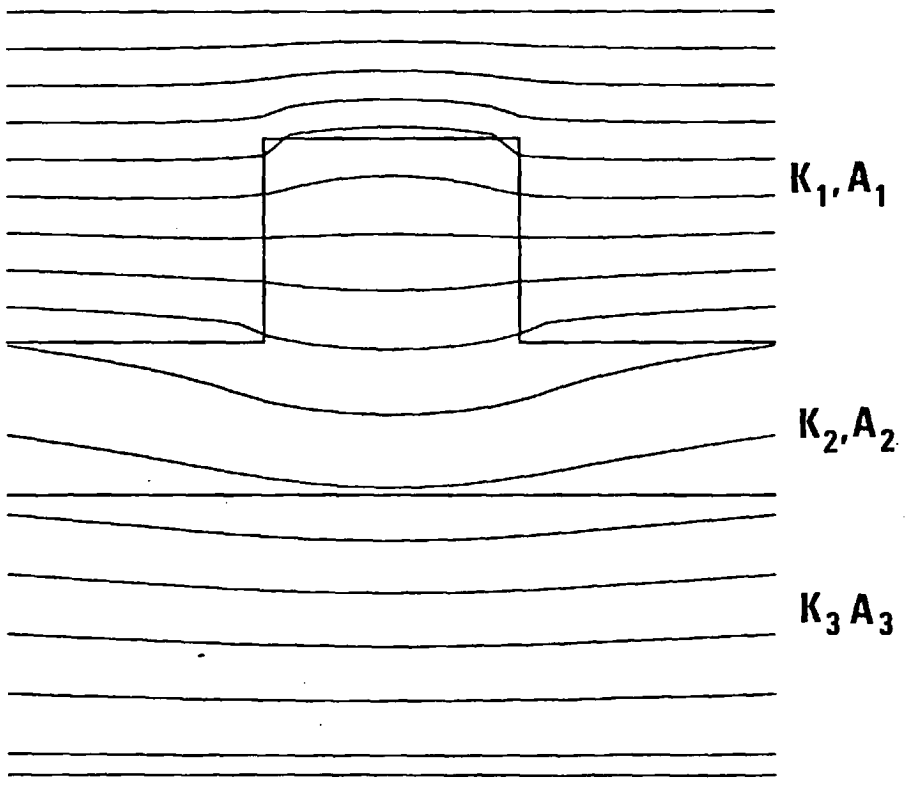
The two North Sea wells, 7/3-1 and 47/15-2, illustrated in Figs. 5.4 and 5.5 respectively, were almost certainly located on some form of a salt structure. The large positive variation of the upper to lower component of heat flow, of the order of 40-80 $mW \cdot m^{-2}$, in the Zechstein (halite) section of these two holes, might easily be explained by such a steady state disturbance of the thermal field.

ANOMALOUS HEAT FLOW
CONTOUR INTERVAL = 10 MW/M.M



negative anomalous heat flow stippled

ISOTHERM CONFIGURATION
CONTOUR INTERVAL = 20 DEG.C.



NORTH SEA SALT DOME

CONDUCTIVITY, $K_1 = 1.74, K_2 = 4.22, K_3 = 2.82$
HEAT PRODUCTION, $A_1 = 0.00, A_2 = 0.00, A_3 = 0.00$
SCALE = 12 KM. SQUARE, STRUCTURE LINES HEAVY

Fig. 5.10

Chapter 6

Conclusions

6.1 Objectives

Three major thesis objectives were outlined in the Introduction. They were:

1. To evaluate the potential of oil exploration well Bottom Hole Temperatures and drill cuttings as a source of raw data for heat flow calculations.

2. To conduct and interpret a regional heat flow survey of Eastern Africa entirely from such data.

3. To conduct a limited survey of the North Sea basin to further evaluate the detailed geothermal gradient maps of this area (Harper, 1971, Evans and Coleman, 1974, Cornelius, 1975).

Objective 1. has, within certain limits, been met. Where care and discrimination are exercised in the gathering of BHT data (Chapter 1), and the measuring of porous rock conductivities from chips (Chapter 2), heat flow values may be calculated and corrected (Chapter 3), such that the end results show internal consistency and are comparable with nearby values obtained by more conventional methods (Chapters 4 and 5). However, it must be emphasized that oil exploration well data derived heat flow values may incorporate significant systematic error. At present, the internal consistency of the data is the only basis on which to estimate the reliability of an individual heat flow determination. Where possible, a number of determinations should be made in a series of closely spaced holes.

Objective 2. has been largely fulfilled (Chapter 4). Sixty-eight determinations of heat flow, thirteen of them in the class A (<15% error)

grade, were made. Several significant results were obtained and are reviewed in section 6.2.

Objective 3. has, in a limited sense, also been achieved (Chapter 5). The computation of three heat flow values and of a large number of sedimentary thermal conductivities has considerably augmented the previously mentioned geothermal gradient studies.

6.2 Significant Results

A number of significant results, both pertaining to the technical aspects of obtaining heat flow values from oil exploration well data and from the two regional studies, have emerged. They are:

1. That Bottom Hole Temperatures (BHTs) are, on average, within $4^{o}C$ of equilibrium during the recording of the final commercial well log (section 1.6). This is sufficiently precise to allow the computation of a geothermal gradient to within 10% - 15%.

2. A rigorous study of porous rock thermal conductivities derived from solid core equivalent chips establishes the validity of the Sass et al. (1971) technique (Chapter 2). It does not support the Sass et al. findings that the geometric mean model is superior to the Maxwell spheres model for computation of whole rock and porous rock chip conductivities.

3. A detailed study of the variation of thermal conductivity with temperature for a wide variety of rocks supports those empirical relations obtained by Tikhomirov (1968) and Anand et al. (1973) on a much more restricted range of rock types (section 3.7).

4. Sixty-eight new heat flow values are presented for coastal Eastern Africa (section 4.7); their preferred mean is 64 ± 26 $mW \cdot m^{-2}$.

5. Eight new Red Sea results have considerably extended the heat flow coverage away from the zone of axial spreading in this young proto-ocean.

The results are consistent with the McKenzie (1967) lithospheric spreading model (section 4.9).

6. A previously unknown thermal low, mean 44 $mW \cdot m^{-2}$, was established for the Eastern Ogaden region (section 4.13).

7. A previously unknown thermal high, 89 $mW \cdot m^{-2}$, was jointly established with Williamson (1975) for the Garissa region of Kenya (section 4.17).

8. The heat flow data was compared with that of the surrounding regions; the 5 x 5 degree average map was updated (section 4.7) and a trend surface analysis of the North-West Indian Ocean and Eastern Africa region was performed (section 4.19). A thermal high over the Mascarene Plateau was found. A positive correlation of gravity-heat flow-magnetics was tentatively proposed (see also section 6.3).

9. One and two dimensional crust and upper mantle temperature profiles were computed for various Eastern Africa models. The Ogaden lithosphere is postulated to be sufficiently thick to impede plate motion. Shallow partial melt zones may exist beneath the Red Sea shelf and the Garissa Region. Both the Garissa Region and Ogaden anomalies may be alternately explained by two dimensional heat production - conductivity contrast structures within the crust, (sections 4.21 and 4.22).

10. Three new heat flow values are presented for the North Sea (section 5.4); their preferred mean is 63 $mW \cdot m^{-2}$.

11. The 191 North Sea conductivity results were used to re-interpret the Evans and Coleman (1974) heat flow profiles, (section 5.5).

12. One and two dimensional crust and upper mantle temperature profiles were computed for various North Sea region models. The results indicate a slightly thin lithosphere under the North Sea (80 km.) while the asthenosphere may be absent under the southern Norway Fenno-Scandia

Shield. A two dimensional model of a high conductivity contrast salt dome emphasizes the importance of local structure on heat flow determinations in oil exploration boreholes (section 5.7).

13. The mechanisms of subsidence for both Eastern Africa and the North Sea are discussed and evaluated in the context of the tectonic setting and surface heat flow of these two regions (sections 4.20 and 5.6). It is the author's opinion that no single mechanism of subsidence is likely to have dominated and/or persisted over the 200-400 million years during which these two regions have more or less continuously subsided. Further, it is concluded that heat flow measurements will not provide any significant insight into the type(s) of subsidence mechanism(s) active at an Atlantic type continental margin (see also section 6.3).

6.3 Suggestions for Future Research

Suggestions for future research connected with technical aspects of the BHTs, conductivity and computation of heat flow, may be found in sections 1.10, 2.17 and 3.10, respectively. Suggestions for extending and improving Chapters 4 and 5 are:

1. An effort should be made to secure conductivity data from the Sinclair holes (Fig. 4.1), and the B-1 and Hol-1 wells. Further, the conductivity data for the Tenneco wells (Fig. 4.1) should be augmented. All of the heat flow values for these wells would be made significantly more reliable with such data.

2. A few new wells, two in Eritrea, one in the Zanzibar channel, might be usefully added to these results. The latter would be most interesting to confirm the low (35 $mW \cdot m^{-2}$) heat flow obtained on Zanzibar Island.

3. An effort might be made to obtain more North Sea data, particularly from the Viking Graben region, which was poorly represented on the

Harper (1971), Evans and Coleman (1974) and Cornelius (1975) gradient maps. As the North Sea oil fields come into production, more reservoir temperature data might usefully be obtained.

4. The tentative gravity-heat flow-magnetic positive correlation from the satellite potential field and trend surface maps deserves further study. An effort might be made to provide a plaussible explanation for this speculative correlation as well as extending the study to other areas.

5. The mechanism of subsidence at an Atlantic type continental margin is clearly complex and, most probably, only indirectly related to the present day crustal temperatures. However, knowledge of the paleogeothermal regime, particularly that established during the initiation and subsequent progressive subsidence of the margin, might provide consider- insight into and differentiation of the possible subsidence mechanism (sections 4.20 and 5.6). Recent developments by oil company researchers have established several techniques for obtaining maximum paleotemperatures from shale type rocks. The implications for heat flow research are obvious.

LIST OF REFERENCES

Admirality, Bathymetric, magnetic and gravity investigations, H.M.S. Owen, 1961-1962, Marine Science Publication, (IIOE), London Hydrographic Department, HD 539, 1963.

Allan, T. D., Magnetic and gravity fields over the Red Sea, Phil. Trans. R. Soc. Lond. A, 267, 153-180, 1970.

American Association of Petroleum Geologists, (AAPG), Geothermal Survey of North America, map, scale 1:1,000,000, 1973.

American Standards of Testing Materials, (ASTM), Manual on the use of thermocouples in temperature measurement, ASTM spec. pub. 470, Phillidelphia, Penn., 1970.

American Standards of Testing Materials, (ASTM), ASTM test number C177, Phillidelphia, Penn., 1971.

Amoco Europe Inc., Personal communication, London, England, 1974.

Amoco (U. K.) Exploration Co., Personal communication, London, England, 1974.

Anand, J., Somerton, W. H., and Gomaa, E., Predicting thermal conductivities of formations from other known properties, Soc. Pet. Eng. J., 13, 267-273, 1973.

Anderson, D. L., and Sammis, C., Partial melting in the upper mantle, Phys. Earth Planet. Interiors, 3, 41-50, 1970.

Anderson, E. M., The loss of heat by conduction from the Earth's crust in Britain, Proc. Roy. Soc. Edinburgh, 60, 192-209, 1940.

Andreae, C., La prevision des temperatures souterraines, Ann. Ponts et Chaussees, 128, 37-85, 1958.

Anglin, F. M., and Beck, A. E., Regional heat flow patterns in western Canada, Can. J. Earth Sci., 2, 176-182, 1965.

Archie, G. E., The electrical resistivity log as an aid in determining some reservoir characteristics, Trans. AIME, 146, 54-60, 1942.

Armstrong, G., Review of the geology of the British continental shelf, Min. Engr., 131, 463-481, 1972.

Artemjev, M. E., and Artyushkov, E. V., Structure and isostasy of the Baikal rift and the mechanism of rifting, J. Geophys. Res., 76, 1197-1211, 1971.

Artyushkov, E. V., Stresses in the lithosphere caused by crustal thickness inhomogeneities, J. Geophys. Res., 78, 7675-7708, 1973.

Assad, Y., A study of the thermal conductivity of fluid bearing rocks, Phd. thesis, University of California, Berkeley, California, 1955.

Azzaroli, A., On the evolution of the Gulf of Aden, 23rd Int. Geol. Cong., Prague, Proc. 1, 125-134, 1968.

Azzaroli, A., and Fois, V., Geological outlines of the northern end of the horn of Africa, 22nd Int. Geol. Cong., New Delhi, 293-314, 1964.

Baker, B. H., and Wohlenberg, J., Structure and evolution of the Kenya rift valley, Nature, 229, 538-542, 1971.

Baker, B. H., Mohr, P. A., and Williams, L. A. J., Geology of the eastern rift system of Africa, Spec. Pap. geol. Soc. Am., 136, 1972.

Baldarassi, G., Troubles triplets, Drilling, 28, 88-91, 1967.

Banks, R. J., and Ottey, P., Geomagnetic depth sounding in and around the Kenya rift, Geophys. J. R. astr. Soc., 36, 321-335, 1974.

Beck, A. E., A steady state method for the rapid measurement of the thermal conductivity of rock, J. scient. Instrum., 40, 452-454, 1957.

Beck, A. E., Techniques of measuring heat flow on land, in; W. H. K. Lee, ed., Terrestrial Heat Flow, Geophysical Monograph Series No. 8, Am. Geophys. Union, Washington, D. C., 24-57, 1965.

Beck, A. E., and Beck, J. M., On the measurement and the thermal conductivities of rocks by observations on a divided bar apparatus, Trans. Am. geophys. Union, 39, 1111-1123, 1958.

Beck, A. E., Jaeger, J. C., and Newstead, G. N., The measurement of the thermal conductvities of rocks by observations in boreholes, Australian J. Phys., 9, 286-296, 1956.

Beck, A. E., Anglin, F. M., and Sass, J. H., Analysis of heat flow data - 'in situ' thermal conductivity measurements, Can. J. Earth Sci., 8, 1-19, 1971.

Beck, J. M., and Beck, A. E., Computing thermal conductivities of rocks from chips and conventional specimens, J. Geophys. Res., 70, 5227-5239, 1965.

Beltrandi, M. D., and Pyre, A., Geological evolution of south west Somalia, in; G. Blant, ed., Sedimentary basins of the African coasts, part 2, South and East coasts, Assoc. Services Geol. Africains, Paris, 159-178, 1973.

Benfield, A. E., Terrestrial heat flow in Great Britain, Proc. Roy. Soc. Lond. A, 173, 428-450, 1939.

Benfield, A. E., The effect of uplift and denudation on underground temperatures, J. appl. Phys., 20, 66-70, 1949a.

Benfield, A. E., A problem of the temperature distribution in a moving medium, Quat. J. appl. Maths., 9, 439-443, 1949b.

Berry, F. A., Bollay, E., and Beers, N. R., Handbook of Meteorology, McGraw-Hill Book Co., New York, 1945.

Bhattacharji, S., and Koide, H., Mechanism model for triple junction fracture geometry, Nature, 255, 21-24, 1975.

Birch, F., Temperature and heat flow in a well near Colorado Springs, Am. J. Sci., 245, 733-753, 1947.

Birch, F., The effect of Pleistocene climatic variations upon geothermal gradients, Am. J. Sci., 246, 729-760, 1948.

Birch, F., Flow of heat in the Front Range, Colorado, Bull. geol. Soc. Am., 61, 567-630, 1950.

Birch, F., Heat From radioactivity, in; F. Faul, ed., Nuclear Geology, John Wiley and Sons Inc., New York, 148-175, 1954.

Birch, F., Low values of oceanic heat flow, J. Geophys. Res., 72, 2261-2262, 1967.

Birch, F., and Clark, H., The thermal conductivity of rocks and its dependence upon temperature and composition, Am. J. Sci., 238, 529-558 and 613-635, 1940.

Birch, F., and Halunen, A. J., Heat flow measurements in the Atlantic Ocean, Indian Ocean, Mediterranean Sea, and Red Sea, J. Geophys. Res., 71, 583-568, 1966.

Birch, F., Roy, R. F., and Decker, E. R., Heat flow and thermal history in New York and New England, in; W. White and E. Anzen, eds., Studies of Appalachian Geology: Northern and Maritime, Interscience, New York, 437-451, 1968.

Bishop, W. W., The late Cenozoic history of East Africa in relation to Homonid evolution, in; K. K. Turekian, ed., Late Cenozoic Glacial Ages, Yale Univ. Press, New Haven, 1971.

Blackwell, D. D., The thermal structure of the continetal crust, in; J. G. Heacock, ed., The structure and physical properties of the Earth's crust, Geophysical Monograph Series No. 14, Am. Geophys. Union, Washington, D. C., 169-184, 1971.

Blackwell, J. H., A transient heat flow method for determination of thermal constants in insulating materials in bulk, J. appl. Phys., 25, 137-144, 1954.

Bott, M. H. P., The Interior of the Earth, Edwards Arnold, London, 1971a.

Bott, M. H. P., Evolution of young continental margins and formation of shelf seas, Tectonophysics, 11, 319-327, 1971b.

Bott, M. H. P., The mantle transition zone as a possible source of global gravity anomalies, Earth Planet. Sci. Letts., 11, 28-34, 1971c.

Bott, M. H. P., Shelf subsidence in relation to the evolution of young continental margins, in; D. H. Tarling and S. K. Runcorn, eds., Implications of continental drift to the earth sciences, 2, Academic Press, London, 675-684, 1973.

Bott, M. H. P., Structure and evolution of the North Scottish Shelf, the Faeroe Block, and the intervening region, in; A. W. Woodland, ed., Petroleum and the continental shelf of North-West Europe, Applied Science Pub., Barking, 105-116, 1975.

Bott, M. H. P., and Dean, D. S., Stress systems at young continental margins, Nature Phys. Sci., 235, 23-25, 1972.

Bott, M. H. P., Johnson, G. A. L., Mansfield, J. and Wheilden, J., Terrestrial heat flow in North-East England, Geophys. J. R. astr. Soc., 27, 277-288, 1972.

Bottinga, Y., and Allegre, C. J., Thermal aspects of sea-floor spreading and the nature of the oceanic crust, Tectonophysics, 18, 1-17, 1973.

Brewer, P. G., Densmore, C. D., Munns, R., and Stanley, G., Hydrography of the Red Sea brines, in; E. T. Degens and D. A. Ross, eds., Hot brines and recent heavy metal deposits in the Red Sea, Springer Verlag, New York, 174-190, 1969.

Briden, J. C., and Gass, I. G., Plate movement and continental magmatism, Nature, 248, 650-653, 1974.

Bridgmann, P. W., The thermal conductivity and compressibility of several rocks under high pressures, Am. J. Sci., 7, 81-102, 1924.

British Petroleum Company, Personal communication, BP Development Ltd., London, England, 1974.

Brock, A., Drifting and rifting: a comment on the Tertiary rotation of Africa, Nature, 219, 599-600, 1968.

Brock, A., Gibson, I. L., and Gacii, P., The paleomagnetism of the Ethiopian flood basalt succession near Addis Ababa, Geophys. J. R. astr. Soc., 19, 485-497, 1970.

Brune, J., and Oorman, J., Seismic waves and earth structure in the Canadian shield, Bull. seis. Soc. Am., 53, 167-210, 1963.

Brunstrom, R. G., and Walmsley, P. G., Permian evaporites in the North Sea basin, Am. Assoc. Pet. Geol. Bull., 53, 870-883, 1969.

Bullard, E. C., Heat flow in South Africa, Proc. Roy. Soc. Lond. A, 173, 474-502, 1939.

Bullard, E. C., The disturbance of the temperature gradient in the earth's crust by inequalities of height, Mon. Not. Roy. astr. Soc., geophys. Suppl., 4, 360-362, 1940.

Bullard, E. C., The time necessary for a borehole to attain temperature equilibrium, Mon. Not. Roy. astr. Soc., geophys. Suppl., 5, 127-130, 1947.

Bullard, E. C., Personal communication, Oept. of Geodesy and Geophysics, University of Cambridge, Cambridge, 1975.

Bullard, E. C., and Niblett, E. R., Terrestrial heat flow in England, Mon. Not. Roy. astr. Soc., geophys. Suppl., 6, 222-238, 1951.

Bunce, E. T., Langseth, M. G., Chase, R. L., and Ewing, M., Structure of the western Somali basin, J. Geophys. Res., 72, 2547-2555, 1967.

Burmah Oil Company, Personal communication, Burmah Oil (Somalia) Ltd., Swindon, 1974.

Cahen, L., and Snelling, N. J., The geochronology of equatorial Africa, North-Holland, Amsterdam, 1966.

Campbell, J. M., Formation Logging, in; J. M. Campbell, ed., Petroleum reservoir property evaluation, Norman, Oklahoma, 1973.

Carella, R., and Scarpa, M., Geological results of exploration in Sudan by AGIP Mineraria, 4th Arab Pet. Conf., Beirut, 1962.

Carre, B. A., The determination of the optimum accelerating factor for successive over-relaxation, Computer J., 4, 73-78, 1961.

Carslaw, H. S., and Jaeger, J. C., Conduction of Heat in Solids, 2nd ed., Oxford University Press, London, 1959.

Casmir, H. B. G., Note on the conduction of heat in crystals, Physica, 5, 495-500, 1938.

Cermak, V., Suggestions for the compilation of European heat flow data, personal communication, The Geophysical Institute, Prague, 1975.

Cermak, V., and Jessop, A. M., Heat flow, heat generation and crustal temperature in the Kapuskasing area of the Canadian shield, Tectonophysics, 11, 287-303, 1971.

Chadwick, P., Heat flow from the earth at Cambridge, Nature, 178, 105-106, 1956.

Chapman, D. S., and Pollack, H. N., 'Cold spot' in west Africa: anchoring the African plate, Nature, 250, 477-478, 1974.

Chayes, F., On deciding whether trend surfaces of progressively higher orders are meaningful, Bull. seis. Soc. Am., 81, 1273-1278, 1970.

Ciaranei, N., Loddo, M., and Mongelli, F., Paleoclimatic effect on the geothermal gradient in never ice-covered Mediterranean regions, Rivista Italiana di Geofisica, 22, 1-7, 1972.

Clark, H., The effects of simple compression and wetting on the thermal conductivity of rocks, Trans. Am. geophys. Union, 22, 543-544, 1941.

Clark, J. D., The later Pleistocene cultures of Africa, Science, 150, 833-847, 1965.

Clark, S. P., Thermal Conductivity, in; S. P. Clark, ed., Handbook of Physical Constants, rev. ed., Geol. Soc. Am. Mem. 97, 459-482, 1966.

Clark, S. P., Heat conductivity in the mantle, in; P. J. Hart, ed., The Earth's crust and upper mantle, Geophysical Monograph Series No. 13, Am. Geophys. Union, Washington, D. C., 622-626, 1969.

Clement, and Peclet, Ann. de chimie de physique, 3, 107, 1841.

Clift, W. O., Sedimentary history of the Ogaden district, Ethiopia, 20th Int. Geol. Conq., Mexico City, Symposium sobre yaciemientos de petroleo y gas, 89-112, 1956.

Coleman, N. C., Thermal recovery and temperature gradients in petroleum exploration boreholes in the North Sea area, BSc. dissertation, University of London, London, 1973.

Coleman, R. G., Geologic background of the Red Sea, in; R. B. Whitmarsh, O. E. Weser, D. A. Ross, et al., eds., Init. Reps. of the Deep Sea Drilling Proj., 23, U. S. Gov. Printing Office, Washington, D. C., 813-820, 1974.

Collette, B. J., The gravity field of the North Sea, in; G. J. Bruins, ed., Gravity Expeditions, 5, Neth. Geod. Comm., Delft, 1960.

Collette, B. J., On the subsidence of the North Sea basin, in; D. T. Donovan, ed., Geology of shelf seas, Oliver and Boyd, London, 15-29, 1968.

Collette, B. J., Lagaay, R. A., and Ritsema, A. R., Depth of the Mohorovicic discontinuity under the North Sea, Nature, 205, 688-689, 1965.

Collette, B. J., Lagaay, R. A., Ritsema, A. R., and Schouten, J. A., Seismic investigations in the North Sea, 1 and 2, Geophys. J. R. astr. Soc., 12, 363-373, 1967.

Collette, B. J., Lagaay, R. A., Ritsema, A. R., and Schouten, J. A., Seismic investigations in the North Sea, 3 to 7, Geophys. J. R. astr. Soc., 19, 183-199, 1970.

Compton, A. H., Physical theory of thermal conductivity of solids, Phys. Rev., 7, 341-348, 1916.

Cooper, L. R., and Jones, C., The determination of virgin strata temperatures from observations in deep survey boreholes, Geophys. J. R. astr. Soc., 2, 116-131, 1959.

Cornelius, C. D., Geothermal aspects of hydrocarbon exploration in the North Sea area, in; A. Whiteman, D. Roberts and M. A. Sellevoll, eds., Petroleum Geology and Geology of the North Sea and Northeast Atlantic continental margin, Norges Geologiske Undersokelse, 316, 29-68, 1975.

Coster, H. P., Terrestrial heat flow in Persia, Mon. Not. Roy. astr. Soc., geophys. Suppl., 5, 131-145, 1947.

Crain, I. K., The glacial effect and the significance of continental terrestrial heat flow measurements, Earth Planet. Sci. Letts., 4, 69-72, 1968.

Cull, J., Rapid measurement of thermal conductivity, Heat Flow Symposium, Imperial College, London, Feb., 1974.

Daniels, J. L., Skiba, W. J., and Sutton, J., The deformation of some banded gabbros in the northern Somalia fold-belt, Quat. J. geol. Soc. Lond., 121, 111-141, 1965.

Davies, T. A., Weser, O. E., Luyendyk, B. P., and Kidd, R. B., Unconformities in the sediments of the Indian Ocean, Nature, 253, 15-19, 1975.

Davis, B. T. C., and England, J. L., The melting of forsterite up to 50 kilobars, J. Geophys. Res., 69, 1113-1116, 1964.

Davis, J. C., Statistics and data analysis in geology, John Wiley and Sons Inc., New York, 1973.

Debye, P., Vortrage uber die kinetische theorie der materie und elektrizitat, Gottinger Wolfskehlvortrage B. G. Tueber, Leipzig and Berlin, 46, 1914.

Defant, A., Physical Oceanography, 1, Permagon Press, Oxford, 116, 1961.

Degens, E. T., Von Herzen, R. P., and Wong, H. K., Lake Tanganyika water chemistry sediments, geological structure, Naturwissenschaften, 58, 229-241, 1971.

De Vries, D. A., Het warmtegeleidingsvermogem van grond, Mededelingen van de Landbouwhogeschool te Wageningen/Nederland, 52, 1-73, 1952.

Devyatkova, E. D., Petrov, A. V., Smirnov, I. A., and Moizhes, B. Y., Fiz. Tverd. Tela, 2, 738, 1960.

Diment, W. H., Thermal regime of a large diameter borehole: Instability of the water column and comparison of air and water-filled conditions, Geophysics, 22, 720-726, 1967.

Diment, W. H., and Robertson, E. C., Temperature, thermal conductivity, and heat flow in a drilled hole near Oak Ridge, Tennessee, J. Geophys. Res., 68, 5035-5047, 1963.

Dobrynin, V. M., Effect of overburden pressure on some properties of sandstones, Soc. Pet. Eng. J., 225, 360-366, 1962.

Doll, H. G., The Microlog, Trans. AIME, 189, 155-164, 1950.

Doll, H. G., The Microlaterolog, J. Pet. Tech., 5, 17-32, 1953.

Domzalski, W., Some geophysical profiles in areas of interest in the North Sea (abstract), in; A. Whiteman, D. Roberts and M. A. Sellevoll, eds., Petroleum Geology and the Geology of the North Sea and Northeast Atlantic continental margin, Norges Geologiske Undersokelse, 316, 165, 1975.

Drake, C. L., and Girdler, R. W., A geophysical study of the Red Sea, Geophys. J. R. astr. Soc., 8, 473-495, 1964.

Duba, A., and Lilley, F. E. M., Effect of an ocean ridge model on geomagnetic variations, J. Geophys. Res., 77, 7100-7105, 1972.

Dubertret, L., Review of structural geology of the Red Sea and surrounding areas, Phil. Trans. R. Soc. Lond., A, 267, 9-20, 1970.

Dunn, W. W., Eha, S., and Heikkla, H. H., North Sea is a tough theater for the oil-hungry industry to explore, Oil and Gas J., 71, 90-93 and 122-128, 1973.

Edwardson, M. J., Girner, H. M., Parkinson, H. R., Williams, C. D., and Mathews, C. S., Calculation of formation temperature disturbance caused by circulation, J. Pet. Tech., 14, 416-426, 1962.

Emiliani, C., Pleistocene temperatures, J. Geol., 63, 538-578, 1955.

Emiliani, C., Cenozoic climatic changes as indicated by stratigraphy and chronology of deep sea cores of globigerina-ooze facies, Ann. N. Y. Acad. Sci., 95, 521-536, 1961.

Emiliani, C., Isotopic Palaeotemperatures, Science, 154, 851-857, 1966.

Emiliani, C., and Shackleton, N. J., The Brunhes Epoch, Isotopic Palaeotemperatures and Geochronology, Science, 183, 511-514, 1974.

Endo, Y., Quantum theory of thermal conductivity of nonmetallic crystals, Sci. Reps. Tokyo Imp. Univ., 11, 183-193, 1922.

Erickson, A. J., and Simmons, G., Thermal measurements in the Red Sea, in; E. T. Degens and D. A. Ross, eds., Hot brines and recent heavy metal deposits in the Red Sea, Springer-Verlag, Berlin, 114-121, 1969.

Evans, T. R., and Coleman, N. C., North Sea geothermal gradients, Nature, 247, 28-30, 1974.

Evans, T. R., and Tammemagi, H. Y., Heat flow and heat production in Northeast Africa, Earth Planet. Sci. Letts., 23, 349-356, 1974.

Fairbridge, R. W., Comm. No. 107, Int. Assoc. Seis., IUGG, Toronto, 1957.

Fairbridge, R. W., Convergence of evidence on climatic changes and ice ages, Ann. N. Y. Acad. Sci., 95, 542-579, 1961.

Fairhead, J. D., and Girdler, R. W., The seismicity of the Red Sea, Gulf of Aden, and Afar triangle, Phil. Trans. R. Soc. Lond., A, 267, 49-74, 1970.

Fairhead, J. D., and Girdler, R. W., The seismicity of Africa, Geophys. J. R. astr. Soc., 21, 271-301, 1971.

Fairhead, J. D., and Girdler, R. W., The seismicity of the East Africa rift system, Tectonophysics, 15, 115-122, 1972.

Falvey, D. A., The development of continental margins in plate tectonic theory, Aust. Pet. Exp. Assoc. J., 14, 95-106, 1974.

Fisher, R. L., Engel, C. E., and Hilde, T. W. C., Basalts dredged from the Admirante Ridge, western Indian Ocean, Deep-Sea Res, 15, 521-534, 1968.

Flavelle, A. J., and Yoshimura, Y., Analysis of gravity data near continental margins, Aust. Pet. Exp. Assoc. J., 14, 114-117, 1974.

Fleischier, U., Surface-ship gravity measurements in the North Sea, Geophys. Prospect., 11, 535-549, 1963.

Flint, R. F., Pleistocene climates in eastern and southern Africa, Geol. Soc. Am. Bull., 70, 343-374, 1959.

Flohn, H., Allgemeine atmospharische Zurkulation und Palaolimatologie, Geol. Rundschau, 40, 153-170, 1952.

Forbes, J. D., Account of some experiments on the temperature of the Earth at different depths and in different soils near Edinburgh, Trans. Roy. Soc. Edinburgh, 16, 189-236, 1845.

Forsythe, G. E., and Wasow, W. R., Finite-difference methods for partial differential equations, John Wiley, New York, 1960.

Foucher, J. P., and LePichon, X., Comments on "Thermal effects of the formation of Atlantic continental margins by continental break-up", by N. H. Sleep, Geophys. J. R. astr. Soc., 29, 43-46, 1972.

Francis, T. J. G., Davies, D., and Hill, M. N., Crustal structure between Kenya and the Seychelles, Phil. Trans. R. Soc. Lond., A, 259, 240-261, 1966.

Gaposchkin, E. M., and Lambeck, K., Earth gravity field to sixteenth degree and station coordinates from satellite and terrestrial data, J. Geophys. Res., 76, 4855-4883, 1971.

Garland, G. D., and Lennox, D. H., Heat flow in western Canada, Geophys. J. R. astr. Soc., 6, 245-262, 1962.

Gass, I. G., The evolution of volcanism in the junction area of the Red Sea, Gulf of Aden and Ethiopian rifts, Phil. Trans. R. Soc. Lond., A, 267, 369-382, 1970.

Gass, I. G., The Red Sea depression: causes and consequences, in; D. H. Tarling and S. K. Runcorn, eds., Implications of continental drift to the earth sciences, 2, Academic Press, London, 779-785, 1973.

Gass, I. G., and Neary, C. R., The granitic association of the North-east Sudan, Geol. Soc. Am. Bull., (in press), 1975.

Gass, I. G., Mallick, D. I. J., and Cox, K. G., Volcanic islands of the Red Sea, J. Geol. Soc., 129, 275-310, 1973.

Geotimes, Deep Sea Drilling Project in Dodo Land, Leg 24, 17, 17-21, 1972.

Gewerkschaft Elwerath, personal communication, Hannover, West Germany, 1973.

Giesel, W., and Holz, A., Das anomale geothermische feld in salz-stocken - quantitative deutung au einem beispiel, Kali u. Steinsalz, 5, 272-274, 1970.

Girdler, R. W., The relationship of the Red Sea to the East Africa rift system, Quat. J. geol. Soc. Lond., 114, 79-105, 1958.

Girdler, R. W., Drifting and rifting of Africa, Nature, 217, 1102-1105, 1968.

Girdler, R. W., The Red Sea - a geophysical background, in; E. T. Degens and D. A. Ross, eds., Hot brines and recent heavy metal deposits in the Red Sea, Springer-Verlag, New York, 38-58, 1969.

Girdler, R. W., A review of Red Sea heat flow, Phil. Trans. R. Soc. Lond., A, 267, 191-203, 1970.

Girdler, R. W., personal communication, School of Physics, University of Newcastle-upon-Tyne, Newcastle, 1975.

Girdler, R. W., and Styles, P., Two stage Red Sea floor spreading, Nature, 247, 7-11, 1974.

Girdler, R. W., Erickson, A. J., and Von Herzen, R. P., Downhole temperature and shipboard thermal conductivity measurements aboard D/V Glomar Challenger in the Red Sea, in; R. B. Whitmarsh, O. E. Weser, D. A. Ross, et al., eds., Init. Reps. of the Deep Sea Drilling Proj., 23, U. S. Gov. Printing Office, Washington, D. C., 879-886, 1974.

Gorshkov, G. P., The seismicity of Africa, in; A review of the natural resources of the African continent, UNESCO, Paris, 101-163, 1963.

Gough, D. I., Heat flow in the southern Karroo, Proc. R. Soc. Lond., A, 272, 207-230, 1963.

Gough, D. I., Electrical conductivity under western North America in relation to heat flow, seismology, and structure, J. Geomag. and Geoelec., 26, 105-123, 1974.

Gouin, P., Seismic and gravity data from Afar in relation to surrounding areas, Phil. Trans. R. Soc. Lond., A, 267, 339-358, 1970.

Green, D. H., and Ringwood, A. E., An experimental investigation of the gabbro eclogite transformation and its petrological applications, Geochim. Cosmochim. Acta, 31, 767-833, 1967.

Greenwood, J. E. G. W., The Inda Ad series of the former Somalialand Protectorate, Overseas Geol. min. Resour., 8, 288-296, 1961.

Gretener, P. E., On the thermal instability of large diameter wells - an observational report, Geophysics, 22, 727-738, 1967.

Griffin, G. M., Tedrick, P. A., Reel, D. A., and Manker, J. P., Geothermal gradients in Florida and southern Georgia, Gulf Coast Assoc. geol. Soc. Trans., 19, 189-193, 1969.

Griffiths, D. H., King, R. F., Khan, M. A., and Blundell, D. J., Seismic refraction line in the Gregory Rift, Nature, 229, 69-71, 1971.

Griffiths, J. F., Eastern Africa, and the Horn of Africa, in; J. F. Griffiths, ed., The Climates of Africa, Elsevier Pub. Co., Amsterdam, 1972.

Grisafi, T. W., Rieke, H. H., and Skidmore, D. R., Approximation of geothermal gradients in northern West Virginia using bottom-hole temperatures from electric logs, Am. Assoc. Pet. Geol. Bull., 58, 321-323, 1974.

Gulf Oil Company, personal communication, Gulf Oil Co. - Eastern Hemisphere, London, 1972.

Gumper, F., and Pomeroy, P. W., Seismic wave velocities and Earth structure on the African continent, Bull. seis. Soc. Am., 60, 651-668, 1970.

Guyod, H., Temperature well logging, Oil Weekly, 8, 1946.

Haenel, R., Eine neue Methode zur Bestimmung der terrestrischen Warmstromdichte in Binnenseen, Z. Geophys., 36, 725-742, 1970.

Haenel, R., Heat flow measurements and a first heat flow map of Germany, Z. Geophys., 37, 975-992, 1971.

Haenel, R., Heat flow measurements in the Red Sea and Gulf of Aden, Z. Geophys., 38, 1035-1047, 1972.

Haenel, R., Heat flow measurements in northern Italy and heat flow maps of Europe, Z. Geophys., 40, 367-380, 1973.

Haenel, R., Gronlie, G., and Heier, K. S., Terrestrial heat flow determinations from lakes in southern Norway, Norsk Geologisk Tidsskrift, 54, 423-428, 1974.

Hales, A. L., Convection currents in geysers, Mon. Not. Roy. astr. Soc., geophys. Suppl., 4, 122-132, 1937.

Haliburton Co., Posimix Cement Data Book, Duncan, Oklahoma.

Hallam, A., Mesozoic geology and opening of the North Atlantic, J. Geol., 79, 129-157, 1971.

Harper, M. L., Approximate geothermal gradients in the North Sea, Nature, 230, 235-236, 1971.

Harper, M. L., personal communication, Amoco Europe Inc., London, 1973.

Harrison, J., and Haw, D., Review of the geology and oil prospects of the Lamu Embayment and adjoining areas, unpub. rep. of the BP-Shell Petroleum Development Company of Kenya Ltd., no. 4338, 1964.

Hashin, Z., and Shtrickman, S. A., Variational approach to the theory of the effective magnetic permeability of multiphase materials, J. appl. Phys., 33, 3125-3131, 1962.

Hedemann, H. A., Beitrage zur Geothermik aus Tiefbohrungen, Freiberger Forsch. H., 228, 63-75, 1968.

Heezen, B. C., Atlantic-type contiental margins, in; C. A. Burk and C. L. Drake, eds., The Geology of Continental Margins, Springer-Verlag, Berlin, 13-24, 1974.

Heezen, B. C., and Tharp, M., Physiographic diagram of the Indian Ocean, Red Sea, the South China Sea, the Sulu Sea, and the Celebes Sea, Geol. Soc. Am., New York, 1964.

Herrin, E., and Clark, S. P., Heat flow in west Texas and eastern New Mexico, Geophysics, 21, 1087-1099, 1956.

Heybroek, F., The Red Sea Miocene evaporite basin, in; Salt basins around Africa, Instit. Pet., London, 17-40, 1965.

Hilchie, D. W., Maximum temperatures recorded in wellbores, The Log Analyst, 9, 21-24, 1968.

Holmes, A., Radioactivity in Earth and Earth's thermal history, Geol. Mag., 2, 60-71, 1915.

Holmes, A., The sequence of Precambrian orogenic belts in south and central Africa, 18th Int. Geol. Cong., London, Rep. 14, 254-268, 1951.

Holmes, A., Principles of Physical Geology, Nelson, London, 1965.

Holmes, C. S., and Swift, S. C., Calculation of circulating mud temperatures, J. Pet. Tech., 22, 670-674, 1970.

Horai, Ki-iti, and Simmons, G., Thermal conductivity of rock-forming minerals, Earth Planet. Sci. Letts., 6, 359-368, 1969.

Hornabrook, J. T., Seismic interpretation of the West Sole gas field, in; A. Whiteman, D. Roberts and M. A. Sellevoll, eds., Petroleum Geology and Geology of the North Sea and Northeast Atlantic continental margin, Norges Geologiske Undersokelse, 316, 121-136, 1975.

Hough, H., and Couvillon, J. A., Deep hot drilling marks Gulf Frio play, Oil and Gas J., 64, 142-158, 1966.

Howitt, F., Aston, E. R., and Jacque, M., The occurrence of Jurassic volcanics in the North Sea, in; A. W. Woodland, ed., Petroleum and the continental shelf of North West Europe, Applied Science Pub., Barking, 379-388, 1875.

Hunt, J. A., Report on the geology of the Berbera-Sheikh area, Somaliland Protectorate Geological Survey, Rep. no. 4, 1960.

Hurtig, E., and Brugger, H., Warmeleitfahigkeitsmessungen unter einaxialem Druck, Tectonophysics, 10, 67-78, 1970.

Hutchins, J. S., and Kading, H., How to interpret temperature surveys, Oil and Gas J., 67, 96-103 and 137-141, 1969.

Ibele, W., Thermophysical properties, in; W. M. Rohsenow and J. P. Hartnett, eds., Handbook of Heat Transfer, McGraw-Hill Book Co., New York, chapter 2, 1973.

Illies, J. H., Graben tectonics as related to crust-mantle interaction, in; J. H. Illies and S. Mueller, eds., Graben Problems, Schweirzerbart, Stuttgart, 1970.

Ingersoll, L. R., Zobel, O. J., and Ingersoll, A. C., Heat Conduction, University of Wisconsin Press, Madison, 1954.

International Business Machines, (IBM), System 360, Scientific Subroutine Package, Version 3, 5th edition, IBM Corp. Tech. Pub., 368-369, 1970.

Irving, E., and Tarling, D. H., The paleomagnetism of the Aden volcanics, J. Geophys. Res., 66, 549-556, 1961.

Jacobs, J. A., and Allan, D. W., Temperatures and heat flow within the Earth, Trans. Roy. Soc. Can., 48, 33-39, 1954.

Jaeger, J. C., The effect of the drilling fluid on temperatures measured in boreholes, J. Geophys. Res., 66, 563-569, 1961.

Jaeger, J. C., Application of the theory of heat conduction to geothermal measurements, in; W. H. K. Lee, ed., Terrestrial Heat Flow, Geophysical Monograph Series No. 8, Am. Geophys. Union, Washington, D. C., 7-23, 1965.

Jamieson, D. T., and Tudhope, J. S., Physical properties of seawater solutions; thermal conductivity, Desalination, 8, 393-401, 1970.

Jeffreys, H., The disturbance of the temperature gradient in the Earth's crust by inequalities of height, Mon. Not. Roy. astr. Soc., geophys. Suppl., 4, 309-312, 1940.

Jessop, A. M., The effect of environment on divided bar measurements, Tectonophysics, 10, 39-49, 1970.

Joly, J., Radioactivity and Geology, Van Nostrand and Co., New York, 1909.

Jones, P. H., Geothermal resources of the northern Gulf of Mexico Basin, Geothermics, 2, 14-26, 1970.

Joyner, W. B., Heat flow in Pennsylvania and West Virginia, Geophysics, 25, 1229-1241, 1960.

Joyner, W. B., Basalt-eclogite transition as a cause for subsidence and uplift, J. Geophys. Res., 72, 4977-4998, 1967.

Judge, A. S., Geothermal measurements in a sedimentary basin, Phd. thesis, University of Western Ontario, London, 1971.

Judge, A. S., and Beck, A. E., An anomolous heat flow layer at London, Ontario, Earth Planet. Sci. Letts., 3, 167-170, 1967.

Kabbani, F. K., Geophysical and structural aspects of the central Red Sea rift valley, Phil. Trans. R. Soc. Lond., A, 267, 89-97, 1970.

Kappelmeyer, O., and Haenel, R., Geothermics with special reference to applications, Gebruder Borntrager, Stuttgart, 1974.

Karnik, V., Seismicity of the European area, D. Reidal Pub. Co., Amsterdam, 1971.

Kaye, G. W. C., and Higgins, W. F., The thermal conductivity of vitreous silica with a note on crystalline quartz, Proc. Roy. Soc. Lond., A, 113, 335-351, 1926.

Kaye, G. W. C., and Laby, T. H., Physical and chemical constants and some mathematical functions, 10th ed., Longmans, Green and Co., London, 1948.

Kaye, G. W. C., and Laby, T. H., Tables of physical and chemical constants, 13th ed., Longmans, London, 1966.

Kazmin, V., The Precambrian of Ethiopia, Nature Phys. Sci., 230, 176-177, 1971.

Kehle, R. O., Schoeppel, R. J., and Oeford, R. K., The AAPG geothermal survey of North America, Geothermics, 2, 358-367, 1970.

Keller, H. H., Couch, E. J., and Berry, P. M., Temperature distribution in circulating mud columns, J. Pet. Tech., 25, 23-30, 1973.

Kennedy, W. Q., The influence of basement structure on the evolution of the coastal (Mesozoic and Tertiary) basins of Africa, in; Salt Basins around Africa, Insit. Pet., London, 7-16, 1965.

Kent, P. E., An evaporite basin in southern Tanzania, in; Salt Basins around Africa, Instit. Pet., London, 41-54, 1965.

Kent, P. E., The Mesozoic history of the east coast of Africa, Nature, 238, 147-148, 1972.

Kent, P. E., Leg 25 results in relation to East Africa coastal stratigraphy, in; E. S. W. Simpson, R. Schlich, et al., eds., Init. Reps. of the Deep Sea Drilling Proj., 25, U. S. Gov. Printing Office, Washington, D. C., 679-684, 1974a.

Kent, P. E., Continental margin of East Africa - a region of vertical movements, in; C. A. Burk and C. L. Drake, eds., The Geology of Continental Margins, Springer-Verlag, Berlin, 313-320, 1974b.

Kent, P. E., The tectonic development of Great Britain and the surrounding seas, in; A. W. Woodland, ed., Petroleum and the continental shelf of North West Europe, Applied Science Pub., Barking, 3-28, 1975.

Kent, P. E., and Perry, J. T. O'B., The development of the Indian Ocean margin in Tanzania, in; G. Blant, ed., Sedimentary basins of the African coasts, part 2, South and East Coasts, Assoc. Services Geol. Africains, Paris, 113-131, 1973.

Kent, P. E., Hunt, J. A., and Johnstone, D. W., The geology and geophysics of coastal Tanzania, Instit. Geol. Sci., London, Geophys. Paper no. 6, 1971.

Kessler, D. W., Building stones, in; E. W. Washburn, ed., Int. Crit. Tables, 2, McGraw Hill Book Co., New York, 47-56, 1927.

King, W., and Simmons, G., Heat flow near Orlando, Florida, and Uvalde, Texas, determined from well cuttings, Geothermics, 1, 133-139, 1972.

Kingery, W. D., and McQuarrie, Thermal conductivity: 1, Concepts of measurement and factors affecting thermal conductivity of ceramic materials, J. Am. Ceram. Soc., 37, 67-72, 1954.

Kittel, C., Interpretation of thermal conductivity of glasses, Phys. Rev., 75, 972-974, 1949.

Klemens, P. G., Thermal conductivity and lattice vibrational modes, Solid State Physics, 7, 1-98, 1958.

Klemme, H. D., Heat influences size of oil giants, Oil and Gas J., 70, 76-78, 1972.

Kline, D. E., Thermal conductivity studies of polymers, J. Polymer Sci., 6, 441-450, 1961.

Kokesh, F. P., Schwartz, R. J., Wall, W. B., and Morris, R. L., A new approach to sonic logging and other acoustic measurements, J. Pet. Tech., 17, 282-286, 1965.

Krenkel, E., Die Seismizitat Afrikas, Zentralblatt fur Min., Geol., Pal., Stuttgart, 6, 173-183, 1923.

Kresl, M., and Vesely, I., Instrument for the automatic measurement of the coefficient of heat conductivity of rocks, Geofysikalini Sbornik, 19, 317-334, 1971.

Kreyszig, E., Advanced Engineering Mathematics, 2nd ed., John Wiley and Sons Inc., London, 1968.

Krige, L. J., Borehole temperatures in the Transvaal and Orange Free State, Proc. Roy. Soc. Lond., A, 173, 450-474, 1939.

Kunz, K. S., and Tixier, M. P., Temperature surveys in gas producing wells, J. Pet. Tech., 204, 111-119, 1955.

Lachenbruch, A. N., Preliminary geothermal model for the Sierra Nevada, J. Geophys. Res., 73, 6977-6989, 1968.

Lachenbruch, A. H., The effect of two-dimensional topography on superficial thermal gradients, Exper. and Theor. Geophys., U. S. Geol. Surv. Bull. 1203-E, 1-63, Washington, D. C., 1969.

Lachenbruch, A. H., Crustal temperature and heat production: implications of the linear heat-flow relation, J. Geophys. Res., 75, 3291-3300, 1970.

Lachenbruch, A. H., and Brewer, M. C., Dissipation of the temperature effect of drilling a well in arctic Alaska, U. S. Geol. Surv. Bull. 1083-C, 73-109, 1959.

Lamb, H. H., The early and medieval warm epoch and its sequel, Palaeogeogr., Palaeoclimatol., Palaeoecol., 1, 13-27, 1965.

Landesberg, K., Pogg. Ann. B., 139, 1, 1853.

Lane, A. C., Geotherms of the Lake Superior copper country, J. Geol., 42, 113-122, 1923.

Langseth, M. G., Measuring heat flow through the ocean floor, in; W. H. K. Lee, ed., Terrestrial Heat Flow, Geophysical Monograph Series No. 8, Am. Geophys. Union, Washington, D. C., 58-77, 1965.

Langseth, M. G., and Taylor, P. T., Recent heat flow measurements in the Indian Ocean, J. Geophys. Res., 72, 6249-6260, 1967.

Langseth, M. G., and Zielinksi, G. W., Marine heat flow measurements in the Norwegian-Greenland Sea and in the vicinity of Iceland, in; L. Kristjanson, ed., Geodynamics of Iceland and the North Atlantic area, D. Reidel Pub. Co., Dordrecht, 277-295, 1974.

Laughton, A. S., The Gulf of Aden, Phil. Trans. R. Soc. Lond., A, 259, 150-171, 1966.

Laughton, A. S., Tectonic evolution of the Northeast Atlantic ocean; a review, in; A. Whiteman, D. Roberts and M. A. Sellevoll, eds., Petroleum Geology and Geology of the North Sea and Northeast Atlantic continental margin, Norges Geologiske Undersokelse, 316, 169-194, 1975.

Laughton, A. S., and Trammontini, C., Recent studies of the crustal structure in the Gulf of Aden, Tectonophysics, 8, 359-375, 1969.

Laughton, A. S., Whitmarsh, R. B., and Jones, M. T., The evolution of the Gulf of Aden, Phil. Trans. R. Soc. Lond., A, 267, 227-266, 1970.

Lawson, A. W., Lowell, R., and Jain, A. L., Thermal conductivity of water at high pressures, J. Chem. Phys., 30, 643-647, 1959.

Lee, W. H. K., On the global variations of terrestrial heat flow, Phys. Earth and Planet. Interiors, 2, 332-341, 1970.

Lee, W. H. K., and Uyeda, S., Review of heat flow data, in; W. H. K. Lee, ed., Terrestrial Heat Flow, Geophysical Monograph Series No. 8, Am. Geophys. Union, Washington, D. C., 87-190, 1965.

Lees, C. H., On the thermal conductivity of crystals and other bad conductors, Phil. Trans. R. Soc. Lond., A, 183, 481-509, 1892.

Lees, C. H., On the shapes of the isogeotherms under mountain ranges in radioactive districts, Proc. Roy. Soc. Lond., A, 83, 339-346, 1910.

LePichon, X., Francheteau, J., and Bonin, J., Plate Tectonics, Elsevier, Amsterdam, 1973.

Lodge, O. J., On a method of measuring the absolute thermal conductivity of crystals and other rare substances, Phil. Mag., 5, 110-117, 1878.

Long, R. E., Backhouse, R. W., Maguire, P. K. H., and Sundarlingham, K., The structure of East Africa using surface wave dispersion and Durham seismic array data, Tectonophysics, 15, 165-178, 1972.

Lowell, S. D., and Genik, G. J., Sea-floor spreading and structural evolution of southern Red Sea, Am. Assoc. Pet. Geol. Bull., 56, 247-259, 1972.

Lubimova, E. A., Thermal history of the Earth, in; P. J. Hart, ed., The Earth's Crust and Upper Mantle, Geophysical Monograph Series No. 13, Am. Geophys.. Union, Washington, D. C., 63-77, 1969.

Lubimova, E. A., and Nikitina, V. N., On heat flow singularities over mid-ocean ridges, J. Geophys. Res., 80, 232-243, 1975.

Maasha, N., and Molnar, P., Earthquake fault parameters in Africa, J. Geophys. Res., 77, 5731-5743, 1972.

Makinson, R. E. B., Thermal conductivity of metals, Proc. Cambridge Phil. Soc., 34, 474-497, 1938.

Marathon Oil Company, personal communication, Marathon International, Findlay, Ohio, 1974.

Mason, J. E., An isolated occurrence of igneous rock at Gorei in the Las Anod district of the Somaliland Protectorate, Geol. Mag., 94, 498-502, 1957.

Matthews, D. H., The Owen Fracture Zone and the northern end of the Carlsberg ridge, Phil. Trans. R. Soc. Lond., A, 259, 172-186, 1966.

Maxwell, J. C., A Treatise on Electricity and Magnetism, 3rd ed., Clarendon Press, Oxford, 1904.

Meisner, A. D., Thompson, L. G. D., and Uffen, R. J., Terrestrial heat flow in Ontario and Quebec, Trans. Am. geophys. Union, 32, 729-738, 1951.

Merriam, D. F., and Cocke, N. C., Computer applications in the Earth Sciences, Kansas Geological Survey Computer Contribution 12, 1967.

Mobil Oil Company, personal communication, Mobil Exploration and Production Services International, Dallas, Texas, 1974.

Mohr, P. A., The geology of Ethiopia, Univ. Coll. Addis Ababa Press, 1962.

Mongelli, F., Considerazioni sulla possibilita' di utilizzare le usuali misure di temperatura nei pozzi petroliferi per lo studio della temperatura della crosta, Bull. di Geofis. Teor. ed Appl., 6, 333-336, 1964.

Montessus de Ballore, F., Les tremblements de terre, La geographie seismologique, Paris, 1-475, 1906.

Moreau, R. E., Africa since the Mesozoic with particular reference to certain biological problems, Lond. Zool. Soc. Proc., 121, 869-913, 1952.

Morgan, P., Disposable thermistor strings for subsurface temperature measurements, (abstr.), Geophys. Prospect., 20, 741-742, 1972.

Morgan, P., Terrestrial heat flow studies in Cyprus and Kenya, Phd. thesis, University of London, London, 1973.

Morgan, P., personal communication, Dept. of Geological Sciences, Southern Methodist University, Dallas, Texas, 1974.

Morgan, W. J., Deep mantle plumes and plate motions, Am. Assoc. Pet. Geol. Bull., 56, 203-213, 1972.

Moses, P. L., Geothermal gradients now known in greater detail, World Oil, 152, 79-82, 1961.

Mullins, R., and Hinsley, F. B., Measurement of geothermic gradients in boreholes, Trans. Instit. Min. Engr., 117, 379-393, 1958.

Mundry, E., Zur Berechnung der gebirgstemperatur bei der grubenbewetterung mit anwendung zur vorausbestimmung von bohrlochtemperaturen, Phd. thesis, Bergakademir Clausthal, 1964.

Mundry, E., Berechnung des gestorten geothermischen feldes mit hilfe relaxations-verfahrens, Z. Geophys., 3, 157-162, 1966.

Munroe, R. J., personal communication, U. S. Geol. Surv., Menlo Park, California, 1972.

Murray, C. G., Magma genesis and heat flow; differences between mid-oceanic ridges and African rift valleys, Earth Planet. Sci. Letts., 9, 34-38, 1970.

MacDonald, G. J. F., Calculation of the thermal history of the Earth, J. Geophys. Res., 64, 1967-2000, 1959.

MacDonald, G. J. F., and Ness, N. F., Stability of phase transitions in the Earth, J. Geophys. Res., 65, 2173-2190, 1960.

McConnell, R. B. Evolution of taphrogenic lineaments in continental platforms, Geol. Rundschau, 63, 389-430, 1974.

McConnell, R. K., Viscosity of the mantle from relaxation time spectra of isostatic adjustment, J. Geophys. Res., 73, 7089-7105, 1968.

McKenzie, D. P., Some remarks on heat flow and gravity anomalies, J. Geophys. Res., 72, 6261-6271, 1967.

McKenzie, D. P., and Morgan, W. J., Evolution of triple junctions, Nature, 224, 125-133, 1969.

McKenzie, D. P., and Sclater, J. G., The evolution of the Indian Ocean since the late Cretaceous, Geophys. J. R. astr. Soc., 25, 437-528, 1971.

McKenzie, D. P., Davies, D., and Molnar, P., Plate tectonics of the Red Sea and East Africa, Nature, 226, 243-248, 1970.

Nicholsen, J. W., A problem in the theory of heat conduction, Proc. Roy. Soc. A, 100, 226-240, 1921.

Oelsner, C., and Sippel, V., Warmeleitfahigkeitsmessungen in situ, Neue Bergbautechnik, 1, 661-664, 1971.

Olausson, E., Evidence in Indian Ocean cores of late Pleistocene climatic changes, in; E. M. van Zinderen Bakker, ed., Palaeoecology of Africa, the surrounding islands and Antarctica, 6, Balkema, Cape Town, 41-44, 1972.

Olausson, E., and Olsson, I. U., Varve stratigraphy in a core from the Gulf of Aden, Palaeogeogr., Palaeoclimatol., Palaeoecol., 6, 87-103, 1969.

Oliver, J., and Isacks, B., Deep earthquake zones, anomolous structure in the upper mantle and the lithosphere, J. Geophys. Res., 72, 4259-4275, 1967.

Oliver, J., Isacks, B., and Barazangi, M., Seismicity at continental margins, in; C. A. Burk and C. L. Drake, eds., The Geology of Continental Margins, Springer-Verlag, Berlin, 85-92, 1974.

Osmaston, M. F., Genesis of ocean ridge median valleys and continental rift valleys, Tectonophysics, 11, 387-405, 1971.

O'Connell, R. J., and Wasserburg, G. J., Dynamics of the motion of a phase change boundary to a change in pressure, Rev. Geophys., 5, 329-410, 1967.

Pallister, J. W., Petroleum in British Somaliland Protectorate, Somaliland Protectorate Geological Survey, unpub. report, 1959.

Pallister, J. W., The Tectonics of East Africa, in; The Tectonics of Africa, UNESCO, Paris, 511-542, 1971.

Papapetru, A., Warmeleitung in kristallen, Physik Z., 35, 527-528, 1934.

Pettijohn, F. J., Sedimentary Rocks, 2nd ed., Harper and Bros., New York, 1957.

Peierls, R., Zur kinetischen theories der warmeleitung in kristallen, Ann. Phys., 3, 1055-1101, 1929.

Phillips, J. D., Woodside, J., and Bowin, C. D., Magnetic and gravity anomalies in the central Red Sea, in; E. T. Degens and D. A. Ross, eds., Hot brines and recent heavy metal deposits in the Red Sea, Springer-Verlag, New York, 98-113, 1969.

Picard, L., Further reflections on graben tectonics in the Levant, in; J. H. Illies and S. Mueller, eds., Graben Problems, Schweizerbart, Stuttgart, 249-267, 1970.

Piper, J. D. A., and Richardson, A., The palaeomagnetism of the Gulf of Guinea volcanic province, West Africa, Geophys. J. R. astr. Soc., 29, 147-172, 1972.

Pirson, S. J., Handbook of well log analysis, Prentice-Hall, New Jersey, 1963.

Pollack, H. N., and Chapman, D. S., To what extent does the lithosphere mask lateral variations of temperature in the asthenosphere, (abstract), Trans. Am. geophys. Union, 56, 1193, 1974.

Popova, A., unpub. research reported in Simmons and Horai (1968), 1968.

Porstendorfer, G., and Kuhn, P., Works for the International Upper Mantle Project on Zanzibar/Tanzania, Monatsberichte der Deutschen Akademie der Wissenschaften zu Berlin, 7, 1-6, 1965.

Powell, R. W., Thermal conductivities and expansion coefficients of ice and water, Advan. in Phys., 7, 276-297, 1958.

Qureshi, I. R., Gravity measurements in the North-Eastern Sudan and the crustal structure of the Red Sea, Geophys. J. R. astr. Soc., 24, 119-135, 1971.

Rasmussen, L. B., Some geological results from the first five Danish exploration wells in the North Sea, Geol. Survey of Denmark, 3rd Series, No. 42, 1974.

Ratcliffe, E. H., Thermal conductivities of fused and crystalline quartz, Brit. J. appl. Phys., 10, 22-25, 1959.

Raymond, L. R., Temperature distribution in a circulating drilling fluid, J. Pet. Tech., 21, 333-341, 1969.

Reel, D. A., and Griffin, G. M., Potentially petroliferous trends in Florida as defined by geothermal gradients, Gulf Coast Assoc. geol. Soc. Trans., 21, 1971.

Regan, R. D., Cain, J. C., and Davis, W. M., A global magnetic anomaly map, J. Geophys. Res., 80, 794-802, 1975.

Rhys, G. H., A proposed standard lithostratigraphic nomenclature for the southern North Sea and an outline structural nomenclature for the whole of the (UK) North Sea, Instit. of Geol. Sci., London, Rept. No. 74/8, 1974.

Richardson, S. W., personal communication, Dept. of Geology and Mineralogy, University of Oxford, Oxford, 1974.

Ringwood, A. E., A model of the upper mantle, 3, Geochim. Cosmochim. Acta, 15, 195-212, 1958.

Ringwood, A. E., Composition and evolution of the upper mantle, in; P. J. Hart, ed., The Earth's Crust and Upper Mantle, Geophysical Monograph Series No. 13, Am. Geophys. Union, Washington, D. C., 1-17, 1969.

Ringwood, A. E., and Green, D. H., Experimental investigations bearing on the nature of the Mohorovicic discontinuity, Nature, 201, 566-567, 1964.

Ross, D. A., and Schlee, J., Shallow structure and development of the southern Red Sea, Geol. Soc. Am. Bull., 84, 3827-3848, 1973.

Roy, R. F., Decker, E. R., Blackwell, D. D., and Birch, F., Heat flow in the United States, J. Geophys. Res., 73, 5207-5221, 1968.

Saggerson, E. P., Metamorphic facies series in Africa; a contrast, Spec. Pub. Geol. Soc. S. Afr., 3, 227-234, 1973.

Sass, J. H., The Earth's heat and internal temperatures, in; I. G. Gass, P. J. Smith, and R. L. Wilson, eds., Understanding the Earth, Artemis Press, Sussex, 81-87, 1972.

Sass, J. H., and LeMarne, A. E., Heat flow at Broken Hill, New South Wales, Geophys. J. R. astr. Soc., 7, 477-489, 1963.

Sass, J. H., Lachenbruch, A. H., and Munroe, R. J., Thermal conductivity of rocks from measurements on fragments and its application to heat flow determinations, J. Geophys. Res., 76, 3391-3401, 1971a.

Sass, J. H., Lachenbruch, A. H., and Jessop, A. M., Uniform heat flow in a deep hole in the Canadian shield and its palaeoclimatic implications, J. Geophys. Res., 76, 8586-8596, 1971b.

Sbrana, F., and Bossolasco, M., Sul regime termico degli strati superiori della crosta terrestre, Geophys. Pura Appl., 23, 3-8, 1952.

Schatz, J. F., and Simmons, G., Thermal conductivity of earth materials at high temperatures, J. Geophys. Res., 77, 6966-6983, 1972.

Scheuch, J., Measurements of heat flow in the Red Sea between 19° and 26° northern latitude (region of the deep brines), Z. Geophys., 39, 859-862, 1973.

Schlich, R., Sea floor spreading history and deep-sea drilling in the Madagascar and Mascarene basins, western Indian Ocean, in; E. S. W. Simpson, R. Schlich et al., eds., Init. Reps. of the Deep Sea Drilling Proj., 25, U. S. Gov. Printing Office, Washington, D. C., 663-678, 1974.

Schlich, R., Aubertin, F., Delteil, J., Leclaire, L., Magnier, P., Montadert, L., Patriat, P., and Valery, P., Donnees nouvelles sur le substratum du Bassin de Somalie a partir d'un profil de sismique reflexion, G. R. Acad. Sci., Paris, 275, 1331-1334, 1972.

Schlumberger, Document 8, Paris, France, 1958.

Schlumberger, Log Interpretation, Vol. 1, Principles, Schlumberger Ltd., New York, 1972.

Schlumberger, Engineered Production Services Manual, Schlumberger Ltd., Paris, France, 1973.

Schlumberger, M., Doll, H. G., and Perebinossoff, A. A., Temperature measurements in oil wells, Instit. Pet. Tech. J., 23, 1-25, 1937.

Schneider, P. J., Conduction, in; W. M. Rohsenow and J. P. Hartnett, eds., Handbook of Heat Transfer, McGraw-Hill Book Co., New York, chapters 1 and 3, 1973.

Schoeppel, R. J., and Gilliranz, S., Use of well log temperatures to evaluate regional geothermal gradients, J. Pet. Tech., 18, 666-673, 1966.

Schurmann, H. M. E., The Precambrian along the Gulf of Suez and northern part of the Red Sea, E. J. Brill., Leiden, 1966.

Sclater, J. G., Heat flow in the northwest Indian Ocean and Red Sea, Phil. Trans. R. Soc. Lond., A, 259, 271-278, 1966.

Sclater, J. G., and Francheteau, J., The implications of terrestrial heat flow observations on current tectonic and geochemical models of the crust and upper mantle of the Earth, Geophys. J. R. astr. Soc., 20, 509-542, 1970.

Searle, R. C., and Gouin, P., An analysis of some local earthquake phases originating near the Afar triple junction, Bull. seis. Soc. Am., 61, 1071-1081, 1971.

Selby, S. M., Sine, Cosine, and Exponential Integrals, in; R. C. Weast and S. M. Selby, eds., Handbook of Tables for Mathematics, 3rd ed., The Chemical Rubber Co., Cleveland, Ohio, 688-692, 1967.

Sellevoll, M. A., Mohorovicic discontinuity beneath Fennoscandia and adjacent parts of the Norwegian Sea, Tectonophysics, 20, 359-366, 1970.

Sellevoll, M. A., and Pomeroy, P., A travel time study for Fennoscandia, Univ. of Bergen pub. no. 9, Norwegian Univ. Press, 1968.

Sestini, J., Cenozoic stratigraphy and depositional history, Red Sea coast Sudan, Am. Assoc. Pet. Geol. Bull., 49, 1453-1472, 1965.

Shackleton, N. J., Ocean palaeotemperature changes around Africa, in; E. M. van Zinderen Bakker, ed., Palaeoecology of Africa, the surrounding islands and Antarctica, 6, Balkema, Cape Town, 37-38, 1972.

Simmons, G., Interpretation of heat flow anomalies, 1, contrasts in heat production, Rev. Geophys., 5, 43-52, 1967.

Simmons, G., and Horai, Ki-iti, Heat flow data, 2, J. Geophys. Res., 73, 6608-6629, 1968.

Sleep, N. H., Thermal effects of the formation of Atlantic continental margins by continental break-up, Geophys. J. R. astr. Soc., 24, 325-350, 1971.

Sleep, N. H., Crustal thinning on Atlantic type continental margins: evidence from older margins, in; D. H. Tarling and S. K. Runcorn, eds., Implications of continental drift to the Earth Sciences, 2, Academic Press, London, 685-692, 1973.

Slettene, R. L., Wilcox, L. E., Blouse, R. S., and Sanders, J. R., Bouguer gravity anomaly map of Africa, Tech. Pap. 73-3, U. S. Def. Mapp. Ag., St. Louis, Missouri, 1973.

Smith, G. D., Numerical solution of partial differential equations, Oxford Univ. Press, London, 1965.

Smithson, S. B., and Decker, E. R., A continental crustal model and its geothermal implications, Earth Planet. Sci. Letts., 22, 215-225, 1974.

Somaliland Oil Exloration Co. Ltd., A geological reconnaissance of the sedimentary deposits of the Protectorate of British Somaliland, Crown Agents, London, 1954.

Somerton, W. H., Some thermal characteristics of porous rocks, J. Pet. Tech., 10, 61-64, 1958.

Somerton, W. H., personal communication, Dept. of Petroleum Engineering, University of California, Berkeley, California, 1974.

Somerton, W. H., and Boozer, G. D., Thermal characteristics of porous rocks at elevated temperatures, J. Pet. Tech., 12, 77-81, 1960.

Sornes, A., Seismic refraction experiments from Norway to Scotland, Phd. thesis, University of Edinburgh, Edinburgh, 1971.

Strachan, P. A., Radiogenic heat production of Cornish granites, (in relation to heat flow), Msc. thesis, University of London, London, 1973.

Strakhov, N. M., Principles of Lithogenesis, Oliver and Boyd, London, 1967.

Struck, B., Zur Kenntnis Afrikanischer Erdbebenvorstellungen, Globus, 1909.

Summers, W. K., Approximation of thermal gradient in southeastern New Mexico using bottom-hole temperatures from electric logs, Am. Assoc. Pet. Geol. Bull., 56, 2072-2074, 1972.

Swanberg, C. A., Chessman, M. D., Simmons, G., Smithson, S. B., Gronlie, G., and Heier, K. S., Heat flow - heat generation studies in Norway, Tectonophysics, 23, 31-48, 1974.

Tarling, D. H., Palaeomagnetism and the origin of the Red Sea and the Gulf of Aden, Phil. Trans. R. Soc. Lond., A, 267, 219-226, 1970.

Tarling, D. H., Sanver, N., and Hutchings, A. M. J., Further palaeomagnetic results from the Federation of South Arabia, Earth Planet. Sci. Letts., 3, 148-154, 1967.

Talwani, M., and Ewing, M., Rapid computation of gravitational attraction of three-dimensional bodies of arbitrary shape, Geophysics, 25, 203-225, 1960.

Tenneco Oil Company, personal communication, Tenneco Ethiopia Inc., Addis Ababa, Ethiopia, 1974.

Thomson, W., On the secular cooling of the Earth, article XCIV, in; Mathematical and Physical Papers, 3, C. J. Clay and Sons, London, 295-311, 1890.

Tikhomirov, V. M., Conductivity of rocks and their relationship with density, saturation, and temperature, Neftianoe Khoziaistro, 46, 36-40, 1968.

Timko, D. J., and Fertl, W. H., How downhole temperatures and pressures affect drilling, part 5, predicting hydrocarbon environments with wireline data, World Oil, 175, 73-88, 1972.

Tittman, J., and Wahl, J. S., The physical foundations of formation density logging (gamma-gamma), Geophysics, 30, 284-294, 1965.

Tittman, J., Sherman, H., Nagel, W. A., and Alger, R. P., The side-wall epithermal neutron porosity log, J. Pet. Tech., 18, 135-1362, 1966.

Tixier, M. P., Alger, R. P., and Tanguy, D. R., New developments in induction and sonic logging, J. Pet. Tech., 12, 79-87, 1960.

Topping, J., Errors of observation and their treatment, The Institute of Physics and the Physical Society Monographs for Students, Chapman and Hall, London, 1962.

Toskoz, M. N., and Arkani-Hamed, J., Seismic delay times: correlation with other data, Science, 158, 783-785, 1967.

Tragesser, A. F., Crawford, P. B., and Crawford, H. R., A method of calculating circulating temperatures, J. Pet. Tech., 19, 1507-1512, 1967.

Trammontini, C., and Davies, D., A seismic refraction survey in the Red Sea, Geophys. J. R. astr. Soc., 17, 225-241, 1969.

Tsederberg, N. V., Thermal conductivity of gases and liquids, M. I. T. Press, Cambridge, Mass., 1965.

United Nations Development Programme, Mineral and Groundwater Survey, Somalia, U. N. Rep. DP/SF/UN/37-Somalia, New York, 1970.

Urey, H. C., The thermodynamic properties of isotopic substances, J. Chem. Soc., 1, 562-581, 1947.

Uyeda, S., and Horai, Ki-iti, Studies of the thermal state of the Earth, 6, Terrestrial heat flow at Innai oil field, Akata Prefecture and at three localities in Kanto District, Japan, Bull. Earthquake Res. Inst., Tokyo Univ., 38, 421-436, 1960.

Van de Lindt, W. J., Movement of the Mohorovicic discontinuity under isostatic conditions, J. Geophys. Res., 72, 1289-1297, 1967.

Van Everdingen, A. F., and Hurst, W., The application of the Laplace transformation to flow problems in reservoirs, Trans. AIME, 186, 305-324, 1949.

Van Orstrand, C. E., Apparatus for measurement of temperature in deep wells by means of a maximum thermometer, Econ. Geol., 19, 229-248, 1924.

Van Orstrand, C. E., Some possible applications of geothermics to geology, Am. Assoc. Pet. Geol. Bull., 18, 13-49, 1934.

Viloria, G., and Ali, S. M. F., Rock thermal conductivity and its variation with density, temperature and fluid saturation, Producers Monthly, 32, 27-30, 1968.

Vine, F. J., Spreading of the ocean floor: new evidence, Science, 154, 1405-1415, 1966.

Von Herzen, R. P., Geothermal heat flow in the Gulfs of Aden and California, Science, 140, 1207-1208, 1963.

Von Herzen, R. P., Heat flow measurements in East Africa (abstract), Tectonophysics, 15, 179, 1972.

Von Herzen, R. P., and Maxwell, A. E., The measurement of thermal conductivity of deep-sea sediments by a needle-probe method, J. Geophys. Res., 64, 1557-1563, 1959.

Von Herzen, R. P., and Uyeda, S., Heat flow through the eastern Pacific floor, J. Geophys. Res., 68, 4219-4250, 1963.

Von Herzen, R. P., and Langseth, M. G., Present status of oceanic heat flow mesurements, Phys. Chem. Earth, 6, 365-407, 1966.

Von Herzen, R. P., and Vacquier, V., Heat flow and magnetic profiles on the mid-Indian Ocean ridge, Phil. Trans. R. Soc. Lond. A, 259, 262-270, 1966.

Von Herzen, R. P., and Vacquier, V., Terrestrial heat flow in Lake Malawi, Africa, J. Geophys. Res., 72, 4221-4226, 1967.

Walcott, R. I., Gravity, flexure and growth of sedimentary basins at a continental edge, Geol. Soc. Am. Bull., 83, 1845-1848, 1972.

Walsh, J. B., and Decker, E. R., Effect of pressure and saturating fluid on the thermal conductivity of compact rocks, J. Geophys. Res., 71, 3053-3061, 1966.

Walters, R., and Linton, R. E., The sedimentary basin of coastal Kenya, in; G. Blant, ed., Sedimentary basins of the African coasts, part 2, South and East coasts, Assoc. Services Geol. Africains, Paris, 133-158, 1973.

Wang, C. Y., Some geophysical implications from gravity and heat flow data, J. Geophys. Res., 70, 5629-5634, 1965.

Warden, A. J., and Daniels, J. L., The Precambrian of the Somalia Republic, unpub. manuscript, 1965.

Watson, G. N., A treatise on the theory of Bessel functions, Cambridge Univ. Press, 2nd ed., 1944.

Watson, G. S., Trend-surface analysis, J. Int. Assoc. Math. Geol., 3, 215-226, 1971.

Weast, R. C., and Selby, S. M., Thermal Conductivity, in; R. C. Weast and S. M. Selby, eds., The Handbook of Chemistry and Physics, The Chemical Rubber Co., Cleveland, Ohio, E-4 and E-11, 1968.

Weertman, J., The creep strenght of the Earth's mantle, Rev. Geophys., 8, 145-168, 1970.

Wetherill, G. W., Steady state calculations bearing on geological implications of a phase transition Mohorovicic discontinuity, J. Geophys. Res., 66, 2983-2993, 1961.

Whiteman, A. J., Rees, G., Naylor, D., and Pegrum, R. P., North Sea troughs and plate tectonics, in; A. Whiteman, D. Roberts and M. A. Sellevoll, eds., Petroleum Geology and Geology of the North Sea and Northeast Atlantic continental margin, Norges Geologiske Undersokelse, 316, 137-162, 1975.

Williamson, K. H., Terrestrial heat flow studies in Kenya, Phd. thesis, University of London, London, 1975.

Willmore, P. L., Crustal structure in the region of the British Isles, Tectonophysics, 20, 341-358, 1973.

Wilson, G. J., and Bush, R. E., Pressure prediction with flowline temperature gradients, J. Pet. Tech., 25, 135-142, 1973.

Wilson, J. T., Did the Atlantic close and then re-open?, Nature, 211, 676-681, 1966.

Wohlenberg, J., Remarks on the seismicity of East Africa between 4^{o}N-12^{o}S and 23^{o}E-40^{o}E, Tectonophysics, 8, 567-578, 1969.

Woodside, W., and Messmer, J. H., The thermal conductivity of porous media, J. appl. Phys., 32, 1688-1706, 1961.

World Oil, The 'boom' returns, 179, 61-64, 1974.

Wright, J. A., and Garland, G. D., In-situ measurements of thermal conductivity in the presence of transverse anisotropy, J. Geophys. Res., 73, 5474-5484, 1968

Wyllie, M. R. J., Gregory, A. R., and Gardiner, G. H. F., An experimental investigation of factors affecting elastic wave velocities in porous media, Geophysics, 23, 459-493, 1958.

Wyllie, P. J., Experimental limits for melting in the Earth's crust and upper mantle, in; J. G. Heacock, ed., The structural and physical properties of the Earth's crust, Geophysical Monograph Series No. 14, Am. Geophys. Union, Washington, D. C., 279-301, 1971.

Yoder, H. S., and Tilley, C. E., Origin of basalt magmas: an experimental study of natural and synthetic rock systems, J. Petrol., 3, 342-532, 1962.

Ziebland, H., Experimental determinations of the thermal conductivity of fluids, in; R. P. Tye, ed., Thermal Conductivity, Academic Press, London, 65-148, 1969.

Ziegler, P. A., The geological evolution of the North Sea area in the tectonic framework of North-western Europe, in; A. Whiteman, D. Roberts and M. A. Sellevoll, eds., Petroleum Geology and Geology of the North Sea and Northeast Atlantic continental margin, Norges Geologiske Undersokelse, 316, 1-28, 1975.

Ziegler, W. H., North Sea basin history in the tectonic framework of North-Western Europe, in; A. W. Woodland, ed., Petroleum and the continental shelf of North West Europe, Applied Science Pub., Barking, 165-190, 1975.

Zierfuss, H., and Van der Vliet, G., Laboratory measurements of heat conductivity of sedimentary rocks, Am. Assoc. Pet. Geol. Bull., 40, 2475-2488, 1956.

Zietz, I., Aeromagnetic investigations of the Earth's crust in the United States, in; P. J. Hart, ed., The Earth's crust and upper mantle, Geophysical Monograph Series No. 13, Am. Geophys. Union, Washington, D. C., 404-414, 1969.

OMISSIONS FROM REFERENCE LIST

American Petroleum Institute (API), Recommended practise for testing oil well cements, RP 108, fifth ed., May, 1956.

Horai, Ki-iti, Effect of past climatic changes on the thermal field of the Earth, Earth Planet. Sci. Letts., 6, 39-42, 1968.

Kent, P. E., and Walmsley, P. J., North Sea progress, Am. Assoc. Pet. Geol. Bull., 54, 168-181, 1970.

Misra, A. K., and Murrell, S. A. F., An experimental study of the effect of temperature and stress on the creep of rocks, Geophys. J. R. astr. Soc., 9, 509-535, 1965.

Polyak, B. G., and Smirnov, Ya. B., Relationship between terrestrial heat flow and the tectonics of continents, Geotectonics, 4, 205-213, 1968.

Sorgenfrei, T., Geological perspectives in the North Sea, Bull. Geol. Soc. Denmark, 19, 160-196, 1969.

Talwani, M., and Eldholm, O., Continental margin off Norway: a geophysical study, Geol. Soc. Am. Bull., 83, 3575-3606, 1972.

Wyllie, M. R. J., Gregory, A. R., and Gardiner, G. H. F., Elastic wave velocities in heterogeneous and porous media, Geophysics, 21, 41-70, 1956.

Bhattacharji, S., and Koide, H., Mechanism model for triple junction fracture geometry, Nature, 255, 21-24, 1975.

Appendix 1

A Discussion of the Paper by E.C. Bullard (1947) entitled 'The Time Necessary for a Borehole To Attain Temperature Equilibrium'

The Bullard (1947) paper on the disturbance due to drilling of the thermal equilibrium in a borehole has long been the standard reference on the subject (cf. Beck, 1965, Kappelmeyer and Haenel, 1974). However, there do appear to be some inconsistencies in the results. Equation (1) from that work,

$$(A.1.1) \qquad T/T_o = \log (1 + t_1/t_2) / (\log 4kt_1/a^2 - .577)$$

which was, in fact, misprinted with the second t_1 appearing as t, is essentially equation (1.12), Section 1.4, where T/T_o is the ratio of the temperature disturbance, t_1 the drilling time, t_2 the time from cessation of drilling to the temperature measurement T, k the thermal diffusivity, a the borehole radius and T_o the initial temperature disturbance. Equation (A.1.1) may be rewritten,

$$(A.1.2) \qquad t_2/t_1 = \left[e^{T/T_o \cdot (\log 4kt_1/a^2 - .577)} \right]^{-1}$$

where the left hand term is the ratio of time that the well must be left to the drilling time in order to reduce the temperature disturbance to a specified value of T/T_o.

Table A.1.1 are those values of t_2/t_1 obtained by Bullard (1947), for a range of t_1 and extreme values of $a^2/4k$; these results being ostensibly calculated from equation (A.1.1). Table A.1.2 are the results which, in fact, should have been calculated by Bullard. The ridiculous value for $t_1 = .1$ and $a^2/4k = 38{,}000$ s., of -49.09, results from the simplification

made by Bullard of ignoring first order and higher terms in calculating the exponential integral, Ei(x), of equations (1.9) - (1.12), Section 1.4. Using sufficient terms to ensure accuracy to 1 part in 10^5 the results were recalculated and are given in table A.1.3 where the bracketed number refers to the highest order term required for the evaluation of (1.9). The value for $a^2/4k = 38{,}000$ and $t_1 = .1$ is no longer negative but is so large as to be obviously wrong. The reason is, of course, that the short drilling time and large borehole radius substantially reduce the initial temperature disturbance at radius a at time t_1. Thus T_o is much less than that for the other cases and in having T to fall to $.01T_o$ we are asking for a much smaller temperature disturbance than we intended (see also Fig. 1.7b).

Finally a comparison calculation for the case of a cylindrical source, Sections 1.5 and 1.6, was made, table A.1.4.

In a recent communication, Bullard (1975, pers. comm.) has confirmed the results presented in Tables A.1.1 - A.1.4. A paper (Evans and Bullard, 1975) to correct the Bullard (1947) work has been prepared.

Table A.1.1 Time necessary for a borehole to return to thermal equilibrium (Bullard, 1947) Determined from Equation (A.1.1)

t_1	.1	1	10	100 (Days)	$a^2/4k$
t_2/t_1	14	11	8.8	7.4	58 seconds
t_2/t_1	51	28	18	13	38,000 seconds

Table A.1.2 Values of t_2/t_1 for Equation (A.1.2) for Bullard's (1947) parameters

t_1	.1	1	10	100 (Days)	$a^2/4k$
t_2/t_1	22.09	14.37	10.58	8.33	58 seconds
t_2/t_1	-49.09	408.66	38.76	20.12	38,000 seconds

Table A.1.3* Values of t_2/t_1 for a line source model insuring sufficient orders of the argument of exponential integral, Equation (A.1.3), for accuracy to within 10^{-5}

t_1	.1	1	10	100 (Days)	$a^2/4k$
t_2/t_1	22.06(1)	14.36(1)	10.58(0)	8.33(0)	58 seconds
t_2/t_1	42,400(21)	155.31(5)	38.06(2)	20.10(1)	38,000 seconds

Table A.1.4 Cylindrical Source Model (See Sections 1.5 and 1.6 for details)

t_1	.1	1	10	100 (Days)	$a^2/4k$
t_2/t_1	24.3	12.7	6.1	2.7	58 seconds
t_2/t_1	185.2	90.5	42.3	22.0	38,000 seconds

*Note - values in brackets refer to the order of the argument (maximum) in the exponential integral to produce the stated accuracy.

Appendix 2

Equations and Tables For The Unit Functions $T(t_d)$, $Q(t_d)$, and $q(t_d)$

The evaluation of the dimensionless temperature disturbance in equation (1.43) required the computation of the dimensionless unit temperature function $T(t_d)$, equation 1.36, and the unit heat flow function $q(t_d)$. Edwardson et al. (1962) have approximated these terms by polynomial functions,

$$(A.2.1) \qquad T(t_d) = \frac{370.529\ t_d^{\frac{1}{2}} + 137.582\ t_d + 5.69549\ t_d^{3/2}}{328.834 + 265.488\ t_d^{\frac{1}{2}} + 45.215\ t_d + t_d^{3/2}}$$

$$(.01 < t_d < 500)$$

$$(A.2.2) \qquad q(t_d) = \frac{26.7544 + 43.5537\ t_d^{\frac{1}{2}} + 13.3813\ t_d + .492949\ t_d^{3/2}}{47.4210\ t_d^{\frac{1}{2}} + 35.5372\ t_d + 2.60967\ t_d^{3/2}}$$

$$(.01 < t_d < 200)$$

where t_d is the dimensionless time factor, equation (1.44), section 1.6.

However, $q(t_d)$ is obviously infinite at $t_d = 0$ so the method of computation of equation (1.43) was by using the unit cumulative heat flow, $Q(t_d)$, equation (1.37), given by,

$$(A.2.3) \qquad Q(t_d) = \frac{1.12834\ t_d^{\frac{1}{2}} + 1.19328\ t_d + .269872\ t_d^{3/2} + .00855294\ t_d^{2}}{1 + .616599\ t_d^{\frac{1}{2}} + .0413008\ t_d}$$

$$(.01 < t_d < 200)$$

The computing scheme was to calculate $Q(t_d)$ at intervals of $t_d = .02$, take the difference and divide by .02 to obtain a $q(t_d^*)$ value where t_d^* is the mean of the two time values. A corresponding value of $T(t_d^*)$ was also computed. Edwardson et al. (1962) have shown this to be a valid technique.

Depending on the length of time t_d, individual calculations of equation (1.43) required one to twenty seconds of central processor time

on a CDC 6400. Stopping circulation was simulated by introducing a negative $q(t_d^*)$ when t_d was equivalent to time t_1 as defined in Section 1.4. A short table of $T(t_d)$ and $Q(t_d)$, after Van Everdingen and Hurst (1949), covering the range used in this study follows.

Table A.2.1

Unit Functions, $Q(t_d)$ and $T(t_d)$

t_d	$Q(t_d)$	$T(t_d)$
0.0	0.0	0.0
0.01	.112	.112
0.05	.278	.229
0.10	.404	.315
0.50	1.020	.616
1.0	1.570	.802
5.0	4.541	1.362
10.0	7.417	1.651
50.0	24.820	2.388
100.0	43.010	2.723

Appendix 3

Derivation of the nonporous rock conductivity from the Maxwell Spheres Relation

The lower limit for the Maxwell spheres model, equation 2.11, is,

$$(A.3.1) \qquad K_l = K_w + (1 - \phi) \cdot \left[(K_r - K_w)^{-1} + \phi \cdot (3K_w)^{-1} \right]^{-1}$$

where ϕ was the volume fraction of water, K_w and K_r the water and nonporous rock conductivities respectively and K_l the lower limit for the aggregate conductivity. Rewriting terms in the bracket of A.3.1 and rearranging,

$$(A.3.2) \qquad \frac{K_l - K_w}{1 - \phi} = \left[\frac{1}{K_r - K_w} + \frac{\phi}{3K_w} \right]^{-1}$$

or,

$$(A.3.3) \qquad (K_r - K_w)^{-1} = (1 - \phi) \cdot (K_l - K_w)^{-1} - \phi \cdot (3K_w)^{-1}$$

and finally,

$$(A.3.4) \qquad K_r = K_w + \left[(1 - \phi) \cdot (K_l - K_w)^{-1} - \phi \cdot (3K_w)^{-1} \right]^{-1}$$

The determination of the nonporous rock conductivity from the upper limit, equation (2.12), is less straight-forward. The upper limit aggregate conductivity, K_u, is given by,

$$(A.3.5) \qquad K_u = K_r + \phi \cdot \left[(K_w - K_r)^{-1} + (1 - \phi) \cdot (3 \cdot K_r)^{-1} \right]^{-1}$$

Rearranging terms we get,

$$(A.3.6) \qquad \frac{K_U - K_r}{K_w - K_r} + \frac{K_U \cdot (1 - \eta)}{3K_r} - \frac{1 + 2\eta}{3} = 0$$

or,

$$(A.3.7) \qquad (2\eta - 2) \cdot K_r^2 + \left[K_U \cdot (2\eta - \eta) - K_w \cdot (1 + 2\eta)\right] \cdot K_r \cdots\cdots$$

$$\cdots\cdots + K_w \cdot K_U \cdot (1 - \eta) = 0$$

Clearly (A.3.7) represents a quadratic in K_r with the solution,

$$(A.3.8) \qquad K_r = \frac{-B \pm (B^2 - AC)^{\frac{1}{2}}}{2A}$$

where,

$$A = 2\eta - 2$$

$$B = K_U \cdot (2 + \eta) - K_w \cdot (1 + 2\eta)$$

$$C = K_w \cdot K_U \cdot (1 - \eta)$$

now, $0 < \eta < 1$

and, $0 < K_w$

and, $0 < K_r$

$\therefore$ $2\eta - 2 = A < 0$

thus, $K_w \cdot K_U \cdot (1 - \eta) = C > 0$

combining the above two lines,

$$4AC < 0$$

by definition,

$$B^2 > 0$$

$$\therefore \qquad (B^2 - 4AC)^{\frac{1}{2}} > B$$

but, $$- B \pm (B^2 - 4AC)^{\frac{1}{2}} < 0$$

since, $$2A < 0$$

and, $$K_r > 0$$

Therefore, the sign must be negative in (A.1.8) and the full solution is,

$$(A.3.9) \qquad K_r = \frac{- B - \left[B^2 - 4 \cdot (2\mathfrak{N} - 2) \cdot \left\{K_w \cdot K_u \cdot (1 - \mathfrak{N})\right\}\right]^{\frac{1}{2}}}{2 \cdot (2\mathfrak{N} - 2)}$$

Now in a manner analogous to that of Horai and Simmon (1969) for the computation of an aggregate conductivity from the mean of the upper and lower bounds, (A.3.1) and (A.3.5), where we measure an aggregate conductivity, K_a we may replace K_u and K_l to obtain the mean value for K_r thus,

$$(A.3.10) \qquad K_r = \tfrac{1}{2} \cdot \left[(K_w \cdot (1 - \mathfrak{N}) \cdot (K_a - K_w)^{-1} - \mathfrak{N} \cdot (3K_w)^{-1}\right]$$

$$+ \tfrac{1}{2} \cdot \left[\frac{- B - \left\{B^2 - 4 \cdot (2\mathfrak{N} - 2) \cdot K_w \cdot K_a (1 - \mathfrak{N})\right\}^{\frac{1}{2}}}{2 \cdot (2\mathfrak{N} - 2)}\right]$$

which is identical with equation (2.22).

Appendix 4

Solution of the Subsidiary Heat Equation For the Semi-Infinite Region Moving With a Velocity, u.

From equation (3.26), section 3.5, we have the nonhomogeneous second order linear partial differential equation,

$$(A.4.1) \qquad \frac{d^2\bar{T}}{dx^2} - \frac{u d\bar{T}}{k dx} - \frac{p\bar{T}}{k} = \frac{-A_o}{Kp} - \frac{V_o + a_x}{k}$$

where $\bar{T}$ is the Laplace transform of the temperature T, A_o, K, and k are the heat production, conductivity and diffusivity respectivity of the semi-infinite region and p is the Laplace operator. The initial and boundary conditions are,

$$(A.4.2) \qquad T = T_o + a_x \qquad x > o, \quad t = o$$

$$(A.4.3) \qquad T = T_1 + b_t \qquad x = o, \quad t > o$$

where we are to solve (A.4.1) with,

$$(A.4.4) \qquad \bar{T} = \frac{T_1}{p} + \frac{b}{p^2} \qquad \text{when } x = o$$

The solution of the homogeneous form of (A.4.1) is given by (cf. Kreysnig, 1968),

$$(A.4.5) \qquad \bar{T}_H = c_1 e^{-x \cdot \left[\frac{-u}{2k} - \left(\frac{u^2}{4k} + \frac{p}{k}\right)^{\frac{1}{2}}\right]} + c_2 e^{-x \cdot \left[\frac{-u}{2k} + \left(\frac{u^2}{4k} + \frac{p}{k}\right)^{\frac{1}{2}}\right]}$$

where c_1 and c_2 are constants. However, as the term $\bar{T} \to o$ as $x \to \infty$, equation (A.4.5) is simplified, as $c_1 = o$, to,

$$(A.4.6) \qquad \bar{T}_H = c_2\, e^{-x\cdot\left[-u/2k + \left(u^2/4k + p/k\right)^{\frac{1}{2}}\right]}$$

The general form of (A.4.1) may be written as,

$$(A.4.7) \qquad \frac{d^2\bar{T}}{dx^2} + \frac{2n\cdot d\bar{T}}{dx} + m^2\bar{T} = f(x)$$

which has a particular solution, where $n^2 > m^2$, of, (Schneider, 1973),

$$(A.4.8) \qquad \bar{T}_p = \left\{ e^{-(n-(n^2-m^2)^{\frac{1}{2}})\times} \cdot\int f(x)e^{(n-(n^2-m^2)^{\frac{1}{2}})x}\,dx \right.$$

$$\left. -e^{-(n+(n^2-m^2)^{\frac{1}{2}})\times} \cdot\int f(x)e^{(n+(n^2-m^2)^{\frac{1}{2}})\times}\,dx \right\} \Big/ 2\cdot(n^2-m^2)^{\frac{1}{2}}$$

where from (A.4.1)

$$(A.4.9) \qquad n = -u/2k$$

$$(A.4.10) \qquad m = (-p/k)^{\frac{1}{2}}$$

$$(A.4.11) \qquad f(x) = -A_o/K_p - (V_o + ax)/k$$

If we let,

$$(A.4.12) \qquad g(x) = (n - (n^2 - m^2)^{\frac{1}{2}})\times$$

$$(A.4.13) \qquad h(x) = (n + (n^2 - m^2)^{\frac{1}{2}})\times$$

then,

$$(A.4.14) \qquad \bar{T}_p = \left\{ e^{-g(x)} \cdot\int f(x)e^{g(x)}\,dx - e^{-h(x)} \cdot\int f(x)e^{h(x)}\,dx \right\} \Big/ 2\cdot(n^2-m^2)^{\frac{1}{2}}$$

which lends itself to solution by integration by parts. Where f(x), g(x), h(x) are linear functions in x as we have here, ie. their first order deriviatives are constants, we obtain;

$$(A.4.15)\quad \bar{T}_p = \frac{\frac{f(x)}{g'(x)} - \frac{f'(x)}{g'(x)^2} - \frac{f(x)}{h'(x)} + \frac{f'(x)}{h'(x)^2}}{2(n^2 - m^2)^{\frac{1}{2}}}$$

which is convenient as it removes terms of x in g(x) and h(x) leaving only constants and f(x), ie.

$$(A.4.16)\quad g'(x) = n - (n^2 - m^2)^{\frac{1}{2}}$$

$$(A.4.17)\quad h'(x) = n + (n^2 - m^2)^{\frac{1}{2}}$$

$$(A.4.18)\quad f'(x) = -a/k$$

We may simplify (A.4.15) by substituting (A.4.16) and (A.4.17) to obtain,

$$(A.4.19)\quad \bar{T}_p = \frac{f(x)}{m^2} - \frac{2n.f'(x)}{m^4}$$

and further substituting (A.4.9 - A.4.11) and (A.4.18) we have,

$$(A.4.20)\quad T_p = \frac{A_o k/K - au}{p^2} + \frac{V_o + ax}{p}$$

Finally, the general solution of (A.4.1) is,

$$(A.4.21)\quad \bar{T} = \bar{T}_h + \bar{T}_p$$

Combining (A.4.6) and A.4.20) we have,

$$(A.4.22)\quad T = c_2 e^{-x \cdot \left[-u/2k \div \left(u^2/4k + p/k \right)^{\frac{1}{2}} \right]} + \frac{A_o k/K - au}{p^2} + \frac{T_o + ax}{p}$$

and invoking (A.4.4) at x = o to obtain the constant c_2 we find,

$$(A.4.23) \qquad \bar{T} = \left[\frac{T_1 - T_o}{\mathcal{P}} + \frac{b + au - A_o k/K}{\mathcal{P}^2} \right] . a \left[ux/2k - x \left(u^2/4k^2 + p/k \right)^{\frac{1}{2}} \right]$$

$$+ \frac{A_o k/K - au}{\mathcal{P}^2} + \frac{T_o + ax}{\mathcal{P}}$$

which is identical with equation (3.28).

Appendix 5

Tabulation of Eastern Africa Temperature and Conductivity Data

The BHT and thermal conductivity data for the sixty-eight Eastern Africa oil exploration boreholes (Figs. 4.1, 4.12, 4.17) are tabulated in the order in which they are presented in tables 4.1, 4.2, 4.3, Chapter 4.

The well name, country, company (the operator), latitude and longitude (degrees/minutes) are given for each borehole. This is followed by a table of the depths (DEPTH) in metres and BHTs (TEMP) in deg. C. Finally there is a second table of the depth ranges (FROM TO) in metres and the measured or assigned conductivities (COND) in $W \cdot m^{-1} \cdot K^{-1}$. The depth range was assigned taking into consideration sample depth, lithologic boundaries and distribution of conductivity measurements (see section 3.2). The conductivity values are followed by a bracketed number (1 through 7) which gives the grade of measurement or method of estimation as discussed in section 3.9 and defined in table 3.11.

The data presented in these tabulations represent all the information (bar lithological) available for the computation of the heat flow values (section 4.7) and the preparation of the composite heat flow plots (sections 4.9 - 4.18).

WELL NAME - DUNGUNAB-1 LATITUDE - 21D 00M N.
COUNTRY - SUDAN LONGITUDE - 37D 05M E.
COMPANY - AGIP

DEPTH	TEMP	DEPTH	TEMP	DEPTH	TEMP
0.0	29.0	1181.0	65.0	1507.0	76.0

DUNGUNAB-1 CONDUCTIVITY DATA

FROM	TO	CONDUCT	FROM	TO	CONDUCT
0.0	396.0	2.16(6)	396.0	495.7	5.53(5)
495.7	838.2	5.27(1)	838.2	1118.0	5.19(1)
1118.0	1142.0	1.40(6)	1142.0	1274.0	3.44(6)
1274.0	1340.0	1.54(3)	1340.0	1371.0	1.46(6)
1371.0	1448.0	3.60(6)	1448.0	1478.0	1.40(5)
1478.0	1567.0	3.60(1)			

WELL NAME - NAGHERSUM-1 LATITUDE - 20D 49M N.
COUNTRY - SUDAN LONGITUDE - 37D 17M E.
COMPANY - AGIP

DEPTH	TEMP	DEPTH	TEMP	DEPTH	TEMP
1093.0	63.0	1760.0	81.0	1956.5	90.0
2284.0	101.0				

NAGHERSUM-1 CONDUCTIVITY DATA

FROM	TO	CONDUCT	FROM	TO	CONDUCT
0.0	18.0	2.10(6)	18.0	116.0	2.52(6)
116.0	674.7	4.73(2)	674.7	874.4	2.16(2)
874.4	1285.0	5.47(5)	1285.0	1507.0	2.63(5)
1507.0	1761.0	2.80(3)	1761.0	1868.5	2.73(1)
1868.5	2042.5	2.93(1)	2042.5	2189.7	3.70(5)
2189.7	2284.0	3.20(3)			

WELL NAME - ABU SHAGARA-1 LATITUDE - 21D 03M N.
COUNTRY - SUDAN LONGITUDE - 37D 17M E.
COMPANY - AGIP

DEPTH	TEMP	DEPTH	TEMP	DEPTH	TEMP
1272.0	64.0	1897.0	82.0	2293.0	95.0

ABU SHAGARA-1 CONDUCTIVITY DATA

FROM	TO	CONDUCT	FROM	TO	CONDUCT
0.0	324.0	2.71(6)	324.0	1024.0	3.64(1)
1024.0	1230.0	3.52(2)	1230.0	1393.7	3.44(2)
1393.7	1580.0	3.22(2)	1580.0	1609.7	2.10(6)
1609.7	1773.5	3.96(2)	1773.5	1939.5	2.84(1)
1939.5	2101.2	2.10(1)	2101.2	2217.5	5.71(1)
2217.5	2293.0	3.59(3)			

WELL NAME - MARAFIT-1 LATITUDE - 10D 19M N.
COUNTRY - SUDAN LONGITUDE - 37D 54M E.
COMPANY - AGIP

DEPTH	TEMP	DEPTH	TEMP	DEPTH	TEMP
0.0	23.0	1525.0	68.0	2256.0	95.0

MARAFIT-1 CONDUCTIVITY DATA

FROM	TO	CONDUCT	FROM	TO	CONDUCT
0.0	2256.0	3.47(6)			

WELL NAME - AMBER-1 LATITUDE - 16D 21M N.
COUNTRY - ETHIOPIA LONGITUDE - 40D 01M E.
COMPANY - MOBIL

DEPTH	TEMP	DEPTH	TEMP	DEPTH	TEMP
893.4	60.0	2541.4	101.7	3525.9	136.0

AMBER-1 CONDUCTIVITY DATA

FROM	TO	CONDUCT	FROM	TO	CONDUCT
0.0	93.4	1.51(5)	93.4	175.6	3.04(5)
175.6	291.7	4.23(5)	291.7	474.6	4.94(5)
474.6	657.5	4.41(5)	657.5	840.3	4.40(5)
840.3	1023.2	4.84(5)	1023.2	1221.3	5.35(5)
1221.3	1419.5	5.11(5)	1419.5	1602.3	5.86(5)
1602.3	1785.2	4.35(5)	1785.2	1968.1	5.42(5)
1968.1	2151.0	5.45(5)	2151.0	2333.9	5.30(5)
2333.9	2516.7	5.12(5)	2516.7	2699.6	4.65(5)
2699.6	2882.5	5.14(5)	2882.5	3065.4	5.29(5)
3065.4	3248.3	5.72(5)	3248.3	3408.3	5.31(5)
3408.3	3522.6	3.37(5)	3522.6	3525.9	2.29(5)

WELL NAME - B-1 LATITUDE - 16D 35M N.
COUNTRY - ETHIOPIA LONGITUDE - 40D 25M E.
COMPANY - MOBIL

DEPTH	TEMP	DEPTH	TEMP	DEPTH	TEMP
880.6	73.3	1310.0	93.3	1371.3	97.8
2432.9	151.1	2880.7	172.2		

B-1 CONDUCTIVITY DATA

FROM	TO	CONDUCT	FROM	TO	CONDUCT
0.0	680.0	2.71(5)	680.0	1234.7	4.99(6)
1234.7	1270.4	1.68(6)	1270.4	1420.7	4.99(6)
1420.7	1445.7	1.68(6)	1445.7	1659.6	2.35(6)
1659.6	1765.1	1.68(6)	1765.1	1903.5	4.99(6)
1903.5	2680.7	1.68(5)			

WELL NAME - C-1 LATITUDE - 16D 49M N.
COUNTRY - ETHIOPIA LONGITUDE - 39D 13M E.
COMPANY - MOBIL

DEPTH	TEMP	DEPTH	TEMP	DEPTH	TEMP
0.0	26.0	1238.7	73.9	2831.0	160.0

C-1 CONDUCTIVITY DATA

FROM	TO	CONDUCT	FROM	TO	CONDUCT
0.0	1076.6	2.71(6)	1076.6	1564.2	2.21(6)
1564.2	2545.7	5.02(6)	2545.7	2831.0	4.99(6)

WELL NAME - C-1A LATITUDE - 16D 49M N.
COUNTRY - ETHIOPIA LONGITUDE - 39D 13M E.
COMPANY - MOBIL

DEPTH	TEMP	DEPTH	TEMP	DEPTH	TEMP
0.0	26.0	653.5	54.4	1906.2	126.9

C-1A CONDUCTIVITY DATA

FROM	TO	CONDUCT	FROM	TO	CONDUCT
0.0	771.8	2.71(6)	771.8	1396.6	2.44(7)
1396.6	1906.2	2.19(7)			

WELL NAME - BERBERA-1 LATITUDE - 10D 25M N.
COUNTRY - SOMALIA LONGITUDE - 44D 59M E.
COMPANY - BP

DEPTH	TEMP	DEPTH	TEMP	DEPTH	TEMP
0.0	30.0	770.2	57.2		

BERBERA-1 CONDUCTIVITY DATA

FROM	TO	CONDUCT	FROM	TO	CONDUCT
0.0	65.5	2.87(7)	65.5	189.6	2.22(7)
189.6	332.2	2.61(7)	332.2	396.8	2.87(7)
396.8	545.3	2.38(7)	545.3	770.2	2.03(7)

WELL NAME - DAGAH SHABEL-1 LATITUDE - 10D 11M N.
COUNTRY - SOMLIA LONGITUDE - 45D 17M E.
COMPANY - MOBIL

DEPTH	TEMP	DEPTH	TEMP	DEPTH	TEMP
0.0	30.0	141.1	36.1	887.9	50.6
1047.6	52.8	1131.1	56.1	1300.6	57.2
1367.3	53.3				

DAGAH SHABEL-1 CONDUCTIVITY DATA

FROM	TO	CONDUCT	FROM	TO	CONDUCT
0.0	487.4	3.03(7)	487.4	784.3	2.27(7)
784.3	844.3	1.81(7)	844.3	904.0	2.72(7)
904.0	984.5	1.81(7)	984.5	1101.5	2.72(7)
1101.5	1293.0	3.03(7)	1293.0	1303.3	1.67(7)
1303.3	1367.3	2.18(7)			

WELL NAME - DAGAH SHABEL-2 LATITUDE - 10D 11M N.
COUNTRY - SOMLIA LONGITUDE - 45D 17M E.
COMPANY - MOBIL

DEPTH	TEMP	DEPTH	TEMP	DEPTH	TEMP
0.0	30.0	311.2	46.7	960.7	50.0
1451.2	62.8				

DAGAH SHABEL-2 CONDUCTIVITY DATA

FROM	TO	CONDUCT	FROM	TO	CONDUCT
0.0	487.7	3.03(7)	487.7	784.6	2.27(7)
784.6	844.6	1.81(7)	844.6	904.3	2.72(7)
904.3	984.8	1.81(7)	984.8	1101.9	2.72(7)
1101.9	1293.3	3.03(7)	1293.3	1303.6	1.67(7)
1303.6	1451.2	2.18(7)			

WELL NAME - DAGAH SHABEL-3 LATITUDE - 10D 11M N.
COUNTRY - SOMLIA LONGITUDE - 45D 17M E.
COMPANY - MOBIL

DEPTH	TEMP	DEPTH	TEMP	DEPTH	TEMP
0.0	30.0	276.1	43.3	985.7	53.9
1505.1	59.6				

DAGAH SHABEL-3 CONDUCTIVITY DATA

FROM	TO	CONDUCT	FROM	TO	CONDUCT
0.0	885.7	2.27(7)	885.7	961.9	2.72(7)
961.9	1280.5	1.81(7)	1289.5	1356.4	2.72(7)
1356.4	1425.2	2.72(7)	1425.2	1505.1	3.03(7)

WELL NAME - BIYO DADER
COUNTRY - SOMALIA
COMPANY - MOBIL

LATITUDE - 10D 15M N.
LONGITUDE - 45D 26M E.

DEPTH	TEMP	DEPTH	TEMP	DEPTH	TEMP
0.0	30.0	828.1	53.3	1474.6	67.8

BIYO DADER CONDUCTIVITY DATA

FROM	TO	CONDUCT	FROM	TO	CONDUCT
0.0	491.6	3.03(7)	491.6	788.5	2.27(7)
788.5	848.6	1.81(7)	848.6	908.3	2.72(7)
908.3	988.8	1.81(7)	988.8	1105.8	2.72(7)
1105.8	1297.2	3.03(7)	1297.2	1307.6	1.67(7)
1307.6	1474.6	2.18(7)			

WELL NAME - BURAN-1 LATITUDE - 100 14M N.
COUNTRY - SOMALIA LONGITUDE - 480 54M E.
COMPANY - AMERADA

DEPTH	TEMP	DEPTH	TEMP	DEPTH	TEMP
0.0	23.9	2432.0	92.2		

BURAN-1 CONDUCTIVITY DATA

FROM	TO	CONDUCT	FROM	TO	CONDUCT
0.0	300.5	2.55(6)	300.5	763.8	2.85(6)
763.8	1390.2	2.66(6)	1390.2	2342.7	2.46(6)
2342.7	2421.3	6.11(6)	2421.3	2432.0	2.26(6)

WELL NAME - BURHISSO-1 LATITUDE - 080 19M N.
COUNTRY - SOMALIA LONGITUDE - 470 54M E.
COMPANY - AMERADA

DEPTH	TEMP	DEPTH	TEMP	DEPTH	TEMP
0.0	23.9	1545.3	97.8		

BURHISSO-1 CONDUCTIVITY DATA

FROM	TO	CONDUCT	FROM	TO	CONDUCT
0.0	245.7	2.55(6)	245.7	670.9	2.85(6)
670.9	1399.3	2.66(6)	1399.3	1483.2	2.46(6)
1483.2	1535.0	6.11(6)	1535.0	1545.3	2.26(6)

WELL NAME - FARO HILLS-1 LATITUDE - 09D 38M N.
COUNTRY - SOMALIA LONGITUDE - 47D 47M E.
COMPANY - AMERADA

DEPTH	TEMP	DEPTH	TEMP	DEPTH	TEMP
0.0	23.9	1611.2	99.4	1632.2	108.9

FARO HILLS-1 CONDUCTIVITY DATA

FROM	TO	CONDUCT	FROM	TO	CONDUCT
0.0	102.4	2.47(6)	102.4	428.5	2.55(6)
428.5	894.9	2.85(6)	894.9	1590.4	2.66(6)
1590.4	1631.0	6.11(6)	1631.0	1632.2	2.18(7)

WELL NAME - LAS ANOD-1 LATITUDE - 08D 28M N.
COUNTRY - SOMALIA LONGITUDE - 47D 12M E.
COMPANY - AMERADA

DEPTH	TEMP	DEPTH	TEMP	DEPTH	TEMP
0.0	23.9	270.1	33.3	1659.0	68.9

LAS ANOD-1 CONDUCTIVITY DATA

FROM	TO	CONDUCT	FROM	TO	CONDUCT
0.0	152.7	2.55(6)	152.7	581.3	2.85(6)
581.3	1213.4	2.66(6)	1213.4	1536.0	2.46(6)
1536.0	1571.5	6.11(6)	1571.5	1659.0	2.26(6)

WELL NAME - YAGURI-1 LATITUDE - 08D 39M N.
COUNTRY - SOMALIA LONGITUDE - 47D 01M E.
COMPANY - AMERADA

DEPTH	TEMP	DEPTH	TEMP	DEPTH	TEMP
0.0	23.9	1436.8	62.2		

YAGURI-1 CONDUCTIVITY DATA

FROM	TO	CONDUCT	FROM	TO	CONDUCT
0.0	131.7	2.55(6)	131.7	502.9	2.85(6)
502.9	1039.7	2.66(6)	1039.7	1331.4	2.46(6)
1331.4	1360.6	6.11(6)	1360.6	1436.8	2.26(6)

WELL NAME - DARIN-1 LATITUDE - 10D 40M N.
COUNTRY - SOMALIA LONGITUDE - 49D 45M E.
COMPANY - AGIP

DEPTH	TEMP	DEPTH	TEMP	DEPTH	TEMP
352.0	44.0	974.0	44.0	1605.0	55.0
2187.5	75.0	2950.0	91.0	2962.7	91.0

DARIN-1 CONDUCTIVITY DATA

FROM	TO	CONDUCT	FROM	TO	CONDUCT
0.0	179.5	3.41(3)	179.5	272.6	2.67(1)
272.8	525.5	2.26(3)	525.5	635.2	2.38(2)
635.2	783.3	2.72(1)	783.3	1014.2	2.88(1)
1014.2	1122.2	2.78(1)	1122.2	1198.2	2.89(1)
1198.2	1353.3	2.38(1)	1353.3	1490.2	2.89(1)
1490.2	1651.2	2.70(2)	1651.2	1751.0	2.62(1)
1751.0	1851.7	2.82(1)	1851.7	1959.9	2.78(1)
1959.9	2020.5	2.54(2)	2020.5	2362.0	5.54(2)
2362.0	2558.5	2.58(3)	2558.5	2692.7	2.56(3)
2692.7	2839.2	2.25(2)	2839.2	2905.5	6.11(1)
2905.5	2962.7	2.26(1)			

WELL NAME - SAGALEH-1 LATITUDE - 09D 29M N.
COUNTRY - SOMALIA LONGITUDE - 50D 48M E.
COMPANY - AGIP

DEPTH	TEMP	DEPTH	TEMP	DEPTH	TEMP
391.8	25.0	950.8	49.0	1862.9	63.0
3045.8	83.0	3263.9	99.0		

SAGALEH-1 CONDUCTIVITY DATA

FROM	TO	CONDUCT	FROM	TO	CONDUCT
0.0	386.6	2.44(2)	386.6	703.0	4.57(2)
703.0	899.9	2.24(2)	899.9	1322.7	1.69(2)
1322.7	1597.9	1.98(1)	1597.9	1982.3	2.56(2)
1982.3	2321.5	2.61(2)	2321.5	2594.0	2.48(2)
2594.0	3059.1	5.48(1)	3059.1	3240.8	2.55(6)
3240.8	3263.9	5.72(1)			

WELL NAME - HORDIO-1 LATITUDE - 10D 37M N.
COUNTRY - SOMALIA LONGITUDE - 51D 00M E.
COMPANY - AGIP

DEPTH	TEMP	DEPTH	TEMP	DEPTH	TEMP
360.3	44.0	1469.0	55.5	2013.1	75.0
2703.3	105.0	3404.8	106.0		

HORDIO-1 CONDUCTIVITY DATA

FROM	TO	CONDUCT	FROM	TO	CONDUCT
0.0	151.5	3.40(5)	151.5	416.3	1.41(4)
416.3	516.8	1.88(4)	516.8	615.8	1.82(4)
615.8	714.8	2.96(5)	714.8	816.3	1.64(4)
816.3	917.3	3.52(5)	917.3	1017.0	2.07(4)
1017.0	1117.0	4.43(5)	1117.0	1216.0	5.29(5)
1216.0	1316.3	4.04(5)	1316.3	1417.0	1.98(4)
1417.0	1547.7	3.11(5)	1547.7	1617.0	2.88(5)
1617.0	1717.3	2.80(5)	1717.3	1823.9	2.77(5)
1823.9	1915.3	2.13(4)	1915.3	2016.5	2.29(4)
2016.5	2116.8	1.58(4)	2116.8	2217.3	1.75(4)
2217.3	2316.8	2.04(4)	2316.8	2416.8	3.46(5)
2416.8	2517.3	3.28(4)	2517.3	2617.8	2.63(4)
2617.8	2717.3	1.93(4)	2717.3	2816.8	2.13(4)
2816.8	2916.8	1.63(4)	2916.8	3017.8	2.55(4)
3017.8	3140.9	2.06(4)	3140.9	3217.3	1.95(4)
3217.3	3318.3	2.60(4)	3318.3	3404.8	2.67(4)

WELL NAME - COTTON-1 LATITUDE - 09D 33M N.
COUNTRY - SOMALIA LONGITUDE - 50D 31M E.
COMPANY - AGIP

DEPTH	TEMP	DEPTH	TEMP	DEPTH	TEMP
348.6	28.0	1148.5	54.0	2203.0	71.0
3306.0	106.0				

COTTON-1 CONDUCTIVITY DATA

FROM	TO	CONDUCT	FROM	TO	CONDUCT
0.0	52.0	2.90(5)	52.0	151.5	3.38(5)
151.5	251.5	3.43(5)	251.5	339.8	1.99(4)
339.8	457.0	2.16(4)	457.0	556.0	1.78(4)
556.0	650.5	1.85(4)	650.5	745.8	1.97(4)
745.8	996.1	2.67(6)	996.1	1214.6	1.69(6)
1214.6	1300.0	2.25(4)	1300.0	1404.0	1.59(4)
1404.0	1507.0	2.40(4)	1507.0	1608.0	2.54(4)
1608.0	1698.9	1.89(4)	1698.9	1802.5	2.21(4)
1802.5	1955.0	2.28(4)	1955.0	2136.3	2.05(4)
2136.3	2208.0	2.30(4)	2208.0	2284.8	2.25(4)
2284.8	2400.5	2.09(4)	2400.5	2508.5	2.90(4)
2508.5	2608.5	3.13(4)	2608.5	2708.5	3.44(4)
2708.5	2808.5	3.96(4)	2808.5	2908.5	2.71(4)
2908.5	3003.5	2.57(4)	3003.5	3109.0	3.26(4)
3109.0	3209.5	1.67(4)	3209.5	3306.0	2.52(4)

WELL NAME - EL HAMURRE-1 LATITUDE - 060 48M N.
COUNTRY - SOMALIA LONGITUDE - 480 50M E.
COMPANY - SINCLAIR

DEPTH	TEMP	DEPTH	TEMP	DEPTH	TEMP
929.6	47.2	1460.9	53.3	2180.2	65.6
3045.0	76.7	3566.8	93.9		

EL HAMURRE-1 CONDUCTIVITY DATA

FROM	TO	CONDUCT	FROM	TO	CONDUCT
0.0	379.8	2.87(7)	379.8	747.4	1.96(7)
747.4	1593.5	4.99(7)	1593.5	3566.8	3.46(7)

WELL NAME - OBBIA-1 LATITUDE - 05D 56M N.
COUNTRY - SOMALIA LONGITUDE - 48D 54M E.
COMPANY - SINCLAIR

DEPTH	TEMP	DEPTH	TEMP	DEPTH	TEMP
613.9	51.7	937.6	52.8	1276.5	55.0
1576.7	57.8	2160.4	80.6	2423.2	82.2
3389.4	112.2	4435.8	146.6	4476.3	148.3
4873.6	153.9				

OBBIA-1 CONDUCTIVITY DATA

FROM	TO	CONDUCT	FROM	TO	CONDUCT
0.0	666.0	2.39(7)	666.0	1117.1	1.76(7)
1117.1	1274.1	1.81(7)	1274.1	2319.5	1.96(7)
2319.5	2701.4	2.18(7)	2701.4	4873.8	2.55(6)

WELL NAME - ENDEBIRRE-1 LATITUDE - 05D 30M N.
COUNTRY - SOMALIA LONGITUDE - 47D 18M E.
COMPANY - SINCLAIR

DEPTH	TEMP	DEPTH	TEMP	DEPTH	TEMP
519.4	48.3	2759.4	81.1	3099.2	101.1
3594.5	118.9				

ENDEBIRRE-1 CONDUCTIVITY DATA

FROM	TO	CONDUCT	FROM	TO	CONDUCT
0.0	886.1	2.39(7)	886.1	1364.6	1.76(7)
1364.6	1695.0	1.81(7)	1695.0	3086.4	1.96(7)
3086.4	3594.5	2.18(7)			

WELL NAME - GIRA-1 LATITUDE - 05D 30M N.
COUNTRY - SOMALIA LONGITUDE - 48D 07M E.
COMPANY - SINCLAIR

DEPTH	TEMP	DEPTH	TEMP	DEPTH	TEMP
766.6	57.2	1985.3	76.1	2141.2	87.8
2656.9	92.2	3253.4	101.7		

GIRA-1 CONDUCTIVITY DATA

FROM	TO	CONDUCT	FROM	TO	CONDUCT
0.0	666.0	2.39(7)	666.0	1117.1	1.76(7)
1117.1	1274.1	1.81(7)	1274.1	2319.5	1.96(7)
2319.5	2701.4	2.18(7)	2701.4	3253.4	2.55(6)

WELL NAME - MARIA ASCIA-1 LATITUDE - 04D 31M N.
COUNTRY - SOMALIA LONGITUDE - 47D 26M E.
COMPANY - SINCLAIR

DEPTH	TEMP	DEPTH	TEMP	DEPTH	TEMP
701.3	56.1	2023.6	88.9	2787.7	112.2
4111.1	166.1				

MARIA ASCIA-1 CONDUCTIVITY DATA

FROM	TO	CONDUCT	FROM	TO	CONDUCT
0.0	666.0	2.39(7)	666.0	1117.1	1.76(7)
1117.1	1274.1	1.81(7)	1274.1	2319.5	1.96(7)
2319.5	2701.4	2.18(7)	2701.4	4111.1	2.55(6)

WELL NAME - XF-5 LATITUDE - 07D 49M N.
COUNTRY - ETHIOPIA LONGITUDE - 45D 37M E.
COMPANY - SINCLAIR

DEPTH	TEMP	DEPTH	TEMP	DEPTH	TEMP
0.0	26.3	1328.9	56.7		

XF-5 CONDUCTIVITY DATA

FROM	TO	CONDUCT	FROM	TO	CONDUCT
0.0	137.3	2.72(7)	137.3	564.8	3.03(7)
564.8	709.1	2.18(7)	709.1	1258.2	2.72(7)
1258.2	1296.9	3.03(7)	1296.9	1328.9	2.26(7)

WELL NAME - BOKH-1 LATITUDE - 07D 30M N.
COUNTRY - ETHIOPIA LONGITUDE - 46D 57M E.
COMPANY - ELMERATH

DEPTH	TEMP	DEPTH	TEMP	DEPTH	TEMP
250.5	35.0	462.6	42.0	734.8	42.0
859.5	44.0	2332.9	71.0	2657.4	77.0
3059.6	85.0				

BOKH-1 CONDUCTIVITY DATA

FROM	TO	CONDUCT	FROM	TO	CONDUCT
0.0	147.5	5.58(5)	147.5	250.0	2.96(5)
250.0	430.0	2.48(5)	430.0	553.5	2.45(5)
553.5	632.5	6.06(5)	632.5	678.0	4.59(5)
678.0	810.0	1.74(5)	810.0	965.0	2.09(5)
965.0	1027.5	2.12(5)	1027.5	1051.9	2.68(5)
1051.9	1200.0	2.32(5)	1200.0	1350.0	2.31(5)
1350.0	1407.5	2.48(5)	1407.5	1490.0	2.36(5)
1490.0	1555.0	2.42(5)	1555.0	1687.5	3.83(5)
1687.5	1750.0	4.32(5)	1750.0	1850.0	3.13(5)
1850.0	1960.0	2.21(5)	1960.0	2072.5	2.32(5)
2072.5	2172.9	1.83(5)	2172.9	2275.0	1.61(5)
2275.0	2370.0	2.61(5)	2370.0	2460.0	2.13(5)
2460.0	2550.0	2.45(5)	2550.0	2652.5	2.73(5)
2652.5	2752.5	2.56(5)	2752.5	2850.0	1.65(5)
2850.0	2910.0	2.55(5)	2910.0	3059.6	3.12(5)

WELL NAME - GALCAIO-2 LATITUDE - 06D 55M N.
COUNTRY - SOMALIA LONGITUDE - 47D 36M E.
COMPANY - MOBIL

DEPTH	TEMP	DEPTH	TEMP	DEPTH	TEMP
0.0	27.5	520.0	49.4	2130.6	73.3

GALCAIO-2 CONDUCTIVITY DATA

FROM	TO	CONDUCT	FROM	TO	CONDUCT
0.0	91.4	1.64(5)	91.4	182.9	2.57(5)
182.9	230.1	5.40(5)	230.1	321.6	2.38(5)
321.6	396.2	3.44(5)	396.2	504.4	2.87(5)
504.4	595.9	2.27(4)	595.9	687.3	2.24(4)
687.3	778.8	2.17(4)	778.8	883.9	2.49(4)
883.9	961.6	1.85(4)	961.6	1053.1	1.24(4)
1053.1	1185.7	1.44(4)	1185.7	1236.0	1.56(4)
1236.0	1327.4	2.23(4)	1327.4	1464.6	1.36(4)
1464.6	1601.7	2.06(5)	1601.7	1667.3	1.59(4)
1667.3	1784.6	1.73(4)	1784.6	1874.5	1.74(4)
1874.5	1967.5	1.52(4)	1967.5	2058.9	1.37(5)
2058.9	2130.6	1.67(4)			

WELL NAME - IDOLE-1 LATITUDE - 06D 10M N.
COUNTRY - SOMALIA LONGITUDE - 47D 02M E.
COMPANY - MOBIL

DEPTH	TEMP	DEPTH	TEMP	DEPTH	TEMP
0.0	27.5	2132.1	75.6		

IDOLE-1 CONDUCTIVITY DATA

FROM	TO	CONDUCT	FROM	TO	CONDUCT
0.0	152.4	2.74(5)	152.4	231.6	1.63(5)
231.6	320.0	2.74(6)	320.0	458.7	1.12(4)
458.7	641.6	1.52(4)	641.6	777.5	1.81(4)
777.5	1028.4	1.50(4)	1028.4	1190.2	2.06(4)
1190.2	1325.9	1.87(4)	1325.9	1575.2	1.98(4)
1575.2	1746.5	1.89(4)	1746.5	2000.7	2.36(4)
2000.7	2058.9	1.97(4)	2058.9	2132.1	2.87(4)

WELL NAME - DUSA MAREB-1 LATITUDE - 050 31M N.
COUNTRY - SOMALIA LONGITUDE - 460 22M E.
COMPANY - MOBIL

DEPTH	TEMP	DEPTH	TEMP	DEPTH	TEMP
0.0	27.5	460.0	40.0	2066.0	67.3

DUSA MAREB-1 CONDUCTIVITY DATA

FROM	TO	CONDUCT	FROM	TO	CONDUCT
0.0	33.9	4.50(5)	33.9	97.9	1.63(6)
97.9	168.0	2.55(5)	168.0	277.8	2.51(5)
277.8	358.5	4.33(5)	358.5	456.1	4.86(5)
456.1	486.6	1.63(6)	486.6	541.4	1.45(5)
541.4	648.1	0.88(5)	648.1	724.3	2.21(5)
724.3	815.7	2.75(5)	815.7	907.2	2.41(5)
907.2	990.1	2.35(5)	990.1	1090.1	2.85(5)
1090.1	1184.5	2.10(5)	1184.5	1245.5	3.39(5)
1245.5	1364.4	3.49(5)	1364.4	1455.8	2.98(5)
1455.8	1561.6	2.17(5)	1561.6	1638.7	4.37(5)
1638.7	1730.1	3.82(5)	1730.1	1821.6	3.11(5)
1821.6	1913.0	2.80(5)	1913.0	2036.5	3.57(5)
2036.5	2066.0	2.92(5)			

WELL NAME - DUSA MAREB-2 LATITUDE - 050 35M N.
COUNTRY - SOMALIA LONGITUDE - 450 53M E.
COMPANY - MOBIL

DEPTH	TEMP	DEPTH	TEMP	DEPTH	TEMP
0.0	27.5	2113.8	66.1		

DUSA MAREB-2 CONDUCTIVITY DATA

FROM	TO	CONDUCT	FROM	TO	CONDUCT
0.0	93.3	1.73(5)	93.3	334.1	1.99(4)
334.1	459.0	3.12(4)	459.0	652.0	3.42(5)
652.0	834.8	1.84(4)	834.8	868.1	2.72(6)
868.1	1007.7	2.22(4)	1007.7	1280.5	2.18(4)
1280.5	1373.4	1.61(4)	1373.4	1556.3	3.08(4)
1556.3	1766.9	2.94(4)	1766.9	1922.1	3.27(4)
1922.1	2056.9	2.02(4)	2056.9	2113.8	1.58(4)

WELL NAME - BULO BURTI-1 LATITUDE - 04D 04M N.
COUNTRY - SOMALIA LONGITUDE - 45D 30M E.
COMPANY - MOBIL

DEPTH	TEMP	DEPTH	TEMP	DEPTH	TEMP
0.0	27.5	224.6	42.2	2134.8	75.0

BULO BURTI-1 CONDUCTIVITY DATA

FROM	TO	CONDUCT	FROM	TO	CONDUCT
0.0	38.1	2.81(5)	38.1	97.5	2.28(5)
97.5	230.1	2.30(4)	230.1	321.6	2.54(4)
321.6	453.5	2.57(4)	453.5	504.4	2.50(4)
504.4	595.9	2.01(4)	595.9	687.3	3.99(4)
687.3	778.8	3.66(4)	778.8	870.2	2.54(4)
870.2	963.2	2.80(4)	963.2	1053.1	2.88(4)
1053.1	1141.5	2.37(4)	1141.5	1236.0	1.50(4)
1236.0	1327.4	1.40(4)	1327.4	1380.7	1.55(4)
1380.7	1510.3	1.93(4)	1510.3	1601.7	1.76(4)
1601.7	1693.2	1.90(4)	1693.2	1784.6	1.72(4)
1784.6	1876.0	2.04(4)	1876.0	1967.5	1.72(4)
1967.5	2058.9	1.99(4)	2058.9	2115.3	2.09(4)
2115.3	2134.8	1.92(4)			

WELL NAME - ABRED-1 LATITUDE - 05D 30M N.
COUNTRY - ETHIOPIA LONGITUDE - 45D 15M E.
COMPANY - ELWERATH

DEPTH	TEMP	DEPTH	TEMP	DEPTH	TEMP
284.4	35.0	735.6	42.0	854.5	44.0
1989.6	66.0	3103.4	80.0		

ABRED-1 CONDUCTIVITY DATA

FROM	TO	CONDUCT	FROM	TO	CONDUCT
0.0	170.0	1.85(6)	170.0	1377.0	2.37(6)
1377.0	2950.0	2.21(6)	2950.0	3070.0	1.99(6)
3070.0	3103.4	2.37(6)			

WELL NAME - CALLAFO-1 LATITUDE - 05D 40M N.
COUNTRY - ETHIOPIA LONGITUDE - 44D 21M E.
COMPANY - TENNECO

DEPTH	TEMP	DEPTH	TEMP	DEPTH	TEMP
694.9	52.2	1668.2	61.1	3237.3	90.0

CALLAFO-1 CONDUCTIVITY DATA

FROM	TO	CONDUCT	FROM	TO	CONDUCT
0.0	679.7	2.72(7)	679.7	1668.2	2.18(7)
1668.2	3237.3	2.81(7)			

WELL NAME - MAGAN-1 LATITUDE - 06D 06M N.
COUNTRY - ETHIOPIA LONGITUDE - 44D 17M E.
COMPANY - TENNECO

DEPTH	TEMP	DEPTH	TEMP	DEPTH	TEMP
773.6	60.6	1245.1	64.4	1352.1	67.2
1777.0	75.6	1851.1	75.6	2320.1	81.1
2522.5	85.6	3376.3	110.6	3573.5	116.1

MAGAN-1 CONDUCTIVITY DATA

FROM	TO	CONDUCT	FROM	TO	CONDUCT
0.0	1245.1	2.72(7)	1245.1	1352.1	1.96(7)
1352.1	1851.1	2.72(7)	1851.1	2320.1	2.87(7)
2320.1	2522.5	3.03(7)	2522.5	3376.3	2.62(7)
3376.3	3573.5	1.93(7)			

WELL NAME - CALUB-1 LATITUDE - 06D 09M N.
COUNTRY - ETHIOPIA LONGITUDE - 44D 32M E.
COMPANY - TENNECO

DEPTH	TEMP	DEPTH	TEMP	DEPTH	TEMP
2065.0	82.2	2986.1	94.4	3290.9	107.2
3659.7	118.3	3674.4	118.3	3699.7	119.4

CALUB-1 CONDUCTIVITY DATA

FROM	TO	CONDUCT	FROM	TO	CONDUCT
0.0	1245.1	2.72(7)	1245.1	1352.1	1.96(7)
1352.1	1851.1	2.72(7)	1851.1	2320.1	2.87(7)
2320.1	2522.5	3.03(7)	2522.5	3376.3	2.62(7)
3376.3	3699.7	1.98(7)			

WELL NAME - GAL TARDO-1 LATITUDE - 03D 05M N.
COUNTRY - SOMALIA LONGITUDE - 45D 45M E.
COMPANY - SINCLAIR

DEPTH	TEMP	DEPTH	TEMP	DEPTH	TEMP
506.3	62.2	1237.5	63.9	2274.4	104.4
2432.0	112.2				

GAL TARDO-1 CONDUCTIVITY DATA

FROM	TO	CONDUCT	FROM	TO	CONDUCT
0.0	298.7	2.61(7)	298.7	527.3	2.16(7)
527.3	909.2	1.90(7)	909.2	1306.5	2.72(7)
1306.5	1337.0	2.72(7)	1337.0	1761.7	2.72(7)
1761.7	2427.7	1.81(7)	2427.7	2432.0	2.55(6)

WELL NAME - BIO ADDO-1 LATITUDE - 02D 57M N.
COUNTRY - SOMALIA LONGITUDE - 45D 52M E.
COMPANY - SINCLAIR

DEPTH	TEMP	DEPTH	TEMP	DEPTH	TEMP
381.0	39.4	1234.4	65.0	2601.8	106.7

BIO ADDO-1 CONDUCTIVITY DATA

FROM	TO	CONDUCT	FROM	TO	CONDUCT
0.0	298.7	2.61(7)	298.7	527.3	2.16(7)
527.3	909.2	1.90(7)	909.2	1761.7	2.72(7)
1761.7	2427.7	1.81(7)	2427.7	2601.8	2.55(6)

WELL NAME - DUDDUMAI-1 LATITUDE - 02D 32M N.
COUNTRY - SOMALIA LONGITUDE - 44D 54M E.
COMPANY - SINCLAIR

DEPTH	TEMP	DEPTH	TEMP	DEPTH	TEMP
1097.3	50.0	1468.8	60.0	2042.8	74.4
2622.8	93.3	3377.8	105.6		

DUDDUMAI-1 CONDUCTIVITY DATA

FROM	TO	CONDUCT	FROM	TO	CONDUCT
0.0	298.7	2.61(7)	298.7	527.3	2.16(7)
527.3	909.2	1.90(7)	909.2	1761.7	2.72(7)
1761.7	2427.7	1.81(7)	2427.7	3377.8	2.55(6)

WELL NAME - WARSCIEK-1 LATITUDE - 02D 13M N.
COUNTRY - SOMALIA LONGITUDE - 45D 27M N.
COMPANY - SINCLAIR

DEPTH	TEMP	DEPTH	TEMP	DEPTH	TEMP
0.0	27.0	2121.7	93.3	2954.7	115.6
4100.8	152.2				

WARSCIEK-1 CONDUCTIVITY DATA

FROM	TO	CONDUCT	FROM	TO	CONDUCT
0.0	648.3	2.61(7)	648.3	1567.3	2.72(7)
1567.3	1837.3	2.39(7)	1837.3	2280.5	2.53(7)
2280.5	3244.6	2.62(7)	3244.6	3480.8	2.40(7)
3480.8	3785.0	2.27(7)	3785.0	4100.8	2.18(7)

WELL NAME - MERCA-1 LATITUDE - 010 52M N.
COUNTRY - SOMALIA LONGITUDE - 440 56M E.
COMPANY - SINCLAIR

DEPTH	TEMP	DEPTH	TEMP	DEPTH	TEMP
0.0	27.0	1686.2	71.7	2124.2	81.7
2479.5	102.2	3202.2	133.3	3800.6	158.9
3956.6	166.7				

MERCA-1 CONDUCTIVITY DATA

FROM	TO	CONDUCT	FROM	TO	CONDUCT
0.0	518.2	2.61(7)	518.2	1255.8	2.72(7)
1255.8	1472.2	2.39(7)	1472.2	1827.3	2.53(7)
1827.3	2272.0	2.62(7)	2272.0	2545.1	2.40(7)
2545.1	2788.9	2.27(7)	2788.9	3032.8	2.18(7)
3032.8	3285.7	1.80(7)	3285.7	3937.4	1.81(7)
3937.4	3956.6	1.67(7)			

WELL NAME - AFGOI-1 LATITUDE - 020 07M N.
COUNTRY - SOMALIA LONGITUDE - 450 03M E.
COMPANY - SINCLAIR

DEPTH	TEMP	DEPTH	TEMP	DEPTH	TEMP
0.0	27.0	3200.4	115.6	3878.9	126.7
4148.3	137.8				

AFGOI-1 CONDUCTIVITY DATA

FROM	TO	CONDUCT	FROM	TO	CONDUCT
0.0	518.2	2.61(7)	518.2	1255.8	2.72(7)
1255.8	1472.2	2.39(7)	1472.2	1827.3	2.53(7)
1827.3	2272.0	2.62(7)	2272.0	2545.1	2.40(7)
2545.1	2788.9	2.27(7)	2788.9	3032.8	2.18(7)
3032.8	3285.7	1.80(7)	3285.7	4148.3	2.17(7)

WELL NAME - DOBEI-1 LATITUDE - 010 49M N.
COUNTRY - SOMALIA LONGITUDE - 440 31M E.
COMPANY - SINCLAIR

DEPTH	TEMP	DEPTH	TEMP	DEPTH	TEMP
0.0	27.0	1708.1	68.3	2125.7	73.3

DOBEI-1 CONDUCTIVITY DATA

FROM	TO	CONDUCT	FROM	TO	CONDUCT
0.0	518.2	2.61(7)	518.2	1255.8	2.72(7)
1255.8	1472.2	2.39(7)	1472.2	1827.3	2.53(7)
1827.3	2125.7	2.62(7)			

WELL NAME - DOBEI-2 LATITUDE - 010 43M N.
COUNTRY - SOMALIA LONGITUDE - 440 28M E.
COMPANY - SINCLAIR

DEPTH	TEMP	DEPTH	TEMP	DEPTH	TEMP
0.0	27.0	1677.6	62.2	2264.4	88.9
2771.5	93.3	3214.7	100.0	3720.1	115.6
3825.2	116.1				

DOBEI-2 CONDUCTIVITY DATA

FROM	TO	CONDUCT	FROM	TO	CONDUCT
0.0	573.6	2.61(7)	573.6	1677.9	2.72(7)
1677.9	2287.5	2.39(7)	2287.5	2590.8	2.53(7)
2590.8	2977.0	2.62(7)	2977.0	3459.5	2.18(7)
3459.5	3825.2	1.98(7)			

WELL NAME - CORIOLE-1 LATITUDE - 010 50M N.
COUNTRY - SOMALIA LONGITUDE - 440 33M E.
COMPANY - SINCLAIR

DEPTH	TEMP	DEPTH	TEMP	DEPTH	TEMP
637.0	48.9	1045.5	64.4	1477.1	70.0
1893.1	82.2	2299.4	86.7	2766.4	104.4
3177.8	120.0	3516.2	123.9		

CORIOLE-1 CONDUCTIVITY DATA

FROM	TO	CONDUCT	FROM	TO	CONDUCT
0.0	518.2	2.61(7)	518.2	1255.8	2.72(7)
1255.8	1472.2	2.39(7)	1472.2	1827.3	2.53(7)
1827.3	2272.0	2.62(7)	2272.0	2545.1	2.40(7)
2545.1	2788.9	2.27(7)	2788.9	3032.8	2.18(7)
3032.8	3285.7	1.80(7)	3285.7	3499.1	1.81(7)
3499.1	3516.2	1.67(7)			

WELL NAME - CORIOLE-2 LATITUDE - 010 49M N.
COUNTRY - SOMALIA LONGITUDE - 440 36M E.
COMPANY - SINCLAIR

DEPTH	TEMP	DEPTH	TEMP	DEPTH	TEMP
0.0	27.0	2377.4	87.8	3561.0	126.7
3992.3	135.0	4063.9	137.8		

CORIOLE-2 CONDUCTIVITY DATA

FROM	TO	CONDUCT	FROM	TO	CONDUCT
0.0	641.0	2.61(7)	641.0	1553.3	2.72(7)
1553.3	1820.9	2.39(7)	1820.9	2260.1	2.53(7)
2260.1	2610.0	2.62(7)	2810.0	3148.0	2.40(7)
3148.0	3449.4	2.27(7)	3449.4	3750.9	1.80(7)
3750.9	4063.9	2.08(7)			

WELL NAME - EL KURAN-1 LATITUDE - 04D 42M N.
COUNTRY - ETHIOPIA LONGITUDE - 42D 05M E.
COMPANY - TENNECO

DEPTH	TEMP	DEPTH	TEMP	DEPTH	TEMP
829.1	80.7	1592.9	77.8	2507.3	91.1
2927.6	100.0	3188.5	104.4		

EL KURAN-1 CONDUCTIVITY DATA

FROM	TO	CONDUCT	FROM	TO	CONDUCT
0.0	1766.8	2.76(1)	1766.8	2340.3	2.52(3)
2340.3	2847.0	2.39(5)	2847.0	3188.5	2.63(5)

WELL NAME - HOL-1 LATITUDE - 03D 28M N.
COUNTRY - SOMALIA LONGITUDE - 41D 57M E.
COMPANY - BURMAH

DEPTH	TEMP	DEPTH	TEMP	DEPTH	TEMP
923.5	73.9	1219.2	85.0	1524.0	90.6
1828.8	96.7	2133.6	102.8	2438.4	110.0
2615.2	106.7	2728.9	110.0	2743.2	117.8
3048.0	124.4	3078.5	120.0	3322.3	126.7
3352.8	131.7	3602.1	134.4	3657.5	141.6
3803.9	135.0	3810.0	147.8	3931.9	141.6
3962.4	166.7	4038.6	171.1		

HOL-1 CONDUCTIVITY DATA

FROM	TO	CONDUCT	FROM	TO	CONDUCT
0.0	178.3	2.15(7)	178.3	814.4	1.78(7)
814.4	1021.4	2.39(7)	1021.4	1422.2	1.78(7)
1422.2	1868.4	5.07(7)	1868.4	2467.4	2.59(7)
2467.4	3800.2	2.52(7)	3800.2	3970.0	2.94(7)
3970.0	4038.6	2.33(7)			

WELL NAME - GHEFERSON-1 LATITUDE - 01D 21M N.
COUNTRY - SOMALIA LONGITUDE - 42D 28M E.
COMPANY - BURMAH

DEPTH	TEMP	DEPTH	TEMP	DEPTH	TEMP
0.0	29.5	2182.7	83.3		

GHEFERSON-1 CONDUCTIVITY DATA

FROM	TO	CONDUCT	FROM	TO	CONDUCT
0.0	2182.7	2.72(7)			

WELL NAME - DAS UEN-1 LATITUDE - 01D 09M N.
COUNTRY - SOMALIA LONGITUDE - 41D 55M E.
COMPANY - BURMAH

DEPTH	TEMP	DEPTH	TEMP	DEPTH	TEMP
0.0	29.5	2222.0	95.0	3060.5	110.0
3249.8	117.8				

DAS JEN-1 CONDUCTIVITY DATA

FROM	TO	CONDUCT	FROM	TO	CONDUCT
0.0	3249.8	2.72(7)			

WELL NAME - LACH BISSIGH-1 LATITUDE - 00D 49M N.
COUNTRY - SOMALIA LONGITUDE - 41D 19M E.
COMPANY - GULF

DEPTH	TEMP	DEPTH	TEMP	DEPTH	TEMP
0.0	29.5	867.8	56.1	3086.1	126.7

LACH BISSIGH-1 CONDUCTIVITY DATA

FROM	TO	CONDUCT	FROM	TO	CONDUCT
0.0	320.0	2.53(7)	320.0	854.4	1.78(7)
854.4	1234.4	2.27(7)	1234.4	1544.1	2.00(7)
1544.1	3066.1	2.27(7)			

WELL NAME - LACH DERA-1 LATITUDE - 00D 29M N.
COUNTRY - SOMALIA LONGITUDE - 41D 32M E.
COMPANY - GULF

DEPTH	TEMP	DEPTH	TEMP	DEPTH	TEMP
707.4	47.8	2757.2	118.3	2868.2	121.1

LACH DERA-1 CONDUCTIVITY DATA

FROM	TO	CONDUCT	FROM	TO	CONDUCT
0.0	505.4	2.53(7)	505.4	1463.0	2.00(7)
1463.0	1785.5	2.27(7)	1785.5	2868.2	2.27(7)

WELL NAME - BRAVA-1 LATITUDE - 000 59M N.
COUNTRY - SOMALIA LONGITUDE - 430 43M E.
COMPANY - SINCLAIR

DEPTH	TEMP	DEPTH	TEMP	DEPTH	TEMP
644.7	42.2	914.4	64.4	1219.2	72.2
1524.0	78.9	1828.8	82.2	2133.6	95.0
2438.4	104.4	2590.8	111.7	3074.8	114.4
3397.6	138.3	3581.1	142.8		

BRAVA-1 CONDUCTIVITY DATA

FROM	TO	CONDUCT	FROM	TO	CONDUCT
0.0	121.9	2.87(7)	121.9	572.4	2.27(7)
572.4	905.3	2.18(7)	905.3	1432.9	1.81(7)
1432.9	1645.3	2.18(7)	1645.3	2590.8	1.81(7)
2590.8	3291.8	2.18(7)	3291.8	3581.1	1.81(7)

WELL NAME - GIAMAMA-1 LATITUDE - 000 05M N.
COUNTRY - SOMALIA LONGITUDE - 420 48M E.
COMPANY - STNCLAIR

DEPTH	TEMP	DEPTH	TEMP	DEPTH	TEMP
593.4	47.8	1937.3	85.0	3329.6	112.8
4126.1	140.6				

GIAMAMA-1 CONDUCTIVITY DATA

FROM	TO	CONDUCT	FROM	TO	CONDUCT
0.0	125.3	2.44(7)	125.3	1085.7	2.53(7)
1085.7	1898.0	1.81(7)	1898.0	2980.6	2.15(7)
2980.6	3393.0	2.27(7)	3393.0	4126.1	1.81(7)

WELL NAME - ODDO ALIMO-1 LATITUDE - 000 04M N.
COUNTRY - SOMALIA LONGITUDE - 420 24M E.
COMPANY - SINCLAIR

DEPTH	TEMP	DEPTH	TEMP	DEPTH	TEMP
634.6	46.1	1605.9	70.0	2256.1	91.7
3354.9	123.3	3789.0	133.3	4460.4	146.1

ODDO ALIMO-1 CONDUCTIVITY DATA

FROM	TO	CONDUCT	FROM	TO	CONDUCT
0.0	70.4	2.44(7)	70.4	609.6	2.53(7)
609.6	1065.6	1.81(7)	1065.6	1673.4	2.15(7)
1673.4	1905.0	2.27(7)	1905.0	2773.4	1.81(7)
2773.4	4460.4	3.03(7)			

WELL NAME - WAL MERER-1 LATITUDE - 00D 07M S.
COUNTRY - KENYA LONGITUDE - 40D 35M E.
COMPANY - BP

DEPTH	TEMP	DEPTH	TEMP	DEPTH	TEMP
1536.2	79.4	2144.6	102.2	2379.9	111.7
3011.4	137.7	3629.9	161.7	3799.0	166.1

WAL MERER-1 CONDUCTIVITY DATA

FROM	TO	CONDUCT	FROM	TO	CONDUCT
0.0	131.1	5.41(5)	131.1	267.3	2.10(5)
267.3	406.9	2.57(5)	406.9	472.4	2.51(5)
472.4	589.8	2.75(5)	589.8	689.6	2.67(5)
689.6	808.6	1.59(2)	808.6	861.8	1.89(4)
861.8	954.0	3.87(5)	954.0	1046.5	1.78(4)
1046.5	1137.5	1.63(4)	1137.5	1260.7	1.78(4)
1260.7	1397.8	3.12(3)	1397.8	1464.6	2.01(4)
1464.6	1591.1	2.51(4)	1591.1	1686.2	1.45(4)
1686.2	1786.1	1.30(4)	1786.1	1846.6	2.03(3)
1846.6	1881.1	2.57(1)	1881.1	1979.1	1.81(4)
1979.1	2043.7	2.12(2)	2043.7	2044.4	1.55(3)
2044.4	2091.8	1.83(4)	2091.8	2163.2	2.68(2)
2163.2	2234.0	1.80(4)	2234.0	2342.4	2.12(4)
2342.4	2413.7	2.43(2)	2413.7	2509.0	3.24(4)
2509.0	2563.4	4.50(4)	2563.4	2652.7	2.81(4)
2652.7	2816.4	5.03(4)	2816.4	2871.2	1.51(4)
2871.2	2966.0	1.64(4)	2966.0	3037.3	2.17(4)
3037.3	3148.6	3.30(4)	3148.6	3301.0	4.18(4)
3301.0	3340.0	3.40(2)	3340.0	3359.4	1.73(2)
3359.4	3423.5	1.66(4)	3423.5	3515.0	2.96(4)
3515.0	3574.7	3.72(4)	3574.7	3628.9	2.45(4)
3628.9	3644.5	2.58(4)	3644.5	3659.7	2.76(4)
3659.7	3675.0	5.12(4)	3675.0	3690.2	2.87(4)
3690.2	3704.7	2.63(4)	3704.7	3719.9	2.45(4)
3719.9	3735.2	4.13(4)	3735.2	3748.1	4.99(4)
3748.1	3754.7	1.34(2)	3754.7	3757.0	2.96(3)
3757.0	3765.7	2.46(4)	3765.7	3779.6	4.38(4)
3779.6	3789.0	3.31(4)			

WELL NAME - GARISSA-1 LATITUDE - 000 22M S.
COUNTRY - KENYA LONGITUDE - 39D 49M E.
COMPANY - BP

DEPTH	TEMP	DEPTH	TEMP	DEPTH	TEMP
0.0	28.5	1214.3	71.1		

GARISSA-1 CONDUCTIVITY DATA

FROM	TO	CONDUCT	FROM	TO	CONDUCT
0.0	129.5	4.83(5)	129.5	240.8	2.75(5)
240.8	306.0	1.66(1)	306.0	334.2	1.57(1)
334.2	423.7	1.52(4)	423.7	472.4	1.45(4)
472.4	522.7	1.65(4)	522.7	589.8	2.17(4)
589.8	681.2	3.27(4)	681.2	772.7	2.15(4)
772.7	864.1	2.07(4)	864.1	1015.6	2.23(4)
1015.6	1082.8	1.92(4)	1082.8	1178.7	2.98(1)
1178.7	1214.3	3.29(2)			

WELL NAME - WALU-2 LATITUDE - 010 38M S.
COUNTRY - KENYA LONGITUDE - 400 15M E.
COMPANY - BP

DEPTH	TEMP	DEPTH	TEMP	DEPTH	TEMP
890.0	71.1	2393.8	105.6	3296.4	132.2
3698.4	146.7	3721.6	152.2		

WALU-2 CONDUCTIVITY DATA

FROM	TO	CONDUCT	FROM	TO	CONDUCT
0.0	131.7	2.12(5)	131.7	241.7	1.59(4)
241.7	306.0	1.57(2)	306.0	307.2	1.55(2)
307.2	334.4	1.47(2)	334.4	406.3	1.81(4)
406.3	470.9	1.60(4)	470.9	588.4	2.87(4)
588.4	680.3	2.01(4)	680.3	771.8	1.98(4)
771.8	876.8	2.23(4)	876.8	967.4	1.62(3)
967.4	1046.7	2.77(4)	1046.7	1136.8	2.70(4)
1136.8	1274.4	2.89(4)	1274.4	1406.7	2.06(4)
1406.7	1473.4	4.25(1)	1473.4	1594.7	2.62(4)
1594.7	1685.8	1.99(4)	1685.8	1797.9	1.91(4)
1797.9	1889.3	1.59(4)	1889.3	1949.2	1.77(4)
1949.2	1984.4	1.47(4)	1984.4	2112.6	1.55(4)
2112.6	2241.3	1.71(3)	2241.3	2245.6	1.93(4)
2245.6	2310.2	1.77(3)	2310.2	2417.4	2.70(4)
2417.4	2464.5	1.14(4)	2464.5	2510.2	1.17(4)
2510.2	2600.2	1.14(4)	2600.2	2703.3	1.33(4)
2703.3	2761.5	1.14(4)	2761.5	2763.5	1.24(4)
2763.5	2818.2	1.21(4)	2818.2	2872.6	1.23(4)
2872.6	2920.1	1.26(4)	2920.1	2967.4	1.25(4)
2967.4	2968.4	1.23(4)	2968.4	2989.9	1.21(4)
2989.9	3045.1	1.37(4)	3045.1	3079.7	1.78(2)
3079.7	3080.3	2.15(2)	3080.3	3148.7	1.87(2)
3148.7	3217.2	1.96(3)	3217.2	3218.5	1.30(2)
3218.5	3252.4	1.42(3)	3252.4	3316.1	1.69(4)
3316.1	3408.0	1.26(4)	3408.0	3612.2	1.36(4)
3612.2	3672.5	2.88(2)	3672.5	3721.6	1.68(4)

WELL NAME - DODORI-1 LATITUDE - 010 49M S.
COUNTRY - KENYA LONGITUDE - 410 11M E.
COMPANY - BP

DEPTH	TEMP	DEPTH	TEMP	DEPTH	TEMP
604.1	45.0	2277.2	87.8	2875.2	108.3
3222.3	113.3	3536.3	122.8	3624.1	123.9
3959.7	131.1	4282.4	140.6		

DODORI-1 CONDUCTIVITY DATA

FROM	TO	CONDUCT	FROM	TO	CONDUCT
0.0	122.5	4.28(5)	122.5	223.0	2.86(5)
223.0	314.4	2.34(5)	314.4	405.8	2.63(5)
405.8	497.3	2.67(5)	497.3	589.5	2.74(5)
589.5	666.4	1.62(4)	666.4	757.1	2.34(5)
757.1	863.0	1.64(4)	863.0	955.2	1.69(4)
955.2	1045.9	2.01(4)	1045.9	1137.4	1.83(4)
1137.4	1207.6	1.79(4)	1207.6	1321.0	2.02(4)
1321.0	1412.4	2.22(5)	1412.4	1503.1	2.31(5)
1503.1	1594.6	1.01(4)	1594.6	1686.8	2.49(4)
1686.8	1777.4	1.44(4)	1777.4	1868.6	1.75(5)
1868.6	1960.8	1.70(4)	1960.8	2060.0	1.50(4)
2060.0	2114.9	2.04(2)	2114.9	2187.2	2.01(4)
2187.2	2276.4	2.33(1)	2276.4	2325.5	2.04(2)
2325.5	2425.6	1.33(4)	2425.6	2480.0	1.93(2)
2480.0	2518.4	2.21(4)	2518.4	2593.7	1.89(4)
2593.7	2633.3	2.38(2)	2633.3	2720.6	2.39(2)
2720.6	2802.9	2.23(4)	2802.9	2870.0	2.37(3)
2870.0	2872.9	2.58(1)	2872.9	2912.5	2.15(4)
2912.5	3006.5	1.72(4)	3006.5	3062.0	2.65(1)
3062.0	3064.6	1.97(3)	3084.6	3132.7	1.50(4)
3132.7	3164.7	2.52(1)	3164.7	3167.3	2.40(1)
3167.3	3248.1	2.49(2)	3248.1	3449.7	2.78(3)
3449.7	3491.3	1.98(2)	3491.3	3507.8	2.29(2)
3507.8	3525.2	4.63(1)	3525.2	3527.9	3.56(2)
3527.9	3531.9	3.91(2)	3531.9	3546.7	4.69(2)
3546.7	3559.8	3.72(2)	3559.8	3574.7	2.18(2)
3574.7	3590.4	3.58(2)	3590.4	3592.7	2.12(2)
3592.7	3741.1	1.91(4)	3741.1	3775.6	2.71(1)
3775.6	3778.0	1.74(2)	3778.0	3846.9	1.24(4)
3846.9	3915.9	2.79(2)	3915.9	3952.5	1.99(2)
3952.5	4049.9	1.94(4)	4049.9	4112.1	1.28(3)
4112.1	4113.7	4.03(2)	4113.7	4157.9	1.49(3)
4157.9	4230.8	1.20(4)	4230.8	4282.4	1.42(4)

WELL NAME - PATE-1
COUNTRY - KENYA
COMPANY - BP

LATITUDE - 02D 04M S.
LONGITUDE - 41D 05M E.

DEPTH	TEMP	DEPTH	TEMP	DEPTH	TEMP
1198.4	51.1	2957.4	91.1	3741.3	124.4

PATE-1 CONDUCTIVITY DATA

FROM	TO	CONDUCT	FROM	TO	CONDUCT
0.0	155.6	4.29(5)	155.6	222.7	2.18(5)
222.7	297.5	2.32(5)	297.5	328.3	2.08(2)
328.3	334.5	2.30(2)	334.5	393.7	1.44(4)
393.7	495.5	1.91(4)	495.5	586.9	1.47(4)
586.9	678.4	1.63(4)	678.4	769.8	1.62(4)
769.8	861.2	1.54(4)	861.2	952.7	1.83(4)
952.7	1044.4	1.65(4)	1044.4	1159.9	1.72(4)
1159.9	1251.4	2.21(2)	1251.4	1319.1	1.94(4)
1319.1	1411.1	2.84(4)	1411.1	1501.9	2.57(4)
1501.9	1636.7	3.05(4)	1636.7	1685.6	2.12(4)
1685.6	1777.8	1.85(4)	1777.8	1829.0	2.10(4)
1829.0	1959.9	1.89(4)	1959.9	2051.3	1.46(4)
2051.3	2142.8	1.99(4)	2142.8	2233.5	1.82(4)
2233.5	2324.9	2.43(4)	2324.9	2388.0	1.28(4)
2388.0	2525.9	2.15(4)	2525.9	2589.3	1.64(2)
2589.3	2591.7	2.44(2)	2591.7	2594.2	2.07(1)
2594.2	2620.1	2.30(1)	2620.1	2690.7	1.94(4)
2690.7	2782.1	1.47(4)	2782.1	2874.3	2.04(4)
2874.3	2966.5	1.79(4)	2966.5	3057.2	1.97(4)
3057.2	3148.6	0.89(4)	3148.6	3240.1	1.37(4)
3240.1	3301.2	2.07(4)	3301.2	3358.9	1.38(4)
3358.9	3361.4	1.88(4)	3361.4	3415.5	1.39(1)
3415.5	3513.6	1.03(4)	3513.6	3605.1	1.39(4)
3605.1	3696.5	1.22(4)	3696.5	3741.3	1.67(5)

WELL NAME - KIPINI-1 LATITUDE - 020 24M S.
COUNTRY - KENYA LONGITUDE - 400 36M E.
COMPANY - BP

DEPTH	TEMP	DEPTH	TEMP	DEPTH	TEMP
1273.4	70.6	2969.7	107.8	3638.6	123.3

KIPINI-1 CONDUCTIVITY DATA

FROM	TO	CONDUCT	FROM	TO	CONDUCT
0.0	170.3	3.70(5)	170.3	222.0	3.17(5)
222.0	313.4	2.54(5)	313.4	405.6	0.94(4)
405.6	497.1	1.49(4)	497.1	588.5	1.58(4)
588.5	679.2	1.60(4)	679.2	770.6	1.56(4)
770.6	862.1	1.67(4)	862.1	953.5	1.67(4)
953.5	1045.7	1.65(4)	1045.7	1137.1	1.59(4)
1137.1	1228.6	1.68(4)	1228.6	1320.0	1.20(4)
1320.0	1411.5	1.79(4)	1411.5	1502.9	1.90(4)
1502.9	1573.6	1.95(4)	1573.6	1685.8	1.17(4)
1685.8	1777.2	1.67(4)	1777.2	1826.9	1.21(4)
1826.9	1960.1	2.18(4)	1960.1	2051.5	2.33(4)
2051.5	2143.0	1.99(4)	2143.0	2234.4	1.29(4)
2234.4	2325.9	1.89(4)	2325.9	2380.1	1.58(4)
2380.1	2641.6	1.43(4)	2641.6	2671.1	2.09(4)
2671.1	2696.7	2.72(1)	2696.7	2697.4	2.23(2)
2697.4	2698.6	2.70(1)	2698.6	2701.2	2.50(1)
2701.2	2765.8	2.19(3)	2765.8	2874.5	2.00(4)
2874.5	3000.4	1.92(4)	3000.4	3111.6	1.84(4)
3111.6	3240.3	1.51(4)	3240.3	3331.7	1.70(4)
3331.7	3411.7	1.69(4)	3411.7	3446.9	1.24(3)
3446.9	3448.3	1.90(3)	3448.3	3449.2	2.12(1)
3449.2	3450.7	1.85(3)	3450.7	3506.1	2.08(3)
3506.1	3605.7	1.44(4)	3605.7	3638.6	2.16(5)

WELL NAME - PEMBA-5 LATITUDE - 05D 16M S.
COUNTRY - TANZANIA LONGITUDE - 39D 42M E.
COMPANY - BP

DEPTH	TEMP	DEPTH	TEMP	DEPTH	TEMP
0.0	26.5	3500.1	173.3	3757.9	182.2
3881.3	187.8				

PEMBA-5 CONDUCTIVITY DATA

FROM	TO	CONDUCT	FROM	TO	CONDUCT
0.0	91.4	2.49(5)	91.4	222.4	1.68(4)
222.4	298.7	1.72(4)	298.7	406.0	1.37(4)
406.0	496.7	1.88(4)	496.7	588.1	2.19(4)
588.1	700.1	2.44(4)	700.1	807.9	1.70(4)
807.9	851.0	1.50(4)	851.0	878.9	1.59(4)
878.9	922.2	1.81(4)	922.2	939.1	1.74(2)
939.1	979.9	1.66(4)	979.9	1055.2	1.42(4)
1055.2	1146.7	2.35(4)	1146.7	1258.8	2.99(2)
1258.8	1324.2	1.47(4)	1324.2	1414.9	1.14(4)
1414.9	1509.7	1.51(4)	1509.7	1601.1	2.36(4)
1601.1	1678.4	1.93(4)	1678.4	1718.5	1.66(2)
1718.5	1720.0	1.73(2)	1720.0	1721.5	2.11(2)
1721.5	1795.3	2.51(2)	1795.3	1869.0	1.70(4)
1869.0	1952.7	1.45(4)	1952.7	2065.9	1.26(4)
2065.9	2138.6	1.59(4)	2138.6	2182.4	1.60(4)
2182.4	2184.0	1.65(3)	2184.0	2232.5	1.66(4)
2232.5	2312.5	1.40(4)	2312.5	2345.3	1.57(2)
2345.3	2404.9	1.38(3)	2404.9	2464.5	1.33(4)
2464.5	2533.3	1.36(3)	2533.3	2602.1	1.54(4)
2602.1	2603.4	1.46(4)	2603.4	2625.2	1.48(4)
2625.2	2701.3	1.34(4)	2701.3	2757.2	1.99(3)
2757.2	2792.9	1.67(4)	2792.9	2878.8	1.18(4)
2878.8	2931.0	2.59(3)	2931.0	2971.2	1.80(2)
2971.2	3061.3	1.68(4)	3061.3	3153.5	1.30(2)
3153.5	3234.7	1.77(4)	3234.7	3348.5	2.63(1)
3348.5	3423.5	1.89(2)	3423.5	3424.7	1.40(1)
3424.7	3447.1	1.45(2)	3447.1	3539.8	1.93(4)
3539.8	3630.5	1.36(2)	3630.5	3749.6	1.70(4)
3749.6	3863.8	2.60(5)	3863.8	3881.3	2.67(5)

WELL NAME - MAFIA-1 LATITUDE - 07D 53M S.
COUNTRY - TANZANIA LONGITUDE - 39D 45M E.
COMPANY - BP

DEPTH	TEMP	DEPTH	TEMP	DEPTH	TEMP
739.4	44.4	1100.6	48.9	1469.4	72.8
1962.0	91.1	2318.3	100.0	2673.4	131.7
2999.5	138.9				

MAFIA-1 CONDUCTIVITY DATA

FROM	TO	CONDUCT	FROM	TO	CONDUCT
0.0	137.0	3.34(5)	137.0	229.2	2.53(5)
229.2	320.6	2.78(5)	320.6	412.1	2.70(5)
412.1	503.5	1.95(4)	503.5	611.3	2.39(4)
611.3	727.9	2.71(3)	727.9	844.3	3.53(5)
844.3	908.0	2.71(1)	908.0	993.6	2.52(4)
993.6	1070.3	2.17(4)	1070.3	1133.2	1.67(4)
1133.2	1234.4	1.58(4)	1234.4	1336.5	1.55(4)
1336.5	1462.9	1.59(4)	1462.9	1633.1	2.12(5)
1633.1	1746.5	2.02(4)	1746.5	1820.9	1.98(4)
1820.9	1958.6	1.96(5)	1958.6	2001.5	1.67(2)
2001.5	2088.2	1.65(4)	2088.2	2140.2	3.20(4)
2140.2	2199.3	1.66(3)	2199.3	2289.0	2.21(3)
2289.0	2350.5	1.43(4)	2350.5	2453.5	1.28(4)
2453.5	2535.9	3.89(2)	2535.9	2681.3	1.39(3)
2681.3	2962.7	1.80(3)	2962.7	2994.5	2.10(4)
2994.5	2999.5	1.88(5)			

WELL NAME - ZANZIBAR-1 LATITUDE - 06D 03M S.
COUNTRY - TANZANIA LONGITUDE - 39D 13M E.
COMPANY - BP

DEPTH	TEMP	DEPTH	TEMP	DEPTH	TEMP
1100.0	51.7	1836.1	70.6	3148.9	92.2
3449.1	107.2	3837.4	117.2		

ZANZIBAR-1 CONDUCTIVITY DATA

FROM	TO	CONDUCT	FROM	TO	CONDUCT
0.0	137.3	5.11(5)	137.3	228.9	4.82(5)
228.9	321.6	5.43(5)	321.6	413.0	4.76(5)
413.0	504.1	4.99(5)	504.1	595.4	4.63(5)
595.4	686.6	3.73(5)	686.6	777.5	5.18(5)
777.5	869.6	4.02(5)	869.6	961.2	3.48(5)
961.2	1059.2	3.32(5)	1059.2	1127.8	2.02(4)
1127.8	1234.6	1.01(4)	1234.6	1325.7	1.54(4)
1325.7	1416.9	1.34(4)	1416.9	1506.9	1.64(4)
1506.9	1598.1	1.29(4)	1598.1	1691.5	1.14(4)
1691.5	1783.8	1.22(4)	1783.8	1875.0	1.27(4)
1875.0	1965.7	1.57(4)	1965.7	2058.2	1.37(4)
2058.2	2150.1	2.37(4)	2150.1	2241.5	1.90(4)
2241.5	2293.6	1.60(4)	2293.6	2448.3	1.42(4)
2448.3	2560.6	1.37(4)	2560.6	2618.7	1.38(4)
2618.7	2703.6	1.43(4)	2703.6	2759.4	2.54(1)
2759.4	2866.5	2.87(4)	2866.5	2964.2	2.51(4)
2964.2	3004.1	2.01(4)	3004.1	3245.1	1.40(4)
3245.1	3357.7	1.52(4)	3357.7	3430.7	2.34(3)
3430.7	3496.1	1.00(4)	3496.1	3618.4	1.24(4)
3618.4	3719.9	1.33(4)	3719.9	3796.6	0.97(4)
3796.6	3837.4	3.06(5)			

WELL NAME - MANDAWA-7 LATITUDE - 09D 25M S.
COUNTRY - TANZANIA LONGITUDE - 39D 25M E.
COMPANY - BP

DEPTH	TEMP	DEPTH	TEMP	DEPTH	TEMP
1103.7	50.0	1389.6	55.6	2502.7	70.0
2859.6	73.3	3171.4	82.2	3476.5	90.6
4057.5	102.8				

MANDAWA-7 CONDUCTIVITY DATA

FROM	TO	CONDUCT	FROM	TO	CONDUCT
0.0	133.0	1.12(4)	133.0	223.6	1.78(4)
223.6	359.4	2.77(4)	359.4	497.1	1.97(4)
497.1	588.0	4.13(4)	588.0	769.9	1.52(4)
769.9	952.5	2.14(4)	952.5	1043.0	2.95(4)
1043.0	1136.0	4.79(4)	1136.0	1229.0	4.10(4)
1229.0	1334.3	4.67(4)	1334.3	1424.5	1.67(2)
1424.5	1547.8	2.28(4)	1547.8	1686.2	3.81(4)
1686.2	1783.4	5.33(4)	1783.4	2007.4	4.39(4)
2007.4	2191.8	5.05(4)	2191.8	2373.2	4.60(4)
2373.2	2554.5	4.04(4)	2554.5	2795.9	4.02(4)
2795.9	2819.1	1.93(2)	2819.1	2862.1	1.79(1)
2862.1	2891.9	1.44(2)	2891.9	3059.3	4.63(4)
3059.3	3073.8	2.60(1)	3073.8	3095.5	1.40(3)
3095.5	3122.2	3.16(1)	3122.2	3169.2	2.29(2)
3169.2	3219.1	2.39(1)	3219.1	3253.0	1.74(2)
3253.0	3365.9	1.65(3)	3365.9	3494.4	4.37(3)
3494.4	3562.0	2.05(2)	3562.0	3642.5	3.18(2)
3642.5	3816.7	2.39(2)	3816.7	3982.4	3.06(2)
3982.4	4036.9	2.01(3)	4036.9	4057.5	2.96(1)

WELL NAME - KISWERE LATITUDE - 09D 27M S.
COUNTRY - TANZANIA LONGITUDE - 39D 31M E.
COMPANY - BP

DEPTH	TEMP	DEPTH	TEMP	DEPTH	TEMP
0.0	26.0	116.9	36.7	350.3	40.0
430.4	40.0	719.3	43.3	734.3	43.3

KISWERE CONDUCTIVITY DATA

FROM	TO	CONDUCT	FROM	TO	CONDUCT
0.0	176.8	2.15(7)	176.8	734.3	1.88(7)

Appendix 6

Tabulation of North Sea Temperature and Conductivity Data

The BHT and thermal conductivity data for the three North Sea oil exploration boreholes (Fig. 5.1) are tabulated in the order in which they are presented in tables 5.1, 5.2, 5.3, Chapter 5.

The presentation format is identical to that previously discussed in Appendix 5 for the Eastern Africa data.

The data presented in this tabulation represent all the data (bar lithological) available for the computation of heat flow values and preparation of the composite heat flow plots (section 5.4).

WELL NAME - 7/3-1 LATITUDE - 57D 51M N.
COUNTRY - NORTH SEA LONGITUDE - 02D 45M E.
COMPANY - AMOCO

DEPTH	TEMP	DEPTH	TEMP	DEPTH	TEMP
0.0	7.0	1462.1	46.9	2626.2	89.4
4289.1	124.4	4486.7	131.1		

7/3-1 CONDUCTIVITY DATA

FROM	TO	CONDUCT	FROM	TO	CONDUCT
0.0	74.1	3.51(5)	74.1	106.1	3.13(5)
106.1	138.1	3.14(5)	138.1	170.1	2.60(5)
170.1	197.5	2.62(5)	197.5	224.9	2.65(5)
224.9	257.7	3.14(5)	257.7	291.2	1.64(4)
291.2	319.4	1.61(4)	319.4	346.9	1.64(4)
346.9	378.9	1.58(4)	378.9	410.9	1.68(4)
410.9	438.3	1.51(4)	438.3	470.3	1.49(4)
470.3	502.3	1.57(4)	502.3	529.7	1.57(4)
529.7	557.2	1.54(4)	557.2	589.2	1.32(4)
589.2	621.2	1.38(4)	621.2	653.2	1.42(4)
653.2	685.2	1.50(4)	685.2	712.6	1.41(4)
712.6	742.3	1.37(4)	742.3	773.6	1.33(4)
773.6	803.3	1.31(4)	803.3	836.1	1.44(4)
836.1	868.1	1.47(4)	868.1	895.5	1.59(4)
895.5	927.5	1.45(4)	927.5	959.5	1.70(4)
959.5	986.9	1.48(4)	986.9	1018.9	1.51(4)
1018.9	1051.0	1.56(4)	1051.0	1078.4	1.65(4)
1078.4	1110.4	1.62(4)	1110.4	1142.4	1.66(4)
1142.4	1174.4	1.79(4)	1174.4	1211.0	1.49(4)
1211.0	1247.5	1.58(4)	1247.5	1284.1	1.84(4)
1284.1	1320.7	1.79(4)	1320.7	1357.3	1.66(4)
1357.3	1393.9	1.65(4)	1393.9	1430.4	1.62(4)
1430.4	1467.0	1.43(4)	1467.0	1503.6	1.44(4)
1503.6	1540.2	1.93(4)	1540.2	1576.7	1.72(4)
1576.7	1613.3	1.98(4)	1613.3	1649.9	1.50(4)
1649.9	1681.9	1.48(4)	1681.9	1718.5	1.49(4)
1718.5	1750.5	1.44(4)	1750.5	1790.1	1.48(4)
1790.1	1817.5	1.97(4)	1817.5	1851.8	2.25(4)
1851.8	1889.2	2.03(4)	1889.2	1925.0	2.11(4)
1925.0	1959.3	1.98(4)	1959.3	1991.3	2.08(4)
1991.3	2018.7	2.14(4)	2018.7	2046.1	2.16(4)
2046.1	2076.6	2.21(4)	2076.6	2107.1	2.21(4)
2107.1	2137.6	2.49(4)	2137.6	2168.0	2.14(4)
2168.0	2198.5	2.19(4)	2198.5	2229.0	2.42(4)
2229.0	2259.5	2.07(4)	2259.5	2293.9	2.14(4)
2293.9	2317.4	2.17(4)	2317.4	2331.1	1.64(4)
2331.1	2363.1	1.92(4)	2363.1	2407.3	1.75(4)
2407.3	2437.8	1.63(4)	2437.8	2469.8	1.62(4)
2469.8	2503.3	1.53(4)	2503.3	2524.7	1.47(4)
2524.7	2547.5	1.52(4)	2547.5	2573.4	0.94(4)
2573.4	2602.4	1.70(4)	2602.4	2639.0	2.46(4)
2639.0	2667.9	4.53(4)	2667.9	2699.2	4.12(4)
2699.2	2855.4	4.35(4)	2855.4	3126.6	4.08(4)
3126.6	3416.2	5.37(4)	3416.2	3730.1	4.89(4)
3730.1	4046.4	5.41(4)	4046.4	4219.3	5.15(4)
4219.3	4248.3	5.16(4)	4248.3	4266.3	4.35(4)
4266.3	4310.0	2.70(4)	4310.0	4340.5	3.11(4)
4340.5	4371.7	1.53(4)	4371.7	4402.2	1.63(4)
4402.2	4432.7	2.00(4)	4432.7	4462.4	2.48(4)
4462.4	4486.7	4.04(4)			

WELL NAME - 47/15-2 LATITUDE - 53D 33M N.
COUNTRY - NORTH SEA LONGITUDE - 00D 54M E.
COMPANY - AMOCO

DEPTH	TEMP	DEPTH	TEMP	DEPTH	TEMP
0.0	9.0	819.3	30.0	2014.4	61.1
2739.8	93.9	2842.9	95.6		

47/15-2 CONDUCTIVITY DATA

FROM	TO	CONDUCT	FROM	TO	CONDUCT
0.0	439.5	1.64(4)	439.5	471.5	1.66(4)
471.5	503.5	1.83(4)	503.5	531.0	1.76(4)
531.0	563.0	1.74(4)	563.0	595.0	1.88(4)
595.0	622.4	1.91(4)	622.4	654.4	1.97(4)
654.4	686.4	2.00(4)	686.4	713.8	2.13(4)
713.8	745.8	2.08(4)	745.8	777.8	2.38(4)
777.8	805.3	2.21(4)	805.3	837.3	2.63(4)
837.3	869.3	2.48(4)	869.3	896.7	2.70(4)
896.7	942.7	2.37(4)	942.7	960.7	2.11(4)
960.7	983.6	2.63(5)	983.6	1020.2	1.13(4)
1020.2	1052.2	1.08(4)	1052.2	1079.6	1.35(4)
1079.6	1111.6	1.32(4)	1111.6	1139.0	1.37(4)
1139.0	1157.3	1.40(4)	1157.3	1181.7	2.18(4)
1181.7	1212.2	1.59(4)	1212.2	1242.7	1.34(4)
1242.7	1273.1	1.87(4)	1273.1	1303.6	1.87(4)
1303.6	1334.1	1.68(4)	1334.1	1362.8	1.51(4)
1362.8	1395.1	1.49(4)	1395.1	1425.5	1.84(4)
1425.5	1456.0	2.15(4)	1456.0	1486.5	1.94(4)
1486.5	1517.0	1.77(4)	1517.0	1547.5	2.05(4)
1547.5	1585.6	2.00(4)	1585.6	1608.4	2.18(4)
1608.4	1638.9	2.58(4)	1638.9	1669.4	1.56(4)
1669.4	1699.9	2.45(4)	1699.9	1730.3	1.98(4)
1730.3	1760.8	1.86(4)	1760.8	1791.3	2.22(4)
1791.3	1824.8	2.68(4)	1824.8	1855.3	2.21(4)
1855.3	1885.8	2.51(4)	1885.8	1916.3	2.44(4)
1916.3	1943.7	2.20(4)	1943.7	1974.2	2.14(4)
1974.2	2007.1	1.92(4)	2007.1	2038.2	2.91(4)
2038.2	2065.6	3.58(4)	2065.6	2098.5	4.58(4)
2098.5	2126.6	3.62(4)	2126.6	2157.1	4.80(4)
2157.1	2175.4	4.11(4)	2175.4	2211.9	4.23(4)
2211.9	2263.7	4.65(4)	2263.7	2309.5	3.80(4)
2309.5	2355.2	4.17(4)	2355.2	2400.9	4.20(4)
2400.9	2446.6	2.93(4)	2446.6	2492.3	4.07(4)
2492.3	2535.9	4.43(4)	2535.9	2564.0	3.81(4)
2564.0	2596.0	3.91(4)	2596.0	2629.8	3.19(4)
2629.8	2643.2	4.02(4)	2643.2	2647.2	4.80(4)
2647.2	2648.6	4.68(4)	2648.6	2651.6	3.97(4)
2651.6	2664.6	3.49(4)	2664.6	2688.9	1.35(4)
2688.9	2719.4	2.30(4)	2719.4	2751.4	1.90(4)
2751.4	2789.5	1.51(4)	2789.5	2829.9	2.20(4)
2829.9	2842.9	4.01(4)			

WELL NAME - 27/3-1 LATITUDE - 56D 56M N.
COUNTRY - NORTH SEA LONGITUDE - 00D 33M W.
COMPANY - AMOCO

DEPTH	TEMP	DEPTH	TEMP	DEPTH	TEMP
0.0	6.5	1888.5	73.9		

27/3-1 CONDUCTIVITY DATA

FROM	TO	CONDUCT	FROM	TO	CONDUCT
0.0	139.0	2.22(7)	139.0	263.0	2.22(7)
263.0	632.2	1.96(7)	632.2	704.1	1.76(7)
704.1	792.2	2.27(7)	792.2	1274.1	5.45(3)
1274.1	1276.3	4.61(3)	1276.3	1297.6	3.90(3)
1297.6	1318.1	3.87(3)	1318.1	1367.9	4.08(3)
1367.9	1518.2	4.00(3)	1516.2	1649.7	4.04(3)
1649.7	1716.2	3.63(3)	1716.2	1791.9	4.39(3)
1791.9	1859.3	3.02(3)	1859.3	1888.5	3.32(3)

(Reprinted from Nature, Vol. 247, No. 5435, pp. 28–30, January 4, 1974)

North Sea Geothermal Gradients

REGIONAL studies of geothermal gradient patterns obtained from bottom hole temperature measurements in deep oil exploration boreholes have been the subject of several recent papers[1–3]. Harper[1] has produced approximate gradients in a study of the North Sea by the direct use of bottom hole temperatures routinely taken during the logging of exploration wells. These temperatures, which are taken with a maximum mercury-in-glass thermometer at a point typically 30 foot from the bottom of the hole, are, in general, less than the true formation temperature as a result of the cooling effect of the circulating drilling fluid.

The effect of such a thermal disturbance in a borehole may be approximated by a constant line heat source in a uniform infinite medium with a solution as a function of time, as derived by Lachenbruch and Brewer[4]. That solution, for a fixed depth in a borehole, is

$$T(t_2) = K\log(1+t_1/t_2) + T(\infty) \qquad (1)$$

where t_1 is the time of cooling the formation by the circulating fluid, t_2 is the interval from cessation of cooling to temperature measurement, $T(t_2)$ is the observed temperature at time t_2, $T(\infty)$ is the true formation temperature and K is a constant. Thus where multiple values of $T(t_2)$, t_1, and t_2 are known, equation (1) may be applied as a semi-log plot of $T(t_2)$ against $(1+t_1/t_2)$ to produce accurate formation temperatures at the linear axis intercept as was recently shown by Timko and Fertl[5].

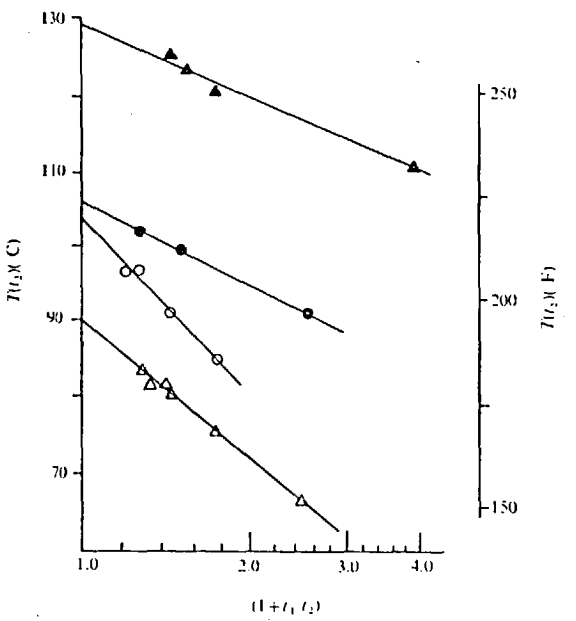


Fig. 1 Thermal recovery of four North Sea exploration boreholes. The temperature intercept is the true formation temperature. ▲, BP, UK; ●, Conoco, UK; ○, Amoco, UK; △, BP, UK.

Bottom hole temperatures from fifty-nine North Sea oil exploration wells, forty in the UK sector, fifteen in the Norwegian, and four in the Dutch, were studied and true formation temperatures calculated by the above method. Figure 1 is a semi-log plot for four typical wells. This method was also applied to a further forty-four results from the previous study by Harper[1]. These were additional data without t_1 values and it was, therefore, necessary to estimate this parameter statistically. The interval t_1, the total time of cooling, is the sum of the time taken to drill the final 30 foot of hole plus any additional time during which fluid circulates after drilling ceases. A log linear relation for drilling rate against depth was observed, while circulation time approximated a normal distribution. These results, based on data from forty-six North Sea wells, allow a satisfactory estimation of t_1 and provide a basis for the application of equation (1).

The determination of all geothermal gradients incorporated the subtraction of sea bottom temperatures from the true formation temperatures with all depths being calculated from sea bottom. Defant[6] showed that the bottom temperature of the central North Sea varies both with water depth and season of the year. Figure 2 shows the transformation of Defant's results to a mean annual temperature at sea bottom as a function of water depth. This result was combined with the true formation temperatures for the calculation of gradients. Geothermal gradients calculated from bottom hole temperatures uncorrected for the thermal disturbance of the drilling fluid would typically be lower than true gradients by 10–15%.

A geothermal gradient contour map, Fig. 3, is based on the total one hundred and three determinations with individual results being averaged over petroleum lease blocks which are 8 by 12 miles in the UK sector and somewhat larger in the others. As stated by Harper[1] and confirmed here, the regional trends seem to be governed by the major structural elements. The major sedimentary basins, English, SW Netherlands, German, Norwegian, East Shetlands, Moray Firth, and Midland Valley are all areas of high geothermal gradients with values locally reaching 44° C km^{-1}. Structural highs including Ringkobing-Fyn, Norwegian Platform, Mid North Sea, Mid Netherlands, and Grampian are characterised by low gradients which, south of Norway, approach 18° C km^{-1}. A geothermal high confirmed by four wells, located at approximately 55° N, 00° E, seems to confirm Armstrong's[7] opinion of the probable presence of Carboniferous coal-bearing rocks at a distance of one hundred miles from the Yorkshire coast trending ESE to fifty miles from the Norfolk coast. A thin stratum of coal above the bottom hole temperature measurement point with thickness 2–3% of that of the total formation would lower the

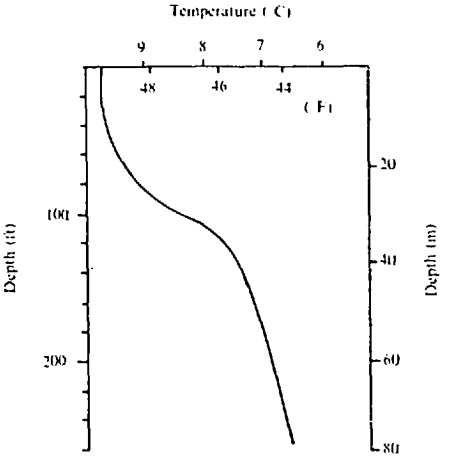


Fig. 2 Mean annual North Sea bottom temperature against water depth.

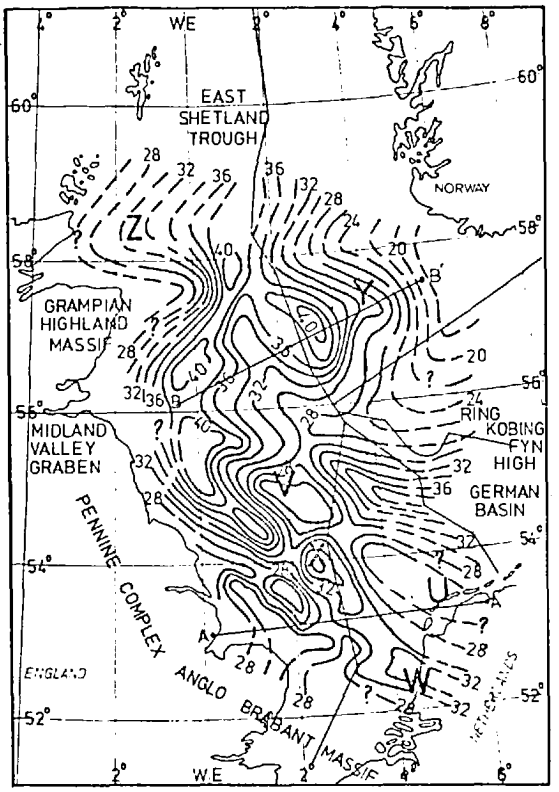


Fig. 3 Geothermal gradients, North Sea. Contour interval 2°C km^{-1}. U, Mid Netherlands Ridge (3%); V, Mid North Sea High (11%); W, S.W. Netherlands Basin (8%); X, English Basin (46%); Y, Norwegian Basin (18%); Z, Moray Firth Basin (2%). Numbers in parentheses refer to percentages of total data in each area. The remaining 12% of data is in the Western (British) extension of the Norwegian Basin.

overall thermal conductivity by approximately 25% due to its very low thermal conductivity[8], and could thus be a viable explanation of this anomaly. In addition there is a strong correlation, north of 56°, with the recently published Palaeocene isopach and base of Tertiary structure maps[9]. The coincidence of high geothermal gradients with the Tertiary depocentres reflects the lower thermal conductivity of this predominantly marine shale sequence.

Figure 4 incorporates diagrammatic cross sections of the

Table 1 Estimates of Thermal Conductivity

Section	Dominant lithology	Thermal conductivity [W m^{-1} K^{-1}]
Quaternary/Tertiary	Shale[11]	1.76 (ref. 3)
Cretaceous (including Danian)	Chalk[7,11]	1.84 (unpublished observations)
Jurassic	Sand/shale[10,11]	2.64 (ref. 3)
Triassic	Sand[7,10,11]	3.10 (ref. 3)
Upper Permian (Zechstein)	Evaporite/carbonate[7,10,11]	3.85 (ref. 12)
Lower Permian (Rotliegendes)	Sand[10,11]	3.10 (ref. 3)
Carboniferous	Shale/limestone[10,11]	1.94 (ref. 12)

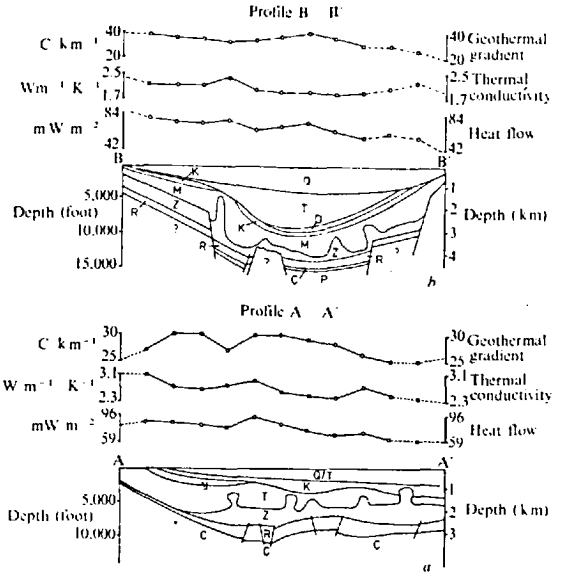


Fig. 4 *a*, Thermal and geological profiles of the southern North Sea. Geology after Armstrong[7]. Data points are samples from the contour map, Fig. 3, taken at equispaced points on profile A–A'. Q, Quaternary; T, Tertiary; D, Basal Tertiary/Upper Cretaceous (Danian); K, Cretaceous; J, Jurassic; T, Triassic; M, undifferentiated Jurassic/Triassic; Z, Upper Permian (Zechstein); R, Lower Permian (Rotliegendes); C, Carboniferous. *b*, As *a* but for central North Sea, profile B–B'.

North Sea in the positions indicated on Fig. 3 as well as the geothermal gradient, conductivity, and heat flow profiles. Estimates of thermal conductivity (Table 1) were made from published descriptions of the major lithological units of the North Sea together with the measured thermal conductivities of similar materials. Mean estimated heat flows of 75 mW m^{-2} from the southern profile (A-A') and 71 mW m^{-2} from the northern profile (B-B') were obtained, thus indicating no significant difference despite the higher gradients observed to the north. The values of heat flow, while slightly higher than the world mean[13], are intermediate in terms of other European basin values[1] and in good agreement with the world-wide mean for marginal seas[14]. A possibly significant aspect of Fig. 4 is that both heat flow profiles show an apparent decrease towards the European continent. This is consistent with world-wide heat flow means of 61.9 mW m^{-2} for post-Precambrian orogenic areas such as Great Britain and 38.5 mW m^{-2} for Precambrian shields such as Norway[14]. Seven recent combined heat flow-heat production measurements in Precambrian and Permian igneous rocks in southern Norway support such a value[15]. But, in general, the paucity of heat flow data in this area limits any attempt to confirm this trend.

Recent oil discoveries in the North Sea such as the Forties (57° 40′ N, 1° 0′ E) and Ekofisk (56° 30′ N, 3° 10′ E) fields seem to support the theories of Klemme[16] that high geothermal gradients enhance petroleum mobility, that is, migration to structural traps, to a greater degree than they adversely affect reservoir quality.

We thank the following oil companies for permission to use temperature data from their North Sea wells: Amoco, BP, Conoco and Phillips. We also thank Drs M. L. Harper and H. Y. Tammemagi for advice.

TOM R. EVANS

Department of Geology,

N. C. COLEMAN

Department of Physics,
Imperial College,
London

Received September 5; revised November 5, 1973.

1 Harper, M. L., *Nature*, **230**, 235 (1971).
2 Summers, W. K., *Am. Assoc. Petrol. Geol. Bull.*, **56**, 2072 (1972).
3 Girdler, R. W., *Phil. Trans. R. Soc.*, **A267**, 191 (1970).
4 Lachenbruch, A. H., and Brewer, M. C., *US Geol. Surv. Bull.*, 1083C, 78 (1959).
5 Timko, J. T., and Fertl, W. M., *Wld. Oil*, **175**, 73 (1972).
6 Defant, A., *Phys. Oceanog.*, **1**, 116 (1961).
7 Armstrong, G., *Min. Eng.*, **131**, 474 (1972).
8 Bullard, E. C., and Niblett, E. R., *Mon. Not. R. astr. Soc. geophys. Supp.*, **6**, 222 (1951).
9 Dunn, W. W., Eha, S., and Heikkila, H. H., *Oil Gas J.*, **71**, 90 (1973).
10 Gill, W. D., *Proc. Seventh W. Petrol. Congr., Mexico*, **2**, 211 (1967).
11 King, R. E., *Wld. Oil.*, **175**, 35 (1972).
12 Clark, S. P., *Handbook of Physical Constants, Mem. 97, Geol. Soc. Am.*, 459 (1966).
13 Lee, W. H. K., and Uyeda, S., *Am. geophys. Monog. Ser.*, **8**, 87 (1965).
14 Lee, W. H. K., and Uyeda, S., *Am. geophys. Monog. Ser.*, **8**, 147 (1965).
15 Swanberg, C. A., Simmons, G., Chessman, M. D., Gronlie, G., and Heier, K. S., *Trans. Am. geophys. Union*, **54**, 464 (1973).
16 Klemme, H. D., *Oil Gas J.*, **70**, 76 (1972).

Earth and Planetary Science Letters, 23 (1974) 349–356
© North-Holland Publishing Company, Amsterdam – Printed in The Netherlands

HEAT FLOW AND HEAT PRODUCTION IN NORTHEAST AFRICA

T.R. EVANS and H.Y. TAMMEMAGI

Geology Department, Imperial College of Science and Technology, London (Great Britain)

Received August 28, 1974

The analysis of both temperature data and thermal conductivity material from seven deep oil exploration boreholes in northeast Africa has allowed the calculation of a heat flow value in the Somalian Horn (average 58 ± 12 mW m^{-2}) and one from the coastal plain of northeast Sudan (average 96 ± 19 mW m^{-2}). Heat production measurements of granites from the Sudanese basement indicate a substantial depletion in the radiogenic heat producing elements.

The heat flow results complement previous measurements from the Gulf of Aden and the Red Sea and are consistent with the geological and geophysical consensus that these two regions are young proto-oceans formed by the mechanisms of spreading lithospheric plates. The heat production evidence suggests that the lithospheric plate beneath the Sudan coastal plain is approximately 30–50 km thick and underlain by a zone of partial or complete melt.

1. Introduction

There is convincing evidence from sub-ocean topography [1,2], magnetic lineations [2–4], and seismic refraction data [5, 6], that both the Red Sea and Gulf of Aden are young proto-oceans formed in the last 40 m.y. Heat flow data [7, 8] further corroborate that the two oceans are being formed by the spreading apart of lithospheric plates with values in qualitative agreement with those predicted analytically for a slab of constant thickness moving with a constant velocity [9]. To date the majority of Red Sea and Gulf of Aden heat flow data have been determined by the oceanic measuring technique [10] with the consequence that its limitations with respect to sea-bottom temperature stability have restricted measurements to water depths [11] typically found only within 100 km of the central ridge/rift. There is a distinct need, in both regions, for reliable data at greater distances from the spreading axes and it is to this purpose that we present these new heat flow values from the northeast African continental margin .

2. Geologic setting

Three of the heat flow sites are situated on the coastal plain of the Sudan in the Ras Abu Shagara region (Fig. 1). The coastal plain consists of Tertiary sediments and Miocene volcanics covered by thin recent sands and gravels [12, 13]. Immediately west of the Sudan coast the crystalline basement outcrops. The oldest rocks of this area are pelitic schists, quartzites, rhyolitic volcanics and marbles into which granites have been intruded in two major phases [14].

The older more extensive Batholithic Granite is, in the main, a leucocratic biotite-hornblende granodiorite which has been dated at 554 ± 54 m.y., while the intrusives, commonly referred to as the Younger Granites, range from sodic syenite through quartz syenite to riebeckite and mica-bearing granite [14] and have been dated at 394 ± 9 m.y. The Batholithic Granite, to the east, unconformably underlies the coastal Tertiary sediments [12, 13] and its total overall extent is greater than 24,000 km^2 [14]. Samples of both granite types were analyzed by gamma-ray spectrometry for uranium, thorium and potassium, the only significant heat producing elements. The radioactive heat contribution of the crust was determined and incorporated in the interpretation of the heat flow data.

The four remaining heat flow sites are located in the Somalia Republic on the Horn of Africa (Fig. 2). This part of Africa has a Lower Jurassic through Lower Miocene marine sedimentary sequence [16] overlying the Palaeozoic metamorphic Inda Ad formation comprising mainly paraschists [17], and the Precambrian crystalline

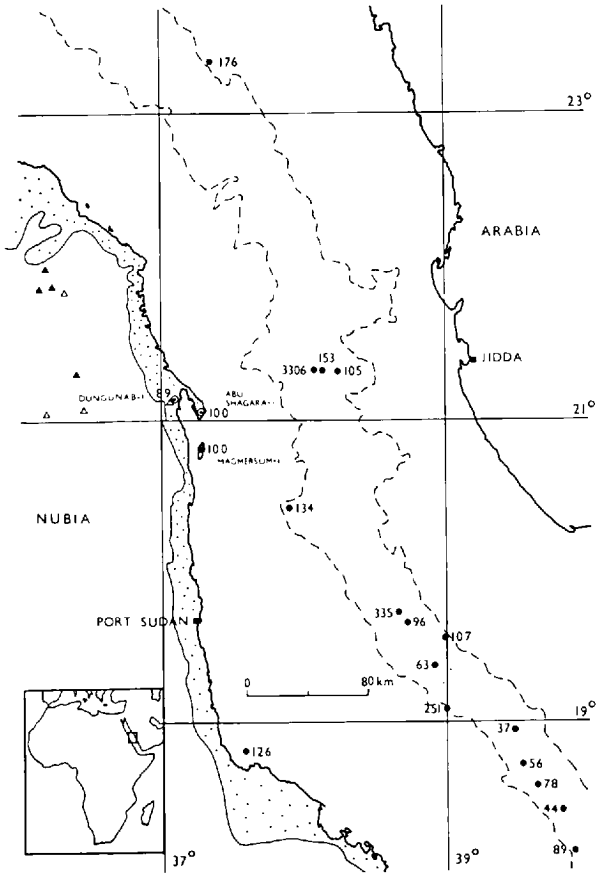


Fig. 1. Heat flow data in the central Red Sea region. The dotted open circles are values presented in this paper, open and closed triangles represent heat production samples of Younger and Batholithic Granite, respectively. The dashed line marks the 500-fathom contour and the stippled region shows the extent of the coastal sediments.

basement. The post-basement tectonics involve block faulting and subsidence of the Indian ocean coastal plain. Volcanism is in evidence with basalts of the Trap (mid Tertiary) and Aden (Quaternary) series along the northern coast and the Somalia Plateau [16]. The drifting apart of Arabia and Somaliland has produced, in addition to the central ridge, graben and marginal scarp [45], much of the Tertiary faulting on the Somalia Horn (12).

3. Basic data and heat flow reduction

Geothermal gradients were determined in all cases from bottom-hole temperatures measured with maximum mercury-in-glass thermometers several hours after drilling fluid ceased to circulate. Recent studies of such temperature data from North Sea oil wells [18, 19] confirm that these measurements yield thermal gradients to an accuracy of about 10%. It should be noted that this accuracy is applicable only to boreholes where the temperature measurement is made at or close to the bottom of the well. For a single well (Sagleh-1) a continuous temperature log was available but the effects of the circulating drilling fluid tended to reduce the actual gradient over most of its length and it was not used. The bottom-hole temperatures are plotted in Fig. 3 (Sudan) and Fig. 4 (Somalia). The average extrapolated surface temperatures, based on available thermal conductivity data, were 27.5 and 25.2°C for the Sudan and Somalia, respectively. These are considered to be in reasonable agreement with the mean annual temperatures of about 29°C.

Thermal conductivity determinations were made on a total of 205 borehole samples using a standard-divided bar apparatus as described by Birch [20]. Cylindrical discs were cut from the solid cores which were available from five of the boreholes. All thermal conductivity samples were saturated with water under a moderate vacuum and subjected to a uniaxial pressure of 70 bars during measurement. As only drill cutting samples, rock chips of about 1 mm, were available for two boreholes (Hordio-1, Cotton-1), the technique of Sass et al. [21] was employed.

Schlumberger micrologs were used to calculate a porosity value at the depth of each cutting sample to allow the correction of nonporous to porous thermal conductivity [21]. In a few instances hole conditions did not permit a porosity estimate and the uncorrected, nonporous, values were used.

Thermal conductivities measured on solid core are accurate to within 2%; values from chips are less reliable with an uncertainty of 5% after the correction for porosity.

Thermal conductivity is dependent, to a degree, on the in-situ temperature whereas the measurements reported here have been made at room temperature. Preliminary results from a study currently in progress suggest that this correction, for the subsurface temperatures and rock types encountered here, will be small, typically leading to a reduction in thermal conductivity of 5%.

A wide range of lithologies were encountered with

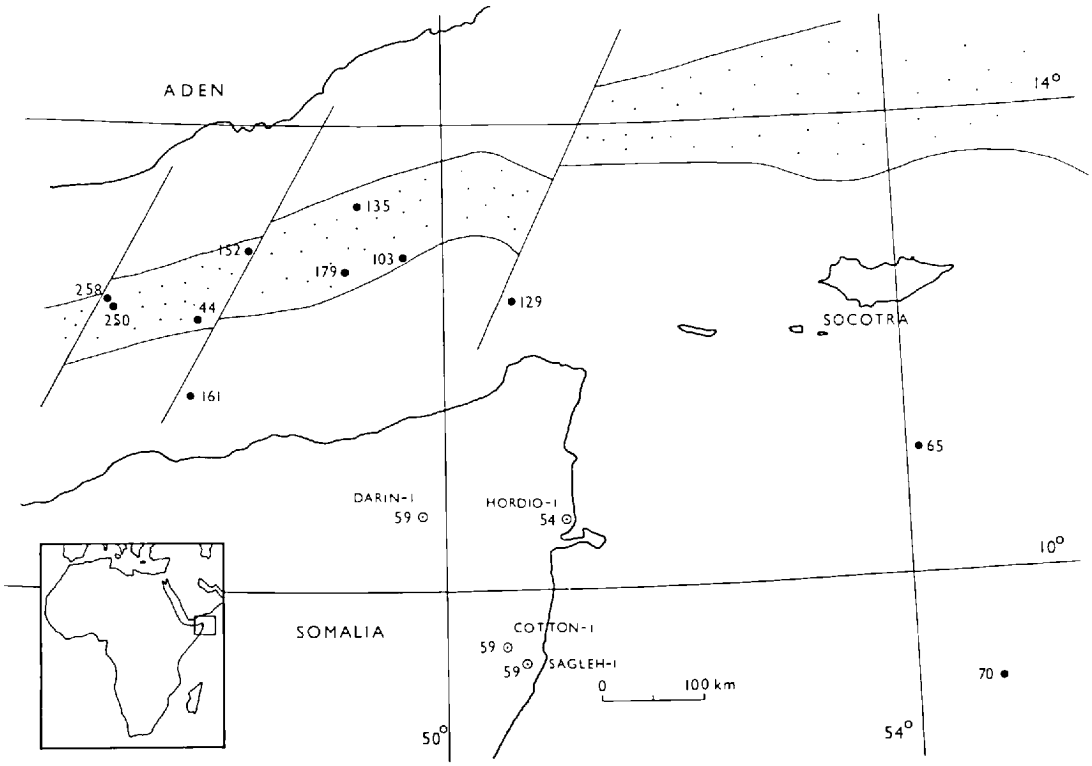
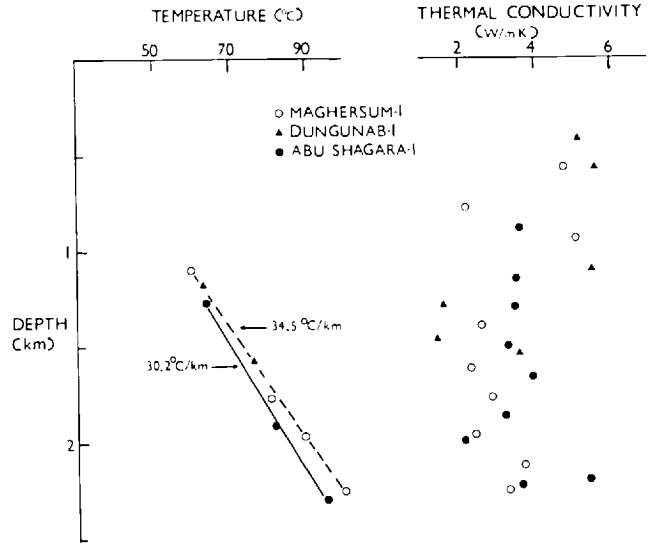
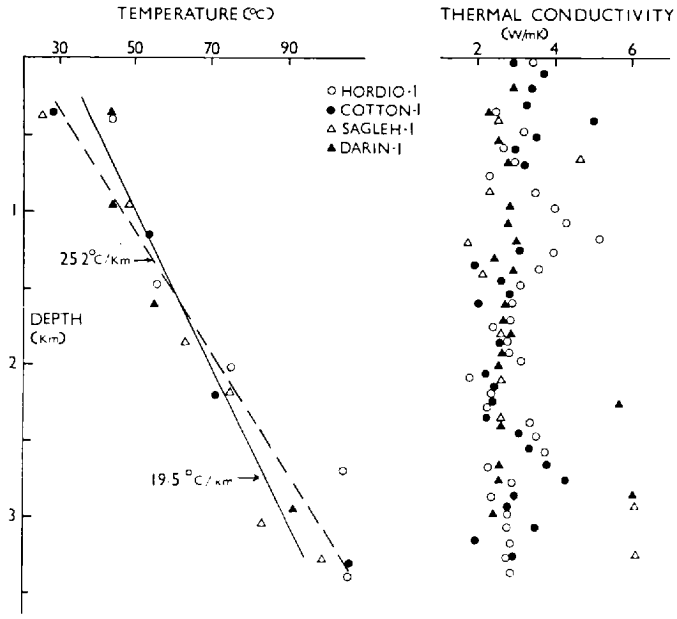


Fig. 2. Heat flow data from the Somalian Horn region. Dotted open circles represent values from this study and the stippled region delineates the approximate zone of new oceanic crust [15].



LITHOLOGY	AGE
SANDS LIMESTONE	PLIO- PLEISTOC.
HALITE	POST MID MIOCENE
LIMESTONE	MID MIOC.
MARLS CONGLOMER. EVAPORITES	MID LOWER MIOCENE
RED SS.	EOCENE
MARLS	CRET.?
BASALTS SERPENTINE GRANITES METAMORPHICS	AGE UNCERTAIN

Fig. 3. Borehole temperature and thermal conductivity data for the three northeast coastal Sudan heat flow sites. Least-squares fits for the maximum (Abu Shagara-1) and minimum (Maghersum-1) geothermal gradients are indicated. The major lithologic units and their ages for northeast coastal Sudan are included (after Carella and Scarpa [12]).



LITHOLOGY	AGE
CONGLOMERATE	MIOCENE
CALCARENITE	U. EOCENE
DOLOMITE ANHYDRITE	L. EOCENE
LIMESTONE	U. PALEOCENE
MARLS	L. PALEOCENE
SANDSTONE	U. CRET.
LIMESTONE MARLS SHALES	L. CRET.
ANHYDRITE	U. JURASSIC
LIMESTONE	L. JURASSIC
SANDSTONE	TRIASSIC?
SCHIST	?

Fig. 4. Borehole temperature and thermal conductivity data for the four Horn of Somalia heat flow sites. Least-squares fits for the maximum (Cotton-1) and minimum (Darin-1) geothermal gradients are indicated. The major lithologic units and their ages for the Horn of Somalia are indicated (after Azzaroli and Fois [16]). Thermal conductivities shown for Cotton-1 and Hordi-1 are uncorrected for porosity.

evaporites and arenaceous materials predominating in the Sudan and argillaceous and carbonate sequences more abundant in Somalia. Values of thermal conductivity ranged from 1.5 W m^{-1} K^{-1} for the more argillaceous material to 6.0 W m^{-1} K^{-1} for the quartzitic and evaporitic samples. The thermal conductivities and lithologies are shown as functions of depth in Fig. 3 (Sudan) and Fig. 4 (Somalia).

Since the lithology, and hence the conductivity, for each borehole is, in general, rather variable, it was necessary to adopt a resistance -integral method of computing heat flow [22]. The temperature T, at depth z, is plotted against the integrated thermal resistance to that depth, and given that the heat flow, q, is constant a linear relationship results of the form:

$$T(z) = T(0) + q \cdot \sum_i z_i/K_i \qquad (1)$$

where z_i is the interval of depth of thermal conductivity K_i. Detailed lithologic logs for both the Sudan [12] and Somalia [16] wells were available for defining upper and lower values of z_i for all conductivity measurements. $T(0)$, the surface temperature, and q are

TABLE 1
Sudanese coast and adjacent Red Sea

Station	Lat.	Long.	Heat flow	Ref.
CH 61	21°22′	38°05′	>3300	[28]
DSDP 227	21°20′	38°08′	153	[46]
DSDP 225	21°19′	38°15′	105	[46]
Dungunab-1	21°08′	37°05′	88.7	this paper
Abu Shagara-1	21°03′	37°17′	99.6	this paper
Maghersum-1	20°49′	37°17′	100.0	this paper
5234	20°27′	37°55′	133.9	[25]
CH 61-153	19°43′	38°41′	335.3	[28]
142	19°38′	38°44′	96.3	[8]
CH 61-154	19°34′	38°59′	106.7	[28]
CH 61-155	19°23′	38°54′	62.8	[28]
DSDP 228	19°05′	39°00′	251?	[46]
146	18°57′	39°26′	38.8	[8]
Durwara 1,2	18°49′	37°38′	126.4	[7]
144	18°42′	39°30′	55.7	[8]
148	18°34′	39°36′	76.6	[8]
5232	18°24′	39°47′	44	[25]
139	18°8′	39°53′	88.7	[8]

TABLE 2
Somalian Horn and adjacent seas

Station	Lat.	Long.	Heat flow	Ref.
Cotton-1	9°33′	50°31′	58.6	this paper
Darin-1	10°40′	49°45′	59.0	this paper
Sagleh-1	9°25′	50°40′	59.0	this paper
Hordio-1	10°37′	51°00′	54.4	this paper
Dis 5226	11°07′	54°03′	64.9	[25]
Z-6	9°08′	54°42′	69.5	[44]
Dis 5229	12°29′	47°2′	257.4	[25]
Z-1	12°27′	47°7′	250.3	[44]
Dis 5227	11°39′	47°50′	161.2	[25]
273	12°21′	47°52′	42.3	[8]
Z-2	12°57′	48°16′	151.5	[44]
269	12°47′	49°08′	178.7	[8]
Z-3	13°17′	49°15′	134.8	[44]
Z-4	12°54′	49°38′	103.4	[44]
Z-5	12°25′	50°33′	129.3	[44]

determined by an application of the least-squares method. The calculated heat flows are listed in Tables 1 and 2 and mapped on Fig. 1 (Sudan) and Fig. 2 (Somalia).

The heat flow values have an estimated error of approximately 20%. This value is composed of a 10% error in geothermal gradient, a 5% error, maximum, in measured thermal conductivity and 5% error as a result of decreased thermal conductivity due to in-situ temperatures. This total error is much less than the observed standard deviation in the least-squares solution of (1) for any of the wells.

4. Discussion

4.1. The Somalia Horn

The four heat flow values from Somalia, the first reported for this country, are consistent and average 58 ± 12 mW m^{-2}. This value is slightly greater than the Indian Ocean mean of 55 mW m^{-2} [23] although significantly less than the Gulf of Aden average of 149 mW m^{-2} [8]. The regional distribution of heat flow is shown in Fig. 1 and listed in Table 2.

The heat flow data for the Gulf of Aden region [44, 25, 8] have been plotted on Fig. 5b superimposed on McKenzie's [9] model for a spreading lithosphere. There is qualitative agreement with a high, but variable, heat flow associated with the zone of new crustal generation. The Somalian values are included for the sake of comparison; these are in agreement with that expected from a province which underwent tectonic activity during the Palaeozoic [36, 37].

4.2. Coastal Sudan

The three values from the coastal plain of the Sudan are in agreement, within expected errors, and yield an average heat flow of 96 ± 19 mW m^{-2}. This value is considerably above the world average of 61.5 mW m^{-2} [23] although lower than the mean for the Red Sea of 116 mW m^{-2} [8]. Heat flow values for the central Red Sea are shown in Fig. 1, and details are given in Table 1. All values have been determined by the oceanic measuring technique with the exception of those of Girdler [7] and this paper. Although very variable the data suggest high heat flow near the central trough; this is consistent with results from other parts of the world oceanic ridge system [24].

McKenzie [9] has obtained solutions for the theoretical heat flow over a lithospheric plate of constant

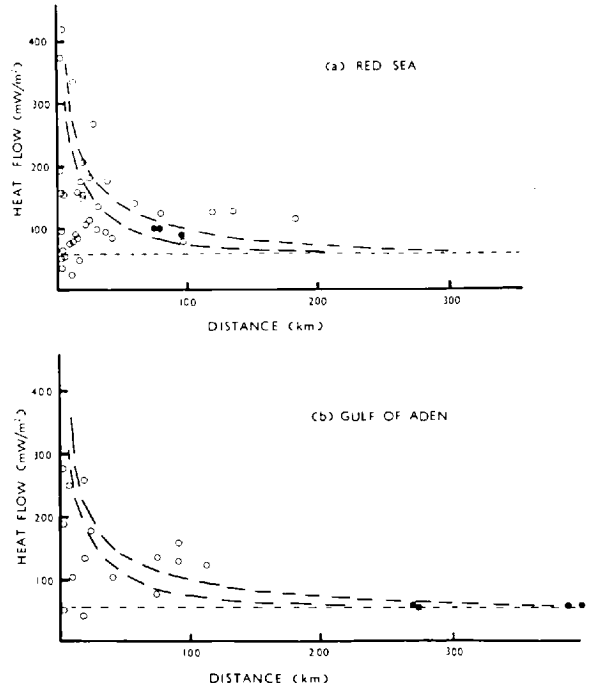


Fig. 5. Model for spreading lithosphere (upper curve in each diagram is for spreading rate of 2 cm a^{-1}, lower for 1 cm a^{-1}) with all available heat flow data superimposed. Solid circles indicate values from this study.

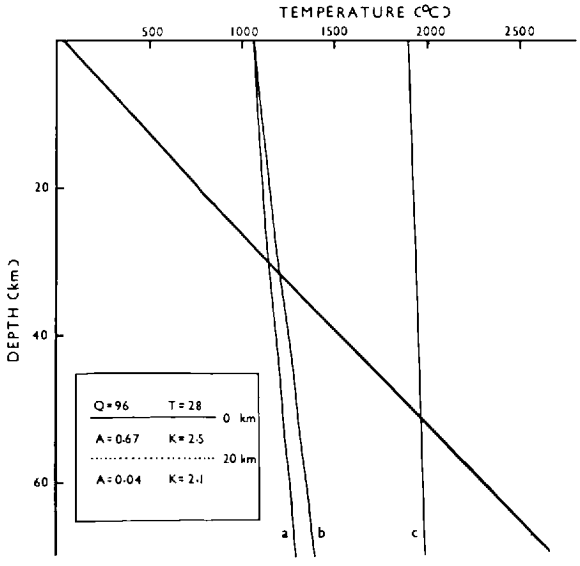


Fig. 6. The temperature profile calculated for the model shown in the inset. Curves a, b, c, are the solidus for dry gabbro [39], the pyrolite solidus [40] and the melting point for forsterite [41], respectively. The symbols Q, T, A and K represent surface heat flow (mW m^{-2}), surface mean temperature (°C), heat production (μW m^{-3}) and thermal conductivity (W m^{-1} °K^{-1}), respectively.

thickness moving at constant velocity with a "dyke intrusion" at constant temperature at one margin. Fig. 5a from McKenzie [9], illustrates the heat flow pattern for a 50-km thick plate with velocities of 1 and 2 cm a^{-1} and superimposed are all the available heat flow data [7, 8, 25–28, 46, this paper] from the Red Sea. These velocities are consistent with the magnetic lineation evidence [3, 4], suggesting a spreading rate of approximately 1 cm a^{-1} for the past few million years. The heat flow data presented here, the first Red Sea continental margin data with measured thermal conductivities, are in agreement with such a spreading rate.

Heat production studies of igneous rocks indicate that surface measurements are representative of the crustal radioactive content to a considerable depth [29–31]. The granitic pluton of northeast Sudan was, therefore, investigated as a potential heat source. A suite of eight granite samples, four Batholithic and four Younger, were analyzed for K, U, and Th with a gamma-ray spectrometer and radioactive heat production calculated using the constants of Birch [32]. The heat production sample sites are shown in Fig. 1 and the results presented below.

	K (%)	U (ppm)	Th (ppm)	Heat production (μ W m^{-3})
Average of 8 granites	1.9	1.0	3.4	0.67 ± 0.49

There was no substantial difference between the Batholithic and Younger Granite. The overall average heat production of 0.67 μW m^{-3} with a standard deviation of 0.49 is considerably less than the 2.5 μW m^{-3} for "typical" granite [33] and indicates that the sialic crust is not contributing significantly to the measured heat flow. This is in contrast to the stable Precambrian granite environment of West Africa where similarly low heat production is found, but the measured heat flow is only 25 mW m^{-2} [34, 35]. This is in agreement with the worldwide correlation of heat flow with tectonic provinces, the older ones having lower heat flow [36, 37].

With the available data and with reasonable assumptions concerning heat production and thermal conduction in the upper mantle it is possible to derive a temperature depth profile for northeast Sudan. Fig. 6 shows a two-layer model with its corresponding temperature profile; the crustal depth of 20 km has been estimated by Qureshi [38]. Although the steady-state model does not account for dynamic plate movement [9, 42], it represents a first-order estimate of the thermal regime. The temperature gradient is high and transgresses the solidus of most relevant materials in the range 30–50 km. The heat flow data thus suggest that the lithosphere of the Red Sea margin, in the region of the northeast Sudan, is of the order of 40 km thick and is underlain by a zone of total or partial melt. Once this zone is reached the mechanism of conductive heat transfer and hence the postulated temperatures of Fig. 6 will probably not be valid. These arguments are in favour of the low-velocity zone being a region of partial melt [43].

Acknowledgements

We are grateful to AGIP (Attivita Minerarie Esplorazione e Produzione Idrocarburi), and in particular Mr. E. Pacchiarotti and Dr. V. Fois, for providing the subsurface temperature data and borehole samples which

made this study possible. We also thank Dr. C. Neary and Prof. I. Gass for kindly providing the heat production samples. Miss R.J. Spragg and Mr. J.S. Dare are thanked for assistance in sample preparation and measurement. We thank Mr. K.H. Williamson for critically reviewing the manuscript. The project has been supported in part by the Natural Environment Research Council.

References

1 A.S. Laughton, A new bathymetric map of the Red Sea, Phil. Trans. R. Soc. Lond. Ser. A, 267 (1970) 21.
2 A.S. Laughton, R.B. Whitmarsh and M.T. Jones, The evolution of the Gulf of Aden, Phil. Trans. R. Soc. Lond. Ser. A, 267 (1970) 227.
3 F.J. Vine, Spreading of the ocean floor: new evidence, Science 154 (1966) 1405.
4 R.W. Girdler and P. Styles, Two stage Red Sea floor spreading, Nature 247 (1974) 7.
5 C. Tramontini and D. Davies, A seismic refraction survey in the Red Sea, Geophys. J.R. Astr. Soc. 17 (1969) 225.
6 A.S. Laughton and C. Tramontini, Recent studies of the crustal structure in the Gulf of Aden, Tectonophysics 8 (1969) 359.
7 R.W. Girdler, A review of Red Sea heat flow, Phil. Trans. R. Soc. Lond. Ser. A, 267 (1970) 191.
8 R. Haenel, Heat flow measurements, Red Sea and Gulf of Aden, Z. Geophysik 38 (1972) 1035.
9 D.P. McKenzie, Some remarks on heat flow and gravity anomalies, J. Geophys. Res. 72 (1967) 6261.
10 M.G. Langseth, Measuring heat flow through the ocean floor, in: W.H.K. Lee, ed., Terrestrial Heat Flow, American Geophysical Union Geophys. Monograph 8 (1965) 58.
11 G. Seidler, General circulation of water masses in the Red Sea, in: E.T. Degens and D.T. Ross, eds., Hot Brines and Recent Heavy Metal Deposits in the Red Sea (Springer-Verlag, Berlin, 1969) 131.
12 R. Carella and M. Scarpa, Geological results of exploration in Sudan by AGIP Mineraria: 4th Arab Petroleum Congr., Beirut (1962).
13 J. Sestini, Cenozoic stratigraphy and depositional history, Red Sea Coast, Sudan, Bull. Am. Assoc. Pet. Geol. 49 (1965) 1453.
14 I.G. Gass and C.R. Neary, The granitic association of the N.E. Sudan, Bull. Geol. Soc. Am. (1974) in press.
15 M.D. Beltrandi and A. Pyre, Geological evolution of south west Somalia, in: G. Blant, ed., Symposium on Sedimentary Basins of the African Coasts, Part II, South and East Coast (Assoc. Services Geol. Africains, Paris, 1972) 159.
16 A. Azzaroli and V. Fois, Geological outlines of the Northern end of the Horn of Africa, XXII Int. Geol. Congr. India, (1964) 293.
17 Somaliland Oil Expl. Co. Ltd., A geological reconnaissance of the sedimentary deposits of the protectorate of British Somaliland, Crown Agents, London (1954).
18 M.L. Harper, Approximate geothermal gradients in the North Sea, Nature 230 (1971) 235.
19 T.R. Evans and N.C. Coleman, North Sea geothermal gradients, Nature 247 (1974) 28.
20 F. Birch, Heat flow in the Front Range, Colorado, Bull. Geol. Soc. Am. 61 (1950) 567.
21 J.H. Sass, A.H. Lachenbruch and R.J. Munroe, Thermal conductivity of rocks from measurements on fragments and its application to heat flow determinations, J. Geophys. Res. 76 (1971) 3391.
22 E.C. Bullard, Heat flow in South Africa, Proc. R. Soc. Lond. Ser. A, 173 (1939) 474.
23 W.H.K. Lee, Global variations of terrestrial heat flow, Phys. Earth Planet. Interiors 2 (1970) 332.
24 M.G. Langseth, X. Le Pichon and M. Ewing, Crustal structure of mid-ocean ridges, 5, Heat flow through the Atlantic ocean floor and convection currents, J. Geophys. Res. 71 (1966) 5321.
25 J.G. Sclater, Heat flow in the Northwest Indian Ocean and Red Sea, Phil. Trans. R. Soc. 259 (1966) 271.
26 F.S. Birch and A.J. Halunen Jr., Heat flow measurements in the Atlantic Ocean, Indian Ocean, Mediterranean Sea, and Red Sea, J. Geophys. Res. 71 (1966) 583.
27 M.G. Langseth, G. Marcus Jr. and P.T. Taylor, Recent heat flow measurements in the Indian Ocean, J. Geophys. Res. 72 (1967) 6249.
28 A.J. Erickson and G. Simmons, Thermal measurements in the Red Sea, in: E.T. Degens and D.T. Ross, eds., Hot Brines and Recent Heavy Metal Deposits in the Red Sea (Springer-Verlag, Berlin, 1969) 114.
29 F. Birch, R.F. Roy and E.R. Decker, Heat flow and thermal history in New England and New York, in: W. White and E. Anzen, eds., Studies of Appalachian Geology: Northern and Maritime (Interscience, New York, 1968) 437.
30 R.F. Roy, D.D. Blackwell and F. Birch, Heat generation of plutonic rocks and continental heat flow provinces, Earth Planet. Sci. Lett. 5 (1968) 1.
31 A.H. Lachenbruch, Preliminary geothermal model of the Sierra Nevada, J. Geophys. Res. 73 (1968) 6977.
32 F. Birch, Heat from radioactivity, in: H. Faul, ed., Nuclear Geology (John Wiley and Sons, New York, 1954) 148.
33 J. Sass, The Earth's heat and internal temperatures, in: I.G. Gass, P.J. Smith and R.C.L. Wilson, eds., Understanding the Earth (Artemis Press, Sussex, 1972) 81.
34 J. Wheildon and H.Y. Tammemagi, Heat flow in Sierra Leone (1974) in preparation.
35 D.S. Chapman and H.N. Pollack, Very low heat flow in the West African sheild (abstract), Trans. Am. Geophys. Union 55 (1974) 424.
36 B.G. Polyak and Ya. B. Smirnov, Relationship between terrestrial heat flow and the tectonics of continents, Geotectonics 4 (1968) 205.
37 J.G. Sclater and J. Francheteau, The implications of terrestrial heat flow observations on current tectonic and geochemical

models of the crust and upper mantle of the Earth, Geophys. J.R. Astr. Soc. 20 (1970) 509.
38 I.R. Qureshi, Gravity measurements in the North-Eastern Sudan and crustal structure of the Red Sea, Geophys. J.R. Astr. Soc. 24 (1971) 119.
39 P.J. Wyllie, Experimental limits for melting in the Earth's crust and upper mantle, in: J.G. Heacock, ed., The structure and Physical Properties of the Earth's Crust, American Geophysical Union Geophys. Monograph 14 (1971) 279.
40 A.E. Ringwood, Composition and evolution of the upper mantle, in: P.J. Hart, ed., The Earth's Crust and Upper Mantle, American Geophysical Union Geophys. Monograph 13 (1969) 1.
41 B.T.C. Davis and J.L. England, The melting of forsterite up to 50 kilobars, J. Geophys. Res. 69 (1964) 1113.
42 Y. Bottinga and C.J. Allegre, Thermal aspects of sea-floor spreading and the nature of the oceanic crust, Tectonophysics 18 (1973)1.
43 D.L. Anderson and C. Sammis, Partial melting in the upper mantle, Phys. Earth Planet. Interiors 3 (1970) 41.
44 R.P. von Herzen and M.G. Langseth, Present status of oceanic heat flow measurements, Phys. Chem. Earth 6 (1966) 365.
45 A. Azzaroli, On the evolution of the Gulf of Aden, Rep. 23rd Int. Geol. Congr., Prague (1968) 125.
46 R.W. Girdler, A.J. Erickson and R. von Herzen, Downhole temperature and shipboard thermal conductivity measurements aboard D/V "Glomar Challenger" in the Red Sea, in: Init. Rep. Deep Sea Drilling Project, 23 (U.S. Government Printing Office, Washington, 1974) 879.